SYSTEMS BIOCATALYSIS FOR BIOPROCESS DESIGN

EDITED BY: Roland Wohlgemuth, Jennifer Ann Littlechild and Byung-Gee Kim

PUBLISHED IN: Frontiers in Bioengineering and Biotechnology

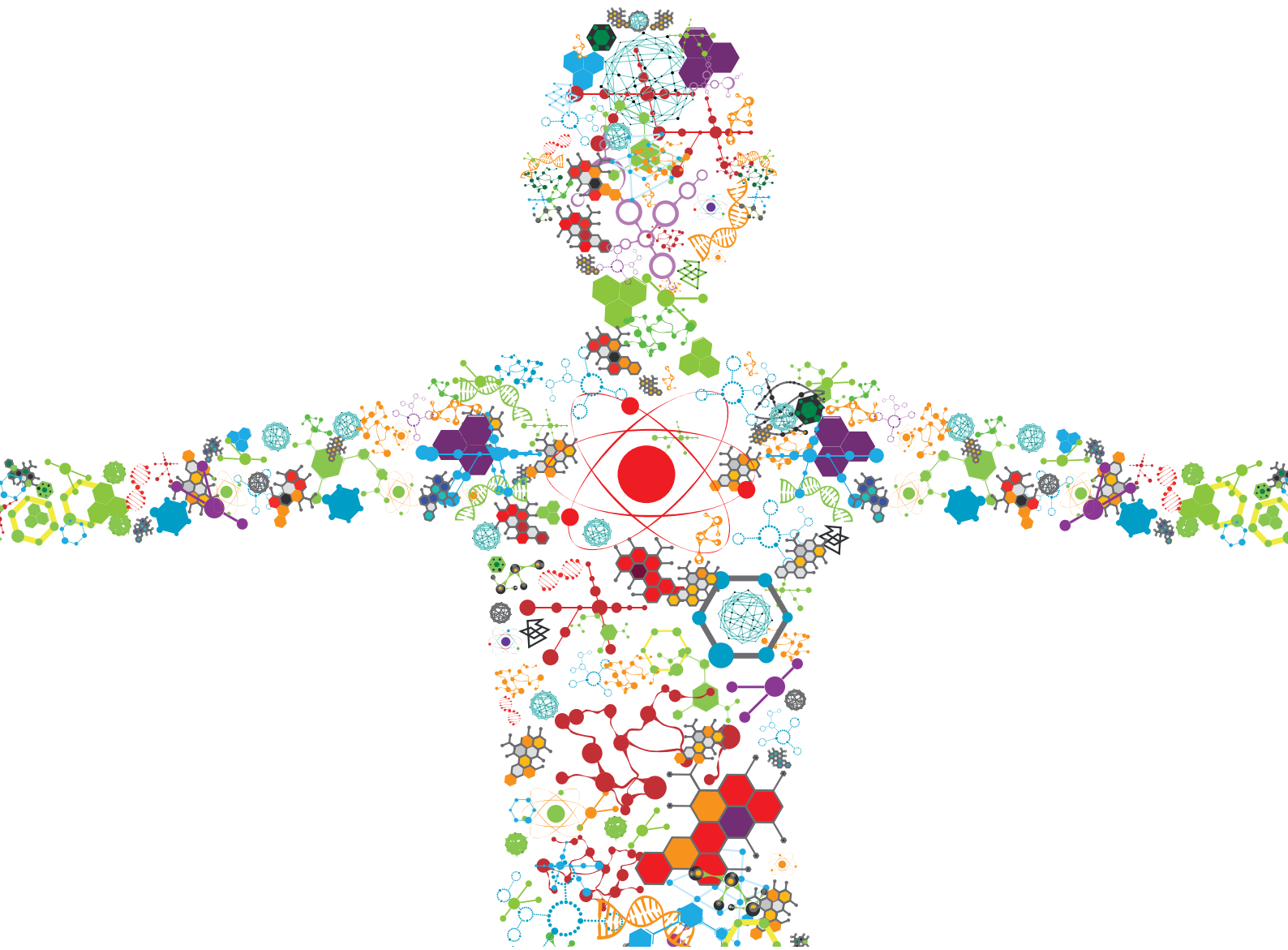

frontiers Research Topics

frontiers

ISSN 1664-8714
ISBN 978-2-83250-842-8
DOI 10.3389/978-2-83250-842-8

About Frontiers

Frontiers is more than just an open-access publisher of scholarly articles: it is a pioneering approach to the world of academia, radically improving the way scholarly research is managed. The grand vision of Frontiers is a world where all people have an equal opportunity to seek, share and generate knowledge. Frontiers provides immediate and permanent online open access to all its publications, but this alone is not enough to realize our grand goals.

Frontiers Journal Series

The Frontiers Journal Series is a multi-tier and interdisciplinary set of open-access, online journals, promising a paradigm shift from the current review, selection and dissemination processes in academic publishing. All Frontiers journals are driven by researchers for researchers; therefore, they constitute a service to the scholarly community. At the same time, the Frontiers Journal Series operates on a revolutionary invention, the tiered publishing system, initially addressing specific communities of scholars, and gradually climbing up to broader public understanding, thus serving the interests of the lay society, too.

Dedication to Quality

Each Frontiers article is a landmark of the highest quality, thanks to genuinely collaborative interactions between authors and review editors, who include some of the world's best academicians. Research must be certified by peers before entering a stream of knowledge that may eventually reach the public - and shape society; therefore, Frontiers only applies the most rigorous and unbiased reviews.
Frontiers revolutionizes research publishing by freely delivering the most outstanding research, evaluated with no bias from both the academic and social point of view. By applying the most advanced information technologies, Frontiers is catapulting scholarly publishing into a new generation.

What are Frontiers Research Topics?

Frontiers Research Topics are very popular trademarks of the Frontiers Journals Series: they are collections of at least ten articles, all centered on a particular subject. With their unique mix of varied contributions from Original Research to Review Articles, Frontiers Research Topics unify the most influential researchers, the latest key findings and historical advances in a hot research area! Find out more on how to host your own Frontiers Research Topic or contribute to one as an author by contacting the Frontiers Editorial Office: frontiersin.org/about/contact

SYSTEMS BIOCATALYSIS FOR BIOPROCESS DESIGN

Topic Editors:
Roland Wohlgemuth, Lodz University of Technology, Poland
Jennifer Ann Littlechild, University of Exeter, United Kingdom
Byung-Gee Kim, Seoul National University, South Korea

Citation: Wohlgemuth, R., Littlechild, J. A., Kim, B.-G., eds. (2022). Systems Biocatalysis for Bioprocess Design. Lausanne: Frontiers Media SA.
doi: 10.3389/978-2-83250-842-8

Table of Contents

frontiers | Frontiers in Bioengineering and Biotechnology

TYPE Editorial
PUBLISHED 09 November 2022
DOI 10.3389/fbioe.2022.1010174

OPEN ACCESS

EDITED AND REVIEWED BY
Manfred Zinn,
HES-SO Valais-Wallis, Switzerland

*CORRESPONDENCE
Roland Wohlgemuth,
roland.wohlgemuth.1@p.lodz.pl
Jennifer Littlechild,
J.A.Littlechild@exeter.ac.uk
Byung-Gee Kim,
byungkim@snu.ac.kr

SPECIALTY SECTION
This article was submitted to Bioprocess Engineering,
a section of the journal
Frontiers in Bioengineering and Biotechnology

RECEIVED 02 August 2022
ACCEPTED 17 October 2022
PUBLISHED 09 November 2022

CITATION
Wohlgemuth R, Littlechild J and Kim B-G (2022), Editorial: Systems biocatalysis for bioprocess design. *Front. Bioeng. Biotechnol.* 10:1010174. doi: 10.3389/fbioe.2022.1010174

Editorial: Systems biocatalysis for bioprocess design

Roland Wohlgemuth[1,2]*, Jennifer Littlechild[3]* and Byung-Gee Kim[4,5]*

[1]Institute of Molecular and Industrial Biotechnology, Lodz University of Technology, Lodz, Poland, [2]Swiss Coordination Committee for Biotechnology, Zurich, Switzerland, [3]Henry Wellcome Building for Biocatalysis, Biosciences, University of Exeter, Exeter, United Kingdom, [4]School of Chemical and Biological Engineering, Institute of Molecular Biology and Genetics, Seoul National University, Seoul, South Korea, [5]Bio-MAX/N-Bio Institute & Institute for Sustainable Development (ISD), Seoul National University, Seoul, South Korea

KEYWORDS

biocatalysis, biotransformation, biosynthesis, biocatalytic process design, biocatalytic reaction engineering

Editorial on the Research Topic
Systems biocatalysis for bioprocess design

Biocatalysis is continuing to be of key importance and relevance for the functioning of natural as well as anthropogenic bioprocesses on planet earth. There is a growing awareness directed to the application of bioprocesses in creating and preserving value, by avoiding loss of value and regenerating new value from waste products. This approach is intended to address climate change and sustainability, which are the great challenges of the 21st century. The favorable features of biocatalytic processes, such as safety, health, environmental sustainability, high selectivity, and resource efficiency, are attracting increasing attention for both synthetic and degradative bioprocesses at a small to large industrial scale.

Bioprocess design and value creation in a sustainable bioeconomy can benefit from an integrated view, which includes the molecular and engineering aspects of the optimal biocatalytic transformation route. The thermodynamics of the biocatalytic transformations and the kinetic characteristics and properties of the involved biocatalysts are key determinants for the resource and energy efficiency of the bioprocesses. This is true whether the transformation route is to be designed for the synthesis of a desired target or from a starting material oriented perspective, and in addition whether it is for a single given target or is oriented towards a diversity of products. The search, design, and optimization of the biocatalysts can benefit from a large diversity of different approaches and methodologies. This can start from biocatalyst identification in biosynthetic pathways already existing in nature, from *de novo* design and evolution of engineered biocatalysts or from a combination of these approaches. The selection of the most suitable starting materials for the bioprocess can be guided by renewable and bio-based raw materials used in natural biosynthetic pathways, by bio-privileged compounds, or by economic factors such as availability, cost, and source of the

starting materials. The range of the desired target products can benefit from the creation of better bio-products containing new functionalities to achieve an improved performance.

Systems approaches provide valuable tools and methodologies for designing new bioprocesses, by offering a thorough insight into the required system components and interactions. Integration of insights into the kinetics and thermodynamics of individual reaction steps within biocatalytic reaction pathways that exist in nature can help new efficient industrial processes to be developed. This process identifies the natural starting materials and their intermediates to obtain the desired products and requires a multidisciplinary approach involving biology, chemistry, and engineering for the bioprocess design. The systems biocatalysis approach includes whole-cell *in vivo* analysis of biocatalytic systems, retrosynthetic analysis, discovery of new biocatalytic functions, development and production of highly active and stable biocatalysts, reaction engineering of individual and multiple biocatalytic reaction steps, downstream processing, and product recovery. Based on the rapidly growing knowledge regarding the structure, function, mechanism, and application of enzymes, the development of biocatalytic reaction pathways using a systems biocatalysis approach can guide the design of resource efficient and sustainable bioprocesses towards the manufacturing of valuable target products. The tasks involved are the discovery of new biocatalysts, the optimization of their function, mutual compatibility and regulation, and the construction of a continuous flux within a synthetic pathway to obtain an optimal efficiency.

This special issue contains a collection of reviews and original research papers that build on the development of this key area of research which strives to achieve a sustainable future worldwide. The contributions range from the development of stable enzyme fusions for improved catalytic performance, and the discovery of new enzyme catalysts and their optimization of substrate specificity using directed and rational mutagenesis, to their use for the biosynthesis of a range of important small metabolites and metabolite-like molecules. The papers within this special topic as outlined below describe a range of new biosynthetic opportunities using either a whole-cell *in vivo* approach or an *in vitro* cell-free approach, using purified enzyme catalysts. In addition, the importance of modelling the biocatalytic process is introduced. This can often be a vital task to carry out at an early stage of development to evaluate the feasibility of the proposed reactions and to allow any subsequent redesign for scale-up to industrial scale to be fully optimized.

Reductive aminases are highly attractive enantioselective biocatalysts in the reductive coupling of carbonyl compounds with primary and secondary amines for synthesizing chiral amines. The broad substrate scope and other favorable properties of two new reductive aminases have been explored and characterized for the direct biocatalytic synthesis of primary and secondary amines, and control of enantioselectivity in rasagiline synthesis has been demonstrated using enzyme engineering by rational design (Zhang et al.). Site-directed mutagenesis has been used in engineering cytochrome P450 monooxygenase CYP153A33 from *Marinobacter aquaeolei* for obtaining increased hydroxylation at the ω-position of 1-dodecanol (Park et al.). The new enzyme variant CYP153A33 P136A has also been investigated with respect to ω-specific hydroxylation of C6 to C16 1-alkanols. A review on methanol dehydrogenases, which catalyze the conversion of methanol to formaldehyde and play a key role in natural or artificial methanol utilization pathways, describes the discovery, properties, and applications of new and newly engineered methanol dehydrogenases (Le et al.). A mini-review on the design of fusion enzymes, which focusses on fusion oxidoreductases with their reported linkers and applications in both aqueous and non-aqueous media, discusses key efficiency and feasibility limitations of aqueous biocatalysis, use of non-aqueous media, and the potential of fusion oxidoreductases in organic media (Ma et al.). A single whole-cell system, which co-expresses the required enzymes in a reaction cascade and the controlled expression level of each enzyme, is demonstrated. This efficiently catalyzes the conversion of ethyl 3-oxo-4-(2,4,5-trifluorophenyl) butanoate to a sitagliptin intermediate, using an esterase, and a transaminase from *Roseomonas deserti*, with benzylamine as amino donor, whereby aldehyde reductase from *Synechocystis* sp. and formate dehydrogenase from *Pseudomonas* sp. were used to resolve the inhibitory effect of benzaldehyde (Khobragade et al.). Despite the natural occurrence of metabolites, new efficient methods for their preparation in adequate amounts are clearly needed to study their biological activities, as described for the enzymatic synthesis of the regiospecific enantiomers 3′-hydroxy-(*S*)-equol, 5-hydroxy-(*S*)-equol, and 6-hydroxy-(*S*)-equol from daidzein and genistein, using daidzein-*(S)*-equol–converting reductases and 4-hydroxyphenylacetate 3-monooxygenase (Song et al.). As α-amino ester hydrolases are of much interest in cephalexin manufacturing, rapid evaluation is desirable regarding the influence of the reactor type and configuration, and on the conversion of the reactant, the cephalexin yield, and the volumetric productivity, taking into account process characteristics such as enzyme deactivation and substrate inhibition (Lagerman et al.). Utilizing inexpensive resources and hetero- or phototrophic metabolic modules for a sustainable supply of the necessary cofactors or co-substrates is attractive for redox-intensive whole-cell biocatalysis. This aims to increase regeneration and supply of redox equivalents, block competing fluxes, and increase the required metabolite availability for the desired biosynthetic routes (Theodosiou et al.). A systems biocatalysis approach and modular cell-free biocatalytic systems offer new opportunities for reducing the complexity of synthesizing metabolites using biological whole-cell approaches or by classical chemical synthesis (Wohlgemuth and Littlechild). The identification of the proteins involved in

inulin utilization by *Faecalibacterium prausnitzii* and a multi-omic study have provided molecular insights with respect to inulin metabolism in *F. prausnitzii* and its connection to improving human intestinal health (Park et al.).

Together, the papers included in this special issue on systems biocatalysis offer important contributions to our drive towards the development of new sustainable industrial bioprocesses. They also provide an overview of the challenges that are involved and how these can be overcome using a systems biocatalysis approach.

Author contributions

JL and RW wrote first drafts of the editorial. All authors, B-GK, JL, and RW, contributed to manuscript revision, read, and approved the submitted version.

Conflict of interest

The authors declare that the research was conducted in the absence of any commercial or financial relationships that could be construed as a potential conflict of interest.

Publisher's note

frontiers in Bioengineering and Biotechnology

ORIGINAL RESEARCH
published: 06 October 2021
doi: 10.3389/fbioe.2021.757062

Synthesis of Sitagliptin Intermediate by a Multi-Enzymatic Cascade System Using Lipase and Transaminase With Benzylamine as an Amino Donor

*Taresh P. Khobragade, Sharad Sarak, Amol D. Pagar, Hyunwoo Jeon, Pritam Giri and Hyungdon Yun **

Department of Systems Biotechnology, Konkuk University, Seoul, South Korea

Herein, we report the development of a multi-enzyme cascade using transaminase (TA), esterase, aldehyde reductase (AHR), and formate dehydrogenase (FDH), using benzylamine as an amino donor to synthesize the industrially important compound sitagliptin intermediate. A panel of 16 TAs was screened using ethyl 3-oxo-4-(2,4,5-trifluorophenyl) butanoate as a substrate (**1**). Amongst these enzymes, TA from *Roseomonas deserti* (TARO) was found to be the most suitable, showing the highest activity towards benzylamine (~70%). The inhibitory effect of benzaldehyde was resolved by using AHR from *Synechocystis* sp. and FDH from *Pseudomonas* sp., which catalyzed the conversion of benzaldehyde to benzyl alcohol at the expense of NAD(P)H. Reaction parameters, such as pH, buffer system, and concentration of amino donor, were optimized. A single whole-cell system was developed for co-expressing TARO and esterase, and the promoter engineering strategy was adopted to control the expression level of each biocatalyst. The whole-cell reactions were performed with varying substrate concentrations (10–100 mM), resulting in excellent conversions (ranging from 72 to 91%) into the desired product. Finally, the applicability of this cascade was highlighted on Gram scale, indicating production of 70% of the sitagliptin intermediate with 61% isolated yield. The protocol reported herein may be considered an alternative to existing methods with respect to the use of cheaper amine donors as well as improved synthesis of (*R*) and (*S*) enantiomers with the use of non-chiral amino donors.

Keywords: sitagliptin, β-amino acid, transaminase, esterase, benzylamine, promoter engineering

OPEN ACCESS

Edited by:
Byung-Gee Kim,
Seoul National University, South Korea

Reviewed by:
Xiaoqiang Ma,
Singapore-MIT Alliance for Research and Technology (SMART), Singapore
Junping Zhou,
Zhejiang University of Technology, China

****Correspondence:***
Hyungdon Yun
hyungdon@konkuk.ac.kr

Specialty section:
This article was submitted to Bioprocess Engineering, a section of the journal Frontiers in Bioengineering and Biotechnology

Received: *11 August 2021*
Accepted: *21 September 2021*
Published: *06 October 2021*

Citation:
Khobragade TP, Sarak S, Pagar AD, Jeon H, Giri P and Yun H (2021) Synthesis of Sitagliptin Intermediate by a Multi-Enzymatic Cascade System Using Lipase and Transaminase With Benzylamine as an Amino Donor. Front. Bioeng. Biotechnol. 9:757062. doi: 10.3389/fbioe.2021.757062

INTRODUCTION

Biocatalysts continue to be explored for consideration as green alternatives to alleviate the environmental issues encountered with the use of methods pertaining to traditional organic chemistry (Patil et al., 2018; Pagar et al., 2021). Thus, multi-enzyme cascade reactions have garnered attention owing to their elegance (Sperl and Sieber, 2018; Hwang and Lee, 2019; Martínez-Montero et al., 2019), comprehensiveness, and involvement in the synthesis of a considerable variety of pharmaceuticals, agrochemicals, and other industrially important chemicals (Sung et al., 2018; Patil et al., 2019; Yoon et al., 2019).

Sitagliptin is a well-reported example of a drug containing a β-amino acid moiety as a key component. Sitagliptin, an inhibitor of dipeptidyl peptidase-4, is used as an oral antidiabetic drug to

treat type 2 diabetes (Yun et al., 2004; Aschner et al., 2006; Desai, 2011; Villegas-Torres et al., 2015). Merck has described the industrial manufacturing method of sitagliptin phosphate. In the first-generation process (chemistry route), the chirality of achiral β-keto ester was introduced in the form of a hydroxy group in β-hydroxy acid through ruthenium-catalyzed asymmetric hydrogenation. The hydroxyl group was then transformed into protected amino acid through several steps, followed by direct coupling to triazolopiperazine to afford sitagliptin. The complete process involves eight steps to enable the production of sitagliptin phosphate with an overall yield of 52% (Hansen et al., 2005; Hansen et al., 2009). In comparison, the second-generation process comprised a three-step one-pot synthesis of dehydro-sitagliptin. The synthesis was initiated with trifluoro phenylacetic acid, followed by serial and controlled addition of other reactants and reagents, resulting in the formation of sitagliptin phosphate. In the last step, the product was crystallized and separated via simple filtration and resulted in the obtainment of 82% overall yield (Hsiao et al., 2004; Xu et al., 2004; Clausen et al., 2006).

The abovementioned chemical process involves the use of hazardous chemicals and other toxic substances. Biocatalysts are environmentally friendly and can be used as an alternative for the chemical process. TA is reportedly a useful and versatile biocatalyst for the selective and sustainable synthesis of amines, including ketones and aldehydes (Mathew and Yun, 2012; Park and Shin, 2013; Guo and Berglund, 2017; Slabu et al., 2017; Hauer, 2020). For the enzymatic synthesis of sitagliptin, the *R*-selective TA derived from *Arthrobacter* sp. was recently engineered using computational modeling and iterative directed evolution tools. The evolved enzyme harbors 27 mutations, highlighting it as a highly active variant, thus enabling its use in the production of the desired sitagliptin at 92% yield (Savile et al., 2010). Another enzymatic route considered for the synthesis of a sitagliptin intermediate using TA (ATA117-rd11 from *Arthrobacter* sp.) was reportedly adopted to produce the desired sitagliptin intermediate at a yield of 82% (Hou et al., 2016). Recently, Zheng and co-workers have reported the asymmetric synthesis of sitagliptin intermediate using TA engineered from *Arthrobacter cumminsii* ZJUT212 (M1+M122H), which helped obtain the target product at ~92% yield (Cheng et al., 2020). Recently, we reported two enzymatic strategies for the synthesis of sitagliptin intermediate using TA from *Ilumatobacter coccineus* (TAIC) and commercial *Candida rugosa* lipase (CRL) in one cascade, as well as using TAIC and esterase from *Pseudomonas stutzeri* (Est PS) in another cascade. In both cascades, (*S*)-α-methylbenzylamine ((*S*)-α-MBA) was used as an amine donor, resulting in ~82% conversion to the desired product (Kim et al., 2019; Khobragade et al., 2021).

Although these TAs are routinely used for the production of various industrially important compounds, including sitagliptin, they present with various inherent problems for large-scale production, such as inhibition of the biocatalyst by co-products and unfavorable thermodynamic equilibrium. (Koszelewski et al., 2010; Park et al., 2013; Voges et al., 2016). Therefore, selection of a suitable amine donor is a crucial step for efficient TA reactions. As such, L-alanine (Ala) has been considered as the most widely utilized amine donor ever since its deaminated product (i.e., pyruvate) was identified with the ability of being recycled. Several enzymes that demonstrate the ability to degrade pyruvate or to convert pyruvate into Ala have been studied, including lactate dehydrogenase, pyruvate decarboxylase, acetolactate synthase, and alanine dehydrogenase, complemented by cofactor recycling using FDH or glucose dehydrogenase (Shin and Kim, 2001; Hoehne et al., 2008; Koszelewski et al., 2008; Koszelewski et al., 2008; Truppo et al., 2009; Truppo et al., 2009; Koszelewski et al., 2010; Mutti et al., 2011; Schätzle et al., 2011; Mutti et al., 2012; Pressnitz et al., 2013; Sayer et al., 2014). Moreover, to shift the reaction equilibrium, a higher amount of Ala was used, and additional enzymes (auxiliary enzymes) were introduced to remove by-products and to recycle the cofactor. However, owing to the high overall cost, this approach is not appealing for industrial applications. Isopropyl amine (IPA) is considered a promising amino donor, as many TAs demonstrate the ability to accept IPA as an efficient amino donor, including *A. citreus* TA mutant, ATA117 mutant, and TAs from *P. aeruginosa, P. denitrificans,* and *A. terreus* (Cassimjee et al., 2010; Savile et al., 2010; Fesko et al., 2013; Park et al., 2013; Simon et al., 2014; Dawood et al., 2018). The advantages of IPA include its achiral nature, which enable its application with either (*S*)- or (*R*)-selective TAs, and the easy elimination of acetone via implementation of physical or chemical approaches (Kelefiotis-Stratidakis et al., 2019). However, IPA also presents with a few limitations, such as the disruption of reactions for final product isolation and purification in the presence of excess amounts of IPA, and the additional assembly required to remove the deaminated product. Recently, 'smart' amine donors such as 3-amino-cyclohexa-1,5-dienecarboxylic acid, o-xylylene diamine, cis-but-2-ene-1,4-diol, cis-but-2-ene-1,4-diamine, and cadaverine have been reported as effective amine donors because they can be used at equimolar quantities (Wang et al., 2013; Green et al., 2014; Gomm et al., 2016; Martínez-Montero et al., 2016; Payer et al., 2017). One of the advantages of these amino donors is the auto-degrading properties of their co-products. However, the separation of product and substrate upon reaction completion can be challenging owing to the similar molecular properties of the amino donors. Moreover, they are costly compared to Ala and IPA. Currently, (*S*)-α-MBA is the most commonly used amine donor for the synthesis of β-amino acids, and the majority of TAs display high activity towards (*S*)-α-MBA, but (*S*)-α-MBA is a relatively expensive co-substrate for transamination reaction; furthermore, the deaminated co-product, acetophenone, is known to inhibit TA (Shon et al., 2014; Mathew et al., 2016). Nevertheless, in a study investigating the amino donor specificity of TA derived from *Vibrio fluvialis* JS17, the biocatalyst exhibited 3.6 and 30% specificity for IPA and Ala, respectively, compared with (*S*)-α-MBA (100%), and benzylamine showed 1.15-fold higher activity than (*S*)-α-MBA (Shin and Kim, 2002)).

However, studies conducted for screening and designing efficient amine donors for the synthesis of β-amino acids compared to chiral amines remains limited. Therefore, exploration of a suitable and cheaper amine donor to shift the reaction equilibrium towards product formation has emerged as a key step in the establishment of multi-enzyme cascade reactions. Benzylamine is considered the cheapest donor among the

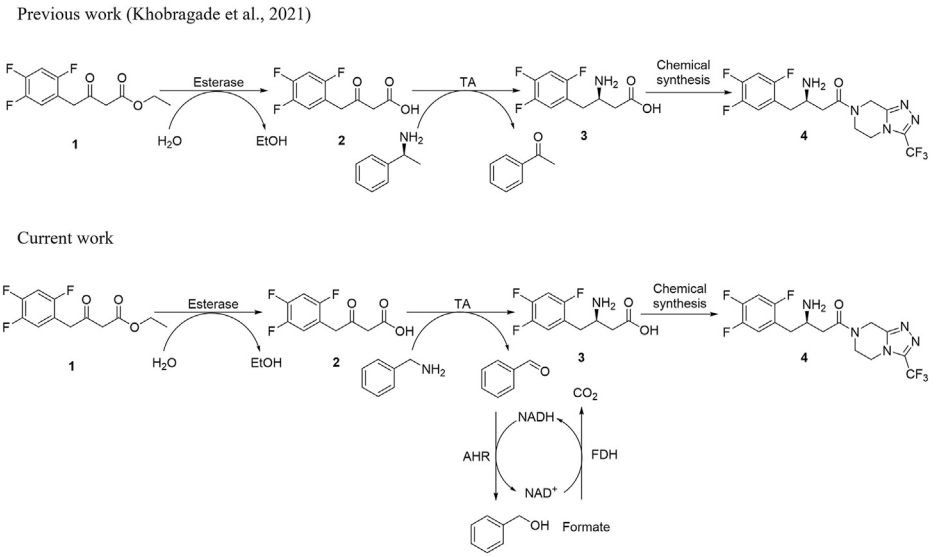

FIGURE 1 | (A) Schematic diagram for the synthesis of sitagliptin phosphate from β-keto ester substrate using (*S*)-α-MBA as an amino donor. **(B)** Schematic diagram for the synthesis of sitagliptin intermediate using benzylamine as an amine donor with the AHR/FDH system.

abovementioned amino donors. Furthermore, it can be used to perform screening of both (*S*)- and (*R*)-selective TAs. Therefore, as a continuation to our previously published work (Kim et al., 2019; Khobragade et al., 2021), the present study was conducted to investigate the effectiveness of benzylamine as an amino donor for the synthesis of sitagliptin intermediate by using **1** as the substrate (**Figure 1**). First, we selected a panel of 16 in-house TAs and assessed their specificity for benzylamine. To shift the reaction equilibrium towards product formation and to minimize enzyme inhibition by the action of the deaminated co-products, the AHR/FDH system was used. In this system, AHR has been considered to catalyze the conversion of benzaldehyde into benzyl alcohol at the expense of NAD(P)H cofactor, and FDH has been considered to supply the depleted NAD(P)H by recycling the corresponding NAD(P)+ cofactor.

MATERIALS AND METHODS

Chemicals and Enzymes

Candida rugosa lipase (Catalog No. L1754), Benzylamine (*S*)-α-methylbenzylamine [(*S*)-α-MBA], 2,3,4,6-Tetra-O-acetyl-β-D-glucopyranosyl isothiocyanate (IPTG), pyridoxal 5′-phosphate hydrate (PLP), perchloric acid (PCA), dimethyl sulfoxide (DMSO) were purchased from Sigma-Aldrich (Sigma-Aldrich Korea, Seoul, South Korea). Ethyl 3-oxo-4-(2,4,5-trifluorophenyl) butanoate was obtained from CKD BiO Corp, Korea.

Expression of the Enzymes

The genes encoding various TAs, AHR, and FDH were synthesized by Bionics (Seoul, Korea). Then gene was inserted into IPTG-inducible pET 24ma vectors (TAs). The AHR and FDH were cloned pET duet vectors (AHR in MCS I site whereas FDH in MCS II site). The plasmids were transformed to *Escherichia coli* (BL21) cells, and the transformants were grown in 0.5 L LB-containing kanamycin or ampicillin (50 or 100 μg/ml) at 37°C. The cells were induced with 0.1 mM IPTG when OD_{600} reached 0.6–0.8 (Kim et al., 2019; Shon et al., 2014; Mathew et al., 2016.). After the overnight induction at 20°C, the cells were harvested by centrifugation (5,000 rpm, 10 min) and washed twice with 200 mM Tris/HCl buffer (pH 8.0).

Determination of Specific Activity of Est PS Using Whole Cells

To examine the specific activity of Est PS, cells were grown in 0.2 L of LB media containing ampicillin (100 μg/ml) at 37°C. When the cell OD_{600} reached 0.6–0.8, 0.1 mM IPTG was added (Kim et al., 2019.), followed by overnight incubation at 20°C. Thereafter, the cells were harvested by centrifugation (4,400 × *g*, 10 min) and were subjected to washing steps two times using 200 mM Tris/HCl buffer (pH 8.0). For the reaction, Est PS (0.15 mg_{DCW}/ml) was incubated at 37°C for 20 min with DMSO 15% and 500 μl Tris-HCl buffer (200 mM, pH 7.0) containing ethyl 3-oxo-4-(2,4,5-trifluorophenyl) butanoate (10 mM) as a substrate. The reaction was terminated by adding 1% perchloric acid at a ratio of 1:1 (v/v). Next, the reaction mixture was centrifuged at 17,000 × *g* for 30 min, and the clear supernatant was analyzed via high-performance liquid chromatography (HPLC) using a C 18 symmetry column.

Whole-Cell Biotransformation Reactions of the Substrate at Different Concentrations

Whole-cell biotransformation reactions were conducted in a reaction volume (5 ml) containing **1** (10 or 50 mM), benzylamine (20 or 150 mM), DMSO (5% (v/v), PLP

(0.5 mM), CRL (10 or 50 mg/ml), Tris-HCl buffer (200 mM, pH 8.0), and whole cells expressing TA only or co-expressing TARO-Est PS. During the reaction, pH was reduced owing to the hydrolysis of an ester substrate. Therefore, the pH of the reaction mixture was adjusted manually by adding 5 M NaOH solution at specific intervals during the 5-h reaction. Subsequently, the sample was collected, and the presence of **3** was detected using HPLC.

Construction of Different Variant of T7 Promoter

The promotor engineering strategy is applied to achieve the optimum expression level of Est PS as described in our previous study (Khobragade et al., 2021). In brief, the gene (Est PS) was cloned in the different strengths of T7 promotors in the pET15b plasmid (Chizzolini et al., 2014). The newly constructed different variant of pET15b plasmid and TARO was co-expressed to develop a single-cell biocatalyst. The specific activity and enzymatic reaction of newly developed co-expressed whole cell was mentioned above.

Whole-Cell Biotransformation Reaction of the Substrate at Different Concentrations Using a pH-Stat System

Whole-cell biotransformation reactions were performed in a reaction volume (30 ml) comprising **1** (100–400 mM), benzylamine (150–300 mM), DMSO (5% (v/v), PLP (0.5 mM), Tris-HCl buffer (200 mM, pH 8.0), and cells co-expressing TARO-Est PS. Similar to the above-mentioned reaction, the hydrolysis of an ester substrate to its corresponding acid caused a decrease in pH in this reaction. Therefore, an 877 Titrino Plus pH-stat system (Metrohm AG, Herisau, Switzerland) for automatic titration with 5 M NaOH was used to ensure a stable pH. Samples were collected at specific intervals for the identification of **3** using HPLC.

Analytical Method

The quantitative analysis of β-amino acid was performed using HPLC with a Crownpak CR column (Daicel Co., Japan) at 210 nm, with an elution of perchloric acid solution (pH 1.5; 0.6 ml/min) as previously reported (Kim et al., 2019; Shon et al., 2014). The β-keto ester (**1**) were analyzed using HPLC with C-18 Column. Mobile phase: 40% water and 60% methanol containing 0.1 TFA. Flowrate: 1.0 ml/min, wavelength: 254 nm.

RESULTS AND DISCUSSION

Screening of TAs for the Synthesis of Sitagliptin Intermediate from β-keto Acid

Generally, (*S*)-selective TAs with specificity for Ala as an amine donor belong to fold-type I (the aspartate aminotransferase superfamily). Among these enzymes (*S*)-β-TAs reportedly possess high activity towards β- and γ-keto acids as a substrate, resulting in the corresponding β- and γ-amino acids. These amine compounds are extensively used for the synthesis of many industrially relevant chiral compounds. Earlier studies have proven that TA exhibits good reactivity towards (*S*)-α-MBA as an amine donor for the transamination step (Mathew et al., 2016; Kim et al., 2019). For screening of suitable TA biocatalysts with high specificity for benzylamine, we selected a panel of our in-house TAs as described previously (Kim et al., 2019). According to previous studies, TAs demonstrating specificity for β-keto acids also possess good reactivity to γ-keto acids, enabling the establishment of improved assay conditions for analysis of γ-amino acids. Therefore, for the initial screening of TAs, 4-oxo-4-phenylbutanoic acid was selected as a substrate, and benzylamine was used as an amine donor. For convenience, whole-cell biocatalysts were used in this assay. Briefly, codon-optimized genes encoding the suitable TAs from 16 desired sources (**Table 1**) were synthesized and cloned into pET24ma vectors and were then expressed using *E. coli* BL21 (DE3) host cells (**Table 1**). Whole-cell biotransformation was performed using 10 mM 4-oxo-4-phenylbutanoic acid substrate, 20 mM benzylamine, 0.5 mM PLP, and 9 mg_{CDW}/ml cells of each TA biocatalyst (**Figure 2**). Among the sixteen enzymes investigated, TAOI and TAIC exhibited the highest conversion 13–15%, whereas eight other TA biocatalysts (TABL, TABU, TARO, TASM, TAHP, TARB, TAAF, and TAPI) led to the achievement of modest conversion of 2–7% into the desired product. On the contrary, the remaining six TAs (TALAB, TAKK3, TAPC, TABV, TAKI, and TASS) resulted in the obtainment of a negligible amount of the desired product (<0.5%). Although few TAs showed comparable activity, the considerably lower conversion could be attributable to enzyme inhibition by benzaldehyde, which was generated as a deaminated co-product of benzylamine during the reaction. However, we examined the enzyme inhibition of benzaldehyde with highly active TAs like TAIC, TARO, and TAOI. As expected, we observed the inhibition of benzaldehyde on the enzyme (**Supplementary Figure S1**). Therefore, we established an aldehyde removal system to minimize the inhibition of TA biocatalyst and to shift the reaction equilibrium towards product formation. Literature reports have evidenced that AHR demonstrates good activity towards benzaldehyde and can efficiently catalyze its conversion into benzyl alcohol at the expense of NAD(P)H; thus, we selected AHR and FDH for recycling of the depleted NAD(P)H cofactor. With the adoption of such a removal system, the reactions were performed using 10 mM 4-oxo-4-phenylbutanoic acid, 20 mM benzylamine, 0.5 mM PLP, and 9 mg_{CDW}/ml of each TA biocatalyst and AHR/FDH cells (**Figure 2**). As expected, utilization of the benzaldehyde removal system improved product formation under conditions of TAOI (~30%) catalysis by 2-fold. Interestingly, product formation via catalysis by TARO and TAHP was significantly enhanced by ~3- and 6-fold, respectively. In contrast, all other TAs did not significantly elevate product formation, resulting in the achievement of only <14% yield of the desired product. These results suggested that benzaldehyde exerted inhibitory effects against the TAs and should be removed to efficiently

TABLE 1 | Various enzymes used in this study.

Entry	Enzyme	Assigned name	GenBank identification number	References
1	*Rhodospirillaceae bacterium*	TARB	WP 092830126.1	Kim et al. (2019)
2	*Labrenziasp*-LAB	TALAB	WP 0841772225.1	
3	*Afipia* sp. P52-10	TAAF	WP 051444297.1	
4	*Oceanibaculum indicum*	TAOI	WP 008945048.1	
5	*Ilumatobacter coccineus*	TAIC	WP 015443725.1	
6	*Variovorax* sp. KK3	TAKK3	WP 076998155.1	
7	*Paraburkholderia caribensis*	TAPC	AMV 45988.1	
8	*Hydrogenophaga palleronii*	TAHP	WP 066271212.1	
9	*Solirubrobacter soli*	TASS	WP 028067622.1	
10	*Kineosporia* sp. *R_H_3*	TAKI	WP 088319003.1	
11	*Roseomonas deserti*	TARO	WP 076960246.1	
12	*Sinorhizobium meliloti*	TASM	WP 018099655.1	
13	*Bosea lupine*	TABL	WP 091836827.1	
14	*Bosea vaviloviae*	TABV	WP 069688334.1	
15	*Pseudacidovorax intermedius*	TAPI	WP 052383549.1	
16	*Burkholderia* sp. *UYPR1.413*	TABU	WP 028368728.1	
17	*Synechocystis* sp	AHR	WP_028949165.1	
18	*Pseudomonas* sp. *101*	FDH	P33160.3	
19	*Pseudomonas stutzeri*	Est PS	WP_020308675.1	Khobragade et al. (2021)

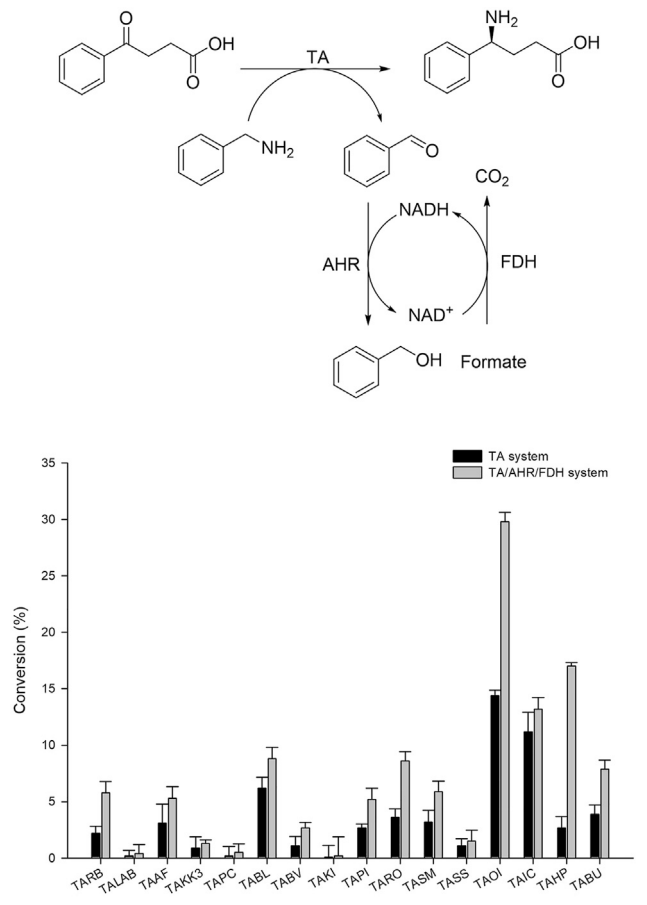

FIGURE 2 | Screening of TAs using benzylamine as an amino donor with TA and the TA/AHR/FDH system. Reaction conditions: 10 mM 4-oxo-4-phenylbutanoic acid, 20 mM benzylamine, 0.1 mM PLP, 9 mg_{CDW}/ml TAs or 9 mg_{CDW}/ml AHR/FDH cells.

improve TA performance. The AHR/FDH system adopted for benzaldehyde removal successfully improved the overall reaction conversion and was thus used for further optimization of the cascade reaction. Finally, the best six TAs (TAHP, TARO, TAOI, TAIC, TABL, and TABV) from the panel were selected for subsequent optimization using coupled enzyme reaction.

Design and Optimization of Coupled Enzyme Reaction (Transaminase/Lipase) for the Synthesis of Sitagliptin Intermediate From the Corresponding β-keto Ester

For the synthesis of sitagliptin intermediate using coupled enzyme reaction, lipase is necessary for hydrolysis of the ester substrate. Previous studies have reported the efficacy of CRL for hydrolysis of an ester substrate. Additionally, to overcome the low intrinsic stability of β-keto acids due to rapid decarboxylation (Rudat et al., 2012), many biocatalytic approaches have been developed by designing the corresponding ester or nitriles as a substrate. Notably, rapid hydrolysis of an ester substrate will cause pH decrease during the reaction, which will affect the optimal conditions of the biocatalysts in the cascade. Therefore, the decreased pH value should be compensated by adding a suitable concentration of base (5 M NaOH) at various time intervals. Considering this, coupled reactions consisting of CRL and six TAs were performed using 10 mM **1** as a substrate. In these reactions, TARO was found to be the best TA, presenting with a conversion of 91%. The other three enzymes exhibited the achievement of 75–82% conversion into the desired product (**Figure 3A**). These results suggested that all selected enzymes except TABU demonstrated a higher specificity for β-keto acid than that for γ-keto acid, and they were therefore selected for further optimization. Next, the reaction parameters, such as pH

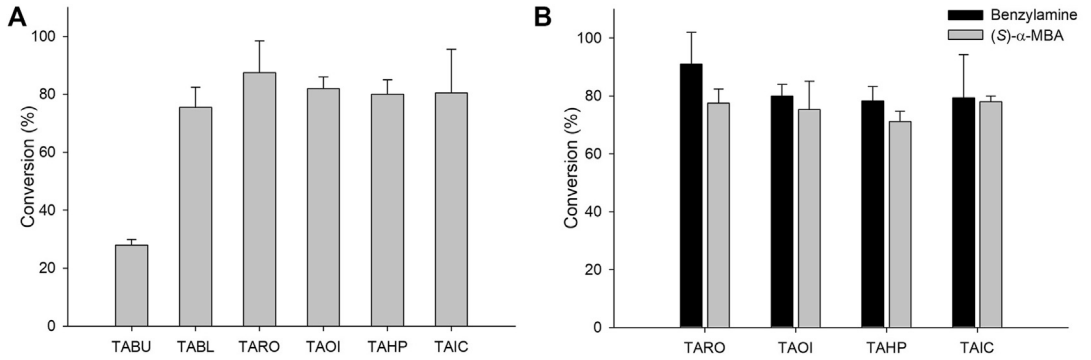

FIGURE 3 | (A) Synthesis of sitagliptin intermediate using the TA/CRL/AHR/FDH system. Reaction conditions: 10 mM **1**, 20 mM benzylamine, 10 mg/ml CRL, 9 mg_{CDW}/ml TAs, 9 mg_{CDW}/ml AHR/FDH cells. **(B)** Comparison of benzylamine and (*S*)-α-MBA as amino donors. Reaction conditions for using benzylamine as an amine donor: 10 mM 1, 20 mM benzylamine, 0.5 mM PLP, 10 mg/ml CRL, 9 mg_{CDW}/ml TAs, 9 mg_{CDW}/ml AHR/FDH, 50 mM sodium formate, 200 mM Tris-HCl Buffer (pH 8.0), 37°C. Reaction conditions for using (*S*)-α-MBA as an amine donor: 10 mM 1, 20 mM (*S*)-α-MBA, 0.5 mM PLP, 10 mg/ml CRL, 9 mg_{CDW}/ml TAs, 200 mM Tris-HCl Buffer (pH 8.0), 37°C.

and buffer system, were optimized for reaction with the four selected TAs (TARO, TAHP, TAOI, and TAIC) (**Supplementary Figure S2**). To determine the optimum pH and suitable buffer species for reaction, three different buffer systems were inspected, namely acetate (pH 4.0–6.0), phosphate (pH 6.0–8.0), and Tris-HCl (pH 7.0–10.0). All four TAs showed the highest activity at pH 8.0 (Tris-HCl buffer); however, for TA from *Vibrio fluvialis* JS17, slightly alkaline pH conditions were necessary, possibly owing to an increase in the effective concentration of deprotonated amine donor, which enhanced the external aldimine formation (Guo and Berglund, 2017).

After optimization of the reaction, we compared the specificity of these TAs for (*S*)-α-MBA. For reactions using benzylamine as an amine donor, the AHR/FDH system was used to remove the benzaldehyde. However, the system was not adopted in reactions with (*S*)-α-MBA used as an amine donor because the removal of acetophenone did not reportedly improve product formation (Khobragade et al., 2021). The reactions consisted of 10 mM **1**, 20 mM benzylamine, 10 mg/ml CRL, 0.5 mM PLP, and 9 mg_{CDW}/ml of each biocatalyst. In reactions using benzylamine as an amine donor, all four TAs led to the obtainment of >80% yield, with TARO showing the highest conversion of 90%. In contrast, reactions using (*S*)-α-MBA led to the achievement of the target product at only ~70% yield, with TARO exhibiting the highest conversion of 77% (**Figure 3B**). The observed 10–15% higher conversion with benzylamine as an amine donor indicated that the four selected TAs possessed higher specificity for benzylamine than that for (*S*)-α-MBA. Encouraged by these results, we performed further reactions with increased substrate concentration (50 mM **1**) and varying CRL concentrations (30–60 mg/ml). Among the four enzymes, TAHP demonstrated the highest conversion of 36% with 40 mg/ml CRL, whereas the other three enzymes resulted in the achievement of <26% yield, with TARO displaying the second-highest conversion (26% at 40 mg/ml of CRL). Therefore, TAOI and TAIC were eliminated, and TAHP and TARO were selected for subsequent studies.

In general, the amount of amine donor plays a vital role in transamination reaction. Increasing the amount of amine donor in the reaction is a commonly used strategy for shifting reaction equilibrium towards product formation. However, such a high amount of amine donor can adversely affect the activity of other enzyme biocatalysts or TA itself in the cascade (Kim et al., 2019). Hence, to determine the optimal concentration of amine donor, reactions were conducted using varying concentrations of benzylamine with 50 mM **1** and 27 mg_{CDW}/mL biocatalyst (**Table 2**). Benzylamine at a concentration of 150 mM (3-fold increase in concentration) was found to be optimal for the reaction, resulting in 38 and 34% conversion into the desired product (**3**) by TARO and TAHP, respectively (**Table 2**, entry 3). On the contrary, further increases in the amount of benzylamine (200–300 mM) led to lower product formation (<30%), indicating that a concentration of more than 150 mM benzylamine inhibited the activity of the enzyme biocatalyst in the cascade. Furthermore, to confirm benzylamine consumption during the reaction, we determined the amount of benzyl alcohol produced. The results suggested that equal amount of the product was formed and amine donor was consumed in the reaction (**Supplementary Figure S3**). Our finding also indicated that the AHR/FDH system could be used to successfully convert the benzaldehyde into benzyl alcohol, thereby shifting the reaction equilibrium towards product formation. Additionally, we examined the effect of different amino donor systems (benzylamine, D-alanine, and IPA) on an (*R*)-selective TA from *Neosartorya fischeri*. The benzylamine amino donor system provided the highest conversion (18%), whereas the D-alanine and IPA amino donor systems resulted in negligible conversion (<0.1%) (**Supplementary Table S1**). Therefore, the benzylamine donor system presented with applicability for both of (*R*)- and (*S*)-selective TAs.

TABLE 2 | Optimization of benzylamine concentration using the TA/CRL/AHR/FDH system.

Entry	Substrate (mM)	Benzylamine (mM)	TARO or TAHP (mg_{CDW}/ml)	Substrate: Donor ratio	Conv. (%)[a] TARO or TAHP	Reaction time (h)
1	50	50	27	1:1	15 ± 4 or 12 ± 2	24
2	50	100	27	1:2	23 ± 2 or 26 ± 7	24
3	50	150	27	1:3	36 ± 5 or 33 ± 9	24
4	50	200	27	1:4	29 ± 4 or 28 ± 4	24
5	50	250	27	1:5	23 ± 2 or 25 ± 5	24
6	50	300	27	1:6	18 ± 3 or 14 ± 8	24

Reaction performed containing 200 mM Tris-HCl buffer (pH 8.0), 0.5 mM PLP, 40 mg/ml CRL, 27 mg_{CDW}/ml AHR/FDH, 100 mM sodium formate; temperature: 37°C.
[a]HPLC analysis.

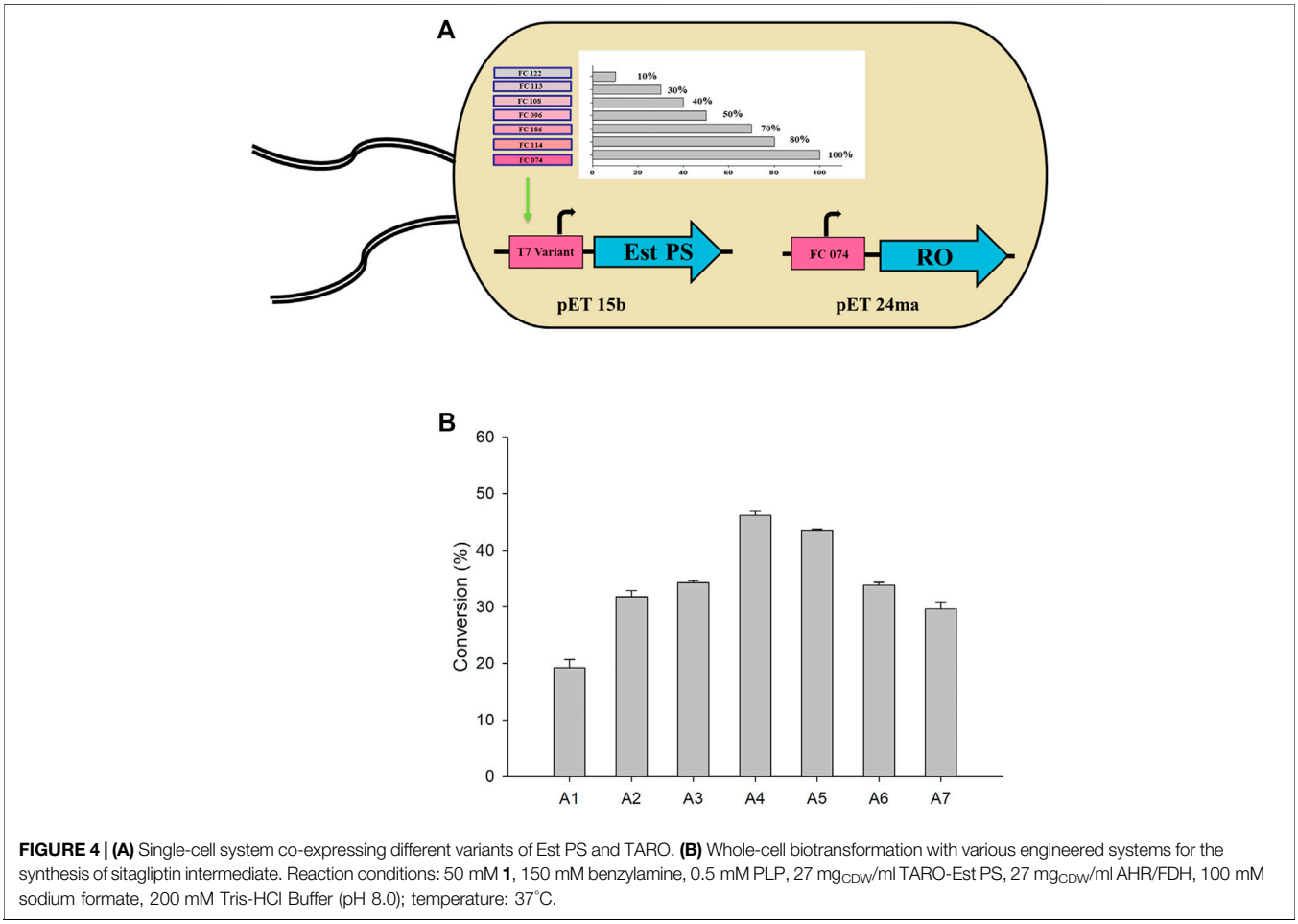

FIGURE 4 | (A) Single-cell system co-expressing different variants of Est PS and TARO. **(B)** Whole-cell biotransformation with various engineered systems for the synthesis of sitagliptin intermediate. Reaction conditions: 50 mM **1**, 150 mM benzylamine, 0.5 mM PLP, 27 mg_{CDW}/ml TARO-Est PS, 27 mg_{CDW}/ml AHR/FDH, 100 mM sodium formate, 200 mM Tris-HCl Buffer (pH 8.0); temperature: 37°C.

Application of Promoter Engineering Strategy for the Synthesis of Sitagliptin Intermediate

Single whole-cell biocatalysts co-expressing multiple enzymes are advantageous in terms of convenient handling and enhanced mass transfer efficiency (Tufvesson et al., 2014; Iglesias et al., 2017; Telzerow et al., 2019). In a previous study, we reported that ratio of esterase to TA should be balanced for fine-tuning of the activity (TAIC-Est PS). Therefore, promotor engineering strategy was developed and applied to control the expression levels of each enzyme (Chizzolini et al., 2014; Yoo et al., 2019). The Est PS used in the study had a specific activity of 3.96 U/mg, which was >12-fold higher than that of CRL. In this experiment, we used a similar strategy by replacing CRL with a biocatalyst co-expressing TARO and Est PS.

Therefore, genes encoding TARO and Est PS were designed and cloned to pET24ma and pET15b vectors, respectively. Whole-cell *E. coli* strains co-expressing variants of Est PS with different promoter strengths and TARO were also developed

TABLE 3 | The co-expression system of TARO and Est PS with different T7 promoter variants.

Entry	Engineered systems	Promoter		Specific activity (U/mg)	
		T7 promoter variant	Relative strength (%)[a]	TARO[b]	Est PS[c]
1	A1	FC 074	100	0.017 ± 0.003	1.69 ± 0.06
2	A2	FC 114	80	0.021 ± 0.002	1.33 ± 0.03
3	A3	FC 186	70	0.023 ± 0.003	1.17 ± 0.04
4	A4	FC 096	50	0.026 ± 0.003	0.97 ± 0.04
5	A5	FC 108	40	0.029 ± 0.002	0.87 ± 0.07
6	A6	FC 113	30	0.031 ± 0.002	0.56 ± 0.03
7	A7	FC 122	10	0.034 ± 0.003	0.44 ± 0.06

[a]*Strength of promoter (Chizzolini et al., 2014).*
[b]*Activity was measured using 200 mM Tris-HCl buffer (pH 7.0) containing 10 mM pyruvate and 20 mM benzylamine at 37°C.*
[c]*Activity was measured using 200 mM Tris-HCl buffer (pH 7.0) containing 10 mM 1 and 15% DMSO at 37°C.*

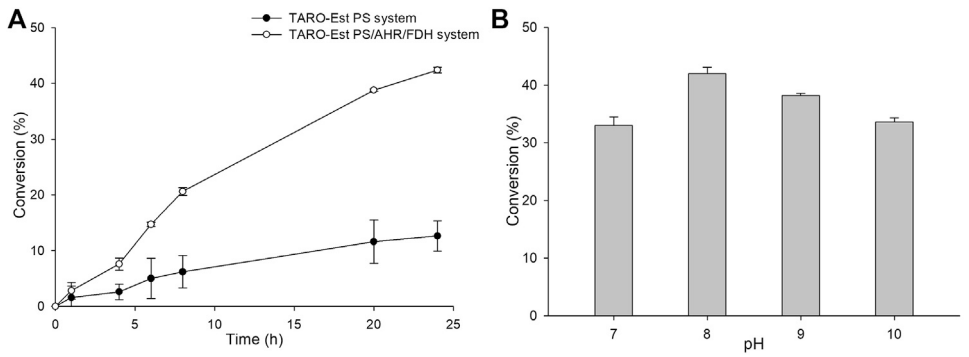

FIGURE 5 | (A) Whole-cell biotransformation reaction with TARO-Est PS and the TARO-Est PS/AHR/FDH system for the synthesis of sitagliptin intermediate. Reaction conditions: 50 mM **1**, 150 mM benzylamine, 0.5 mM PLP, 27 mg_{CDW}/ml TARO-Est PS or 27 mg_{CDW}/ml AHR/FDH or 100 mM sodium formate, 200 mM Tris-HCl Buffer (pH 8.0); temperature: 37°C. **(B)** Whole-cell reaction for the synthesis of sitagliptin intermediate using different pH. Reaction conditions: 50 mM 1, 150 mM benzylamine, 0.5 mM PLP, 27 mg_{CDW}/ml TARO-Est PS, 27 mg_{CDW}/ml AHR/FDH, 100 mM sodium formate; temperature: 37°C.

(**Figure 4A**). The specific activity of the cells expressing TARO and Est PS alone was estimated to be 0.014 U/mg and 3.56 U/mg, respectively. Similarly, the specific activity of whole cells co-expressing TARO-Est PS was measured (**Table 3**), and the results showed that the specific activity decreased with decreasing order of Est PS promotor strength, indicating reduced expression level of the enzyme; in contrast, the specific activity of TARO was enhanced, suggesting that TARO expression was higher than that of Est PS in the single-cell system. For Est PS, the highest specific activity (1.69 U/mg) was achieved with the A1 system, and the lowest activity (0.44 U/mg) was obtained with the A7 system. On the contrary, for TARO, the A7 system exhibited the highest activity of 0.034 U/mg and A1 demonstrated the lowest activity of 0.017 U/mg (**Table 3,** entry 1–7).

Considering the findings obtained herein, subsequent whole-cell reactions were performed to determine the optimum single-cell system for the synthesis of sitagliptin intermediate. The reactions were conducted using 50 mM of **1**, 150 mM of benzylamine, and 27 mg_{CDW}/ml of each cell system (A1-A7) (**Figure 4B**). The highest yield of 46% of the desired product **3**) was obtained by using the A4 system, whereas use of the A2, A3, A5, and A7 systems led to the achievement of moderate conversion of ~27–34%. Conversely, the A1 system exhibited extremely low product formation (11%). Therefore, the A4 system was selected for further optimization.

Furthermore, to improve the reaction productivity, other reaction parameters, such as co-solvents and the loading amount of the whole-cell biocatalyst, were optimized (**Supplementary Figure S4**). Our results suggested that 5% (v/v) of DMSO and 27 mg_{CDW}/mL of whole cells were optimum, resulting in the achievement of ~44% yield of the sitagliptin intermediate. In comparison, the same reaction in the absence of AHR/FDH system led to the achievement of a significantly lower conversion rate of 10% into the desired product (**3**) (**Figure 5A**), further confirming that benzaldehyde inhibited the action of the enzyme biocatalyst. Next, as a key factor affecting the productivity of the reaction, pH was optimized by performing the reactions at a pH range of 7.0–10 with 200 mM of Tris-HCl buffer, 50 mM of **1,** and 27 mg_{CDW}/ml of the biocatalyst. A pH value of 8.0 was found to be suitable, leading to the highest conversion rate of 42%, whereas alkaline pH values of 9.0 and 10 resulted in the achievement of only 38 and 34% conversion rates, respectively.

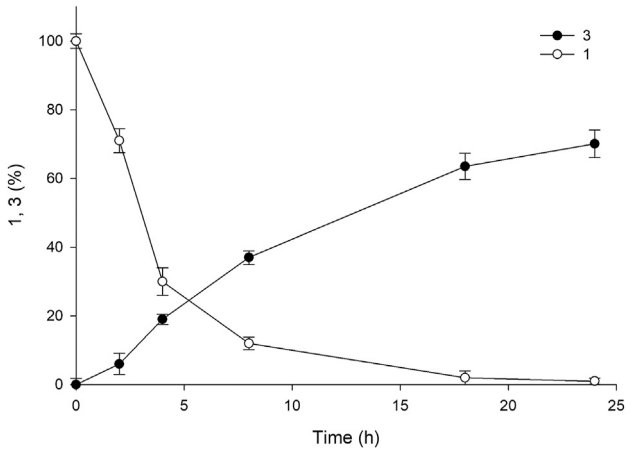

FIGURE 6 | Time course of the reaction using 100 mM **1** for the synthesis of sitagliptin intermediate. Reaction conditions: 100 mM **1**, 300 mM benzylamine, 0.5 mM PLP, 60 mg_{CDW}/mL TARO-Est PS, 60 mg_{CDW}/mL AHR/FDH, 200 mM sodium formate, 200 mM Tris-HCl Buffer (pH 8.0); temperature: 37°C.

Synthesis of Sitagliptin Intermediate Using the pH-Stat System

As mentioned above, pH plays a crucial role in the reaction, and the value consistently decreases owing the hydrolysis of ester into a carboxylic acid group. The pH values of the reactions in earlier experiments were controlled using 5 M NaOH via manual addition at an interval of 30 min for 5 h. However, the hydrolysis reaction catalyzed by esterase occurs more rapidly, resulting in a rapid decline in pH during the reaction. Therefore, manual pH adjustment is inefficient. Hence, to minimize pH fluctuation and to maintain the optimal pH value (8.0), we used a pH-stat system in the subsequent experiments. The reactions were performed using three systems (A1, A4, and A6) with 50 mM of **1** in 30 ml of the total reaction volume (**Supplemenatry Figure S5**). Sample analysis at various time points revealed almost complete consumption of the substrate within 18 h, resulting in the achievement of ~80% yield of the desired product. The use of such a pH-stat system enhanced production by almost 50%, indicating that a fine-tuned control of pH is necessary for optimum product formation. The concentration of benzyl alcohol formed was comparable to the amount of product obtained (79%), indicating that an equal amount of amine donor was consumed during the reaction. On the contrary, A1 and A6 exhibited 36 and 56% yield of the sitagliptin intermediate, respectively, suggesting that the promoter engineering strategy enabled fine-tuned control of the expression level of each biocatalyst, which was beneficial for improving the reaction productivity (**Supplemenatry Figure S6**). Encouraged by these results, we selected the A4 system for conducting further reactions with elevated substrate concentrations of 100–200 mM of **1**. Our findings showed that the reaction with 100 mM substrate provided 72% yield of the sitagliptin intermediate and led to the achievement of nearly equal amount of benzyl alcohol (~71%) (**Figure 6**), whereas reaction with 200 mM substrate rection produced only 37% yield of the desired product (**Supplementary Figure S7**).

Finally, the applicability of this coupled enzyme reaction was investigated on Gram scale via utilization of the A4 system using 100 mM (1.0 g) of substrate in 40 ml of the reaction volume. This preparative scale reaction led to the achievement of ~70% yield of the sitagliptin intermediate (70 mM; 0.7 g) without major accumulation of reaction intermediates. After successful completion of the reaction, the sitagliptin intermediate was isolated and purified. First, the reaction mixture containing ~0.7 g of the desired product was acidified using 5°N HCl (pH 2.0) to terminate the reaction, and the enzyme biocatalysts were precipitated. The reaction mixture was then centrifuged for 15 min to remove the cell mass, and the supernatant was subsequently neutralized by using 5 M NaOH and was then extracted with ethyl acetate (2 times) to remove the unreacted amine donor and other reaction intermediates that are soluble in organic solvents. Next, the separated aqueous layer was evaporated to dryness to obtain the crude product mixture, which was then solubilized into methanol to separate the buffer salts and other aqueous impurities. Finally, this methanol solution was concentrated to obtain the desired product, which was further purified by recrystallization using an ethanol:water system, yielding a pure white solid. The solid was then characterized by using ^{1}H NMR and HPLC (61% isolated yield).

CONCLUSION

In conclusion, we report benzylamine as an efficient alternative amine donor for transamination in the synthesis of sitagliptin intermediate. We performed screening of TAs with high specificity for benzylamine and optimized the reaction parameters such as pH, buffer system, and amine donor concentration. The inhibition of TAs or lipase by benzaldehyde was resolved by the application of an AHR/FDH system, which efficiently improved product formation. The promotor engineering strategy was designed and established for improved control of the expression levels of each biocatalyst, and a single whole-cell system for TA and esterase was developed. Whole-cell biotransformation using various substrate concentrations (10–100 mM **1**) led to the achievement of excellent conversion rates (72–91%) to yield the sitagliptin intermediate. Fine-tuned pH control during the reaction by using a pH-stat system improved the yield by ~50% at a substrate concentration of 100 mM. The optimized cascade with 100 mM substrate resulted in the achievement of 61% yield, as determined by spectroscopic and chromatographic methods. The protocol developed in this study can be considered an alternative to existing methods, with the advantages of obtainment of a cheap amine donor and simultaneous synthesis of (*R*) and (*S*) enantiomers with the use of a non-chiral amino donor. This novel method can be used to synthesize industrially valuable compounds, such as substituted β- and γ-amino acids, from the

corresponding esters as the building blocks of many pharmaceutical compounds.

DATA AVAILABILITY STATEMENT

The original contributions presented in the study are included in the article/**Supplementary Material**, further inquiries can be directed to the corresponding author.

AUTHOR CONTRIBUTIONS

TK: Experiment, methodology, data collection and analysis, writing original draft preparation. SS, AP, HJ, and PG: Methodology and experiment. HY: Conceptualization, methodology, writing, review and editing, project administration. All authors have read and agreed to the published version of the manuscript.

FUNDING

This research was supported by Konkuk University Researcher Fund (#2017-A019-0607) in 2017.

SUPPLEMENTARY MATERIAL

The Supplementary Material for this article can be found online at: https://www.frontiersin.org/articles/10.3389/fbioe.2021.757062/full#supplementary-material

REFERENCES

Aschner, P., Kipnes, M. S., Lunceford, J. K., Sanchez, M., Mickel, C., and Williams-Herman, D. E. (2006). Effect of the Dipeptidyl Peptidase-4 Inhibitor Sitagliptin as Monotherapy on Glycemic Control in Patients with Type 2 Diabetes. *Diabetes Care* 29 (12), 2632–2637. doi:10.2337/dc06-0703

Cassimjee, K. E., Branneby, C., Abedi, V., Wells, A., and Berglund, P. (2010). Transaminations with Isopropyl Amine: Equilibrium Displacement with Yeast Alcohol Dehydrogenase Coupled to *In Situ* Cofactor Regeneration. *Chem. Commun.* 46 (30), 5569–5571. doi:10.1039/C0CC00050G

Cheng, F., Chen, X.-L., Li, M.-Y., Zhang, X.-J., Jia, D.-X., Wang, Y.-J., et al. (2020). Creation of a Robust and R-Selective ω-amine Transaminase for the Asymmetric Synthesis of Sitagliptin Intermediate on a Kilogram Scale. *Enzyme Microb. Tech.* 141, 109655. doi:10.1016/j.enzmictec.2020.109655

Chizzolini, F., Forlin, M., Cecchi, D., and Mansy, S. S. (2014). Gene Position More Strongly Influences Cell-free Protein Expression from Operons Than T7 Transcriptional Promoter Strength. *ACS Synth. Biol.* 3 (6), 363–371. doi:10.1021/sb4000977

Clausen, A. M., Dziadul, B., Cappuccio, K. L., Kaba, M., Starbuck, C., Hsiao, Y., et al. (2006). Identification of Ammonium Chloride as an Effective Promoter of the Asymmetric Hydrogenation of a β-Enamine Amide. *Org. Process. Res. Dev.* 10 (4), 723–726. doi:10.1021/op050232o

Dawood, A. W. H., Weiß, M. S., Schulz, C., Pavlidis, I. V., Iding, H., de Souza, R. O. M. A., et al. (2018). Isopropylamine as Amine Donor in Transaminase-Catalyzed Reactions: Better Acceptance through Reaction and Enzyme Engineering. *ChemCatChem* 10 (18), 3943–3949. doi:10.1002/cctc.201800936

Desai, A. A. (2011). Sitagliptin Manufacture: A Compelling Tale of green Chemistry, Process Intensification, and Industrial Asymmetric Catalysis. *Angew. Chem. Int. Ed.* 50 (9), 1974–1976. doi:10.1002/anie.201007051

D. Patil, M., Grogan, G., Bommarius, A., and Yun, H. (2018). Recent Advances in ω-Transaminase-Mediated Biocatalysis for the Enantioselective Synthesis of Chiral Amines. *Catalysts* 8 (7), 254. doi:10.3390/catal8070254

Fesko, K., Steiner, K., Breinbauer, R., Schwab, H., Schürmann, M., and Strohmeier, G. A. (2013). Investigation of One-Enzyme Systems in the ω-transaminase-catalyzed Synthesis of Chiral Amines. *J. Mol. Catal. B: Enzymatic* 96, 103–110. doi:10.1016/j.molcatb.2013.06.015

Gomm, A., Lewis, W., Green, A. P., and O'Reilly, E. (2016). A New Generation of Smart Amine Donors for Transaminase-Mediated Biotransformations. *Chem. Eur. J.* 22, 12692–12695. doi:10.1002/chem.201603188

Green, A. P., Turner, N. J., and O'Reilly, E. (2014). Chiral Amine Synthesis Using ω-Transaminases: An Amine Donor that Displaces Equilibria and Enables High-Throughput Screening. *Angew. Chem.* 126 (40), 10890–10893. doi:10.1002/ange.201406571

Guo, F., and Berglund, P. (2017). Transaminase Biocatalysis: Optimization and Application. *Green. Chem.* 19 (2), 333–360. doi:10.1039/C6GC02328B

Hansen, K. B., Balsells, J., Dreher, S., Hsiao, Y., Kubryk, M., Palucki, M., et al. (2005). First Generation Process for the Preparation of the DPP-IV Inhibitor Sitagliptin. *Org. Process. Res. Dev.* 9 (5), 634–639. doi:10.1021/op0500786

Hansen, K. B., Hsiao, Y., Xu, F., Rivera, N., Clausen, A., Kubryk, M., et al. (2009). Highly Efficient Asymmetric Synthesis of Sitagliptin. *J. Am. Chem. Soc.* 131 (25), 8798–8804. doi:10.1021/ja902462q

Hauer, B. (2020). Embracing Nature's Catalysts: A Viewpoint on the Future of Biocatalysis. *ACS Catal.* 10 (15), 8418–8427. doi:10.1021/acscatal.0c01708

Höhne, M., Kühl, S., Robins, K., and Bornscheuer, U. T. (2008). Efficient Asymmetric Synthesis of Chiral Amines by Combining Transaminase and Pyruvate Decarboxylase. *ChemBioChem* 9 (3), 363–365. doi:10.1002/cbic.200700601

Hou, A., Deng, Z., Ma, H., and Liu, T. (2016). Substrate Screening of Amino Transaminase for the Synthesis of a Sitagliptin Intermediate. *Tetrahedron* 72 (31), 4660–4664. doi:10.1016/j.tet.2016.06.039

Hsiao, Y., Rivera, N. R., Rosner, T., Krska, S. W., Njolito, E., Wang, F., et al. (2004). Highly Efficient Synthesis of β-Amino Acid Derivatives via Asymmetric Hydrogenation of Unprotected Enamines. *J. Am. Chem. Soc.* 126 (32), 9918–9919. doi:10.1021/ja047901i

Hwang, E. T., and Lee, S. (2019). Multienzymatic Cascade Reactions via Enzyme Complex by Immobilization. *ACS Catal.* 9 (5), 4402–4425. doi:10.1021/acscatal.8b04921

Iglesias, C., Panizza, P., and Rodriguez Giordano, S. (2017). Identification, Expression and Characterization of an R-ω-Transaminase from Capronia Semiimmersa. *Appl. Microbiol. Biotechnol.* 101 (14), 5677–5687. doi:10.1007/s00253-017-8309-2

Kelefiotis-Stratidakis, P., Tyrikos-Ergas, T., and Pavlidis, I. V. (2019). The challenge of Using Isopropylamine as an Amine Donor in Transaminase Catalysed Reactions. *Org. Biomol. Chem.* 17 (7), 1634–1642. doi:10.1039/C8OB02342E

Khobragade, T. P., Yu, S., Jung, H., Patil, M. D., Sarak, S., Pagar, A. D., et al. (2021). Promoter Engineering-mediated Tuning of Esterase and Transaminase Expression for the Chemoenzymatic Synthesis of Sitagliptin Phosphate at the Kilogram-scale. *Biotechnol. Bioeng.* 118 (8), 3263–3268. doi:10.1002/bit.27819

Kim, G.-H., Jeon, H., Khobragade, T. P., Patil, M. D., Sung, S., Yoon, S., et al. (2019). Enzymatic Synthesis of Sitagliptin Intermediate Using a Novel ω-transaminase. *Enzyme Microb. Tech.* 120, 52–60. doi:10.1016/j.enzmictec.2018.10.003

Kim, G. H., Jeon, H., Khobragade, T. P., Patil, M. D., Sung, S., Yoon, S., et al. (2019). Glutamate as an Efficient Amine Donor for the Synthesis of Chiral β- and γ-Amino Acids Using Transaminase. *ChemCatChem* 11 (5), 1437–1440. doi:10.1002/cctc.201802048

Koszelewski, D., Gã¶ritzer, M., Clay, D., Seisser, B., and Kroutil, W. (2010). Synthesis of Optically Active Amines Employing Recombinant Ï‰-Transaminases inE.Â€ coliCells. *ChemCatChem* 2 (1), 73–77. doi:10.1002/cctc.200900220

Koszelewski, D., Lavandera, I., Clay, D., Guebitz, G. M., Rozzell, D., and Kroutil, W. (2008). Formal Asymmetric Biocatalytic Reductive Amination. *Angew. Chem.* 120 (48), 9477–9480. doi:10.1002/ange.200803763

Koszelewski, D., Lavandera, I., Clay, D., Rozzell, D., and Kroutil, W. (2008). Asymmetric Synthesis of Optically Pure Pharmacologically Relevant Amines Employing ω-Transaminases. *Adv. Synth. Catal.* 350 (17), 2761–2766. doi:10.1002/adsc.200800496

Koszelewski, D., Tauber, K., Faber, K., and Kroutil, W. (2010). ω-Transaminases for the Synthesis of Non-racemic α-chiral Primary Amines. *Trends Biotechnol.* 28 (6), 324–332. doi:10.1016/j.tibtech.2010.03.003

Martínez-Montero, L., Gotor, V., Gotor-Fernández, V., and Lavandera, I. (2016). But-2-ene-1,4-diamine and But-2-Ene-1,4-Diol as Donors for Thermodynamically Favored Transaminase- and Alcohol Dehydrogenase-Catalyzed Processes. *Adv. Synth. Catal.* 358 (10), 1618–1624. doi:10.1002/adsc.201501066

Martínez-Montero, L., Schrittwieser, J. H., and Kroutil, W. (2019). Regioselective Biocatalytic Transformations Employing Transaminases and Tyrosine Phenol Lyases. *Top. Catal.* 62 (17), 1208–1217. doi:10.1007/s11244-018-1054-7

Mathew, S., Jeong, S.-S., Chung, T., Lee, S.-H., and Yun, H. (2016). Asymmetric Synthesis of Aromatic β-amino Acids Using ω-transaminase: Optimizing the Lipase Concentration to Obtain Thermodynamically Unstable β-keto Acids. *J. Biotechnol.* 11 (1), 185–190. doi:10.1002/biot.201500181

Mathew, S., and Yun, H. (2012). ω-Transaminases for the Production of Optically Pure Amines and Unnatural Amino Acids. *ACS Catal.* 2 (6), 993–1001. doi:10.1021/cs300116n

Mutti, F. G., Fuchs, C. S., Pressnitz, D., Sattler, J. H., and Kroutil, W. (2011). Stereoselectivity of Four (R)-Selective Transaminases for the Asymmetric Amination of Ketones. *Adv. Synth. Catal.* 353 (17), 3227–3233. doi:10.1002/adsc.201100558

Mutti, F. G., Fuchs, C. S., Pressnitz, D., Turrini, N. G., Sattler, J. H., Lerchner, A., et al. (2012). Amination of Ketones by Employing Two New (S)-Selective ω-Transaminases and the His-Tagged ω-TA from Vibrio Fluvialis. *Eur. J. Org. Chem.* 2012, 1003–1007. doi:10.1002/ejoc.201101476

Pagar, A. D., Patil, M. D., Flood, D. T., Yoo, T. H., Dawson, P. E., and Yun, H. (2021). Recent Advances in Biocatalysis with Chemical Modification and Expanded Amino Acid Alphabet. *Chem. Rev.* 121 (10), 6173–6245. doi:10.1021/acs.chemrev.0c01201

Park, E.-S., Malik, M. S., Dong, J.-Y., and Shin, J.-S. (2013). One-Pot Production of Enantiopure Alkylamines and Arylalkylamines of Opposite Chirality Catalyzed by ω-Transaminase. *ChemCatChem* 5 (7), 1734–1738. doi:10.1002/cctc.201300052

Park, E.-S., and Shin, J.-S. (2013). ω-Transaminase from Ochrobactrum Anthropi Is Devoid of Substrate and Product Inhibitions. *Appl. Environ. Microbiol.* 79 (13), 4141–4144. doi:10.1128/aem.03811-12

Patil, M. D., Yoon, S., Jeon, H., Khobragade, T. P., Sarak, S., Pagar, A. D., et al. (2019). Kinetic Resolution of Racemic Amines to Enantiopure (S)-amines by a Biocatalytic cascade Employing Amine Dehydrogenase and Alanine Dehydrogenase. *Catalysts* 9 (7), 600. doi:10.3390/catal9070600

Payer, S. E., Schrittwieser, J. H., and Kroutil, W. (2017). Vicinal Diamines as Smart Cosubstrates in the Transaminase-Catalyzed Asymmetric Amination of Ketones. *Eur. J. Org. Chem.* 2017 (17), 2553–2559. doi:10.1002/ejoc.201700253

Pressnitz, D., Fuchs, C. S., Sattler, J. H., Knaus, T., Macheroux, P., Mutti, F. G., et al. (2013). Asymmetric Amination of Tetralone and Chromanone Derivatives Employing ω-Transaminases. *ACS Catal.* 3 (4), 555–559. doi:10.1021/cs400002d

Rudat, J., Brucher, B. R., and Syldatk, C. (2012). Transaminases for the Synthesis of Enantiopure Beta-Amino Acids. *AMB express* 2 (1), 11–10. doi:10.1186/2191-0855-2-11

Savile, C. K., Janey, J. M., Mundorff, E. C., Moore, J. C., Tam, S., Jarvis, W. R., et al. (2010). Biocatalytic Asymmetric Synthesis of Chiral Amines from Ketones Applied to Sitagliptin Manufacture. *Science* 329 (5989), 305–309. doi:10.1126/science.1188934

Sayer, C., Martinez-Torres, R. J., Richter, N., Isupov, M. N., Hailes, H. C., Littlechild, J. A., et al. (2014). The Substrate Specificity, Enantioselectivity and Structure of the (R)-selective Amine : Pyruvate Transaminase fromNectria Haematococca. *Febs J.* 281 (9), 2240–2253. doi:10.1111/febs.12778

Schätzle, S., Steffen-Munsberg, F., Thontowi, A., Höhne, M., Robins, K., and Bornscheuer, U. T. (2011). Enzymatic Asymmetric Synthesis of Enantiomerically Pure Aliphatic, Aromatic and Arylaliphatic Amines with (R)-Selective Amine Transaminases. *Adv. Synth. Catal.* 353 (13), 2439–2445. doi:10.1002/adsc.201100435

Shin, J.-S., and Kim, B.-G. (2001). Comparison of the ω-Transaminases from Different Microorganisms and Application to Production of Chiral Amines. *Biosci. Biotechnol. Biochem.* 65 (8), 1782–1788. doi:10.1271/bbb.65.1782

Shin, J.-S., and Kim, B.-G. (2002). Exploring the Active Site of Amine:Pyruvate Aminotransferase on the Basis of the Substrate Structure−Reactivity Relationship: How the Enzyme Controls Substrate Specificity and Stereoselectivity. *J. Org. Chem.* 67 (9), 2848–2853. doi:10.1021/jo016115i

Shon, M., Shanmugavel, R., Shin, G., Mathew, S., Lee, S.-H., and Yun, H. (2014). Enzymatic Synthesis of Chiral γ-amino Acids Using ω-transaminase. *Chem. Commun.* 50 (84), 12680–12683. doi:10.1039/C3CC44864A

Simon, R. C., Richter, N., Busto, E., and Kroutil, W. (2014). Recent Developments of Cascade Reactions Involving ω-Transaminases. *ACS Catal.* 4, 129–143. doi:10.1021/cs400930v

Slabu, I., Galman, J. L., Lloyd, R. C., and Turner, N. J. (2017). Discovery, Engineering, and Synthetic Application of Transaminase Biocatalysts. *ACS Catal.* 7, 8263–8284. doi:10.1021/acscatal.7b02686

Sperl, J. M., and Sieber, V. (2018). Multienzyme Cascade Reactions-Status and Recent Advances. *ACS Catal.* 8 (3), 2385–2396. doi:10.1021/acscatal.7b03440

Sung, S., Jeon, H., Sarak, S., Ahsan, M. M., Patil, M. D., Kroutil, W., et al. (2018). Parallel Anti-sense Two-step cascade for Alcohol Amination Leading to ω-amino Fatty Acids and α,ω-diamines. *Green. Chem.* 20 (20), 4591–4595. doi:10.1039/C8GC02122H

Telzerow, A., Hobisch, M., Müller, M., Schürmann, M., Schwab, H., and Steiner, K. (2019). A Co-expression System to Shift the Equilibrium of Transamination Reactions toward the Synthesis of Enantiomerically Pure Amines. *Mol. Catal.* 471, 38–43. doi:10.1016/j.mcat.2019.04.006

Truppo, M. D., Rozzell, J. D., Moore, J. C., and Turner, N. J. (2009). Rapid Screening and Scale-Up of Transaminase Catalysed Reactions. *Org. Biomol. Chem.* 7 (2), 395–398. doi:10.1039/B817730A

Truppo, M. D., Turner, N. J., and Rozzell, J. D. (2009). Efficient Kinetic Resolution of Racemic Amines Using a Transaminase in Combination with an Amino Acid Oxidase. *Chem. Commun.* (16), 2127–2129. doi:10.1039/B902995H

Tufvesson, P., Bach, C., and Woodley, J. M. (2014). A Model to Assess the Feasibility of Shifting Reaction Equilibrium by Acetone Removal in the Transamination of Ketones Using 2-propylamine. *Biotechnol. Bioeng.* 111 (2), 309–319. doi:10.1002/bit.25017

Villegas-Torres, M. F., Martinez-Torres, R. J., Cázares-Körner, A., Hailes, H., Baganz, F., and Ward, J. (2015). Multi-step Biocatalytic Strategies for Chiral Amino Alcohol Synthesis. *Enzyme Microb. TechnologyTechnol* 81, 23–30. doi:10.1016/j.enzmictec.2015.07.003

Voges, M., Schmidt, F., Wolff, D., Sadowski, G., and Held, C. (2016). Thermodynamics of the Alanine Aminotransferase Reaction. *Fluid Phase Equilibria* 422, 87–98. doi:10.1016/j.fluid.2016.01.023

Wang, B., Land, H., and Berglund, P. (2013). An Efficient Single-Enzymatic cascade for Asymmetric Synthesis of Chiral Amines Catalyzed by ω-transaminase. *Chem. Commun.* 49 (2), 161–163. doi:10.1039/C2CC37232K

Xu, F., Armstrong, J. D., Zhou, G. X., Simmons, B., Hughes, D., Ge, Z., et al. (2004). Mechanistic Evidence for an α-Oxoketene Pathway in the Formation of β-Ketoamides/Esters via Meldrum's Acid Adducts. *J. Am. Chem. Soc.* 126 (40), 13002–13009. doi:10.1021/ja046488b

Yoo, H.-W., Kim, J., Patil, M. D., Park, B. G., Joo, S.-y., Yun, H., et al. (2019). Production of 12-hydroxy Dodecanoic Acid Methyl Ester Using a Signal Peptide Sequence-Optimized Transporter AlkL and a Novel Monooxygenase. *Bioresour. Tech.* 291, 121812. doi:10.1016/j.biortech.2019.121812

Yoon, S., Patil, M. D., Sarak, S., Jeon, H., Kim, G. H., Khobragade, T. P., et al. (2019). Deracemization of Racemic Amines to Enantiopure (R)- and (S)-amines by Biocatalytic Cascade Employing ω-Transaminase and Amine Dehydrogenase. *ChemCatChem* 11 (7), 1898–1902. doi:10.1002/cctc.201900080

Yun, H., Lim, S., Cho, B.-K., and Kim, B.-G. (2004). ω-Amino Acid:Pyruvate Transaminase from Alcaligenes Denitrificans Y2k-2: a New Catalyst for Kinetic Resolution of β-Amino Acids and Amines. *Appl. Environ. Microbiol.* 70 (4), 2529–2534. doi:10.1128/aem.70.4.2529-2534.2004

Conflict of Interest: The authors declare that the research was conducted in the absence of any commercial or financial relationships that could be construed as a potential conflict of interest.

Publisher's Note: All claims expressed in this article are solely those of the authors and do not necessarily represent those of their affiliated organizations, or those of the publisher, the editors and the reviewers. Any product that may be evaluated in this article, or claim that may be made by its manufacturer, is not guaranteed or endorsed by the publisher.

frontiers in Bioengineering and Biotechnology

ORIGINAL RESEARCH
published: 01 November 2021
doi: 10.3389/fbioe.2021.703399

Catechol 1,2-Dioxygenase From *Paracoccus* sp. MKU1—A Greener and Cleaner Bio-Machinery for *cis, cis*-Muconic Acid Production by Recombinant *E. coli*

Manikka Kubendran Aravind[1], *Perumal Varalakshmi*[2], *Swamidoss Abraham John*[3] *and Balasubramaniem Ashokkumar*[1]*

[1]Department of Genetic Engineering, School of Biotechnology, Madurai Kamaraj University, Madurai, India, [2]Department of Molecular Microbiology, School of Biotechnology, Madurai Kamaraj University, Madurai, India, [3]Centre for Nanoscience and Nanotechnology, Department of Chemistry, Gandhigram Rural Institute, Gandhigram, India

OPEN ACCESS

Edited by:
Jennifer Ann Littlechild,
University of Exeter, United Kingdom

Reviewed by:
Roland Wohlgemuth,
Lodz University of Technology, Poland
Si Jae Park,
Ewha Womans University, South Korea
Johnson Lin,
University of KwaZulu-Natal, South Africa

***Correspondence:**
Balasubramaniem Ashokkumar
rbashokkumar@yahoo.com

Specialty section:
This article was submitted to Bioprocess Engineering, a section of the journal Frontiers in Bioengineering and Biotechnology

Received: 30 April 2021
Accepted: 19 October 2021
Published: 01 November 2021

Citation:
Aravind MK, Varalakshmi P, John SA and Ashokkumar B (2021) Catechol 1,2-Dioxygenase From Paracoccus sp. MKU1—A Greener and Cleaner Bio-Machinery for cis, cis-Muconic Acid Production by Recombinant E. coli. Front. Bioeng. Biotechnol. 9:703399. doi: 10.3389/fbioe.2021.703399

Cis, *cis*-muconic acid (ccMA) is known for its industrial importance as a precursor for the synthesis of several biopolymers. Catechol 1,2-dioxygenase (C12O) is involved in aromatic compounds catabolism and ccMA synthesis in a greener and cleaner way. This is the first study on *C12O* gene from a metabolically versatile *Paracoccus* sp. MKU1, which was cloned and expressed in *E. coli* to produce ccMA from catechol. From the *E. coli* transformant, recombinant C12O enzyme was purified and found to be a homotrimer with a subunit size of 38.6 kDa. The apparent K_m and V_{max} for C12O was 12.89 μM and 310.1 U.mg^{-1}, respectively, evidencing high affinity to catechol than previously reported C12Os. The predicted 3D-structure of C12O from MKU1 consisted of five α-helices in N-terminus, one α-helix in C-terminus, and nine β-sheets in C-terminus. Moreover, a unique α-helix signature 'EESIHAN' was identified in C-terminus between 271 and 277 amino acids, however the molecular insight of conservative α-helix remains obscure. Further, fed-batch culture was employed using recombinant *E. coli* expressing *C12O* gene from *Paracoccus* sp. MKU1 to produce ccMA by whole-cells catalyzed bioconversion of catechol. With the successive supply of 120 mM catechol, the transformant produced 91.4 mM (12.99 g/L) of ccMA in 6 h with the purity of 95.7%. This single step conversion of catechol to ccMA using whole-cells reactions of recombinants did not generate any by-products in the reaction mixtures. Thus, the recombinant *E. coli* expressing high activity C12O from *Paracoccus* sp. MKU1 holds promise as a potential candidate for yielding high concentrations of ccMA at faster rates in low cost settings.

Keywords: *cis, cis*-muconic acid, bioplastics, catechol 1, 2-dioxygenase, *Paracoccus* sp., recombinant *E. coli*, fed-batch culture

1 INTRODUCTION

Cis, cis-Muconic acid (ccMA), a C6 unsaturated dicarboxylic acid, is an industrially important precursor molecule employed for the synthesis of a broad range of economically valuable compounds of polymeric in nature (Salvachúa et al., 2018). The functionally active dual-acid structure and open benzene frame of ccMA triggers multiple chemical reactions, which lead to the formation of numerous synthetic polymers and pharmaceuticals (Vardon et al., 2016). Muconic acid can be converted into adipic acid and terephthalic acid by direct hydrogenation and Diels-Alder reaction followed by oxidation, respectively (Lu et al., 2015). The adipic acid and terephthalic acid are the major platform chemicals used primarily for the production of bioplastics and polyesters including polyethylene terephthalate and nylon-6,6. Annually 73.8 million tonnes were produced worldwide, yet the demand was increasing drastically due to its extensive applications in various industrial sector (Curran et al., 2013). Thus, various methodologies were developed for the chemical synthesis of ccMA by oxidation of petroleum derived benzene as a feedstock. However, ccMA synthesis by oxidation of benzene starts from a carcinogen and involves many hazardous and toxic chemicals. Besides, the production of an economically important chemical constituent by non-renewable sources appears miserable and such chemical methods require high energy inputs to produce ccMA, and also liberate harmful greenhouse gases into the environment (Weber et al., 2012). In this concern, the biological method seems to be a promising and eco-friendly approach for the production of ccMA. To date, many microorganisms were employed to produce ccMA through the conversion of various biomass feedstock rich in sugars and aromatic compounds (Han et al., 2015; Becker et al., 2018; Salvachúa et al., 2018). In the meantime, *Escherichia coli—Escherichia coli* co-culture systems were developed to achieve enhanced production of ccMA from a glucose/xylose mixture (Zhang et al., 2015). Recently, several attempts were made to develop microbial cell factories through genetic modifications, metabolic engineering by constructing artificial biosynthetic pathways, and process optimizations of metabolic pathways, which has resulted promising increase in the yield of ccMA (Xie et al., 2014; Wang et al., 2018; Choi et al., 2020). Nevertheless, such bioconversions require multiple enzyme-catalyzed reactions, the recovered yields were inadequate and their purification fold appeared to be exiguous due to other metabolic intermediates (Vardon et al., 2016). As an alternate, biosynthesis of ccMA through catechol by single enzymatic conversion using recombinant bacteria could be a superior strategy to achieve maximum production of ccMA.

Catechol is one of the most common dihydroxylated intermediates of aromatic compounds metabolism, which readily undergoes various chemical reactions due to its redox potential, results in the generation of reactive oxygen species that could harm cells and other organisms, if not eliminated from the environment (Schweigert et al., 2001). Catechol is generally metabolized through *ortho* (β-ketoadipate) and *meta* cleavage pathways, in which the intradiol cleavages are catalyzed by catechol 1,2-dioxygenase (C12O) to produce ccMA and extradiol cleavages are catalyzed by catechol 2,3-dioxygenase (C23O) to produce hydroxymuconic semialdehyde, respectively (Bugg, 2003). ccMA has been produced in a single step by the ring cleavage of catechol through the β-ketoadipate pathway by certain bacteria belonging to the genus *Pseudomonas*, *Corynebacterium*, and *Stenotrophomonas* (Guzik et al., 2013; Becker et al., 2018; Kohlstedt et al., 2018). Additionally, the crystal structures of C12O (PDB: 1DMH and 2BOY) have been determined from *Acinetobacter* sp. ADP1 and *Rhodococcus opacus* 1CP, respectively, which enabled better understanding about the interaction of the enzyme C12O with the substrate catechol (Vetting and Ohlendorf, 2000; Di Nardo et al., 2004; Matera et al., 2010). Gaining of structural information provides opportunities to redesign tailor-made enzymes with modifications in the active sites with improved catalytic activities and other related functions. Thus, the microorganisms that produce high activity C12O enzymes enable it as a suitable choice for bio-based production of high titre of ccMA in a direct single-step conversion without any by-products.

Paracoccus sp. MKU1 is a chemo-lithotrophic bacterium that has a unique potential to metabolize various organic compounds for its energy consumption by their peculiar nature of its genome architecture (Nisha et al., 2015). The whole-genome sequences of the *Paracoccus* sp. MKU1 substantiate the existence of three different intradiol cleavage dioxygenases such as Catechol 1,2-dioxygenase (AQY21_07,895), 6-Chlorohydroxyquinol 1,2-dioxygenase (AQY21_23,320), and Hydroxyquinol 1,2-dioxygenase (AQY21_15,640), and extradiol cleavage dioxygenases like Catechol 2,3-dioxygenase (AQY21_02,980) (Nisha et al., 2016). Moreover, the expression of gene clusters corresponding to intradiol (*C12O*) and extradiol cleavage (*C23O*) at the transcriptional levels were found to be constitutive in *Paracoccus* sp. MKU1 and their expressions were significantly induced in the presence of catechol in a concentration dependent manner (Aravind et al., 2020). The wild-type *Paracoccus* sp. MKU1 also contains genes corresponding to cis, *cis*-muconate cycloisomerase and muconolactone lyase, which could further metabolize the ccMA produced by C12O from catechol into the intermediates of the citrate cycle. Hence, it is essential to clone and overexpress *C12O* gene in a better strain heterologously, which is devoid of ccMA catabolising activity, could produce recombinant C12O enzyme in larger quantities industrially for the enhanced ccMA production. The intradiol cleavage of catechol by C12O seems to be advantageous since it is a direct single-step conversion of catechol into ccMA. Moreover, C12O catalysed conversion of catechol to ccMA looks attractive in terms of ccMA recovery with high purity even in large scale processes because it doesn't generate any other by-products as contaminants. On the other hand, C12O efficiently catalyses the conversion of catechol in to ccMA, which is estimated to produce up to 100% molar yield of ccMA by complete utilization of catechol (Van Duuren et al., 2011). In this study, *C12O* gene from *Paracoccus* sp. MKU1 was cloned in pET30b(+) vector and transformed in to *E. coli* BL21. Initially, the biochemical properties of the purified recombinant C12O enzyme in terms of their catalytic activity and stability were characterized under

different conditions prior to fed-batch fermentation. Further, the recombinant *E. coli* was employed for the fed-batch fermentation with the continuous supply of catechol as a feedstock under optimistic conditions resulted in prodigious titre of ccMA, which was successfully recovered with maximum purity.

2 MATERIALS AND METHODS

2.1 Materials

4-Aminoantipyrine and Isopropyl ß-D-1-thiogalactopyranoside (IPTG) from Hi-Media, India; Catechol (extra pure, 99%) from SRL, India and ccMA from Sigma-Aldrich, India were purchased. Restriction endonuclease enzymes and T_4 DNA Ligase enzyme were purchased from NEB, United States. pGEM-T Easy Vector Systems (Promega, United States) was used for TA cloning. *E. coli* DH5α, *E. coli* BL21 and pET30b(+) vector were procured from the original stock of our lab. Ni-NTA Agarose resin from Qiagen, Germany; Sephacryl S-300 HR resin from Cytiva, United States and NativeMark™ Unstained Protein Standards were obtained from Invitrogen, United States.

2.2 PCR Amplification of Putative C12O Gene From *Paracoccus* sp. MKU1

Genomic DNA was obtained from *Paracoccus* sp. MKU1 grown in LB medium at 37°C for 24 h using HiPurA Bacterial Genomic DNA Purification Kit (Hi-Media, India). A set of primers were designed from the genome sequences of *Paracoccus* sp. MKU1 (NCBI accession number LLWQ00000000.1) to PCR amplify full length of *C12O* gene: *C12O*F 5′-GCGGATCCCATGACTGT CAAGATTTTCGAC-3′; and *C12O*R 5′- TACTCGAGTCAGG CGGCAGCGCGAC-3′. The *C12O* gene was amplified with according to the following PCR conditions: initial denaturation for 5 min at 94°C, followed by 35 cycles of denaturation at 94°C for 45 s, annealing at 54°C for 60 s, and extension at 72°C for 2 min with a final extension of 10 min at 72°C. The PCR products were then electrophoresed and gel purified using Favorgen-PCR purification kit.

2.3 Heterologous Expression and Purification of C12O

The amplified products of *C12O* was cloned into pGEM-T easy vector and transformed into *E. coli* DH5α. Positive clones containing plasmids with inserts were extracted and sequence verified (SciGenom Labs, India) to confirm the presence of the *C12O* gene. The sequence-verified clones were digested using *Bam*HI and *Xho*I for release of the *C12O* gene, which was sub-cloned into pET30b(+) vector to transform into *E. coli* BL21 (DE3). Subsequently, the positive clones were sequence verified with a pair of primers from the T7 promoter region. The recombinant *E. coli* BL21 (DE3) harbouring *C12O* gene was cultured under shaking conditions at 150 rpm in LB medium (10 g/L of tryptone, 5 g/L of yeast extract, 10 g/L of NaCl; pH 7.5 ± 0.2) containing kanamycin (50 mg/L) until the culture reached an OD600 of 0.5–0.6, and the expression of the *C12O* gene was induced with IPTG (0.2–1.0 mM) by culturing at 25°C for about 3 h. Later, cells were harvested by centrifugation for 5 min at 4°C and 8,000 rpm, resuspended in lysis buffer [50 mM Tris-HCl pH 7.6; 10% glycerol; 0.1% Triton X-100; 100 µg/ml (1000 U) of lysozyme (Thermo Scientific, United States) for cell wall lysis; 1 mM PMSF as serine protease inhibitor] and sonicated at ice-cold conditions. Insoluble debris was removed by centrifugation at 12,000 rpm for 20 min at 4°C to score the supernatant containing crude enzyme. The supernatant was applied to a column packed with Ni-NTA agarose resins for purification of the recombinant enzyme with His-tag by metal-affinity chromatography, according to the manufacturer's instructions (Qiagen, Germany). The homogeneity and molecular mass of the purified C12O enzyme was analyzed using SDS-PAGE. To determine the molecular mass of purified C12O under non-denatured conditions, Size exclusion chromatography (SEC) was performed using BioLogic DuoFlow™ Chromatography FPLC System. For this, sephacryl S-300 HR column was equilibrated with 50 mM Tris-HCl buffer at pH 8.5. The conditions for SEC were set at the flow rate of 1 ml/min at 9 PSI pressure and the absorbance was measured at 280 nm with QuadTec UV/Vis Detector. NativeMark™ Unstained Protein Standards having molecular weight in the range of 20–1,236 kDa (LC0725, Invitrogen) was used as reference protein for the calibration. The purified recombinant enzymes were stored at 20°C and used for further characterization.

2.4 Catechol Dioxygenase Assay

Enzymatic conversion of catechol into ccMA through intradiol cleavage mediated by the purified C12O were spectrophotometrically determined using 4-aminoantipyrine assay by measuring the reduction in the level of catechol as reported earlier (Larue et al., 1964). For this, the enzyme-substrate reactions were initiated by adding 20 µL of purified C12O enzymes with 960 µL of Tris-HCl buffer pH 7.6 containing 20 µL of 50 mM concentration of catechol, and the reaction mixture was incubated at 37°C for 20 min. After the enzyme substrate reactions, the residual catechol was measured by adding 4-aminoantipyrine and the absorbance was measured at 540 nm. The protein concentration was determined by Bradford assay. One unit of enzyme activity was defined as the amount of enzyme that required to convert 1 µmol of the catechol into ccMA per min at pH 7.5 and 37°C. Specific activity of the enzyme was defined as units per mg of protein. Each assay was performed in triplicates.

2.5 Effect of pH and Temperature on Activity and Stability

The optimum pH of purified recombinant C12O enzyme was determined by measuring the enzyme activity at 37°C over the pH ranges from 3.5 to 9.0, using the following buffers: 0.05 M sodium citrate (pH 3.5–4.5); 0.05 M sodium acetate (pH 5.0–6.0); 0.05 M potassium phosphate (pH 6.5–7.5); 0.05 M Tris-HCl (8.0–9.0). The optimum temperature on C12O activity was determined by recording the enzyme activity at various temperatures ranging

from 15°C to 65°C. The stability of C12O at different pH/temperature was determined by incubating the enzymes at various pH conditions for 3 h at 4°C or various temperatures ranging from 10°C to 70°C for 6 h and the enzyme activity was assayed at standard conditions. The maximum stability was considered as 100% and other activities were expressed as the relative maximum activities.

2.6 Effect of Metal Ions on Enzyme Activity

The impact of metal ions on the catalytic conversion of catechol into ccMA by C12O was measured at standard assay conditions in the presence of trivalent and divalent metal complexes Fe^{3+}, Fe^{2+}, Mg^{2+}, Hg^{2+}, Cu^{2+}, and Mn^{2+} (0.1 mM each). The reactions were carried out with 50 mM Tris-HCl buffer solution (pH 7.5) containing each of the metal ions individually at 37°C. The activity assessed in the absence of metal ions was treated as control.

2.7 Determination of Kinetic Constants

The kinetic parameters (K_m and V_{max}) were determined by measuring the initial rate of enzymatic activity with different concentrations of catechol (0–200 μM) in Tris-HCl buffer solution (50 mM; pH 7.5) at 37°C for 20 min. Three independent assays were performed for each substrate concentration. The K_m and V_{max} values were calculated from Michaelis-Menten equation using GraphPad Prism 8 and verified with Lineweaver-Burk plots by applying the reciprocal values obtained from Michaelis-Menten equation. The k_{cat} value of C12O was calculated based on the molecular weight of the enzyme subunit (38.6 kDa).

2.8 *In silico* Analysis of C12O

The amino acid sequence of catechol 1,2-dioxygenase was retrieved from the whole genome sequence of *Paracoccus* sp. MKU1 (Accession number LLWQ00000000.1), which was subjected to PROSITE analysis to predict the active sites, substrate binding sites, and functional domains of C12O. The conservation of domains across various species was demonstrated phylogenetically by the construction of a neighbourhood joining tree with 1,000 bootstrap confidence level using MEGA 8 software. Later, the 3D structure of C12O was generated by homology modelling strategy using I-TASSER server. Concurrently, the homology modelling was validated by Ramachandran plot to assess the quality of predicted structural configuration by analysing the sterically allowed region of amino acids in the core graph. The 3D structure of ligand (catechol) was retrieved from the PubChem database and converted into PDB format using UCSF chimera. Molecular docking studies were carried out using AutoDock Tools 1.5.7 (ADT). Initially, the deletion of water, addition of polar hydrogen, merging of nonpolar hydrogen and insertion of Kollman charges were performed to pre-prepare of grid parameter file (GPF). Later, the docking parameter was outlined using the Lamarckian genetic algorithm (LMA) that comprises a maximum number of 25×10^5 energy appraisals with 0.02 mutation rates and 0.8 crossover rates. The docking parameter file (DPF) was finally designated with a total 50 independent runs and programmed in the Cygwin platform. The catechol molecule docked with the 3D model of C12O was analyzed in Biovia Discovery Studio to determine the substrate binding site, amino acids interaction, the types of bond formation, and catechol cleavage upon binding with the amino acid residue of C12O enzyme in *Paracoccus* sp. MKU1.

2.11. Process Optimization and ccMA Production

Overnight cultures of recombinant *E. coli* BL21 transformed with pET30b(+)-*C12O* expression constructs were inoculated in the M9 modified minimal media (pH 7.5) containing glycerol (1%) as a major carbon source and 100 μM $FeCl_3$. The composition of M9 modified minimal media is 1.8 g/L of K_2HPO_4; 1.2 g/L of KH_2PO_4; 4 g/L of NH_4Cl; 0.2 g/L of MgSO4; 0.1 g/L of NaCl. The culture broth was incubated at 37°C for 6 h. Subsequently, *C12O* expression was induced with 0.2 mM IPTG and 0.2% of lactose for 6 h at 30°C. To determine the conversion of efficiency of catechol to ccMA, the induced cultures of recombinants were supplied with different concentrations of catechol ranging from 10 to 50 mM and incubated for 1 h at 35°C separately. After incubation, cultures were centrifuged and their supernatant was analyzed for the residual catechol concentration by 4-aminoantipyrine assay.

The fed-batch fermentation was further carried out in a 1 L shake flask supplied with 20 mM catechol at 1 h interval until 6 h under above described media and conditions. The growth of recombinant *E. coli*, media pH, reduction of catechol, and ccMA production was monitored for 6 h at 1 h interval. Metabolites in the culture supernatant were harvested, filtered through 0.22 μm filters, and analyzed for the detection of ccMA by GC-MS. GC-MS was performed with Agilent GCMS 5977B instrument using GC-capillary column (0.32 mm × 50 m fused silica) in auto injection mode with helium as the carrier gas at 100 kPa (1 bar. 14.3 psi) at the column temperature of 40°C for 2 min and raised to 250°C by an increase of 10°C/min. Further, the Mass spectrum was carried out using Agilent triple-axis detector (TAD) with electron multiplier (EM) by the scan range of 30–600 at 230°C with the electron ionization of 70 eV.

2.12 Purification and Recovery of ccMA

The ccMA produced in the fed-batch culture was scored by centrifugation at 6,000 rpm for 5 min to remove the bacterial biomass. The supernatant was collected in a screw cap bottle and treated with activated charcoal carbon for 1 h, which was passed through 0.22 μm filters. The flow-through liquid from 0.22 μm filtration was colorless and watery in nature, which was subjected for the acid-temperature shift (pH 2 by H_2SO_4 at 5°C) that allowed precipitation of ccMA. Later, the precipitate containing ccMA was dried in a vacuum oven (Spinco, India) at 50°C and washed twice with ethanol to remove the impurities if any. Finally, the quantity and purity of ccMA was analyzed by Reverse-phase High-Performance Liquid Chromatography (RP-HPLC). Shortly, RP-HPLC was performed on a

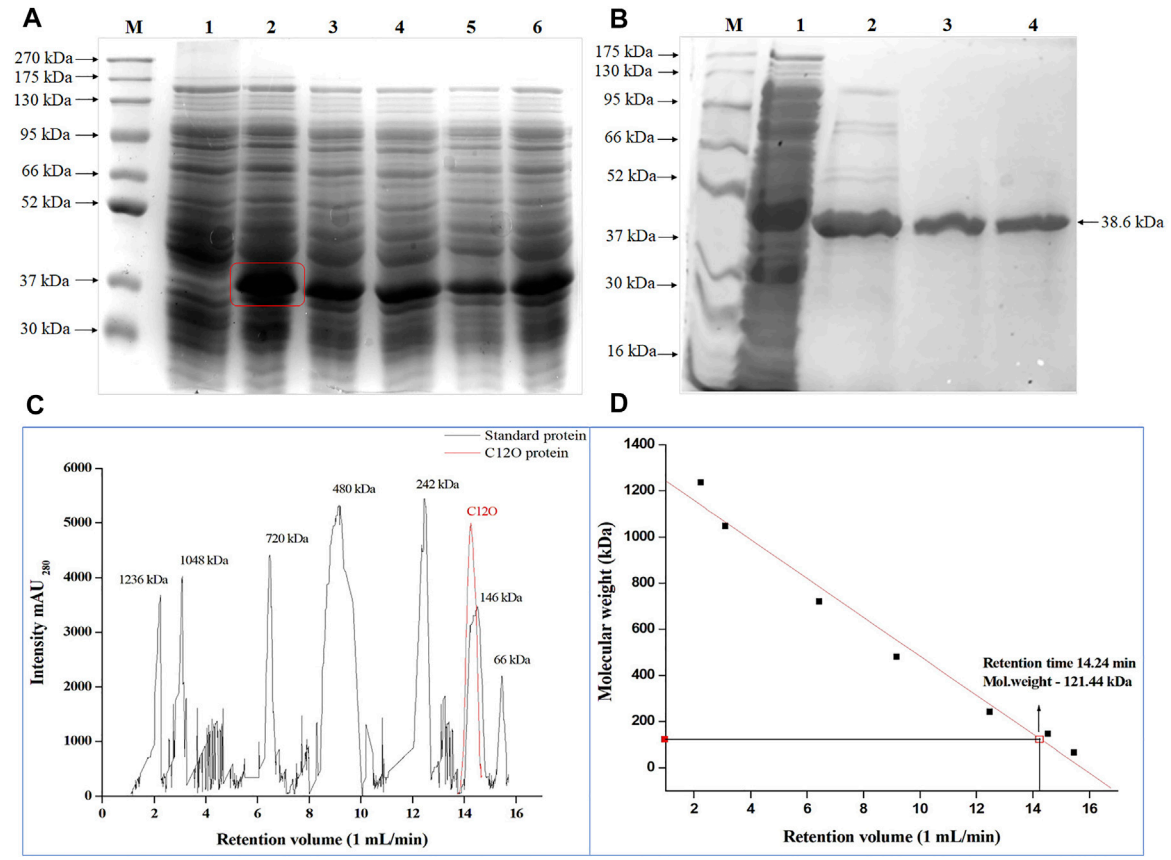

FIGURE 1 | Over-expression of *C12O* from *Paracoccus* sp. MKU1 in *E. coli*. **(A)** SDS-PAGE analysis of IPTG induced cell lysate. Lane M—Protein Ladder; Lane 1—Uninduced; Lane 2—0.2 mM IPTG; Lane 3—0.4 mM IPTG; Lane 4—0.6 mM IPTG; Lane 5—0.8 mM IPTG; Lane 6—1.0 mM IPTG. **(B)** SDS-PAGE analysis of Ni-NTA column purified recombinant C12O protein after 0.2 mM IPTG induction. M—Marker, Lane 1—Crude extract, Lane 2—Eluate 1, Lane 3—Eluate 2, Lane 4—Eluate 3. **(C)**—Size exclusion chromatography analysis of purified of C12O and reference proteins. **(D)** Calibration graph for C12O.

Shimadzu HPLC (Prominence LC-20AT, Japan) using Suplex column (15 cm × 4.6 mm, 5 µm). The mobile phase was carried out with [A] 20 mM phosphoric acid: [B] acetonitrile; with a ratio of 75:25. The column temperature was maintained at 30°C with a flow rate of 1.5 ml/min. The sample was detected at 260 nm by diode array detector.

3 RESULTS AND DISCUSSION

3.1 Cloning of C12O From *Paracoccus* sp. MKU1

Paracoccus sp. MKU1 is metabolically versatile bacteria that possess higher flexibility in utilizing wide range of recalcitrant xenobiotics (Aravind et al., 2020). Genome analysis of *Paracoccus* sp. MKU1 predicted at least 28 different putative dioxygenase genes (Nisha et al., 2016). Of which, the existence of genes corresponding to the catabolism of catechol and protocatechuate branches of the β-ketoadipate pathway has gained much significance in the biodegradation of diverse aromatic pollutants. The extradiol dioxygenase encoding *C12O* gene (AQY21_07895) corresponding to the conversion of catechol into ccMA was PCR amplified using genomic DNA as the template and gene-specific primer sets. The *C12O* gene consisted of an open reading frame (ORF) spanning about 939 bp (**Supplementary Figure S1A**) that encodes a protein of 312 amino acid residues with a theoretical molecular mass of 34.1 kDa and pI of 4.84. The BLAST analysis of C12O nucleotide sequence of *Paracoccus* sp. MKU1 with various closely related bacteria using mega X software revealed maximum identity with *Paracoccus pantotrophus* (90.1%) and *Paracoccus denitrificans* (89.36%), respectively. Likewise, the other bacteria genera such as *Martelella* sp. AD-3, *Rhizobium* sp. WL3 and *Labrys neptuniae* strain KNU-23 shared second-order higher homology with *C12O* gene of *Paracoccus* sp. MKU1. To our surprise, the C12O gene was chromosomally encoded in most of the bacteria except *Rhodobacter* sp. CZR27 and *Ensifer adhaerens* strain Corn53, where it was encoded in the plasmids. The PCR amplicons were cloned in pGEM-T Easy vector and transformed into *E. coli* DH5α. From the transformants, the recombinant plasmids were isolated and digested with *EcoRI* to release the insert, which confirmed the presence of *C12O* ORF (**Supplementary Figure S1B**). Subsequently, the pGEM-T vector carrying *C12O*

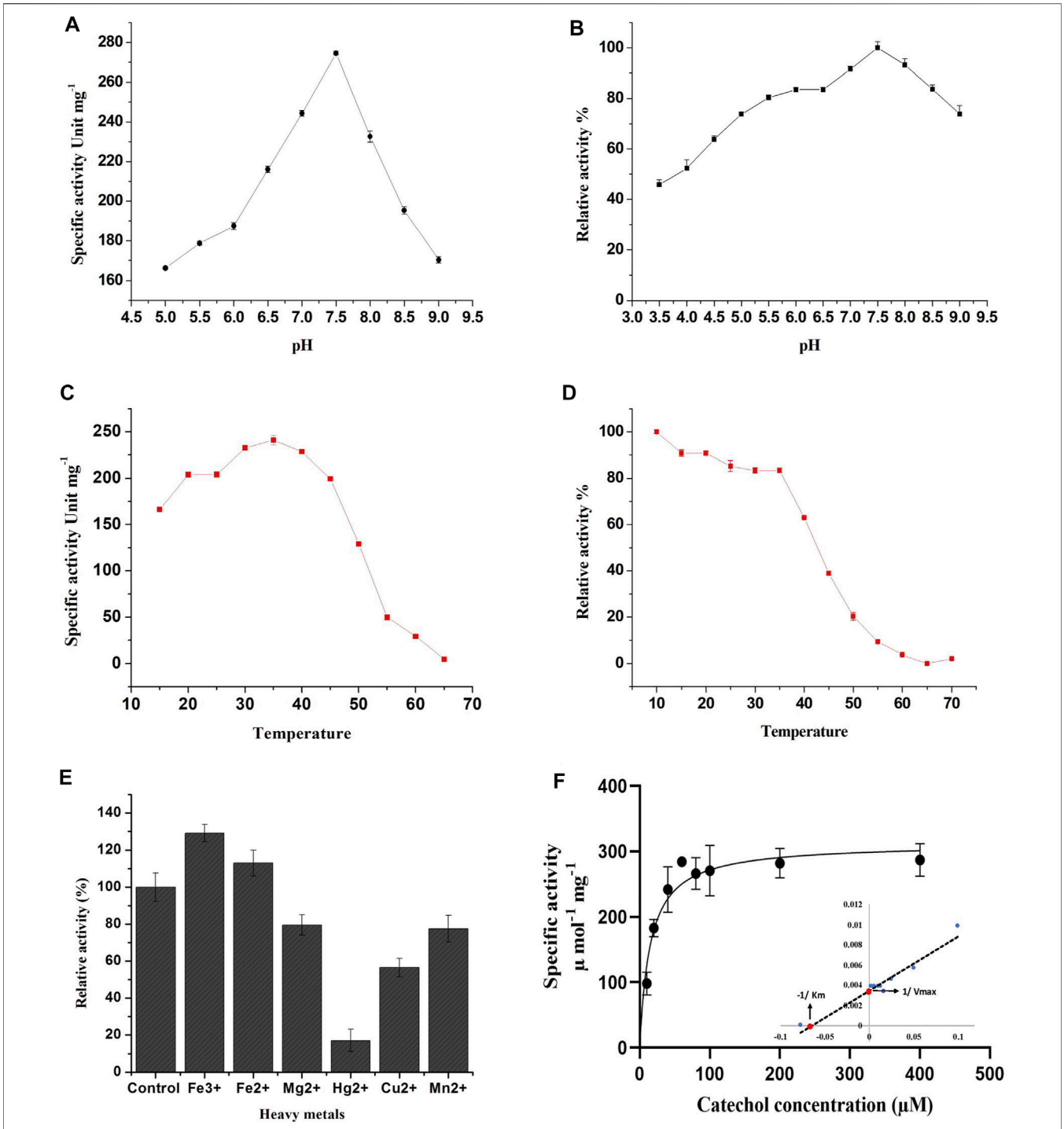

FIGURE 2 | Effect of pH, temperature and metal ions on recombinant C12O activity. **(A)** pH optima, **(B)** pH stability, **(C)** Temperature optima, **(D)** Temperature stability, **(E)** Effect of metal ions, **(F)** Determination of enzyme kinetic constants. Inlet: Lineweaver-Burk plot for the determination of K_m and V_{max}. The residual relative activity of enzyme was determined by the standard assay and compared with the highest activity of the enzyme displayed at different conditions. All the assays were performed in triplicate and the values are presented as mean ± SEM.

ORF was digested with *BamHI* and *XhoI* to release the ORF fragment of *C12O*, which was sub-cloned in pET30b(+) expression vector (**Supplementary Figure S2**). The positive clones carrying a full-length coding region of *C12O* was bidirectionally sequenced and verified to contain no mutations (**Supplementary Figure S3**).

3.2 Expression and Purification of C12O From *E. coli*

The *C12O* ORF of *Paracoccus* sp. MKU1 cloned in pET30b(+) vector was successfully transformed into *E. coli* BL21 (DE3), and was expressed as an active protein upon induction with 0.2 mM IPTG (**Figure 1A**). With the 50 ml of culture, the induced expression of recombinant C12O obtained from the crude cell lysate of *E. coli* transformant was 122.48 U/ml with total activity of 6,124 Units. The recombinant C12O enzyme was purified to apparent homogeneity with a promising purification fold and recovery of 2.11 and 84.4%, respectively. The total concentration of protein in the purified fraction was 376 µg/ml. The enzyme activity of purified enzyme was decreased from 122.8 U/ml to 103 U/ml whereas, the specific activity of the purified enzyme was found to be increased from 129.9 U mg^{-1} to 274.6 U mg^{-1}. The molecular mass of the purified C12O under denatured conditions on SDS-PAGE was estimated to be 38.6 kDa (**Figure 1B**), while the molecular mass of C12O under non-denatured conditions was determined to be 121.4 kDa by size exclusion chromatography (**Figures 1C,D**), suggesting that the nature of native C12O is a homotrimer. The molecular mass of C12O isolated from *Paracoccus* sp. MKU1 is similar to those of some C12Os (38.6 kDa) from *A. radioresistens* (Briganti et al., 2000; Pessione et al., 2001) but lower than those of C12O (40 kDa) from *R. rhodochrous* (Strachan et al., 1998), *A. calcoaceticus* (Patel et al., 1976) and *R. erythropolis* (Aoki et al., 1984). It should be also noted that the purified C12O from various bacteria existed mostly as dimers having two identical subunits with a molecular mass of about 29.0–38.6 kDa (Guzik et al., 2013). Exceptionally, they are present in trimeric or tetrameric structures in some bacteria including *A. radioresistens* (Briganti et al., 2000) and *R. erythropolis* (Aoki et al., 1984), respectively. Thus, C12O from *Paracoccus* sp. MKU1 is predicted to be a trimer with each monomeric unit of 38.6 kDa.

3.4 pH Optima and Stability

The effect of pH on enzyme activity of the purified C12O was also investigated since pH is the crucial factor that influences spatial configuration in enzymes, which directly affects enzyme-catalyzed reactions. The purified C12O displayed a higher catalytic activity over a broad range of pH with optimum activity at pH 7.5. The C12O had maximum enzyme activity of 274.6 U mg^{-1} of protein. The enzyme activity was gradually decreased with the changes in pH towards both acidic and alkaline conditions and retained 60–65% of activity at pH 5.0 and pH 9.0 (**Figure 2A**). The purified C12O of MKU1 was highly active at pH 7.5 and tolerated different pH efficiently by displaying decent enzyme activity even at acidic pH of 3.5 and alkaline pH of 9.0 (**Figure 2B**). The reduced catalytic activity at lower branches of acidic and alkaline conditions could be attributed to the conformational changes in the C12O protein. In comparison, C12O of *Paracoccus* sp. MKU1 is more stable than C12O from other genera, as it retained 43.7% of its activity at pH 3.5. This broad range pH tolerance and stability is the unique property of this dioxygenase from *Paracoccus* sp. MKU1, since C120 purified from *P. aeruginosa* (Wang et al., 2006), *A. calcoaceticus* (Patel et al., 1976), and *Rhodococcus* sp. NCIM2891 (Nadaf and Ghosh, 2011) had shown lesser enzyme activity at acidic and alkaline pH conditions. Meantime, the pH stability of C12O was found consistent with the enzymes from *Pseudomonas* sp. AW-2 (Murakami et al., 1998) and *P. aeruginosa* (Wang et al., 2006).

3.5 Temperature Optima and Stability

Temperature plays a key role in maintaining the kinetic energy of an enzyme against the rate of catalytic reaction. To understand the influence of reaction temperature on enzyme activity, an assay was performed at different temperatures in the range of 15°C–65°C using catechol as substrate. The C12O enzymes exhibited maximum catalytic activity at 35°C, while enzyme activity was gradually decreased with increasing temperature (inversely proportional) and displayed less than 3% of activity at 65°C (**Figure 2C**). This result corroborates with observations of temperature optima for C12O from *P. putida* N6 (Guzik et al., 2011) and *A. calcoaceticus* (Patel et al., 1976). Exceptionally, thermophilic C12Os were characterized earlier from *S. xenophaga* with 50°C (Gou et al., 2009), and *Geobacillus* sp. with 60°C as temperature optima (Giedraityte and Kalėdienė, 2009).

The thermal stability of the recombinant C12O was analyzed by incubating the enzyme at different temperatures ranging from 10°C to 70°C for 3 h to evaluate the temperature stability of C12O relative to the maximum activity. The recombinant C12O enzyme stored at 10°C for 3 h poses greater stability by exhibiting maximum activity. Comparably, the enzyme stored at the temperature ranging from 15°C to 35°C had lost only 8–17% of activity. More than 81–90% of enzyme activity was lost at 50–55°C and there was complete loss of enzyme activity at 65 °C (**Figure 2D**). A similar effect had been previously observed for C12O from *P. aeruginosa* (Wang et al., 2006), *Arthrobacter* sp. BA-5-17 (Murakami et al., 1998) and *S. maltophilia* (Guzik et al., 2013).

3.6 Effect of Metal Ions on C12O Activity

The effect of different metal ions on enzyme activity of C12O was tested using catechol as a substrate (**Figure 2E**). The results evidenced that the presence of Fe^{3+} ($FeCl_3$) and Fe^{2+} ($FeSO_4$) enhanced the catalytic activity of C12O, while $MgCl_2$, $CuSO_4$, and $MnSO_4$ slightly inhibited the activity (15–30%). $HgCl_2$ was the only tested metal that strongly inhibited the catalytic activity of C12O enzyme (82.5%). Many studies evidenced previously that Hg^{2+} is an extremely effective inhibitor of the activity of C12O obtained from several microbial sources (Li et al., 2018; Setlhare et al., 2019). Moreover, the addition of Hg^{2+} (0.1 mM) resulted in complete loss of C12O activity especially in several species of *Rhodococcus* (Aoki et al., 1984; Matsumura et al., 2004; Nadaf and Ghosh, 2011) and *Arthrobacter* sp. BA-5-17 (Murakami et al., 1998). Hg^{2+} ions display high affinity towards sulfur groups of cysteine, and thus the disulfide bonds between cysteines are disrupted, which leads to structural modifications in a protein. Such modifications in the protein structure could affect the active site leading to loss of catalytic activity of enzymes. The enhanced activity by Fe^{3+} was higher than Fe^{2+} for C12O, whereas a significant increase in the presence of Fe^{3+} and Fe^{2+} had been

TABLE 1 | Enzyme kinetic parameters K_m and V_{max} for Catechol 1,2-dioxygenase from various bacterial sources.

Bacterial source	K_m (μM)	V_{max} (U mg^{-1})	References
Paracoccus sp. MKU1	12.89	310.1	This study
Pseudomonas putida	85.19	14.54	Guzik et al. (2011)
Pseudomonas chlororaphis	35.76	16.67	Setlhare et al. (2019)
*Pseudomonas aeruginosa TK*U002	5.9	–	Wang et al. (2006)
Pseudomonas putida ND6	0.019	1.434	Zhao et al. (2007)
Acinetobacter radioresistens	2.82	25.8	Briganti et al. (2000)
Rhodococcus rhodochrous	1.1	19	Strachan et al. (1998)
Rhodococcus opacus	1.4	22.6	Shumkova et al. (2009)
Rhodococcus sp. NCIM 2891	5	62.5	Nadaf and Ghosh, (2011)
Stenotrophomonas maltophila	12.18	1,218.8	Guzik et al. (2013)
Acinetobacter sp. Y64	17.53	1.95	Lin and Milase (2015)
Acinetobacter sp. DS002	1.58	2	Pandeeti and Siddavattam (2011)
Sphingomonas xenophaga QYY	52.85	0.25 μM L^{-1} mg^{-1} min^{-1}	Gou et al. (2009)
Geobacillus sp. G27	28	9.4 (k_{cat})	Giedraityte and Kalėdienė (2009)

reported previously for C12O from *Acinetobacter* sp. Y64 (Lin and Milase, 2015), *P. aeruginosa* (Wang et al., 2006), and *P. putida* (Li et al., 2018). However, the presence of Fe^{3+} and Fe^{2+} resulted in complete loss or decrease of C12O activities in *Rhodococcus* sp. (Aoki et al., 1984; Nadaf and Ghosh, 2011). C12O are metalloenzymes containing non-heme iron (Fe^{3+}) as a cofactor to catalyze intradiol cleavage of catechol (Bugg, 2003). It is apparent that metal ion interactions in these enzymes play crucial role in their catalytic activity or in the structural stabilization. Replacement of Fe^{3+} and Fe^{2+} ions with other metal ions have destabilized the enzyme conformation and led to partial or a complete loss of enzyme activity (Di Nardo et al., 2004). However, the response of bacterial enzymes from various sources in the presence of heavy metals was largely varied, which indicates that the structural organizations of such enzymes from various sources might be different in response to different environmental stimulations. With respect to *Paracoccus* sp. MKU1, these findings demonstrate that none of the metal ions tested, except Hg^{2+}, inhibited the activity of C12O significantly.

3.7 Kinetic Properties of CDOs

The Michaelis-Menten kinetics studies were determined to delineate the minimal concentration of catechol required to attain optimal catalytic cleavage by recombinant C12O enzyme. The kinetic constants for the purified C12O were determined by measuring the initial linear rates of enzymatic reaction at different concentrations of catechol (0–200 μM). The apparent K_m and V_{max} values for C12O were 12.89 μM and 310.1 U.mg^{-1} (**Figure 2F**). During kinetic characteristics determinations for C12O, substrate-level inhibition was noticed at 80 μM of catechol (**Figure 2F**), which corroborated with previous observations in *S. maltophilia* (Guzik et al., 2013). In comparison, the K_m of C12O was lower than a few other bacterial species (**Table 1**) suggesting a higher affinity of C12O to catechol than others. The K_m value of C12O from *Paracoccus* sp. MKU1 was similar to that of *S. maltophilia* and *Acinetobacter* sp. Y64 (Guzik et al., 2013; Lin and Milase, 2015), lower than in *P. chlororaphi*, *P. putida*, and *S. xenophaga* (Guzik et al., 2011; Setlhare et al., 2019) and higher than in *Rhodococcus* sp. NCIM 2891 and *Acinetobacter radioresistens* (Briganti et al., 2000; Nadaf and Ghosh, 2011). Since the K_m value of C12O from different bacterial sources varied greatly (0.19–85.19 μM), the K_m value of C12O from MKU1 signifies that the enzyme has a better affinity for catechol. Likewise, the V_{max} of recombinant C12O from MKU1 was several folds higher than the activity of previously reported C12O except *S. maltophilia* (Guzik et al., 2013) (**Table 1**). Further, the turnover number (k_{cat}) and catalytic efficiency (k_{cat}/K_m) obtained for C12O were 199.5 s^{-1} and 1.54 x 10^7 M^{-1} s^{-1}, respectively under the optimum conditions. Previously, Rodríguez-Salazar et al. (2020) reported that the k_{cat} and k_{cat}/K_m values of purified trimeric C12O from *P. stutzeri* were 16.13 s^{-1} and 1.2 × 10^6 M^{-1} s^{-1}. Likewise, k_{cat} values of two different isoforms of the dimeric C12O (IsoA and IsoB) from *A. radioresistens* LGM S13 were 48.7 and 31.3 s^{-1} (Briganti et al., 2000). In terms of catalytic efficiency and substrate turnover number, C12O from *Paracoccus* sp. MKU1 reflects comparatively higher catalytic proficiency than those from *P. stutzeri, A. radioresistens and* (Briganti et al., 2000; Caglio et al., 2009; Rodríguez-Salazar et al., 2020).

3.8 Sequence Alignment, Structural and Functional Prediction of Catechol Dioxygenases

C12O from *Paracoccus* sp. MKU1 shared about 91–95% homology at the amino acid level with the sequences from other species of the same genus, besides it showed only 69–80% of homology with other genera (**Supplementary Figure S4**). The amino acid sequence alignment across different genera revealed the presence of a highly conserved particular stretch of sequence (101-TPRTIEGPLYVAGAP-115) in all the enzyme sequences aligned (**Supplementary Figure S5**). This conservation of a particular stretch of sequence at a different location between 144–158 aa had also been reported earlier (Caposio et al., 2002; Lin and Milase, 2015), where the majority of the source of enzymes were from *Acinetobacter* sp. Furthermore, it has been reported that the amino acids Ile148, Pro151, and Leu152 (highlighted in bold) in the conserved sequence encompasses the active site of C12O, and Pro151 interacts with the aromatic ring of the substrate (Vetting and

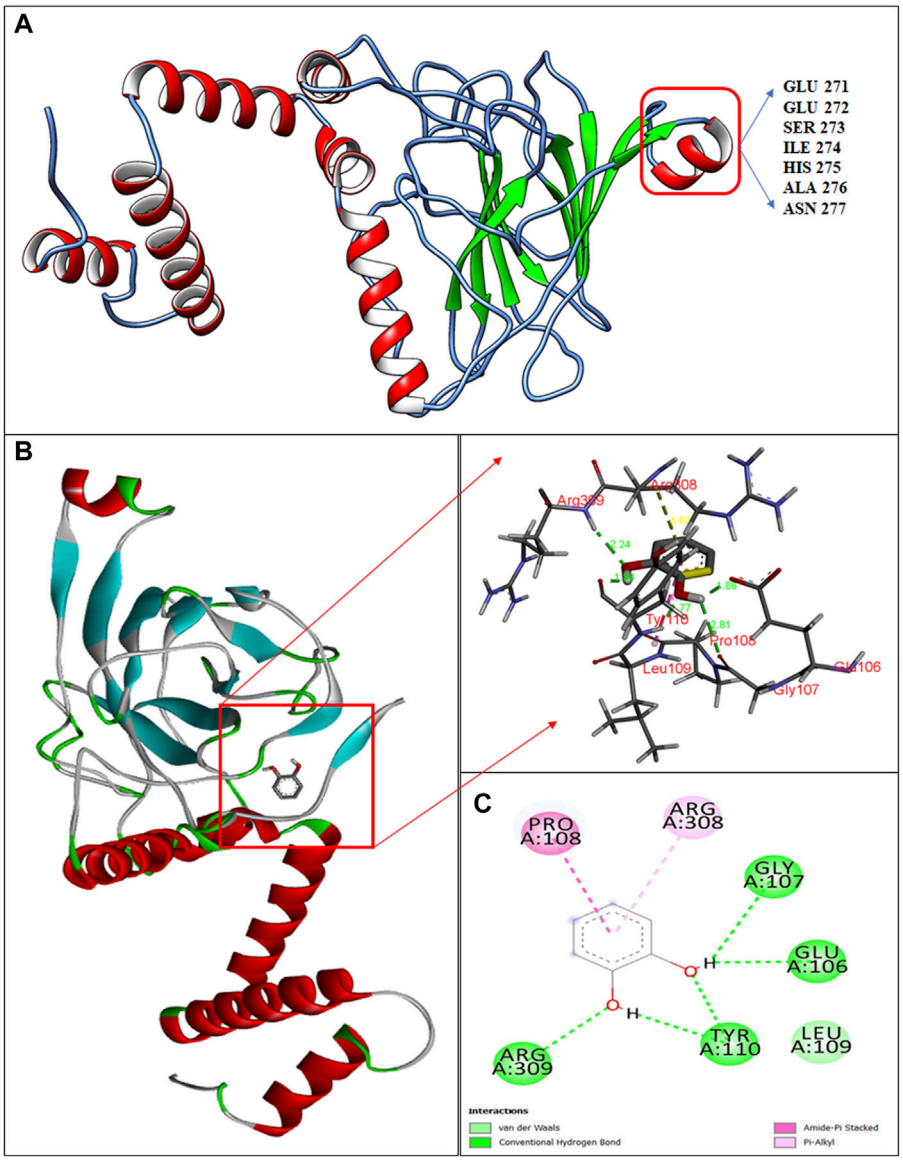

FIGURE 3 | Structural insights in to catechol binding sites in C12O enzyme from *Paracoccus* sp. MKU1. **(A)** 3D structure of C12O with catechol, **(B)** Enlarged image of molecular interaction of C12O with catechol, **(C)** 2D interaction of catechol with specific amino acids of C12O enzyme.

Ohlendorf, 2000). The presence of a similar kind of amino acid stretch and its conservation in the C12O of *Paracoccus* sp. MKU1 demonstrated their common ancestry. The Prosite analysis for binding domains revealed the presence of stretches of amino acid sequences 136-MHGVVHGADGQPLPGAKVEVWHCDTRG FY-164, which is known as the intradiol signature of C12O enzyme that has a major role in the enzyme function such as activation and incorporation of molecular oxygen (Liang et al., 2017).

The 3D-structure of C12O from *Paracoccus* sp. MKU1 was predicted by homology modeling using I-TASSER tool that evidenced the presence of five α-helices in the N-terminus and one α-helix in the C-terminus, whereas nine anti-parallel β-sheets appeared in the C-terminus only, which is depicted by color code using UCSF chimera as shown in **Figure 3A**. The quality of the homology modelling was investigated by Ramachandran plot, which evidenced 99.2% of amino acids were positioned in the favorable and core region of graph plot except GLU116 and VAL140 amino acid residues as shown in the **Supplementary Figure S6**. Similar molecular structures are reported previously for the C12O enzyme from several bacterial sources except for the presence of α-helix in the C-terminus (Earhart et al., 2005; Matera et al., 2010; Guzik et al., 2011). It is interesting to highlight that this unique α-helix signature in the C-terminus was located in between 271-EESIHAN-277 amino acids in C12O from *Paracoccus* and *Martelella* species only (**Figure 3A**; **Supplementary Figure S5**). The molecular insight of this conservative α-helix in the C-terminus of C12O enzyme

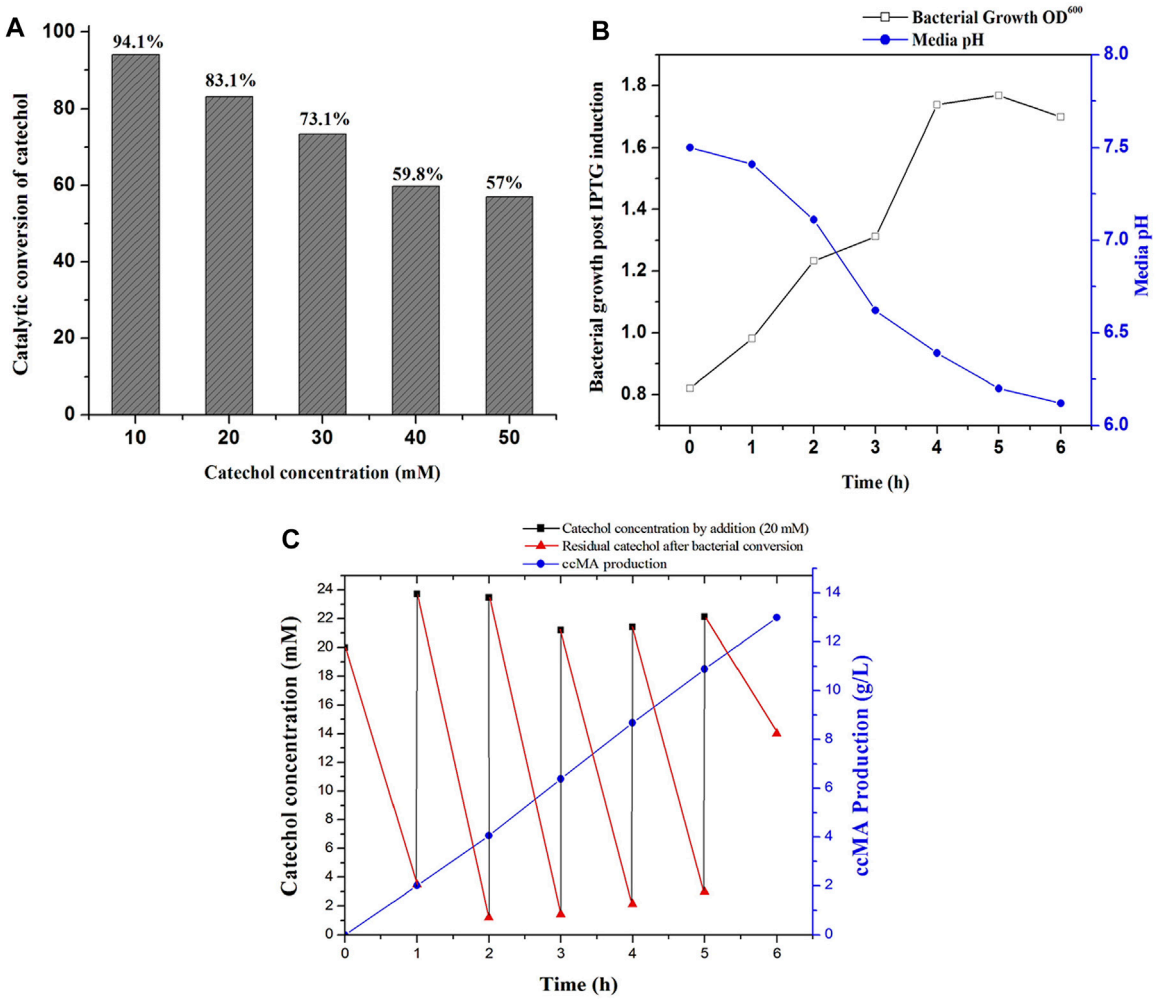

FIGURE 4 | ccMA production by fed-batch fermentation. **(A)** Determination of substrate concentration for catalytic conversion by whole-cells catalyzed reactions at 1 h, **(B)** Bacterial growth profile and media pH during fed-batch fermentation, **(C)** ccMA production and catechol reduction followed by successive supply of 20 mM catechol at 1 h interval up to 6 h.

still remains unclear. Subsequent molecular docking analysis using Auto dock tools 1.5.7 revealed that hydrogen bonding and Van-der walls interactions were formed between catechol and C12O with the binding energy of −5.07 kcal/mol. Particularly, amino acid residues Arg309, Gly107, Glu106, and Tyr110 (2 H bonds in Tyr110) were predicted to interact with the functional group of ligand molecule (catechol) through hydrogen bonds with the distance covered by the length of 2.44 Å, 2.81 Å, 2.86, and 1.84 Å and 1.77 Å, respectively (**Figures 3B**,C). Whereas, the Pro108 interacts with the ligand by Amide Pi stacked bond with the length of 4.17 Å and Arg308 amino acid interacts with the ligand by a pi-alkyl bond with the length of 4.80 Å (**Figures 3B**,C). Surprisingly, these substrate binding sites of C12O enzymes include Glu106, Gly107, Pro108, Leu109, and Tyr110 were also positioned at the conserved region in the C12Os family as shown in **Supplementary Figure S5**. Likewise, Han et al. (2015) had determined the presence binding pocket configured with the stretches of amino acids Leu73, Pro76, Ile105, Pro108, Leu109, Arg221, Phe253, and Ala254 facilitating the interaction between catechol and C12O from *Acinetobacter* sp. ADP1.

3.9 Process Optimization for Whole-Cells Catalyzed ccMA Production

Microbial synthesis of ccMA by the IPTG induced recombinant *E. coli* expressed with *C12O* was optimized by growing them in M9 medium (100 ml) containing glycerol and different concentrations of catechol ranging from 10 to 50 mM to determine the efficiency of whole-cells catalyzed conversion of catechol to ccMA. The whole-cell catalyzed catechol conversions were performed at 35°C since the purified recombinant C12O enzyme exhibited maximum catalytic activity at 35°C only. As shown in **Figure 4A**, the whole-cells catalyzed conversion achieved up to 83.1% at 1 h of incubation with initial concentration of 20 mM catechol, whereas only 57.0%

conversion was attained with 50 mM of initial catechol concentration at same time. Meantime, it was also confirmed that *E. coli* BL21(DE3) cells without *C12O* did not exhibit any activity towards catechol and ccMA. Likewise, Kaneko et al. (2011) reported that the whole-cells reactions by the recombinant *E. coli* expressed with *catA* gene from *P. putida* mt-2 efficiently converted 40 mM catechol in 2 h of incubation. Additionally, the culture filtrate was analyzed by GC-MS to substantiate the microbial production of ccMA by the recombinant *E. coli*, while a noticeable peak with a higher confidence level was detected at the molecular mass of 142.1 in the chromatogram, which evidenced the presence of ccMA (**Supplementary Figure S7**).

3.10 Fed-Batch Fermentation of Whole-Cells Catalyzed ccMA Production

Biosynthesis of ccMA by recombinant *E. coli* was successfully accomplished by fed-batch fermentation (1 L) with whole cells, which produces ccMA through the continuous expression of recombinant protein over a prolonged time by both IPTG and lactose autoinduction. Moreover, whole-cells catalyzed conversions do not require any additional pre-treatment like cell lysis and purification of recombinant enzymes for reactions (Kaneko et al., 2011). During fermentation, changes in the bacterial growth, media pH, catechol concentration, and ccMA production were monitored regularly at 1 h intervals until 6 h. As shown in **Figure 4B**, the bacterial growth was increased until 5 h of incubation and started to decline later. In the meantime, the pH of the fed-batch culture was decreased from 7.5 to 6.2, which indicated the production of ccMA as an end product of catechol conversion. The slight decrease in the pH during fermentation may inhibit the catalytic conversion efficiency, however C12O restored more than 81% of relative activity at pH 6.0–6.5 (**Figure 2B**). Later, cell-free extracts were harvested and processed for the recovery of ccMA, which was further analyzed by HPLC to determine its quality and quantity (**Supplementary Figure S8**). The productivity of ccMA was linearly increased with time and the maximum yield obtained was 12.99 g/L ccMA with 95.7% purity (**Figure 4C**). The quantification of ccMA synthesized during fed-batch fermentation evidenced 2.01 g/L of ccMA yield within an hour of fermentation, which confers its efficiency in producing ccMA at faster rates. The molar conversion yield of ccMA was 91.41 mM with the total successive supply of 120 mM of catechol in 6 h. The reduction in the levels of catechol was more than 90% until the 5th supply, which was directly proportional to ccMA production. However, at the 6th supply, only ~30% of catechol was reduced and the remaining ~70% was retained in the fermentation media over an hour (**Figure 4C**), and this reduced conversion of catechol might be due to the inhibitory effects on the growth of culture by the prevailing concentrations of ccMA produced and decrease in the media pH. Previously, Kaneko et al. (2011) produced 59.0 g/L ccMA in 12 h with a continuous supply of 480 mM (10 mM for 48 times at 15 min interval) catechol in a fed-batch process using a genetically engineered *E. coli* expressed with *C12O* (*catA*) gene from *P. putida* mt-2. Likewise, *K. pneumoniae* was genetically modified by deleting *catB* gene and overexpressed *C12O* that produced 2.1 g/L of ccMA from catechol endogenously (Jung et al., 2015). Lee et al. (2018) had reported the yield of 34 g/L and 54 g/L of ccMA from 7 to 50 L of the feed stock culture using a genetically engineered *C. glutamicum*, which was heterologously expressed with foreign protocatechuate decarboxylase followed by the deletion of *AroE*, *pcaG/H* and, *catB* genes for the accumulation of ccMA. ccMA was produced from vanillic acid and 4-hydroxybenzoic acid (lignin derivatives) by genetically engineered *P. putida* IDPC, which yielded 22.9–31.4 mg/L/h of ccMA (Sonoki et al., 2018). Choi et al. (2019), constructed a recombinant *E. coli* expressing a cluster of gene from different bacterial sources (*asbF* from *B. thuringiensis*; *aroY* from *K. pneumoniae*, and *catA* from *A. calcoaceticus*) for the conversion of 3-dehydroshikimate to ccMA in the fed batch fermentation, which yielded 64 g/L of ccMA with accumulation of other intermediates. Though, ccMA has been produced using certain microbes previously by metabolizing aromatic compounds including phenol, PCA and toluene, benzoate, and vanillic acid, bioconversion of catechol to ccMA in a single step by the whole-cell catalytic process using recombinant bacteria expressing high activity C12O seems to be advantageous since no other contaminants accumulated as a by-product in the fermented culture broth. Thus, the recombinant *E. coli* expressing high activity C12O from *Paracoccus* sp. MKU1 looks as a promising candidate for producing contaminant-free ccMA in higher concentrations within shorter duration and under low-cost conditions through continuous batch fermentation. However, the use of recombinant bacteria for continuous batch fermentation is not commonly employed in the industries due to the difficulties that include instability of the recombinant proteins in the host cells, risk of genetic drift in the culture, lack of process optimization, and uncharacteristic intracellular fluxes (Peebo and Neubauer, 2018). This study has successfully demonstrated the possibility of optimization of recombinant protein expression, characterization enzyme activity and stability, efficiency of catalytic conversion, determination of substrate levels, and its saturation in the fed-batch fermentation itself. It is evident from these observations that the strategies employed for the ccMA production seems logical to transfer the technology from fed-batch to continuous batch fermentation using recombinant *E. coli* and would also be a remarkable choice for the industrial operations for large scale productions.

4 CONCLUSION

In this work, we have generated a genetically stable *E. coli* transformant carrying high activity C12O gene from a metabolically versatile *Paracoccus* sp. MKU1, which is capable of producing ccMA from catechol. The purified recombinant C12O displayed high catalytic efficiency towards catechol, reasonable stability at various pH and tempearture,

and excellent kinetic properties that makes it as a suitable microbial cell factory for the production of ccMA. The whole-cells catalyzed reactions (1 L) with the recombinant *E. coli* has yielded 12.99 g/L of ccMA with 95.7% purity from 120 mM of catechol in 6 h of incubation. Bio-based ccMA production using various other substrates with genetically modified organisms is regarded promising with higher yield, but the pre-treatment strategies and recovery of ccMA is a bottleneck to achieve the anticipated purity due to the existence of numerous metabolic intermediates. This direct one step enzymatic conversion of catechol to ccMA in a shorter duration without any contaminating by-products would be a better choice for many industrial applications. Though various chemical and biological methods were inspected for ccMA synthesis, still there is a great deal for constructing an optimistic strategy to synthesize ccMA to overcome its demand, especially while producing through the continuous batch fermentation. Thus, the recombinant *E. coli* transformant carrying C12O from *Paracoccus* sp. MKU1 seems to be a systemic tool with excellent flexibility for various parameters, and could be employed for the synthesis of ccMA in a greener and cleaner way by continuous fed-batch fermentation in large scale**.**

DATA AVAILABILITY STATEMENT

The datasets presented in this study can be found in online repositories. The names of the repository/repositories and accession number(s) can be found in the article/**Supplementary Material**.

AUTHOR CONTRIBUTIONS

MA: Experimentation, Data curation, Formal analysis, Validation, and Writing—original draft. PV: Data curation, Writing—review, and editing. SJ: Writing—review and editing. BA: Conceptualization, Supervision, Project administration, Writing—review, and editing.

FUNDING

Authors sincerely acknowledge the financial support by Department of Biotechnology, Government of India, New Delhi through a research grant to BA and SAJ (BT/PR20469/BCE/8/1394/2016).

ACKNOWLEDGMENTS

We gratefully acknowledge DST-PURSE and MKU-UPE programs of Madurai Kamaraj University for the infrastructure and other facilities.

SUPPLEMENTARY MATERIAL

The Supplementary Material for this article can be found online at: https://www.frontiersin.org/articles/10.3389/fbioe.2021.703399/full#supplementary-material

REFERENCES

Aoki, K., Konohana, T., Shinke, R., and Nishira, H. (1984). Purification and Characterization of Catechol 1,2-Dioxygenase from Aniline-Assimilating Rhodococcus Erythropolis AN-13†. *Agric. Biol. Chem.* 48, 2087–2095. doi:10.1080/00021369.1984.10866453

Aravind, M. K., Kappen, J., Varalakshmi, P., John, S. A., and Ashokkumar, B. (2020). Bioengineered Graphene Oxide Microcomposites Containing Metabolically Versatile *Paracoccus* Sp. MKU1 for Enhanced Catechol Degradation. *ACS Omega* 5, 16752–16761. doi:10.1021/acsomega.0c01693

Becker, J., Kuhl, M., Kohlstedt, M., Starck, S., and Wittmann, C. (2018). Metabolic Engineering of *Corynebacterium Glutamicum* for the Production of Cis, Cis-Muconic Acid from Lignin. *Microb. Cel Fact.* 17, 115. doi:10.1186/s12934-018-0963-2

Briganti, F., Pessione, E., Giunta, C., Mazzoli, R., and Scozzafava, A. (2000). Purification and Catalytic Properties of Two Catechol 1,2-dioxygenase Isozymes from Benzoate-Grown Cells of *Acinetobacter Radioresistens*. *J. Protein Chem.* 19, 709–716. doi:10.1023/a:1007116703991

Bugg, T. D. H. (2003). Dioxygenase Enzymes: Catalytic Mechanisms and Chemical Models. *Tetrahedron* 59, 7075–7101. doi:10.1016/s0040-4020(03)00944-x

Caglio, R., Valetti, F., Caposio, P., Gribaudo, G., Pessione, E., and Giunta, C. (2009). Fine-tuning of Catalytic Properties of Catechol 1,2-Dioxygenase by Active Site Tailoring. *Chembiochem* 10 (6), 1015–1024. doi:10.1002/cbic.200800836

Caposio, P., Pessione, E., Giuffrida, G., Conti, A., Landolfo, S., Giunta, C., et al. (2002). Cloning and Characterization of Two Catechol 1,2-dioxygenase Genes from *Acinetobacter Radioresistens* S13. *Res. Microbiol.* 153, 69–74. doi:10.1016/s0923-2508(01)01290-6

Choi, S.-S., Seo, S.-Y., Park, S.-O., Lee, H.-N., Song, J.-s., Kim, J.-y., et al. (2019). Cell Factory Design and Culture Process Optimization for Dehydroshikimate Biosynthesis in *Escherichia coli*. *Front. Bioeng. Biotechnol.* 7, 241. doi:10.3389/fbioe.2019.00241

Choi, S., Lee, H.-N., Park, E., Lee, S.-J., and Kim, E.-S. (2020). Recent Advances in Microbial Production of Cis,cis-Muconic Acid. *Biomolecules* 10 (9), 1238. doi:10.3390/biom10091238

Curran, K. A., Leavitt, J. M., Karim, A. S., and Alper, H. S. (2013). Metabolic Engineering of Muconic Acid Production in *Saccharomyces cerevisiae*. *Metab. Eng.* 15, 55–66. doi:10.1016/j.ymben.2012.10.003

Di Nardo, G., Pessione, E., Cavaletto, M., Anfossi, L., Vanni, A., Briganti, F., et al. (2004). Effects of Surface Hydrophobicity on the Catalytic Iron Ion Retention in the Active Site of Two Catechol 1,2-dioxygenase Isoenzymes. *Biometals* 17, 699–706. doi:10.1007/s10534-004-1208-x

Earhart, C. A., Vetting, M. W., Gosu, R., Michaud-Soret, I., Que, L., Jr, and Ohlendorf, D. H. (2005). Structure of Catechol 1,2-dioxygenase from Pseudomonas Arvilla. *Biochem. Biophysical Res. Commun.* 338 (1), 198–205. doi:10.1016/j.bbrc.2005.08.221

Giedraityte, G., and Kalėdienė, L. (2009). Catechol 1,2-dioxygenase from α-naphthol Degrading Thermophilic Geobacillus Sp. Strain: Purification and Properties. *Cent. Eur. J. Biol.* 4, 68–73. doi:10.2478/s11535-008-0049-y

Gou, M., Qu, Y., Zhou, J., Li, A., and Salah Uddin, M. (2009). Characterization of Catechol 1,2-dioxygenase from Cell Extracts of *Sphingomonas Xenophaga* QYY. *Sci. China Ser. B-chem.* 52, 615–620. doi:10.1007/s11426-008-0149-6

Guzik, U., Greń, I., Hupert-Kocurek, K., and Wojcieszyńska, D. (2011). Catechol 1,2-dioxygenase from the New Aromatic Compounds - Degrading *Pseudomonas Putida* Strain N6. *Int. Biodeterioration Biodegradation* 65, 504–512. doi:10.1016/j.ibiod.2011.02.001

Guzik, U., Hupert-Kocurek, K., Sitnik, M., and Wojcieszyńska, D. (2013). High Activity Catechol 1,2-dioxygenase from *Stenotrophomonas Maltophilia* Strain KB2 as a Useful Tool in Cis,cis-Muconic Acid Production.

Antonie van Leeuwenhoek 103, 1297–1307. doi:10.1007/s10482-013-9910-8

Han, L., Liu, P., Sun, J., Wu, Y., Zhang, Y., Chen, W., et al. (20152015). Engineering Catechol 1, 2-dioxygenase by Design for Improving the Performance of the Cis, Cis-Muconic Acid Synthetic Pathway in *Escherichia coli*. *Sci. Rep.* 5, 13435. doi:10.1038/srep13435

Jung, H.-M., Jung, M.-Y., and Oh, M.-K. (2015). Metabolic Engineering of *Klebsiella pneumoniae* for the Production of Cis,cis-Muconic Acid. *Appl. Microbiol. Biotechnol.* 99 (12), 5217–5225. doi:10.1007/s00253-015-6442-3

Kaneko, A., Ishii, Y., and Kirimura, K. (2011). High-yield Production Ofcis,cis-Muconic Acid from Catechol in Aqueous Solution by Biocatalyst. *Chem. Lett.* 40, 381–383. doi:10.1246/cl.2011.381

Kohlstedt, M., Starck, S., Barton, N., Stolzenberger, J., Selzer, M., Mehlmann, K., et al. (2018). From Lignin to Nylon: Cascaded Chemical and Biochemical Conversion Using Metabolically Engineered *Pseudomonas Putida*. *Metab. Eng.* 47, 279–293. doi:10.1016/j.ymben.2018.03.003

Larue, T. A., and Blakley, E. R. (1964). Spectrophotometric Determination of Catechols with 4-Aminoantipyrine. *Anal. Chim. Acta.* 31, 400–403. doi:10.1016/S0003-2670(00)88845-5

Lee, H. N., Shin, W. S., Seo, S. Y., Choi, S. S., Song, J. S., Kim, J. Y., et al. (2018). *Corynebacterium* Cell Factory Design and Culture Process Optimization for Muconic Acid Biosynthesis. *Sci. Rep.* 8 (1), 18041. doi:10.1038/s41598-018-36320-4

Li, S., Qin, K., Li, H., Guo, J., Li, D., Liu, F., et al. (2018). Cloning and Characterisation of Four catA Genes Located on the Chromosome and Large Plasmid of *Pseudomonas Putida* ND6. *Electron. J. Biotechnol.* 34, 83–90. doi:10.1016/j.ejbt.2018.06.001

Liang, Y., Wan, N., Cheng, Z., Mo, Y., Liu, B., Liu, H., et al. (2017). Whole-genome Identification and Expression Pattern of the Vicinal Oxygen Chelate Family in Rapeseed (*Brassica Napus* L.). *Front. Plant Sci.* 8, 745. doi:10.3389/fpls.2017.00745

Lin, J., and Milase, R. N. (2015). Purification and Characterization of Catechol 1,2-dioxygenase from *Acinetobacter* Sp. Y64 Strain and *Escherichia coli* Transformants. *Protein J.* 34, 421–433. doi:10.1007/s10930-015-9637-7

Lu, R., Lu, F., Chen, J., Yu, W., Huang, Q., Zhang, J., et al. (2015). Production of Diethyl Terephthalate from Biomass-Derived Muconic Acid. *Angew. Chem.* 128, 257–261. doi:10.1002/ange.201509149

Matera, I., Ferraroni, M., Kolomytseva, M., Golovleva, L., Scozzafava, A., and Briganti, F. (2010). Catechol 1,2-dioxygenase from the Gram-Positive Rhodococcus Opacus 1CP: Quantitative Structure/activity Relationship and the crystal Structures of Native Enzyme and Catechols Adducts. *J. Struct. Biol.* 170 (3), 548–564. doi:10.1016/j.jsb.2009.12.023

Matsumura, E., Ooi, S., Murakami, S., Takenaka, S., and Aoki, K. (2004). Constitutive Synthesis, Purification, and Characterization of Catechol 1,2-dioxygenase from the Aniline-Assimilating Bacterium *Rhodococcus* Sp. AN-22. *J. Biosci. Bioeng.* 98, 71–76. doi:10.1016/s1389-1723(04)70245-5

Murakami, S., Wang, C. L., Naito, A., Shinke, R., and Aoki, K. (1998). Purification and Characterization of Four Catechol 1,2-dioxygenase Isozymes from the Benzamide-Assimilating Bacterium *Arthrobacter* Species BA-5-17. *Microbiol. Res.* 153, 163–171. doi:10.1016/s0944-5013(98)80036-0

Nadaf, N. H., and Ghosh, J. S. (2011). Purification and Characterization of Catechol 1 , 2-dioxygenase from *Rhodococcus* Sp. NCIM 2891. *Res. J. Environ. Earth Sci.* 3, 608–613.

Nisha, K. N., Devi, V., Varalakshmi, P., and Ashokkumar, B. (2015). Biodegradation and Utilization of Dimethylformamide by Biofilm Forming *Paracoccus* Sp. Strains MKU1 and MKU2. *Bioresour. Technol.* 188, 9–13. doi:10.1016/j.biortech.2015.02.042

Nisha, K. N., Sridhar, J., Varalakshmi, P., and Ashokkumar, B. (2016). Draft Genome Sequence of *Paracoccus* Sp. MKU1, a New Bacterial Strain Isolated from an Industrial Effluent with Potential for Bioremediation. *J. Genomics* 4, 13–15. doi:10.7150/jgen.14847

Pandeeti, E. V. P., and Siddavattam, D. (2011). Purification and Characterization of Catechol 1,2-Dioxygenase from Acinetobacter Sp. DS002 and Cloning, Sequencing of Partial catA Gene. *Indian J. Microbiol.* 51 (3), 312–318. doi:10.1007/s12088-011-0123-4

Patel, R. N., Hou, C. T., Felix, A., and Lillard, M. O. (1976). Catechol 1,2-dioxygenase from *Acinetobacter Calcoaceticus*: Purification and Properties. *J. Bacteriol.* 127, 536–544. doi:10.1128/jb.127.1.536-544.1976

Peebo, K., and Neubauer, P. (2018). Application of Continuous Culture Methods to Recombinant Protein Production in Microorganisms. *Microorganisms* 6 (3), 56. doi:10.3390/microorganisms6030056

Pessione, E., Giuffrida, M. G., Mazzoli, R., Caposio, P., Landolfo, S., Conti, A., et al. (2001). The Catechol 1,2 Dioxygenase System of *Acinetobacter Radioresistens*: Isoenzymes, Inductors and Gene Localisation. *Biol. Chem.* 382, 1253–1261. doi:10.1515/BC.2001.156

Rodríguez-Salazar, J., Almeida-Juarez, A. G., Ornelas-Ocampo, K., Millán-López, S., Raga-Carbajal, E., Rodríguez-Mejía, J. L., et al. (2020). Characterization of a Novel Functional Trimeric Catechol 1,2-Dioxygenase from a Pseudomonas Stutzeri Isolated from the Gulf of Mexico. *Front. Microbiol.* 11, 1100. doi:10.3389/fmicb.2020.01100

Salvachúa, D., Johnson, C. W., Singer, C. A., Rohrer, H., Peterson, D. J., Black, B. A., et al. (2018). Bioprocess Development for Muconic Acid Production from Aromatic Compounds and Lignin. *Green. Chem.* 20, 5007–5019. doi:10.1039/c8gc02519c

Schweigert, N., Zehnder, A. J. B., and Eggen, R. I. L. (2001). Chemical Properties of Catechols and Their Molecular Modes of Toxic Action in Cells, from Microorganisms to Mammals. Minireview. *Environ. Microbiol.* 3, 81–91. doi:10.1046/j.1462-2920.2001.00176.x

Setlhare, B., Kumar, A., Mokoena, M. P., and Olaniran, A. O. (2019). Catechol 1,2-dioxygenase Is an Analogue of Homogentisate 1,2-dioxygenase in *Pseudomonas Chlororaphis* Strain UFB2. *Int. J. Mol. Sci.* 20, 61. doi:10.3390/ijms20010061

Shumkova, E. S., Solyanikova, I. P., Plotnikova, E. G., and Golovleva, L. A. (2009). Phenol Degradation by *Rhodococcus Opacus* Strain 1G. *Appl. Biochem. Microbiol.* 45 (1), 43–49. doi:10.1134/s0003683809010086

Sonoki, T., Takahashi, K., Sugita, H., Hatamura, M., Azuma, Y., Sato, T., et al. (2018). Glucose-free Cis,cis-Muconic Acid Production via New Metabolic Designs Corresponding to the Heterogeneity of Lignin. *ACS Sustain. Chem. Eng.* 6, 1256–1264. doi:10.1021/acssuschemeng.7b03597

Strachan, P. D., Freer, A. A., and Fewson, C. A. (1998). Purification and Characterization of Catechol 1,2-dioxygenase from *Rhodococcus Rhodochrous* NCIMB 13259 and Cloning and Sequencing of its catA Gene. *Biochem. J.* 333, 741–747. doi:10.1042/bj3330741

Van Duuren, J. B. J. H., Brehmer, B., Mars, A. E., Eggink, G., Dos Santos, V. A. P. M., and Sanders, J. P. M. (2011). A Limited LCA of Bio-Adipic Acid: Manufacturing the Nylon-6,6 Precursor Adipic Acid Using the Benzoic Acid Degradation Pathway from Different Feedstocks. *Biotechnol. Bioeng.* 108 (6), 1298–1306. doi:10.1002/bit.23074

Vardon, D. R., Rorrer, N. A., Salvachúa, D., Settle, A. E., Johnson, C. W., Menart, M. J., et al. (2016). cis,cis-Muconic Acid: Separation and Catalysis to Bio-Adipic Acid for Nylon-6,6 Polymerization. *Green. Chem.* 18, 3397–3413. doi:10.1039/c5gc02844b

Vetting, M. W., and Ohlendorf, D. H. (2000). The 1.8 Å crystal Structure of Catechol 1,2-dioxygenase Reveals a Novel Hydrophobic Helical Zipper as a Subunit Linker. *Structure* 8, 429–440. doi:10.1016/s0969-2126(00)00122-2

Wang, C.-L., You, S.-L., and Wang, S.-L. (2006). Purification and Characterization of a Novel Catechol 1,2-dioxygenase from *Pseudomonas aeruginosa* with Benzoic Acid as a Carbon Source. *Process Biochem.* 41, 1594–1601. doi:10.1016/j.procbio.2006.03.008

Wang, S., Bilal, M., Zong, Y., Hu, H., Wang, W., and Zhang, X. (2018). Development of a Plasmid-free Biosynthetic Pathway for Enhanced Muconic Acid Production in *Pseudomonas Chlororaphis* HT66. *ACS Synth. Biol.* 7 (4), 1131–1142. doi:10.1021/acssynbio.8b00047

Weber, C., Brückner, C., Weinreb, S., Lehr, C., Essl, C., and Boles, E. (2012). Biosynthesis of Cis , Cis -Muconic Acid and its Aromatic Precursors, Catechol and Protocatechuic Acid, from Renewable Feedstocks by *Saccharomyces cerevisiae*. *Appl. Environ. Microbiol.* 78, 8421–8430. doi:10.1128/aem.01983-12

Xie, N.-Z., Liang, H., Huang, R.-B., and Xu, P. (2014). Biotechnological Production of Muconic Acid: Current Status and Future Prospects. *Biotechnol. Adv.* 32, 615–622. doi:10.1016/j.biotechadv.2014.04.001

Zhang, H., Pereira, B., Li, Z., and Stephanopoulos, G. (2015). Engineering *Escherichia coli* Coculture Systems for the Production of Biochemical Products. *Proc. Natl. Acad. Sci. USA* 112 (27), 8266–8271. doi:10.1073/pnas.1506781112

Zhao, H. B., Chen, W., and Cai, B. L. (2007). Cloning and Expression of catA Gene from Pseudomonas Putida ND6 and Study on the Catechol Cleavage Pathway. *Wei Sheng Wu Xue Bao* 47 (3), 387–391.

Conflict of Interest: The authors declare that the research was conducted in the absence of any commercial or financial relationships that could be construed as a potential conflict of interest.

Publisher's Note: All claims expressed in this article are solely those of the authors and do not necessarily represent those of their affiliated organizations, or those of the publisher, the editors and the reviewers. Any product that may be evaluated in this article, or claim that may be made by its manufacturer, is not guaranteed or endorsed by the publisher.

frontiers in Bioengineering and Biotechnology

ORIGINAL RESEARCH
published: 22 December 2021
doi: 10.3389/fbioe.2021.798147

Engineering of Reductive Aminases for Asymmetric Synthesis of Enantiopure Rasagiline

Kai Zhang, Yuanzhi He, Jiawei Zhu, Qi Zhang, Luyao Tang, Li Cui and Yan Feng**

State Key Laboratory of Microbial Metabolism, Joint International Research Laboratory of Metabolic and Developmental Sciences, School of Life Sciences and Biotechnology, Shanghai Jiao Tong University, Shanghai, China

Reductive aminases (RedAms) for the stereoselective amination of ketones represent an environmentally benign and economically viable alternative to transition metal–catalyzed asymmetric chemical synthesis. Here, we report two RedAms from *Aspergillus calidoustus* (*Ac*RedAm) and bacteria (*Ba*RedAm) with NADPH-dependent features. The enzymes can synthesize a set of secondary amines using a broad range of ketone and amine substrates with up to 97% conversion. To synthesize the pharmaceutical ingredient (*R*)-rasagiline, we engineered *Ac*RedAm through rational design to obtain highly stereoselective mutants. The best mutant Q237A from *Ac*RedAm could synthesize (*R*)-rasagiline with >99% enantiomeric excess with moderate conversion. The features of *Ac*RedAm and *Ba*RedAm highlight their potential for further study and expand the biocatalytic toolbox for industrial applications.

Keywords: reductive aminase, chiral amine, site saturation mutagenesis, rational design, rasagiline

OPEN ACCESS

Edited by:
Jennifer Ann Littlechild, University of Exeter, United Kingdom

Reviewed by:
Aitao Li, Hubei University, China
Dirk Tischler, Ruhr University Bochum, Germany

****Correspondence:***
Li Cui
cuili@sjtu.edu.cn
Yan Feng
yfeng2009@sjtu.edu.cn

Specialty section:
This article was submitted to Bioprocess Engineering, a section of the journal Frontiers in Bioengineering and Biotechnology

Received: *19 October 2021*
Accepted: *24 November 2021*
Published: *22 December 2021*

Citation:
Zhang K, He Y, Zhu J, Zhang Q, Tang L, Cui L and Feng Y (2021) Engineering of Reductive Aminases for Asymmetric Synthesis of Enantiopure Rasagiline. Front. Bioeng. Biotechnol. 9:798147. doi: 10.3389/fbioe.2021.798147

INTRODUCTION

Chiral amines are valuable building blocks of numerous natural products, active pharmaceuticals, and other high-value chemicals (Afanasyev et al., 2019; Newman and Cragg, 2020; Guo et al., 2021; Li et al., 2021; Nguyen and Kou, 2021). Constituting approximately 40% of new drugs approved by the FDA in recent years, chiral amines constituted a market value of USD 14 billion in 2020 (de Gonzalo and Lavandera, 2021). Numerous chemical strategies have been established for the preparation of chiral amines, which suffer limitations such as low efficiency, low selectivity, and adverse environmental impact. In contrast, enzymes from renewable resources can afford excellent stereo- and regioselectivity and catalyze reactions under mild aqueous conditions (Bornscheuer et al., 2012; Matzel et al., 2017; Wu et al., 2021). Because biochemical reactions can take place without using toxic reagents and extensive protection and deprotection steps, enzymes are always employed as catalysts for developing green chemistry; consequently, biosynthesis has received considerable attention (Ran et al., 2008; Wohlgemuth, 2010; Choi et al., 2015).

Over the last 20 years, a significant number of enzymatic routes have been developed for the synthesis of chiral amines, among which are enzymes that catalyze the reductive amination of prochiral ketones into amines: transaminases (TAs), amine dehydrogenases (AmDHs), and imine reductases (IREDs) have attracted considerable interest (Schrittwieser et al., 2015; Sharma et al., 2017; D Patil et al., 2018; Grogan, 2018; Liu et al., 2020; Montgomery et al., 2020). Both TAs and AmDHs are currently limited to the synthesis of primary amines, necessitating subsequent alkylation chemistry for the synthesis of chiral secondary and tertiary amines (Dold et al., 2016; Knaus et al., 2017). In particular, IREDs can catalyze the NAD(P)H-dependent reduction of prochiral imines to

chiral amines (Mitsukura et al., 2010) and prefer the reduction of cyclic imine substrates but lead to poor conversion with the amination of prochiral ketones (Huber et al., 2014; Wetzl et al., 2016).

Notably, Turner et al. reported an NADPH-dependent reductive aminase (*Asp*RedAm) from *Aspergillus oryzae* in 2017, which was identified as a subclass of IREDs and could catalyze intermolecular reductive amination of a wider range of ketones and amines with high activity in aqueous media (Aleku et al., 2017). Compared to the multistep chemical routes and other biocatalysts, including TAs and AmDHs, the RedAm approaches show considerable efficiency in producing all types of chiral amines from ketones and amines in a single condensation step with new C-N single bond formation. In particular, *Asp*RedAm enabled the formation of the anti-Parkinson's agent (*R*)-rasagiline directly from indanone and propargylamine. In some cases, *Asp*RedAm also displayed high reactivity by catalyzing reductive amination with ketone: amine ratios as low as 1:1 (Aleku et al., 2017).

Subsequently, Turner's group also disclosed new thermotolerant fungal RedAms that could utilize cheap ammonium salts as amine donors to produce primary amines and perform continuous flow biotransformation under mild conditions (Mangas-Sanchez et al., 2020). Taking advantage of an NADPH cofactor regeneration system and a variety of amines as amino donors, the RedAm-catalyzing process of reductive amination maximizes the atom economy, thereby contributing to environmentally sustainable development. These study results showed that RedAms possess prominent industrial advantages, such as broad substrate scope and excellent stereoselectivity for the synthesis of chiral amines. The remarkable features of known RedAms highlight their great potential for application and have already been successfully applied in industry (Schober et al., 2019).

Currently, the development of RedAms is still limited. Herein, we aimed to apply a sequence structure mining strategy to explore new RedAms for enabling the synthesis of some active pharmaceutical ingredients and scaffolds and engineer them for the synthesis of desired enantiopure products combined with directed evolution. The asymmetric synthesis of rasagiline was chosen as the model reaction because (*R*)-rasagiline is an effective anti-Parkinson's agent, and (*S*)-rasagiline has also been proven to provide prominent cardioprotective activity (Chen et al., 2007; Berdichevski et al., 2010; Leegwater-Kim and Bortan, 2010; Weinreb et al., 2010; Ertracht et al., 2011).

In this study, the enzymatic properties of the candidate RedAms were investigated, they were successfully engineered to produce enantiopure rasagiline, and their synthetic potential as catalysts for accessing rasagiline in one step was explored.

MATERIAL AND METHODS

Strains, Plasmids, and Chemicals

Commercially available chemicals and reagents were purchased from Bidepharm (Shanghai, China), Macklin (Shanghai, China), Energy Chemical (Anhui, China), TCI (Shanghai, China), Kai Wei Chemical (Shanghai, China), Aladdin (Shanghai, China), J&K (Beijing, China), Amethyst (Beijing, China), Collins (Shanghai, China), Adamas (Shanghai, China), Sigma-Aldrich (St. Louis, MO, United States), or Acros Organics (Geel, Belgium) unless stated otherwise. Glucose dehydrogenase (GDH) was purchased from Aladdin (Shanghai, China). Restriction enzymes, T4 DNA ligase, and DNA polymerases were purchased from New England Biolabs or Takara Bio. Chemically competent *E. coli* Trans5α and BL21(DE3) were purchased from TransGen Biotech (Beijing, China). pET28a was obtained from our laboratory. The codon-optimized genes for the candidate RedAms were synthesized and cloned into pUC18 using GenScript (Nanjing, China). All kits for mini-preparation of DNA, PCR purification, and gel extraction were purchased from Axygen (Hangzhou, China).

Phylogenetic Tree Building and Protein Sequence Structure Analysis

Homologous protein sequences were searched using the BLASTP algorithm (Altschul et al., 2005). The previously reported protein sequences of *Asp*RedAm (accession no. XP_001827659) and *At*RedAm (accession no. XP_001217087) were used as search queries in the GenBank non-redundant protein sequence database. Multiple sequence alignments were performed using ClustalW (Thompson et al., 1994). The phylogenetic tree was constructed using MEGA7 with maximum likelihood algorithms (Kumar et al., 2016). The protein sequences in the phylogenetic tree were submitted to SWISS-MODEL for modeling (Waterhouse et al., 2018). The predicted protein structures were aligned using PyMOL to analyze and compare the structural similarities and active pockets with *Asp*RedAm.

Gene Cloning, Expression, and Protein Purification

The codon-optimized genes encoding the candidate RedAms were incorporated into the vector pET28a between *Nde*I and *Xho*I restriction sites. The constructed plasmids were confirmed by sequencing and then transformed into *Escherichia coli* BL21(DE3) chemically competent cells by heat shock. The transformed *E. coli* cells were cultivated in 500 ml LB medium with 50 μg/ml kanamycin at 37°C with shaking at 220 rpm. At OD_{600} between 0.6 and 0.8, isopropyl-β-D-thiogalactopyranoside (IPTG) was added to a final concentration of 0.5 mM to induce protein expression. Incubation was continued at 18°C and 220 rpm for 12 h. The cells were then harvested by centrifugation and disrupted by ultrasonication in 100 mM Tris–HCl buffer (pH 8.0). Recombinant proteins were purified from the supernatant by Ni-affinity chromatography. Purified proteins were examined by SDS-PAGE. The concentration of proteins was measured based on the absorbance at 280 nm by using a NanoDrop spectrophotometer (ThermoFisher), and the extinction coefficients were determined by the selected sample type and baseline correction.

RedAm-Catalyzing Biotransformation

The reductive amination reaction was performed in 100 mM Tris–HCl buffer (pH 9.0) containing 1 mg/ml purified RedAm,

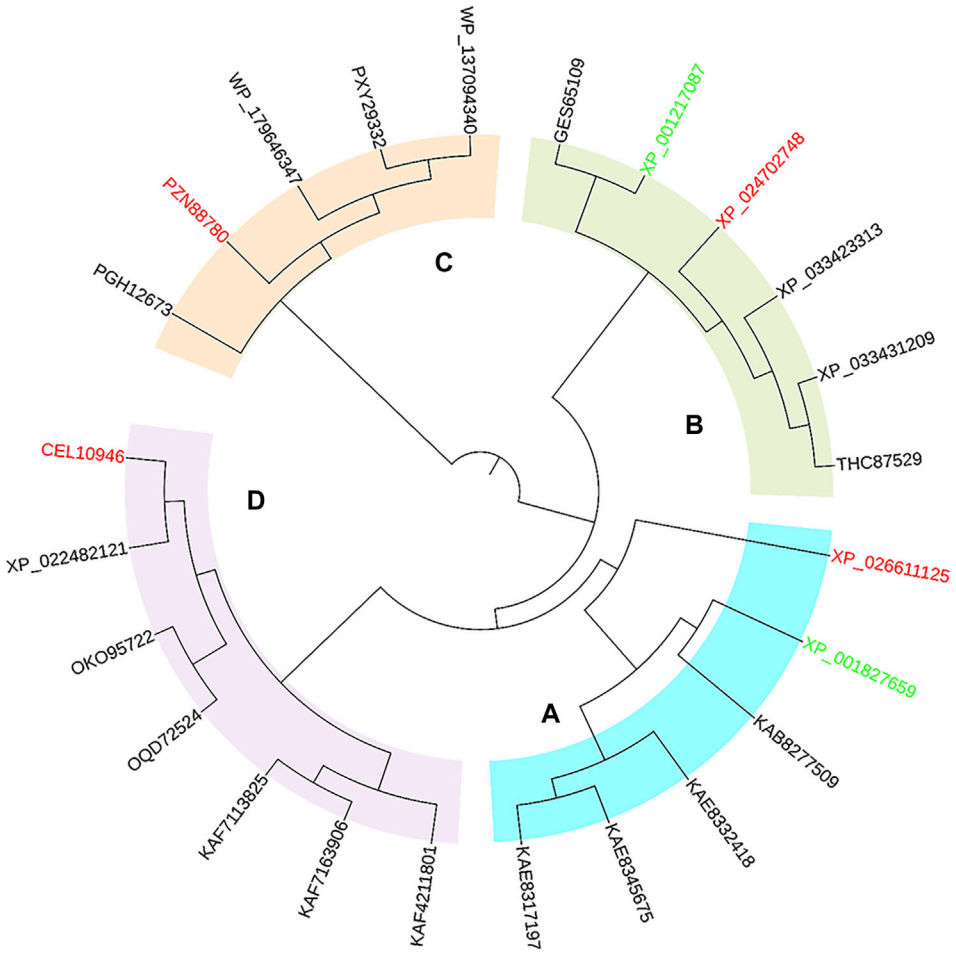

FIGURE 1 | Phylogenetic tree of *Asp*RedAm, *At*RedAm, and potential RedAms. Four major clades were observed, in which four sequences from distinct clades were selected as candidates. The start sequences and candidate sequences are highlighted in green and red, respectively.

0.7 mg/ml GDH (Aladdin), 30 mM D-glucose, 1 mM $NADP^+$, 5 mM ketone, an appropriate ratio of amine (in buffer adjusted to pH 9.0), and 2% (v/v) DMSO. The final reaction volume was made up to 500 µL using Tris–HCl buffer. The reaction mixture was incubated at 25°C with shaking at 220 rpm for 24 h. Then 30 µL of 10 M NaOH was added to quench the reaction. The reaction mixture was extracted twice with 500 µL of *tert*-butyl methyl ether. The organic fractions were combined, dried over anhydrous $MgSO_4$, and analyzed using HPLC or GC-FID (Aleku et al., 2017).

Large-scale reactions for synthesizing rasagiline were carried out using 1 mg/ml purified wild-type RedAms or variant, 0.7 mg/ml GDH, 100 mM D-glucose, 1 mM $NADP^+$, 5 mM indanone, 250 mM propargylamine, and 2% (v/v) DMSO in 100 mM pH 9.0 Tris buffer. The final reaction volume was made up to 50 ml using Tris–HCl buffer. The reaction mixture was incubated at 25°C with shaking at 220 rpm for 180 h. Then 200 µL of the sample was taken at different time points from 2 to 180 h. The sample was quenched by adding 10 µL of 10 M NaOH and extracted twice with 200 µL of *tert*-butyl methyl ether. The organic layers were combined, dried over anhydrous $MgSO_4$, and analyzed using HPLC or GC-FID (Mangas-Sanchez et al., 2020).

Kinetic Assays

To determine the kinetic parameters of *Ac*RedAm and variants for indanone 9, a typical reaction mixture contained 0.002–10 mM of ketone 9, 20 mM propargylamine e from buffer stock adjusted to pH 9.0, 0.2 mM NADPH, 1% DMSO, and purified enzymes at appropriate concentrations in a total volume of 200 µL (100 mM Tris-HCl, pH 9.0). Activity measurements were performed in triplicate at 340 nm (ε = 6.22 mM^{-1} cm^{-1}) using a UV-2550 spectrophotometer (Shimadzu, Japan). The kinetic constants were obtained through nonlinear regression based on the Michaelis–Menten equation (GraphPad Prism 8.0).

Homology Modeling and Docking Analysis

The homology model of *Ac*RedAm was constructed based on the X-ray structure of *Asp*RedAm (PDB code: 5G6S), using SWISS-MODEL. The docking of the NADPH cofactor, substrates, or product rasagiline into the simulation structure of *Ac*RedAm was performed using the Glide SP program in the Schrödinger

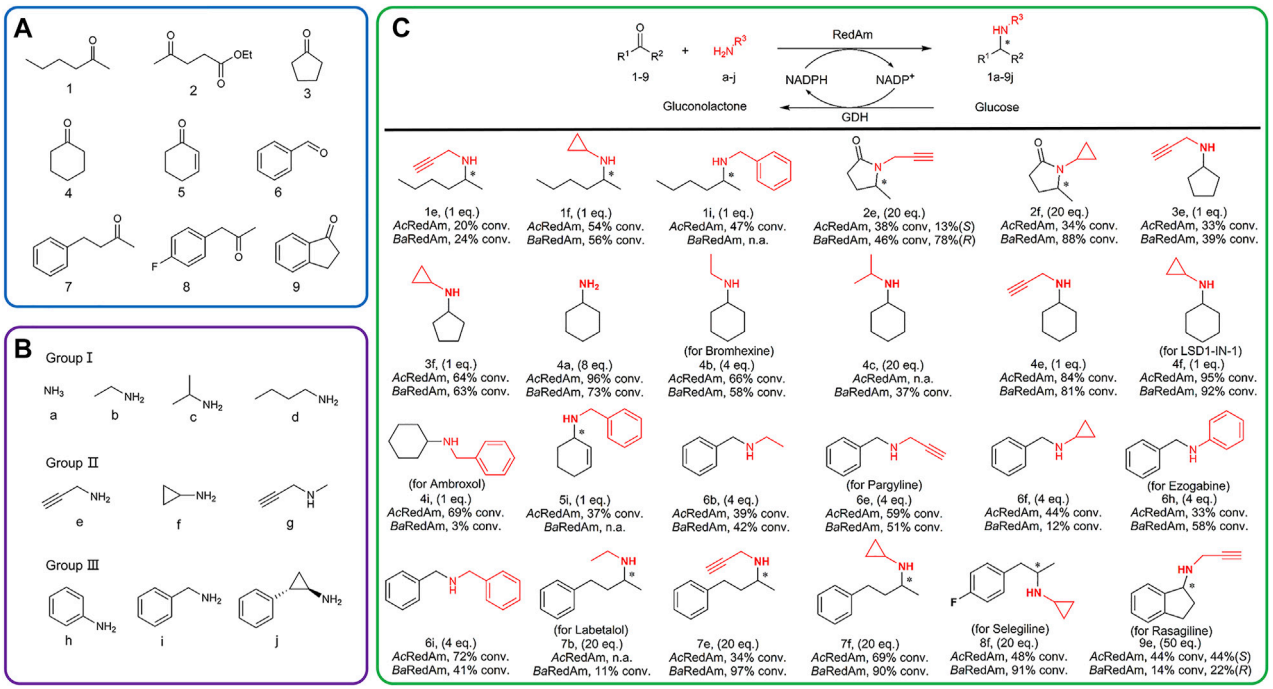

FIGURE 2 | Selected ketones **(A)** and amines **(B)** for the substrate screening of RedAms. **(C)** RedAm-catalyzing reductive amination using selected substrates to access different amines. Reaction conditions: ketone/aldehyde (5 mM), amine (1–50 eq.), RedAm (1 mg ml^{-1}), $NADP^+$ (1 mM), GDH (0.7 mg ml^{-1}), D-glucose (30 mM), and Tris–HCl buffer (100 mM, pH 9.0), 25°C, 220 rpm, 24 h. Conversion determined by HPLC or GC-FID analysis.

package. The residues were evaluated and analyzed using Molecular Operating Environment (MOE) software.

Library Construction and Expression

Site saturation mutagenesis libraries were constructed by overlap extension PCR with primers containing NNK degenerate codons (Horton et al., 2013), which are listed in **Supplementary Section S6**. All transformed libraries were plated to single colony density on LB agar plates containing 50 μg/ml kanamycin and grown overnight at 37°C. To obtain the other 19 amino acid exchange mutants from each library, single colonies were picked and confirmed by sequencing. Expression and purification of the confirmed mutants were performed as previously described.

RESULTS AND DISCUSSION

Computational Exploration of the Novel RedAms Basing on the Sequence and Structure

Protein exploration based on inquiring sequences and structures is an effective strategy to discover novel enzymes from gene or protein databases. As representative reductive aminases, *Asp*RedAm and *At*RedAm have been well studied for their structure and catalytic mechanism (Aleku et al., 2017; Sharma et al., 2018). To inform the survey, the sequences of *Asp*RedAm (accession no. XP_001827659) and *At*RedAm (accession no. XP_001217087) were used as query sequences for a BLAST search of the databases. Bioinformatics filters (identity >45% and <90%; align length >90%; containing key motifs of RedAms; host of different microorganisms) were used to recruit potential protein sequences. The results of the homologous sequences were then processed by phylogenetic analysis (**Figure 1**). The phylogenetic tree consisted of four major clades, in which the starting sequences *Asp*RedAm and *At*RedAm belonged to clades A and B, respectively.

Subsequently, a systematic computational analysis of the sequence and structural characteristics of proteins in each major clade was conducted to predict the activity and structure-related enzymatic properties of these proteins. The protein of each major clade was submitted to SWISS-MODEL to model their three-dimensional structures, and then each simulated structure was aligned to the crystal structure of *Asp*RedAm (PDB code: 5G6S). Three reductive aminases from eukaryotic sources and one from bacteria were finally identified based on their similar folding and conservative active pockets to *Asp*RedAm through structural alignment. *As*RedAm (from *Aspergillus steynii*, accession no. XP_024702748), *Ac*RedAm (from *Aspergillus calidoustus*, accession no. CEL10946), *Ath*RedAm (from *Aspergillus thermomutatus*, accession no. XP_026611125) and *Ba*RedAm (from bacterium, accession no. PZN88780) displayed 63, 62, 54, and 46% overall sequence homology with *Asp*RedAm, respectively. As potential RedAm targets, they all possessed conserved residues such as N93, D169, Y177, and Q240 in *Asp*RedAm, which were suggested to be

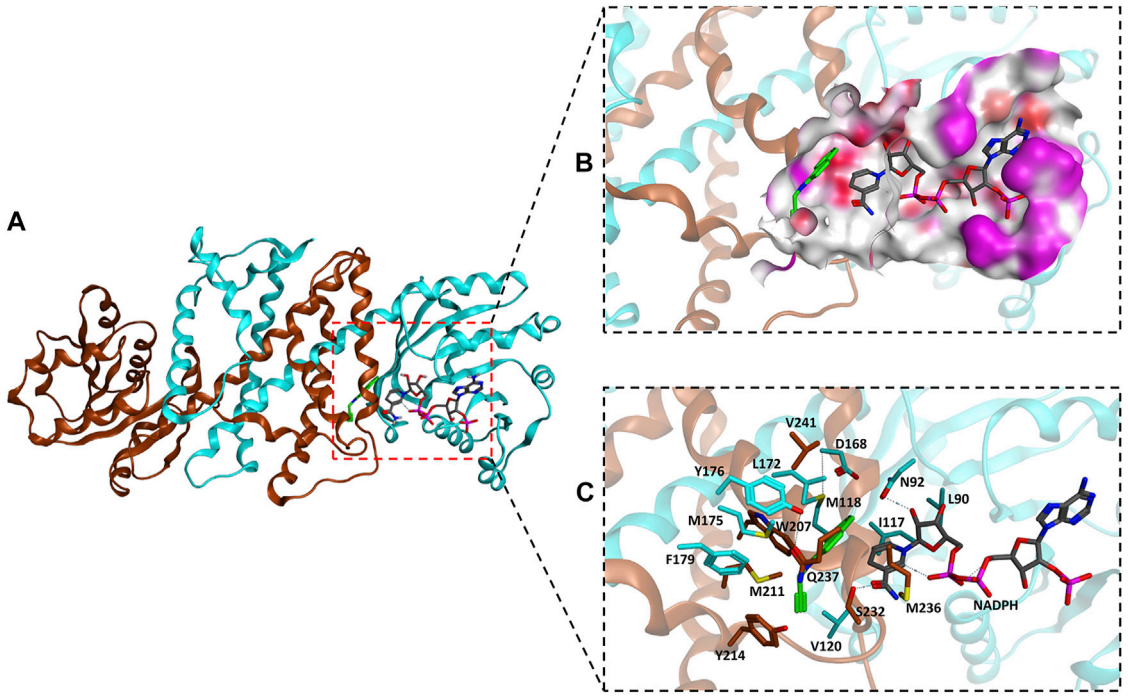

FIGURE 3 | (A) Homology model of the *Ac*RedAm dimeric structure in complex with NADPH (gray) and the iminium intermediate of 9e (green) incorporated by docking. **(B)** The binding pocket of *Ac*RedAm is shown, which is at the dimer interface (red, polar; white, hydrophobic; magenta, exposed). **(C)** The residues located within 8 Å of the iminium intermediate are shown as sticks. Carbon atoms of subunits A and B are shown in cyan and orange, respectively.

important in catalysis in the template model (**Supplementary Figure S1**) (Aleku et al., 2017; Sharma et al., 2018). Furthermore, the phylogenetic relationships of four candidates with known IREDs and RedAms revealed that they belonged to the subclass of IREDs, which might possess the capability for reductive amination reactions (**Supplementary Figure S2**). In the following experiments, the genes of the target RedAms were cloned and expressed in *E. coli* BL21 (DE3); *Ac*RedAm from *Aspergillus calidoustus*, and *Ba*RedAm from bacteria displayed high levels of soluble expression, but the other two were expressed in an insoluble form in inclusion bodies (**Supplementary Figure S4**). Therefore, soluble *Ac*RedAm and *Ba*RedAm were purified by Ni-NAT affinity chromatography for *in vitro* enzymatic assays.

Combinatorial Biosynthesis for Chiral Amines Conducted by the New Explored *Ac*RedAm and *Ba*RedAm

A panel of structurally diverse ketones 1-9 and amines a-j was selected to study the reductive amination activity of the novel enzymes (**Figures 2A,B**). The ketones and amines were arranged according to the properties of their chains. The substrate scope of *Ac*RedAm and *Ba*RedAm was initially assessed by combining a set of ketones (1–9) with different amines. A clear preference for amines e and f was observed (**Supplementary Table S2**). Subsequently, enzyme-catalyzed reductive amination reactions were conducted with the substrates in an appropriate ratio (**Figure 2C**). Reductive amination reactions with both aliphatic ketones and aromatic ketones catalyzed by these two RedAms afforded amine products with moderate to excellent conversion (**Figure 2C**).

In several cases, even equimolar concentrations of ketone and amine resulted in high conversion of 81–95% (**Figure 2C**, products 4e, 4f); hexan-2-one 1 and cyclopentanone 3 were aminated with one equivalent of e, f, or i by each enzyme with a conversion between 20 and 64%; one equivalent of benzylamine i aminated with ketone 4 or 5 yielded 3–69% conversion to the secondary amine, which was indicative of the genuine reductive amination capacity of these enzymes (Sharma et al., 2018). Ester 2 was aminated with 20 equivalents of e or f by each enzyme with a conversion between 34 and 88%.

In the case of 2e, enantiomeric excess (ee) values between 13 and 78% were observed. Ammonia a was also directly accepted as a donor, giving 96% and 73% conversion by *Ac*RedAm and *Ba*RedAm when coupled with carbonyl acceptor 4, respectively. Benzaldehyde 6 gave secondary amines with 4 equivalents of b, e, f, h, or i, with a conversion of 12–72%. In the presence of some carbonyl acceptors (e.g., 2, 7, and 8), amination with various amines, including ethylamine b, propargylamine e, and cyclopropylamine f, proceeded with higher conversion of up to 97% when using *Ba*RedAm compared to *Ac*RedAm. Products 4a, 4b, 4f, 4i, 6e, 6h, 7b, and 8f could also be used as relevant scaffolds for the manufacture of some pharmaceuticals (**Figure 2C**). Furthermore, *Ac*RedAm and *Ba*RedAm were both able to directly produce rasagiline 9e starting from 1-indanone 9 and propargylamine e in 44%

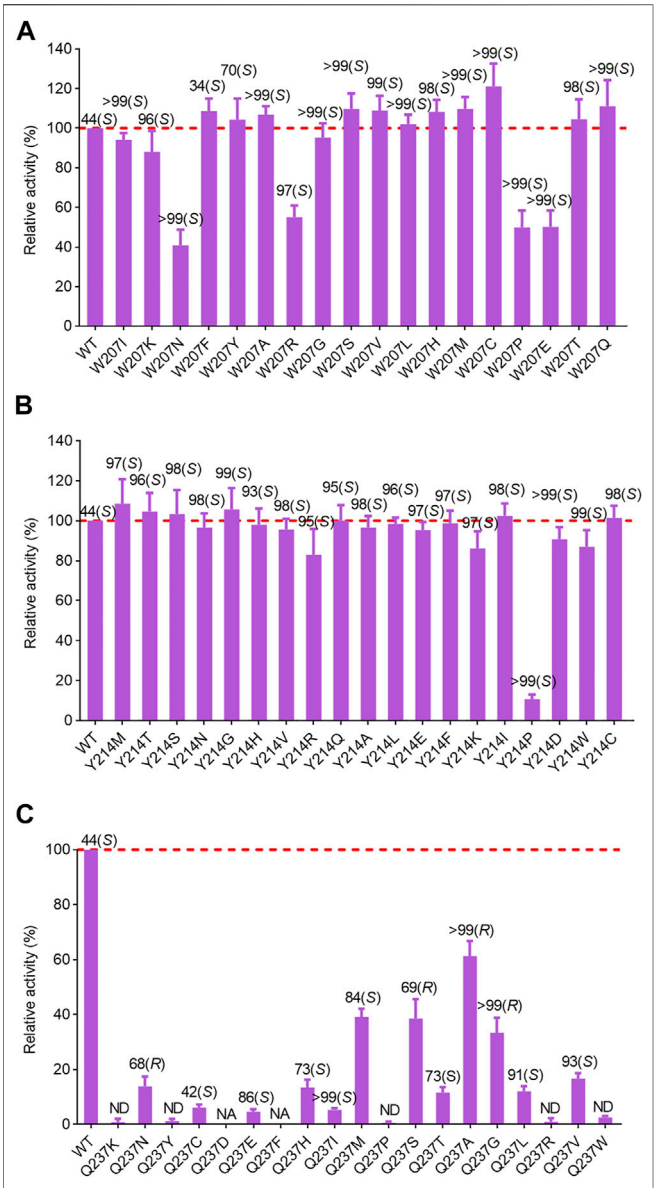

FIGURE 4 | Relative activity and ee values of saturation variants from site 207 **(A)**, 214 **(B)** and 237 **(C)** of *Ac*RedAm for the synthesis of rasagiline. Mutant W207D formed insoluble inclusion bodies. NA indicates no activity; ND indicates not determined for ee value. The activity of the wild-type enzyme was set as 100%. Error bars represent the standard deviations of three replicates.

conversion (44% ee (*S*)-rasagiline) and 14% conversion (22% ee (*R*)-rasagiline), respectively.

Rational Engineering of RedAms for Enantiospecific Improvement of the Rasagiline Synthesis

The initial results not only suggested that *Ac*RedAm and *Ba*RedAm displayed activity for producing rasagiline 9e starting from 1-indanone 9 and propargylamine e but also prompted in-depth engineering of these enzymes for the synthesis of enantiopure rasagiline as the pharmaceutical ingredient (*R*)-rasagiline is an anti-Parkinson's agent, and (*S*)-rasagiline provides prominent cardioprotective activity. *Ac*RedAm was first selected for engineering because it afforded higher conversion to rasagiline 9e than *Ba*RedAm.

The homology model of *Ac*RedAm was generated by SWISS-MODEL using the crystal structure of *Asp*RedAm (PDB code: 5G6S) as the template, and the iminium intermediate of 9e and cofactor NADPH were docked to determine residues near or in the binding pocket (**Figures 3A,B**). The residues located within 8 Å of the iminium intermediate were obtained (**Figure 3C**). By limiting the analysis of this subset of residues, two amino acids (L90 and I117) and five amino acids (L172, W207, Y214, M236, and Q237) might potentially affect amine e and 1-indanone 9 binding and are involved in product recognition, respectively (**Figure 3C**; **Supplementary Figure S8**). Therefore, these 7 amino acids were targeted for single-site saturation mutagenesis. The remaining positions were discounted because they (N92, D168, and Y176) might have important roles in catalysis according to the structure alignment of *Ac*RedAm and *Asp*RedAm. M118 forms a hydrogen bond with the carbon atom of amine e, and others are far from the substrates compared to the target amino acids (**Supplementary Figure S8**).

Mutant Characterization of RedAms for the Synthesis of Enantiopure Rasagiline

After identification of the saturation mutagenesis at position 90, a total of 10 variants were purified with soluble expression, indicating that position 90 is a key residue influencing the correct folding of *Ac*RedAm and has a slight effect on the enantioselectivity of the product rasagiline (**Supplementary Figure S9**). Other positive mutations were identified at positions 207 and 214, with several variants showing slightly improved activity and most of the variants with a high degree of enantioselectivity toward the enantiomer (*S*)-9e (up to >99% ee) (**Figures 4A,B**). W207C showed the highest activity, which was 1.2-fold that of the wild-type enzyme. In case of single-site saturation mutations at positions 117, 172, 236, and 237, most of the mutants exhibited decreased activity, but several variants such as L172V, Q237N, Q237S, Q237G, and Q237A had moderate to excellent enantioselectivity toward the desired enantiomer (*R*)-9e, with values of 40% ee up to >99% ee (**Figure 4C**; **Supplementary Figure S9**).

The best-performing mutant was Q237A, which retained 70% activity and had excellent activity toward (*R*)-9e with values > 99% ee (**Figure 4C**). To investigate the molecular mechanisms of these beneficial mutations, the product (*S*)- or (*R*)-rasagiline and cofactor NADPH were docked into the binding pocket of mutant W207C and Q237A, respectively. The small side chain of C207 was likely to avoid steric hindrance at the bulky indane ring of (*S*)-9e and accommodate the enantiomer (*S*)-9e, leading to the distance between the reactive carbon atom of (*S*)-9e and the hydride donating carbon (C4) of the nicotinamide of NADPH being reduced,

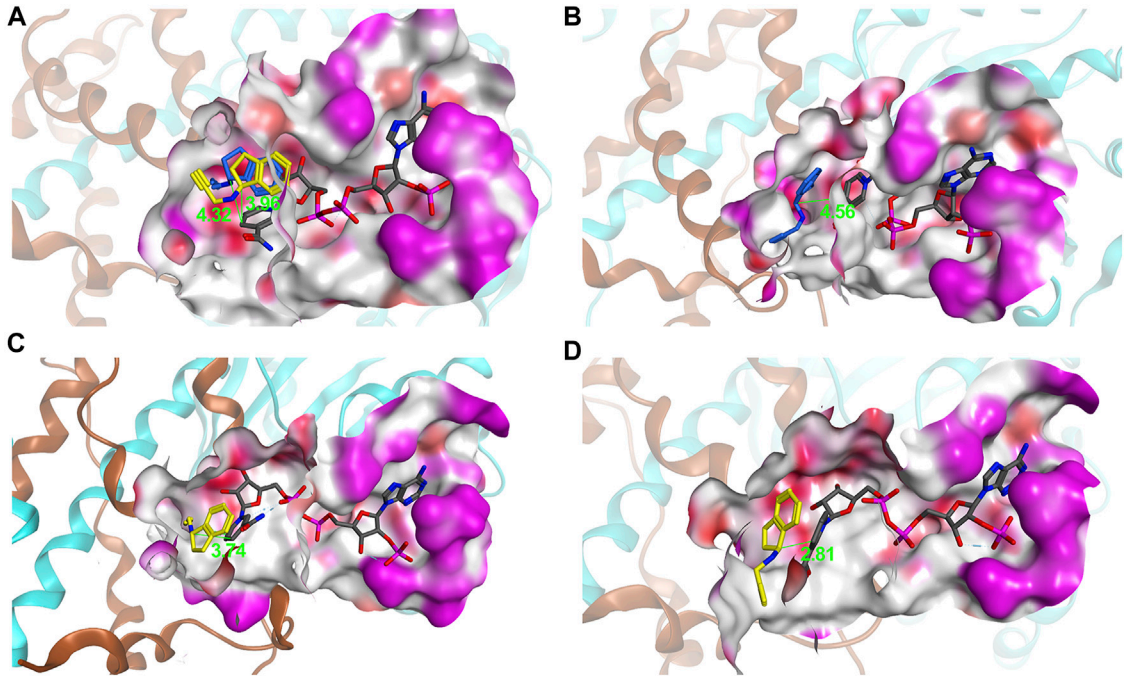

FIGURE 5 | Binding pockets (red, polar; white, hydrophobic; magenta, exposed) and distance between the reactive carbon atom of 9e and the hydride donating carbon (C4) of the nicotinamide of NADPH. **(A)** *Ac*RedAm; **(B)** *Ac*Q237A; **(C)** *Ac*W207C; **(D)** *Ac*W207S/Y214C. NADPH, (*R*)-rasagiline, and (*S*)-rasagiline are shown in gray, blue, and yellow, respectively.

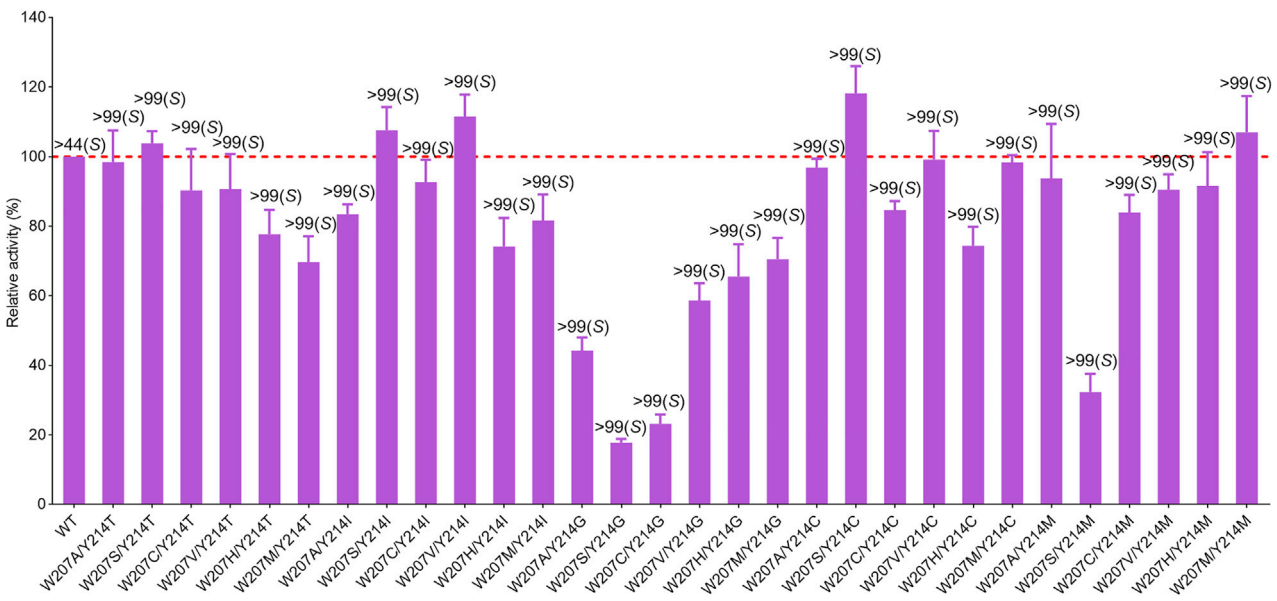

FIGURE 6 | Relative activity and ee values of the double-point mutants for rasagiline synthesis. The activity of wild-type enzyme was set as 100%. Error bars represent the standard deviations of three replicates.

which is conducive to the reduction of the iminium ion intermediate, thereby improving the activity (**Figures 5A,C**) (Sharma et al., 2018; Wang et al., 2021).

However, the small side chain (from alanine, glycine, or serine) at site 237 could also avoid steric hindrance at the bulky indane ring of (*R*)-9e and could accommodate the

TABLE 1 | Kinetic constants of *Ac*RedAm and its variants toward 1-indanone 9.

Enzyme	K_m (mM)	k_{cat} (s^{-1})	k_{cat}/K_m ($s^{-1}mM^{-1}$)
Wild type	0.016 ± 0.004	0.017 ± 0.001	1.063 ± 0.041
Q237A	0.009 ± 0.001	0.007 ± 0.001	0.778 ± 0.021
Q237G	0.004 ± 0.001	0.002 ± 0.001	0.500 ± 0.030
W207C	0.018 ± 0.002	0.022 ± 0.001	1.222 ± 0.044
Y214M	0.012 ± 0.004	0.014 ± 0.002	1.167 ± 0.021
W207S/Y214C	0.021 ± 0.004	0.026 ± 0.002	1.238 ± 0.026

Conditions: 0.002-10 mM 1-indanone 9 concentration, 20 mM propargylamine e, RedAm (5-250 ug), NADPH (0.2 mM), 1%(v/v) DMSO, and Tris buffer (100 mM, pH 9.0).

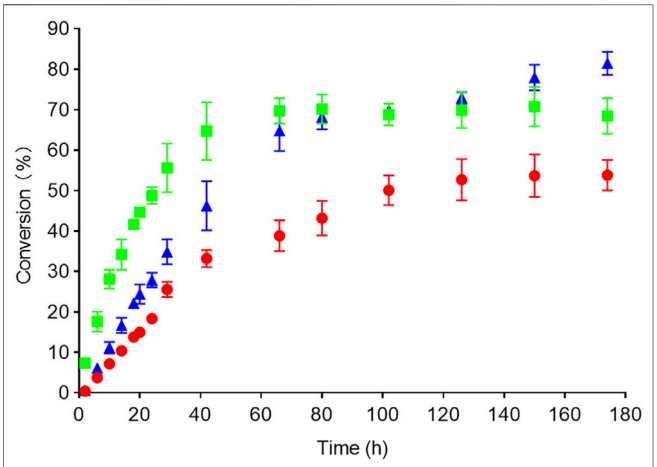

FIGURE 7 | Time course of the reactions. Conversion over time to rasagiline was measured with HPLC and GC (AcRedAm green, Q237A red, BaRedAm blue). Conditions: 5 mM 1-indanone 9, 250 mM propargylamine e, RedAm 1 mg/ml, 100 mM glucose, 1 mM $NADP^+$, and 0.7 mg/ml glucose dehydrogenase. Reactions were incubated at 25°C, 220 rpm.

enantiomer (*R*)-9e; however, the distance between the reactive carbon atom of (*R*)-9e and the hydride donating carbon (C4) of the nicotinamide of NADPH increased, resulting in decreased reaction efficiency (**Figures 5A,B**) (Sharma et al., 2018; Wang et al., 2021). Moreover, the corresponding residue Q257 from *Ba*RedAm was selected for single-site saturation mutagenesis to investigate its role. Interestingly, the mutants of Q257 could also confer a complete inversion of enantioselectivity toward rasagiline (**Supplementary Figure S11**), further proving that the residue plays a key role in RedAms.

To obtain the optimal mutant with better activity, the mutants showing slightly improved activity were recombined. Although there was no significant increase in activity, all double-point mutants displayed excellent enantioselectivity toward the enantiomer (*S*)-9e (>99% ee) (**Figure 6**). W207S/Y214C was the best-performing mutant, with a 1.3-fold increase in the activity of the wild-type enzyme. For mutant W207S/Y214C, substitution of these two residues with less polar residues could also avoid steric hindrance at the bulky indane ring of (*S*)-9e and alter the microenvironment of the binding pocket to accommodate the enantiomer (*S*)-9e; the distance between the reactive carbon atom of (*S*)-9e and the hydride donating carbon (C4) of the nicotinamide of NADPH was reduced, thereby improving the activity (**Figures 5A,D**).

Determination of the kinetic parameters showed that both Q237A and Q237G displayed a decrease in K_m and k_{cat} for indanone 9 compared to the wild type, which indicated that they had increased affinity but decreased activity for substrate 9 (**Table 1**). In contrast to the results for both Q237A and Q237G mutants, W207C and W207S/Y214C showed a slight increase in K_m and k_{cat} for ketone 9 compared to the wild type, suggesting that they exhibited increased activity but decreased affinity for substrate 9 (**Table 1**).

Synthetic Potential Evaluation of RedAms for Producing Rasagiline in Large Scale

Rasagiline has been reported to be synthesized in high conversion (up to 91%) using IREDs on a preparative scale but failed to obtain enantiopure products (Matzel et al., 2017). Although the known *Asp*RedAm and its variants were reported to have high enantioselectivity for rasagiline (ee value up to 98%), their potential for the preparative scale has not been explored (Aleku et al., 2017). The approach of enantiopure rasagiline bioproduction has become more attractive.

To test the synthetic potential of the candidate RedAms and mutants in this study, a series of large-scale reactions were performed. By applying 9 and e as substrates, the reaction conditions were investigated on an analytical scale prior to conducting the large-scale reaction. The concentrations of ketone, amine, and enzyme loading were investigated as described in detail in **Supplementary Section S7** and **Supplementary Figure S12**. Under optimal conditions, rasagiline 9e was obtained with 70% conversion (yield: 60%) employing *Ac*RedAm after 60 h, and enantiopure (*R*)-rasagiline (ee > 99%) was also successfully synthesized with the Q237A variant on a large scale to afford a product with a conversion of 51% (yield: 42%) after 120 h (**Figure 7**). Interestingly, 83% conversion (yield: 72%) was achieved using *Ba*RedAm for 180 h, which was consistent with the previous result that *Ba*RedAm possessed greater thermal stability than *Ac*RedAm (**Figure 7** and **Supplementary Figure S7**).

CONCLUSION

In summary, the exploration and characterization of two new reductive aminases, *Ac*RedAm, from *A. calidoustus*, and *Ba*RedAm, from bacteria are reported. Both showed a broad substrate scope and could directly produce primary and secondary amines, including some pharmaceutically relevant scaffolds and valuable amine enantiomer rasagiline in a one-pot reaction. Moreover, *Ba*RedAm displayed greater thermostability than the previously reported RedAms, which highlights its potential as a biocatalyst in industrial processes. *Ac*RedAm was successfully engineered for the synthesis of the pharmaceutically enantiopure rasagiline through rational design. Some key residues were identified, which could confer a significant improvement or a complete inversion of enantioselectivity toward rasagiline by a single-site mutant of *Ac*RedAm, such as W207, Y214, and Q237. Finally, the synthetic potential of rasagiline synthesis was explored through a large-scale reaction using *Ac*RedAm, *Ba*RedAm, or *Ac*RedAm Q237A mutants. Taken together, our work paved the way for further engineering other RedAms and developed a biocatalytic

toolbox for eco-friendly enzymatic asymmetric synthesis of pharmaceuticals containing chiral amines.

DATA AVAILABILITY STATEMENT

The datasets presented in the study are included in the article/**Supplementary Material**, further inquiries can be directed to the corresponding author/s. Additionally, sequence data have been deposited in Genbank with the accession number OL468622 and OL468617.

AUTHOR CONTRIBUTIONS

YF and KZ designed the experiments. KZ, YH, JZ, and QZ conducted the experiments. YF, LC, and LT helped with the data analysis. KZ, LC, and YF wrote the manuscript. All authors read and approved the final manuscript.

FUNDING

This work was financially supported by the National Key Research and Development Program of China 2020YFA0907700, National Natural Science Foundation of China 31620103901, 31770098, and 21977067.

SUPPLEMENTARY MATERIAL

The Supplementary Material for this article can be found online at: https://www.frontiersin.org/articles/10.3389/fbioe.2021.798147/full#supplementary-material

REFERENCES

Afanasyev, O. I., Kuchuk, E., Usanov, D. L., and Chusov, D. (2019). Reductive Amination in the Synthesis of Pharmaceuticals. *Chem. Rev.* 119 (23), 11857–11911. doi:10.1021/acs.chemrev.9b00383

Aleku, G. A., France, S. P., Man, H., Mangas-Sanchez, J., Montgomery, S. L., Sharma, M., et al. (2017). A Reductive Aminase from *Aspergillus oryzae*. *Nat. Chem.* 9 (10), 961–969. doi:10.1038/nchem.2782

Altschul, S. F., Wootton, J. C., Gertz, E. M., Agarwala, R., Morgulis, A., Schäffer, A. A., et al. (2005). Protein Database Searches Using Compositionally Adjusted Substitution Matrices. *FEBS J.* 272 (20), 5101–5109. doi:10.1111/j.1742-4658.2005.04945.x

Berdichevski, A., Meiry, G., Milman, F., Reiter, I., Sedan, O., Eliyahu, S., et al. (2010). TVP1022 Protects Neonatal Rat Ventricular Myocytes against Doxorubicin-Induced Functional Derangements. *J. Pharmacol. Exp. Ther.* 332 (2), 413–420. doi:10.1124/jpet.109.161158.10

Bornscheuer, U. T., Huisman, G., Kazlauskas, R., Lutz, S., Moore, J., and Robins, K. (2012). Engineering the Third Wave of Biocatalysis. *Nature* 485 (7397), 185–194. doi:10.1038/nature11117

Chen, J. J., Swope, D. M., and Dashtipour, K. (2007). Comprehensive Review of Rasagiline, a Second-Generation Monoamine Oxidase Inhibitor, for the Treatment of Parkinson's Disease. *Clin. Ther.* 29 (9), 1825–1849. doi:10.1016/j.clinthera.2007.09.021

Choi, J. M., Han, S. S., and Kim, H. S. (2015). Industrial Applications of Enzyme Biocatalysis: Current Status and Future Aspects. *Biotechnol. Adv.* 33 (7), 1443–1454. doi:10.1016/j.biotechadv.2015.02.014

D Patil, M., Grogan, G., Bommarius, A., and Yun, H. (2018). Recent Advances in ω-transaminase-mediated Biocatalysis for the Enantioselective Synthesis of Chiral Amines. *Catalysts* 8 (7), 254. doi:10.3390/catal8070254

de Gonzalo, G., and Lavandera, I. (2021). *Biocatalysis for Practitioners: Techniques, Reactions and Applications*. Hoboken, New Jersey, US: John Wiley & Sons.

Dold, S. M., Syldatk, C., and Rudat, J. (2016). Transaminases and Their Applications. *Green. Biocatalysis* 24, 715–746. doi:10.1002/9781118828083.ch29

Ertracht, O., Liani, E., Bachner-Hinenzon, N., Bar-Am, O., Frolov, L., Ovcharenko, E., et al. (2011). The Cardioprotective Efficacy of TVP1022 in a Rat Model of Ischaemia/reperfusion. *Br. J. Pharmacol.* 163 (4), 755–769. doi:10.1111/j.1476-5381.2011.01274.x

Grogan, G. (2018). Synthesis of Chiral Amines Using Redox Biocatalysis. *Curr. Opin. Chem. Biol.* 43, 15–22. doi:10.1016/j.cbpa.2017.09.008

Guo, Z., Xie, J., Hu, T., Chen, Y., Tao, H., and Yang, X. (2021). Kinetic Resolution of N-Aryl β-amino Alcohols via Asymmetric Aminations of Anilines. *Chem. Commun.* 57 (74), 9394–9397. doi:10.1039/D1CC03117A

Horton, R. M., Cai, Z., Ho, S. N., and Pease, L. R. (2013). Gene Splicing by Overlap Extension: Tailor-Made Genes Using the Polymerase Chain Reaction. *Biotechniques* 54 (3), 129–133. doi:10.2144/000114017

Huber, T., Schneider, L., Präg, A., Gerhardt, S., Einsle, O., and Müller, M. (2014). Direct Reductive Amination of Ketones: Structure and Activity of *S*-selective Imine Reductases from *Streptomyces*. *ChemCatChem* 6 (8), 2248–2252. doi:10.1002/cctc.201402218

Knaus, T., Böhmer, W., and Mutti, F. G. (2017). Amine Dehydrogenases: Efficient Biocatalysts for the Reductive Amination of Carbonyl Compounds. *Green. Chem.* 19 (2), 453–463. doi:10.1039/c6gc01987k

Kumar, S., Stecher, G., and Tamura, K. (2016). MEGA7: Molecular Evolutionary Genetics Analysis Version 7.0 for Bigger Datasets. *Mol. Biol. Evol.* 33 (7), 1870–1874. doi:10.1093/molbev/msw054

Leegwater-Kim, J., and Bortan, E. (2010). The Role of Rasagiline in the Treatment of Parkinson's Disease. *Clin. interventions Aging* 5, 149. doi:10.2147/cia.s4145

Li, F., Liang, Y., Wei, Y., Zheng, Y., Du, Y., and Yu, H. (2021). Biochemical and Structural Characterization of an (*R*)-Selective Transaminase in the Asymmetric Synthesis of Chiral Hydroxy Amines. *Adv. Synth. Catal.* 363 (19), 4582–4589. doi:10.1002/adsc.202100636

Liu, L., Wang, D. H., Chen, F. F., Zhang, Z. J., Chen, Q., Xu, J. H., et al. (2020). Development of an Engineered Thermostable Amine Dehydrogenase for the Synthesis of Structurally Diverse Chiral Amines. *Catal. Sci. Tech.* 10 (8), 2353–2358. doi:10.1039/D0CY00071J

Mangas-Sanchez, J., Sharma, M., Cosgrove, S. C., Ramsden, J. I., Marshall, J. R., Thorpe, T. W., et al. (2020). Asymmetric Synthesis of Primary Amines Catalyzed by Thermotolerant Fungal Reductive Aminases. *Chem. Sci.* 11 (19), 5052–5057. doi:10.1039/D0SC02253E

Matzel, P., Gand, M., and Höhne, M. (2017). One-step Asymmetric Synthesis of (*R*)-and (*S*)-rasagiline by Reductive Amination Applying Imine Reductases. *Green. Chem.* 19 (2), 385–389. doi:10.1039/C6GC03023H

Mitsukura, K., Suzuki, M., Tada, K., Yoshida, T., and Nagasawa, T. (2010). Asymmetric Synthesis of Chiral Cyclic Amine from Cyclic Imine by Bacterial Wshole-Cell Catalyst of Enantioselective Imine Reductase. *Org. Biomol. Chem.* 8 (20), 4533–4535. doi:10.1039/C0OB00353K

Montgomery, S. L., Pushpanath, A., Heath, R. S., Marshall, J. R., Klemstein, U., Galman, J. L., et al. (2020). Characterization of Imine Reductases in Reductive Amination for the Exploration of Structure-Activity Relationships. *Sci. Adv.* 6 (21), eaay9320doi:10.1126/sciadv.aay9320

Newman, D. J., and Cragg, G. M. (2020). Natural Products as Sources of New Drugs over the Nearly Four Decades from 01/1981 to 09/2019. *J. Nat. Prod.* 83 (3), 770–803. doi:10.1021/acs.jnatprod.9b01285

Nguyen, V. K., and Kou, K. G. (2021). The Biology and Total Syntheses of Bisbenzylisoquinoline Alkaloids. *Org. Biomol. Chem.* 19 (35), 7535–7543. doi:10.1039/D1OB00812A

Ran, N., Zhao, L., Chen, Z., and Tao, J. (2008). Recent Applications of Biocatalysis in Developing green Chemistry for Chemical Synthesis at the Industrial Scale. *Green. Chem.* 10 (4), 361–372. doi:10.1039/B716045C

Schober, M., MacDermaid, C., Ollis, A. A., Chang, S., Khan, D., Hosford, J., et al. (2019). Chiral Synthesis of LSD1 Inhibitor GSK2879552 Enabled by Directed Evolution of an Imine Reductase. *Nat. Catal.* 2 (10), 909–915. doi:10.1038/s41929-019-0341-4

Schrittwieser, J. H., Velikogne, S., and Kroutil, W. (2015). Biocatalytic Imine Reduction and Reductive Amination of Ketones. *Adv. Synth. Catal.* 357 (8), 1655–1685. doi:10.1002/adsc.201500213

Sharma, M., Mangas-Sanchez, J., France, S. P., Aleku, G. A., Montgomery, S. L., Ramsden, J. I., et al. (2018). A Mechanism for Reductive Amination Catalyzed by Fungal Reductive Aminases. *ACS Catal.* 8 (12), 11534–11541. doi:10.1021/acscatal.8b03491

Sharma, M., Mangas-Sanchez, J., Turner, N. J., and Grogan, G. (2017). NAD(P)H-Dependent Dehydrogenases for the Asymmetric Reductive Amination of Ketones: Structure, Mechanism, Evolution and Application. *Adv. Synth. Catal.* 359 (12), 2011–2025. doi:10.1002/adsc.201700356

Thompson, J. D., Higgins, D. G., and Gibson, T. J. (1994). CLUSTAL W: Improving the Sensitivity of Progressive Multiple Sequence Alignment through Sequence Weighting, Position-specific gap Penalties and Weight Matrix Choice. *Nucleic Acids Res.* 22 (22), 4673–4680. doi:10.1093/nar/22.22.4673

Wang, L., Diao, S., Sun, Y., Jiang, S., Liu, Y., Wang, H., et al. (2021). Rational Engineering of *Acinetobacter Tandoii* Glutamate Dehydrogenase for Asymmetric Synthesis of L-Homoalanine through Biocatalytic Cascades. *Catal. Sci. Tech.* 11 (12), 4208–4215. doi:10.1039/D1CY00376C

Waterhouse, A., Bertoni, M., Bienert, S., Studer, G., Tauriello, G., Gumienny, R., et al. (2018). SWISS-MODEL: Homology Modelling of Protein Structures and Complexes. *Nucleic Acids Res.* 46 (W1), W296–W303. doi:10.1093/nar/gky427

Weinreb, O., Amit, T., Bar-Am, O., and Youdim, M. B. (2010). Rasagiline: a Novel Anti-parkinsonian Monoamine Oxidase-B Inhibitor with Neuroprotective Activity. *Prog. Neurobiol.* 92 (3), 330–344. doi:10.1016/j.pneurobio.2010.06.008

Wetzl, D., Gand, M., Ross, A., Müller, H., Matzel, P., Hanlon, S. P., et al. (2016). Asymmetric Reductive Amination of Ketones Catalyzed by Imine Reductases. *ChemCatChem* 8 (12), 2023–2026. doi:10.1002/cctc.201600384

Wohlgemuth, R. (2010). Biocatalysis-key to Sustainable Industrial Chemistry. *Curr. Opin. Biotechnol.* 21 (6), 713–724. doi:10.1016/j.copbio.2010.09.016

Wu, S., Snajdrova, R., Moore, J. C., Baldenius, K., and Bornscheuer, U. T. (2021). Biocatalysis: Enzymatic Synthesis for Industrial Applications. *Angew. Chem. Int. Edition* 60 (1), 88–119. doi:10.1002/anie.202006648

Conflict of Interest: The authors declare that the research was conducted in the absence of any commercial or financial relationships that could be construed as a potential conflict of interest.

Publisher's Note: All claims expressed in this article are solely those of the authors and do not necessarily represent those of their affiliated organizations, or those of the publisher, the editors, and the reviewers. Any product that may be evaluated in this article, or claim that may be made by its manufacturer, is not guaranteed or endorsed by the publisher.

frontiers in Bioengineering and Biotechnology

REVIEW
published: 24 December 2021
doi: 10.3389/fbioe.2021.787791

Methanol Dehydrogenases as a Key Biocatalysts for Synthetic Methylotrophy

Thien-Kim Le[1†], *Yu-Jin Lee*[1,2†], *Gui Hwan Han*[3*] *and Soo-Jin Yeom*[1,2*]

[1]School of Biological Sciences and Technology, Chonnam National University, Gwangju, South Korea, [2]School of Biological Sciences and Biotechnology, Graduate School, Chonnam National University, Gwangju, South Korea, [3]Center for Industrialization of Agricultural and Livestock Microorganisms (CIALM), Jeollabuk-do, South Korea

One-carbon (C1) chemicals are potential building blocks for cheap and sustainable resources such as methane, methanol, formaldehyde, formate, carbon monoxide, and more. These resources have the potential to be made into raw materials for various products used in our daily life or precursors for pharmaceuticals through biological and chemical processes. Among the soluble C1 substrates, methanol is regarded as a biorenewable platform feedstock because nearly all bioresources can be converted into methanol through syngas. Synthetic methylotrophy can be exploited to produce fuels and chemicals using methanol as a feedstock that integrates natural or artificial methanol assimilation pathways in platform microorganisms. In the methanol utilization in methylotrophy, methanol dehydrogenase (Mdh) is a primary enzyme that converts methanol to formaldehyde. The discovery of new Mdhs and engineering of present Mdhs have been attempted to develop synthetic methylotrophic bacteria. In this review, we describe Mdhs, including in terms of their enzyme properties and engineering for desired activity. In addition, we specifically focus on the application of various Mdhs for synthetic methylotrophy.

Keywords: methanol dehydrogenase, synthetic methylotrophy, C1 gas, assimilation, formaldehyde

OPEN ACCESS

Edited by:
Roland Wohlgemuth, Lodz University of Technology, Poland

Reviewed by:
Nathan M. Good, University of California, Berkeley, United States
Benjamin Michael Woolston, Northeastern University, United States

***Correspondence:**
Gui Hwan Han
ghhan@cialm.or.kr
Soo-Jin Yeom
soojin258@chonnam.ac.kr

[†]*These authors have contributed equally to this work*

Specialty section:
This article was submitted to Bioprocess Engineering, a section of the journal Frontiers in Bioengineering and Biotechnology

Received: *01 October 2021*
Accepted: *03 December 2021*
Published: *24 December 2021*

Citation:
Le T-K, Lee Y-J, Han GH and Yeom S-J (2021) Methanol Dehydrogenases as a Key Biocatalysts for Synthetic Methylotrophy. Front. Bioeng. Biotechnol. 9:787791. doi: 10.3389/fbioe.2021.787791

INTRODUCTION

One-carbon (C1) substrates are potential feedstocks and have recently gained attention and preference in industrial fields due to their natural abundance, low production cost, and availability as industrial by-products (Jiang et al., 2021). Among C1 chemicals, methanol is a potentially renewable feed stock for microorganisms as it is electron rich and can be derived from methane or CO_2 (Chen et al., 2020). In nature, methylotrophs, such as *Methylobacterium extorquens* and *Bacillus methanolicus*, can utilize methanol, and their biochemical function have been characterized (Brautaset et al., 2007; Bennett et al., 2018). However, so far, there are limitations in the engineering of native methylotrophs to produce heterologous products at high rates and titers due to the lack of genetic tools available. Recent advances in synthetic biology, integration of efficient methanol converting enzymes, genome engineering, and laboratory evolution are enabling the first steps toward the creation of synthetic methanol-utilizing microorganisms (Heux et al., 2018; Meyer et al., 2018; Bennett et al., 2020; Chen et al., 2020; Keller et al., 2020; Wang et al., 2020).

In the methanol utilization in methylotrophy, one of the key steps is the oxidation of methanol to formaldehyde by oxidoreductase (Zhang et al., 2017), and methanol dehydrogenases (Mdhs) are the main enzymes as they catalyze the oxidation of methanol to form formaldehyde with two electrons

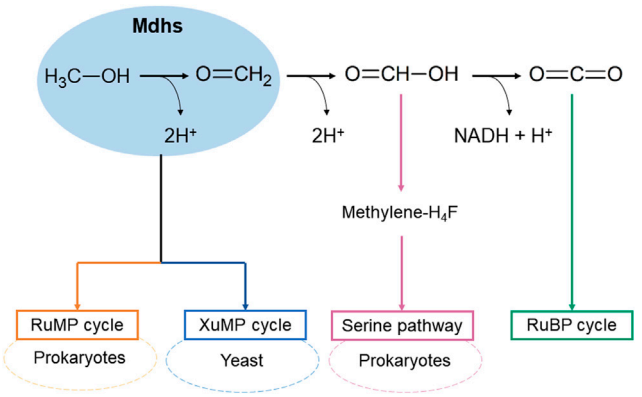

FIGURE 1 | Natural methane and methanol utilization pathways in methylotrophs.

and $2H^+$ (Le et al., 2021) (**Figure 1**). There are three native pathways of formaldehyde assimilation, that have been discovered and biochemically described for growth support of microorganisms in methanol, as follows: the ribulose monophosphate (RuMP) cycle, serine pathway, and xylulose monophosphate (XuMP) cycle (**Figure 1**) (Zhang et al., 2017). The RuMP and serine cycles mainly occur in prokaryotes, the XuMP cycle is found in yeasts. Among them, the RuMP cycle of hexulose-6-phosphate synthases (HPS) and 6-phospho-3-hexulose isomerase (PHI) has been identified as the best combination because of its highest theoretical growth rate; thus, it has received the most attention (Heux et al., 2018; Claassens et al., 2019). Meanwhile, there have been a modified serine cycle in *Escherichia coli* was reported (Yu and Liao 2018) and only one study on XuMP in *Saccharomyces cerevisiae* (Dai et al., 2017).

Various hypotheses have been proposed regarding potential bottlenecks to efficient methanol assimilation. In particular, the concentration of Mdhs is a limitation, and poor kinetic and thermodynamic properties of methanol oxidation by nicotinamide adenine dinucleotide (NAD)- Mdh is widely acknowledged (Whitaker et al., 2017; Woolston et al., 2018). The low activity and substrate affinity of Mdh fundamentally limits methanol assimilation flux, while a high NADH/NAD^+ ratio negatively impacts the Gibbs free energy of methanol oxidation (Wang et al., 2020). Thus, the development of efficient Mdhs presents a significant challenge to synthetic methylotrophy. In this review, we summarize the current classifications, enzyme properties, and engineering of reported Mdhs. Additionally, we provide a comprehensive overview of recent advances in the use of Mdhs in engineering synthetic methylotrophy.

Class of Methanol Dehydrogenases

Depending on the electron acceptors, Mdhs in methylotrophs are classified into three groups: NAD^+-dependent Mdh, PQQ (pyrrolo-quinoline quinone)-dependent Mdh, and O_2-dependent **AOX** (alcohol oxidase) (**Figure 2**).

NAD^+-dependent Mdh

NAD^+-dependent Mdh in thermophilic Gram-positive methylotrophs uses NAD^+ as the cofactor for the methanol oxidation. The first NAD^+-dependent Mdh was reported in 1989 (Arfman et al., 1989). NAD^+-dependent Mdhs also obtained from non-methylotrophic bacteria. To date, several NAD^+-dependent Mdhs have been isolated from *Bacillus* sp. (such as *B. methanolicus* (Arfman et al., 1989; Arfman et al., 1991; Müller et al., 2015; Witthoff et al., 2015; Price et al., 2016) and *B. stearothermophilus* (Whitaker et al., 2017)), *Lysinibacillus* sp. (such as *L. xylanilyticus* (Lee et al., 2020)), and *Cupriavidus* sp. (such as *C. necator* (Wu et al., 2016)). In particular, their NAD^+-dependent Mdhs have been focused and reported for studies of recombinant *E. coli* as synthetic methylotrophs (Müller et al., 2015; Wu et al., 2016; Whitaker et al., 2017; Lee et al., 2020; Le et al., 2021). Three NAD^+-dependent Mdhs have been found in *B. methanolicus* MGA3 (Mdh, Mdh2, and Mdh3). Moreover, the activity of all three Mdhs is modulated by an endogenous Mdh activator protein (ACT). *In vitro* studies suggest that ACT

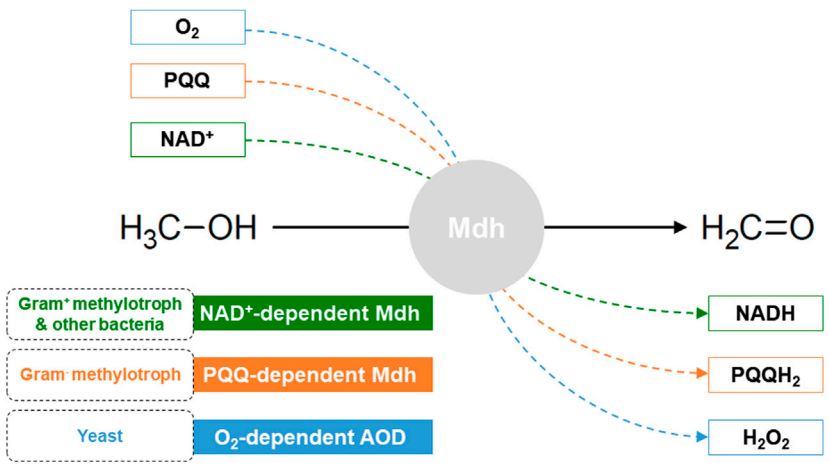

FIGURE 2 | Three classes of methanol dehydrogenases (Mdhs).

enhances the methanol affinity, oxidation rate, and catalytic activity of Mdhs; however, the detailed mechanism for activation is currently unclear (Hektor et al., 2002; Witthoff et al., 2015) and no effect has been shown *in vivo* in a synthetic methylotrophy (Müller et al., 2015) because detail research for the activator protein functions in native host has not been tested. To enable the assimilation of methanol as the carbon source in metabolic engineering, ACT-independent Mdhs and their mutants from *C. necator* (Wu et al., 2016; Chen et al., 2018) and *L. xylanilyticus* (Lee et al., 2020; Le et al., 2021) have been reported and introduced into *E. coli* for methanol assimilation. As best candidate for synthetic methylotrophy, NAD^+-dependent Mdh that can perform its function under both aerobic and anaerobic conditions (Zhang et al., 2017). Besides, it uses NAD^+, which is ubiquitous and can provide electrons for metabolite products, as the cofactor. Therefore, it may be the best candidate for recombinant-based synthetic methylotrophs (Zhang et al., 2017).

PQQ-dependent Mdh

In Gram-negative methylotrophs, the oxidation of methanol occurs in the periplasmic space by PQQ-dependent Mdh (Skovran et al., 2019). Pure PQQ-dependent Mdh was first described in 1967 (Anthony and Zatman 1967). To date, PQQ-dependent Mdh has been isolated and purified from several different strains of microorganisms including *Pseudomonas* sp. (Anthony and Zatman 1965; Anthony and Zatman 1967; Patel et al., 1972), *Methylococcus capsulatus* (Patel et al., 1972), *Hyphomicrobium denitrificans* (Nojiri et al., 2006), *Methylorubrum extorquens* (formerly *Methylobacterium extorquens*) (Anthony 2004; Liu et al., 2006; Nakagawa et al., 2012), *Methyloversatilis universalis* FAM5 (Kalyuzhnaya et al., 2008), *Methylibium petroleiphilum* (Kalyuzhnaya et al., 2008), *Methylophaga aminisulfidivorans* (Kim et al., 2012; Cao et al., 2018), *Methylobacterium nodulans* (Kuznetsova et al., 2012), *Methylophilus* sp. (Leopoldini et al., 2007; Li et al., 2011), *Burkholderiales* sp. (Kalyuzhnaya et al., 2008), *Paracoccus denitrificans* (Xia et al., 2003), *M. radiotolerans* (Hibi et al., 2011), *Bradyrhizobium* sp. (Fitriyanto et al., 2011), *M. aquaticum* (Masuda et al., 2018), *Methylomicrobium buryatense* (Deng et al., 2018), *M. fumariolicum* (Jahn et al., 2018), and *Bradyrhizobium diazoefficiens* (Wang et al., 2019). The PQQ-dependent Mdh contains a PQQ prosthetic group. The chemical structure of the PQQ prosthetic group has been confirmed by two independent research groups using a wide range of chemical and physical techniques, such as X-ray, UV/Vis absorption spectra, and HPLC (Anthony 1982). The role of the PQQ prosthetic group is capturing electrons from methanol oxidation and passing them to the cytochrome (Anthony 2004). The biggest disadvantage is the requirement of molecular oxygen for PQQ bio-synthesis (Velterop et al., 1995), while some desired intermediates as precursors of value-added products such as lactate must be produced under anaerobic conditions. Therefore, this limits the application of PQQ-dependent Mdhs.

In genomes of methylotrophs, PQQ-dependent Mdhs are generally encoded by MxaFI and XoxF. MxaFI consists of small (MxaI) and large (MxaF) subunits, encoding PQQ-dependent Mdh using calcium (Ca^{2+}) as a cofactor (MxaFI-Mdh) (Anthony 2004). Another PQQ-dependent Mdh, which uses lanthanides (Ln^{3+}) instead of Ca^{2+}, is encoded by XoxF (XoxF-type Mdh) (Chistoserdova 2016; Skovran et al., 2019). XoxF-Mdh from *M. extorquens* AM1 is a representative of Ln^{3+}-dependent Mdh that it was studied carefully to show the biochemical characterization. XoxF of M. extorquens AM1 showed better activity when La^{3+} or Ca^{2+} and La^{3+} were added together than when Ca^{2+} was used alone as part of the cofactor complex (Vu et al., 2016; Good et al., 2020). In addition, other elements of lanthanide (Ce^{3+}, Nd^{3+}, Pr^{3+}, Sm^{3+}, Eu^{3+}, or Gd^{3+}) were also found to be involved in the methanol oxidation activity (Pol et al., 2014). Lanthanides as important factor was suggested in regulatory and catalytic functions because the XoxF genes are required for transcription of the MxaFI (Vu et al., 2016).

O_2-dependent AOX

Unlike NAD^+-dependent and PQQ-dependent Mdhs, O_2-dependent **AOX** is obtained from eukaryotic methylotrophs and is located in the peroxisome of yeasts (Egli et al., 1980). First, formaldehyde and hydrogen peroxide (H_2O_2), which are highly toxic chemicals for cells, are created from methanol oxidation by O_2-dependent **AOX**. To protect the cells, dihydroxyacetone synthase (DAS) and catalase (CTA) work to transform them into non-toxic chemicals (Zhang et al., 2017). O_2-dependent **AOX** only function under aerobic conditions and thus, has limitations similar to those of PQQ-dependent Mdh. In addition, another important limitation AOX's is that the electrons from methanol are not captured as useable energy by the cell, but wasted in the generation of peroxide.

BIOCHEMICAL CHARACTERIZATION OF METHANOL DEHYDROGENASES

Among three classes of Mdhs, enzyme properties of NAD^+- and PQQ-dependent Mdhs are summarized in **Table 1**.

Optimal Conditions for Methanol Oxidation Reaction by Mdhs

The most important factor, which has a considerable effect on the activity of Mdhs, is cofactor binding. For NAD^+-dependent Mdhs, a metal ion is involved in cofactor binding which may influence enzymatic activity (Hektor et al., 2002). Several metal ions have been examined for the effects on the methanol oxidation activity of Mdhs, such as Fe^{2+}, Mn^{2+}, Zn^{2+}, Cu^{2+}, Co^{2+}, Ni^{2+}, or Mg^{2+} ions (Sridhara et al., 1969; Arfman et al., 1991; Montella et al., 2005; Müller et al., 2015; Wu et al., 2016; Whitaker et al., 2017; Lee et al., 2020; Le et al., 2021). In general, the supplementation of Fe^{2+} or Mn^{2+} ions increase enzyme activity, and Mdh activity is inhibited by Cu^{2+}, Co^{2+}, or Zn^{2+} (Sridhara et al., 1969; Montella et al., 2005). In the case of Mdhs from *Lysinibacillus xylanilyticus* (Lxmdh), Mn^{2+} or Fe^{2+} reduce its activity, whereas and Zn^{2+}, Cu^{2+}, or Co^{2+} inhibit Lxmdh activity (Lee et al., 2020). For almost all NAD^+-dependent

TABLE 1 | Enzyme properties of NAD^+-Dependent Mdhs (EC number: 1.1.1.244) and PQQ-Dependent Mdhs (EC number: 1.1.2.7).

Enzyme	Source	Optimum tem. (°C)	Optimum pH	Molecular weight (kDa)		Association form	Metal ion	Refs
				Subunit	Native			
NAD^+-Dependent Mdhs	*Bacillus methanolicus* C1	57–59	9.5	4.3	43	Decamer	Mg^{2+}	Arfman et al. (1991)
	Bacillus methanolicus MGA3	37	7.4	N.I.	43	Decamer	Mg^{2+}	Müller et al. (2015)
		45	9.5	N.I.	N.I.	Decamer	Mg^{2+}	Krog et al. (2013)
		50	9.5	N.I.	43	Decamer	Mg^{2+}	Witthoff et al. (2015)
		50	9.0	N.I.	N.I.	Decamer	Mg^{2+}	Ochsner et al. (2014)
	Bacillus methanolicus PB1	37	7.4	N.I.	43	Decamer	Mg^{2+}	Müller et al. (2015)
		45	9.5	N.I.	N.I.	Decamer	Mg^{2+}	Krog et al. (2013)
	Bacillus stearothermophilus	37	7.4	N.I.	N.I.	N.I.	Mg^{2+}	Whitaker et al. (2017)
	Lysinibacillus xylanilyticus	55	9.5	N.I.	42.8	N.I.	Mg^{2+}	Lee et al. (2020)
	Cupriavidus necator N-1	30	9.5	N.I.	40.7	N.I.	Ni^{2+}	Wu et al. (2016)
PQQ-Dependent Mdhs	*Pseudomonas* sp. M27	N.I.	9.0	α: 62, β: N.I.	120	N.I.	N.I.	Patel et al. (1972)
	Methylococcus capsulatus (Texas strain)	N.I.	9.0	α: 62, β: N.I.	120	N.I.	N.I.	
	Hyphomicrobium denitrificans A3151	25	7.0	α: 65, β: 9	148	Heterotetramer	N.I.	Nojiri et al. (2006)
	Methylorubrum extorquens	N.I.	7.0	α: 66, β: 8.5	149	Heterotetramer	Ca^{2+}	Anthony (2004)
	Methylorubrum extorquens AM1	N.I.	9.0	α: 62, β: 7.5	139	Heterotetramer	Ca^{2+}	Liu et al. (2006)
		30	8.0	N.I.	117	Homodimer	La^{3+}	Nakagawa et al. (2012)
		N.I.	8.0	N.I.	N.I.	N.I.	La^{3+}, Nd^{3+}	Good et al. (2019)
		N.I.	8.0	N.I.	N.I.	N.I.	Gd^{3+}	Good et al. (2021)
	Methyloversatilis universalis FAM5	22	7.5	α: 65, β: N.I.	N.I.	Monomer	N.I.	Kalyuzhnaya et al. (2008)
	Methylibium petroleiphilum PM1	22	7.5	α: 65, β: N.I.	N.I.	Monomer	N.I.	Kalyuzhnaya et al. (2008)
	Burkholderiales strains Z18-153	R.T	8.8	α: 65, β: N.I.	N.I.	Monomer	N.I.	Kim et al. (2012)
	Burkholderiales strains FAM1	R.T	8.8	α: 65, β: N.I.	N.I.	Monomer	N.I.	
	Methylophaga aminisulfidivorans MP^T	30	8.0	α: 65.98, β: 7.58	147.12	Tetramer	Ca^{2+}	
	Methylophaga aminisulfidivorans MP^T Mdh_{Mas}	N.I.	N.I.	α: 65, β: 7.5	145	Heterotetramer	Mg^{2+}	Cao et al. (2018)
	Methylobacterium nodulans ORS 2060T	50	9–10	α: 60, β: 6.5	70	Heterodimer	No metal	Kuznetsova et al. (2012)
	Methylophilus methylotrophus W3A1	N.I.	N.I.	α: 62, β: 8	140	Heterotetramer	Ca^{2+}	Leopoldini et al. (2007)
	Paracoccus denitrificans	N.I.	N.I.	α: 67, β: 9.5	153	Heterotetramer	Ca^{2+}	Xia et al. (2003)
	Methylobacterium radiotolerans NBRC15690	N.I.	N.I.	α: 63, β: N.I.	120	Homodimer	La^{3+}	Hibi et al. (2011)
	Methylobacterium radiotolerans NBRC15690	N.I.	N.I.	α: 60, β: 10	114	Heterotetramer	Ca^{2+}	Hibi et al. (2011)
	Bradyrhizobium sp. MAFF211645	N.I.	N.I.	α: 68, β: N.I.	108	Homodimer	Ce^{3+}	Fitriyanto et al. (2011)
	Methylobacterium aquaticum strain 22A	N.I.	N.I.	N.I.	N.I.	N.I.	La^{3+}	Masuda et al. (2018)
	Methylomicrobium buryatense 5GB1C	N.I.	N.I.	α: 67.2, β: N.I.	N.I.	Homodimer	La^{3+}	Deng et al. (2018)
	Methylacidiphilum fumariolicum SolV	45	7.2	N.I.	63.6	Homodimer	Eu^{3+}	Jahn et al. (2018)
	Bradyrhizobium diazoefficiens strain USDA110	N.I.	N.I.	α: 64, β: N.I.	136	N.I.	Ce^{3+}	Wang et al. (2019)

R.T—Room temperature; N.I—No information.

Mdhs, Mg^{2+} increases the effect of enzyme activity (Arfman et al., 1989; Arfman et al., 1991; Müller et al., 2015; Whitaker et al., 2017; Lee et al., 2020; Le et al., 2021). For Mdhs from *Cupriavidus necator* (Cnmdh), Ni^{2+} is typically the chosen cofactor (Wu et al., 2016).

For PQQ-dependent Mdhs, Ca^{2+} plays a role in the active site (Anthony and Zatman 1967; Anthony 2004). The X-ray structure of Mdhs from *M. extorquens*, *M. nodulans*, *Methylophilus* sp, and *P. denitrificans* has been determined to have one molecule of PQQ and one Ca^{2+} ion in each large α-subunit, which is encoded

by MxaF (Anthony and Williams 2003; Anthony 2004). Moreover, some types of Mdhs, which are encoded by XoxF, use Ln^{3+} instead of Ca^{2+}, which is a part of cofactor complex for Mdhs encoded by MxaF (Egli et al., 1980; Skovran et al., 2019). Ln^{3+} was first suggested as a metal ion of the cofactor complex for PQQ-dependent Mdhs obtained from *M. radiotolerans* (Hibi et al., 2011) and *Bradyrhizobium* sp. (Fitriyanto et al., 2011) in 2011. Furthermore, Mdhs from *M. extorquens* AM1 (Nakagawa et al., 2012), *M. aquaticum* (Masuda et al., 2018), *M. buryatense* (Deng et al., 2018), *M. fumariolicum* (Jahn et al., 2018), and *B. diazoefficiens* (Wang et al., 2019) have been observed to be Ln^{3+}-dependent Mdhs. Interestingly, the subunits of PQQ-dependent Mdh from *M. aminisulfidivorans* MP^T are coordinated by an Mg^{2+} ion instead of a Ca^{2+} ion or Ln^{3+} group (Cao et al., 2018). In addition, the activity of PQQ-dependent Mdhs under aerobic conditions with artificial electron acceptors *in vitro* requires the presence of an activator (e.g., ammonium salt) (Anthony 1982; Anthony and Williams 2003; Anthony 2004; Kuznetsova et al., 2012).

The other most important factors are the temperature and pH of the buffer in the enzyme assay. Almost all methanol dehydrogenases have high activity at high temperatures (~55°C) and high pH (9–10). Mdhs from *M. nodulans* (Mnmdh) exhibits maximal activity at pH 9–10, and it increases linearly with increasing temperature from 20°C to 50°C (Kuznetsova et al., 2012). The optimum pH for Mdh from *Pseudomonas* sp. M27 (Patel et al., 1972), *M. capsulatus* (Patel et al., 1972), and *M. extorquens* AM1 (Liu et al., 2006) are also 9. Similarly, an assay involving NAD^+-dependent Mdhs from thermotolerant methylotrophic *Bacillus* strains is performed at 45–50°C, using glycine/KOH buffer at pH 9.5 (Arfman et al., 1991; Krog et al., 2013). Lxmdh and its mutant or Cnmdh also function better in buffers with a pH of 9.5; however, Lxmdh and its mutant exhibit high activity at 55°C (Lee et al., 2020; Le et al., 2021), while the temperature for testing Cnmdh activity is 30°C (Wu et al., 2016). On the other hand, the conditions for the Mdhs from *M. methanolicus* (Bmmdh) and *B. stearothermophilus* (Bsmdh) reactions are similar, at pH 7.4 and 37°C (Müller et al., 2015; Whitaker et al., 2017). When examining the activity of Mdhs obtained from *L. xylanilyticus* or *Burkholderiales* using spectrometer experiments to detect the changes in absorbance, room temperature is preferred (Kalyuzhnaya et al., 2008; Le et al., 2021). Moreover, buffer systems with a pH of 8.8 are used for *Burkholderiales* Mdh assays (Kalyuzhnaya et al., 2008). On the whole, the Mdh assay requires the presence of an ion as the binding cofactor. This depends on the type and source of Mdh. For PQQ-dependent Mdhs, the activator for enzyme activity is required under aerobic conditions.

Molecular Weight of Methanol Dehydrogenases

The molecular weight of most PQQ-dependent Mdhs has been identified as being between 112 and 158 kDa. The associated form of almost all PQQ-dependent Mdhs, which are Ca^{2+}-dependent Mdhs, is a tetramer ($\alpha_2\beta_2$). Therefore, it can be dissociated to α-subunits (56–76 kDa) and β-subunits (very small, ≤ 10 kDa) by a low pH or sodium dodecyl sulfate (SDS) (Anthony 1982), such as the Mdh from *H. denitrificans* (α: 65 kDa, β: 9 kDa) (Nojiri et al., 2006), *M. extorquens* (α: 62–65 kDa, β: 7.5–8.5 kDa) (Anthony 2004; Liu et al., 2006), *M. aminisulfidivorans* MP^T (α: 65–66 kDa, β: 7.5–7.6 kDa) (Kim et al., 2012; Cao et al., 2018), *M. methylotrophus* (α: 62 kDa, β: 8 kDa) (Leopoldini et al., 2007; Li et al., 2011), and *M. radiotolerans* (α: 60 kDa, β: 10 kDa) (Hibi et al., 2011). There are also some special cases with the heterodimer form (αβ), for example, Mdh from *M. nodulans* (α: 60 kDa, β: 6.5 kDa) (Kuznetsova et al., 2012). Besides, the associated form of La^{3+}-dependent Mdhs is a homodimer (formed by two identical proteins), e. g, Mdhs from *M. radiotolerans* (120 kDa) (Hibi et al., 2011), *Bradyrhizobium* sp. (108 kDa) (Fitriyanto et al., 2011), *M. extorquens* AM1 (117 kDa) (Nakagawa et al., 2012), *Methylacidiphilum fumariolicum* SolV (63.6 kDa) (Jahn et al., 2018), and *M. buryatense* (Deng et al., 2018). On the other hand, the NAD^+-dependent Mdh with a single subunit has a molecular weight of around 40 kDa. For instance, the molecular weight of NAD^+-dependent Mdh from *Bacillus* sp. C1 (a thermotolerant methylotrophic *Bacillus*) is 43 kDa (Arfman et al., 1989; Arfman et al., 1991). Other *B. methanolicus* strains (MGA3 and PB1) show a similar molecular weight at 43 kDa (Müller et al., 2015; Witthoff et al., 2015; Price et al., 2016). Moreover, Cnmdh from *C. necator* N-1 (Wu et al., 2016) or Lxmdh from *L. xylanilyticus* (Lee et al., 2020) show respective molecular subunits at 40.7 or 42.8 kDa (**Table 1**). According to the previous report, NAD^+-dependent Mdhs has decameric association structure (430 kDa) as native form (Vonck et al., 1991).

Substrate Affinity Toward Methanol of Wild-type or Engineered NAD-Mdh

Although, MxaFI-Mdhs from *M. extorquens* AM1, with a high efficiency (k_{cat}/K_M) of methanol production, has been suggested as the best choice for engineering *E. coli* (Anthony and Williams 2003), it requires at least 11 gene products for its functional assembly (Chistoserdova et al., 2003). In addition, XoxF-Mdhs from *M. extorquens* AM1 would be required only three genes with a high catalytic efficiency (Keltjens et al., 2014), PQQ-dependent Mdhs are not suitable for synthetic methylotrophy using engineered *E. coli*. Because, PQQ as critical cofactor is critical limit that specially *E. coli* is not able to synthesize PQQ (Anthony 2004). In the case of O_2-dependent **AOX**, its product, H_2O_2, is also challenging because it is the highly toxic to most hosts. Therefore, only NAD^+-dependent Mdh has been considered as the best candidate for synthetic methylotrophs (Zhang et al., 2017), which requires only one gene for functional production and can generate the reducing equivalent (NADH) to promote strain growth under both aerobic and anaerobic conditions. To successfully achieve methanol assimilation, the Mdh kinetics, including substrate affinity and catalytic activity, should be improved for methanol assimilation through directed evolution or rational approach based engineering. Various NAD^+-dependent Mdhs from *B. methanolicus* (Vonck et al., 1991; De Vries et al., 1992; Hektor et al., 2002; Krog et al.,

TABLE 2 | Summary of substrate affinity for methanol by NAD^+-Dependent Mdhs.

Enzyme type	Strain	Type of enzyme	V_{max} (U/mg)	k_{cat} (s^{-1})	K_M (mM)	Evolution method	Refs
Wild type Mdh	*B. methanolicus* MGA3	*Mdh*	0.06 ± 0.002	N.I.	170 ± 20	WT	Krog et al. (2013)
		Mdh 2	0.09 ± 0.003	N.I.	360 ± 30	WT	
		Mdh 3	0.07 ± 0.005	N.I.	200 ± 70	WT	
		Mdh + ACT	0.4 ± 0.02	N.I.	26 ± 7	WT	
		Mdh 2 + ACT	0.2 ± 0.008	N.I.	200 ± 20	WT	
		Mdh 3 + ACT	0.4 ± 0.008	N.I.	150 ± 10	WT	
		Mdh	0.151 ± 0.008	0.11 ± N.I.	150 ± 25	WT	Ochsner et al. (2014)
		Mdh 2	0,151 ± 0.012	0.12 ± N.I.	416 ± 97	WT	
		Mdh + ACT	0.474 ± 0.032	0.32 ± N.I.	9 ± 2	WT	
		Mdh 2 + ACT	0.394 ± 0.016	0.27 ± N.I.	96 ± 12	WT	
	B. methanolicus PB1	*Mdh*	0.03 ± 0.001	N.I.	220 ± 30	WT	Krog et al. (2013)
		Mdh 1	0.015 ± 0.001	N.I.	170 ± 60	WT	
		Mdh 2	0.08 ± 0.004	N.I.	330 ± 0.05	WT	
		Mdh + ACT	0.2 ± 0.003	N.I.	10 ± 1	WT	
		Mdh 1 + ACT	0.05 ± 0.002	N.I.	5 ± 1	WT	
		Mdh 2 + ACT	0.38 ± 0.04	N.I.	110 ± 50	WT	
	C. necator N-1 WT	*Mdh* 2	0.32 ± N.I.	0.22 ± 0.01	132 ± 15.4	WT	Wu et al. (2016)
	B. stearothermophilus	*Mdh*	2.1 ± N.I.	N.I.	20 ± N.I.	WT	Whitaker et al. (2017)
	L. xylanilyticus	*Mdh* 2	0.3027 ± 0.0169	0.21 ± 0.01	3.23 ± 1.05	WT	Lee et al. (2020)
Engineered Mdh	*B. methanolicus* MGA3 S98G	*Mdh*	0.44 ± 0.053	0.35 ± N.I.	1,151 ± 274	Rational approach	Ochsner et al. (2014)
	B. methanolicus MGA3 S98G + ACT	*Mdh*	0.819 ± 0.082	0.59 ± N.I.	847 ± 190	Rational approach	
	C. necator N-1 CT4-1	*Mdh* 2	0.29 ± N.I.	0.20 ± 0.01	21.6 ± 1.5	Directed evolution	Wu et al. (2016)
	L. xylanilyticus Mdh -S101V	*Mdh* 2	0.3423 ± 0.02167	0.24 ± 0.01	10.35 ± 3.87	Rational approach	Lee et al. (2020)
	L. xylanilyticus Mdh -T141S	*Mdh* 2	0.4629 ± 0.0576	0.33 ± 0.04	51.24 ± 23.95	Rational approach	
	L. xylanilyticus Mdh -A164F	*Mdh* 2	0.4753 ± 0.05072	0.33 ± 0.03	36.83 ± 15.82	Rational approach	
	L. xylanilyticus Mdh -E396V	*Mdh* 2	N.I.	0.020 ± 0.002	0.010 ± 0.003	Directed evolution	Le et al. (2021)
	L. xylanilyticus Mdh -K318N	*Mdh* 2	N.I.	0.027 ± 0.005	0.046 ± 0.072	Directed evolution	
	L. xylanilyticus Mdh -E396V + K318N	*Mdh* 2	N.I	0.022 ± 0.002	0.233 ± 0.107	Directed evolution	
	B. methanolicus (WT)	*Mdh* 2	0.0365 ± 0.0017	N.I.	636 ± 74	Directed evolution	Roth et al. (2019)
	B. methanolicus Q5L E123G	*Mdh* 2	0.0366 ± 0.0016	N.I.	615 ± 66	Directed evolution	
	B. methanolicus Q5L M163V	*Mdh* 2	0.055 ± 0.0031	N.I.	627 ± 89	Directed evolution	
	B. methanolicus Q5L A164P	*Mdh* 2	0.0754 ± 0.0023	N.I.	440 ± 39	Directed evolution	
	B. methanolicus Q5L A363L	*Mdh* 2	0.127 ± 0.0033	N.I.	432 ± 32	Directed evolution	
	B. methanolicus Q5L A164P A363L	*Mdh* 2	0.0885 ± 0.0023	N.I.	329 ± 28	Directed evolution	
Wild type ADH	*C. glutamicum* R AdhA	Class I	0.29 ± N.I.	0.20 ± 0.01	97 ± 9.8	WT	Wu et al. (2016)
	L. sphaericus C3-41	N.I.	0.0029 ± N.I.	N.I.	N.I.	WT	Müller et al. (2015)
	L. fusiformis ZC1	N.I.	0.0038 ± N.I.	N.I.	N.I.	WT	
	B. coagulans 36D1	N.I.	0.0058 ± N.I.	N.I.	N.I.	WT	
	D. hafniense Y51	N.I.	0.0018 ± N.I.	N.I.	N.I.	WT	

N.I.—No information.

2013; Ochsner et al., 2014; Müller et al., 2015; Witthoff et al., 2015), *C. necator* (Wu et al., 2016), *B. stearothermophilus* (Whitaker et al., 2017), *L. xylanilyticus* (Lee et al., 2020) were reported in methanol conversion. Researchers are searching for NAD^+-dependent Mdhs with higher activity and lower K_M from different microorganisms and improving their characteristics by a rational approach and directed evolution (Hektor et al., 2002; Ochsner et al., 2014; Roth et al., 2019; Lee et al., 2020; Le et al., 2021) (**Table 2**). Specially, the improvement of substrate affinity toward low concentration methanol is focused in the development of Mdh-driven synthetic methylotrophy because of the high toxicity of methanol for *E. coli* (Dyrda et al., 2019).

NAD^+-dependent Mdhs from *B. methanolicus* that has been studied a lot (Vonck et al., 1991; De Vries et al., 1992; Hektor et al., 2002; Krog et al., 2013; Ochsner et al., 2014; Müller et al., 2015; Witthoff et al., 2015). They support cell growth and methanol uptake with high speed in native *B. methanolicus*. However, the catalytic activity of Mdhs from *B. methanolicus in vitro* and *in vivo* are limited because of the unclear mechanism of ACT (Hektor et al., 2002; Witthoff et al., 2015), even though

ACT significantly improve the K_M value of Bmmdh (reduced from 1.8- to 14.0-fold) (Krog et al., 2013; Ochsner et al., 2014). Second, an ACT-independent Mdh from *C. necator* was developed and characterized for the kinetics and substrate specificity on 2016 (Wu et al., 2016). It showed the low affinity to methanol (132 mM for K_M) compared to that of Mdhs from *B. methanolicus* (170–360 mM for K_M) (Krog et al., 2013; Ochsner et al., 2014; Müller et al., 2015; Wu et al., 2016). Another study showed an Mdh from *B. stearothermophilus*, which shares 21–23% amino acid identity with the Mdh from *B. methanolicus* (Whitaker et al., 2017). The affinity of Mdh from *B. stearothermophilus* showed a lower value than that from Bmmdh and Cnmdh (20 mM for K_M), thus, it had superior performance *in vivo* than previously published Mdhs. In particular, Lee et al. found an Mdh from *L. xylanilyticus*, that had higher substrate specificity towards methanol than Bmmdh, Cnmdh and Bsmdh (Lee et al., 2020). In addition, it is also an ACT-independent Mdh with an impressively low affinity (3.23 mM for K_M).

To improve the activity of Mdhs, site-directed (Hektor et al., 2002; Ochsner et al., 2014), site-saturation (Wu et al., 2016) or random mutagenesis (Le et al., 2021) is used for creating Mdh mutants. In 2002, Hektor et al. used site-directed mutagenesis to confirm the role of various amino acid residues in the NAD(H) binding site in Mdh from *B. methanolicus* C1 (Hektor et al., 2002). All mutants are impaired in cofactor NAD(H) binding, though, some mutants (G95A, S97G, and S97T) retained Mdh activity. Finally, only the S97G mutant displayed as "fully activated" in Mdh reaction rates. Another study from Ochsner et al. investigated the effect of site-directed mutations in the predicted active site of Mdh from *B. methanolicus* MGA3 (Ochsner et al., 2014). The V_{max} of Bmmdh S98G increased two-fold compared with that of its wild-type (WT), yet its K_M value also increased in the absence of ACT. Even upon adding ACT, the catalytic efficiency of Bmmdh S98G was similar to that of WT (a doubling of V_{max} with a slight reduction in K_M). Meanwhile, Bmmdh2 S101G lost the activity on methanol. For Mdh from *C. necator*, the site-saturation mutagenesis on the Mdh2 A169 site was constructed (Wu et al., 2016). In the first round of screening, eight possible positive variants with over 50% activity improvement (based on the Nash reaction) were selected from 2000 screened variants, and, finally, CT1-2 was used as the template for another error-prone PCR library in the second round of screening. Afterward, CT4-1, the recombinant of three mutations (A169V, A31V and A26V), which showed a low K_M (21.6 mM) and an unchanged k_{cat} (0.2 s^{-1}) compared with WT Mdh2, was created by various rounds of high throughput screening (HTS). For studying the activity of Mdh from *L. xylanilyticus*, eight residues within 4.5 Å of the center of the docked substrate were selected to contribute toward site-directed mutagenesis (Lee et al., 2020). Finally, the mutations S101V (K_M = 10.35), T141S (K_M = 51.24) and A164F (K_M = 36.83) improved the enzyme's specific activity towards methanol compared to that of the Lxmdh WT. Furthermore, a random mutant library of *L. xylanilyticus* Mdh was constructed and high throughput screened by an formaldehyde detectible biosensor (Le et al., 2021). As a result, several mutants were characterized by high catalytic efficiency and low K_M compared with Lxmdh WT and its published mutants. Thus, mutant Lxmdh E396V, which has the highest catalytic efficiency (79-fold that of WT catalytic efficiency) and an impressive K_M value (0.01 mM), was found. Moreover, the K_M value of another Lxmdh mutant, K318N, was also impressive (0.046 mM). Nevertheless, the recombinant of two mutations (E396V and K318N) had a higher K_M value compared with each mutant (0.233 mM).

Many alcohol dehydrogenases (ADHs), which can catalyze methanol oxidation, may be treated as Mdhs. Although, the catalytic efficiency of methanol oxidation by ADHs is low, it is another good candidate for synthetic methylotrophy. As an example, the AdhA from *Corynebacterium glutamicum* R has shown a low K_M value of methanol activity (97 mM) compared with Bmmdh and Cnmdh (Kotrbova-Kozak et al., 2007; Wu et al., 2016). A number of ADH enzymes has been tested for the methanol oxidation activity without kinetic values, such as ADHs from *Lysinibacillus sphaericus*, L*ysinibacillus fusiformis*, *Bacillus coagulans* and *Desulfitobacterium hafniense* (Müller et al., 2015).

Furthermore, critically, improving methanol oxidation rates by kinetically improved Mdh variants would only be enabled in cells where there is sufficiently fast of formaldehyde assimilation (Woolston et al., 2018). This is important for the development of Mdh-directed evolution approaches. This is covered in the synthetic methylotrophy section of this review.

APPLICATION OF MDHS IN SYNTHETIC METHYLOTROPHY

C1 feed stocks are inexpensive abiotic resources for microbial bio production. Among all C1, the soluble C1 substrates, such as methanol, may be more suitable feed stocks because of the avoidance of mass transfer limitation (Claassens et al., 2019). Synthetic methylotrophy using the integration of Mdhs for the assimilation of methanol as a carbon source into non methylotrophs such as *E. coli* and *C. glutamicum* has been investigated further in recent studies.

For the design of synthetic methylotrophy, a number of biochemical and practical considerations should be considered. Compared to PQQ-dependent Mdhs and O2-dependent Aods, NAD-dependent Mdhs require only enzyme for its functional assembly in both aerobic and anaerobic conditions. Although, PQQ-dependent Mdhs has very high substrate affinity and activity toward methanol, PQQ biosynthesis requires molecular oxygen (Velterop et al., 1995), which will restrict the applications of PQQ-dependent Mdhs as some of metabolites must be produced only under anaerobic conditions. Unfortunately, there are no PQQ biosynthesis pathway in *E. coli* and *C. glutamicum* as candidate for synthetic methylotrophy. NAD-dependent Mdhs can be utilize a ubiquitous cofactor (NAD) that can be generate reducing equivalents in the form of NADH and used to provide electron for metabolite production under both aerobic and anaerobic conditions and generate reducing equivalents (NADH), which can help promote strain growth. In this

TABLE 3 | Strategies and advancements in improving methanol bioconversion efficiency of synthetic methylotrophy in recent literature.

Host	Carbon source/substrate	Used Mdh	Refs
E.coli	0.4% glucose and 1 M methanol	Mdh from *B. methanolicus* MGA3 and PB1	Müller et al. (2015)
	5 mM sodium gluconate, 20 mM sodium pyruvate, 0.1 g/L yeast extract and 500 mM methanol	Mdh from *B. methanolicus* PB1	Meyer et al. (2018)
	60 mM methanol and 1 g/L yeast extract	Mdh from *B. stearothermophilus*	Whitaker et al. (2017)
	250 mM methanol, 10 g/L glucose		Bennett et al. (2020)
	60 mM methanol and 0.5 g/L yeast extract or 4 g/L glucose		Bennett et al. (2018)
	100 mM methanol and 0.5 g/L yeast extract		Rohlhill et al. (2020)
	6 g/L xylose and 250 mM methanol	Mdh 2 from *C. necator* N-1	Woolston et al. (2018)
	250 mM methanol, 50 mM ribose or xylose, 0.05% casamino acids	Mdh 2 CT4-1 from *C. necator* N-1	Chen et al. (2018)
	400 mM methanol and 20 mM xylose		Chen et al. (2020)
	500 mM methanol and 20 mM pyruvate		Keller et al. (2020)
C. glutamicum	120 mM methanol and 55 mM glucose	Mdh and MD3 from *B. methanolicus* MGA3	Witthoff et al. (2015)
	500 mM methanol and 20 mM co-substrates (ribose, xylose or gluconate)	Mdh from *B. methanolicus*	Hennig et al. (2020)
	96.90 mM methanol and 25.32 mM xylose	Mdh from *B. stearothermophilus*	Tuyishime et al. (2018)
		Mdh 3 from *B. methanolicus* MGA3	
		Mdh 2 CT4-1 from *C. necator* N-1	
S. cerevisiae	10 g/L methanol, 20 g/L glucose, 10 g/L yeast extract and 20 g/L peptone	Mdh from *B. methanolicus* MGA3	Dai et al. (2017)

point, NAD-dependent MDHs may be the best candidates for synthetic methylotrophy (Zhang et al., 2017).

For instance, introducing NAD^+-dependent Mdhs is the simplest way to engineer methanol oxidation for all reasons mentioned above. Many researchers are also trying to improve the methanol bioconversion efficiency of synthetic methylotrophy by searching for the NAD^+-dependent Mdhs with better characteristics from different organisms via directed evolution (**Table 3**). The Mdhs from *B. methanolicus* (Müller et al., 2015; Witthoff et al., 2015; Dai et al., 2017; Meyer et al., 2018; Tuyishime et al., 2018; Hennig et al., 2020), *B. stearothermophilus* (Whitaker et al., 2017; Bennett et al., 2018; Tuyishime et al., 2018; Bennett et al., 2020; Rohlhill et al., 2020), and *C. necator* (Chen et al., 2018; Tuyishime et al., 2018; Woolston et al., 2018; Chen et al., 2020; Keller et al., 2020) have been used for synthetic methylotrophy in recent studies with *E. coli* as the most popular host (Müller et al., 2015; Whitaker et al., 2017; Bennett et al., 2018; Chen et al., 2018; Meyer et al., 2018; Woolston et al., 2018; Bennett et al., 2020; Chen et al., 2020; Keller et al., 2020; Rohlhill et al., 2020), besides *C. glutamicum* (Witthoff et al., 2015; Tuyishime et al., 2018; Hennig et al., 2020) and *S. cerevisiae* (Dai et al., 2017). *In vitro* system to mimic synthetic methylotrophy using scaffold system by enzyme assembly for enhancement of methanol utilization have been also attempt (Price et al., 2016).

Although, NAD-dependent MDHs are their favored MDHs for synthetic methylotrophy according to the recent study, the PQQ MDH XoxF has revealed novel activities, such as the oxidation of formaldehyde *in vivo* (Pol et al., 2014; Good et al., 2019). This shows that these enzymes also can generate novel activities for synthetic methylotrophy, even if PQQ must be added; and further, these enzymes may yet reveal undiscovered activities that cannot be generated by NAD-dependent MDHs that would be of great interest to the field.

This consideration could be extended to other steps for engineering synthetic methylotrophy. As mentioned, the speed of formaldehyde assimilation has a big effect on improving methanol oxidation rates. For example, Whitaker et al. combined NAD^+-dependent Mdh from *B. stearothermophilus* and RuMP pathway enzymes from *B. methanolicus* to engineer *E. coli*, which can grow with methanol as the carbon source. Through their engineered *E. coli* strain (BW25113 Δ*frmA* expressing *B. stearothermophilus* Mdh and *B. methanolicus* RuMP), the amount of biomass derived from methanol was determined to be 0.289 ± 0.028 gCDW/gMeOH in media, including 60 mM methanol and 1 g/L yeast extract. A similar increase of biomass in the presence of yeast extract and methanol at a larger scale was confirmed by bioreactor experiments (0.344 ± 0.012 gCDW/gMeOH) (Whitaker et al., 2017).

SYSTEM BIOLOGY BASED PATHWAY OPTIMIZATION

System-wide consideration of engineering strategies is necessary. To address the complexity and identify the best combination of genes for a given host, several computational tools have been developed for the *in silico* design of metabolic pathways (Medema et al., 2012; Vieira et al., 2014; Carbonell et al., 2016). They help identify the best combinations of genes and pathways and optimize the host metabolism, such as transport, cofactors, C1 acceptor regeneration, and chemical toxicity. Müller et al. used the OptFlux software for *in silico* modeling approaches to test the preferred choice of enzymes and pathways by modifying a stoichiometric genome-scale *E. coli* model. A model containing 1,271 gene products and reactions with 1,676 metabolites was established and modified to find a solution for efficient methanol metabolism as a carbon source with a maximal μ of 0.88 h^{-1}

(Müller et al., 2015). Later, in 2018, Meyer et al. performed reaction knockout (KO) analyses using FlexFlux based on the *E. coli* models iAF1260 and iML1515 containing additional reactions for NAD^+-dependent Mdh, HPS and PHI (Meyer et al., 2018). As another example, Keller et al. used cobra python for flux balance analysis (FBA) of the core metabolism of an *E. coli* model from BiGG (Keller et al., 2020).

In methylotrophs, the absence of methanol (or formaldehyde) controls the expression of genes involved, so microorganisms can adapt to the changing of carbon sources (Selvamani et al., 2017). For this reason, regulating the gene expression of methanol and the formaldehyde response is also important. Another important factor is the efficient regeneration of formaldehyde acceptors for methanol assimilation (Woolston et al., 2018). In this regard, it is worth mimicking native methylotrophs (Wang et al., 2019). Five enzymes of the nonoxidative pentose phosphate pathway (PPP) from *B. methanolicus* were introduced into *E. coli* (Bennett et al., 2018). The whole PPP is usually kept for formaldehyde acceptor regeneration, however, it prevents methanol consumption in the absence of a cosubstrate (such as glucose). Therefore, synthetic methanol-dependent strains are engineered for methanol as a co-consumption regime. This leads to the cell growth being bound to methanol assimilation to improve methanol utilization via adaptive laboratory evolution (ALE) (Chen et al., 2020; Wang et al., 2020).

CONCLUSION

In this review, the enzymatic properties of various reported Mdhs and their applications in synthetic methylotrophy were discussed. Protein engineering and molecular modifications using site-directed mutagenesis, random mutagenesis, HTS, and direct evolution can potentially advance further studies in this field by improving the properties (i.e., activity, thermos ability, and substrate-binding affinity) of existing Mdh enzymes and discovering new Mdh enzymes. The proposal for engineering Mdh-based synthetic methylotrophy is providing value-added products from methanol. Until now, several useful metabolites of methanol have been produced, proving the potential of methanol-based bio-manufacturing. Therefore, we may take advantage of Mdhs for the utilization of methanol as feedstock for high value chemicals, which is a methanol-based bio economy.

AUTHOR CONTRIBUTIONS

T-KL, GH, and S-JY initiated the project. T-KL and Y-JL searched the data base. T-KL wrote the first drafts of the manuscript and Y-JL, GH, and S-JY contributed to further revisions and the final version. All authors have made a direct intellectual contribution to the work and approved it for publication.

FUNDING

This work was supported by the C1 Gas Refinery Program funded by the Ministry of Science and ICT (NRF-2018M3D3A1A01056181), the National Research Foundation of Korea (NRF- 2020R1C1C1004178), Chonnam National University (Grant number : 2020-2070), Korea Institute of Planning and Evaluation for Technology in Food, Agriculture and Forestry (IPET) through Useful Agricultural Life Resources Industry Technology Development Program, funded by Ministry of Agriculture, Food and Rural Affairs(MAFRA)(318012-4), and "Cooperative Research Program for Agriculture Science and Technology Development (Project No. PJ01489702)" Rural Development Administration, Republic of Korea.

REFERENCES

Anthony, C., and Williams, P. (2003). The Structure and Mechanism of Methanol Dehydrogenase. *Biochim. Biophys. Acta* 1647 (1-2), 18–23. doi:10.1016/s1570-9639(03)00042-6

Anthony, C. (1982). *The Biochemistry of Methylotrophs*. London, England: Academic Press.

Anthony, C. (2004). The Quinoprotein Dehydrogenases for Methanol and Glucose. *Arch. Biochem. Biophys.* 428 (1), 2–9. doi:10.1016/j.abb.2004.03.038

Anthony, C., and Zatman, L. J. (1967). Prosthetic Group of Alcohol Dehydrogenase of *Pseudomonas* Sp. M27-A New Oxidoreductase Prosthetic Group. *Biochem. J.* 104 (3), 960. doi:10.1042/bj1040960

Anthony, C., and Zatman, L. (1965). The Microbial Oxidation of Methanol. The Alcohol Dehydrogenase of Pseudomonas Sp. M27. *Biochem. J.* 96, 808–812. doi:10.1042/bj0960808

Arfman, N., Van Beeumen, J., De Vries, G. E., Harder, W., and Dijkhuizen, L. (1991). Purification and Characterization of an Activator Protein for Methanol Dehydrogenase from Thermotolerant *Bacillus* Spp. *J. Biol. Chem.* 266 (6), 3955–3960. doi:10.1016/s0021-9258(19)67886-5

Arfman, N., Watling, E. M., Clement, W., Van Oosterwijk, R. J., De Vries, G. E., Harder, W., et al. (1989). Methanol Metabolism in Thermotolerant Methylotrophic *Bacillus* Strains Involving a Novel Catabolic NAD-dependent Methanol Dehydrogenase as a Key Enzyme. *Arch. Microbiol.* 152 (3), 280–288. doi:10.1007/bf00409664

Bennett, R. K., Dillon, M., Gerald Har, J. R., Agee, A., von Hagel, B., Rohlhill, J., et al. (2020). Engineering *Escherichia coli* for Methanol-dependent Growth on Glucose for Metabolite Production. *Metab. Eng.* 60, 45–55. doi:10.1016/j.ymben.2020.03.003

Bennett, R. K., Gonzalez, J. E., Whitaker, W. B., Antoniewicz, M. R., and Papoutsakis, E. T. (2018). Expression of Heterologous Non-oxidative Pentose Phosphate Pathway from Bacillus Methanolicus and Phosphoglucose Isomerase Deletion Improves Methanol Assimilation and Metabolite Production by a Synthetic *Escherichia coli* Methylotroph. *Metab. Eng.* 45, 75–85. doi:10.1016/j.ymben.2017.11.016

Brautaset, T., Jakobsen, Ø. M., Josefsen, K. D., Flickinger, M. C., and Ellingsen, T. E. (2007). Bacillus Methanolicus: a Candidate for Industrial Production of Amino Acids from Methanol at 50°C. *Appl. Microbiol. Biotechnol.* 74 (1), 22–34. doi:10.1007/s00253-006-0757-z

Cao, T.-P., Choi, J. M., Kim, S. W., and Lee, S. H. (2018). The crystal Structure of Methanol Dehydrogenase, a Quinoprotein from the marine Methylotrophic Bacterium Methylophaga Aminisulfidivorans MPT. *J. Microbiol.* 56 (4), 246–254. doi:10.1007/s12275-018-7483-y

Carbonell, P., Currin, A., Jervis, A. J., Rattray, N. J. W., Swainston, N., Yan, C., et al. (2016). Bioinformatics for the Synthetic Biology of Natural Products: Integrating across the Design-Build-Test Cycle. *Nat. Prod. Rep.* 33 (8), 925–932. doi:10.1039/c6np00018e

Chen, C.-T., Chen, F. Y.-H., Bogorad, I. W., Wu, T.-Y., Zhang, R., Lee, A. S., et al. (2018). Synthetic Methanol Auxotrophy of *Escherichia coli* for Methanol-dependent Growth and Production. *Metab. Eng.* 49, 257–266. doi:10.1016/j.ymben.2018.08.010

Chen, F. Y.-H., Jung, H.-W., Tsuei, C.-Y., and Liao, J. C. (2020). Converting *Escherichia coli* to a Synthetic Methylotroph Growing Solely on Methanol. *Cell* 182 (4), 933–946.e914. doi:10.1016/j.cell.2020.07.010

Chistoserdova, L. (2016). Lanthanides: New Life Metals? *World J. Microbiol. Biotechnol.* 32 (8), 138. doi:10.1007/s11274-016-2088-2

Chistoserdova, L., Chen, S.-W., Lapidus, A., and Lidstrom, M. E. (2003). Methylotrophy in *Methylobacterium Extorquens* AM1 from a Genomic point of View. *J. Bacteriol.* 185 (10), 2980–2987. doi:10.1128/jb.185.10.2980-2987.2003

Claassens, N. J., He, H., and Bar-Even, A. (2019). Synthetic Methanol and Formate Assimilation via Modular Engineering and Selection Strategies. *Curr. Issues Mol. Biol.* 33 (1), 237–248. doi:10.21775/cimb.033.237

Dai, Z., Gu, H., Zhang, S., Xin, F., Zhang, W., Dong, W., et al. (2017). Metabolic Construction Strategies for Direct Methanol Utilization in *Saccharomyces cerevisiae*. *Bioresour. Technol.* 245, 1407–1412. doi:10.1016/j.biortech.2017.05.100

De Vries, G. E., Arfman, N., Terpstra, P., and Dijkhuizen, L. (1992). Cloning, Expression, and Sequence Analysis of the *Bacillus Methanolicus* C1 Methanol Dehydrogenase Gene. *J. Bacteriol.* 174 (16), 5346–5353. doi:10.1128/jb.174.16.5346-5353.1992

Deng, Y. W., Ro, S. Y., and Rosenzweig, A. C. (2018). Structure and Function of the Lanthanide-dependent Methanol Dehydrogenase XoxF from the Methanotroph *Methylomicrobium Buryatense* 5GB1C. *J. Biol. Inorg. Chem.* 23 (7), 1037–1047. doi:10.1007/s00775-018-1604-2

Dyrda, G., Boniewska-Bernacka, E., Man, D., Barchiewicz, K., and Słota, R. (2019). The Effect of Organic Solvents on Selected Microorganisms and Model Liposome Membrane. *Mol. Biol. Rep.* 46 (3), 3225–3232. doi:10.1007/s11033-019-04782-y

Egli, T. H., Van Dijken, J. P., Veenhuis, M., Harder, W., and Fiechter, A. (1980). Methanol Metabolism in Yeasts: Regulation of the Synthesis of Catabolic Enzymes. *Arch. Microbiol.* 124 (2), 115–121. doi:10.1007/bf00427715

Fitriyanto, N. A., Fushimi, M., Matsunaga, M., Pertiwiningrum, A., Iwama, T., and Kawai, K. (2011). Molecular Structure and Gene Analysis of Ce3+-Induced Methanol Dehydrogenase of Bradyrhizobium Sp. MAFF211645. *J. Biosci. Bioeng.* 111 (6), 613–617. doi:10.1016/j.jbiosc.2011.01.015

Good, N. M., Moore, R. S., Suriano, C. J., and Martinez-Gomez, N. C. (2019). Contrasting *In Vitro* and *In Vivo* Methanol Oxidation Activities of Lanthanide-dependent Alcohol Dehydrogenases XoxF1 and ExaF from Methylobacterium Extorquens AM1. *Sci. Rep.* 9 (1), 4248. doi:10.1038/s41598-019-41043-1

Good, N. M., Fellner, M., Demirer, K., Hu, J., Hausinger, R. P., and Martinez-Gomez, N. C. (2020). Lanthanide-dependent Alcohol Dehydrogenases Require an Essential Aspartate Residue for Metal Coordination and Enzymatic Function. *J. Biol. Chem.* 295 (24), 8272–8284. doi:10.1074/jbc.ra120.013227

Good, N. M., Lee, H., Hawker, E. R., Gilad, A. A., and Martinez-Gomez, N. C. (2021). Harnessing Methylotrophs as a Bacterial Platform to Reduce Adverse Effects of the Use of the Heavy Lanthanide Gadolinium in Magnetic Resonance Imaging. *bioRxiv*.

Hektor, H. J., Kloosterman, H., and Dijkhuizen, L. (2002). Identification of a Magnesium-dependent NAD(P)(H)-binding Domain in the Nicotinoprotein Methanol Dehydrogenase from Bacillus Methanolicus. *J. Biol. Chem.* 277 (49), 46966–46973. doi:10.1074/jbc.m207547200

Hennig, G., Haupka, C., Brito, L. F., Rückert, C., Cahoreau, E., Heux, S., et al. (2020). Methanol-essential Growth of Corynebacterium Glutamicum: Adaptive Laboratory Evolution Overcomes Limitation Due to Methanethiol Assimilation Pathway. *Int. J. Mol. Sci.* 21 (10), 3617. doi:10.3390/ijms21103617

Heux, S., Brautaset, T., Vorholt, J. A., Wendisch, V. F., and Portais, J. C. (2018). "Synthetic Methylotrophy: Past, Present, and Future," in *Methane Biocatalysis: Paving the Way to Sustainability* (Berlin, Germany: Springer), 133–151. doi:10.1007/978-3-319-74866-5_9

Hibi, Y., Asai, K., Arafuka, H., Hamajima, M., Iwama, T., and Kawai, K. (2011). Molecular Structure of La3+-Induced Methanol Dehydrogenase-like Protein in Methylobacterium Radiotolerans. *J. Biosci. Bioeng.* 111 (5), 547–549. doi:10.1016/j.jbiosc.2010.12.017

Jahn, B., Pol, A., Lumpe, H., Barends, T. R. M., Dietl, A., Hogendoorn, C., et al. (2018). Similar but Not the Same: First Kinetic and Structural Analyses of a Methanol Dehydrogenase Containing a Europium Ion in the Active Site. *ChemBioChem* 19 (11), 1147–1153. doi:10.1002/cbic.201800130

Jiang, W., Hernández Villamor, D., Peng, H., Chen, J., Liu, L., Haritos, V., et al. (2021). Metabolic Engineering Strategies to Enable Microbial Utilization of C1 Feedstocks. *Nat. Chem. Biol.* 17 (8), 845–855. doi:10.1038/s41589-021-00836-0

Kalyuzhnaya, M. G., Hristova, K. R., Lidstrom, M. E., and Chistoserdova, L. (2008). Characterization of a Novel Methanol Dehydrogenase in Representatives of Burkholderiales : Implications for Environmental Detection of Methylotrophy and Evidence for Convergent Evolution. *J. Bacteriol.* 190 (11), 3817–3823. doi:10.1128/jb.00180-08

Keller, P., Noor, E., Meyer, F., Reiter, M. A., Anastassov, S., Kiefer, P., et al. (2020). Methanol-dependent *Escherichia coli* Strains with a Complete Ribulose Monophosphate Cycle. *Nat. Commun.* 11 (1), 5403–5410. doi:10.1038/s41467-020-19235-5

Keltjens, J. T., Pol, A., Reimann, J., and Op den Camp, H. J. M. (2014). PQQ-dependent Methanol Dehydrogenases: Rare-Earth Elements Make a Difference. *Appl. Microbiol. Biotechnol.* 98 (14), 6163–6183. doi:10.1007/s00253-014-5766-8

Kim, H. G., Han, G. H., Kim, D., Choi, J.-S., and Kim, S. W. (2012). Comparative Analysis of Two Types of Methanol Dehydrogenase fromMethylophaga aminisulfidivoransMPTgrown on Methanol. *J. Basic Microbiol.* 52 (2), 141–149. doi:10.1002/jobm.201000479

Kotrbova-Kozak, A., Kotrba, P., Inui, M., Sajdok, J., and Yukawa, H. (2007). Transcriptionally Regulated adhA Gene Encodes Alcohol Dehydrogenase Required for Ethanol and N-Propanol Utilization in *Corynebacterium Glutamicum* R. *Appl. Microbiol. Biotechnol.* 76 (6), 1347–1356. doi:10.1007/s00253-007-1094-6

Krog, A., Heggeset, T. M. B., Müller, J. E. N., Kupper, C. E., Schneider, O., Vorholt, J. A., et al. (2013). Methylotrophic Bacillus Methanolicus Encodes Two Chromosomal and One Plasmid Born NAD+ Dependent Methanol Dehydrogenase Paralogs with Different Catalytic and Biochemical Properties. *PloS one* 8 (3), e59188. doi:10.1371/journal.pone.0059188

Kuznetsova, T. A., Beschastny, A. P., Ponamoreva, O. N., and Trotsenko, Y. A. (2012). Purification and Characterization of Methanol Dehydrogenase of *Methylobacterium Nodulans* Rhizosphere Phytosymbionts. *Appl. Biochem. Microbiol.* 48 (6), 546–551. doi:10.1134/s0003683812060063

Le, T.-K., Ju, S.-B., Lee, H., Lee, J.-Y., Oh, S.-H., Kwon, K.-K., et al. (2021). Biosensor-Based Directed Evolution of Methanol Dehydrogenase from *Lysinibacillus Xylanilyticus*. *Int. J. Mol. Sci.* 22 (3), 1471. doi:10.3390/ijms22031471

Lee, J.-Y., Park, S.-H., Oh, S.-H., Lee, J.-J., Kwon, K. K., Kim, S.-J., et al. (2020). Discovery and Biochemical Characterization of a Methanol Dehydrogenase from *Lysinibacillus Xylanilyticus*. *Front. Bioeng. Biotechnol.* 8, 67. doi:10.3389/fbioe.2020.00067

Leopoldini, M., Russo, N., and Toscano, M. (2007). The Preferred Reaction Path for the Oxidation of Methanol by PQQ-Containing Methanol Dehydrogenase: Addition-Elimination versus Hydride-Transfer Mechanism. *Chem. Eur. J.* 13 (7), 2109–2117. doi:10.1002/chem.200601123

Li, J., Gan, J.-H., Mathews, F. S., and Xia, Z.-X. (2011). The Enzymatic Reaction-Induced Configuration Change of the Prosthetic Group PQQ of Methanol Dehydrogenase. *Biochem. Biophysical Res. Commun.* 406 (4), 621–626. doi:10.1016/j.bbrc.2011.02.107

Liu, Q., Kirchhoff, J. R., Faehnle, C. R., Viola, R. E., and Hudson, R. A. (2006). A Rapid Method for the Purification of Methanol Dehydrogenase from *Methylobacterium Extorquens*. *Protein Expr. Purif.* 46 (2), 316–320. doi:10.1016/j.pep.2005.07.014

Masuda, S., Suzuki, Y., Fujitani, Y., Mitsui, R., Nakagawa, T., Shintani, M., et al. (2018). Lanthanide-Dependent Regulation of Methylotrophy in Methylobacteriumaquaticum Strain 22A. *Msphere* 3 (1), e00462–00417. doi:10.1128/mSphere.00462-17

Medema, M. H., Van Raaphorst, R., Takano, E., and Breitling, R. (2012). Computational Tools for the Synthetic Design of Biochemical Pathways. *Nat. Rev. Microbiol.* 10 (3), 191–202. doi:10.1038/nrmicro2717

Meyer, F., Keller, P., Hartl, J., Gröninger, O. G., Kiefer, P., and Vorholt, J. A. (2018). Methanol-essential Growth of *Escherichia coli*. *Nat. Commun.* 9 (1), 1508–1510. doi:10.1038/s41467-018-03937-y

Montella, C., Bellsolell, L., Pe´rez-Luque, R., Badi´a, J., Baldoma, L., Coll, M., et al. (2005). Crystal Structure of an Iron-dependent Group III Dehydrogenase that Interconverts L -Lactaldehyde and L -1,2-Propanediol in *Escherichia coli*. *J. Bacteriol.* 187 (14), 4957–4966. doi:10.1128/jb.187.14.4957-4966.2005

Müller, J. E. N., Meyer, F., Litsanov, B., Kiefer, P., Potthoff, E., Heux, S., et al. (2015). Engineering *Escherichia coli* for Methanol Conversion. *Metab. Eng.* 28, 190–201. doi:10.1016/j.ymben.2014.12.008

Nakagawa, T., Mitsui, R., Tani, A., Sasa, K., Tashiro, S., Iwama, T., et al. (2012). A Catalytic Role of XoxF1 as La3+-dependent Methanol Dehydrogenase in Methylobacterium Extorquens Strain AM1. *PloS one* 7 (11), e50480. doi:10.1371/journal.pone.0050480

Nojiri, M., Hira, D., Yamaguchi, K., Okajima, T., Tanizawa, K., and Suzuki, S. (2006). Crystal Structures of Cytochrome cL and Methanol Dehydrogenase from Hyphomicrobium Denitrificans: Structural and Mechanistic Insights into Interactions between the Two Proteins,. *Biochemistry* 45 (11), 3481–3492. doi:10.1021/bi051877j

Ochsner, A. M., Müller, J. E. N., Mora, C. A., and Vorholt, J. A. (2014). *In Vitro* activation of NAD-dependent Alcohol Dehydrogenases by Nudix Hydrolases Is More Widespread Than Assumed. *FEBS Lett.* 588 (17), 2993–2999. doi:10.1016/j.febslet.2014.06.008

Patel, R. N., Bose, H. R., Mandy, W. J., and Hoare, D. S. (1972). Physiological Studies of Methane- and Methanol-Oxidizing Bacteria: Comparison of a Primary Alcohol Dehydrogenase from Methylococcus Capsulatus (Texas Strain) and Pseudomonas Species M27. *J. Bacteriol.* 110 (2), 570–577. doi:10.1128/jb.110.2.570-577.1972

Pol, A., Barends, T. R. M., Dietl, A., Khadem, A. F., Eygensteyn, J., Jetten, M. S. M., et al. (2014). Rare Earth Metals Are Essential for Methanotrophic Life in Volcanic Mudpots. *Environ. Microbiol.* 16 (1), 255–264. doi:10.1111/1462-2920.12249

Price, J. V., Chen, L., Whitaker, W. B., Papoutsakis, E., and Chen, W. (2016). Scaffoldless Engineered Enzyme Assembly for Enhanced Methanol Utilization. *Proc. Natl. Acad. Sci. USA* 113 (45), 12691–12696. doi:10.1073/pnas.1601797113

Rohlhill, J., Gerald Har, J. R., Antoniewicz, M. R., and Papoutsakis, E. T. (2020). Improving Synthetic Methylotrophy via Dynamic Formaldehyde Regulation of Pentose Phosphate Pathway Genes and Redox Perturbation. *Metab. Eng.* 57, 247–255. doi:10.1016/j.ymben.2019.12.006

Roth, T. B., Woolston, B. M., Stephanopoulos, G., and Liu, D. R. (2019). Phage-Assisted Evolution of *Bacillus Methanolicus* Methanol Dehydrogenase 2. *ACS Synth. Biol.* 8 (4), 796–806. doi:10.1021/acssynbio.8b00481

Selvamani, V., Maruthamuthu, M. K., Arulsamy, K., Eom, G. T., and Hong, S. H. (2017). Construction of Methanol Sensing *Escherichia coli* by the Introduction of Novel Chimeric MxcQZ/OmpR Two-Component System from *Methylobacterium Organophilum* XX. *Korean J. Chem. Eng.* 34 (6), 1734–1739. doi:10.1007/s11814-017-0063-8

Skovran, E., Raghuraman, C., and Martinez-Gomez, N. C. (2019). Lanthanides in Methylotrophy. *Curr. Issues Mol. Biol.* 33 (1), 101–116. doi:10.21775/cimb.033.101

Sridhara, S., Wu, T. T., Chused, T. M., and Lin, E. C. C. (1969). Ferrous-activated Nicotinamide Adenine Dinucleotide-Linked Dehydrogenase from a Mutant of *Escherichia coli* Capable of Growth on 1,2-Propanediol. *J. Bacteriol.* 98 (1), 87–95. doi:10.1128/jb.98.1.87-95.1969

Tuyishime, P., Wang, Y., Fan, L., Zhang, Q., Li, Q., Zheng, P., et al. (2018). Engineering *Corynebacterium Glutamicum* for Methanol-dependent Growth and Glutamate Production. *Metab. Eng.* 49, 220–231. doi:10.1016/j.ymben.2018.07.011

Velterop, J. S., Sellink, E., Meulenberg, J. J., David, S., Bulder, I., and Postma, P. W. (1995). Synthesis of Pyrroloquinoline Quinone *In Vivo* and *In Vitro* and Detection of an Intermediate in the Biosynthetic Pathway. *J. Bacteriol.* 177 (17), 5088–5098. doi:10.1128/jb.177.17.5088-5098.1995

Vieira, G., Carnicer, M., Portais, J.-C., and Heux, S. (2014). FindPath: a Matlab Solution for In Silico Design of Synthetic Metabolic Pathways. *Bioinformatics* 30 (20), 2986–2988. doi:10.1093/bioinformatics/btu422

Vonck, J., Arfman, N., De Vries, G. E., Van Beeumen, J., Van Bruggen, E. F., and Dijkhuizen, L. (1991). Electron Microscopic Analysis and Biochemical Characterization of a Novel Methanol Dehydrogenase from the Thermotolerant *Bacillus* Sp. C1. *J. Biol. Chem.* 266 (6), 3949–3954. doi:10.1016/s0021-9258(19)67885-3

Vu, H. N., Subuyuj, G. A., Vijayakumar, S., Good, N. M., Martinez-Gomez, N. C., and Skovran, E. (2016). Lanthanide-dependent Regulation of Methanol Oxidation Systems in *Methylobacterium Extorquens* AM1 and Their Contribution to Methanol Growth. *J. Bacteriol.* 198 (8), 1250–1259. doi:10.1128/jb.00937-15

Wang, L., Suganuma, S., Hibino, A., Mitsui, R., Tani, A., Matsumoto, T., et al. (2019). Lanthanide-dependent Methanol Dehydrogenase from the Legume Symbiotic Nitrogen-Fixing Bacterium *Bradyrhizobium Diazoefficiens* Strain USDA110. *Enzyme Microb. Technol.* 130, 109371. doi:10.1016/j.enzmictec.2019.109371

Wang, Y., Fan, L., Tuyishime, P., Zheng, P., and Sun, J. (2020). Synthetic Methylotrophy: a Practical Solution for Methanol-Based Biomanufacturing. *Trends Biotechnol.* 38 (6), 650–666. doi:10.1016/j.tibtech.2019.12.013

Whitaker, W. B., Jones, J. A., Bennett, R. K., Gonzalez, J. E., Vernacchio, V. R., Collins, S. M., et al. (2017). Engineering the Biological Conversion of Methanol to Specialty Chemicals in *Escherichia coli*. *Metab. Eng.* 39, 49–59. doi:10.1016/j.ymben.2016.10.015

Witthoff, S., Schmitz, K., Niedenführ, S., Nöh, K., Noack, S., Bott, M., et al. (2015). Metabolic Engineering of *Corynebacterium Glutamicum* for Methanol Metabolism. *Appl. Environ. Microbiol.* 81 (6), 2215–2225. doi:10.1128/aem.03110-14

Woolston, B. M., King, J. R., Reiter, M., Van Hove, B., and Stephanopoulos, G. (2018). Improving Formaldehyde Consumption Drives Methanol Assimilation in Engineered *E. coli*. *Nat. Commun.* 9 (1), 2387. doi:10.1038/s41467-018-04795-4

Wu, T.-Y., Chen, C.-T., Liu, J. T.-J., Bogorad, I. W., Damoiseaux, R., and Liao, J. C. (2016). Characterization and Evolution of an Activator-independent Methanol Dehydrogenase from *Cupriavidus Necator* N-1. *Appl. Microbiol. Biotechnol.* 100 (11), 4969–4983. doi:10.1007/s00253-016-7320-3

Xia, Z.-X., Dai, W.-W., He, Y.-N., White, S. A., Mathews, F. S., and Davidson, V. L. (2003). X-ray Structure of Methanol Dehydrogenase from *Paracoccus Denitrificans* and Molecular Modeling of its Interactions with Cytochrome C-551i. *J. Biol. Inorg. Chem.* 8 (8), 843–854. doi:10.1007/s00775-003-0485-0

Yu, H., and Liao, J. C. (2018). A Modified Serine Cycle in *Escherichia coli* Coverts Methanol and CO2 to Two-Carbon Compounds. *Nat. Commun.* 9 (1), 3992. doi:10.1038/s41467-018-06496-4

Zhang, W., Zhang, T., Wu, S., Wu, M., Xin, F., Dong, W., et al. (2017). Guidance for Engineering of Synthetic Methylotrophy Based on Methanol Metabolism in Methylotrophy. *RSC Adv.* 7 (7), 4083–4091. doi:10.1039/c6ra27038g

Conflict of Interest: The authors declare that the research was conducted in the absence of any commercial or financial relationships that could be construed as a potential conflict of interest.

Publisher's Note: All claims expressed in this article are solely those of the authors and do not necessarily represent those of their affiliated organizations, or those of the publisher, the editors, and the reviewers. Any product that may be evaluated in this article, or claim that may be made by its manufacturer, is not guaranteed or endorsed by the publisher.

frontiers in Bioengineering and Biotechnology

ORIGINAL RESEARCH
published: 03 January 2022
doi: 10.3389/fbioe.2021.817455

Engineering of CYP153A33 With Enhanced Ratio of Hydroxylation to Overoxidation Activity in Whole-Cell Biotransformation of Medium-Chain 1-Alkanols

Hyuna Park[1], Doyeong Bak[2], Wooyoung Jeon[3], Minjung Jang[3], Jung-Oh Ahn[3,4] and Kwon-Young Choi[1,2]**

[1]Department of Environmental Engineering, College of Engineering, Ajou University, Suwon, South Korea, [2]Department of Environmental and Safety Engineering, College of Engineering, Ajou University, Suwon, South Korea, [3]Biotechnology Process Engineering Center, Korea Research Institute of Biosceince and Biotechnology (KRIBB), Cheongju, South Korea, [4]Department of Bioprocess Engineering, University of Science and Technology (UST), Daejeon, South Korea

OPEN ACCESS

Edited by:
Byung-Gee Kim,
Seoul National University, South Korea

Reviewed by:
Aitao Li,
Hubei University, China
Dirk Tischler,
Ruhr University Bochum, Germany

***Correspondence:**
Jung-Oh Ahn
ahnjo@kribb.or.kr
Kwon-Young Choi
kychoi@ajou.ac.kr

Specialty section:
This article was submitted to Bioprocess Engineering, a section of the journal Frontiers in Bioengineering and Biotechnology

Received: 18 November 2021
Accepted: 13 December 2021
Published: 03 January 2022

Citation:
Park H, Bak D, Jeon W, Jang M, Ahn J-O and Choi K-Y (2022) Engineering of CYP153A33 With Enhanced Ratio of Hydroxylation to Overoxidation Activity in Whole-Cell Biotransformation of Medium-Chain 1-Alkanols. Front. Bioeng. Biotechnol. 9:817455. doi: 10.3389/fbioe.2021.817455

α,ω-Dodecanediol is a versatile material that has been widely used not only as an adhesive and crosslinking reagent, but also as a building block in the pharmaceutical and polymer industries. The biosynthesis of α,ω-dodecanediol from fatty derivatives, such as dodecane and dodecanol, requires an ω-specific hydroxylation step using monooxygenase enzymes. An issue with the whole-cell biotransformation of 1-dodecanol using cytochrome P450 monooxygenase (CYP) with ω-specific hydroxylation activity was the low conversion and production of the over-oxidized product of dodecanoic acid. In this study, CYP153A33 from *Marinobacter aquaeolei* was engineered to obtain higher ω-specific hydroxylation activity through site-directed mutagenesis. The target residue was mutated to increase flux toward α,ω-dodecanediol synthesis, while reducing the generation of the overoxidation product of dodecanoic acid and α,ω-dodecanedioic acid. Among the evaluated variants, CYP153A33 P136A showed a significant increase in 1-dodecanol conversion, i.e., 71.2% (7.12 mM from 10 mM 1-dodecanol), with an increased hydroxylation to over-oxidation activity ratio, i.e., 32.4. Finally, the applicability of this engineered enzyme for ω-specific hydroxylation against several 1-alkanols, i.e., from C6 to C16, was investigated and discussed based on the structure-activity relationship.

Keywords: enzyme engineering, CYP153A33, α,ω-alkanediol, over-oxidation, whole-cell biotransformation

INTRODUCTION

Cytochrome P450 monooxygenases (CYPs) are oxidoreductases that catalyze the insertion of an oxygen atom into diverse substrates, with excellent regio-/stereo-selectivity (Park et al., 2020b); CYP consists of heme-thiolate structures in its catalytic core. CYP enzymes are classified into several groups depending on the electron transfer system of redox proteins. In general, bacterial CYPs belong to the class I system, which consists of a CYP core harboring a heme domain, ferredoxin, and ferredoxin reductase, which require independent expression during the oxidation reaction (Finnigan et al., 2020).

Its substrate spectrum includes fatty derivatives such as fatty alkanes, alcohols, and acids (Jung et al., 2016; Hsieh et al., 2018), of which fatty alcohols are a promising feedstock in the chemical and

biochemical industries. Several fatty alcohols have been used as repeating monomers in the polymer industry, or as solvents, lubricants, surfactants, and precursors for organic synthesis (Lee et al., 2018). In particular, α,ω-alkanediols are versatile chemicals that can be obtained *via* the consecutive oxidation of alkanes/1-alkanol or the reduction of diacids by carboxylic acid reductase (Kirillova et al., 2009; Olmedo et al., 2016; Hsieh et al., 2018). They are also widely used as monomer precursors for polyesters, polyamides, and polyurethane, through cascade oxidation, amination, and polymerization reactions (Ahsan et al., 2018). For example, α,ω-alkanediols are widely used as building blocks for polyester synthesis through direct esterification reactions (Dai et al., 2017).

During the oxidation of long-chain fatty derivatives, however, regioselectivity is critical for obtaining high-purity products, varying depending on the CYP enzyme family and its carbon chains (Munday et al., 2016); for example, the most well-known CYP102A1, also called BM3, was reported to prefer ω-1 or ω-2 regioselectivity over the ω-position (Whitehouse et al., 2011; Whitehouse et al., 2012; Li and Wong, 2019). In addition, CYP505 and CYP102A showed distinct preferable ratios at the ω-1, ω-2, and ω-3 positions; a CYP enzyme responsible for ω-carbon-specific hydroxylation has also been identified (Whitehouse et al., 2012). The CYP153 family, for example, has been isolated and characterized to function as an ω-specific hydroxylase of long-chain fatty derivatives; additionally, CYP2E1, CYP4A1, and CYP153A G307, all prefer ω-specific hydroxylation on the ω-1, 2, and 3 positions (Holmes et al., 2004; Kuzgun et al., 2020). The CYP153A family is classified as a class I CYP enzyme, requiring redox proteins to mediate electron transfer (Van Beilen et al., 2006). Several CYP153 subfamily members, such as CYP153A7 and CYP153A33, showed a wide range of substrate specificities, such as ω- and ω-1 specific hydroxylation activity against C12 fatty acids, and have demonstrated a high degree of structural plasticity and flexibility in substate recognition sites (Fujita et al., 2009; Fiorentini et al., 2018).

To utilize the CYP153 family for preparing α,ω-alkanediols from alkanes or 1-alkanol, it is necessary to secure the active CYP153 enzyme with high regioselectivity against the targeted chain of substrates. Another limiting factor in such bioconversion is the overoxidation activity of the CYP153 enzyme, which is known to proceed with the continuous oxidation of the produced alcohols into acid *via* aldehyde. Although the oxidation of alcohol and aldehyde reportedly occurs *via* alcohol dehydrogenase or fatty alcohol oxidase and aldehyde dehydrogenase enzymes, respectively, some CYP enzymes have also been reported to catalyze overoxidation reactions as well (Scheller et al., 1998; Eschenfeldt et al., 2003). Although the exact reaction mechanisms of overoxidation are not clearly understood and need clarification, the overoxidation products can be attributed to the catalytic activity of CYP in converting alcohol to aldehyde, followed by oxidation to acids. According to previous reports, purified CYP52A3 from *Candida maltose* could oxidize the first oxidation product of 1-hexadecanol, thus generating 1,16-hexadecanedioic acids without the intervention of other enzymes such as ADH and FAO (Scheller et al., 1998). Similarly, studies demonstrated that CYP52A13 and CYP52A17 isolated from *Candida tropicalis* (ATCC20336) displayed overoxidation activity on long-chain saturated and unsaturated fatty acids; postulating the path of the NADPH-dependent conversion of fatty acids to corresponding fatty aldehydes and α,ω-dicarboxylic acid (Eschenfeldt et al., 2003).

Previously, our group reported the production of 1,12-dodecanediol from 1-dodecanol or dodecane as a substrate, using CYP153A from *Marinobacteri aquaeolei* and Nfa22290 from *Nocardia farcinica* (IFM10152) in combination with putida ferredoxin and ferredoxin reductase (CamA) (Park and Choi, 2020). During the biotransformation of dodecane, the conversion to diol was less than 10%, and its overoxidation products, i.e., dodecanoic acid (lauric acid) and 12-hydroxydodecanoic acid were observed as byproducts. This suggests that overoxidation limited the production of α,ω-alkanediols, and needs to be engineered to obtain CYP153A deficient in overoxidation activity.

Based on our structural understanding, CYP153A enzymes appear to have a high degree of structural plasticity and flexibility in the catalytic core site that hosts the substrate recognition site. Structural analysis of the CYP153A33 enzyme to enhance terminal hydroxylation of fatty acids has also been reported; the substrate-binding pocket of the enzyme has an inverted conical shape. It has thus been suggested that the fatty acid substrate can be vertically combined (Sara et al., 2016). In this study, the activity ratio of ω-site-specific hydroxylation to overoxidation by CYP153A33 variants was increased by mutation of the substrate-binding pocket, i.e., by substituting key amino acids through the destruction of proline-proline linkages. In addition, whole-cell biotransformation by wild-type CYP153A33 and its mutants was investigated with medium- and long-chain fatty alkanols. Interestingly, the CYP153A33 mutant displayed significantly higher ω-specific hydroxylation activity on dodecanoic acid and a low ratio of overoxidation activity, when compared to the wild-type. These results would be of great help for further research on the CYP-dependent oxidation of fatty derivatives.

MATERIALS AND METHODS

Chemical Reagents and Media

All fatty alcohols, fatty acids, and solvents were obtained from Sigma-Aldrich (Seoul, South Korea) and Sejin CI (Seoul, South Korea). The culture media used in this research were obtained from Becton, Dickinson, and Company, U.S., and the ethyl acetate solvent was obtained from Samchun Chemical Co. Ltd., South Korea.

Site-Directed Mutagenesis of CYP153A33 and Construction of Expression System in *E. coli*

Mutations in the protein structure were induced through site-directed mutagenesis, using the pair of primers, 5′-CAGCCC CTCCGCAGGGTCACCGAG-3′, and 5′-CTCGGTGACCCT

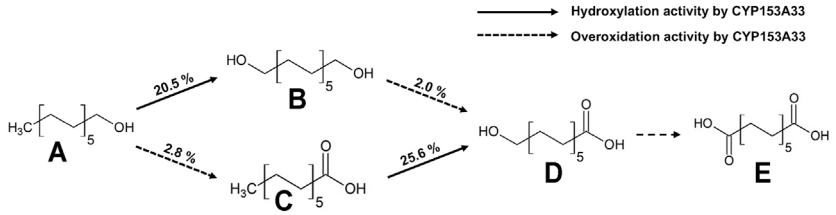

FIGURE 1 | Multistep cascade reaction of 1-dodecanol by CYP153A33-dependent whole-cell transformation. Conversion was calculated when CYP153A33 reached the highest α,ω-dodecanediol production. Conversion of dodecanoic acid to ω-hydroxydodecanoic acid was conducted independently, using dodecanoic acid as a substrate; **(A)** 1-dodecanol, **(B)** α,ω-dodecanediol, **(C)** dodecanoic acid, **(D)** ω-hydroxydodecanoic acid, **(E)** dodecanedioic acid.

GCGGAGGGGCTG-3′. After the preparation of two PCR templates, the final PCR was conducted using another pair of primers (i.e., 5′-AAA CAT ATG ATG CCA ACA CTG CCC AGA-3′, and 5′-AAA CTC GAG TTA ACT GTT CGG TGT CAG-3′); restriction sites were NdeI and XhoI. The enzyme expression system was identical to that used in previous research (Park et al., 2020b). Putidaredoxin *camB* and putidatedoxin reductase *camA* from *Pseudomonas putida* were overexpressed as the redox proteins for CYP catalysis, and the long-chain fatty acid transporter *fadL* from *Escherichia coli* was overexpressed in *E. coli* BW25113(DE3)Δ*fadD* (Bae et al., 2014; Park and Choi, 2020). The CYP153A33 and mutant genes were each inserted into a pET-24ma (+) expression vector, and the *camA* and *camB* genes were cloned into a pETduet-1 expression vector; the *fadL* gene was cloned into pCDFduet-1 MCS1. The mutant CYP153A33 P136A was also inserted into a pET-24ma (+) expression vector, and was included in an identical whole-cell transformation system (Park and Choi, 2020).

Enzyme Expression and Whole-Cell Reaction of Primary Fatty Alcohols Using Recombinant *E. coli* Cells

Recombinant *E. coli* BW25113(DE3)Δ*fadD* was cultured in a Luria-Bertani medium containing kanamycin, ampicillin, and spectinomycin at 37°C for 9 h with shaking at 200 rpm (Bae et al., 2014; Park and Choi, 2020). The cells were then grown in 50 ml of Terrific Broth containing the same antibiotics, at 37°C for approximately 4 h until an OD_{600} of 2.4, was reached; Erlenmeyer baffled flasks were used for culturing. Next, 0.5 mM 5-aminolevulinic acid (ALA), 0.25 mM of isopropyl-β-D-thiogalactopyranoside (IPTG), and 0.1 mM iron (II) sulfate were added for protein expression. Induced cells were incubated at 30°C for 10 h with shaking at 200 rpm. For whole-cell reaction, the cells were harvested by centrifugation at 8,000 rpm for 10 min and then washed twice with a 0.1 M potassium phosphate buffer (pH 7.0). The cell pellets thus obtained were resuspended in 0.1 M potassium phosphate buffer containing 1% (w/v) D-glucose and diluted to an OD_{600} of 30. Reactant (10 ml) containing 10 mM of 1-alkanol was incubated at 30°C and 200 rpm using a 100-ml Erlenmeyer baffled flask.

Gas Chromatography Analysis

Whole-cell reaction samples were analyzed using gas chromatography. Ingredients in the samples were extracted with an equal amount of ethyl acetate at 50°C. The supernatant was separated by centrifugation and derivatized into N,O-bis(trimethylsilyl) trifluoroacetamide at 70°C for 40 min. The derivatized sample was analyzed using a 6500 GC gas chromatography system (Younglin, Suwon, South Korea); an Agilent J&W GC column (CP-Sil 5 CB, 30 m, 0.25 mm i.d.; 0.25 μm film thickness) was used for its analysis. The conditions for the detection of 1-dodecanol, α,ω-dodecanediol, dodecanoic acid, and ω-hydroxydodecanoic acid are mentioned below (Park and Choi, 2020). The initial column temperature was 80°C, which was then increased to 230°C at 20°C/min and maintained for 1.5 min. The capillary flow rate was 2 ml/min, and the carrier gas was nitrogen (N_2); the same column was used for the detection of other extracts as well. The initial column temperature was 130°C, which was then increased to 230°C at 20°C/min and maintained for 3 min.

Structural Analysis of Enzyme and Enzyme-Substrate Docking Simulation

Enzyme-substrate docking simulation was conducted using PyMOL2 (Schrödinger, Inc., US). Structural analysis of CYP153A33 was conducted using AutoDockTools-1.5.6 (Scripps Research, San Diego, CA), using PDB 5FYF (DOI**:** 10.2210/pdb5FYF/pdb) as the template.

RESULTS

Whole-Cell Transformation of 1-Dodecanol by CYP153A33 Expressing *E. coli*

The CYP153A33-encoding gene was co-expressed with CamAB redox proteins for the whole-cell biotransformation of 1-dodecanol. 10 mM of 1-Dodecanol (A) was used as the substrate, and the whole-cell bioconversion resulted in diverse production profiles, including α,ω-dodecanediol (B), dodecanoic acid (C), ω-hydroxydodecanoic acid (D), and α,ω-dodecanedioic acid (E) (**Figure 1**). After 3 h of reaction, the production titer of α,ω-dodecanediol was the highest, and each product was

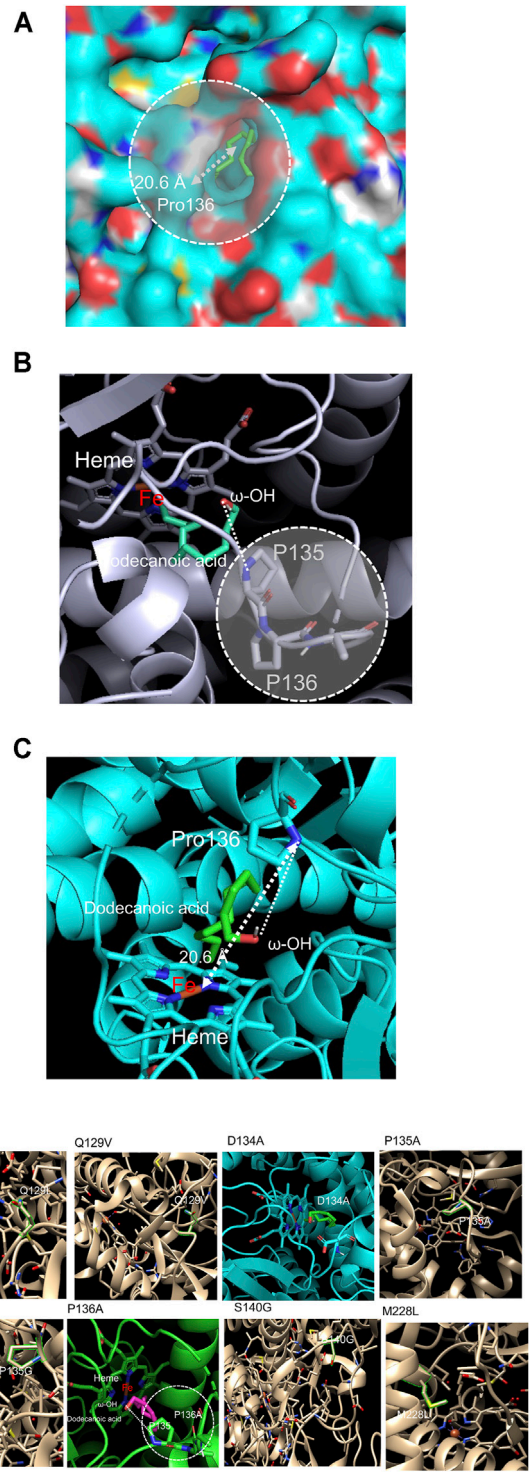

FIGURE 2 | (A) Construction of a CYP153A33 structure model, used to calculate the distance between the heme center and hydroxyl functional group of docked dodecanoic acid. **(B)** 1-dodecanol-docked CYP153A33 structural model; P135-P136 linkage was found at the substate recognition site which holds ω-OH terminal of the docked dodecanoic acid. **(C)** Among two proline residues, Pro136 has direct interaction with the ω-OH terminal of docked dodecanoic acid. **(D)** Selection of target residues in the active site and

(*Continued*)

FIGURE 2 | substrate binding site of CYP153A33. Among the screened residues, D134A and P136A were finally selected for the evaluation of 1-dodecanol bioconversion.

separated by gas chromatography for simultaneous quantitative analysis. The production profile with conversion included 20.5% α,ω-dodecanediol, 2.8% dodecanoic acid, 2.0% ω-hydroxydodecanoic acid, plus miscible amounts of α,ω-dodecanedioic acid. The conversion of ω-hydroxydodecanoic acids to dodecanedioic acid was also observed as less than 5%, indicating that ω-specific hydroxylation to the terminal carbon of the fatty substrate is the most dominant reaction. The relatively lower dodecanoic acid accumulation might be due to the reduction reaction of the aldehyde to alcohol by endogenous enzymes in the host strain of *E. coli* BW25113(DE3)Δ*fadD*.

The major product was identified as α,ω-dodecanediol, but the conversion was low, i.e., only 23.3%. Although one of the overoxidation products of 1-dodecanal was not detected in the whole-cell biotransformation, another overoxidation product of ω-hydroxydodecanoic acid was generated with a similar amount of dodecanoic acid, whose hydroxylation ratio to overoxidation activity was calculated as 13.7. In a control experiment that converted 1-dodecanol to dodecanoic acid by using *E. coli* BW25113(DE3)Δ*fadD* cells harboring an empty vector, less than 0.1 mM of dodecanoic acid was produced, suggesting that this conversion was attributed to both CYP153A33 and the endogenous oxidase enzymes in host cells. In addition, a separate experiment for dodecanoic acid bioconversion *via* CYP153A33-expressing cells resulted in 25.6% conversion to ω-hydroxydodecanoic acid, while 2% conversion was observed in the 1-dodecanol bioconversion. This suggests that CYP153A33 favors fatty acid forms as a substrate, rather than 1-alkanol and overoxidation activity, which was higher with α,ω-dodecanediol (9.8%) than it was with 1-dodecanol (2.8%).

Overoxidation Activity of CYP153A33 and Sequence Analysis With CYP52A Family

Understanding the correlation between end-point production and rate at each step revealed that the highest rate could be observed in the 1-dodecanol conversion, while the lowest was observed in the ω-hydroxydodecanoic acid conversion. These oxidation patterns are in accordance with previous results by Scheller et al., wherein the purified CYP52A3 displayed overoxidation activity during the oxidation of hexadecane, which was further confirmed using kinetic studies demonstrating higher V_{max} values against alkane, 1-alkanol, 1-alkanal, and lower V_{max} against acid, diol, and hydroxy acid.

CYP153A33 showed slight homology (around 20%) with CYP52A3, CYP52A13, and CYP52A17, which were all previously proven to have good overoxidation activity; however, some conserved regions were found in the substrate-binding domains and the active site. Firstly, the residues at the entrance of the substrate access channel may differentiate in their

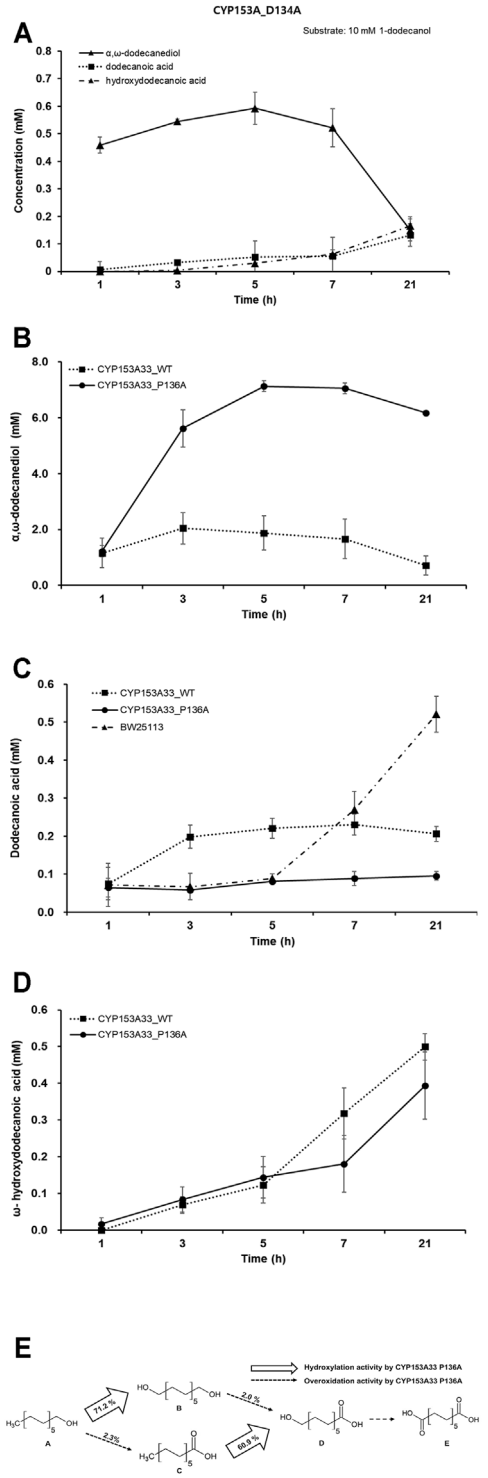

FIGURE 3 | Evaluation of 1-dodecanol bioconversion by whole-cell reaction of CYP153A33 mutant strains. **(A)** Whole-cell biotransformation of 1-dodecanol by CYP153A33 D134A. The production time-profile includes α,ω-dodecanediol, dodecanoic acid, and ω-hydroxydodecanoic acid, from 10 mM of 1-dodecanol substrate. **(B)** Production of α,ω-dodecanediol, **(C)** dodecanoic acid, and **(D)** ω-hydroxydodecanoic acid from 10 mM of 1-dodecanol substrate, through whole-cell biotransformation of 1-dodecanol using CYP153A33 P136A (solid line) and wild-type (dotted line) strains. **(E)** Multistep cascade reaction of 1-dodecanol by CYP153A33 P136A-dependent whole-cell transformation. Conversion was calculated when CYP153A33 P136A reached the highest α,ω-dodecanediol production. Conversion of dodecanoic acid to ω-hydroxydodecanoic acid was conducted independently, using dodecanoic acid as a substrate; **(A)** 1-dodecanol, **(B)** α,ω-dodecanediol, **(C)** dodecanoic acid, **(D)** ω-hydroxydodecanoic acid, **(E)** dodecanedioic acid.

(*Continued*)

substrate specificity and binding affinity with the -OH functional group of the hydroxylated product. Secondly, the CYP153A33 and CYP52A families contain a conserved sequence (i.e., NXXLLXIVXGXDTT) in the central I-helix, suggesting that these residues might be responsible for the high ω-regioselectivity of the CYP153A33 and CYP52A families. One important clue about this overoxidation activity appears to lie in the feedback regulation, as the final product (i.e., α,ω-dodecanedioic acid) acts as a competitive inhibitor of 1-dodecanol binding and may be important for the metabolic regulation of P450 activity (Scheller et al., 1998).

Selection of Key Residue in Substrate Binding Pocket and Site-Directed Mutagenesis of CYP153A33

Based on the analysis of conserved sequences of the CYP153A33 and CYP53A families, we attempted to engineer CYP153A to lower the overoxidation activity by mutating key residues binding the generated hydroxyl functional group. Firstly, a structural model of CYP153A33 was constructed based on the crystal structure of CYP153A (PDB code: 5FYF), followed by docking simulation with a dodecanoic acid substrate. The constructed model showed an obvious path from the hydroxyl functional group of dodecanoic acid to the heme active site, allowing the long-chain fatty acids to access and bind to one another without hindrances. Additionally, the distance of the linear path was calculated to be 20.6 Å (**Figure 2A**).

On the active site in the pocket of the dodecanoic acid-docked CYP153A33 model, proline-proline contiguous amino acid sequences at Pro135 and Pro136 were identified (**Figure 2B**). Proline residues are known to act as structural disruptors in the middle of regular secondary structure elements such as α-helices and β-sheets, thereby increasing the rigidity of protein structures and inhibiting the flexibility of enzymes when incorporated into peptide bonds in the active site (Morgan and Rubenstein, 2013). Since Pro135 and Pro136 were located in the heme active site, bound to the expected hydroxylated carbon atom of α,ω-dodecanediol to facilitate further oxidation to aldehyde by holding and facing the substrate-enzyme complex to the heme active site, Pro136 in the proline-proline linkage was selected as the first target for a mutation (**Figure 2C**). In addition, key residues including Gln129, Asp134, Met129, and Ser140 in the substrate recognition site were identified, and their mutation was first investigated via docking simulation with 1-dodecanol. The selected residues were exchanged with smaller, hydrophobic residues to minimize the effect on pocket polarity and to

increase the chance of substrate access to the active site by lowering the rigidity of the substrate access path. Mutated CYP153A33 structures—Q129L, Q129V, D134A, P135A, P135G, P136A, S140G, and M228L—were generated and evaluated (**Figure 2D**). Excluding D134A and P136A, the docking model did not show a dramatic decrease in the affinity energy and distance from the heme iron center. Next, CYP153A33 D134A and P136A mutants were constructed and their whole-cell activities were investigated.

Whole-Cell Transformation of 1-Dodecanol by CYP153A33 D134A and P136A

Whole-cell biotransformation of 10 mM 1-dodecanol was performed with a recombinant *E. coli* system expressing each CYP153A33 variant of D134A and P136A; however, no significant increase in bioconversion activity was observed in the mutant strains of D134A. The highest tier could be reached after 5 h of reaction, and less than 0.7 mM of α, ω-dodecanediol was produced from 10 mM 1-dodecanol, which was much less than that of wild-type CYP153A33 (**Figure 3A**). Other oxidative metabolites of dodecanoic acid and ω-hydroxydodecanoic acid were produced less than 2% conversion.

Interestingly, among the mutant strains, only the CYP153A33 P136A mutant showed a significant increase in α,ω-dodecanediol production, while also having a dramatic decrease in the overoxidation ratio. The conversion of 1-dodecanol to α,ω-dodecanediol was increased up to 71.2% within 5 h of the whole-cell reaction, and it was 3.47 times higher than that of the wild-type CYP153A33 (**Figure 3B**). Therefore, the hydroxylation ratio over overoxidation activity dramatically increased to 32.4, which was a 2.3-folds increase compared to that of the CYP153A33 wild type. In addition, the conversion of dodecanoic acid to ω-hydroxydodecanoic acid by the P136A mutant independently increased up to 2.38 times with 60.9% conversion. The final overoxidation production of α,ω-dodecanedioic acid was not completely converted by P136A; direct conversion to dodecanoic acid was less than 3% by both CYP153A33 and P136A (**Figure 3C**). This seems to be because 1-dodecanol was mostly consumed by the P136A mutant for hydroxylation and could be due to the increased amount of conversion to α,ω-dodecanediol, by increasing the access opportunity to the active site of 1-dodeacanol results from the flexibility of the pocket. Similarly, dodecanoic acid accumulated at higher concentrations after 5 h, through wild-type CYP153A33 and *E. coli* control strains not harboring any CYP-redox plasmids than P136A (**Figure 3D**).

The overall conversion values of CYP153A33 P136A, when the highest conversion of α,ω-dodecanediol production reached, are summarized in **Figure 3E** for easy comparison with those of wild-type CYP153A33. It is worth noting that the hydroxylation activity against 1-dodecanol and dodecanoic acid was significantly increased and the hydroxylation ratio with overoxidation activity also increased significantly.

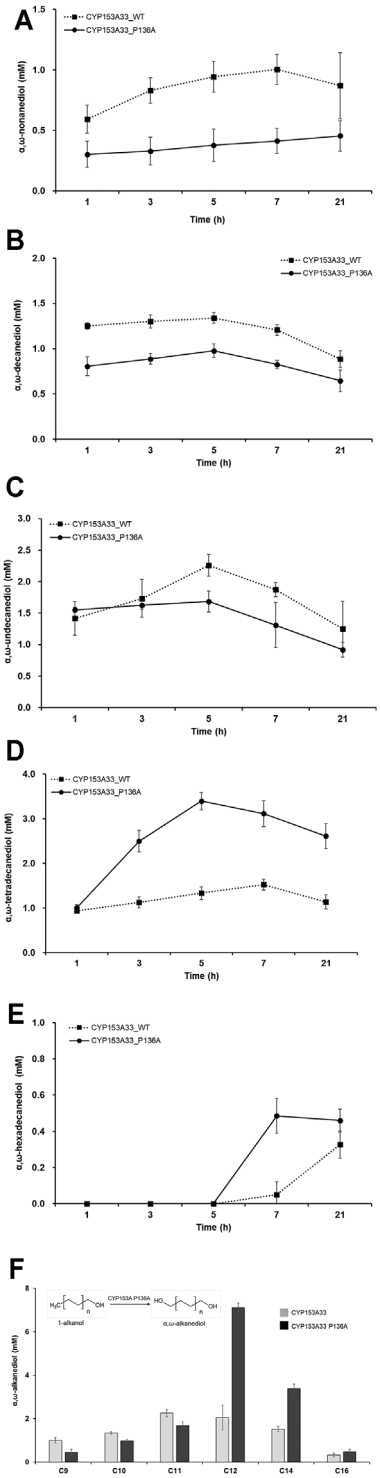

FIGURE 4 | Whole-cell biotransformation of medium- and long-chain 1-alkanols into corresponding α,ω-alkanediols. Time-dependent production profile of α,ω-alkanediol in bioconversion of: **(A)** 1-nonanol, **(B)** 1-decanol, **(C)** 1-undecanol, **(D)** 1-tetradecanol, and **(E)** 1-hexadecanol, using CYP153A33 P136A (solid line) and wild-type (dotted line) strains. **(F)** Summary and comparison of α,ω-alkanediol production using CYP153A33 P136A (black bar) and wild-type (grey bar) strains.

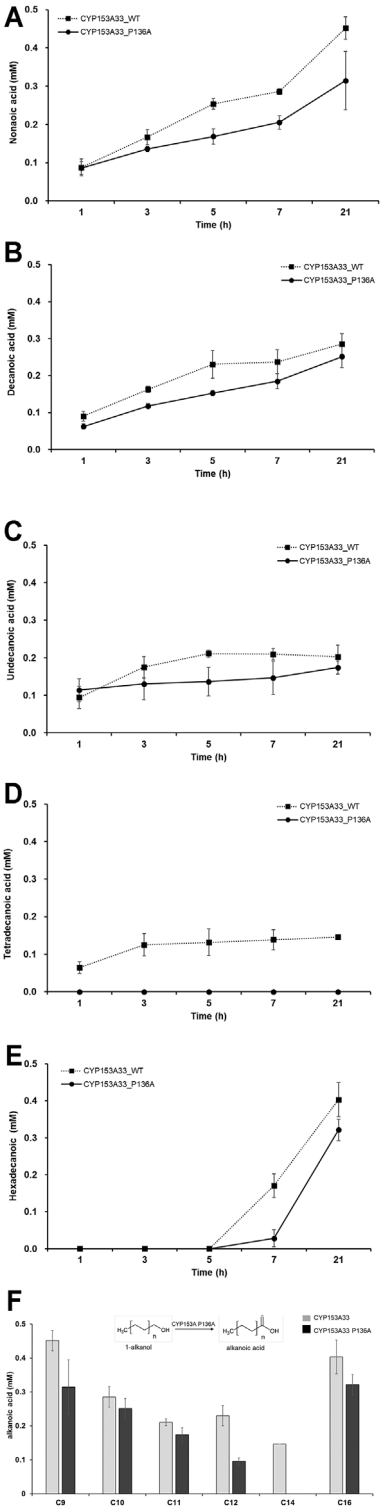

FIGURE 5 | Whole-cell biotransformation of medium- and long-chain 1-alkanols into corresponding fatty acids through overoxidation. Time-dependent production profile of fatty acids in bioconversion of: **(A)** 1-nonanol, **(B)** 1-decanol, **(C)** 1-undecanol, **(D)** 1-tetradecanol, and **(E)** 1-hexadecanol, using CYP153A33 P136A (dotted line) and wild-type (solid line) strains. **(F)** Summary and comparison of fatty acids production using CYP153A33 P136A (black bar) and wild-type (grey bar) strains.

Evaluation of Substrate Specificity of CYP153A33 P136A Against Medium and Long-Chain Fatty Alkanols

The bioconversion activity of CYP153A33 P136A against medium-and long-chain 1-alkanols was then evaluated. Under similar reaction conditions, the whole-cell reaction was conducted in the presence of 1-alkanol substrates including 1-hexanol (C6), 1-nonanol (C9), 1-decanol (C10), 1-undecanol (C11), 1-tetradecanol (C14), and 1-hexadecanol (C16). The production of each α,ω-alkanediol was first evaluated and compared with the bioconversion activity of the wild-type CYP153A33 (**Figures 4A–E**). No oxidation product could be found in the C6 bioconversion; CYP153A33 showed higher α,ω-alkanediol production with C9, C10, and C11 1-alkanol, while P136A showed higher conversion with C12, C14, and C16 1-alkanol. In particular, the maximum yield was more than double that of the wild-type, and 3.4 mM of α,ω-tetradecanediol can be produced via 1-tetradecanol bioconversion within 5 h of reaction. In most cases, however, bioconversion was much lower than C12 of 1-dodecanol, suggesting that CYP153A33 P136A accepts C12 fatty alcohol as the most favorable substrate with exceptionally high conversion (**Figure 4F**), unlike for C14 and C16.

The overoxidation activity of CYP153A P136A with C9 to C16 1-alkanols was also investigated (**Figures 5A–E**). The lowest overoxidation activity was observed for the P136A mutant against tetradecanoic acid, while the highest was observed for CYP153A33 against nonanoic acid. In general, the P136A mutant displayed lower overoxidation activity throughout the examined (C9 to C16) 1-alkanols compared to the CYP153A33 wild-type. Interestingly, the overoxidation activity of both wild-type CYP153A33 and the P136A mutants decreased as the carbon chain increased from C9 to C12 and increased as the carbon chain increased from C14 to C16, suggesting that the lowest activity is between the C12 and C14 chain-lengths of 1-alkanol. In the 1-tetradecanol bioconversion, no overoxidation product(s) of tetradecanoic acid were observed.

DISCUSSION

In this study, CYP153A33, a well-known enzyme with ω-specific hydroxylation activity in fatty primary alcohols, was engineered to obtain a higher hydroxylation activity with 1-dodecanol, along with increased α,ω-dodecanediol conversion. As a result, the best variant of CYP153A33 P136A could be selected, and the bioconversion of 1-dodecnaol increased significantly. The overoxidation product decreased significantly or was not observed in 1-alkanol bioconversion by CYP153A P136A, suggesting that the ratio of hydroxylation to overoxidation activity is also critical if it is mediated by endogenous

enzymes. One thing that should be addressed here is that the origin of CYP153A33 is bacterial, i.e., it is not from a yeast host. Since overoxidation activity was observed by the CYP52A family from *Candida* species of yeast, the catalytic activity and overoxidation-related mechanisms could differ (Scheller et al., 1998; Eschenfeldt et al., 2003). The sequence identity between the CYP52A family and CYP153A33 was less than 20%, and both have different electron transfer systems. Although this study targeted the production of α,ω-alkanediol, the overoxidation product of α,ω-alaknedioic acid is also a very useful biochemical for the chemical industry, potentially being used as polymer building blocks, surfactants, and lubricants. Therefore, if extensive, overoxidation could be beneficial for such purposes, by providing a direct route to the α,ω-alkanedioic acid.

In terms of the rates of conversion and production, conversion of more than 70% within 3 h of the whole-cell reaction is very promising, especially in bioprocesses that include CYP bioconversion. In addition, most CYP-dependent oxyfunctionalizations have low turnover rates and NAD(P)H cofactor utilization. The engineered CYP153A33 P136A strain can produce α,ω-dodecanediol with a productivity of 0.29 g/L/h. This value is very promising, considering the reported space-time yields of CYP-dependent whole-cell biotransformation (Park et al., 2020a).

The application of overoxidation deficient CYP enzymes for alkane oxidation is very diverse. For example, direct use of alkanediol for various monomers for polyesters, polyamides, and polyurethane can be possible. Also, preparation of diamine, which can be applied for polyamide monomers, by introducing an amine functional group through cascade oxidation and transamination can be possible. This diamine synthesis is very competitive compared to the method by fatty acid decarboxylase enzymes (Cha et al., 2021). However, there are still more rooms to be engineered for the more efficient whole-cell biotransformation of the CYP153A P136A. For example, engineering approach could be made available by providing additional redox potentials or by introducing transporting channels into the host cell membrane (Choi et al., 2014; Park and Choi, 2020); this would contribute to a higher production titer, as previously reported. A limitation of the CYP-dependent oxidation process is the use and additional and required feeding of aminolevulinic acid as a heme precursor to activate the CYP core structure (Kim et al., 2017; Namgung et al., 2019). This heme precursor is expensive and must be fed extracellularly during induction. Also, the supply of oxygen, which is one of the co-substrates in CYP-dependent oxidation reaction, could be one of the limiting factors. Altogether, there are still challenges to be overcome and solutions to be potentially engineered in further research.

DATA AVAILABILITY STATEMENT

The original contributions presented in the study are included in the article/Supplementary Material, further inquiries can be directed to the corresponding authors.

AUTHOR CONTRIBUTIONS

K-YC and J-OA designed the study. HP, DB, MJ, and WJ conducted bioconversion experiments and analyzed the products. K-YC and J-OA wrote and revised the manuscript.

FUNDING

This study was performed with the support of the R&D Program of MOTIE/KEIT (grant number 20014350 and 20002734).

REFERENCES

Ahsan, M. M., Jeon, H., Nadarajan, S. P., Chung, T., Yoo, H. W., Kim, B. G., et al. (2018). Biosynthesis of the Nylon 12 Monomer, omega-Aminododecanoic Acid with Novel CYP153A, AlkJ, and omega-TA Enzymes. *Biotechnol. J.* 13, e1700562. doi:10.1002/biot.201700562

Bae, J. H., Park, B. G., Jung, E., Lee, P.-G., and Kim, B.-G. (2014). fadD Deletion and fadL Overexpression in Escherichia coli Increase Hydroxy Long-Chain Fatty Acid Productivity. *Appl. Microbiol. Biotechnol.* 98, 8917–8925. doi:10.1007/s00253-014-5974-2

Cha, T.-Y., Yong, Y., Park, H., Yun, H.-J., Jeon, W., Ahn, J.-O., et al. (2021). Biosynthesis of C12 Fatty Alcohols by Whole Cell Biotransformation of C12 Derivatives Using Escherichia coli Two-Cell Systems Expressing CAR and ADH. *Biotechnol. Bioproc. E* 26, 392–401. doi:10.1007/s12257-020-0239-7

Choi, K.-Y., Jung, E., Yun, H., Yang, Y.-H., and Kim, B.-G. (2014). Engineering Class I Cytochrome P450 by Gene Fusion with NADPH-dependent Reductase and S. Avermitilis Host Development for Daidzein Biotransformation. *Appl. Microbiol. Biotechnol.* 98, 8191–8200. doi:10.1007/s00253-014-5706-7

Dai, L., Tao, F., Tang, H., Guo, Y., Shen, Y., and Xu, P. (2017). Directing Enzyme Devolution for Biosynthesis of Alkanols and 1,n-Alkanediols from Natural Polyhydroxy Compounds. *Metab. Eng.* 44, 70–80. doi:10.1016/j.ymben.2017.09.005

Eschenfeldt, W. H., Zhang, Y., Samaha, H., Stols, L., Eirich, L. D., Wilson, C. R., et al. (2003). Transformation of Fatty Acids Catalyzed by Cytochrome P450 Monooxygenase Enzymes of Candida tropicalis. *Appl. Environ. Microbiol.* 69, 5992–5999. doi:10.1128/aem.69.10.5992-5999.2003

Finnigan, J. D., Young, C., Cook, D. J., Charnock, S. J., and Black, G. W. (2020). Cytochromes P450 (P450s): A Review of the Class System with a Focus on Prokaryotic P450s. *Adv. Protein Chem. Struct. Biol.* 122, 289–320. doi:10.1016/bs.apcsb.2020.06.005

Fiorentini, F., Hatzl, A.-M., Schmidt, S., Savino, S., Glieder, A., and Mattevi, A. (2018). The Extreme Structural Plasticity in the CYP153 Subfamily of P450s Directs Development of Designer Hydroxylases. *Biochemistry* 57, 6701–6714. doi:10.1021/acs.biochem.8b01052

Fujita, N., Sumisa, F., Shindo, K., Kabumoto, H., Arisawa, A., Ikenaga, H., et al. (2009). Comparison of Two Vectors for Functional Expression of a Bacterial Cytochrome P450 Gene inEscherichia coliUsingCYP153Genes. *Biosci. Biotechnol. Biochem.* 73, 1825–1830. doi:10.1271/bbb.90199

Holmes, V. E., Bruce, M., Shaw, P. N., Bell, D. R., Qi, F. M., and Barrett, D. A. (2004). A Gas Chromatography-Mass Spectrometry Method for the Measurement of Fatty Acid ω and ω−1 Hydroxylation Kinetics by CYP4A1 Using an Artificial Membrane System. *Anal. Biochem.* 325, 354–363. doi:10.1016/j.ab.2003.10.046

Hsieh, S. C., Wang, J. H., Lai, Y. C., Su, C. Y., and Lee, K. T. (2018). Production of 1-Dodecanol, 1-Tetradecanol, and 1,12-Dodecanediol through Whole-Cell

Biotransformation in Escherichia coli. *Appl. Environ. Microbiol.* 84, e01806. doi:10.1128/AEM.01806-17

Jung, E., Park, B. G., Ahsan, M. M., Kim, J., Yun, H., Choi, K.-Y., et al. (2016). Production of ω-hydroxy Palmitic Acid Using CYP153A35 and Comparison of Cytochrome P450 Electron Transfer System *In Vivo*. *Appl. Microbiol. Biotechnol.* 100, 10375–10384. doi:10.1007/s00253-016-7675-5

Kim, H.-J., Jang, S., Kim, J., Yang, Y.-H., Kim, Y.-G., Kim, B.-G., et al. (2017). Biosynthesis of Indigo in *Escherichia coli* Expressing Self-Sufficient CYP102A from *Streptomyces Cattleya*. *Dyes Pigm.* 140, 29–35. doi:10.1016/j.dyepig.2017.01.029

Kirillova, M. V., Kirillov, A. M., Kuznetsov, M. L., Silva, J. A. L., Fraústo da Silva, J. J. R., and Pombeiro, A. J. L. (2009). Alkanes to Carboxylic Acids in Aqueous Medium: Metal-free and Metal-Promoted Highly Efficient and Mild Conversions. *Chem. Commun.* 17, 2353–2355. doi:10.1039/b900853e

Kuzgun, G., Başaran, R., Arıoğlu İnan, E., and Can Eke, B. (2020). Effects of Insulin Treatment on Hepatic CYP1A1 and CYP2E1 Activities and Lipid Peroxidation Levels in Streptozotocin-Induced Diabetic Rats. *J. Diabetes Metab. Disord.* 19, 1157–1164. doi:10.1007/s40200-020-00616-y

Lee, H., Han, C., Lee, H.-W., Park, G., Jeon, W., Ahn, J., et al. (2018). Development of a Promising Microbial Platform for the Production of Dicarboxylic Acids from Biorenewable Resources. *Biotechnol. Biofuels* 11, 310. doi:10.1186/s13068-018-1310-x

Li, Y., and Wong, L. L. (2019). Multi-Functional Oxidase Activity of CYP102A1 (P450BM3) in the Oxidation of Quinolines and Tetrahydroquinolines. *Angew. Chem. Int. Ed.* 58, 9551–9555. doi:10.1002/anie.201904157

Morgan, A. A., and Rubenstein, E. (2013). Proline: the Distribution, Frequency, Positioning, and Common Functional Roles of Proline and Polyproline Sequences in the Human Proteome. *PLoS One* 8, e53785. doi:10.1371/journal.pone.0053785

Munday, S. D., Maddigan, N. K., Young, R. J., and Bell, S. G. (2016). Characterisation of Two Self-Sufficient CYP102 Family Monooxygenases from Ktedonobacter Racemifer DSM44963 Which Have New Fatty Acid Alcohol Product Profiles. *Biochim. Biophys. Acta (Bba) - Gen. Subjects* 1860, 1149–1162. doi:10.1016/j.bbagen.2016.01.023

Namgung, S., Park, H. A., Kim, J., Lee, P.-G., Kim, B.-G., Yang, Y.-H., et al. (2019). Ecofriendly One-Pot Biosynthesis of Indigo Derivative Dyes Using CYP102G4 and PrnA Halogenase. *Dyes Pigm.* 162, 80–88. doi:10.1016/j.dyepig.2018.10.009

Olmedo, A., Aranda, C., del Río, J. C., Kiebist, J., Scheibner, K., Martínez, A. T., et al. (2016). From Alkanes to Carboxylic Acids: Terminal Oxygenation by a Fungal Peroxygenase. *Angew. Chem. Int. Ed.* 55, 12248–12251. doi:10.1002/anie.201605430

Park, H., Park, G., Jeon, W., Ahn, J. O., Yang, Y. H., and Choi, K. Y. (2020b). Whole-cell Biocatalysis Using Cytochrome P450 Monooxygenases for Biotransformation of Sustainable Bioresources (Fatty Acids, Fatty Alkanes, and Aromatic Amino Acids). *Biotechnol. Adv.* 40, 107504. doi:10.1016/j.biotechadv.2020.107504

Park, H. A., and Choi, K.-Y. (2020). A, ω-Oxyfunctionalization of C12 Alkanes via Whole-Cell Biocatalysis of CYP153A from Marinobacter Aquaeolei and a New CYP from Nocardia Farcinica IFM10152. *Biochem. Eng. J.* 156, 107524. doi:10.1016/j.bej.2020.107524

Park, H., Park, G., Jeon, W., Ahn, J.-O., Yang, Y.-H., and Choi, K.-Y. (2020a). Whole-cell Biocatalysis Using Cytochrome P450 Monooxygenases for Biotransformation of Sustainable Bioresources (Fatty Acids, Fatty Alkanes, and Aromatic Amino Acids). *Biotechnol. Adv.* 40, 107504. doi:10.1016/j.biotechadv.2020.107504

Sara, M., Hoffmann, H.-R. D.-A., Spandolf, C., Weissenborn, M. J., Grogan, G., and Hauer, B. (2016). Structure-Guided Redesign of CYP153AM.Aq for the Improved Terminal Hydroxylation of Fatty Acids. *ChemCatChem* 8, 3234–3239. doi:10.1002/cctc.201600680

Scheller, U., Zimmer, T., Becher, D., Schauer, F., and Schunck, W.-H. (1998). Oxygenation Cascade in Conversion of N-Alkanes to α,ω-Dioic Acids Catalyzed by Cytochrome P450 52A3. *J. Biol. Chem.* 273, 32528–32534. doi:10.1074/jbc.273.49.32528

Van Beilen, J. B., Funhoff, E. G., Van Loon, A., Just, A., Kaysser, L., Bouza, M., et al. (2006). Cytochrome P450 Alkane Hydroxylases of the CYP153 Family Are Common in Alkane-Degrading Eubacteria Lacking Integral Membrane Alkane Hydroxylases. *Appl. Environ. Microbiol.* 72, 59–65. doi:10.1128/aem.72.1.59-65.2006

Whitehouse, C. J. C., Bell, S. G., and Wong, L.-L. (2012). P450BM3(CYP102A1): Connecting the Dots. *Chem. Soc. Rev.* 41, 1218–1260. doi:10.1039/c1cs15192d

Whitehouse, C. J. C., Yang, W., Yorke, J. A., Tufton, H. G., Ogilvie, L. C. I., Bell, S. G., et al. (2011). Structure, Electronic Properties and Catalytic Behaviour of an Activity-Enhancing CYP102A1 (P450BM3) Variant. *Dalton Trans.* 40, 10383–10396. doi:10.1039/c1dt10098j

Conflict of Interest: The authors declare that the research was conducted in the absence of any commercial or financial relationships that could be construed as a potential conflict of interest.

Publisher's Note: All claims expressed in this article are solely those of the authors and do not necessarily represent those of their affiliated organizations, or those of the publisher, the editors and the reviewers. Any product that may be evaluated in this article, or claim that may be made by its manufacturer, is not guaranteed or endorsed by the publisher.

frontiers in Bioengineering and Biotechnology

ORIGINAL RESEARCH
published: 18 January 2022
doi: 10.3389/fbioe.2022.825399

An Integrative Multiomics Approach to Characterize Prebiotic Inulin Effects on *Faecalibacterium prausnitzii*

*Ji-Hyeon Park[1†], Won-Suk Song[1†], Jeongchan Lee[2], Sung-Hyun Jo[1], Jae-Seung Lee[1], Hyo-Jin Jeon[1], Ji-Eun Kwon[1], Ye-Rim Kim[1], Ji-Hyun Baek[1], Min-Gyu Kim[1], Yung-Hun Yang[3], Byung-Gee Kim[2] and Yun-Gon Kim[1]**

[1]Department of Chemical Engineering, Soongsil University, Seoul, South Korea, [2]School of Chemical and Biological Engineering, Seoul National University, Seoul, South Korea, [3]Department of Biological Engineering, Konkuk University, Seoul, South Korea

OPEN ACCESS

Edited by:
Ken'ichiro Matsumoto, Hokkaido University, Japan

Reviewed by:
Takaaki Horinouchi, National Institute of Advanced Industrial Science and Technology (AIST), Japan
Mireia Lopez Siles, Instituto de Salud Carlos III (ISCIII), Spain

***Correspondence:**
Yun-Gon Kim
ygkim@ssu.ac.kr

[†]These authors have contributed equally to this work

Specialty section:
This article was submitted to Bioprocess Engineering, a section of the journal Frontiers in Bioengineering and Biotechnology

Received: *30 November 2021*
Accepted: *24 January 2022*
Published: *18 January 2022*

Citation:
Park J-H, Song W-S, Lee J, Jo S-H, Lee J-S, Jeon H-J, Kwon J-E, Kim Y-R, Baek J-H, Kim M-G, Yang Y-H, Kim B-G and Kim Y-G (2022) An Integrative Multiomics Approach to Characterize Prebiotic Inulin Effects on Faecalibacterium prausnitzii. Front. Bioeng. Biotechnol. 10:825399. doi: 10.3389/fbioe.2022.825399

Faecalibacterium prausnitzii, a major commensal bacterium in the human gut, is well known for its anti-inflammatory effects, which improve host intestinal health. Although several studies have reported that inulin, a well-known prebiotic, increases the abundance of *F. prausnitzii* in the intestine, the mechanism underlying this effect remains unclear. In this study, we applied liquid chromatography tandem mass spectrometry (LC-MS/MS)-based multiomics approaches to identify biological and enzymatic mechanisms of *F. prausnitzii* involved in the selective digestion of inulin. First, to determine the preference for dietary carbohydrates, we compared the growth of *F. prausnitzii* in several carbon sources and observed selective growth in inulin. In addition, an LC-MS/MS-based intracellular proteomic and metabolic profiling was performed to determine the quantitative changes in specific proteins and metabolites of *F. prausnitzii* when grown on inulin. Interestingly, proteomic analysis revealed that the putative proteins involved in inulin-type fructan utilization by *F. prausnitzii*, particularly β-fructosidase and amylosucrase were upregulated in the presence of inulin. To investigate the function of these proteins, we overexpressed *bfrA* and *ams,* genes encoding β-fructosidase and amylosucrase, respectively, in *Escherichia coli,* and observed their ability to degrade fructan. In addition, the enzyme activity assay demonstrated that intracellular fructan hydrolases degrade the inulin-type fructans taken up by fructan ATP-binding cassette transporters. Furthermore, we showed that the fructose uptake activity of *F. prausnitzii* was enhanced by the fructose phosphotransferase system transporter when inulin was used as a carbon source. Intracellular metabolomic analysis indicated that *F. prausnitzii* could use fructose, the product of inulin-type fructan degradation, as an energy source for inulin utilization. Taken together, this study provided molecular insights regarding the metabolism of *F. prauznitzii* for inulin, which stimulates the growth and activity of the beneficial bacterium in the intestine.

Keywords: *Faecalibacterium prausnitzii*, inulin, prebiotics, LC-MS/MS, beta-fructosidase, amylosucrase, ABC transporter, PTS transporter

INTRODUCTION

In the human gastrointestinal tract (GI), there is a complex and dense microbial community that maintains a symbiotic relationship with the host (Bäckhed et al., 2005; Eckburg et al., 2005; El Kaoutari et al., 2013). It degrades monosaccharides and dietary carbohydrates, which are resistant to human digestive enzymes and ferments them into short-chain fatty acids (SCFAs) (Flint et al., 2012; Nyangale et al., 2012). Among the microbial-derived SCFAs, butyrate acts as an energy source for colonocytes and plays an important role in regulating intestinal health and host immune system by providing anti-carcinogenic, anti-inflammatory, and barrier protection in the intestine (Roediger, 1980; Hamer et al., 2008; Fung et al., 2012; Wang et al., 2012). Recently, based on the correlation between host health and fermentation metabolites produced by beneficial gut bacteria, there is a growing interest in intentionally increasing the proportion of butyrate-producing bacteria in the gut.

Faecalibacterium prausnitzii, a member of Clostridium cluster IV in Bacillota (previously known as Firmicutes), is one of the major butyrate-producing bacteria in the intestine (Miquel et al., 2013; Oren and Garrity, 2021). It has recently emerged as a potential next-generation probiotic that plays an important role in regulating intestinal inflammatory responses and maintaining host gut health (Walker et al., 2011; O'Toole et al., 2017). *F. prausnitzii* is one of the most abundant microbial species, accounting for approximately 5–15% of the human gut microbiota and is less abundant in the intestines of individuals suffering from irritable bowel syndrome, obesity, type 2 diabetes, and inflammatory bowel diseases such as ulcerative colitis, and Crohn's disease (Jia et al., 2010; Willing et al., 2010; Joossens et al., 2011; Miquel et al., 2013; Miquel et al., 2014; Lopez-Siles et al., 2016). In addition, regulating the intestinal proportion of *F. prausnitzii* is expected to alleviate or treat these diseases. The bacterium has been reported to reduce the severity of intestinal inflammation through anti-inflammatory metabolites in a colitis mouse model (Sokol et al., 2008; Martín et al., 2015; Miquel et al., 2015). However, several constraints need to be addressed prior to commercialization, such as the need to minimize contact with external oxygen since *F. prausnitzii*, an obligate anaerobe, loses viability within 2 min of exposure to ambient air (Duncan et al., 2002; Khan et al., 2014). Therefore, to increase the abundance and activity of *F. prausnitzii* in the intestine, a dietary carbohydrate that can selectively stimulate the metabolic activity and proliferation of *F. prausnitzii* is required.

Prebiotics are nutrients that are not digested by the human gastrointestinal tract, but can improve human health by selectively stimulating the growth and activity of the gut microbiota (Gibson and Roberfroid, 1995). Inulin is one of the most widely used prebiotics as a component of food and nutritional supplements. It consists of β-2,1-linked fructosyl residues with an α-1,2-linked glucose terminus and has a linear structure with a degree of polymerization (DP) of 2–60 (Roberfroid and Delzenne, 1998; Roberfroid, 2005). An *in vitro* study has demonstrated the degradation of inulin by *F. prausnitzii*, and ingestion of a diet containing inulin-type fructan increased the abundance of *F. prausnitzii* in the human gut (Duncan et al., 2002; Ramirez-Farias et al., 2008; Dewulf et al., 2013; Moens and De Vuyst, 2017). Furthermore, increased butyrate production by consuming an inulin-rich diet has been observed in a mouse model, and increasing evidence support the effect of inulin on intestinal health in various *in vivo* models (Campbell et al., 1997; Koleva et al., 2012; Holscher et al., 2014). However, despite considerable interest in the role of *F. prausnitzii* as an efficient degrader of inulin and the subsequent

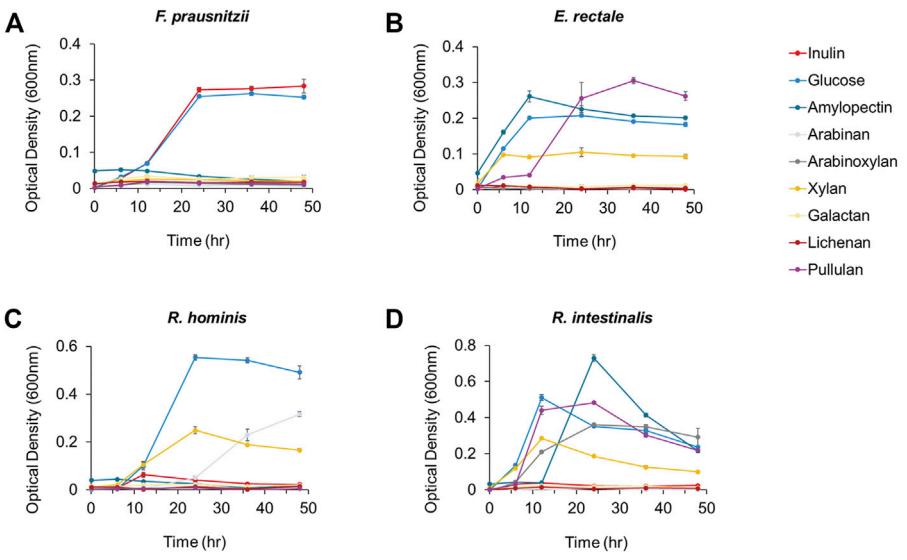

FIGURE 1 | The growth analysis of butyrate-producing bacteria **(A)** *F. prausnitzii* **(B)** *E. rectale* **(C)** *R. hominis* and **(D)** *R. intestinalis* cultured in mYCFA supplemented with either inulin, glucose, amylopectin, arabinan, arabinoxylan, xylan, galactan, lichenan, or pullulan. All experiments were performed in triplicates for each experiment.

effect on improving intestinal health, molecular-level studies to determine the mechanisms whereby *F. prausnitzii* utilizes dietary inulin and undergoes physiological changes are still insufficient.

In this study, integrative multiomics analysis was performed on proteins and metabolites, to identify the biological mechanism involved in the selective digestion of inulin in the intestine by *F. prausnitzii*. To investigate molecular-level cellular metabolic changes using multiomics approaches, we used *F. prausnitzii* strain A2-165, whose complete genome sequence has already been well reported (Miquel et al., 2013; Fitzgerald et al., 2018; Ueda et al., 2021). First, to confirm the preference for dietary carbohydrates in *F. prausnitzii*, we compared the growth of the bacterium in the presence of several carbon sources and confirmed significant growth in inulin. In addition, liquid chromatography with tandem mass spectrometry (LC-MS/MS)-based intracellular proteome analysis was performed to determine quantitative changes in the protein content of *F. prausnitzii* during growth on inulin as the sole carbon source. The results showed that the proteins involved in inulin degradation and intracellular transport were upregulated, and fructan hydrolysis enzymes, β-fructosidase and amylosucrase, were significantly upregulated. Expression levels of the genes encoding these two enzymes were determined using quantitative real time polymerase chain reaction (qRT-PCR). The activity of the enzymes against inulin and sucrose degradation was demonstrated by overexpression in *Escherichia coli*. Analysis of enzyme activity and subcellular location showed that fructan hydrolases are cytoplasmic enzymes that degrade the inulin-type fructan taken up by the fructan ATP-binding cassette (ABC) transporters, which are upregulated in proteomic data. In addition, upregulation of the fructose phosphotransferase system (PTS) transporter, which transports fructose into cells, indicates that *F. prausnitzii* can also enhance the uptake fructose through inulin metabolism. Furthermore, intracellular metabolome analysis demonstrated that *F. prausnitzii* used fructose, the final degradation product of inulin-type fructan, as an efficient energy source during the inulin utilization process. In this study, we characterized the functional roles of proteins upregulated in inulin metabolism by *F. prausnitzii* on a molecular scale; based on these data, we were able to outline a model in which *F. prausnitzii* utilizes inulin in the intestinal ecosystem. Finally, understanding these metabolic pathways is expected to provide evidence for the development of targeted prebiotics for enhancing intestinal microorganisms classified as beneficial bacteria.

MATERIALS AND METHODS

Bacterial Strain and Culture Condition

The bacterial strains used in this study were *F. prausnitzii* A2-165 (DSM 17677), *Eubacterium rectale* (KCTC 5835), *Roseburia hominis* (KCTC 5845), and *Roseburia intestinalis* (KCTC 15746). *F. prausnitzii* A2-165 (DSM 17677) was purchased from German collection of microorganisms and cell cultures (DSMZ, Braunschweig, Germany) and cultured in modified YCFA medium, hereafter referred to as mYCFA medium. All components were added as the referenced method, but the final concentration of short-chain fatty acids (SCFA) in the medium was modified (Duncan et al., 2002). 30 mM of acetic acid, sterilized by syringe filter (PVDF, pore size 0.45 μm, JETbiofil), was added to the sterilized medium. If 5 g/L glucose (Sigma-Aldrich, MO, United States) was supplemented as a carbon source, hereafter referred to as mYCFAG.

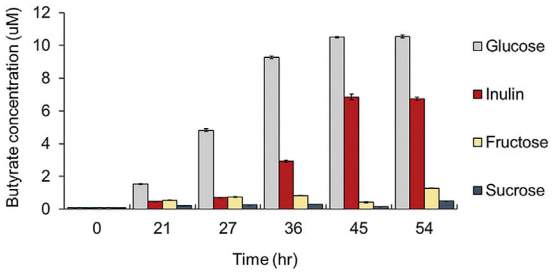

FIGURE 2 | Comparison of butyrate productivity of *F. prausnitzii* grown in mYCFA supplemented with either glucose, inulin, fructose, or sucrose. All experiments were performed in triplicates for each experiment.

F. prausnitzii was cultured on mYCFA agar and a preculture was prepared by inoculating single colony of *F. prausnitzii* in 5 ml of mYCFAG broth. Precultured *F. prausnitzii* was diluted in 30 ml of fresh mYCFAG broth to an initial optical density of 0.05 at 600 nm and cultured in 37°C anaerobic chamber (Coy Laboratory Products, MI, United States) containing 86% N_2, 7% CO_2 and 7% H_2. Optical densities were measured by an UV spectrophotometry (Thermo Fisher Scientific, MA, United States). To culture *F. prausnitzii* in mYCFA containing a carbohydrate source, 300 μL in the mid-log phase cultured in mYCFAG medium was inoculated in the 30 ml of mYCFA containing a carbohydrate source at 0.3% (w/v) final concentration. Glucose (Sigma-Aldrich, MO, United States), inulin (Megazyme, IL, United States), amylopectin (Sigma-Aldrich, MO, United States), arabinan (Megazyme, IL, United States), arabinoxylan (Sigma-Aldrich, MO, United States), xylan (Sigma-Aldrich, MO, United States), galactan (Sigma-Aldrich, MO, United States), lichenan (Sigma-Aldrich, MO, United States), and pullulan (Sigma-Aldrich, MO, United States) were used as sole carbon sources, respectively. These were sterilized through membrane filtration using syringe filter (CA, pore size 0.2 μm, Hyundai Micro), then added to the sterilized mYCFA medium.

SCFAs Analysis by LC-MS/MS

For the SCFAs analysis, we followed the referenced method with some modifications (Song et al., 2020). The culture supernatants of *F. prausnitzii* were harvested by centrifugation at each time points and filtrated with a syringe filter (PVDF, pore size 0.45 μm, Millipore). Then 50 μL of filtered supernatant was mixed with 450 μL HPLC-grade water (Fisher Scientific, NH, United States). Butyrate-d7 (CDN isotopes, QC, Canada) was used as internal standard compound, and dissolved in 50% Acetonitrile (ACN, Fisher Scientific, NH, United States) to 1 mM. Girard's reagent T (GT, Sigma-Aldrich, MO, United States), used for chemical

derivatization, was dissolved in 50% ACN with 40 μL/ml pyridine (Sigma-Aldrich, MO, United States) and 18 μL/ml HCl (Junsei, Tokyo, Japan) to 100 mM. Also 100 mM 1-ethyl-3-(3-dimethylaminopropyl)carbodiimide (EDC, Sigma-Aldrich, MO, United States) were dissolved in 50% ACN. GT derivatization reaction conditions were prepared as follows. First, 20 μL of diluted supernatant was mixed with 10 μL of butyrate-d7, 40 μL of 100 mM GT, 40 μL of 100 mM EDC, and 50 μL 50% of ACN followed by incubation at 40°C for 1 h. After incubation, it was diluted 100-fold with 50% ACN and analyzed by LC–MS/MS. To analyze the quantitative curve of GT-labeled butyrate, the SCFA standard mixture consists of acetate, propionate, butyrate, valerate, caproate (Sigma-Aldrich, MO, United States) was dissolved in 50% ACN (100 nmol/ml). It was serially diluted, and 20 μL of the diluted SCFA standard mixture was GT derivatizated and incubated as above. After incubation, it was diluted 20-fold with 50% ACN and analyzed by LC–MS/MS. The number of molecules of GT-labeled SCFA injected into LC–MS/MS was as follows: 1,000 pmol, 200 pmol, 50 pmol, 10 pmol, 2 pmol, 500 fmol, 100 fmol, 20 fmol, 5 fmol, 1 fmol, and 0 fmol.

LC–MS/MS analysis was performed using an integrated system composed of Acquity UPLC H-Class (Waters, MA, United States) and LTQ XL™ Linear Ion Trap Mass Spectrometer (Thermo Fisher Scientific, MA, United States). Then 5 μL of reaction mixture of GT-labeled butyrate was injected into Zorbax HILIC plus column (4.6 × 100 mm, 3.5 μm, Agilent, CA, United States). Solvent C comprised water containing 20 mM ammonium acetate and 20 mM acetic acid while solvent D was 100% ACN. GT-labeled SCFAs were separated on the analytical column at a flow rate of 0.3 ml/min. The LC gradient method was set as follows: t = 0 min, 70% D; 1 min, 70% D; 10 min, 30% D; 15 min, 30% D; 15.1 min, 70% D; and 20 min, 70% D. The mass spectrometer was operated in positive ion mode. The normalized collision energy was 35.

Preparation of Intracellular Proteomic Analysis

For the preparation of intracellular proteomic analysis, we used the filter-aided sample preparation (FASP) method with some modifications (Wiśniewski et al., 2009). Cell pellets of *F. prausnitzii* were harvested by centrifugation at the mid-log phase and were washed two times with phosphate-buffered saline (PBS) at 4°C. Cell pellets were resuspended with RIPA buffer (Thermo Fisher Scientific, MA, United States) supplemented with 0.1% protease inhibitor cocktail (Sigma-Aldrich, MO, United States) and sonicated on ice by a probe sonicator (Sonics & Materials, Inc., CT, United States) for cell lysis. After cell lysates were centrifuged at 4,000 rpm for 10 min at 4°C, supernatants were obtained. The protein concentration was measured by the bicinchoninic acid protein assay kit (BCA assay; Thermo Fisher Scientific, MA, United States) according to the manufacturer's instructions. For protein reduction, dithiothreitol (DTT) was added to a final concentration of 50 mM and incubated for 5 min at 95°C. 200 μg of reduced proteins were transferred to 30 k filter units (Microcon; Millipore, MA, United States). 200 μL of UA buffer (8 M urea in 0.1 M Tris-HCl, pH 8.5) was added to the device and centrifuged at 10,000 xg for 15 min at 20°C. This step was repeated 3 times, and proteins were alkylated by addition of 100 μL of 0.05 M iodoacetamide (IAM) in UA buffer and incubation in the dark and at room temperature for 20 min. After centrifugation, the concentrate was diluted with 100 μL of UA buffer and centrifuged and repeated this step twice. Subsequently, 100 μL 0.05 M Tris-HCl, pH 8.5 were added to filter unit and centrifuged again. This step was repeated 2 times, and the prepared proteins were digested by trypsin. To collect the digests, 250 μL of 0.05 M Tris-HCl, pH 8.5 was added to filter unit and centrifuged. Then the digests were desalted on Pierce Peptide Desalting Spin Columns (Thermo Fisher Scientific, MA, United States) according to the instructions provided by the manufacturer. Purified samples were dried with a centrifugal vacuum concentrator (Vision Scientific, Seoul, Korea) and stored at −80°C until used for analysis.

Intracellular Proteome Analysis by LC-MS/MS

Proteomic analysis was performed as described previously (Jo et al., 2020). Briefly, the dried samples were dissolved in solvent A (0.1% v/v formic acid in water) before the analysis. Proteomic analysis was performed using nano-HPLC, Ultimate 3,000 RSLCnano LC system (Thermo Scientific, MA, United States). Q Exactive Hybrid Quadrupole-Orbitrap (Thermo Scientific, MA, United States) equipped with a nano-electrospray ionization source was used in combination with the nano-HPLC. Samples were trapped in an Acclaim PepMap 100 trap column (100 μm × 2 cm, nanoViper C18, 5 μm, 100 Å, Thermo Scientific, MA, United States). Then, solvent A (98%) was used to wash the column at a flow rate of 4 μL/min for 6 min. After washing, the samples were separated at a flow rate 350 nL/min. An Acclaim PepMap 100 capillary column (75 μm × 15 cm, nanoViper C18, 3 μm, 100 Å, Thermo Scientific, MA, United States) was used for LC separation. The LC gradient was as follows: 0 min, 2% B; 30 min, 35% B; 40 min 90% B, 45 min, 90% B; 60 min, 5% B. Solvent A (0.1% formic acid in water) and solvent B (0.1% formic acid in acetonitrile) were used. The ion spray voltage was 2,100 eV. MS data were collected using Xcaliber software. The Orbitrap analyzer scanned precursor ions with a mass range of 350–1800 m/z and a resolution of 70,000 at m/z 200. For collision-induced dissociation (CID), up to the 15 most abundant precursor ions were selected. The normalized collision energy was 32.

Protein identification and label-free quantification (LFQ) were performed using MaxQuant software (Cox et al., 2014). Proteins were identified by searching MS and MS/MS data of peptides against the UniProt database. Statistical analysis of LFQ data was processed with the R statistical programming environment (Shah et al., 2020). Quantified protein data were processed with Perseus software, and the significance was determined using the adjusted *p*-value (Tyanova et al., 2016).

Intracellular Metabolite Extraction

A cell pellet was obtained from 10 ml of culture by centrifugation at 3,000 rpm at 4°C for 10 min and washed twice with the sterile

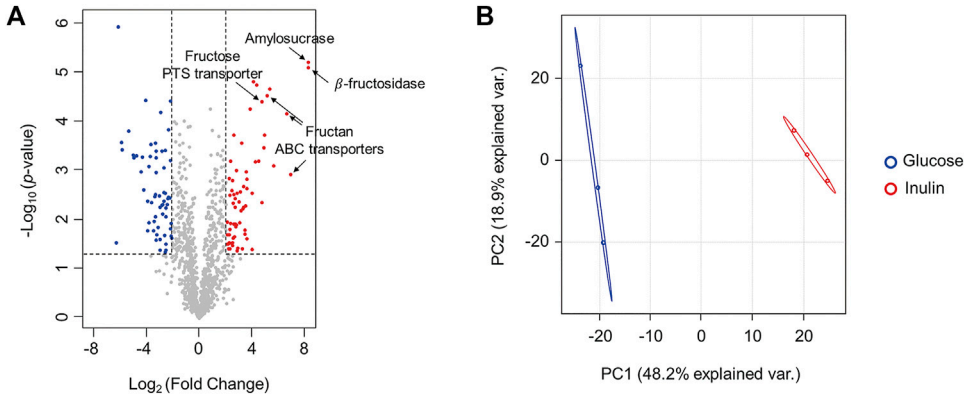

FIGURE 3 | Comparison of proteomic changes of *F. prausnitzii* grown in mYCFA supplemented with glucose or inulin. **(A)** Volcano plot for proteomic changes of *F. prausnitzii* grown in mYCFA supplemented with glucose or inulin. Volcano plots indicate the upregulated proteins of inulin-grown *F. prausnitzii* in red circles and downregulated proteins in blue circles. Indications are proteins discussed in this study. **(B)** Principal component analysis (PCA) plot of proteomic analysis for *F. prausnitzii* grown in each carbon source. Proteomic analysis was performed in triplicates.

PBS at 4°C. Then, 1 ml of 80% cold methanol (−80°C, HPLC grade, Fisher Scientific, NJ, United States) was added to each cell pellet to extract intracellular metabolites. After samples were vortexed for 1 min, they were incubated at −80°C for 1 h. The supernatant was obtained after centrifugation at 13,000 rpm for 3 min at 4°C. For re-extraction, cold 80% methanol was added to cell pellets remained and they were incubated at −80°C for 1 h. Next, supernatant was obtained as described above, and the extraction step of 1 h was repeated one more. Finally, the metabolite samples were dried using centrifugal vacuum concentrator (Hanil Science Industrial, Gimpo, Korea) and stored at −80°C before analysis.

Intracellular Metabolome Analysis by LC-MS/MS

The metabolite samples were dissolved in 50% methanol containing 10 μg/mL L-Phenylalanine $^{13}C_9$, ^{15}N (Sigma-Aldrich, MO, United States) as an internal standard (IS). They were filtrated with a syringe filter (PVDF, pore size 0.45 μm, Millipore). Prepared samples were transferred to LC vials, and LC-MS/MS analysis was performed. Analysis was performed using a 1,260 Infinity Binary HPLC system (Agilent, CA, United States) combined with a 6,420 Triple Quadrupole LC-MS system (Agilent, CA, United States). Injected metabolites were separated using an Xbridge amide column (4.6 × 100 mm, 3.5 μm particle size, Waters, MA, United States) with solvent A (25 mM ammonium acetate (HPLC grade, Fisher Scientific, NJ, United States) and 25 mM ammonium hydroxide (HPLC grade, Fisher Scientific, NJ, United States) in 95: 5 = water: ACN) and solvent B (100% ACN) given a gradient to analysis. The flow rate was 0.4 ml/min and the electrospray ionization voltage was 4 kV. The LC gradient was as follows: 0 min, 85% B; 5 min, 45% B; 16 min, 0% B; 24 min, 0% B; 25 min, 85% B; 32 min, 85% B. MS peak areas were extracted using Agilent MassHunter Qualitative Analysis software. The peak area was normalized using the peak area of internal standard. The False Discovery Rate (FDR)-corrected *p*-values were provided using the Statistical analysis module of Metaboanalyst 5.0 (Pang et al., 2021).

mRNA Isolation and Quantitative Analysis by qRT-PCR

Cell pellets *of F. prausnitzii* in the mid-log phase were harvested by centrifugation at 4°C and total RNA was isolated by using TRIzol reagent (Takara, Tokyo, Japan), following the supplier's instructions. The RNA concentration and the purity were measured by spectrophotometry (Thermo Fisher Scientific, MA, United States). The extracted RNA was reverse transcribed into cDNA using a cDNA synthesis kit (Bio-Rad, CA, United States). PCR primer sequences for β-fructosidase, amylosucrase, and GAPDH were designed in this study by using SnapGene software (Version 3.1; GSL Bio-tech, snapgene.com) and shown in **Supplementary Table S6**. GAPDH was used as an internal control for normalize the mRNA expression levels of all genes. The sample mixtures for qRT-PCR were prepared with SsoAdvanced Universal SYBR Green Supermix (Bio-Rad, CA, United States). The qRT-PCR was performed using the CFX connect (Bio-Rad, CA, United States) under the following conditions: 40 cycles of denaturation at 95°C for 15 s, annealing at 60°C for 30 s. The results were analyzed using CFX Maestro software (Bio-Rad, CA, United States). All experiments were performed in three biological replicates for each experiment.

Cloning of *bfrA* Gene and *ams* Gene

The β-fructosidase gene was amplified from genomic DNA of *F. prausnitzii* using primer *bfrA*_F (5′-ATATGGATCCATGAA CGATTTGACTTTACA-3′) and *bfrA*_R (5′-ATATCTCGA GTTACAGATTCAGTTCAAACT-3′). And the amylosucrase gene was amplified from genomic DNA of *F. prausnitzii* using *ams*_F (5′-ATATGGATCCATGGCAGCAAAACAGGAATT-3′) and *ams*_R (5′-ATATCTCGAGTTATTTGTTTTTTACCA GCA-3′). The DNA fragments were amplified by PCR with an

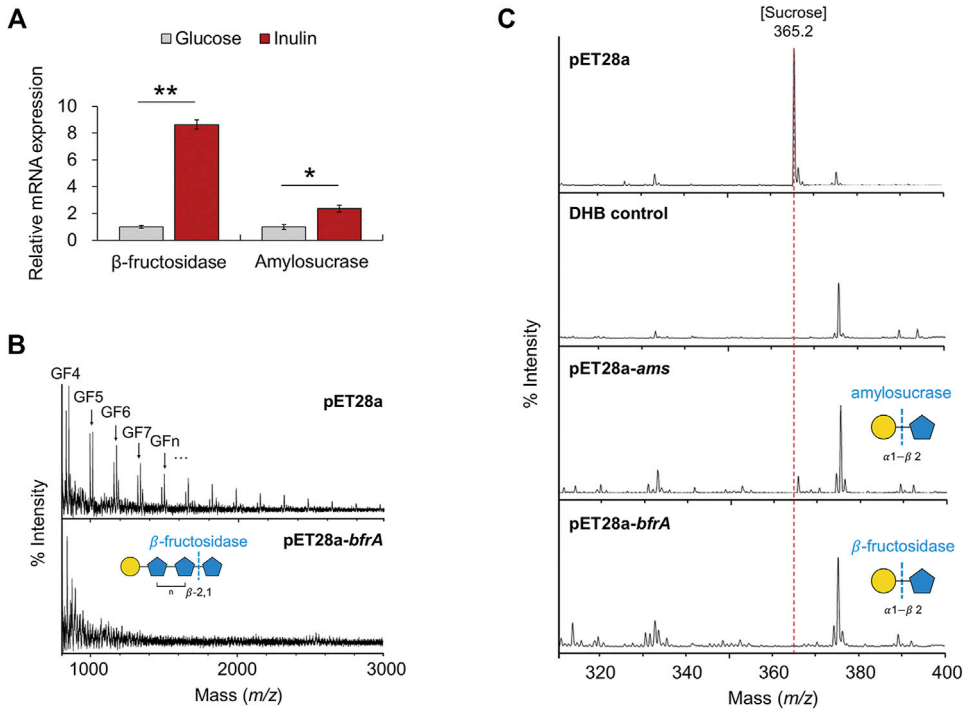

FIGURE 4 | Mass spectrometry analysis of cell lysates. **(A)** mRNA expression of glycoside hydrolases (β-fructosidase, amylosucrase). The error bars indicate the standard deviation of triplicate samples. $^{*}p < 0.05$, $^{**}p < 0.01$. **(B)** MALDI-TOF-MS spectra of inulin degraded by cell lysates of pET28a-*bfrA*. Peaks are labeled by DP. G, glucose; F, fructose. All molecular ions are $[M + Na]^+$. **(C)** MALDI-TOF-MS spectra of sucrose degraded by cell lysates of pET28a-*ams*, and pET28a-*bfrA*. All molecular ions are $[M + Na]^+$.

Automated Thermal Cycler (Thermo Fisher Scientific, MA, United States) from the following PCR mixture: 50 ng genomic DNA, 1 μM of each primer, 0.2 mM of each dNTP, polymerase buffer, and herculase II Fusion DNA Polymerase (Agilent, CA, United States). PCR conditions were 95°C for 5 min, followed by 25 cycles of 95°C for 30 s, 50°C for 30 s, and 72°C for 1 min, with a final extension period of 5 min at 72°C. The PCR products were purified and cloned into the pET28a, yielding pET28a-*bfrA* and pET28a-*ams*. The cloning products were heat-transformed into *E. coli* strain DH5α. After the colony selection on LB agar plate with ampicillin, the selected colony was grown overnight in LB broth at 37°C. Constructed vectors were extracted and stored at −70°C.

Protein Expression

β-fructosidase and amylosucrase were expressed using *E. coli* BL21 (DE3). The constructed vectors were transformed into competent cells of *E. coli* BL21. *E. coli* BL21 cells containing pET28a-*bfrA* and pET28a-*ams* were cultured at 37°C in LB medium containing 100 μg/ml ampicillin until OD600 nm reached 0.6–0.8. Expressions of *bfrA* and *ams* were induced by addition of 0.5 mM isopropyl-β-d-thiogalactoside (IPTG) with subsequent overnight incubation at 18°C. The cells were harvested by centrifugation (3,500 xg, 10 min, 4°C), and the pellet was resuspended in Tris buffer solution containing 50 mM Tris-HCl (pH 8.0), 200 mM NaCl and 10% (v/v) glycerol. After ultrasonification in ice-chilled water, the extracts were centrifuged (13,000 xg, 30 min, 4°C) and the supernatants were harvested. To confirm the protein molecular weight, the soluble fraction of lysates was loaded into 12% sodium dodecyl sulfate-polyacrylamide gel electrophoresis (SDS–PAGE) at 50 V for 15 min and 130 V for 60 min after the denaturation process (**Supplementary Figure S1**). Protein concentrations were measured using the Bradford assay.

Enzymatic Function Assay

The enzymatic functions were measured in a 50 μL volume that contained 36 ng of proteins in soluble fractions of the cell lysates and 10 mg/ml of sucrose or inulin in 50 mM sodium phosphate buffer. The reaction was performed at 37°C for 10 min and stopped by heating at 95°C for 10 min. The reaction products were centrifuged (16,000 xg, 5 min, 4°C) and mass spectra of the supernatant were analyzed by matrix-assisted laser desorption ionization-time of flight mass spectrometry (MALDI-TOF-MS, Bruker Daltonics, MA, United States). Briefly, 1 μL of the supernatants was mixed with 1 μL of 2,5-dihydroxybenzoic acid (DHB) solution. And 1 μL of the mixture was spotted and dried on a stainless steel MALDI plate. MALDI spectra was obtained by scanning a total of 600 shots from six different spots in positive ion mode. The operating conditions were as follows: accelerating voltage 20 kV; laser frequency 60 Hz; ion

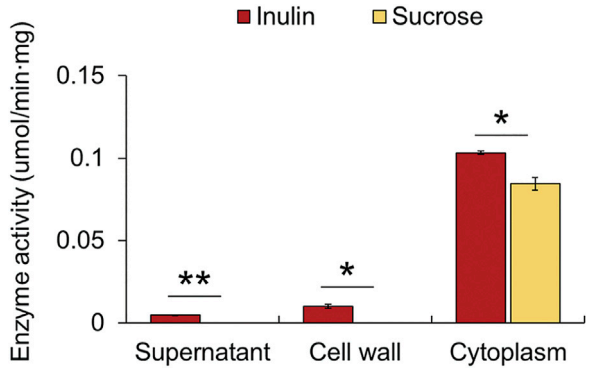

FIGURE 5 | Fructan hydrolase enzyme activities in three fractions of the cell: cell-free supernatant, cell wall extract, and cytoplasmic extract. The activity was measured by determining the amount of fructose released per min per mg of protein. The error bars indicate the standard deviation of duplicate samples. *$p < 0.05$, **$p < 0.01$.

source 1 voltage 19 kV; ion source 2 voltage 16 kV; lens voltage 9.8 kV; detector gain 5.8 and laser power 70%. The average spectrum profiles obtained were visualized with FlexAnalysis 3.3 software (Bruker Daltonics, MA, United States).

Fructan Hydrolysis Assay

Fructan hydrolysis assay was performed following the referenced methods with some modifications (Goh et al., 2007; Fang et al., 2021). After the cell pellet of *F. prausnitzii* cultured in the mYCFAG was washed and re-suspended in carbohydrate-free mYCFA, 300 µL was inoculated in the 30 ml of mYCFA medium supplemented with 0.3% (w/v) inulin. Cell fractionation was performed when the *F. prausnitzii* was in the mid-log phase. The cells were harvested by centrifugation at 3,000 xg for 15 min at 4°C. The culture supernatant was filtered and sterilized with a syringe filter (PES, pore size 0.2 µm, Hyundai Micro), and concentrated using an Amicon Ultra-4 ultrafiltration centrifuge tube (30 k; Millipore, MA, United States). The cell pellet was washed twice in 100 mM potassium phosphate buffer (pH 7.0) and resuspended in 1 ml of the same buffer. The cell suspension was transferred into microtube and sonicated on ice by a probe sonicator (Sonics & Materials, Inc., CT, United States). Then, the cell lysate was transferred into a new tube, and the fraction containing cell wall fragments was separated from the cytoplasmic fraction by centrifuging at 13,800 xg for 10 min at room temperature. Then the cell wall fraction was resuspended in 1 ml of phosphate buffer, and the cytoplasmic extract was concentrated by using an Amicon Ultra-4 ultrafiltration centrifuge tube.

The concentrated culture supernatant, cell wall fraction, or cytoplasmic extract was added to 190 µL of 0.3% (w/v) sucrose or inulin solution. The reaction mixture was incubated at 37°C for 3 h, and inactivated at 95°C for 3 min. The fructan hydrolysis activity was measured by determining the amount of fructose released per min per mg of protein. The fructose concentration was determined by high-performance liquid chromatography using an Xbridge amide column (Waters, MA, United States). The protein concentration was measured by the BCA assay kit according to the manufacturer's instructions.

Fermentation Experiments

For the comparison of the growth of *F. prausnitzii* according to the sole carbon source, the cell pellet of *F. prausnitzii* cultured in the mYCFAG was washed twice with carbohydrate-free mYCFA and re-suspended in carbohydrate-free mYCFA. 300 µL of this suspension was inoculated onto 30 ml of mYCFA containing 0.3% (w/v) glucose, fructose, sucrose, and inulin as the sole carbon source, respectively. Inulin was sterilized at 121°C for 15 min and the others were sterilized through membrane filtration using CA syringe filter, then they were added to the sterilized mYCFA medium. Glucose, fructose was purchased from Sigma-Aldrich (MO, United States), sucrose was purchased from Junsei (Tokyo, Japan), and inulin was purchased from Megazyme (IL, United States). According to the information supplied by the company, the DP of the inulin chains is varied between 2 and 60. *F. prausnitzii* was

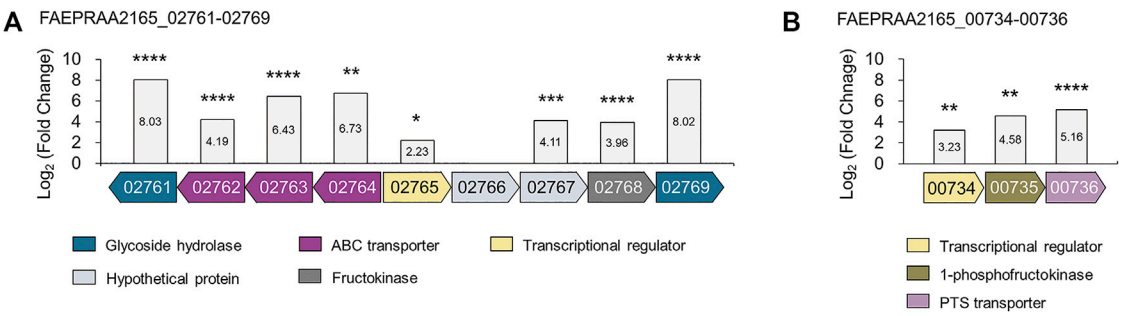

FIGURE 6 | The gene organization of proteins upregulated from proteomic analyses of *F. prausnitzii* grown on inulin relative to glucose. Proteins involved in **(A)** inulin-type fructan utilization and **(B)** fructose uptake were annotated. The locus tag numbers FAEPRAA2165_XXXXX are abbreviated with the last numbers after the hyphen. Proteins with similar predicted functions are colored by the same color. The $\log_2$ (fold-change) relative to *F. prausnitzii* grown on glucose is shown on the *y*-axis. The proteomic analysis was performed in triplicates. *$p < 0.05$, **$p < 0.01$, ***$p < 0.001$, ****$p < 0.0001$., Protein annotation: β-fructosidase (02761); fructan ABC transporters (02762–02764); LacI family transcriptional regulator (02765); hypothetical proteins (02766–02767); fructokinase (02768); amylosucrase (02769); DeoR family transcriptional regulator (00734); 1-phosphofructokinase (00735); fructose PTS transporter (00736).

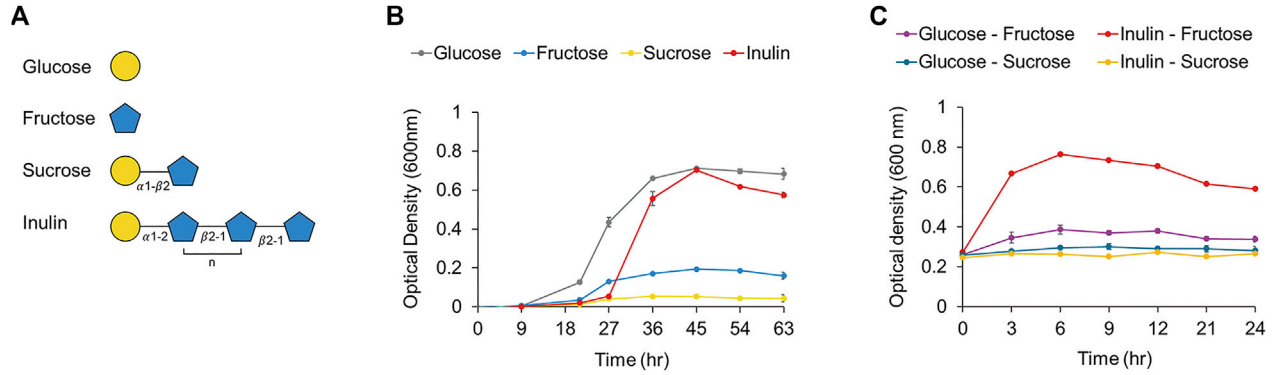

FIGURE 7 | (A) Structures of the components (i.e., glucose, fructose, sucrose, inulin). of inulin were shown. **(B)** The growth curve of *F. prausnitzii* cultured in mYCFA supplemented with either glucose, fructose, sucrose, or inulin. **(C)** The growth curve of *F. prausnitzii* cultured in mYCFA supplemented with either fructose or sucrose. Cells cultured in inulin or glucose were harvested and inoculated in fructose or sucrose. Each point on the curves represents the average of three independent experiments. Error bars represent standard deviations (s.d.).

cultured anaerobically at 37°C and optical densities of the cultures were measured at 600 nm.

Also, the bacterial pellet cultured in mYCFA supplemented with 0.3% (w/v) glucose or inulin was re-suspended in carbohydrate-free mYCFA when the OD600 nm reached 1.11 or 0.57, respectively. Then, 300 µL of this suspension was inoculated onto 30 ml of mYCFA containing 0.3% (w/v) fructose or sucrose. Culture was performed anaerobically at 37°C and optical densities at 600 nm were measured.

Comparative Genomic Analysis

A BLAST search using the UniProt database was applied to determine the protein sequence alignments and the BLAST hits with a cut-off of E-value <0.0001. The output of sequences producing significant alignments (E-value <0.0001) against other *F. prausnitzii* strains was determined by NCBI BLASTP online tool.

Statistical Analysis

Statistical analysis was performed using R statistical programming environment. Data was expressed as the means ± s.d. All data was normalized with mean of control, and significant differences of between two groups was assessed to the unpaired two-tailed Student's *t* test. $p < 0.05$ were defined as quantitatively significant. Statistical comparison was indicated with *, **, ***, **** for $p < 0.05$, $p < 0.01$, $p < 0.001$, $p < 0.0001$ respectively.

RESULTS AND DISCUSSION

Increased Fermentation Ability and Butyrate Productivity of *F. prausnitzii* Grown on Inulin

First, we added glucose and eight polysaccharides (i.e., inulin, amylopectin, arabinan, arabinoxylan, xylan, galactan, lichenan, and pullulan) as the sole carbon source to a carbohydrate-free medium and observed the growth of four major compositional species among human intestinal butyrate-producing bacteria (i.e., *F. prausnitzii, E. rectale, R. hominis,* and *R. intestinalis*), to explore the preference for dietary fibers. Among these butyrate-producing bacteria, only *F. prausnitzii* could grow on inulin as the sole carbon source. While the growth of all strains was enhanced when grown on glucose, *F. prausnitzii* was also able to grow on glucose and inulin, as previously reported (**Figure 1**) (Duncan et al., 2002; Desai et al., 2016; Louis and Flint, 2017). We also measured the production of butyrate, a beneficial metabolite to the intestine, from *F. prausnitzii* grown on each carbon source; high butyrate productivity was observed when glucose or inulin was used as the sole carbon source (**Figure 2**). The highest productivity of butyrate was observed after culturing for 45 h on inulin, which was 65% of that produced by using glucose as the carbon source.

To efficiently produce butyrate by using a substrate in a non-competitive manner with other bacteria in the intestine, it was preferable to use highly selective inulin, instead of glucose, as the carbon source for *F. prausnitzii*, which has excellent growth ability against most of the other gut bacteria. Findings from *in vivo* inflammatory models have proved that the ingestion of prebiotics, such as inulin, is effective in promoting host health, by inducing selective growth of butyrate-producing *F. prausnitzii*

TABLE 1 | The metabolomic changes involved in the energy metabolism of *F. prausnitzii* according to fermentation of inulin or glucose. Data are presented with different four samples (n = 4) by LC-MS/MS. *$p < 0.05$, **$p < 0.01$, ***$p < 0.001$ by two-tailed Student's t-test.

Name	Log_2FC (Inulin/Glucose)
Citrate	1.23***
Aconitate	0.98*
Fructose 6-phosphate	0.92*
Succinyl-CoA	0.92*
Glucose 6-phosphate	0.89*
Fructose 1,6-bisphosphate	−0.6**
Adenosine triphosphate	−0.66***
Acetyl-CoA	−1.22**
Succinate	−1.76***
Malate	−1.92***

and possessing immunomodulatory properties, such as intestinal barrier protection and anti-inflammatory effects in (Sokol et al., 2008; Varela et al., 2013; Martín et al., 2015; Miquel et al., 2015; Lopez-Siles et al., 2016). However, research on the precise mechanism and degrading enzymes involved in the selective utilization of inulin in *F. prausnitzii* remains limited; molecular-based characterization is required to induce butyrate production *in vivo* using *F. prausnitzii* and for the commercial use of related strains and enzymes in future. Therefore, we applied integrative proteomics-metabolomics approaches, to explore the changes occurring at the molecular level in inulin utilization by *F. prausnitzii* and to characterize the related degrading enzymes.

Proteomic Changes of *F. prausnitzii* Grown on Inulin

To investigate proteins involved in inulin utilization by *F. prausnitzii*, we investigated the intracellular proteomic changes in *F. prausnitzii* after culturing them using inulin or glucose, which showed growth potential as the sole carbon source. A total of 1,125 proteins were identified, of which 68 proteins were significantly upregulated ($\log_2$ (fold-change) >2, $p < 0.05$), and 62 proteins were significantly downregulated ($\log_2$ (fold-change) <-2, $p < 0.05$) during growth in inulin, compared to growth in glucose (**Figure 3A**, **Supplementary Table S1**). In addition, principal component analysis revealed that proteomic results of *F. prausnitzii* were significantly different when glucose and inulin were cultured as the sole carbon source (**Figure 3B**). Proteomic analysis showed that the function of upregulated proteins in inulin media was mainly associated with carbohydrate metabolism. In particular, glycoside hydrolases and ABC transporters were involved in inulin-type fructan degradation and intracellular transport, and the PTS transporter involved in fructose uptake were significantly upregulated.

Glycoside Hydrolases Upregulated in *F. prausnitzii* Grown on Inulin

Proteomic analysis revealed that the most upregulated protein during growth in inulin compared to growth in glucose was a 261-fold upregulated enzyme, which belongs to glycoside hydrolase family 32 (GH32) (**Figure 3A**). A Basic Local Alignment Search Tool (BLAST) search for the amino acid sequence of this protein revealed ≥85% sequence identity with β-fructosidases (levanase/invertase), sucrose-6-phosphate hydrolase (sacA), and β-fructofuranosidase of *F. prausnitzii* L2-6, *F. prausnitzii,* and *Gemmiger formicilis*, respectively (**Supplementary Table S2**). All of them are hydrolytic enzymes belonging to the GH32 family and function as β-fructosidase (EC 3.2.1.26), which hydrolyzes the β-D-fructofuranoside bond of sucrose or inulin-type fructan and degrades them into fructose monosaccharides. A BLAST search also confirmed that the query sequence of this protein was highly conserved with the aligned sequences even in other *F. prausnitzii* strains (**Supplementary Table S3**). In addition, the second upregulated protein was an α-amylase catalytic domain protein that was upregulated 260-fold during growth in inulin compared to growth in glucose. A BLAST search revealed a sequence identity of

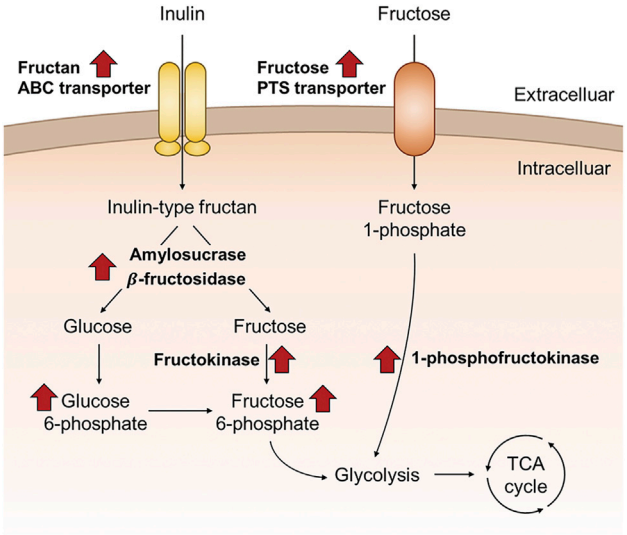

FIGURE 8 | Schematic overview of the proposed inulin utilization pathway of *F. prausnitzii* that were discovered in this study, based on the proteomic and metabolomic data of *F. prausnitzii* grown on inulin relative to glucose.

≥98% with amylosucrase (ams) and the degree of conservation of this protein among different *F. prausnitzii* strains (**Supplementary Tables S4, S5**). Amylosucrase (EC 2.4.1.4) is a hydrolase belonging to the GH13 family and is a glucose transference, which cleaves sucrose into glucose and fructose and transfers glucosyl residues to the glucan chain to form α-1,4-linked glucan (Montalk et al., 1999; Tian et al., 2018). Therefore, putative β-fructosidase and amylosucrase are enzymes capable of hydrolyzing inulin-type fructan and sucrose. However, while amylosucrase is a hydrolase, which uses sucrose as a substrate, β-fructosidase could degrade both the β-2,1 fructose-glucose bond and the β-2,1 bond between fructose, when a polymer such as inulin-type fructan is present as the substrate. β-fructosidase (EC 3.2.1.26) of *Thermotoga maritima* can release fructose from the inulin terminus by an exo-type mechanism and form sucrose (Liebl et al., 1998). In contrast, β-fructofuranosidase (EC 3.2.1.26) of *Bifidobacterium breve* UCC2003 cleaves the β-2,1 bond of glucose-fructose in sucrose and fructooligosaccharide (FOS) substrates, but not the β-2,1 bond between fructose (Ryan et al., 2005). Thus, even the same enzyme may have different functions depending on the source species and the substrate on which it acts. Therefore, we attempted to characterize the exact function of putative β-fructosidase and amylosucrase of *F. prausnitzii* by analyzing the enzyme activity and substrate specificity.

Intracellular Inulin-type Fructan Degrading Enzymes Upregulated in *F. prausnitzii* Grown on Inulin

To characterize putative β-fructosidase and amylosucrase upregulated during the growth of *F. prausnitzii* on inulin, we investigated mRNA expression levels of the genes encoding each

hydrolase, using quantitative real time polymerase chain reaction analysis. The mRNA expression levels of β-fructosidase and amylosucrase significantly increased by 8.64-fold and 2.35-fold, respectively, during growth in inulin, compared to the levels observed during growth in glucose, similar to the data obtained from proteome analysis (**Figure 4A**). In addition, to evaluate the degradation activity of these enzymes on inulin and sucrose substrates, we cloned *bfrA* and *ams* into the pET28a vector and transformed them into *E. coli* BL21. The activity of the purified enzyme obtained after overexpression in *E. coli* was determined by treating the extracted cell lysate with inulin and sucrose, followed by analysis of the final product using matrix-assisted laser desorption/ionization-time of flight mass spectrometry. It was found that all lengths of inulin (DP = 2–60) were hydrolyzed by the pET28a-*bfrA* recombinant strain lysate regardless of the DP (**Figure 4B**). Thus, the putative β-fructosidase could cleave all of the β-2,1 bonds between the fructose of inulin-type fructan. In addition, sucrose was degraded by the pET28a-*ams* and pET28a-*bfrA* recombinant strains (**Figure 4C**). These results showed that putative amylosucrase and putative β-fructosidase were enzymes capable of cleaving the α1- β2 bond between α-D-glucose and β-D-fructose. However, although we established the hydrolytic activity of the two hydrolases on inulin-type fructan and sucrose through the recombinant strains, it remains unclear whether the degradation in the metabolic pathway of the enzyme was intracellular or extracellular.

It is predicted that many cell wall-associated proteins of Gram-positive bacteria are anchored to the cell wall through the LPxTG (where x is any amino acid) cell wall anchor motif located in the C-terminal region of the amino acid sequence (Navarre and Schneewind, 1994). A cell wall anchor motif is present in the β-fructosidase of *Lactiplantibacillus plantarum* P14 and P76 and *Lacticaseibacillus paracasei* 1,195, and it has been confirmed that a cell wall-anchored β-fructosidase degrades fructan outside the cell (Goh et al., 2007; Buntin et al., 2017). In contrast, it is known that β-fructosidase of *Lactobacillus acidophilus* NCFM is a cytoplasmic protein, since it does not contain the LPxTG sequence and hence is expected to be an intracellular enzyme (Barrangou et al., 2003). However, we could not identify a specific sequence corresponding to the characteristic cell wall anchor motif from the amino acid sequences of β-fructosidase and amylosucrase (data not shown). Therefore, it could be predicted that both these enzymes are intracellular, which degrade inulin-type fructan transported into cells. Additionally, subcellular localization of the protein through PSORT Version 3.0.3 revealed that the two hydrolases were >99.7% cytoplasmic (Yu et al., 2010). To determine the location of the hydrolases more accurately, *F. prausnitzii*, cultured in inulin as a sole carbon source, was extracted by dividing it into three fractions: cell-free supernatant, cell wall extract, and cytoplasmic extract, and the amount of fructose released was measured when inulin and sucrose were used as substrates. When inulin was used as a substrate, the cytoplasmic extract showed 22 times more hydrolytic activity than the supernatant and 10 times more hydrolytic activity than the cell wall extract; when sucrose was used as a substrate, only the cytoplasmic extract showed activity (**Figure 5**). Therefore, it was confirmed that the enzyme that degraded inulin-type fructan in inulin metabolism of *F. prausnitzii* was an intracellular enzyme, which degrades inulin-type fructan transported into the cell.

Uptake of Inulin-Type Fructans by Upregulated Fructan ABC Transporters in *F. prausnitzii* Grown on Inulin

From the proteomic results, we confirmed that glycoside hydrolases and proteins involved in the intracellular transport of sugars were upregulated 18-fold or more during growth in inulin (**Figures 6A**,**B**). A BLAST search confirmed that these proteins were ABC transporters, which transport substrates using ATP as an energy source, and the PTS transporter that transports sugar into cells and simultaneously phosphorylates it (**Supplementary Table S7**) (Saurin et al., 1999; Deutscher et al., 2006). The metabolism of sugar using transport systems, such as ABC and PTS transporters, generally follows two metabolic pathways. Interestingly, various studies have reported that transport systems are involved in inulin-type fructan utilization together with β-fructosidase in various probiotic bacteria. First, inulin-type fructan enters the cell, in an undigested state through the transporter, and is degraded by the cytoplasmic enzyme, which can be mainly taken up by the ABC transporter in this case. Tsujikawa et al. reported that *Lactobacillus delbrueckii* JCM 1002T transported inulin (DP > 8) into cells in an undigested state through the inulin ABC transporter (Tsujikawa et al., 2013; Tsujikawa et al., 2021). In addition, the ABC transport system of *Lactobacillus acidophilus* NCFM is involved in FOS (DP 2–4) utilization, together with intracellular β-fructosidase (*bfrA*) (Barrangou et al., 2003). Second, after the substrate is degraded by enzymes present in the extracellular space or the cell wall, the product enters the cell through the PTS transporter. Goh Yong et al. showed that when *Lactobacillus paracasei* 1,195 degrades FOS (DP < 10) extracellularly through cell wall-anchored β-fructosidase, the generated fructose and sucrose are taken up into cells through each PTS transporter (Goh et al., 2006; Goh et al., 2007). In addition, in fructan utilization by *Roseburia inulinivorans* A2-194, inulin-type fructan (DP 2–60) is transported into cells by the ABC transporter and degraded by β-fructofuranosidase, while the PTS transporter is reported to be involved in the uptake of fructose (Scott et al., 2011). This study confirmed the intracellular activity of β-fructosidase of *F. prausnitzii* using an enzyme assay. Therefore, it is predicted that the inulin-type fructan enters into cells in its original state through the putative ABC transporter and is then degraded by cytoplasmic β-fructosidase.

Furthermore, bacterial carbohydrate utilization is generally caused by the co-regulation of genes encoding carbohydrate hydrolases, transporters, and transcriptional regulators in adjacent positions (Barrangou et al., 2003; Goh et al., 2007). We found that the location of the genes encoding β-fructosidase, amylosucrase, and putative ABC transporters were located adjacent to those of the putative fructokinase and putative

LacI family regulator (locus tag FAEPRAA2165_02761-02769), which were upregulated 15.56-fold and 4.69-fold, respectively, during growth in inulin (**Figure 6A**, **Supplementary Table S7**). Interestingly, these proteins had a similar gene organization to β-fructofuranosidase, ABC transporters, 6-phosphofructokinase, and LacI family regulators, belonging to the fructan utilization gene cluster induced during inulin growth in *R. inulinivorans*. Especially, β-fructofuranosidase, and three ABC transport system components shared 45–66% identity with β-fructofuranosidase and ABC transporters in this study (**Supplementary Table S8**). Accordingly, we suggest that *F. prausnitzii* utilizes inulin-type fructan (DP 2–60) by uptake into cells through fructan ABC transporter and degradation by cytoplasmic β-fructosidase, similar to fructan utilization by *R. inulinivorans*. However, further research is needed to determine the exact DP of inulin-type fructan taken up into the cell through the fructan ABC transporter.

Upregulated Fructose Uptake Ability in *F. prausnitzii* Grown on Inulin

We confirmed that the putative PTS transporter was upregulated 35-fold in *F. prausnitzii* grown on inulin (**Figure 6B**). A BLAST search confirmed that this transporter responds specifically to fructose; a recent study has reported that a fructose-specific PTS transporter participates in the intracellular transport of fructose and is induced when *F. prausnitzii* is grown in the presence of fructose (**Supplementary Table S7**) (Kang et al., 2021). In addition, proteomic data confirmed that the transcriptional regulator and 1-phosphofructokinase encoded by the gene adjacent to the gene of the fructose PTS transporter were upregulated (**Figure 6B**). Because the PTS transporter transports sugar into the cell and simultaneously phosphorylates it, *F. prausnitzii* is expected to take up fructose into the cell through the fructose PTS transporter and phosphorylate it to fructose 1-phosphate, which is subsequently converted into fructose 1,6-bisphosphate by 1-phosphofructokinase and enters the glycolytic pathway (Kang et al., 2021). To explore the activity of the fructose PTS transporter, we compared the growth ability of *F. prausnitzii* on glucose, fructose, sucrose, and inulin produced during the digestion process of inulin (**Figure 7A**). As a result, *F. prausnitzii* showed a significant growth ability on glucose and inulin substrates, but a relatively low growth ability in fructose, and growth was difficult in sucrose (**Figure 7B**). These results demonstrated that *F. prausnitzii* preferred to utilize inulin, which has a higher DP than fructose and sucrose, and the transport of inulin-type fructan through the fructan ABC transporter was more dominant than that of fructose through the fructose PTS transporter. In addition, to investigate whether inulin induced upregulation of the fructose PTS transporter in *F. prausnitzii* results in increased uptake of fructose by cells, we inoculated *F. prausnitzii*, isolated in the mid-log phase grown on glucose or inulin, to a new medium supplemented with fructose and sucrose, and compared the growth. The growth ability of inulin-grown *F. prausnitzii* on fructose was significantly higher than that of glucose-grown *F. prausnitzii*. (**Figure 7C**). These results suggested that when *F. prausnitzii* utilized inulin, and the fructose PTS transporter was upregulated, thereby enhancing the ability to uptake fructose into cells. Interestingly, *F. prausnitzii* could not uptake sucrose despite the upregulation of the fructose PTS transporter and fructan ABC transporter. These results revealed that sucrose could not be transported through the fructose PTS transporter because it was not degraded into fructose outside the cell and was not directly transported into the cell even in the state of undigested sucrose. In summary, we demonstrated that when *F. prausnitzii* metabolized inulin, the fructose PTS transporter, which can specifically uptake fructose into the cell, was upregulated; however, we confirmed that the transport of inulin-type fructan by the ABC transporter was more dominant. This suggested that the main pathway for inulin utilization in *F. prausnitzii* was the selective transport of inulin-type fructan into the cell through the fructan ABC transporter and the degradation of inulin-type fructan into fructose by the cytoplasmic degrading enzyme.

Metabolomic Changes of *F. prausnitzii* Grown on Inulin

We compared quantitative changes in the intracellular metabolome of *F. prausnitzii* incubated with inulin or glucose as the sole carbon source, to observe changes in metabolites related to inulin utilization in *F. prausnitzii*. In total, 129 metabolite changes were observed, and when inulin was grown as a sole carbon source, 21 metabolites were significantly upregulated (fold-change >1.5, $p < 0.05$), and 51 metabolites were downregulated (fold-change < −1.5, $p < 0.05$) (**Supplementary Figure S2**, **Supplementary Table S9**). Proteomic data have earlier revealed that when *F. prausnitzii* grows on inulin, the fructose utilization system is also activated. Thus, it could be inferred that fructokinase phosphorylates fructose, which is produced by the degradation of inulin-type fructan that is transported inside the cell by fructan ABC transporter, and converts it into fructose-6-phosphate. In addition, 1-phosphofructokinase converts phosphorylated fructose, which is produced by the fructose PTS transporter while taken up into fructose 1,6-bisphosphate, which could be metabolized to the glycolytic pathway. Metabolomic analysis showed that fructose-6-phosphate was significantly upregulated 1.89-fold when *F. prausnitzii* was grown on inulin compared to that obtained with growth on glucose (**Table 1**). In addition, glucose-6-phosphate, which is produced by the phosphorylation of intracellular glucose and is converted into fructose-6-phosphate to enter the glycolysis pathway, was also significantly upregulated by 1.85 times. This indicated that the increase in intracellular fructose through inulin-type fructan metabolism was eventually induced in the glycolysis pathway and the tricarboxylic acid (TCA) cycle for energy production, which is essential for cell growth. In addition, the metabolite expression pattern of the TCA cycle, which is important for the production of ATP and the chemical energy produced by carbohydrate metabolism, was quantitatively confirmed. It was found that citrate, aconitate, and succinyl-CoA were upregulated by 2.35, 1.98, and 1.89-fold, respectively; malate, succinate, and

acetyl-CoA were downregulated by 0.26, 0.30, and 0.43-fold, respectively. In addition, ATP decreased by 0.63-fold, which is believed to result in relative differences in ATP due to the energy consumption required for inulin metabolism by *F. prausnitzii* compared to the growth of *F. prausnitzii* on glucose. However, these results suggest that inulin can be selectively used as a carbohydrate source by *F. prausnitzii* in a targeted manner compared to glucose, which other gut bacterial species can utilize.

CONCLUSION

Based on a molecular perspective, this study attempted to elucidate the biological mechanism whereby *F. prausnitzii*, a human health-promoting intestinal butyrate-producing bacterium, can selectively digest prebiotic inulin. *F. prausnitzii* could selectively digest inulin among various dietary fibers, and when grown in inulin as the sole carbon source, it has an excellent butyrate production capacity of about 65% of that when grown on glucose. In addition, intracellular proteomic data revealed that proteins involved in inulin-type fructan degradation and intracellular transport were upregulated in *F. prausnitzii* grown on inulin. First, β-fructosidase and amylosucrase, which can completely degrade inulin-type fructan, were significantly upregulated, and the activity of enzymes against fructan and sucrose degradation was verified in *E. coli* using genetic recombination. In addition, analysis of the subcellular location of enzymes demonstrated that the inulin-type fructan degrading enzymes were present intracellularly. We found that fructan ABC transporters, which could directly uptake inulin-type fructan into cells for intracellular degradation, were upregulated. In addition, the fructose transporter transporting fructose into cells was upregulated, implying that *F. prausnitzii* improved not only inulin-type fructan utilization but also the fructose uptake ability through inulin metabolism. In addition, intracellular metabolomics confirmed that *F. prausnitzii* efficiently used fructose, the final degradation product of inulin-type fructan, for energy production during growth using inulin as a carbon source. In conclusion, we conducted a study by a multiomics approach to identify the proteins involved in inulin utilization by *F. prausnitzii* and were able to present a molecular scale model of *F. prausnitzii* utilizing inulin in the intestine (**Figure 8**). Thus, the results have potential applications in the selection and development of optimized prebiotics in the future to enhance human health by improving the survival of *F. prausnitzii*, which has useful metabolic productivity as compared to other intestinal microorganisms.

DATA AVAILABILITY STATEMENT

The mass spectrometry proteomics data generated in this study have been deposited in the ProteomeXchange Consortium via the PRIDE (Perez-Riverol et al., 2019) partner repository with the dataset identifier "PXD030078".

AUTHOR CONTRIBUTIONS

J-HP, W-SS, and Y-GK conceptualized the research and contributed to this work. J-HP, W-SS, JL, S-HJ, J-SL, H-JJ, J-EK, Y-RK, J-HB, and M-GK carried out the experiment and interpreted the results under the guidance. J-HP, W-SS wrote the manuscript with support from Y-GK. Y-HY, B-GK, and Y-GK revised the manuscript and provided critical feedback.

FUNDING

This work was supported by the Basic Science Research Program through the National Research Foundation of Korea (NRF-2019M2C8A2058418, NRF-2018R1D1A1B07048185, NRF-2017M3A9E4077235, and NRF-2020R1A6A1A03044977) and a grant of the Korea Health Technology R&D Project through the Korea Health Industry Development Institute (KHIDI), funded by the Ministry of Health & Welfare, Republic of Korea (Grant Number: HP20C0210).

SUPPLEMENTARY MATERIAL

The Supplementary Material for this article can be found online at: https://www.frontiersin.org/articles/10.3389/fbioe.2022.825399/full#supplementary-material

REFERENCES

Bäckhed, F., Ley, R. E., Sonnenburg, J. L., Peterson, D. A., and Gordon, J. I. (2005). Host-bacterial Mutualism in the Human Intestine. *Science* 307 (5717), 1915–1920. doi:10.1126/science.1104816

Barrangou, R., Altermann, E., Hutkins, R., Cano, R., and Klaenhammer, T. R. (2003). Functional and Comparative Genomic Analyses of an Operon Involved in Fructooligosaccharide Utilization by Lactobacillus Acidophilus. *Proc. Natl. Acad. Sci.* 100 (15), 8957–8962. doi:10.1073/pnas.1332765100

Buntin, N., Hongpattarakere, T., Ritari, J., Douillard, F. P., Paulin, L., Boeren, S., et al. (2017). An Inducible Operon Is Involved in Inulin Utilization in Lactobacillus Plantarum Strains, as Revealed by Comparative Proteogenomics and Metabolic Profiling. *Appl. Environ. Microbiol.* 83 (2), e02402-16. doi:10.1128/AEM.02402-16

Campbell, J. M., Fahey, G. C., Jr., and Wolf, B. W. (1997). Selected Indigestible Oligosaccharides Affect Large Bowel Mass, Cecal and Fecal Short-Chain Fatty Acids, pH and Microflora in Rats. *J. Nutr.* 127 (1), 130–136. doi:10.1093/jn/127.1.130

Cox, J., Hein, M. Y., Luber, C. A., Paron, I., Nagaraj, N., and Mann, M. (2014). Accurate Proteome-wide Label-free Quantification by Delayed Normalization and Maximal Peptide Ratio Extraction, Termed MaxLFQ. *Mol. Cell Proteomics* 13 (9), 2513–2526. doi:10.1074/mcp.M113.031591

Desai, M. S., Seekatz, A. M., Koropatkin, N. M., Kamada, N., Hickey, C. A., Wolter, M., et al. (2016). A Dietary Fiber-Deprived Gut Microbiota Degrades the Colonic Mucus Barrier and Enhances Pathogen Susceptibility. *Cell* 167 (5), 1339–1353. e1321. doi:10.1016/j.cell.2016.10.043

Deutscher, J., Francke, C., and Postma, P. W. (2006). How Phosphotransferase System-Related Protein Phosphorylation Regulates Carbohydrate Metabolism in Bacteria. *Microbiol. Mol. Biol. Rev.* 70 (4), 939–1031. doi:10.1128/mmbr.00024-06

Dewulf, E. M., Cani, P. D., Claus, S. P., Fuentes, S., Puylaert, P. G., Neyrinck, A. M., et al. (2013). Insight into the Prebiotic Concept: Lessons from an Exploratory, Double Blind Intervention Study with Inulin-type Fructans in Obese Women. *Gut* 62 (8), 1112–1121. doi:10.1136/gutjnl-2012-303304

Duncan, S. H., Hold, G. L., Harmsen, H. J. M., Stewart, C. S., and Flint, H. J. (2002). Growth Requirements and Fermentation Products of Fusobacterium Prausnitzii, and a Proposal to Reclassify it as Faecalibacterium Prausnitzii Gen. nov., Comb. Nov. *Int. J. Syst. Evol. Microbiol.* 52 (6), 2141–2146. doi:10.1099/00207713-52-6-2141

Eckburg, P. B., Bik, E. M., Bernstein, C. N., Purdom, E., Dethlefsen, L., Sargent, M., et al. (2005). Diversity of the Human Intestinal Microbial flora. *Science* 308 (5728), 1635–1638. doi:10.1126/science.1110591

Fang, S., Yan, B., Tian, F., Lian, H., Zhao, J., Zhang, H., et al. (2021). β-Fructosidase FosE Activity in Lactobacillus Paracasei Regulates Fructan Degradation during Sourdough Fermentation and Total FODMAP Levels in Steamed Bread. *LWT* 145, 111294. doi:10.1016/j.lwt.2021.111294

Fitzgerald, C. B., Shkoporov, A. N., Sutton, T. D. S., Chaplin, A. V., Velayudhan, V., Ross, R. P., et al. (2018). Comparative Analysis of Faecalibacterium Prausnitzii Genomes Shows a High Level of Genome Plasticity and Warrants Separation into New Species-Level Taxa. *BMC Genomics* 19 (1), 931. doi:10.1186/s12864-018-5313-6

Flint, H. J., Scott, K. P., Louis, P., and Duncan, S. H. (2012). The Role of the Gut Microbiota in Nutrition and Health. *Nat. Rev. Gastroenterol. Hepatol.* 9 (10), 577–589. doi:10.1038/nrgastro.2012.156

Fung, K. Y. C., Cosgrove, L., Lockett, T., Head, R., and Topping, D. L. (2012). A Review of the Potential Mechanisms for the Lowering of Colorectal Oncogenesis by Butyrate. *Br. J. Nutr.* 108 (5), 820–831. doi:10.1017/s0007114512001948

Gibson, G. R., and Roberfroid, M. B. (1995). Dietary Modulation of the Human Colonic Microbiota: Introducing the Concept of Prebiotics. *J. Nutr.* 125 (6), 1401–1412. doi:10.1093/jn/125.6.1401

Goh, Y. J., Lee, J.-H., and Hutkins, R. W. (2007). Functional Analysis of the Fructooligosaccharide Utilization Operon in Lactobacillus Paracasei 1195. *Appl. Environ. Microbiol.* 73 (18), 5716–5724. doi:10.1128/AEM.00805-07

Goh, Y. J., Zhang, C., Benson, A. K., Schlegel, V., Lee, J.-H., and Hutkins, R. W. (2006). Identification of a Putative Operon Involved in Fructooligosaccharide Utilization by Lactobacillus Paracasei. *Appl. Environ. Microbiol.* 72 (12), 7518–7530. doi:10.1128/AEM.00877-06

Hamer, H. M., Jonkers, D., Venema, K., Vanhoutvin, S., Troost, F. J., and Brummer, R. J. (2008). Review Article: the Role of Butyrate on Colonic Function. *Aliment. Pharmacol. Ther.* 27 (2), 104–119. doi:10.1111/j.1365-2036.2007.03562.x

Holscher, H. D., Doligale, J. L., Bauer, L. L., Gourineni, V., Pelkman, C. L., Fahey, G. C., et al. (2014). Gastrointestinal Tolerance and Utilization of Agave Inulin by Healthy Adults. *Food Funct.* 5 (6), 1142–1149. doi:10.1039/C3FO60666J

Jia, W., Whitehead, R. N., Griffiths, L., Dawson, C., Waring, R. H., Ramsden, D. B., et al. (2010). Is the Abundance of Faecalibacterium Prausnitzii Relevant to Crohn's Disease. *FEMS Microbiol. Lett.* 310 (2), 138–144. doi:10.1111/j.1574-6968.2010.02057.x

Jo, S.-H., Song, W.-S., Park, H.-G., Lee, J.-S., Jeon, H.-J., Lee, Y.-H., et al. (2020). Multi-omics Based Characterization of Antibiotic Response in Clinical Isogenic Isolates of Methicillin-Susceptible/-Resistant *Staphylococcus aureus*. *RSC Adv.* 10 (46), 27864–27873. doi:10.1039/D0RA05407K

Joossens, M., Huys, G., Cnockaert, M., De Preter, V., Verbeke, K., Rutgeerts, P., et al. (2011). Dysbiosis of the Faecal Microbiota in Patients with Crohn's Disease and Their Unaffected Relatives. *Gut* 60 (5), 631–637. doi:10.1136/gut.2010.223263

Kang, D., Ham, H. I., Lee, S. H., Cho, Y. J., Kim, Y. R., Yoon, C. K., et al. (2021). Functional Dissection of the Phosphotransferase System Provides Insight into the Prevalence of Faecalibacterium Prausnitzii in the Host Intestinal Environment. *Environ. Microbiol.* 23 (8), 4726–4740. doi:10.1111/1462-2920.15681

Kaoutari, A. E., Armougom, F., Gordon, J. I., Raoult, D., and Henrissat, B. (2013). The Abundance and Variety of Carbohydrate-Active Enzymes in the Human Gut Microbiota. *Nat. Rev. Microbiol.* 11 (7), 497–504. doi:10.1038/nrmicro3050

Khan, M. T., van Dijl, J. M., and Harmsen, H. J. M. (2014). Antioxidants Keep the Potentially Probiotic but Highly Oxygen-Sensitive Human Gut Bacterium Faecalibacterium Prausnitzii Alive at Ambient Air. *PLoS One* 9 (5), e96097. doi:10.1371/journal.pone.0096097

Koleva, P. T., Valcheva, R. S., Sun, X., Gänzle, M. G., and Dieleman, L. A. (2012). Inulin and Fructo-Oligosaccharides Have Divergent Effects on Colitis and Commensal Microbiota in HLA-B27 Transgenic Rats. *Br. J. Nutr.* 108 (9), 1633–1643. doi:10.1017/S0007114511007203

Liebl, W., Brem, D., and Gotschlich, A. (1998). Analysis of the Gene for β-fructosidase (Invertase, Inulinase) of the Hyperthermophilic Bacterium Thermotoga Maritima , and Characterisation of the Enzyme Expressed in *Escherichia coli*. *Appl. Microbiol. Biotechnol.* 50 (1), 55–64. doi:10.1007/s002530051256

Lopez-Siles, M., Martinez-Medina, M., Surís-Valls, R., Aldeguer, X., Sabat-Mir, M., Duncan, S. H., et al. (2016). Changes in the Abundance of Faecalibacterium Prausnitzii Phylogroups I and II in the Intestinal Mucosa of Inflammatory Bowel Disease and Patients with Colorectal Cancer. *Inflamm. Bowel Dis.* 22 (1), 28–41. doi:10.1097/mib.0000000000000590

Louis, P., and Flint, H. J. (2017). Formation of Propionate and Butyrate by the Human Colonic Microbiota. *Environ. Microbiol.* 19 (1), 29–41. doi:10.1111/1462-2920.13589

Martín, R., Miquel, S., Chain, F., Natividad, J. M., Jury, J., Lu, J., et al. (2015). Faecalibacterium Prausnitzii Prevents Physiological Damages in a Chronic Low-Grade Inflammation Murine Model. *BMC Microbiol.* 15 (1), 67–12. doi:10.1186/s12866-015-0400-1

Miquel, S., Leclerc, M., Martin, R., Chain, F., Lenoir, M., Raguideau, S., et al. (2015). Identification of Metabolic Signatures Linked to Anti-inflammatory Effects of Faecalibacterium Prausnitzii. *Mbio* 6(2), e00300-00315. doi:10.1128/mBio.00300-15

Miquel, S., Martín, R., Bridonneau, C., Robert, V., Sokol, H., Bermúdez-Humarán, L. G., et al. (2014). Ecology and Metabolism of the Beneficial Intestinal Commensal bacteriumFaecalibacterium Prausnitzii. *Gut Microbes* 5 (2), 146–151. doi:10.4161/gmic.27651

Miquel, S., Martín, R., Rossi, O., Bermúdez-Humarán, L., Chatel, J., Sokol, H., et al. (2013). Faecalibacterium Prausnitzii and Human Intestinal Health. *Curr. Opin. Microbiol.* 16 (3), 255–261. doi:10.1016/j.mib.2013.06.003

Moens, F., and De Vuyst, L. (2017). Inulin-type Fructan Degradation Capacity ofClostridiumcluster IV and XIVa Butyrate-Producing colon Bacteria and Their Associated Metabolic Outcomes. *Beneficial Microbes* 8 (3), 473–490. doi:10.3920/bm2016.0142

Navarre, W. W., and Schneewind, O. (1994). Proteolytic Cleavage and Cell wall Anchoring at the LPXTG Motif of Surface Proteins in Gram-Positive Bacteria. *Mol. Microbiol.* 14 (1), 115–121. doi:10.1111/j.1365-2958.1994.tb01271.x

Nyangale, E. P., Mottram, D. S., and Gibson, G. R. (2012). Gut Microbial Activity, Implications for Health and Disease: the Potential Role of Metabolite Analysis. *J. Proteome Res.* 11 (12), 5573–5585. doi:10.1021/pr300637d

Oren, A., and Garrity, G. M. (2021). Valid Publication of the Names of Forty-Two Phyla of Prokaryotes. *Int. J. Syst. Evol. Microbiol.* 71 (10). doi:10.1099/ijsem.0.005056

O'Toole, P. W., Marchesi, J. R., and Hill, C. (2017). Next-generation Probiotics: the Spectrum from Probiotics to Live Biotherapeutics. *Nat. Microbiol.* 2 (5), 17057. doi:10.1038/nmicrobiol.2017.57

Pang, Z., Chong, J., Zhou, G., de Lima Morais, D. A., Chang, L., Barrette, M., et al. (2021). MetaboAnalyst 5.0: Narrowing the gap between Raw Spectra and Functional Insights. *Nucleic Acids Res.* 49 (W1), W388–W396. doi:10.1093/nar/gkab382

Perez-Riverol, Y., Csordas, A., Bai, J., Bernal-Llinares, M., Hewapathirana, S., Kundu, D. J., et al. (2019). The PRIDE Database and Related Tools and Resources in 2019: Improving Support for Quantification Data. *Nucleic Acids Res.* 47 (D1), D442–D450. doi:10.1093/nar/gky1106

Potocki De Montalk, G., Remaud-Simeon, M., Willemot, R. M., Planchot, V., and Monsan, P. (1999). Sequence Analysis of the Gene Encoding Amylosucrase from Neisseria Polysaccharea and Characterization of the Recombinant Enzyme. *J. Bacteriol.* 181 (2), 375–381. doi:10.1128/jb.181.2.375-381.1999

Ramirez-Farias, C., Slezak, K., Fuller, Z., Duncan, A., Holtrop, G., and Louis, P. (2008). Effect of Inulin on the Human Gut Microbiota: Stimulation ofBifidobacterium adolescentisandFaecalibacterium Prausnitzii. *Br. J. Nutr.* 101 (4), 541–550. doi:10.1017/S0007114508019880

Roberfroid, M. B., and Delzenne, N. M. (1998). Dietary Fructans. *Annu. Rev. Nutr.* 18, 117–143. doi:10.1146/annurev.nutr.18.1.117

Roberfroid, M. B. (2005). Introducing Inulin-type Fructans. *Br. J. Nutr.* 93 (Suppl. 1), S13–S25. doi:10.1079/bjn20041350

Roediger, W. E. (1980). Role of Anaerobic Bacteria in the Metabolic Welfare of the Colonic Mucosa in Man. *Gut* 21 (9), 793–798. doi:10.1136/gut.21.9.793

Ryan, S. M., Fitzgerald, G. F., and van Sinderen, D. (2005). Transcriptional Regulation and Characterization of a Novel β-Fructofuranosidase-Encoding Gene from Bifidobacterium Breve UCC2003. *Appl. Environ. Microbiol.* 71 (7), 3475–3482. doi:10.1128/AEM.71.7.3475-3482.2005

Saurin, W., Hofnung, M., and Dassa, E. (1999). Getting in or Out: Early Segregation between Importers and Exporters in the Evolution of ATP-Binding Cassette (ABC) Transporters. *J. Mol. Evol.* 48 (1), 22–41. doi:10.1007/pl00006442

Scott, K. P., Martin, J. C., Chassard, C., Clerget, M., Potrykus, J., Campbell, G., et al. (2011). Substrate-driven Gene Expression in Roseburia Inulinivorans: Importance of Inducible Enzymes in the Utilization of Inulin and Starch. *Proc. Natl. Acad. Sci.* 108 (Suppl. 1), 4672–4679. doi:10.1073/pnas.1000091107

Shah, A. D., Goode, R. J. A., Huang, C., Powell, D. R., and Schittenhelm, R. B. (2020). LFQ-analyst: An Easy-To-Use Interactive Web Platform to Analyze and Visualize Label-free Proteomics Data Preprocessed with MaxQuant. *J. Proteome Res.* 19 (1), 204–211. doi:10.1021/acs.jproteome.9b00496

Sokol, H., Pigneur, B., Watterlot, L., Lakhdari, O., Bermúdez-Humarán, L. G., Gratadoux, J.-J., et al. (2008). Faecalibacterium Prausnitzii Is an Anti-inflammatory Commensal Bacterium Identified by Gut Microbiota Analysis of Crohn Disease Patients. *Proc. Natl. Acad. Sci.* 105 (43), 16731–16736. doi:10.1073/pnas.0804812105

Song, W.-S., Park, H.-G., Kim, S.-M., Jo, S.-H., Kim, B.-G., Theberge, A. B., et al. (2020). Chemical Derivatization-Based LC-MS/MS Method for Quantitation of Gut Microbial Short-Chain Fatty Acids. *J. Ind. Eng. Chem.* 83, 297–302. doi:10.1016/j.jiec.2019.12.001

Tian, Y., Xu, W., Zhang, W., Zhang, T., Guang, C., and Mu, W. (2018). Amylosucrase as a Transglucosylation Tool: From Molecular Features to Bioengineering Applications. *Biotechnol. Adv.* 36 (5), 1540–1552. doi:10.1016/j.biotechadv.2018.06.010

Tsujikawa, Y., Ishikawa, S., Sakane, I., Yoshida, K.-I., and Osawa, R. (2021). Identification of Genes Encoding a Novel ABC Transporter in Lactobacillus Delbrueckii for Inulin Polymers Uptake. *Sci. Rep.* 11 (1), 16007. doi:10.1038/s41598-021-95356-1

Tsujikawa, Y., Nomoto, R., and Osawa, R. (2013). Difference in Degradation Patterns on Inulin-type Fructans Among Strains of Lactobacillus Delbrueckii and Lactobacillus Paracasei. *Biosci. Microbiota Food Health* 32 (4), 157–165. doi:10.12938/bmfh.32.157

Tyanova, S., Temu, T., Sinitcyn, P., Carlson, A., Hein, M. Y., Geiger, T., et al. (2016). The Perseus Computational Platform for Comprehensive Analysis of (Prote)omics Data. *Nat. Methods* 13 (9), 731–740. doi:10.1038/nmeth.3901

Ueda, A., Shinkai, S., Shiroma, H., Taniguchi, Y., Tsuchida, S., Kariya, T., et al. (2021). Identification of Faecalibacterium Prausnitzii Strains for Gut Microbiome-Based Intervention in Alzheimer's-type Dementia. *Cel Rep. Med.* 2 (9), 100398. doi:10.1016/j.xcrm.2021.100398

Varela, E., Manichanh, C., Gallart, M., Torrejón, A., Borruel, N., Casellas, F., et al. (2013). Colonisation byFaecalibacterium Prausnitziiand Maintenance of Clinical Remission in Patients with Ulcerative Colitis. *Aliment. Pharmacol. Ther.* 38 (2), 151–161. doi:10.1111/apt.12365

Walker, A. W., Ince, J., Duncan, S. H., Webster, L. M., Holtrop, G., Ze, X., et al. (2011). Dominant and Diet-Responsive Groups of Bacteria within the Human Colonic Microbiota. *ISME J.* 5 (2), 220–230. doi:10.1038/ismej.2010.118

Wang, H.-B., Wang, P.-Y., Wang, X., Wan, Y.-L., and Liu, Y.-C. (2012). Butyrate Enhances Intestinal Epithelial Barrier Function via Up-Regulation of Tight junction Protein Claudin-1 Transcription. *Dig. Dis. Sci.* 57 (12), 3126–3135. doi:10.1007/s10620-012-2259-4

Willing, B. P., Dicksved, J., Halfvarson, J., Andersson, A. F., Lucio, M., Zheng, Z., et al. (2010). A Pyrosequencing Study in Twins Shows that Gastrointestinal Microbial Profiles Vary with Inflammatory Bowel Disease Phenotypes. *Gastroenterology* 139 (6), 1844–1854. e1841. doi:10.1053/j.gastro.2010.08.049

Wiśniewski, J. R., Zougman, A., Nagaraj, N., and Mann, M. (2009). Universal Sample Preparation Method for Proteome Analysis. *Nat. Methods* 6 (5), 359–362. doi:10.1038/nmeth.1322

Yu, N. Y., Wagner, J. R., Laird, M. R., Melli, G., Rey, S., Lo, R., et al. (2010). PSORTb 3.0: Improved Protein Subcellular Localization Prediction with Refined Localization Subcategories and Predictive Capabilities for All Prokaryotes. *Bioinformatics* 26 (13), 1608–1615. doi:10.1093/bioinformatics/btq249

Conflict of Interest: The authors declare that the research was conducted in the absence of any commercial or financial relationships that could be construed as a potential conflict of interest.

Publisher's Note: All claims expressed in this article are solely those of the authors and do not necessarily represent those of their affiliated organizations, or those of the publisher, the editors and the reviewers. Any product that may be evaluated in this article, or claim that may be made by its manufacturer, is not guaranteed or endorsed by the publisher.

frontiers in Bioengineering and Biotechnology

ORIGINAL RESEARCH
published: 02 March 2022
doi: 10.3389/fbioe.2022.826357

Reactor Design and Optimization of α-Amino Ester Hydrolase- Catalyzed Synthesis of Cephalexin

*Colton E. Lagerman, Martha A. Grover, Ronald. W. Rousseau and Andreas S. Bommarius**

School of Chemical and Biomolecular Engineering, Georgia Institute of Technology, Atlanta, GA, United States

Pharmaceutical production quality has recently been a focus for improvement through incorporation of end-to-end continuous processing. Enzymatic ß-lactam antibiotic synthesis has been one focus for continuous manufacturing, and α-amino ester hydrolases (AEHs) are currently being explored for use in the synthesis of cephalexin due to their high reactivity and selectivity. In this study, several reactors were simulated to determine how reactor type and configuration impacts reactant conversion, fractional yield toward cephalexin, and volumetric productivity for AEH-catalyzed cephalexin synthesis. The primary reactor configurations studied are single reactors including a continuous stirred-tank reactor (CSTR) and plug flow reactor (PFR) as well as two CSTRS and a CSTR + PFR in series. Substrate concentrations fed to the reactors as well as enzyme concentration in the reactor were varied. The presence of substrate inhibition was found to have a negative impact on all reactor configurations studied. No reactor configuration simultaneously allowed high substrate conversion, high fractional yield, and high productivity; however, a single PFR was found to enable the highest substrate conversion with higher fractional yields than all other reactor configurations, by minimizing substrate inhibition. Finally, to further demonstrate the impact of substrate inhibition, an AEH engineered to improve substrate inhibition was simulated and Pareto optimal fronts for a CSTR catalyzed with the current AEH were compared to Pareto fronts for the improved AEH. Overall, reduced substrate inhibition would allow for high substrate conversion, fractional yield, and productivity with only a single CSTR.

Keywords: α-amino ester hydrolase, Xanthomonas campestris pv. campestris, ß-lactam antibiotics, reactor modelling, reactor optimization

OPEN ACCESS

Edited by:
Byung-Gee Kim,
Seoul National University, South Korea

Reviewed by:
Blaž Likozar,
National Institute of Chemistry, Slovenia
Aitao Li,
Hubei University, China
Hui Li,
Nanjing Tech University, China

****Correspondence:***
Andreas S. Bommarius
andreas.bommarius@chbe.gatech.edu

Specialty section:
This article was submitted to Bioprocess Engineering, a section of the journal Frontiers in Bioengineering and Biotechnology

Received: *30 November 2021*
Accepted: *14 February 2022*
Published: *02 March 2022*

Citation:
Lagerman CE, Grover MA, Rousseau RW and Bommarius AS (2022) Reactor Design and Optimization of α-Amino Ester Hydrolase- Catalyzed Synthesis of Cephalexin. Front. Bioeng. Biotechnol. 10:826357. doi: 10.3389/fbioe.2022.826357

1 INTRODUCTION

End-to end continuous processing has recently become a target for improving production quality in the pharmaceutical industry. Continuous processing often has distinct advantages over batch processing in terms of improvement in overall drug quality, efficiency, and controllability (Mascia et al., 2013; Lee et al., 2015; Myerson et al., 2015). ß-lactam antibiotics are promising candidates for continuous production due to the high volume of their consumption worldwide and the development of single-step enzymatic synthesis routes (Kasche 1986; Hernandez-Justiz et al., 1999; Youshko and Svedas 2000; Wegman et al., 2001; Youshko et al., 2002a; Elander 2003; Kallenberg et al., 2005; Chandel et al., 2008; Srirangan et al., 2013; Thakuria and Lahon 2013). Specifically, consumption of cephalosporins grew 94% between 2000 and 2010 and global production of cephalexin currently exceeds approximately 4,000 tons each year (Laxminarayan 2014; Van

Boeckel et al., 2014). Recent studies have focused specifically on developing a continuous operation in simulations of continuous reactor designs using both enzymatic reaction and crystallization kinetics (Valencia et al., 2012; Encarnación-Gómez et al., 2016; McDonald et al., 2017; McDonald et al., 2019a; McDonald et al., 2019b; McDonald et al., 2019c; Cuthbertson et al., 2019; Salami et al., 2020).

β-lactam antibiotics are typically synthesized enzymatically using penicillin G acylase (PGA) due to its high thermostability, efficiency, and selectivity toward antibiotic synthesis. α-amino ester hydrolases (AEHs, EC 3.1.1.43), another class of enzymes, are also capable of stereoselective synthesis of *ß*-lactam antibiotics and have recently been shown to be particularly useful for cephalexin synthesis (Takahashi et al., 1972; Takahashi et al. 1974; Takahashi et al. 1977; Kato et al., 1980; Nam et al., 1985; Ryu and Ryu 1988; Polderman-Tijmes et al., 2002). AEH has been studied far less than PGA, and a kinetic model describing AEH-catalyzed synthesis of cephalexin has only recently been established (Lagerman et al., 2021). While AEH can synthesize cephalexin at a much faster rate than PGA and has a lower optimum pH of activity beneficial for *ß*-lactam stability (Barends et al., 2003), AEH also suffers from low thermostability and strong substrate inhibition (Blum and Bommarius 2010; Blum et al., 2012; Lagerman et al., 2021). While PGA is currently the favored enzyme for *ß*-lactam antibiotic synthesis, the synthesis potential of AEH has not been fully realized. Overall, cephalexin is the strongest candidate for synthesis by AEH, and understanding how AEH can be used in common reactor configurations is a prerequisite for developing AEH-catalyzed synthesis processes.

Well-developed kinetic models for the enzyme(s) involved in a reactor are required for successful prediction and design of optimal reactor configuration prior to construction and operation. Useful kinetic models describe reaction kinetics across a wide range of conditions relevant to large-scale processes. While numerous studies for simulation of enzymatic reactors exist, many models are generalized or developed for single-substrate or single-product reactions (Vasic-Racki et al., 2003; Harmand and Dochain 2005; Andrić et al., 2010; Lindeque and Woodley 2019), whereas enzymatic synthesis of *ß*-lactam antibiotics is a complex reaction network with multiple substrates, products, and inhibitions (Youshko and Svedas 2000; Youshko et al., 2002b; McDonald et al., 2017; Lagerman et al., 2021). The complexities of *ß*-lactam synthesis by AEH render even the simplest reactor design studies both non-trivial and necessary prior to reactor construction.

Enzymatic reactor modelling also allows for development of whole process models and coupled reaction-isolation systems in addition to reactor optimization. Accurate models for downstream processing of active pharmaceutical ingredients (APIs) rely on proper modelling of all upstream units, including reactors. Several studies have discussed complex reaction-isolation systems (Salami et al., 2020; Ma et al., 2021) as well as upstream process modelling for generation of reaction substrates (Caşcaval et al., 2012) and downstream process modelling from fermentation broths (Likozar et al., 2012; Likozar et al., 2013), which could all be coupled with reactor modelling for whole process models of API production and isolation.

In this work, reactor design considerations were studied for continuous synthesis of cephalexin using previously determined kinetics for an AEH from *Xanthomonas campestris pv. campestris*. The effects of inlet substrate concentrations, reactor enzyme concentration, and reactor configuration including the use of reactors in series were the primary focus. Multiple combinations of continuous stirred-tank reactors (CSTRs) and plug flow reactors (PFRs) were compared in terms of reactant conversion, fractional yield toward cephalexin, and volumetric productivity. To demonstrate the current limitations of AEH and demonstrate how reactor engineering and improvements in catalytic properties through protein engineering can positively impact the system, several reactor configurations were studied. Several substrate and enzyme concentrations were considered. Finally, a CSTR operated with an engineered AEH demonstrating reduced substrate inhibition was simulated to demonstrate the synthetic potential of an improved AEH.

2 METHODS

2.1 Model Development

The reaction model used in this study is based on the mechanism and kinetics for AEH-catalyzed cephalexin synthesis previously studied (Lagerman et al., 2021). Briefly, AEH catalyzes the synthesis of cephalexin by direct coupling of two substrates: an activated acyl donating electrophile, phenylglycine methyl ester (PGME), and a *ß*-lactam ring containing nucleophile, (7-ADCA). In addition to the primary synthesis reaction, AEH also catalyzes the hydrolysis of PGME into the byproduct phenylglycine (PG) as well as hydrolysis of cephalexin into PG and 7-ADCA. Substrate inhibition by PGME had been found to have a significant impact on the synthesis potential of AEH at high concentrations of PGME through both competitive inhibition to form a nonreactive species, *EPGME·PGME,* as well as a partial competitive inhibition that still allows for hydrolysis of a PGME-bound acyl-enzyme complex, *EAPGME,* to PG (**Scheme 10**).

The rate equations for each reactant and product involved in the reaction were formulated as a system of differential equations connected through the acyl group and *ß*-lactam nuclei mass balances as previously described (Lagerman et al., 2021). Each reactor simulation was solved by setting the inlet concentrations of 7-ADCA ($C_{7\text{-ADCA},0}$) and PGME ($C_{\text{PGME},0}$) and the reactor enzyme concentration ($[E]_0$). Reactor configurations were set by the respective design equations for each reactor system as described below. Residence time (τ), productivity (space-time yield, *s.t.y.*), and fractional yield were then solved and studied as the primary reactor metrics. Both a CSTR and a PFR were simulated using the rate equations from the model described above. In addition to

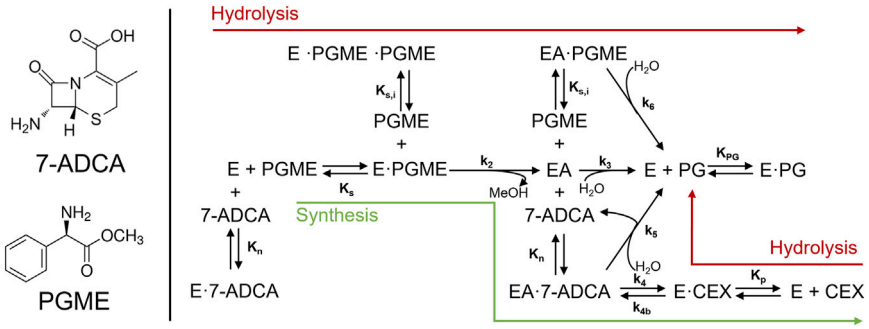

SCHEME 1 | Reaction network from Lagerman *et al.* describing the reactions involved in the synthesis of cephalexin catalyzed by AEH. In addition to the primary synthesis reaction (green arrow), AEH catalyzes both the hydrolysis of PGME as well as cephalexin.

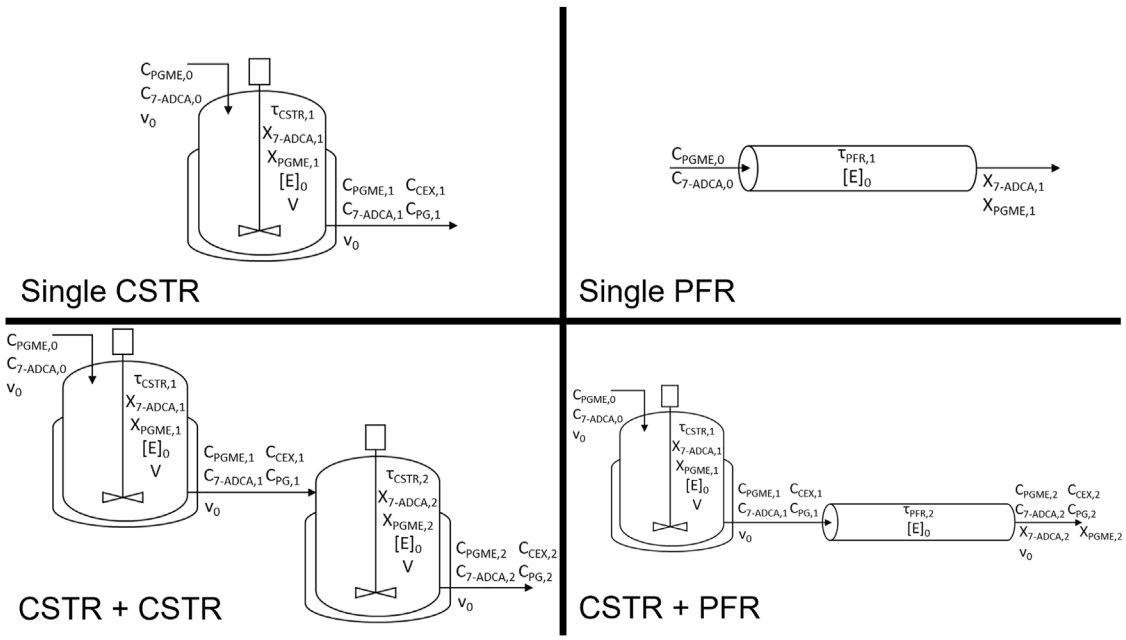

FIGURE 1 | Reactor configurations simulated and corresponding variables tracked for each system. Reactor configurations include a single CSTR, single PFR, CSTR + CSTR, and a CSTR + PFR.

the single reactors, two CSTRs in series as well as a CSTR followed by a PFR were also considered (**Figure 1**). All CSTRs were assumed to be well-mixed, implying that reactor and product concentrations in CSTR outlets are equal to their concentrations in the bulk reactor. The system of equations was solved using *vpasolve* in MATLAB R2021b for the single CSTR and two CSTR simulations. Systems containing a PFR were solved using *ode45* in MATLAB. All rate equations were calculated using previously determined model parameters (Lagerman et al., 2021).

Mass balances were derived for 7-ADCA and PGME consumption in a single CSTR and written in residence time format (Fogler 1999). To develop the design equation, each derived mass balance was set equal to the other, as a single CSTR configuration must satisfy both mass balances simultaneously. For the single CSTR (**Scheme 10**), the design equation

$$\frac{X_{7-ADCA,1}C_{7-ADCA,0}}{(-R_{7-ADCA,1})} = \frac{X_{PGME,1}C_{PGME,0}}{(-R_{PGME,1})} \quad (1)$$

equates the mass balance for 7-ADCA consumption (left-hand side of **Eq. 1**) and PGME consumption (right-hand side of **Eq. 1**) in a single CSTR. $X_{PGME,1}$ is PGME conversion, $X_{7\text{-}ADCA,1}$ is 7-

ADCA conversion, and $R_{PGME,1}$ and $R_{7-ADCA,1}$ are the rate equations for PGME and 7-ADCA evaluated at the CSTR exit conditions such that

$$\begin{aligned} \boldsymbol{R_{PGME,1}} = &-\frac{k_2[E]C_{PGME,1}}{K_s} \\ &-\frac{k_6 C_{PGME,1}}{K_{s,i}}\left(\frac{k_2[E]C_{PGME,1}}{K_s}+\frac{k_{4b}[E]C_{CEX,1}}{K_p}\right) \\ &\left(\frac{1}{\frac{k_4 C_{7-ADCA,1}}{K_n}+\frac{k_5 C_{7-ADCA,1}}{K_n}+\frac{k_6 C_{PGME,1}}{K_{si}}+k3}\right) \end{aligned} \tag{2}$$

$$\begin{aligned} \boldsymbol{R_{7-ADCA,1}} = &-\frac{k_2[E]C_{PGME,1}}{K_s} \\ &+\left(\frac{[E]}{\frac{k_4 C_{7-ADCA,1}}{K_n}+\frac{k_5 C_{7-ADCA,1}}{K_n}+\frac{k_6 C_{PGME,1}}{K_{si}}+k3}\right) \\ &\left(\frac{k_2 C_{PGME,1}}{K_s}+\frac{k_{4b}C_{CEX,1}}{K_p}\right)\left(k_3+\frac{k_5 C_{7-ADCA,1}}{K_n}\right) \end{aligned} \tag{3}$$

where $[E]$ is the concentration of free AEH in the system derived from an enzyme balance (**Supplementary Equation S3**). Values for all kinetic parameters can be found in the **Supplementary Table S1**. It should be noted that all rate equations account for all reactions in the network shown in **Scheme 10**. For example, R_{CEX} accounts for both cephalexin production and consumption and R_{7-ADCA} accounts for both 7-ADCA production and consumption. Each rate is evaluated with the outlet concentrations of PGME, 7-ADCA, cephalexin, and PG ($C_{PGME,1}, C_{7-ADCA,1}, C_{CEX,1}, C_{PG,1}$, respectively) and the concentration of AEH in the reactor, $[E]_0$. The additional equations to describe the single CSTR include rate equations for cephalexin and PG ($R_{CEX,1}$ and $R_{PG,1}$) and the outlet reactor concentrations of PGME, 7-ADCA, cephalexin, and PG ($C_{PGME,1}, C_{7-ADCA,1}, C_{CEX,1}, C_{PG,1}$, respectively) were solved simultaneously with the design equation such that

$$\boldsymbol{R_{CEX,1}} = -\boldsymbol{R_{7-ADCA,1}} \tag{4}$$

$$\boldsymbol{R_{PG,1}} = -\boldsymbol{R_{PGME,1}} - \boldsymbol{R_{CEX,1}} \tag{5}$$

$$\boldsymbol{C_{PGME,1}} = \boldsymbol{C_{PGME,0}} - \boldsymbol{C_{PGME,0}X_{PGME,1}} \tag{6}$$

$$\boldsymbol{C_{7-ADCA,1}} = \boldsymbol{C_{7-ADCA,0}} - \boldsymbol{C_{7-ADCA,0}X_{7-ADCA,1}} \tag{7}$$

$$\boldsymbol{C_{CEX,1}} = \boldsymbol{X_{7-ADCA,1}C_{7-ADCA,0}} \tag{8}$$

$$\boldsymbol{C_{PG,1}} = \boldsymbol{X_{PGME,1}C_{PGME,0}} - \boldsymbol{C_{CEX,1}} \tag{9}$$

Finally, residence time (τ_{CSTR}), fractional yield, and productivity were calculated as

$$\boldsymbol{\tau_{CSTR,1}} = \frac{\boldsymbol{X_{7-ADCA,1}C_{7-ADCA,0}}}{\left(-\boldsymbol{R_{7-ADCA,1}}\right)} \tag{10}$$

$$\textbf{\textit{Fractional Yield}} = \frac{\boldsymbol{C_{CEX,1}}}{\boldsymbol{C_{PGME,0}} - \boldsymbol{C_{PGME,1}}} \tag{11}$$

$$\textbf{\textit{Productivity}}\ \left(\boldsymbol{g/L/hr}\right) = \frac{\left(347.4\frac{\boldsymbol{g}}{\boldsymbol{mol}}\right)\left(60\frac{\boldsymbol{min}}{\boldsymbol{hr}}\right)\boldsymbol{C_{CEX,1}}}{\left(1000\frac{\boldsymbol{mmol}}{\boldsymbol{mol}}\right)\boldsymbol{\tau_{CSTR,1}}} \tag{12}$$

The PFR was simulated by solving the rate equations simultaneously in MATLAB using *ode45* to solve the system of rate equations for each substrate and product and obtain the outlet concentrations of all species at a wide range of residence times corresponding to the full conversion profiles of both substrates. At each residence time ($\tau_{PFR,1}$), 7-ADCA and PGME conversion were calculated as

$$\boldsymbol{X_{7-ADCA,1}} = \frac{\boldsymbol{C_{7-ADCA,0}} - \boldsymbol{C_{7-ADCA,1}}}{\boldsymbol{C_{7-ADCA,0}}} \tag{13}$$

$$\boldsymbol{X_{PGME,1}} = \frac{\boldsymbol{C_{PGME,0}} - \boldsymbol{C_{PGME,1}}}{\boldsymbol{C_{PGME,0}}} \tag{14}$$

where $C_{7-ADCA,1}$ and $C_{PGME,1}$ are the outlet 7-ADCA and PGME concentrations for a given $\tau_{PFR,1}$. Finally, fractional yield was calculated using **Eq. 11** as for a CSTR and productivity was calculated as

$$\textbf{\textit{Productivity}}\ \left(\boldsymbol{g/L/hr}\right) = \frac{\left(347.4\frac{\boldsymbol{g}}{\boldsymbol{mol}}\right)\left(60\frac{\boldsymbol{min}}{\boldsymbol{hr}}\right)\boldsymbol{C_{CEX,1}}}{\left(1000\frac{\boldsymbol{mmol}}{\boldsymbol{mol}}\right)\boldsymbol{\tau_{PFR,1}}} \tag{15}$$

For the two-CSTR system, the design equation for the first CSTR remains the same (**Eq. 1**) and the second CSTR design equation derived from a mass balance around the second CSTR is

$$\frac{\left(\boldsymbol{X_{7-ADCA,2}} - \boldsymbol{X_{7-ADCA,1}}\right)\boldsymbol{C_{7-ADCA,0}}}{\left(-\boldsymbol{R_{7-ADCA,2}}\right)} = \frac{\left(\boldsymbol{X_{PGME,2}} - \boldsymbol{X_{PGME,1}}\right)\boldsymbol{C_{PGME,0}}}{\left(-\boldsymbol{R_{PGME,2}}\right)} \tag{16}$$

where $X_{7-ADCA,2}$ and $X_{PGME,2}$ are the total 7-ADCA and PGME conversions after leaving the second CSTR and $R_{7-ADCA,2}$ and $R_{PGME,2}$ are the rates of consumption of 7-ADCA and PGME. To solve the CSTR + CSTR system, **Eqs. 1–9**) to describe the first CSTR as well as **Eq 16** and

$$\begin{aligned} \boldsymbol{R_{PGME,2}} = &-\frac{k_2[E]C_{PGME,2}}{K_s} - \frac{k_6 C_{PGME,2}}{K_{s,i}} \\ &\left(\frac{k_2[E]C_{PGME,2}}{K_s}+\frac{k_{4b}[E]C_{CEX,2}}{K_p}\right) \\ &\left(\frac{1}{\frac{k_4 C_{7-ADCA,2}}{K_n}+\frac{k_5 C_{7-ADCA,2}}{K_n}+\frac{k_6 C_{PGME,2}}{K_{si}}+k3}\right) \end{aligned} \tag{17}$$

$$\begin{aligned} \boldsymbol{R_{7-ADCA,2}} = &-\frac{k_2[E]C_{PGME,2}}{K_s} \\ &+\left(\frac{[E]}{\frac{k_4 C_{7-ADCA,2}}{K_n}+\frac{k_5 C_{7-ADCA,2}}{K_n}+\frac{k_6 C_{PGME,2}}{K_{si}}+k3}\right) \\ &\left(\frac{k_2 C_{PGME,2}}{K_s}+\frac{k_{4b}C_{CEX,2}}{K_p}\right)\left(k_3+\frac{k_5 C_{7-ADCA,2}}{K_n}\right) \end{aligned} \tag{18}$$

where $[E]$ is the concentration of free AEH in the system derived from an enzyme balance (**Supplementary Equation S3**). Each equation evaluated with the reactor two outlet concentrations of PGME, 7-ADCA, cephalexin, and PG

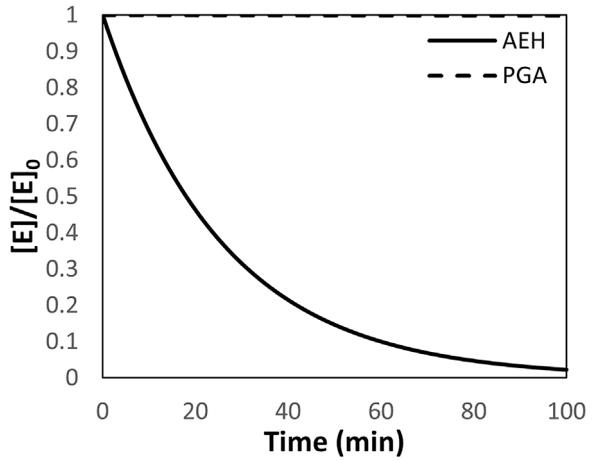

FIGURE 2 | The deactivation of AEH and PGA depicted as the ratio of enzyme at time, t, relative to the initial concentration of enzyme assuming first order deactivation kinetics. The deactivation constant for AEH is 0.0386 min^{-1} while the deactivation constant for PGA is 7E-8 min^{-1} (McDonald et al., 2018). PGA is shown for comparison.

($C_{PGME,2}, C_{7-ADCA,2}, C_{CEX,2}, C_{PG,2}$, respectively) and the concentration of AEH in the reactor, $[E]_0$. The following equations

$$R_{CEX,2} = -R_{7-ADCA,2} \tag{19}$$

$$R_{PG,2} = -R_{PGME,2} - R_{CEX,2} \tag{20}$$

$$C_{CEX,2} = X_{7-ADCA,2} C_{7-ADCA,0} \tag{21}$$

$$C_{PG,2} = X_{PGME,2} C_{PGME,0} - C_{CEX,2} \tag{22}$$

$$X_{7-ADCA,2} = \frac{C_{7-ADCA,0} - C_{7-ADCA,2}}{C_{7-ADCA,0}} \tag{23}$$

$$X_{PGME,2} = \frac{C_{PGME,0} - C_{PGME,2}}{C_{PGME,0}} \tag{24}$$

are required to completely solve the design equation. $C_{7-ADCA,0}$, $C_{PGME,0}$, $[E]_0$, $X_{7-ADCA,1}$, and $X_{7-ADCA,2}$ were all specified to solve the system of equations. Finally, residence times of the first and second CSTR ($\tau_{CSTR,1}$ and $\tau_{CSTR,2}$, respectively), productivity, and fractional yield were solved using

$$\tau_{CSTR,1} = \frac{X_{7-ADCA,1} C_{7-ADCA,0}}{(-R_{7-ADCA,1})} \tag{25}$$

$$\tau_{CSTR,2} = \frac{(X_{7-ADCA,2} - X_{7-ADCA,1}) C_{7-ADCA,0}}{(-R_{7-ADCA,2})} \tag{26}$$

$$Fractional\ Yield = \frac{C_{CEX,2}}{C_{PGME,0} - C_{PGME,2}} \tag{27}$$

$$Productivity\ (g/L/hr) = \frac{\left(347.4 \frac{g}{mol}\right)\left(60 \frac{min}{hr}\right) C_{CEX,2}}{\left(1000 \frac{mmol}{mol}\right)(\tau_{CSTR,1} + \tau_{CSTR,2})} \tag{28}$$

Finally, the CSTR + PFR system was solved using **Eqs. 1–9** to describe the CSTR and the PFR was solved using *ode45* for the rate equations with the inlet condition being the outlet concentrations from the CSTR to directly solve for $\tau_{PFR,2}$, $C_{PGME,2}$, $C_{7-ADCA,2}$, $C_{CEX,2}$, and $C_{PG,2}$. $X_{7-ADCA,2}$ and $X_{PGME,2}$ are solved using **Eq. 23** and **Eq. 24** $\tau_{CSTR,1}$ is calculated from **Eq. 10**, fractional yield is calculated from **Eq. 27**, and productivity is calculated as

$$Productivity\ (g/L/hr) = \frac{\left(347.4 \frac{g}{mol}\right)\left(60 \frac{min}{hr}\right) C_{CEX,2}}{\left(1000 \frac{mmol}{mol}\right)(\tau_{CSTR,1} + \tau_{PFR,2})} \tag{29}$$

3 RESULTS

3.1 AEH Deactivation

One of the primary assumptions in the design and simulation of a reactor system built around AEH is a constant enzyme concentration. However, AEH deactivates very rapidly at 25°C and pH 7.0 where 50% of activity is lost in around 20 min based on 1st order deactivation kinetics (**Figure 2**) (Lagerman et al., 2021). For comparison, PGA, a more readily used enzyme for synthesis of ß-lactam antibiotics, has <1% deactivation over 100 min under these conditions based on current deactivation data (McDonald et al., 2018). In the following simulations, it is assumed that AEH can be replaced at a rate that compensates for deactivation to assume constant enzyme activity in the reactor.

3.2 Single Reactor Simulations

In the following discussion, Levenspiel plots were used to easily visualize the relationship between substrate conversion, reaction rates, and reactor residence times. Levenspiel plot curves are constructed as the ratio of initial substrate concentration divided by the rate of substrate consumption, $C_{7\text{-ADCA},0}/(-R_{7\text{-ADCA}})$, plotted as a function of conversion, $X_{7\text{-}ADCA}$, and used to determine the residence time, τ, of each reactor at a given conversion. As reciprocal rates are used in Levenspiel plots, a negative slope signifies increasing reaction rates with increasing conversion. For a PFR, residence time (**Figure 4B**, red line) is calculated as the area under the Levenspiel curve for a given conversion (**Figure 4A**, red line). For a CSTR, residence time (**Figure 4B**, black line) is calculated as the product of the conversion and corresponding $C_{7\text{-ADCA},0}/(-R_{7\text{-ADCA}})$, or the area of the rectangle under the Levenspiel curve (**Figure 4A**, black line).

3.2.1 Single CSTR

A single CSTR is perhaps the simplest operation of an enzymatic reactor and has been simulated and operated for PGA previously (McDonald et al., 2019a; McDonald et al., 2019b). Here, simulations involving AEH were performed by varying reactor residence times and inlet PGME and 7-ADCA concentrations from 25–1,000 mM and 25–500 mM respectively to study how conversion, fractional yield, and productivity are affected by easily tunable operating conditions. Focus was given to maximizing 7-ADCA conversion as the cost of 7-ADCA is much greater than the cost of PGME.

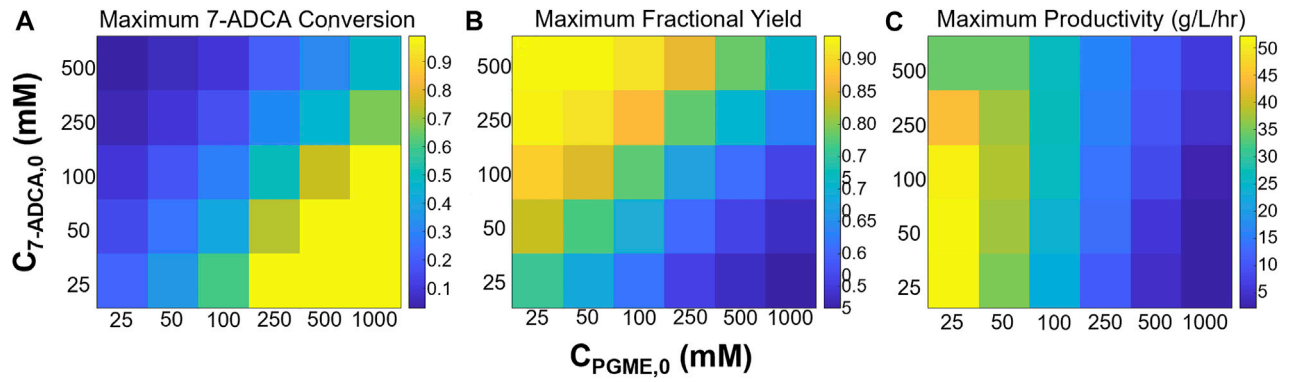

FIGURE 3 | Maximum **(A)** 7-ADCA conversion, **(B)** fractional yield of cephalexin from PGME, and **(C)** productivity in g/L/hr is shown for different combinations of inlet substrate concentrations for a single CSTR. PGME concentrations range from 25–1,000 mM while 7-ADCA concentrations range from 25–500 mM.

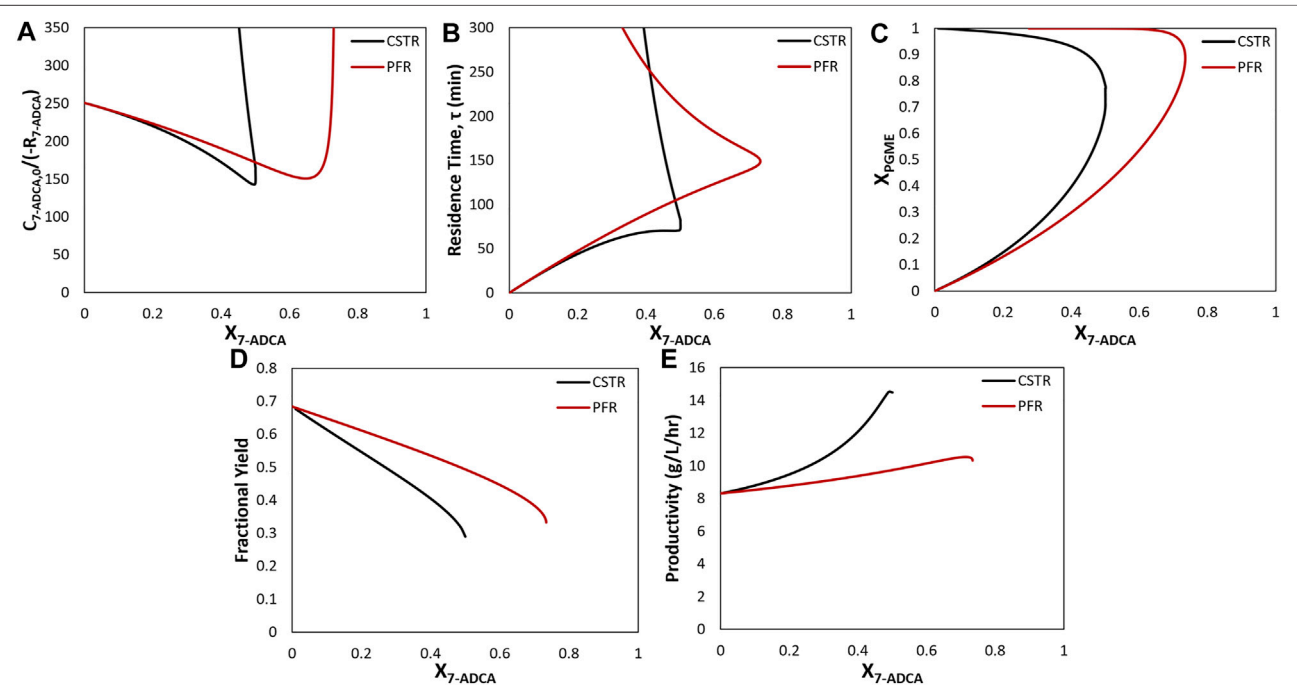

FIGURE 4 | Comparison of a CSTR (black) and PFR (red) for inlet conditions of 250 mM PGME and 100 mM 7-ADCA **(A)** Levenspiel plots showing the inverse 7-ADCA reaction rate as a function of 7-ADCA conversion ($X_{7\text{-}ADCA}$) **(B)** Residence times (τ) as a function of 7-ADCA conversion ($X_{7\text{-}ADCA}$) derived from the Levenspiel plots. Residence time is calculated as the area under the curve for a PFR at a given $X_{7\text{-}ADCA}$. For the CSTR, residence time is calculated as the product of $X_{7\text{-}ADCA}$ and the corresponding $C_{7\text{-}ADCA}/(-R_{7\text{-}ADCA})$ or the area of the rectangle under the curve at a given $X_{7\text{-}ADCA}$ **(C)** PGME conversions (X_{PGME}) corresponding to each $X_{7\text{-}ADCA}$ in panel **(A)**. **(D)** Fractional yields obtained for $X_{7\text{-}ADCA}$ in panel **(A)**. **(E)** Productivities obtained from **Eq. 12** for the CSTR and **Eq. 15** for the PFR at all $X_{7\text{-}ADCA}$ values.

Figure 3 shows the maximum 7-ADCA conversions (**Figure 3A**), maximum fractional yields (**Figure 3B**), and maximum productivities (**Figure 3C**) obtainable using a single CSTR for various combinations of inlet PGME and 7-ADCA concentrations. The highest maximum 7-ADCA conversions were found to occur at high inlet concentrations of PGME relative to 7-ADCA. When PGME is in excess, most of the 7-ADCA can be converted to cephalexin despite some PGME being converted to byproduct, PG. Greater than 99% of 7-ADCA can be converted to cephalexin when PGME is supplied at a 10:1 ratio (or greater) of PGME:7-ADCA. When PGME and 7-ADCA are supplied at equal concentrations to the inlet of the reactor, 7-ADCA conversion does not exceed 40% due to low fractional yield of PGME to cephalexin.

Maximum fractional yields (that is, the ratio of moles of cephalexin to moles of PG plus moles of cephalexin) can exceed 0.9 when 7-ADCA is supplied in large excess relative to PGME in contrast to excess PGME giving the highest

maximum 7-ADCA conversion; however, it should be noted that the maximum fractional yield for a given combination of inlet concentrations can only be obtained at low conversion (<1%) when 7-ADCA remains at high concentration in the reactor. As more 7-ADCA is converted, selectivity toward cephalexin relative to PG production is decreased resulting in lower fractional yield at higher 7-ADCA conversion. In other words, to obtain the maximum 7-ADCA conversion for a given set of substrate inlet concentrations, fractional yield must be sacrificed and vice versa.

The largest maximum productivities (**Figure 3C**) were found to occur at low concentrations of both PGME and 7-ADCA with the highest cephalexin productivities occurring in a CSTR with only 25 mM PGME. As the concentration of PGME is increased, productivity drops off substantially as PGME inhibition increases. In other words, to produce the same amount of cephalexin with higher inlet concentrations of PGME, a much longer residence time is required due to the slower rates of reaction caused by substrate inhibition which results in lower productivities. In addition, at low PGME concentrations, 7-ADCA concentration has little effect on productivity unless in large excess (>250 mM). However, at high PGME concentration (>250 mM), increases in inlet 7-ADCA concentration leads to slightly higher productivities due to the higher production of cephalexin that occurs when higher 7-ADCA is supplied.

The maximum productivity for a given set of inlet concentrations is obtained at the maximum conversion for all combinations of substrate concentrations. While data for all substrate concentrations is not shown, a representative example can be found in **Figure 4** (black curves). At high 7-ADCA conversion and therefore high PGME conversion (**Figure 4C**), the cephalexin synthesis rate achieves a maximum value (minimum y-value) as shown for the example Levenspiel plot for a single CSTR operating with an inlet concentration of 100 mM 7-ADCA and 250 mM PGME (**Figure 4A**, black curve). The corresponding productivity is also at a maximum at this conversion (**Figure 4E**, black curve). As PGME is consumed (i.e. higher X_{PGME}), substrate inhibition decreases and the rate of reaction increases, so a CSTR configured with a larger residence time for higher $X_{7\text{-}ADCA}$ operates at a higher rate of reaction and therefore higher productivity than a CSTR operating at low $X_{7\text{-}ADCA}$.

3.2.2 Single PFR

For many of the following comparisons of reactor configuration, an example system with inlet concentrations of 250 mM PGME and 100 mM 7-ADCA at a constant reactor enzyme concentration of 200 nM is used to demonstrate representative trends across all inlet substrate concentration. **Figure 4** shows simulation results for a single CSTR and single PFR using the example inlet concentrations. Based on the Levenspiel plot for 250 mM PGME, 100 mM 7-ADCA (**Figure 4A**), a CSTR operates at a higher reaction rate than a PFR at identical 7-ADCA conversions ($X_{7\text{-}ADCA}$). Because of the higher reaction rates, a CSTR provides a more efficient synthesis than a PFR in terms of lower residence time (**Figure 4B**) and higher productivity (**Figure 4E**) for the same $X_{7\text{-}ADCA}$. A PFR, however, allows for higher conversion of 7-ADCA relative to a CSTR (**Figure 4A**). For this example, a CSTR can only be used to convert 50% of 7-ADCA whereas a PFR can drive conversion up to 73%.

A PFR will have a higher concentration of 7-ADCA throughout the reactor compared to a CSTR because a CSTR operates at the exit conditions of the reactor whereas a PFR is used to gradually consume substrate. For a PFR, this higher 7-ADCA concentration leads to more efficient PGME consumption relative to 7-ADCA consumption (**Figure 4C**) which in turn leads to much higher fractional yield toward cephalexin when compared to a CSTR (**Figure 4D**). The reaction rate for a PFR, however, is always lower than that of a CSTR, so a higher residence time is required to reach high conversions (**Figure 4B**). Productivity is much lower due to the high residence times required to reach a given conversion (**Figure 4E**). A single CSTR can reach nearly 15 g/L/hr at 50% 7-ADCA conversion whereas a PFR operating at 50% 7-ADCA conversion can only reach about 10 g/L/hr.

3.3 Multiple Reactor Simulations

Reactors in series are often used to reach higher substrate conversion than is possible in a single reactor, and CSTRs and PFRs can be used interchangeably in series. Design of reactors in series is often focused on minimization of total reactor volume or total reactor residence time, and residence time is minimized by adjusting conversion in each reactor to achieve the same total conversion. While focus is often given to improving conversion, for AEH-catalyzed cephalexin synthesis, consideration must also be given to tradeoffs in fractional yield and productivity in addition to substrate conversion.

3.3.1 Two CSTRs in Series

Two CSTRs in series were simulated while varying 7-ADCA conversion in the first CSTR ($X_{7\text{-}ADCA,1}$) and the total 7-ADCA exiting the second CSTR ($X_{7\text{-}ADCA,2}$). **Figure 5** shows the maximum attainable 7-ADCA conversion (**Figure 5A**) and improvement in maximum conversion (**Figure 5B**) defined as the difference in total conversion for a CSTR + CSTR system relative to a single CSTR. In general, addition of a second CSTR allows for higher possible 7-ADCA conversion than a single CSTR for all inlet substrate concentrations. At intermediate concentrations of both 7-ADCA and PGME, possible 7-ADCA conversion is increased by up to 14% points. At low 7-ADCA inlet concentrations and high PGME concentrations, 7-ADCA conversions already reach >99%, so improvements are limited, and a second reactor adds no benefit to 7-ADCA conversion. For the previous example of 250 mM PGME and 100 mM 7-ADCA, 7-ADCA conversion is increased from 50 to 58%.

Two CSTRs in series allow for an additional degree of freedom as each reactor can be sized separately while achieving the same total 7-ADCA conversion. To study how the configuration of the first CSTR impacts productivity, fractional yield, and total residence time, a two-CSTR system was simulated at several total 7-ADCA conversions ($X_{7\text{-}ADCA,2}$) while varying conversion achieved in the first CSTR ($X_{7\text{-}ADCA,1}$) using the example inlet conditions of 250 mM PGME and 100 mM 7-ADCA and constant enzyme concentration of 200 nM in each reactor. **Figure 6** shows the fractional yield (**Figure 6A**), total

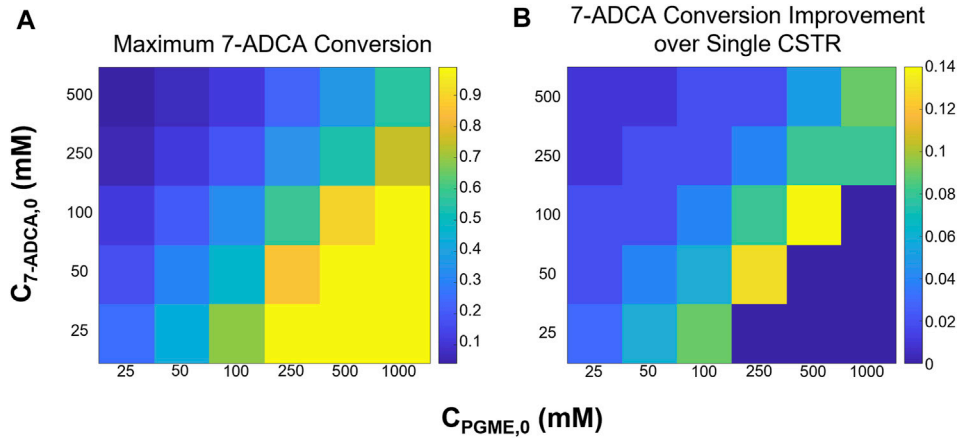

FIGURE 5 | (A) Maximum 7-ADCA conversion and **(B)** improvement in maximum 7-ADCA conversion when compared to a single CSTR is shown for a two CSTR system for several combinations of inlet substrate concentrations. PGME concentrations range from 25–1,000 mM while 7-ADCA concentrations range from 25–500 mM.

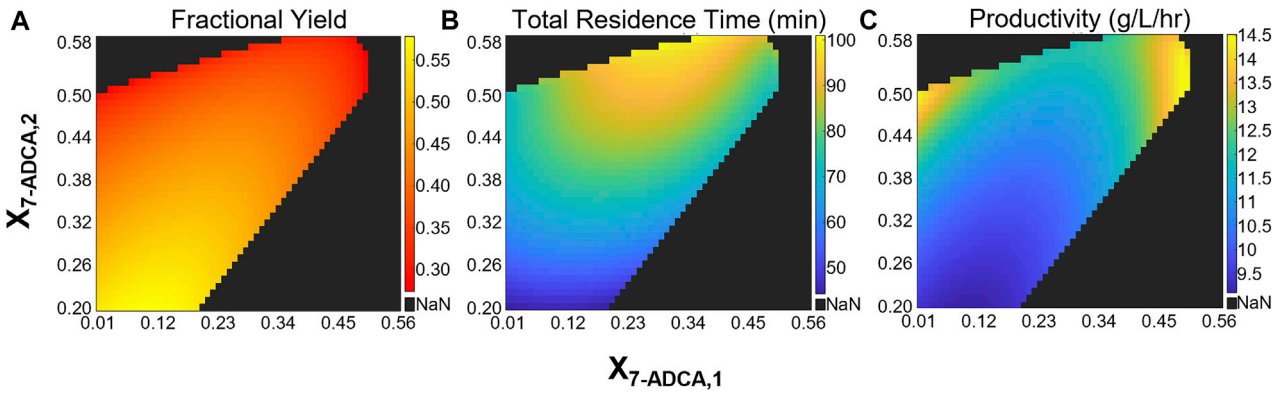

FIGURE 6 | Heatmaps showing the **(A)** fractional yield **(B)** productivity and **(C)** total residence time for a CSTR + CSTR system at various combinations of 7-ADCA conversions in each reactor. The *x*-axis shows the total conversion reached in the first CSTR and the *y*-axis shows the total 7-ADCA conversion exiting reactor two assuming an inlet 7-ADCA concentration of 100 mM and inlet PGME concentration of 250 mM. The AEH concentration in both reactors is constant at 200 nM.

residence time (**Figure 6B**), and productivity (**Figure 6C**) obtained for several combinations of CSTR configurations. As established for a single CSTR, high total 7-ADCA conversion ($X_{7\text{-}ADCA,2}$) limits fractional yield and no combination of two CSTRs operating at a high $X_{7\text{-}ADCA,2}$ (**Figure 6A**) improves fractional yield significantly over a single CSTR (**Figure 4B**, black curve). For example, when total 7-ADCA conversion is 0.58, varying $X_{7\text{-}ADCA,1}$ does not improve fractional yield above 0.3. Significant improvement in fractional yield can be obtained at lower total 7-ADCA conversions ($X_{7\text{-}ADCA,2} \leq 0.50$) when 50% of the total conversion is achieved in the first CSTR (i.e. $X_{7\text{-}ADCA,1} \approx 0.5X_{7\text{-}ADCA,2}$) (**Figure 6A**). Such a configuration of CSTRs, however, impacts productivity and residence time significantly. With two similarly sized CSTRs achieving similar conversion ($X_{7\text{-}ADCA,1} \approx 0.5X_{7\text{-}ADCA,2}$), the total residence time is maximized (**Figure 6B**), and productivity is minimized (**Figure 6C**). For example, when $X_{7\text{-}ADCA,2} = 0.50$, the total residence time is approximately 75 min and productivity is 14.5 g/L/hr when $X_{7\text{-}ADCA,1} < 0.05$ or when $X_{7\text{-}ADCA,1} > 0.45$ compared to a residence time of 92 min and productivity of 11 g/L/hr when $X_{7\text{-}ADCA,1} = 0.25$. In other words, productivity is maximized when one CSTR is much smaller than the other to minimize total residence time. Overall, a second small CSTR should only be used to drive conversion farther than a single CSTR is capable.

3.3.2 Comparison of Reactors in Series to Single CSTR and Single PFR

Figure 7 shows how different reactor configurations impact maximum 7-ADCA conversion (**Figure 7A**) and the associated fractional yields (**Figure 7B**) and productivities (**Figure 7C**) at the maximum conversion for inlet substrate concentrations of 250 mM PGME and 100 mM 7-ADCA at a constant AEH concentration of 200 nM in all reactors. As mentioned previously, two CSTRs can drive 7-ADCA

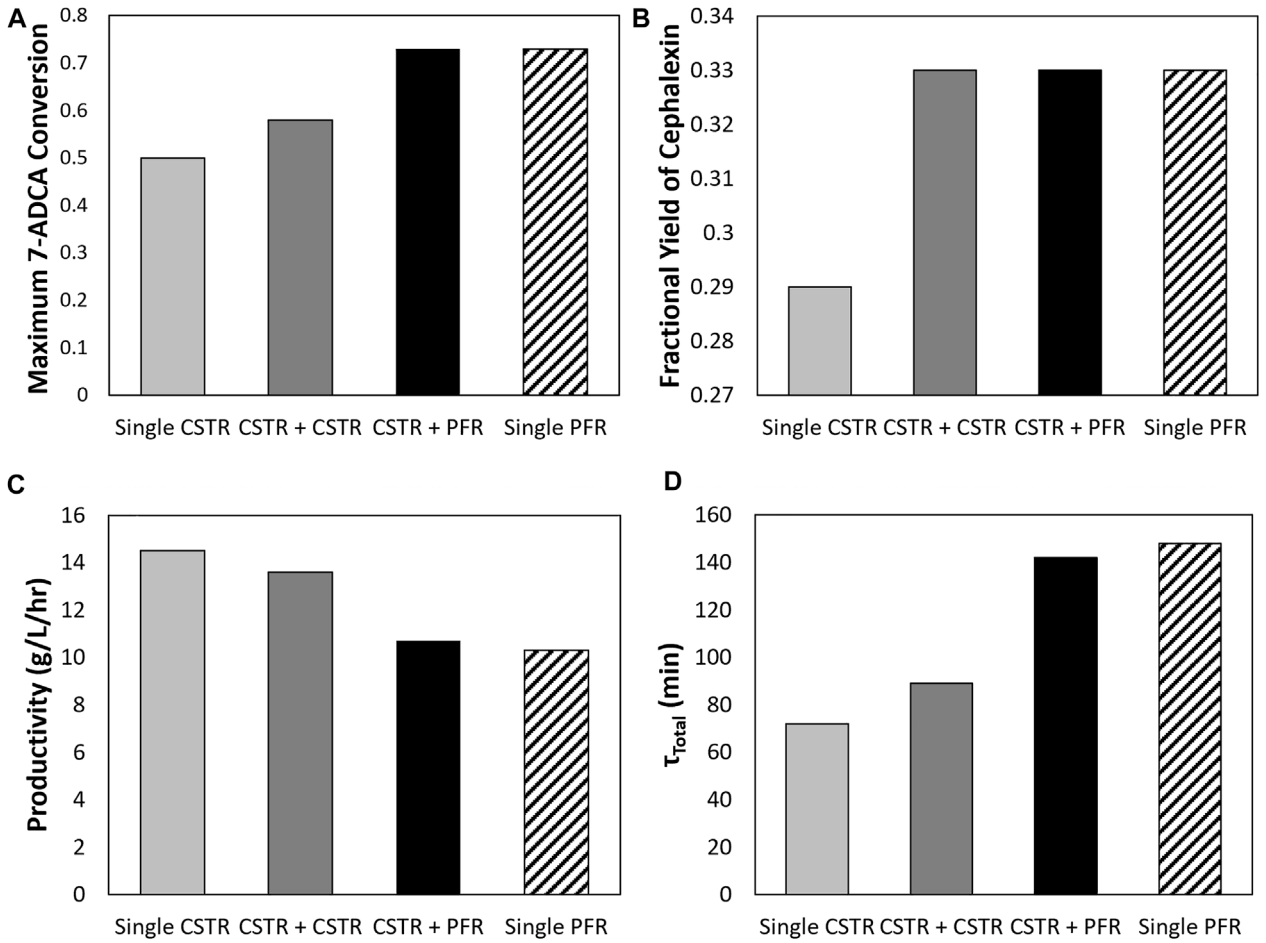

FIGURE 7 | A comparison is shown of the **(A)** maximum 7-ADCA conversion as well as the **(B)** fractional yield at the maximum 7-ADCA conversion, **(C)** productivity at maximum 7-ADCA conversion, and **(D)** total residence time at maximum 7-ADCA conversion for an inlet reactor concentration of 250 mM PGME and 100 mM 7-ADCA and AEH concentration of 200 nM is shown for the single CSTR, single PFR, CSTR plus CSTR, and CSTR plus PFR systems.

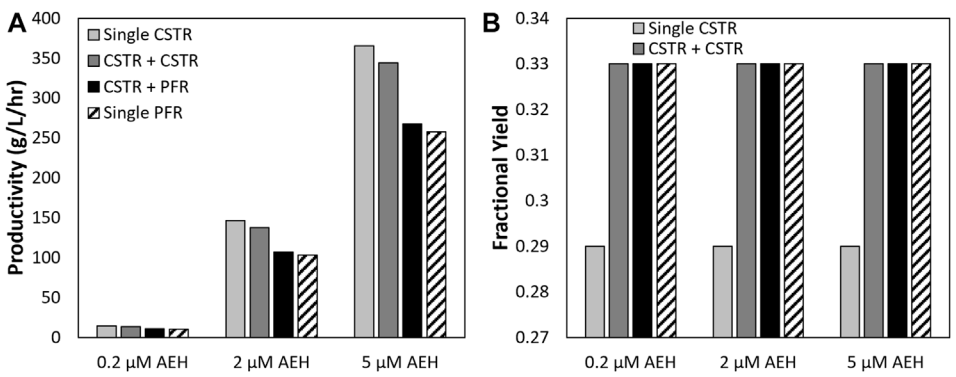

FIGURE 8 | (A) productivities and **(B)** fractional yields obtained for a single CSTR, single PFR, and CSTR + PFR are shown at varying concentrations of AEH at the maximum 7-ADCA conversion for each respective reactor configuration assuming 250 mM PGME and 100 mM 7-ADCA inlet concentrations.

conversions higher to 58% when compared to a single CSTR conversion of 50%. While driving 7-ADCA conversion higher typically has negative impact on fractional yield due to the lower concentration of 7-ADCA in the reactor, the two CSTR configuration shows slightly improved fractional yield at 58% 7-ADCA conversion than a single CSTR at 50% conversion. The

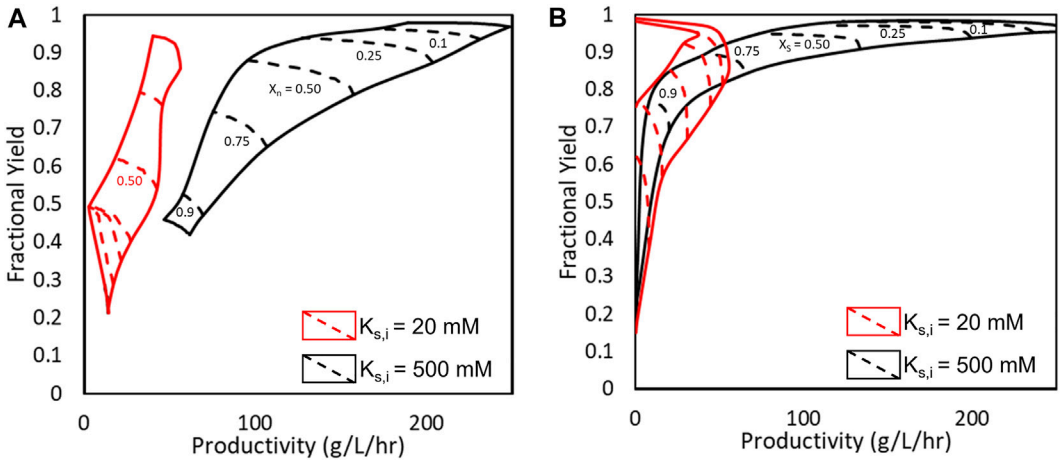

FIGURE 9 | Pareto optimal fronts for fractional yield and productivity under **(A)** varying 7-ADCA conversion ($X_{7\text{-}ADCA}$) and **(B)** varying PGME conversion. The red curves show the obtainable fractional yields, productivities, and conversions for the current AEH ($K_{S,I}$ = 20 mM) while the black curves represent an engineered AEH with minimized substrate inhibition ($K_{S,I}$ = 500 mM).

increase in conversion, however, does have a slight negative impact on productivity, reducing cephalexin productivity from 14.5 g/L/hr to 13.6 g/L/hr. The addition of a CSTR prior to a PFR provides no advantage to fractional yield or 7-ADCA conversion than a PFR alone; however, the CSTR helps reduce total residence time and thus provides a higher overall productivity when compared to a PFR operating at the same conversion.

3.4 Effects of Enzyme Concentration on Reactor Design

AEH concentration was varied using the 250 mM PGME, 100 mM 7-ADCA example to study how the concentration of enzyme affects productivity, 7-ADCA conversion, and fractional yield. **Figure 8** shows the impact of AEH concentration on productivity. Productivity is proportional to the concentration of enzyme supplied to the reactor as more enzyme increases the speed of the reaction and thus requires a much smaller residence time to convert the same amount of reactant as a smaller concentration of enzyme would require. This in turn increases cephalexin productivity and has no impact on fractional yield (**Figure 8B**) as the rate of PG and cephalexin production scale equally with enzyme concentration. This data shows that fractional yield and conversion can be set by the reactor conditions (residence time, inlet concentrations, reactor configurations, etc.) and productivity can be scaled accordingly with the concentration of enzyme to match production requirements.

3.5 Simulation of a Single CSTR With an Improved AEH

Finally, to demonstrate the impacts of substrate inhibition on AEH catalyzed cephalexin synthesis, an engineered AEH was simulated assuming substrate inhibition could be reduced through protein engineering. This was simulated by increasing $K_{S,I}$ to 500 mM while keeping all other model parameters constant. In **Figure 9**, Pareto plots comparing 7-ADCA conversion (**Figure 9A**) and PGME conversion (**Figure 9B**) to both fractional yield and productivity. The Pareto curves show either the maximum fractional yields or productivities that can be obtained without sacrificing the other parameter at a given conversion by changing the reactor conditions and still obtaining a given conversion. The red curves show the Pareto curves for a single CSTR simulated with wildtype AEH from *Xanthomonas campestris pv. campestris.* (Lagerman et al., 2021), and the black curves show the hypothetical improved AEH with reduced substrate inhibition. All Pareto plots are simulated with 200 nM AEH.

With the wildtype AEH, high conversion of 7-ADCA cannot be reached without sacrificing both fractional yield and productivity. Past 50% 7-ADCA conversion, equal amounts of both byproduct PG and cephalexin are produced rendering an overall inefficient process with just a single CSTR as previously discussed. With an improved AEH, a single CSTR can be designed for 75% conversion of 7-ADCA while still reaching fractional yields up to 75% and productivities between 80–110 g/L/hr. The single CSTR operated with an improved AEH can also reach much higher conversions of PGME while maintaining high fractional yield, which is not possible with the current AEH.

4 DISCUSSION AND CONCLUSION

The design of an efficient reactor network for the synthesis of cephalexin catalyzed by AEH is a difficult task due to rapid deactivation of AEH (**Figure 2**) and strong substrate inhibition by PGME. While addition of AEH over time into the reactor is a possible solution for constant enzyme concentration, such a process would be relatively expensive and, overall, an infeasible solution. Instead, improvements to the stability of AEH can be achieved through protein engineering and should

be pursued to further enable AEH catalyzed synthesis of cephalexin.

Substrate inhibition should also be a focus for AEH engineering efforts. Based on the current kinetic model, the inhibition constant for AEH toward PGME ($K_{S,I}$) is 20 mM and reactor configurations require PGME well above 100 mM for selective and efficient production of cephalexin (**Figure 3**). Further understanding of the underlying mechanism for PGME inhibition and modifications to alleviate this inhibition are necessary to further pursue AEH for synthesis of cephalexin. If substrate inhibition can be reduced through protein engineering, a single CSTR could be operated to obtain high fractional yield, substrate conversion, and productivity (**Figure 8**). Other reactor configurations may further optimize use of an improved AEH; however, this is currently outside the scope of this work.

Careful design of an AEH-catalyzed reactor network can help alleviate the effects of substrate inhibition with the current AEH; however, tradeoffs between high substrate conversion and high fractional yield still exist. While maintaining a high inlet ratio of 7-ADCA to PGME improves selectivity toward cephalexin, doing so reduces maximum 7-ADCA conversion (**Figures 3**, **4**, **6**) and leads to a large amount of wasted substrate. As 7-ADCA is the more expensive reactant, conversion of 7-ADCA should be maximized without sacrifice of selectivity toward cephalexin which is currently not attainable given the current substrate inhibition.

Based on these simulations, no single optimum design can be found that maximizes productivity, fractional yield, and 7-ADCA conversion (**Figure 3**). With a single CSTR, the highest productivity is achieved at low concentrations of both 7-ADCA and PGME as substrate inhibition is not as prevalent (**Figure 3C**). High fractional yield occurs at high concentrations of 7-ADCA and low concentrations of PGME to shift production away from PG and toward cephalexin (**Figure 3B**); however, this comes at a cost to 7-ADCA conversion as PGME becomes the limiting substrate. Finally, high 7-ADCA conversion is attainable with low 7-ADCA and high PGME (**Figure 3A**), but much more byproduct PG is produced which lowers fractional yield.

A single PFR allows for higher conversion and fractional yield over a single CSTR, but total residence time and productivity suffer (**Figure 4**). Productivity can be improved through an increase in AEH supplied to the reactor (**Figure 7**) but operating at high 7-ADCA conversion still reduces fractional yields to inefficient values as the production of PG increases drastically as 7-ADCA is consumed (**Figure 4D**). Multi-reactor configurations allow for increases in 7-ADCA conversion relative to a single CSTR but cannot achieve higher 7-ADCA conversions than can be obtained with a single PFR. Higher fractional yields are also attainable relative to a single CSTR (**Figure 5**, **Figures 6A, B**); however, this conversion increase comes at the cost of productivity (**Figure 6C**) and increased residence time (**Figure 6D**). Ultimately, a single PFR provides the highest fractional yield at the highest 7-ADCA conversion and should be considered for AEH catalyzed synthesis of cephalexin.

DATA AVAILABILITY STATEMENT

Publicly available datasets were analyzed in this study. This data can be found here: doi.org/10.1016/j.cej.2021.131816.

AUTHOR CONTRIBUTIONS

CL. conducted the simulations, interpreted the results, and wrote the draft of the manuscript, MG. guided the design of simulations, AB. conceived the study, and MG, RR, and AB. critically accompanied the writing of the manuscript.

FUNDING

This work was supported by the U.S. Food and Drug Administration (FDA), Center for Drug Evaluation and Research (CDER), Office of Pharmaceutical Quality (OPQ), through Grant U01FD006484, which is gratefully acknowledged. CL. gratefully acknowledges funding by the U.S National Science Foundation through the Graduate Research Fellowship Program (GRFP) under Grant No. DGE-1650044.

SUPPLEMENTARY MATERIAL

The Supplementary Material for this article can be found online at: https://www.frontiersin.org/articles/10.3389/fbioe.2022.826357/full#supplementary-material

REFERENCES

Andrić, P., Meyer, A. S., Jensen, P. A., and Dam-Johansen, K. (2010). Reactor Design for Minimizing Product Inhibition during Enzymatic Lignocellulose Hydrolysis: I. Significance and Mechanism of Cellobiose and Glucose Inhibition on Cellulolytic Enzymes. *Biotechnol. Adv.* 28 (3), 308–324. doi:10.1016/j.biotechadv.2010.01.003

Barends, T. R. M., Polderman-Tijmes, J. J., Jekel, P. A., Hensgens, C. M. H., de VriesDe Vries, E. J., JanssenJanssen, D. B., et al. (2003). The Sequence and Crystal Structure of the α-Amino Acid Ester Hydrolase from Xanthomonas Citri Define a New Family of β-Lactam Antibiotic Acylases. *J. Biol. Chem.* 278 (25), 23076–23084. doi:10.1074/jbc.m302246200

Blum, J. K., and Bommarius, A. S. (2010). Amino Ester Hydrolase from Xanthomonas Campestris Pv. Campestris, ATCC 33913 for Enzymatic Synthesis of Ampicillin. *J. Mol. Catal. B Enzym* 67 (1-2), 21–28. doi:10.1016/j.molcatb.2010.06.014

Blum, J. K., Ricketts, M. D., and Bommarius, A. S. (2012). Improved Thermostability of AEH by Combining B-FIT Analysis and Structure-Guided Consensus Method. *J. Biotechnol.* 160 (3-4), 214–221. doi:10.1016/j.jbiotec.2012.02.014

Caşcaval, D., Turnea, M., Galaction, A.-I., and Blaga, A. C. (2012). "6-Aminopenicillanic Acid Production in Stationary Basket Bioreactor with Packed Bed of Immobilized Penicillin Amidase—Penicillin G Mass Transfer and Consumption Rate under Internal Diffusion Limitation. *Biochem. Eng. J.* 69, 113–122. doi:10.1016/j.bej.2012.09.004

Chandel, A. K., Rao, L. V., Narasu, M. L., and Singh, O. V. (2008). The Realm of Penicillin G Acylase in β-lactam Antibiotics. *Enzyme Microb. Techn.* 42 (3), 199–207. doi:10.1016/j.enzmictec.2007.11.013

Cuthbertson, A. B., Rodman, A. D., Diab, S., and Gerogiorgis, D. I. (2019). Dynamic Modelling and Optimisation of the Batch Enzymatic Synthesis of Amoxicillin. *Processes* 7 (6), 318. doi:10.3390/pr7060318

Elander, R. P. (2003). Industrial Production of Beta-Lactam Antibiotics. *Appl. Microbiol. Biotechnol.* 61 (5-6), 385–392. doi:10.1007/s00253-003-1274-y

Encarnación-Gómez, L. G., Bommarius, A. S., and Rousseau, R. W. (2016). Reactive Crystallization of β-lactam Antibiotics: Strategies to Enhance Productivity and Purity of Ampicillin. *React. Chem. Eng.* 1 (3), 321–329. doi:10.1039/C5RE00092K

Fogler, H. S. (1999). *Elements of Chemical Reaction Engineering*. Third edition. Upper Saddle River, N.J.: Prentice Hall PTR.

Harmand, J., and Dochain, D. (2005). The Optimal Design of Two Interconnected (Bio)chemical Reactors Revisited. *Comput. Chem. Eng.* 30 (1), 70–82. doi:10.1016/j.compchemeng.2005.08.003

Hernandez-Justiz, O., Terreni, M., Pagani, G., Garcia, J. L., Guisan, J. M., and Fernandez-Lafuente, R. (1999). "Evaluation of Different Enzymes as Catalysts for the Production of Beta-Lactam Antibiotics Following a Kinetically Controlled Strategy. *Enzyme Microb. Techn.* 25 (3-5), 336–343. doi:10.1016/s0141-0229(99)00050-2

Kallenberg, A. I., van Rantwijk, F., and Sheldon, R. A. (2005). "Immobilization of Penicillin G Acylase: The Key to Optimum Performance. *Adv. Synth. Catal.* 347 (7-8), 905–926. doi:10.1002/adsc.200505042

Kasche, V. (1986). Mechanism and Yields in Enzyme Catalysed Equilibrium and Kinetically Controlled Synthesis of β-lactam Antibiotics, Peptides and Other Condensation Products. *Enzyme Microb. Techn.* 8 (1), 4–16. doi:10.1016/0141-0229(86)90003-7

Kato, K., Kawahara, K., Takahashi, T., and Igarasi, S. (1980). Enzymatic Synthesis of Amoxicillin by the Cell-Bound .ALPHA.-amino Acid Ester Hydrolase of Xanthomonas Citri. *Agric. Biol. Chem.* 44 (4), 821–825. doi:10.1080/00021369.1980.1086404210.1271/bbb1961.44.821

Lagerman, C. E., Grover, M. A., Rousseau, R. W., and Bommarius, A. S. (2021). Kinetic Model Development for α-amino Ester Hydrolase (AEH)-catalyzed Synthesis of β-lactam Antibiotics. *Chem. Eng. J.* 426, 131816. doi:10.1016/j.cej.2021.131816

Laxminarayan, R. (2014). Antibiotic Effectiveness: Balancing Conservation against Innovation. *Science* 345 (6202), 1299–1301. doi:10.1126/science.1254163

Lee, S. L., O'Connor, T. F., Yang, X., Cruz, C. N., Chatterjee, S., Madurawe, R. D., et al. (2015). Modernizing Pharmaceutical Manufacturing: from Batch to Continuous Production. *J. Pharm. Innov.* 10 (3), 191–199. doi:10.1007/s12247-015-9215-8

Likozar, B., Senica, D., and Pavko, A. (2012). Comparison of Adsorption Equilibrium and Kinetic Models for a Case Study of Pharmaceutical Active Ingredient Adsorption from Fermentation Broths: Parameter Determination, Simulation, Sensitivity Analysis and Optimization. *Braz. J. Chem. Eng.* 29, 635–652. doi:10.1590/S0104-66322012000300020

Likozar, B., Senica, D., and Pavko, A. (2013). Interpretation of Experimental Results for Vancomycin Adsorption on Polymeric Resins in a Fixed Bed Column by Mathematical Modeling with Independently Estimated Parameters. *Ind. Eng. Chem. Res.* 52 (26), 9247–9258. doi:10.1021/ie400832p

Lindeque, R., and Woodley, J. (2019). Reactor Selection for Effective Continuous Biocatalytic Production of Pharmaceuticals. *Catalysts* 9 (3), 262. doi:10.3390/catal9030262

Ma, Y., Yang, Z., El-Khoruy, A., Zhang, N., Li, J., Zhang, B., et al. (2021). Simultaneous Synthesis and Design of Reaction-Separation-Recycle Processes Using Rigorous Models. *Ind. Eng. Chem. Res.* 60 (19), 7275–7290. doi:10.1021/acs.iecr.1c00250

Mascia, S., Heider, P. L., Zhang, H., Lakerveld, R., Benyahia, B., Barton, P. I., et al. (2013). End-to-End Continuous Manufacturing of Pharmaceuticals: Integrated Synthesis, Purification, and Final Dosage Formation. *Angew. Chem. Int. Ed.* 52 (47), 12359–12363. doi:10.1002/anie.201305429,

McDonald, M. A., Bommarius, A. S., Grover, M. A., and Rousseau, R. W. (2019b). Continuous Reactive Crystallization of β-lactam Antibiotics Catalyzed by Penicillin G Acylase. Part II: Case Study on Ampicillin and Product Purity. *Comput. Chem. Eng.* 126, 332–341. doi:10.1016/j.compchemeng.2019.04.005

McDonald, M. A., Bommarius, A. S., Rousseau, R. W., and Grover, M. A. (2019c). Continuous Reactive Crystallization of β-lactam Antibiotics Catalyzed by Penicillin G Acylase. Part I: Model Development. *Comput. Chem. Eng.* 123, 331–343. doi:10.1016/j.compchemeng.2018.12.029

McDonald, M. A., Bommarius, A. S., and Rousseau, R. W. (2017). Enzymatic Reactive Crystallization for Improving Ampicillin Synthesis. *Chem. Eng. Sci.* 165, 81–88. doi:10.1016/j.ces.2017.02.040

McDonald, M. A., Bromig, L., Grover, M. A., Rousseau, R. W., and Bommarius, A. S. (2018). Kinetic Model Discrimination of Penicillin G Acylase thermal Deactivation by Non-isothermal Continuous Activity Assay. *Chem. Eng. Sci.* 187, 79–86. doi:10.1016/j.ces.2018.04.046

McDonald, M. A., Marshall, G. D., Bommarius, A. S., Grover, M. A., and Rousseau, R. W. (2019a). Crystallization Kinetics of Cephalexin Monohydrate in the Presence of Cephalexin Precursors. *Cryst. Growth Des.* 19 (9), 5065–5074. doi:10.1021/acs.cgd.9b00429

Myerson, A. S., Krumme, M., Nasr, M., Thomas, H., and Braatz, R. D. (2015). Control Systems Engineering in Continuous Pharmaceutical Manufacturing May 20-21, 2014 Continuous Manufacturing Symposium. *J. Pharm. Sci.* 104 (3), 832–839. doi:10.1002/jps.24311

Nam, D. H., Kim, C., and Ryu, D. D. Y. (1985). Reaction Kinetics of Cephalexin Synthesizing Enzyme fromXanthomonas Citri. *Biotechnol. Bioeng.* 27 (7), 953–960. doi:10.1002/bit.260270705

Polderman-Tijmes, J. J., Jekel, P. A., de Vries, E. J., van Merode, A. E. J., Floris, R., van der Laan, J.-M., et al. (2002). Cloning, Sequence Analysis, and Expression in Escherichia coli of the Gene Encoding an α-Amino Acid Ester Hydrolase from Acetobacter Turbidans. *Appl. Environ. Microbiol.* 68 (1), 211–218. doi:10.1128/aem.68.1.211-218.2002

Ryu, Y. W., and Ryu, D. D. Y. (1988). Semisynthetic β-lactam Antibiotic Synthesizing Enzyme from Acetobacter Turbidans: Catalytic Properties. *Enzyme Microb. Techn.* 10 (4), 239–245. doi:10.1016/0141-0229(88)90073-7

Salami, H., Lagerman, C. E., Harris, P. R., McDonald, M. A., Bommarius, A. S., Rousseau, R. W., et al. (2020). Model Development for Enzymatic Reactive Crystallization of β-lactam Antibiotics: a Reaction-Diffusion-Crystallization Approach. *React. Chem. Eng.* 5 (11), 2064–2080. doi:10.1039/D0RE00276C

Srirangan, K., Orr, V., Akawi, L., Westbrook, A., Moo-Young, M., and Chou, C. P. (2013). Biotechnological Advances on Penicillin G Acylase: Pharmaceutical Implications, Unique Expression Mechanism and Production Strategies. *Biotechnol. Adv.* 31 (8), 1319–1332. doi:10.1016/j.biotechadv.2013.05.006

Takahashi, T., Kato, K., Yamazaki, Y., and Isono, M. (1977). Synthesis of Cephalosporins and Penicillins by Enzymatic Acylation. *Jpn. J. Antibiot.* 30, 230–238.

Takahashi, T., Yamazaki, Y., Kato, K., and Isono, M. (1972). Enzymic Synthesis of Cephalosporins. *J. Am. Chem. Soc.* 94 (11), 4035–4037. doi:10.1021/ja00766a076

Takahashi, T., Yamazaki, Y., and Kato, K. (1974). Substrate Specificity of an α-amino Acid Ester Hydrolase Produced by Acetobacter Turbidans A.T.C.C. 9325. *Biochem. J.* 137 (3), 497–503. doi:10.1042/bj1370497

Thakuria, B., and Lahon, K. (2013). The Beta Lactam Antibiotics as an Empirical Therapy in a Developing Country: An Update on Their Current Status and Recommendations to Counter the Resistance against Them. *J. Clin. Diagn. Res.* 7 (6), 1207–1214. doi:10.7860/JCDR/2013/5239.3052

Valencia, P., Flores, S., Wilson, L., and Illanes, A. (2012). Batch Reactor Performance for the Enzymatic Synthesis of Cephalexin: Influence of Catalyst Enzyme Loading and Particle Size. *New Biotechnol.* 29 (2), 218–226. doi:10.1016/j.nbt.2011.09.002

Van Boeckel, T. P., Ashok, A., Caudron, Q., Grenfell, B. T., Levin, S. A., Laxminarayan, R., et al. (2014). Global Antibiotic Consumption 2000 to 2010: an Analysis of National Pharmaceutical Sales Data. *Lancet Infect. Dis.* 14 (8), 742–750. doi:10.1016/s1473-3099(14)70780-7

Vasic-Racki, D., Kragl, U., and Liese, A. (2003). Benefits of Enzyme Kinetics Modelling. *Chem. Biochem. Eng. Q.* 17, 7–18.

Wegman, M. A., Janssen, M. H. A., van Rantwijk, F., and Sheldon, R. A. (2001). "Towards Biocatalytic Synthesis of β-Lactam Antibiotics. *Adv. Synth. Catal.*343(6–7), 559–576. doi:10.1002/1615-4169(200108)343:6/7<559::AID-ADSC559>3.0.CO;2-Z

Youshko, M. I., Chilov, G. G., Shcherbakova, T. A., and Svedas, V. K. (2002a). Quantitative Characterization of the Nucleophile Reactivity in Penicillin Acylase-Catalyzed Acyl Transfer Reactions. *Biochim. Biophys. Acta* 1599 (1-2), 134–140. doi:10.1016/s1570-9639(02)00413-2

Youshko, M. I., and Švedas, V. K. (2000). Kinetics of Ampicillin Synthesis Catalyzed by Penicillin Acylase from E. coli in Homogeneous and Heterogeneous Systems. Quantitative Characterization of Nucleophile Reactivity and Mathematical Modeling of the Process. *Biochemistry (Mosc)* 65 (12), 1367–1375. doi:10.1023/a:1002896621567

Youshko, M. I., van Langen, L. M., de Vroom, E., van Rantwijk, F., Sheldon, R. A., and Svedas, V. K. (2002b). Penicillin Acylase-Catalyzed Ampicillin Synthesis Using a pH Gradient: A New Approach to Optimization. *Biotechnol. Bioeng.* 78 (5), 589–593. doi:10.1002/bit.10234

Conflict of Interest: The authors declare that the research was conducted in the absence of any commercial or financial relationships that could be construed as a potential conflict of interest.

frontiers in Bioengineering and Biotechnology

ORIGINAL RESEARCH
published: 24 March 2022
doi: 10.3389/fbioe.2022.830712

Regioselective One-Pot Synthesis of Hydroxy-(*S*)-Equols Using Isoflavonoid Reductases and Monooxygenases and Evaluation of the Hydroxyequol Derivatives as Selective Estrogen Receptor Modulators and Antioxidants

Hanbit Song[1,2†], *Pyung-Gang Lee*[1,2,3†], *Junyeob Kim*[1,2], *Joonwon Kim*[1,2], *Sang-Hyuk Lee*[1,2], *Hyun Kim*[1,2], *Uk-Jae Lee*[1,2], *Jin Young Kim*[1,2], *Eun-Jung Kim*[4] and *Byung-Gee Kim*[1,2,4,5*]

[1]School of Chemical and Biological Engineering, Seoul National University, Seoul, South Korea, [2]Institute of Molecular Biology and Genetics, Seoul National University, Seoul, South Korea, [3]Institute of Engineering Research, Seoul National University, Seoul, South Korea, [4]Bio-MAX/N-Bio Institute, Seoul National University, Seoul, South Korea, [5]Institute for Sustainable Development (ISD), Seoul National University, Seoul, South Korea

Several regiospecific enantiomers of hydroxy-(*S*)-equol (HE) were enzymatically synthesized from daidzein and genistein using consecutive reduction (four daidzein-to-equol–converting reductases) and oxidation (4-hydroxyphenylacetate 3-monooxygenase, HpaBC). Despite the natural occurrence of several HEs, most of them had not been studied owing to the lack of their preparation methods. Herein, the one-pot synthesis pathway of 6-hydroxyequol (6HE) was developed using HpaBC (*Ec*HpaB) from *Escherichia coli* and (*S*)-equol-producing *E. coli*, previously developed by our group. Based on docking analysis of the substrate or products, a potential active site and several key residues for substrate binding were predicted to interpret the (*S*)-equol hydroxylation regioselectivity of *Ec*HpaB. Through investigating mutations on the key residues, the T292A variant was verified to display specific mono-*ortho*-hydroxylation activity at C6 without further 3′-hydroxylation. In the consecutive oxidoreductive bioconversion using T292A, 0.95 mM 6HE could be synthesized from 1 mM daidzein, while 5HE and 3′HE were also prepared from genistein and 3′-hydroxydaidzein (3′HD or 3′-ODI), respectively. In the following efficacy tests, 3′HE and 6HE showed about 30~200-fold higher EC_{50} than (*S*)-equol in both ER_α and ER_β, and they did not have significant SERM efficacy except 6HE showing 10% lower β/α ratio response than that of 17β-estradiol. In DPPH radical scavenging assay, 3′HE showed the highest antioxidative activity among the examined isoflavone derivatives: more than 40% higher than the well-known 3′HD. In conclusion, we demonstrated that HEs could be produced efficiently and regioselectively through the one-pot bioconversion platform and evaluated estrogenic and antioxidative activities of each HE regio-isomer for the first time.

Keywords: hydroxy-(S)-equol, oxidoreductases, isoflavonoids, SERM (selective estrogen receptor modulator), antioxidants, one-pot synthesis, enzyme engineering

OPEN ACCESS

Edited by:
Didier Laurent Buisson, Centre National de la Recherche Scientifique (CNRS), France

Reviewed by:
Yasushi Ogasawara, Hokkaido University, Japan
Dirk Tischler, Ruhr University Bochum, Germany

***Correspondence:**
Byung-Gee Kim
byungkim@snu.ac.kr

[†]*These authors have contributed equally to this work*

Specialty section:
This article was submitted to Bioprocess Engineering, a section of the journal Frontiers in Bioengineering and Biotechnology

Received: *07 December 2021*
Accepted: *31 January 2022*
Published: *24 March 2022*

Citation:
Song H, Lee P-G, Kim J, Kim J, Lee S-H, Kim H, Lee U-J, Kim JY, Kim E-J and Kim B-G (2022) Regioselective One-Pot Synthesis of Hydroxy-(S)-Equols Using Isoflavonoid Reductases and Monooxygenases and Evaluation of the Hydroxyequol Derivatives as Selective Estrogen Receptor Modulators and Antioxidants. Front. Bioeng. Biotechnol. 10:830712. doi: 10.3389/fbioe.2022.830712

INTRODUCTION

Anaerobic equol-producing bacteria such as *Slackia isoflavoniconvertens*, *Eggerthella* sp. YY7918, and *Lactococcus garvieae* can convert daidzein (or genistein) into (*S*)-equol (or (-)-5-hydroxyequol) in the human intestine with a strict enantioselective manner (Uchiyama et al., 2007; Yokoyama and Suzuki, 2008; Matthies et al., 2012). When such gut bacterial metabolites reach their biological target organs or tissues, they function as a selective estrogen receptor modulator (SERM) based on their selective binding affinity for ER_β over ER_α (Setchell et al., 2005). The functional phytoestrogen (*S*)-equol has been clinically verified to be effective against estrogen or testosterone-related health problems including women's menopausal symptoms, ovarian/prostate cancers, osteoporosis, and even hair loss (Lund et al., 2004; Jackson et al., 2011). However, its metabolism in the human body has not been completely understood yet. R.J. Schwen *et al.* observed that (*S*)-equol in rats, monkeys, and humans is mainly metabolized through the 4′-glucuronide conjugated form or 7-sulfated form in minor (Schwen et al., 2012). Otherwise, most researchers believe that it is just diluted and eventually removed along with urine, but a study suggests that hydroxylation of equol in the liver might be another route to discard equol in the human body (Marrian and Haslewood, 1932; Rufer et al., 2006). According to the observation, equol is mainly hydroxylated at C-3′, six or 8 *ortho*-positions of its inherent hydroxyl groups by enzymes, possibly cytochrome P450s (CYPs) present in the liver microsome.

Phytochemicals comprising multiple phenol groups on their backbone are called 'polyphenols'. Flavonoids or isoflavonoids are the representatives of the plant polyphenol, and their physiological activities against the human body vary along with the position or number of the hydroxyl groups on their aromatic backbone. For example, one of the major isoflavones in soybean, namely daidzein (7,4′-dihydroxyisoflavone), has moderate antioxidative activity; Also, *ortho*-dihydroxyisoflavone (ODI) derivatives such as 7,3′,4′-trihydroxyisoflavone (3′-hydroxydaidzein), 6,7,4′-trihydroxyisoflavone (6-hydroxydaidzein) and 7,8,4′-trihydroxyisoflavone (8-hydroxydaidzein) display superior antioxidative characters and unique biological functions caused by their actions on different signaling pathways such as anti-skin cancer (3′-hydroxydaidzein), anti-colon cancer, anti-adipogenesis (6-hydroxydaidzein), and anti-atopic dermatitis (8-hydroxydaidzein) pathways (Park et al., 2008; Park et al., 2010; Lee et al., 2011a; Lee et al., 2011b; Seo et al., 2013; Kim et al., 2014). In order to synthesize such hydroxylated polyphenols efficiently, scientists isolated several microbial enzymes and constructed the respective biocatalytic reaction systems. Those studies harnessed microbial cytochrome P450s, flavin-dependent monooxygenases (FMO), or tyrosinases in their natural or mutated forms for an efficient and regioselective production of plant polyphenols (Pandey et al., 2010; Lee et al., 2012; Lee et al., 2014; Lee S.-H. et al., 2016; Lee et al., 2019). In recent studies, a two-component FMO called HpaBC derived from *E. coli* or *P. aeruginosa* has been introduced as another potent candidate to hydroxylate aromatic chemicals. The two component FMO exhibited broad substrate specificities toward plant polyphenols so that naringenin and resveratrol were readily functionalized into eriodictyol (3′-hydroxynaringenin) and piceatannol (3-hydroxyresveratrol), respectively (Furuya and Kino, 2014; Lin and Yan, 2014).

Herein, we focused on the potential estrogenic and antioxidative activity of HEs which had not been studied due to the lack of proper synthetic methods. One study reported a single-step hydroxylation reaction of equol to 3′HE and 6HE, but the percent yields were quite low (<50%) probably due to the over-oxidation arising from adding too many HpaBC-expressing cells (Hashimoto et al., 2019). To overcome such limitations, herein, a set of polyphenol-hydroxylating enzymes from microbial monooxygenases including cytochrome P450, FMO and HpaBC was tested (**Figure 1**). Among the candidates, *Ec*HpaBC (HpaBC from *Escherichia coli*) was selected for its relatively high activity toward (*S*)-equol. Then, site-directed mutagenesis was performed for the key residues identified by ligand-docking analysis to modulate its regioselectivity. Finally, regioselective synthesis of 6-hydroxy-(*S*)-equol from daidzein was achieved using recombinant equol-producing and equol-hydroxylating strains simultaneously as whole-cell catalysts.

Other hydroxyequols including 3′-hydroxy-(*S*)-equol (3′HE) and 5-hydroxy-(*S*)-equol (5HE) were also prepared using the same recombinant equol-producing strain (Lee P.-G. et al., 2016; Lee S.-H. et al., 2016; Lee et al., 2017). The synthesized hydroxyequols as well as (*S*)-equol were subjected to the evaluation of their estrogenic activities using yeast two hybrid (Y2H) assay, which examined dose-responsive agonism of two ERs according to interactions with steroid receptor coactivator 1 (SRC1), and DPPH radical scavenging assay was used for the antioxidative efficacy test.

RESULTS AND DISCUSSION

Screening of (*S*)-Equol-Hydroxylating Monooxygenases

Since no specific oxygenases responsible for hydroxylation of equol have been reported yet, we examined several microbial monooxygenase candidates including cytochrome P450, FMO, and HpaBC. Because of the unfavorable diphenolase activity, tyrosinase was excluded in this study (Lee et al., 2012). CYP102G4 is a self-sufficient microbial cytochrome P450 isolated from *Streptomyces cattelya*. Similar to other self-sufficient P450s, CYP102G4 directly consumes NAD(P)H as an electron source to activate heme, forming 'Compound I' Fe=O (IV) that finally breaks the substrate C-H bond for monooxygenation (Rittle and Green, 2010; Kim et al., 2018). In our previous study, the CYP102G4, was characterized to show a naturally high monooxygenation activity for various polyaromatic substrates including benzophenone and flavone owing to its wide cavity in the active site that enables bulky substrates to easily access the activated heme species (Kim et al., 2018). Whole-cells expressing CYP102G4, however, gave poor conversion of (*S*)-equol (ca. < 1%) with minor detection of

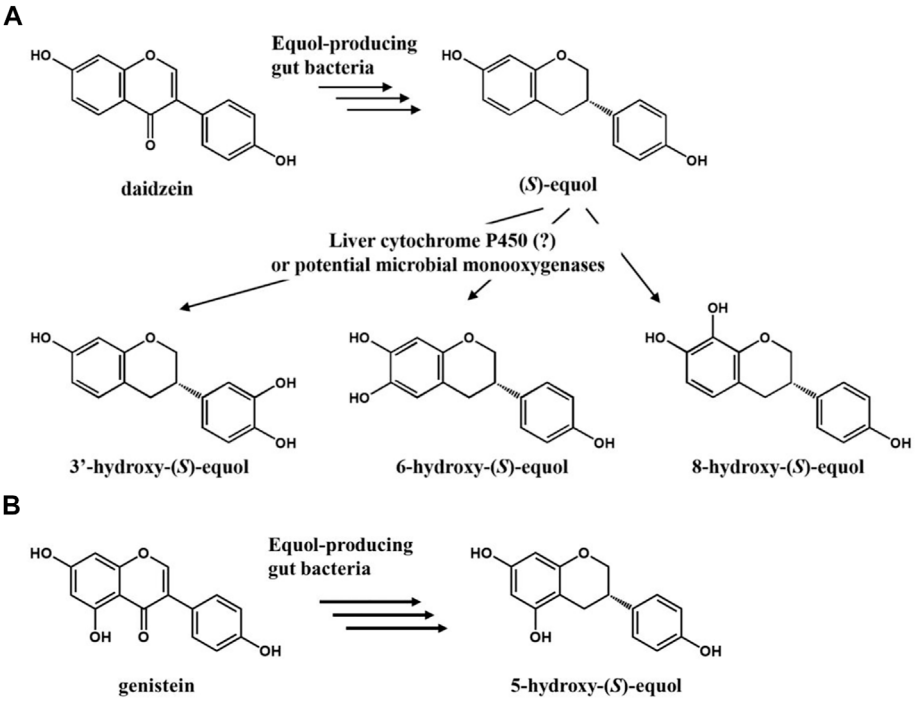

FIGURE 1 | (A) Potential scheme of (*S*)-equol hydroxylation after metabolism of daidzein into (*S*)-equol by gut bacteria. **(B)** Metabolism of genistein into 5-hydroxy-(*S*)-equol by gut bacteria.

3′-hydroxy-(*S*)-equol (3′HE), 6-hydroxy-(*S*)-equol (6HE), and 8-hydroxy-(*S*)-equol (8HE) as reaction products (**Figure 2** and **Figure 3**).

Next, flavin-containing monooxygenases (FMOs) are potent catalysts to prepare hydroxylated phytochemicals. In former studies, monooxygenation of daidzein, naringenin, and stilibene was achieved using FMOs from various microbial sources (Lee et al., 2014). We selected an FMO derived from *Methylophaga aminisulfidivorans* (*Ma*FMO), which was mainly examined for hydroxylation of indole to form indigo, an aromatic natural dye (Han et al., 2008). Although *Ma*FMO has been shown to exhibit superior activity for indole, no detectable monooxygenation activity for (*S*)-equol was found (**Figure 2**). Instead, we paid attention to a two-component FAD-dependent monooxygenase called *Ec*HpaBC that was previously identified as a 4-hydroxyphenylacetate 3-monooxygenase in *E. coli* (Prieto and Garcia, 1994). The two-component FMO showed excellent hydroxylation activity for plant-derived polyphenols such as naringenin, resveratrol, and afzelechin with high efficiency (Lin and Yan, 2014; Jones et al., 2016). Interestingly, *Ec*HpaBC-expressing whole cells resulted in remarkable consumption of (*S*)-equol (for OD_{600} = 10, ca. 79% conversion in 4 h) and generated three products with single or multiple hydroxyl group(s), which were finally identified as 6HE, 3′HE, and 6,3′-dihydroxy-(*S*)-equol (6,3′diHE) based on GC-MS analysis (**Figure 2** and **Figure 3**). The EI-MS fragmentation patterns of the hydroxyequols (HEs) corresponded to those of previously identified products, and the fragment ions of *m/z 280* and *295* generated from *m/z 562* mother peak in the 6,3′diHE mass spectrum indicated the presence of hydroxyl groups at C3' (B-ring) and C6 (A-ring), respectively (Rufer et al., 2006).

The unexpected high conversion rate of *Ec*HpaBC from enterobacterium, *E. coli*, for (*S*)-equol led us to assume that the enzyme might be potentially involved in isoflavone metabolism in the human intestine as well as biodegradation of aromatic compounds by *E. coli* (Diaz et al., 2001). However, a BLAST search of *Ec*HpaB for the human microbiome database (MetaQuery) revealed that the abundance and prevalence of HpaB in the human gut microbiome was only 0.089 and 33.19%, respectively, whereas those of daidzein reductase from *Slackia isoflavoniconvertens* were 0.26 and 100%, respectively. Even though several homologous HpaB proteins were observed in Proteobacteria including genus *Escherichia*, *Klebsiella*, *Enterobacter*, and *Providencia* with >50% sequence identity, the apparent low occurrence of HpaB might lead to infrequent detection of such HEs in the gut. Otherwise, generation of HEs might occur in the human liver *via* human cytochrome P450(CYP) enzymes, and the produced HEs would be estrogenic ligands such as (*S*)-equol or biologically active compounds with different roles from the parent compound (Rufer et al., 2006).

Modulation of Regioselectivity of HpaB

According to the *Ec*HpaBC-WT whole-cell reaction profile, *Ec*HpaBC catalyzed (*S*)-equol into 6HE and 3′HE as major and minor products, respectively, and then, the mono-hydroxylated HEs were subjected to consecutive second hydroxylation, being converted into 6,3′diHE. To interpret the

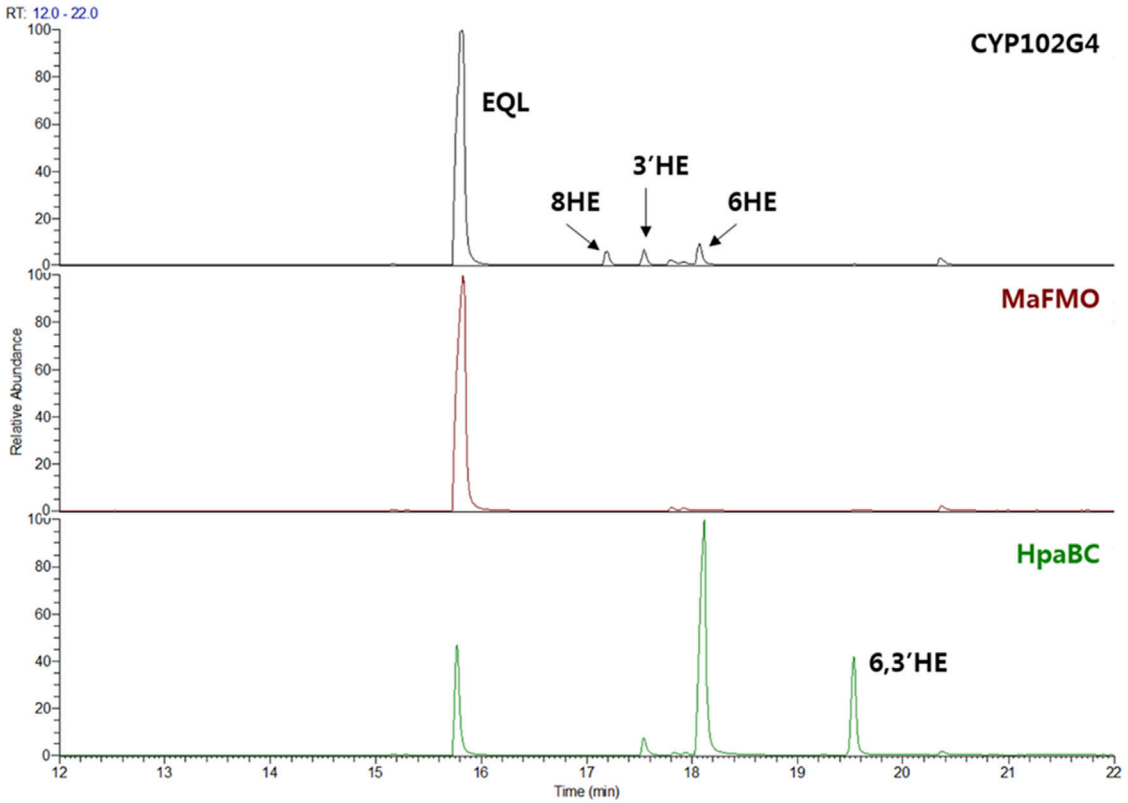

FIGURE 2 | (*S*)-equol (EQL) monooxygenation assay using whole-cells expressing three microbial monooxygenases: CYP102G4, *Ma*FMO, and *Ec*HpaBC. 200 μM of (*S*)-equol was initially used for the whole-cell (OD_{600} = 10) biotransformation, and reaction extracts at 4 h were analyzed using GC-MS.

regioselectivity of *Ec*HpaB, biochemical regiospecific analysis of the reaction products was carried out using protein–ligand docking analysis. The two-component HpaBC consists of HpaB, a catalytic component containing flavin adenine dinucleotide (FAD) as a prosthetic group, and HpaC, a NAD(P)H:flavin oxidoreductase component that regenerates $FADH_2$ for complete oxidation of the substrate and reduction of molecular oxygen by HpaB (Kim et al., 2007). In a recent report, the well-known broad substrate specificity of *Ec*HpaB toward various aromatic phytochemicals was explained by identifying the crystal structure (PDB code: 6QYI) (Deng et al., 2020). As proposed earlier, $FAD(H_2)$ freely associates and dissociates in between HpaB and HpaC to complete a cycle of the catalysis, explaining a loosely bound FAD in the active site of *Ec*HpaB (Kim et al., 2007; Deng et al., 2020). Arg164 and Arg333 stabilize diphosphate and adenine moieties, respectively, by constructing a substrate binding site in a groove of *Ec*HpaB. The possible substrate binding site on the *re* face (over flavin) of FAD, partially exposed to the protein surface, was predicted from the binding mode of 4-hydrophenylacetate in *Thermus thermophilus* HB8 HpaB (PDB code: 2YYI) (Kim et al., 2007). Based on the hypothesis that (*S*)-equol would bind to the same *re* face of FAD, energetically minimized (*S*)-equol was docked into the substrate binding region, which resulted in highly probable two binding modes of (*S*)-equol for 3′ and 6-hydroxylation with binding energy -7.6 and -7.4 kcal/mol, respectively (**Figure 4**). This computational prediction intuitively explains the production of both 3′HE and 6HE by *Ec*HpaBC. Moreover, the generation of another major product of *Ec*HpaBC, 6,3′diHE, could be rationalized by assuming a potential binding of 6HE in the binding pocket for the second hydroxylation at C-3′ and *vice versa* with low probability (**Supplementary Figure S1**). In the predicted bindings, virtual interactions between the bound substrate and enzyme residues were observed at R113, Y117, H155, I157, T292, and Y301. Among them, R113 and Y117 are the key residues to possibly stabilize 4′- or 7-OH of (*S*)-equol by hydrogen bondings in the respective two binding modes. The other residues might be involved in hydrophobic interactions with the aromatic substrate backbone.

Site-Directed Mutagenesis of HpaB to Enhance Its Regioselectivity

Given the possible binding mode of (*S*)-equol to *Ec*HpaB, we investigated the role of several active site residues that might determine the regioselectivity of *Ec*HpaB toward (*S*)-equol. Because the native regioselectivity of *Ec*HpaB favored 6-hydroxylation of (*S*)-equol, to generate 6HE as a sole product, we first focused on the effect of the residues contributing to

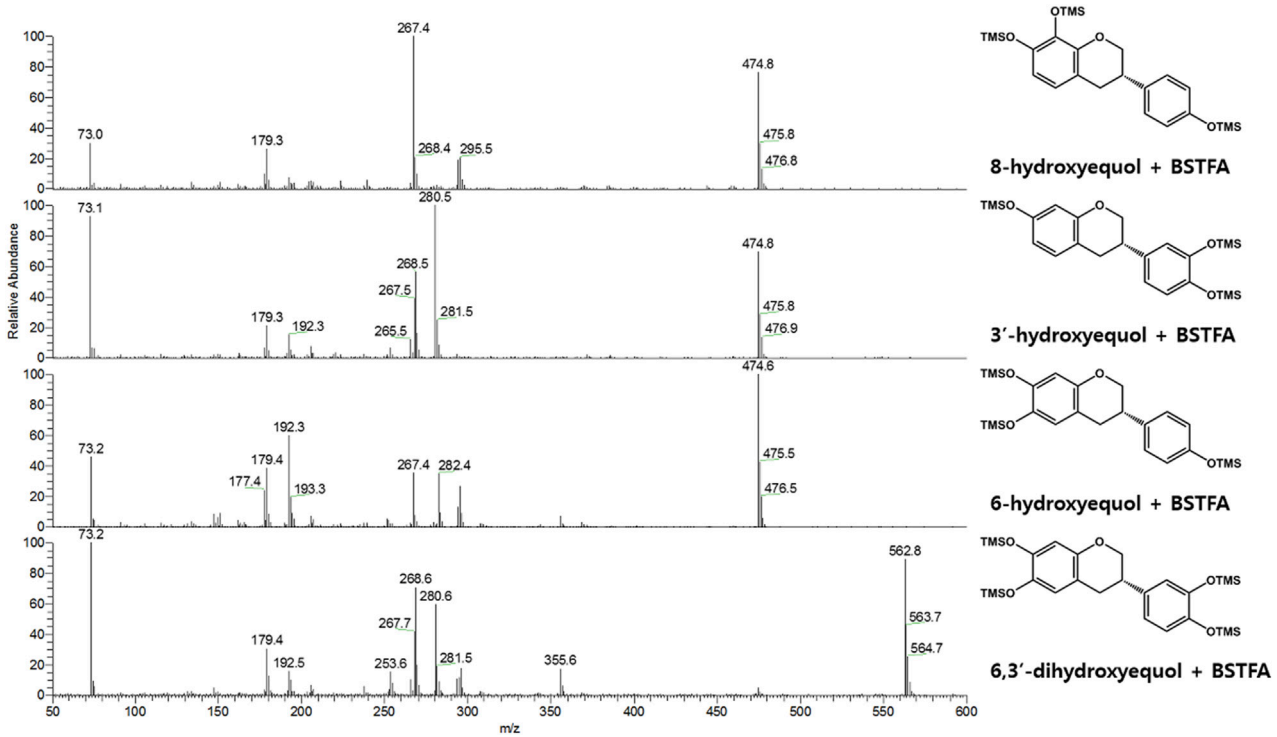

FIGURE 3 | EI-mass spectra (BSTFA: N, O-bis(trimethylsilyl)trifluoroacetamide) of trimethylsilylated hydroxy-(*S*)-equols biosynthesized by CYP0102G4 and *Ec*HpaBC. 3′-hydroxyequol and 6-hydroxyequol were detected in both enzyme reaction samples, while 8-hydroxyequol and 6,3′-dihydroxyequol were detected in the reaction extracts of CYP102G4 and *Ec*HpaBC, respectively.

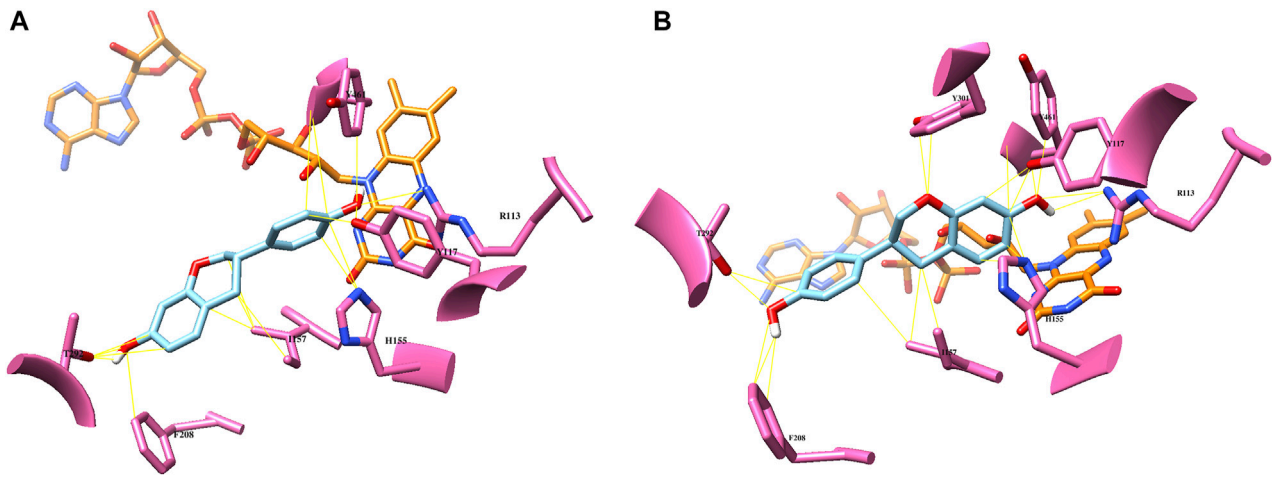

FIGURE 4 | Computational docking analysis of (*S*)-equol (cyan) of the crystal structure of *Ec*HpaB (PDB code: 6QYI) **(A)**: binding mode of 3′-hydroxylation **(B)**: binding mode of 6-hydroxylation. Potential substrate binding residues are highlighted with pink, and the FAD cofactor is shown as orange.

generate 3′HE or 6,3′diHE as minor or major products, respectively. If the residues stabilize the binding mode of (*S*)-equol for 3′-hydroxylation, any possible mutations on the residues might reduce the hydroxylation activity at C3′ at (*S*)-equol (*via* losing hydrogen bonding), while maintaining hydroxylation activity at C6. Because we did not want to lose the robust (*S*)-equol hydroxylation activity of *Ec*HpaB, the residues allowing hydrogen bonds or hydrophobic interactions with (*S*)-equol in both binding modes were excluded from the mutation candidates. An interaction between O1 of 6HE and

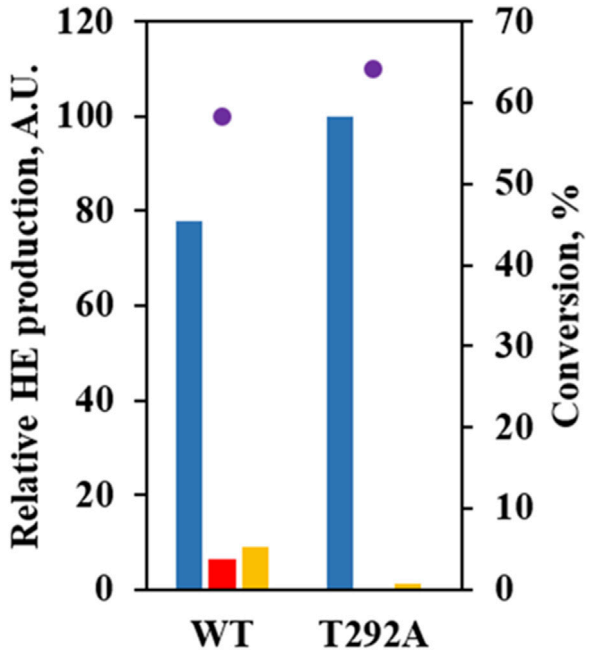

FIGURE 5 | Mutational study to investigate the role of T292 in (*S*)-equol hydroxylations. Relative abundances of 6HE (blue bar), 3′HE (red bar), and 6,3′diHE (yellow bar) were shown with (*S*)-equol conversion at 4 h (purple dot) for *Ec*HpaBC-WT and T292A. The 6HE production level was arbitrarily set to 100, and relative concentrations of the other HEs were estimated with peak areas on gas chromatogram.

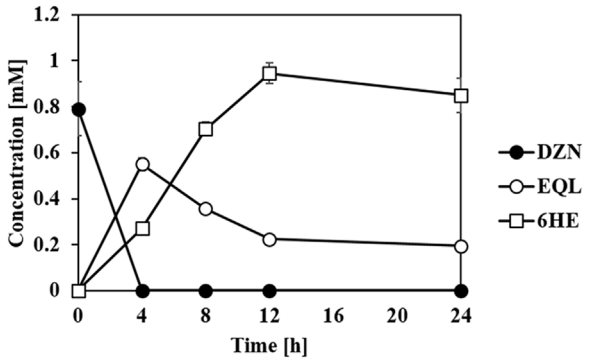

FIGURE 6 | Whole-cell biotransformation of daidzein (DZN) into (*S*)-equol (EQL) and subsequently to 6HE. The tDDDT strain (previously developed by Lee *et al.* (2016)) and t*Ec*HpaBC-T292A strain set up in one-pot reaction catalyzed daidzein (initial concentration: 1 mM) into equol (reduction step), and then subsequently into 6HE (oxidation step) in a highly regioselective manner. All the data were recorded using mean values with standard deviations for triplicates.

Y301 was the sole difference between the two binding modes. However, mutation of Y301 might deteriorate the activity of *Ec*HpaB on 6HE because Y301 seems to stabilize the binding of 6HE *via* hydrogen bonding.

Instead, we paid attention to T292 potentially forming a hydrogen bond with 6-OH when 6HE was docked. T292 appeared to contribute more stability to the binding of 6HE than (*S*)-equol due to hydroxylation at C3' (**Supplementary Figure S1**). In order to confirm our predictions, the T292A mutant was constructed and evaluated by using whole-cell assay. The mutant showed no detectable production of 3′HE compared to WT, but yielded 6HE as the major product (ca. 98%) and significantly diminished the production of 6,3′diHE (**Figure 5**), suggesting that the binding of (*S*)-equol or 6HE to wild-type *Ec*HpaB for hydroxylation at C3′ is likely to be stabilized by possible interactions with T292. Especially, hydrogen bonds between 6-OH of 6HE and T292-OH could explain the diminished production of 6,3′diHE by *Ec*HpaB T292A.

One-Pot Synthesis of *Ortho*-hydroxylated (*S*)-Equols From Daidzein

In previous studies, we suggested that an equol-producing recombinant *E. coli* strain that converted daidzein into (*S*)-equol would be a useful biocatalytic platform to prepare various equol analogs because the whole-cell biotransformation system of the transformant, tDDDT tolerated aerobic production of equol from daidzein (or 5-hydroxyequol from genistein) and displayed a high yield (g/L titer) and productivity (Lee P.-G. et al., 2016; Lee et al., 2017; Lee et al., 2018). It would be fascinating to synthesize novel HEs rarely found in the human body, but with unknown new biological roles, from common soy isoflavone daidzein. The previous development of the whole-cell catalysts and plasmids drove us to investigate the possibility of a combined use of equol and HE producing strains developed in this study in one-pot reaction. Then, one *E. coli* strain could perform the series of reduction steps of daidzein to (*S*)-equol, and the other strain could subsequently oxidize (*S*)-equol into HEs. The concept has proven to be valid in combinatorial whole-cell biotransformation exploiting tDDDT and the transformant with t*Ec*HpaBC-T292A strains as biocatalysts (**Figure 6**). All the initial amount of daidzein (ca. 1 mM) was consumed in 4 h, converted into (*S*)-equol rapidly, and then finally 0.95 mM of 6HE (ca. 244 mg/L) was synthesized in a highly regioselective manner. During the whole-cell biotransformation, no significant intermediates or byproducts were detected. This interesting finding shows that *Ec*HpaBC monooxygenase selectively reacts with (*S*)-equol rather than other isoflavone intermediates including daidzein, dihydrodaidzein, and tetrahydrodaidzein, which helped in maintaining the regioselectivity of *Ec*HpaBC-T292A in the microbial cells. This is the first study of one-pot synthesis involving oxidation and reduction of isoflavones using two individual whole cells. Because isoflavone derivatives including equol freely pass through the cell membrane, the two whole-cell compartments can perform simultaneous oxidoreductions of isoflavone with high efficiency (Lee et al., 2017). As a result, it becomes an efficient biocatalytic platform to prepare diverse equol derivatives including hydroxyequols or other chemically modified equols if active equol-catalyzing enzymes are provided. In addition, this platform is an economical choice for producing invaluable hydroxyequol derivatives, for example, the price of

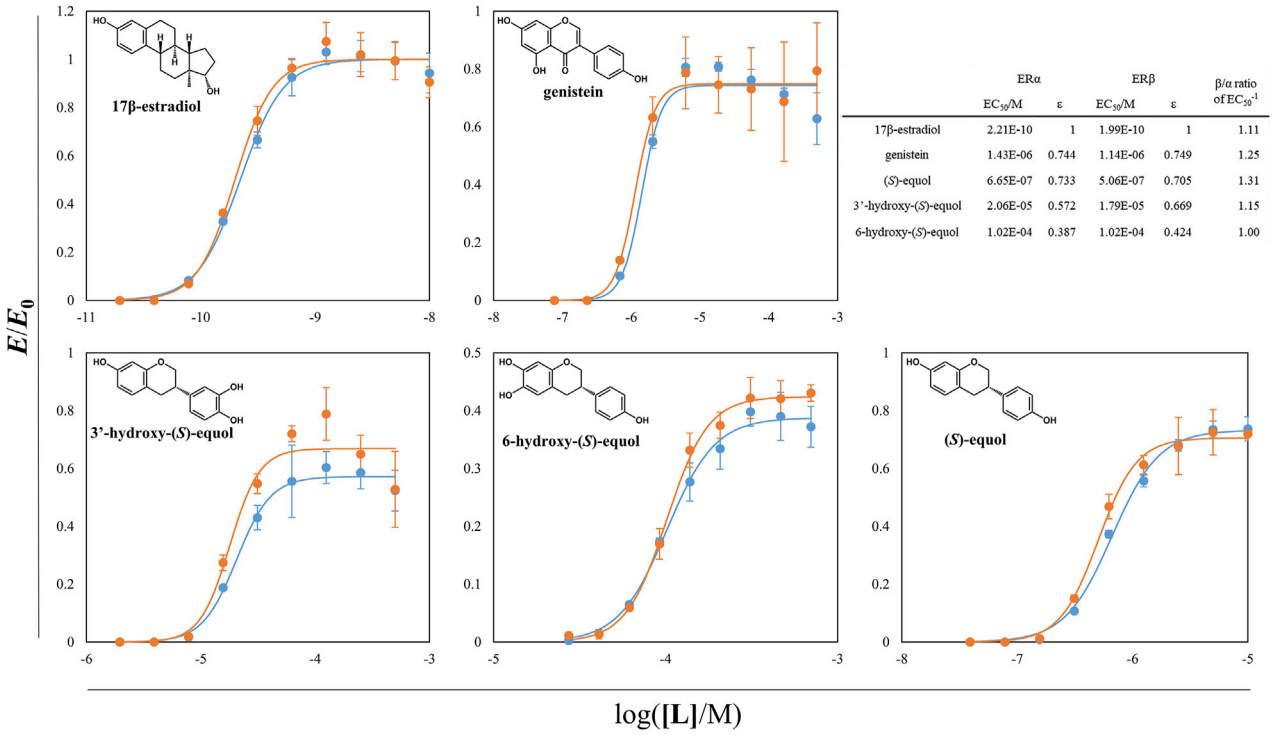

	ERα		ERβ		β/α ratio of EC_{50}^{-1}
	EC_{50}/M	ε	EC_{50}/M	ε	
17β-estradiol	2.21E-10	1	1.99E-10	1	1.11
genistein	1.43E-06	0.744	1.14E-06	0.749	1.25
(*S*)-equol	6.65E-07	0.733	5.06E-07	0.705	1.31
3'-hydroxy-(*S*)-equol	2.06E-05	0.572	1.79E-05	0.669	1.15
6-hydroxy-(*S*)-equol	1.02E-04	0.387	1.02E-04	0.424	1.00

FIGURE 7 | ER-SRC1 agonistic Y2H assay of equol derivatives and the other estrogenic compounds. *β*-galactosidase activity of yeast L40 cells harboring $ER_α$ (or $ER_β$) LBD hybrid and tSRC1 hybrid protein was assessed. The normalized responses of $ER_α$-SRC1 and $ER_β$-SRC1 interaction were expressed as blue and orange circles, respectively. The lines with two different colors were the regressed values. The inward table is the summary of EC_{50}s, *ε*s, and *β*/*α* ratios of each compounds. All the data were recorded using mean values with standard deviations for triplicates.

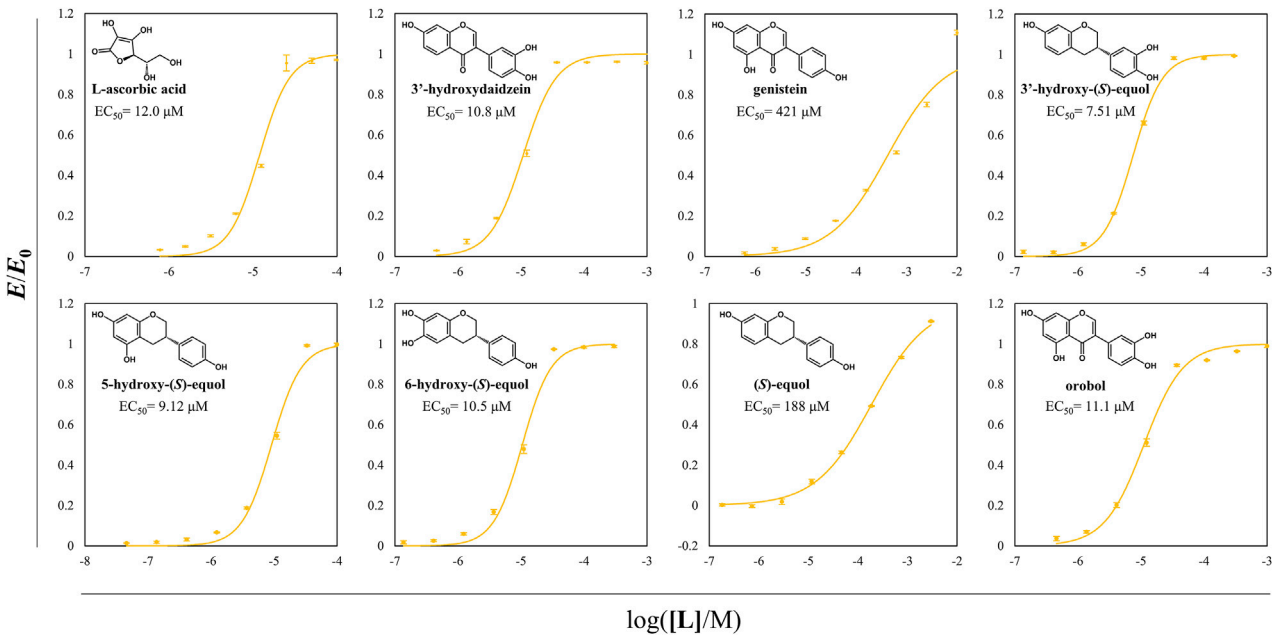

FIGURE 8 | DPPH radical scavenging assay of probable direct antioxidative compounds including HEs. DPPH radical scavenging activity of direct antioxidants was assessed according to the changes in the value of OD_{520}/OD_{495}. EC_{50} of DPPH radical scavenging of each compound was written in the plots. The normalized OD ratio change values were expressed as yellow circles, and the lines of yellow color were the regressed values. All the data were recorded using mean values with standard deviations for triplicates.

non-derivatized (*S*)-equol (>97%, in Sigma, St. Louis, MO, US at 01/10/2022) is $329/25 mg which is about 4.5 fold higher than daidzein (>98%, in Sigma at 01/10/2022, $73.5/25 mg).

Estrogenic Efficacies of (*S*)-Equol and Hydroxyequol Derivatives

With the aid of tDDDT whole-cell biotransformation, the other HEs including 3′HE and 5HE were synthesized through the conversion of corresponding isoflavones and purified to evaluate their estrogenic efficacies. The yeast-two-hybrid (Y2H) systems between ERs and SRC1 were exploited and agonistic activities of the estrogenic compounds synthesized throughout this study were measured (**Supplementary Figure S3** and **Figure 7**). In these systems, EC_{50}s of 17β-estradiol (E2) were about 0.2 nM for two ER isotypes with a slight potency preference on ER_β. Genistein and (*S*)-equol had about 3-orders of magnitude weaker estrogenic activity both on ER_α and ER_β than E2 but had SERM activity with the preference to ER_β with the β/α ratio of 1.25 and 1.31, respectively. 3′ and 6HE showed much lower activities than the other examined compounds having their EC_{50}s with concentrations in the range of 10^{-5}~10^{-4} M and had weaker SERM efficacies than (*S*)-equol displaying β/α ratios of 1.15 and 1.00, respectively, indicating that 6HE is a slightly ER_α preferring SERM compared to E2. 5HE did not show any response with concentrations in the range of 10^{-8}~10^{-3} M. However, a previous report demonstrated that 5HE had a higher binding affinity to ER_α than ER_β, suggesting that 5HE is an ER_α-selective antagonist (Lee et al., 2017). In general, all tested HEs did not show prominent estrogenic activity, which suggests that equol loses its estrogenic activity through metabolism in the liver (Rufer et al., 2006).

Antioxidative Effect of Hydroxyequol Derivatives

Antioxidative effects of the HEs and the prominent antioxidants were assessed through DPPH radical scavenging assay (**Figure 8**). Among the examined compounds, the compounds with a catechol moiety showed better radical scavenging activity even among the equol derivatives. Especially, all the HEs of interest had EC_{50} values in the range of 7–11 μM and had superior scavenging activities than 3′HD which is a well-known antioxidative isoflavone. 5HE and 3′HE had lower EC_{50} values than their original isoflavones, suggesting that the backbone of isoflavanes tends to be more potent direct antioxidants than the backbone of isoflavones.

CONCLUSION

Despite the possible presence of HEs in the human body, the lack of the synthetic methods of HE has prohibited us from pursuing further studies on their biological roles in hormonal regulation or intended nutritional effect in the human gut microbiome. In this study, we demonstrated that *Ec*HpaBC exhibited significant catalytic activity toward (*S*)-equol (a dominant form of equol enantiomer in the gut), generating 6HE and 6,3′diHE as major products. To enhance the yield of regioselective synthesis of 6HE from (*S*)-equol or daidzein, protein engineering of *Ec*HpaBC using the semi-rational approach, such as ligand-docking analysis and site-directed mutagenesis on the selected target residues, was carried out. Based on this approach, we achieved a 95% yield of 6-hydroxy-(*S*)-equol in 4 h from 1 mM daidzein with a one-pot synthesis procedure. Along with 6HE, the other HEs such as 3′HE and 5HE were synthesized from daidzein and genistein and were assessed for ER binding efficacy and antioxidant efficiency. This work provides valuable information on the construction of an efficient biocatalytic platform to prepare diverse HEs and evaluation of the synthesized HE compounds for ER-binding assays, for the first time. On the basis of our findings, other studies such as the evaluation of HEs' antagonism and/or *in vivo* testing for exploring novel activities of HEs could be supported, and a facile one-pot high-titer production of another equol derivatives is anticipated.

Experimental Methods

Chemicals. Daidzein and genistein were purchased from Sigma Aldrich, and (*S*)-equol was purchased from Tocris Bioscience. L-Ascorbic acid was purchased from Junsei. 2,2-Diphenyl-1-(2,4,6-trinitrophenyl)hydrazin-1-yl (DPPH) radical and 17β-estradiol (E2) were purchased from Sigma Aldrich. 3′-Hydroxydaidzein and orobol were prepared from daidzein and genistein respectively using the reported method (Lee S.-H. et al., 2016).

Microbial strains. Cloning information and used primers for the construction of *Ec*HpaBC and *Ma*FMO encoded vectors are listed in **Supplementary Table S1**. In brief, a two-component flavin-dependent monooxygenase, *Ec*HpaBC, was newly cloned from the genomic DNA of *Escherichia coli* ATCC 8739, and *Ma*FMO was cloned from the genomic DNA of *Methylophaga aminisulfidivorans*. The vector encoding CYP102G4 was previously constructed (Kim et al., 2018). Respective *E. coli* BL21 (DE3) transformants were verified for the soluble expression in SDS-PAGE (**Supplementary Figure S2**) and were then used as microbial strains for the whole-cell biotransformation. Three *Ec*HpaB mutants were made by site-directed mutagenesis using the listed overlapping primer-containing intended mutations. *Saccharomyces cerevisiae* L40 (*MATa his3*-200 *trp1*-901 *leu2*-3,112 *ade2 lys2*-801a.m. *URA3*(*lexAop*)8- *lacZ LYS2*(*lexAop*)4-*HIS3*) strain was utilized as a host for yeast-two-hybrid (Y2H) assays. The bait hybrid proteins were cloned in the pBTM116 vector as fusions of LexA DNA-binding domain (DBD)-human estrogen receptor *a* ligand-binding domain (ER_α LBD, 312–595) or LexA DBD-ER_β LBD (264–510). The prey hybrid protein was cloned in the pVP16 vector as a fusion of the VP16 activator domain (AD)-$(Gly_4Ser)_2$ linker-truncated steroid receptor coactivator 1 (tSRC1) (613–773). These sets of two vectors (pBTM116:LexA DBD-ER_α LBD & pVP16:VP16 AD-$(Gly_4Ser)_2$-tSRC1 or pBTM116: LexA DBD-ER_β LBD & pVP16:VP16 AD-$(Gly_4Ser)_2$-tSRC1) were transformed in the L40 strains.

Whole-cell biotransformation (GC-MS analysis). The aforementioned *E. coli* transformants were grown overnight, 1 ml of which was transferred to 50 ml of LB containing appropriate antibiotics. When the optical density (OD_{600}) of the cells reached 0.6 to 0.8, addition of 0.1 mM isopropyl-thio-β-D-galactopyranoside (IPTG) or 0.5 mM 5-aminolevulinic acid for heme formation of CYP102G4 induced the heterologous expression of monooxygenases overnight at 18°C. The monooxygenase-expressing cells were harvested *via* centrifugation (4°C, 4,000 rpm; 3,480 rcf for 10 min), washed with phosphate buffer saline (0.5x volume), and then centrifuged again for subsequent whole-cell catalysis.

The prepared whole cells were resuspended in the reaction solution (final OD_{600} = 10, total volume = 5 ml) composed of 0.1 M potassium phosphate buffer (KPB) pH 7.0, 1% (w/v) glucose, 5 mM L-ascorbic acid, and 0.2 mM (*S*)-equol. Whole-cell biotransformation was performed in the baffled flask shaken by 180 rpm at 30°C. In the case of consecutive oxidoreduction of daidzein into HEs, the reaction condition was slightly modified by referring to apreviously reported study (0.2 M KPB pH 8.0, 2% (w/v) glucose, 1% (v/v) glycerol, and polyvinylpyrrolidone 1% (w/v) in a 140 rpm shaking incubator) (Lee et al., 2018). The equol-producing whole-cells were also prepared following the previously reported method (Lee P.-G. et al., 2016).

Preparation of hydroxyequols. 6-Hydroxyequol (6HE) was synthesized with the aforementioned method. 5HE was synthesized with the previously reported method using genistein as the initial substrate (Lee P.-G. et al., 2016; Lee et al., 2017). 3′HE was synthesized using the same method from 3′-hydroxydaidzein which was prepared by *ortho*-hydroxylation of the tyrosianse derived from *Bacillus megaterium* with borate chelation (Lee P.-G. et al., 2016; Lee S.-H. et al., 2016). All of the isoflavonoids were purified through EA extraction, HPLC preparation (Econosil C18 prep column, 10 μm, 22 × 250 mm; Alltech, United States), and freeze-drying. The final purity of 6HE, 3′HE, and 5HE was confirmed with GC-MS or HPLC and ^{1}H-NMR analysis.

6-Hydroxy-(*S*)-equol: ^{1}H-NMR [$(CD_3)_2SO$, 400 MHz] δ 2.73 (m, 2H, H-4), 2.98 (m, 1H, H-3), 3.81 (t, *J* = 10.4 Hz, 1H, H-$2_β$), 4.05 (m, 1H, H-$2_α$), 6.19 (s, 1H, H-8), 6.44 (s, 1H, H-5), 6.71 (d, *J* = 8.4 Hz, 2H, H-3′), 7.09 (d, *J* = 8.4 Hz, 2H, H-2'), 8.26 (s, 1H, OH), 8.69 (s, 1H, OH), and 9.26 (s, 1H, OH).

5-Hydroxy-(*S*)-equol: ^{1}H-NMR [$(CD_3)_2SO$, 400 MHz] δ 2.47 (dd, *J* = 16.1, 10.9 Hz, 1H, H-$4_β$), 2.73 (ddd, *J* = 16.1, 5.5, 1.4 Hz, 1H, H-$4_α$), 2.95 (m, 1H, H-3), 3.83 (t, *J* = 10.4 Hz, 1H, H-$2_β$), 4.10 (dq, *J* = 10.4, 1.6 Hz, 1H, H-$2_α$), 5.70 (d, *J* = 2.3 Hz, 1H, H-6), 5.90 (d, *J* = 2.3 Hz, 1H, H-8), 6.72 (d, *J* = 8.5 Hz, 2H, H-3′), 7.11 (d, *J* = 8.5 Hz, 2H, H-2'), 8.93 (s, 1H, OH), 9.17 (s, 1H, OH), and 9.25 (s, 1H, OH).

3′-Hydroxy-(*S*)-equol: ^{1}H-NMR [$(CD_3)_2SO$, 400 MHz] δ 2.78 (m, 2H, H-4), 2.94 (m, 1H, H-3), 3.87 (t, *J* = 10.5 Hz, 1H, H-$2_β$), 4.15 (m, 1H, H-$2_α$), 6.19 (d, *J* = 2.4 Hz, 1H, H-8), 6.29 (dd, *J* = 8.2, 2.4 Hz, 1H, H-6), 6.56 (dd, *J* = 8.2, 2.2 Hz, 1H, H-6′), 6.67 (d, *J* = 2.3 Hz, 1H, H-2′), 6.69 (d, *J* = 8.2 Hz, 1H, H-5′), 6.87 (d, *J* = 8.2 Hz, 1H, H-5), 8.78 (s, 2H, OH), and 9.14 (s, 1H, OH).

Ligand-docking simulation. AutoDock Vina 1.1.2 (Trott and Olson, 2010) predicted docking modes of (*S*)-equol or 6HE in the reported *Ec*HpaB crystal structure (PDB code: 6QYI) (Deng et al., 2020), which were visualized by using Chimera 1.15.

Bioinformatic analyses. MetaQuery, an open-source web server for quantitative analysis of a given gene in the human gut microbiome, was utilized to calculate the abundance and prevalence of HpaB (from *E. coli*) and daidzein reductase (from *Slakia isoflavoniconvertens*, reference) in a human gut microbiome database (Nayfach et al., 2015). The minimum percent identity/maximum E-value/query alignment coverage/target alignment coverage were set to 30%/1e-5/70%/70% (web default values), respectively.

Yeast-two-hybrid assay. The transformed L40 strains were grown in synthetic leucine and tryptophan drop-out (SD L^-W^-) media. In 96-deep well plates, each well with the cultural medium of 500 μL SD L^-W^- contained initial OD_{600} = 0.1 of L40 preculture, 2% (v/v) DMSO, and specific amount of isoflavonoids or 17β-estradiol (E2). These plates were incubated at 30 °C with shaking of 1,000 rpm for overnight (~20 h). After the incubation, the cultures were centrifuged, and the supernatants were discarded. In each well, 500 μL Z-buffer (60 mM Na_2HPO_4, 40 mM NaH_2PO_4, 10 mM KCl, and 1 mM $MgSO_4$; pH 7.0) with 1 mM dithiothreitol (DTT) was filled and resuspended. 50 μL of each suspension was taken for OD_{600} measurement before chloroform treatment. (This value was not used for the measurement of the Miller unit.) Chloroform 50 μL was added to each 450 μL of the suspension, and the solution mixture was shaked for 1 min at 1,000 rpm to disrupt the cell membrane. The disrupted suspensions were kept still at room temperature for 2 min, and 50 μL aqueous aliquots were taken. In polystyrene flat-bottomed 96-well plate, each well was charged with 100 μL of Z-buffer with 1 mM DTT, 50 μL aqueous aliquot, and 50 μL of Z-buffer with 1 mM DTT and 0.4 mg/ml *ortho*-nitrophenyl-β-galactoside (ONPG). Initially, OD_{600} of all the wells was measured, and subsequently, OD_{420} of the same wells was measured for 30 min with a minute interval. The Miller units ($dOD_{420}/dt/OD_{600}$) of all the wells were calculated and normalized by using the value of the positive control (10 nM E2). The data were triplicated, and the points of average values were regressed using the following formula (Buchwald, 2020).

$$\frac{E}{E_0} = \frac{\varepsilon}{1 + 10^{n\left(\log(EC_{50}) - \log([L])\right)}},$$

where E/E_0 is the normalized Miller unit and ε is the maximum response relative to E2 (ε(E2) = 1). [L] is the concentration of ligands and *n* is the Hill's coefficient. EC_{50} is the value of effective concentration at $E/E_0 = 0.5\varepsilon$.

DPPH radical scavenging assay. In each well of polystyrene flat-bottom 96-well plates, 200 μL of solution containing 0.1 mM 2,2-diphenyl-1-(2,4,6-trinitrophenyl)hydrazin-1-yl (DPPH) radical, 50% (v/v) MeOH, 10% (v/v) DMSO, specific amount of compounds, and 1x concentration of phosphate buffered saline (PBS) was made. The PBS was prepared with 4x concentration of its original recipe with pH 7.4 and diluted by adding 50 μL in the solution mixture. The plates were incubated at 37°C for 30 min. The OD_{520} and OD_{495} of incubated plates were measured. The radical scavenging activity was defined as $(OD_{520}/OD_{495})_{DMSO}$-$OD_{520}/OD_{495}$. $(OD_{520}/OD_{495})_{DMSO}$ is the OD_{520}/OD_{495} of the

DMSO control without antioxidative compounds. The radical scavenging activity values were normalized with the value of the positive control (1 mM of L-ascorbic acid). The data were triplicated, and the average values were regressed using the following formula.

$$\frac{E}{E_0} = \frac{1}{1 + 10^{n\left(\log(EC_{50}) - \log([L])\right)}},$$

where E/E_0 is the normalized radical scavenging activity, [L] is the concentration of compounds, and n is the Hill's coefficient, and EC_{50} is the value of effective concentration at $E/E_0 = 0.5$.

DATA AVAILABILITY STATEMENT

The original contributions presented in the study are included in the article/**Supplementary Material**; further inquiries can be directed to the corresponding author.

AUTHOR CONTRIBUTIONS

HS and P-GL: conceptualization, experimentation, data curation, formal analysis, validation, and writing—original draft. JK: experimentation, data curation, formal analysis and writing—review, and editing. JK and S-HL: data curation and writing—review and editing. HK, U-JL, and JK: writing—review and editing. E-JK: experimentation, data curation, and formal analysis. Byung-gee Kim: conceptualization, supervision, project administration, writing—review, and editing.

FUNDING

This research was supported by the Korean Medical Device Development Fund grant funded by the Korean government (the Ministry of Science and ICT, the Ministry of Trade, Industry and Energy, the Ministry of Health and Welfare, and the Ministry of Food and Drug Safety) (Project Number. KMDF_PR_20200901_0151) and the Korean Fund for Regenerative Medicine (KFRM) grant funded by the Korean government (the Ministry of Science and ICT and the Ministry of Health and Welfare) (21A0301L1).

SUPPLEMENTARY MATERIAL

The Supplementary Material for this article can be found online at: https://www.frontiersin.org/articles/10.3389/fbioe.2022.830712/full#supplementary-material

REFERENCES

Buchwald, P. (2020). A Single Unified Model for Fitting Simple to Complex Receptor Response Data. *Sci. Rep.* 10 (1), 13386. doi:10.1038/s41598-020-70220-w

Deng, Y., Faivre, B., Back, O., Lombard, M., Pecqueur, L., and Fontecave, M. (2020). Structural and Functional Characterization of 4-Hydroxyphenylacetate 3-Hydroxylase from *Escherichia coli*. *Chembiochem* 21 (1-2), 163–170. doi:10.1002/cbic.201900277

Dı´az, E., Ferra´ndez, A., Prieto, M. A., and Garcı´a, J. L. (2001). Biodegradation of Aromatic Compounds by *Escherichia coli*. *Microbiol. Mol. Biol. Rev.* 65 (4), 523–569. doi:10.1128/MMBR.65.4.523-569.2001

Furuya, T., and Kino, K. (2014). Regioselective Synthesis of Piceatannol from Resveratrol: Catalysis by Two-Component Flavin-dependent Monooxygenase HpaBC in Whole Cells. *Tetrahedron Lett.* 55 (17), 2853–2855. doi:10.1016/j.tetlet.2014.03.076

Han, G. H., Shin, H.-J., and Kim, S. W. (2008). Optimization of Bio-Indigo Production by Recombinant *E. coli* Harboring Fmo Gene. *Enzyme Microb. Technology* 42 (7), 617–623. doi:10.1016/j.enzmictec.2008.02.004

Hashimoto, T., Nozawa, D., Mukai, K., Matsuyama, A., Kuramochi, K., and Furuya, T. (2019). Monooxygenase-catalyzed Regioselective Hydroxylation for the Synthesis of Hydroxyequols. *RSC Adv.* 9 (38), 21826–21830. doi:10.1039/c9ra03913a

Jackson, R. L., Greiwe, J. S., and Schwen, R. J. (2011). Emerging Evidence of the Health Benefits of S-Equol, an Estrogen Receptor β Agonist. *Nutr. Rev.* 69 (8), 432–448. doi:10.1111/j.1753-4887.2011.00400.x

Jones, J. A., Collins, S. M., Vernacchio, V. R., Lachance, D. M., and Koffas, M. A. G. (2016). Optimization of Naringenin Andp-Coumaric Acid Hydroxylation Using the nativeE. Colihydroxylase Complex, HpaBC. *Biotechnol. Prog.* 32 (1), 21–25. doi:10.1002/btpr.2185

Kim, H., Kim, J. R., Kang, H., Choi, J., Yang, H., Lee, P., et al. (2014). 7,8,4′-Trihydroxyisoflavone Attenuates DNCB-Induced Atopic Dermatitis-like Symptoms in NC/Nga Mice. *PloS one* 9 (8), e104938. doi:10.1371/journal.pone.0104938

Kim, J., Lee, P.-g., Jung, E.-o., and Kim, B.-G. (2018). *In Vitro* characterization of CYP102G4 from Streptomyces Cattleya: A Self-Sufficient P450 Naturally Producing Indigo. *Biochim. Biophys. Acta (BBA) - Proteins Proteomics* 1866 (1), 60–67. doi:10.1016/j.bbapap.2017.08.002

Kim, S.-H., Hisano, T., Takeda, K., Iwasaki, W., Ebihara, A., and Miki, K. (2007). Crystal Structure of the Oxygenase Component (HpaB) of the 4-hydroxyphenylacetate 3-monooxygenase from Thermus Thermophilus HB8. *J. Biol. Chem.* 282 (45), 33107–33117. doi:10.1074/jbc.M703440200

Lee, D. E., Lee, K. W., Byun, S., Jung, S. K., Song, N., Lim, S. H., et al. (2011a). 7,3′,4′-Trihydroxyisoflavone, a Metabolite of the Soy Isoflavone Daidzein, Suppresses Ultraviolet B-Induced Skin Cancer by Targeting Cot and MKK4. *J. Biol. Chem.* 286 (16), 14246–14256. doi:10.1074/jbc.M110.147348

Lee, D. E., Lee, K. W., Jung, S. K., Lee, E. J., Hwang, J. A., Lim, T.-G., et al. (2011b). 6,7,4'-trihydroxyisoflavone Inhibits HCT-116 Human colon Cancer Cell Proliferation by Targeting CDK1 and CDK2. *Carcinogenesis* 32 (4), 629–635. doi:10.1093/carcin/bgr008

Lee, H., Kim, B.-G., and Ahn, J.-H. (2014). Production of Bioactive Hydroxyflavones by Using Monooxygenase from Saccharothrix Espanaensis. *J. Biotechnol.* 176, 11–17. doi:10.1016/j.jbiotec.2014.02.002

Lee, N., Kim, E. J., and Kim, B.-G. (2012). Regioselective Hydroxylation of Trans-resveratrol via Inhibition of Tyrosinase from Streptomyces Avermitilis MA4680. *ACS Chem. Biol.* 7 (10), 1687–1692. doi:10.1021/cb300222b

Lee, P.-G., Kim, J., Kim, E.-J., Jung, E., Pandey, B. P., and Kim, B.-G. (2016a). P212A Mutant of Dihydrodaidzein Reductase Enhances (S)-Equol Production and Enantioselectivity in a Recombinant *Escherichia coli* Whole-Cell Reaction System. *Appl. Environ. Microbiol.* 82 (7), 1992–2002. doi:10.1128/AEM.03584-15

Lee, P.-G., Kim, J., Kim, E.-J., Lee, S.-H., Choi, K.-Y., Kazlauskas, R. J., et al. (2017). Biosynthesis of (−)-5-Hydroxy-Equol and 5-Hydroxy-Dehydroequol from Soy Isoflavone, Genistein Using Microbial Whole Cell Bioconversion. *ACS Chem. Biol.* 12 (11), 2883–2890. doi:10.1021/acschembio.7b00624

Lee, P.-G., Lee, S.-H., Kim, J., Kim, E.-J., Choi, K.-Y., and Kim, B.-G. (2018). Polymeric Solvent Engineering for Gram/liter Scale Production of a Water-Insoluble Isoflavone Derivative, (S)-equol. *Appl. Microbiol. Biotechnol.* 102 (16), 6915–6921. doi:10.1007/s00253-018-9137-8

Lee, P. G., Lee, S. H., Hong, E. Y., Lutz, S., and Kim, B. G. (2019). Circular Permutation of a Bacterial Tyrosinase Enables Efficient Polyphenol-specific Oxidation and Quantitative Preparation of Orobol. *Biotechnol. Bioeng.* 116, 19–27. doi:10.1002/bit.26795

Lee, S.-H., Baek, K., Lee, J.-E., and Kim, B.-G. (2016b). Using Tyrosinase as a Monophenol Monooxygenase: A Combined Strategy for Effective Inhibition of Melanin Formation. *Biotechnol. Bioeng.* 113 (4), 735–743. doi:10.1002/bit.25855

Lin, Y., and Yan, Y. (2014). Biotechnological Production of Plant-specific Hydroxylated Phenylpropanoids. *Biotechnol. Bioeng.* 111 (9), 1895–1899. doi:10.1002/bit.25237

Lund, T. D., Munson, D. J., Haldy, M. E., Setchell, K. D. R., Lephart, E. D., and Handa, R. J. (2004). Equol Is a Novel Anti-androgen that Inhibits Prostate Growth and Hormone Feedback1. *Biol. Reprod.* 70 (4), 1188–1195. doi:10.1095/biolreprod.103.023713

Marrian, G. F., and Haslewood, G. A. D. (1932). Equol, a New Inactive Phenol Isolated from the Ketohydroxyoestrin Fraction of Mares' Urine. *Biochem. J.* 26 (4), 1227–1232. doi:10.1042/bj0261227

Matthies, A., Loh, G., Blaut, M., and Braune, A. (2012). Daidzein and Genistein Are Converted to Equol and 5-Hydroxy-Equol by Human Intestinal Slackia Isoflavoniconvertens in Gnotobiotic Rats. *J. Nutr.* 142 (1), 40–46. doi:10.3945/jn.111.148247

Nayfach, S., Fischbach, M. A., and Pollard, K. S. (2015). MetaQuery: a Web Server for Rapid Annotation and Quantitative Analysis of Specific Genes in the Human Gut Microbiome. *Bioinformatics* 31 (20), 3368–3370. doi:10.1093/bioinformatics/btv382

Pandey, B. P., Roh, C., Choi, K. Y., Lee, N., Kim, E. J., Ko, S., et al. (2010). Regioselective Hydroxylation of Daidzein Using P450 (CYP105D7) from Streptomyces Avermitilis MA4680. *Biotechnol. Bioeng.* 105 (4), 697–704. doi:10.1002/bit.22582

Park, J.-S., Kim, D. H., Lee, J. K., Lee, J. Y., Kim, D. H., Kim, H. K., et al. (2010). Natural Ortho-Dihydroxyisoflavone Derivatives from Aged Korean Fermented Soybean Paste as Potent Tyrosinase and Melanin Formation Inhibitors. *Bioorg. Med. Chem. Lett.* 20 (3), 1162–1164. doi:10.1016/j.bmcl.2009.12.021

Park, J.-S., Park, H. Y., Kim, D. H., Kim, D. H., and Kim, H. K. (2008). ortho-dihydroxyisoflavone Derivatives from Aged Doenjang (Korean Fermented Soypaste) and its Radical Scavenging Activity. *Bioorg. Med. Chem. Lett.* 18 (18), 5006–5009. doi:10.1016/j.bmcl.2008.08.016

Prieto, M. A., and Garcia, J. L. (1994). Molecular Characterization of 4-hydroxyphenylacetate 3-hydroxylase of *Escherichia coli*. A Two-Protein Component Enzyme. *J. Biol. Chem.* 269 (36), 22823–22829. doi:10.1016/s0021-9258(17)31719-2

Rittle, J., and Green, M. T. (2010). Cytochrome P450 Compound I: Capture, Characterization, and C-H Bond Activation Kinetics. *Science* 330 (6006), 933–937. doi:10.1126/science.1193478

Rüfer, C. E., Glatt, H., and Kulling, S. E. (2006). Structural Elucidation of Hydroxylated Metabolites of the Isoflavan Equol by Gas Chromatography-Mass Spectrometry and High-Performance Liquid Chromatography-Mass Spectrometry. *Drug Metab. Dispos* 34 (1), 51–60. doi:10.1124/dmd.105.004929

Schwen, R. J., Nguyen, L., and Jackson, R. L. (2012). Elucidation of the Metabolic Pathway of S-Equol in Rat, Monkey and Man. *Food Chem. Toxicol.* 50 (6), 2074–2083. doi:10.1016/j.fct.2012.03.048

Seo, S. G., Yang, H., Shin, S. H., Min, S., Kim, Y. A., Yu, J. G., et al. (2013). A Metabolite of Daidzein, 6,7,4′-trihydroxyisoflavone, Suppresses Adipogenesis in 3T3-L1 Preadipocytes via ATP-Competitive Inhibition of PI3K. *Mol. Nutr. Food Res.* 57 (8), 1446–1455. doi:10.1002/mnfr.201200593

Setchell, K. D., Clerici, C., Lephart, E. D., Cole, S. J., Heenan, C., Castellani, D., et al. (2005). S-equol, a Potent Ligand for Estrogen Receptor β, Is the Exclusive Enantiomeric Form of the Soy Isoflavone Metabolite Produced by Human Intestinal Bacterial flora. *Am. J. Clin. Nutr.* 81 (5), 1072–1079. doi:10.1093/ajcn/81.5.1072

Trott, O., and Olson, A. J. (2010). AutoDock Vina: Improving the Speed and Accuracy of Docking with a New Scoring Function, Efficient Optimization, and Multithreading. *J. Comput. Chem.* 31 (2), 455–461. doi:10.1002/jcc.21334

Uchiyama, S., Ueno, T., and Suzuki, T. (2007). Identification of a Newly Isolated Equal-Producing Lactic Acid Bacterium from the Human Feces. *J. Intestinal Microbiol.* 21 (3), 217. doi:10.11209/jim.21.217

Yokoyama, S.-i., and Suzuki, T. (2008). Isolation and Characterization of a Novel Equol-Producing Bacterium from Human Feces. *Biosci. Biotechnol. Biochem.* 72 (10), 2660–2666. doi:10.1271/bbb.80329

Conflict of Interest: The authors declare that the research was conducted in the absence of any commercial or financial relationships that could be construed as a potential conflict of interest.

Publisher's Note: All claims expressed in this article are solely those of the authors and do not necessarily represent those of their affiliated organizations or those of the publisher, the editors, and the reviewers. Any product that may be evaluated in this article, or claim that may be made by its manufacturer, is not guaranteed or endorsed by the publisher.

frontiers | Frontiers in Bioengineering and Biotechnology

REVIEW
published: 13 April 2022
doi: 10.3389/fbioe.2022.855715

Exploitation of Hetero- and Phototrophic Metabolic Modules for Redox-Intensive Whole-Cell Biocatalysis

Eleni Theodosiou[1], *Adrian Tüllinghoff*[2], *Jörg Toepel*[2] *and Bruno Bühler*[2]*

[1]Institute of Applied Biosciences, Centre for Research and Technology Hellas, Thessaloniki, Greece, [2]Department of Solar Materials, Helmholtz Centre for Environmental Research GmbH—UFZ, Leipzig, Germany

The successful realization of a sustainable manufacturing bioprocess and the maximization of its production potential and capacity are the main concerns of a bioprocess engineer. A main step towards this endeavor is the development of an efficient biocatalyst. Isolated enzyme(s), microbial cells, or (immobilized) formulations thereof can serve as biocatalysts. Living cells feature, beside active enzymes, metabolic modules that can be exploited to support energy-dependent and multi-step enzyme-catalyzed reactions. Metabolism can sustainably supply necessary cofactors or cosubstrates at the expense of readily available and cheap resources, rendering external addition of costly cosubstrates unnecessary. However, for the development of an efficient whole-cell biocatalyst, in depth comprehension of metabolic modules and their interconnection with cell growth, maintenance, and product formation is indispensable. In order to maximize the flux through biosynthetic reactions and pathways to an industrially relevant product and respective key performance indices (i.e., titer, yield, and productivity), existing metabolic modules can be redesigned and/or novel artificial ones established. This review focuses on whole-cell bioconversions that are coupled to heterotrophic or phototrophic metabolism and discusses metabolic engineering efforts aiming at 1) increasing regeneration and supply of redox equivalents, such as NAD(P/H), 2) blocking competing fluxes, and 3) increasing the availability of metabolites serving as (co)substrates of desired biosynthetic routes.

Keywords: whole-cell redox biocatalysis, central metabolism, TCA cycle, metabolic engineering, cyanobacteria, redox balance

OPEN ACCESS

Edited by:
Jennifer Ann Littlechild, University of Exeter, United Kingdom

Reviewed by:
Lian He, University of Washington, United States
Konstantinos Vavitsas, National and Kapodistrian University of Athens, Greece

***Correspondence:**
Bruno Bühler
bruno.buehler@ufz.de

Specialty section:
This article was submitted to Bioprocess Engineering, a section of the journal Frontiers in Bioengineering and Biotechnology

Received: *15 January 2022*
Accepted: *09 March 2022*
Published: *13 April 2022*

Citation:
Theodosiou E, Tüllinghoff A, Toepel J and Bühler B (2022) Exploitation of Hetero- and Phototrophic Metabolic Modules for Redox-Intensive Whole-Cell Biocatalysis. Front. Bioeng. Biotechnol. 10:855715. doi: 10.3389/fbioe.2022.855715

1 INTRODUCTION

Living microbial cells have at their disposal active enzymes and metabolic pathways that allow the catalysis of synthetically interesting reactions in an economically feasible way and, in many cases, the simultaneous *in situ* regeneration of required cofactors or cosubstrates. They can theoretically produce all the metabolites present in their metabolic network from simple carbon sources such as sugars, organic acids, or even CO_2. If naturally occurring microorganisms are employed, the production efficiencies typically are rather low (Chae et al., 2017). For the successful development of robust, productive, and efficient whole-cell biocatalysts, whole-cell systems have to be considered in their entire complexity (Lee et al., 2013; Schrewe et al., 2013; Ladkau et al., 2014;

Volmer et al., 2015; Kadisch et al., 2017). Cell physiology is intrinsically optimized to secure growth and not the envisaged bioconversion. The maximization of the crucial process performance parameters titer, yield, and productivity thus typically requires the engineering of metabolic machineries *via* the redesign of existing metabolic pathways and/or the introduction of novel/artificial ones (Chae et al., 2017).

The present review focuses on the exploitation and engineering of modules of hetero- and phototrophic metabolism as well as artificial modules for redox-intensive production schemes. In heterotrophs, the central carbon metabolism provides carbon building blocks as well as redox power and energy by making use of simple organic molecules such as sugars and thus constitutes the hub for nearly all catabolic and anabolic processes. It includes the Embden–Meyerhof–Parnas pathway (EMPP), the Entner-Doudoroff pathway (EDP), the pentose phosphate pathway (PPP), as well as the tricarboxylic acid (TCA) cycle (Macnab, 1990), with few individual variations depending on the ecological niche in which the organism lives (Sudarsan et al., 2014). During aerobic growth, a maximum of 24 reducing equivalents (electrons) in the form of 12 molecules of NADH, NADPH, or $FADH_2$ is theoretically obtained per molecule of glucose oxidized to CO_2 (Blank et al., 2010). Their transfer to O_2 *via* the respiratory electron transport chain then generates the majority of the metabolic energy. In contrast, photoautotrophic metabolism relies on differing resources for carbon, electrons, and energy, i.e., CO_2, water, and light, respectively. The light reactions of photosynthesis gather electrons from water using light energy (photosynthetic water oxidation), generate a proton gradient *via* the photosynthetic electron transport chain (PETC), and thereby regenerate NADPH and ATP to fuel CO_2 fixation *via* the Calvin-Benson-Bassham cycle (Lassen et al., 2014a). The latter feeds glycderaldehyde-3-phosphate (G3P) into gluconeogenesis and lower glycolysis, thereby connecting to EMPP, EDP, and PPP and indirectly also the TCA cycle. In both heterotrophs and photoautotrophs, the central carbon metabolism produces biomass precursors (Chen et al., 2016) and is highly connected to redox and energy metabolism (Liao et al., 2016; Wang et al., 2017).

Phototrophic organisms are increasingly attracting attention as hosts for the sustainable production of C-based products, as they can rely on light, CO_2, and water for growth and product formation. This allows biocatalyst production, regeneration, and operation at minimal economical and ecological costs in overall carbon neutral and land-saving processes. Recent results show the high potential of cyanobacteria, green algae, and other phototrophs to produce biomass (Tsuzuki et al., 2019), biofuels (Arias et al., 2021; Kato et al., 2022), chemicals (Vavitsas et al., 2021; Jaiswal et al., 2022), and high value compounds (Tanvir et al., 2021). Respective advantages and disadvantages are intensely discussed, and new strategies have been developed to overcome limitations in carbon fixation (Batista-Silva et al., 2020). In particular, electron consuming reactions are prone to benefit from electrons derived from photosynthetic water oxidation, with H_2 formation as a prominent example (Appel et al., 2020; Lupacchini et al., 2021). Maximal electron transfer rates in phototrophs illustrate their high potential to fuel biocatalytic reactions (Grund et al., 2019). Additionally, the photosynthesis product O_2 can be utilized to support O_2-dependent reactions (Hoschek et al., 2017; Hoschek et al., 2018; Tüllinghoff et al., 2022), with the potential to overcome O_2 limitation, a major bottleneck in many processes based on heterotrophs (Baldwin and Woodley, 2006; Ouyang et al., 2018). However, C- (Angermayr et al., 2015) and e^--based (Jodlbauer et al., 2021) processes with phototrophic organisms are still limited by several factors, ranging from the lack of advanced molecular biology tools and a poor understanding of the cellar metabolism and its regulation to the lack of bioreactor systems enabling high cell density cultivation (Yu et al., 2013; Till et al., 2020). Generally heterotrophic organisms can still be considered the favored hosts for most production processes due to 1) higher growth rates, 2) a considerably deeper understanding of metabolic and regulatory networks, 3) a more expanded molecular biology tool box, 4) a very active metabolism, i.e., a high glucose consumption rate, and 5) the high cell density cultivation options. These advantages allow elaborate processes like *in vivo* cascades (Ladkau et al., 2014; Ladkau et al., 2016; Woo et al., 2018) and the production of fine and bulk chemicals at industrial scale. However, as stated above, phototrophic organisms have a high potential as hosts for electron demanding reactions, making glucose or other reduced C-compounds for the regeneration of reduction equivalent dispensable. Thus, bioprocesses based on phototrophs profit from low land use demands. Whereas heterotrophic hosts require—beside a low area demand for the bioreactor plants—arable land for the rather area-inefficient production of glucose or other organic substrates, phototrophs show comparably high areal productivity and can also be applied on non-arable land and buildings (Brandenburg et al., 2021; Fernández et al., 2021; Schipper et al., 2021). As long as glucose remains a rather cheap resource, it will be difficult for photobiotechnology to compete; but facing a growing global population with an increasing demand for food, energy, and chemicals, photobiotechnology can be attributed a high future potential making research on respective molecular biology tools, metabolic and regulatory modules, and high cell density cultivation highly valuable.

Since the synthesis of most target products make use of metabolic modules either providing carbon or energy, maximizing respective fluxes is pivotal. This requires knowledge on structure and function of the metabolic network as well as its response upon environmental or genetic perturbations (Jahan et al., 2016; Aslan et al., 2017). In case of redox-dependent production systems, the rate of redox cofactor regeneration is intrinsically linked with the entirety of metabolic modules producing and consuming redox cofactors (Blank et al., 2010) and thus depends on the chosen microbial production system. Whereas

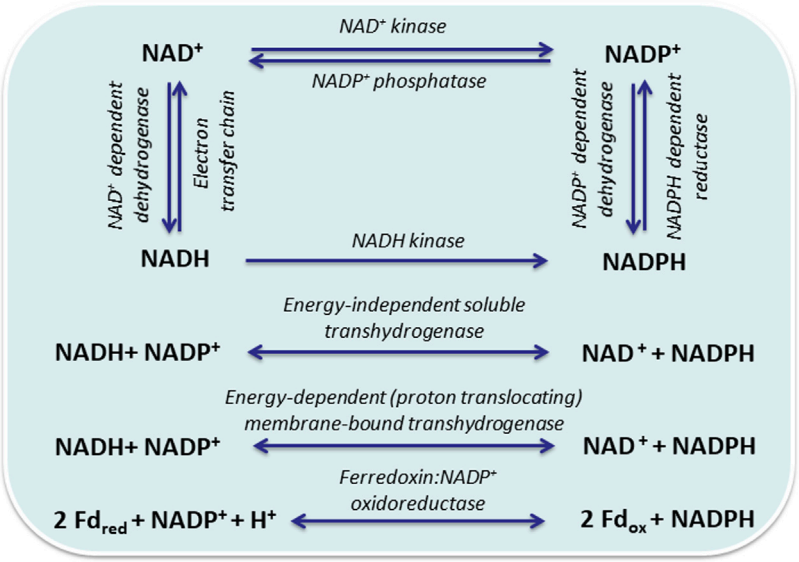

FIGURE 1 | Interconversion and regeneration of redox equivalents via reactions that are not directly coupled to the central carbon metabolism: NAD^+ kinase (EC 2.7.1.23); NADH kinase (EC 2.7.1.86), $NADP^+$ phosphatase (EC 2.7.1.23); NAD^+-dependent dehydrogenase (EC:1.12.1.2); $NADP(H)^+$-dependent dehydrogenases (EC 1.12.1.3); energy-independent soluble pyridine nucleotide transhydrogenase (UdhA, EC 1.6.1.1); energy-dependent proton translocating membrane-bound pyridine nucleotide transhydrogenase (PntAB, EC 1.6.1.2); ferredoxin:$NADP^+$ oxidoreductase (FNR, EC 1.18.1.2).

heterotrophs rely on the central carbon metabolism with a bias for NADH over NADPH supply, phototrophs involve the light reaction as main module with a bias for NADPH instead of NADH supply, both with respective challenges in redox balancing. In phototrophs, the light reactions often generate more reducing power than their primary metabolism needs, i.e., their metabolism is sink-limited, so that excess reducing power can be exploited for light-driven biosyntheses (Lassen et al., 2014a). Metabolic cofactor regeneration can become limiting, when the target reaction runs at high rates and has to compete with NAD(P)H demands for maintenance and biomass formation. It is obvious that the bioprocess objective to maximize target product formation is not in line with the natural objective of a cell to exploit its redox and energy metabolism for optimized growth and maintenance (Schrewe et al., 2013). To overcome metabolic and cofactor imbalances that impede whole-cell biocatalyst performance, various engineering strategies have been employed, which will be summarized and discussed in this review. These strategies either aim at increasing regeneration and supply of redox equivalents or at blocking competing fluxes. Thereby, heterotrophic, phototrophic, and introduced modules are considered and discussed regarding their potential to fuel whole-cell redox biocatalysis, including strategies to improve them.

2 Rerouting Electron Transfer Using Enzymatic Modules

In microbial metabolism, redox cofactors serve as electron carriers providing the cell with the reducing power needed in energy and/or anabolic metabolism. Furthermore, they play critical roles in maintaining intracellular redox homeostasis and are key players for the production of many, fuels, chemicals, and pharmaceuticals *via* redox biocatalysis (Duetz et al., 2001; Zhao and van der Donk, 2003; Park, 2007; Schroer et al., 2009). Their essential role in host metabolism and the complexity and flexibility of their turnover give metabolism-based cofactor regeneration a high potential, but make respective analyses and metabolic engineering towards efficient microbial cell factories a complex task (Blank et al., 2008; Holm et al., 2010; Lee et al., 2013).

Redox balancing is pivotal for living cells and is affected by any respective manipulation. An important aspect is the different roles, which NAD(H) and NADP(H) play in heterotrophic and phototrophic cells. In the latter, NADPH constitutes a main product of the photosynthetic light reaction, the electron donor for CO_2 fixation, and thus the central electron carrier under illumination (Ishikawa and Kawai-Yamada, 2019). This changes in the dark, when maintenance metabolism mainly relies on NADH and respiration. In heterotrophs, NADH is the main electron carrier for catabolism and NADPH for anabolism. Both, hetero- and phototrophs can balance pool sizes and reroute electrons between different electron carriers, involving transhydrogenases and NAD kinases (**Figure 1**). The different roles of transhydrogenases and NAD kinases in hetero- and phototrophs, as well as the usage of heterologous NAD(P)H regeneration systems will be discussed below. Biotechnological approaches based on living cells have to consider not only the electron donor dependency of synthetic reactions and pathways, but also

the presence of competing pathways and the cellular responses upon electron drain.

2.1 Engineering by Means of NAD(P/H) Transhydrogenases

The function of NAD(P/H) transhydrogenases differs among organisms, especially between phototrophic and heterotrophic bacteria, and is not completely understood, yet. The transhydrogenase reaction (NADH + $NADP^+$ ↔ NAD^+ + NADPH) is catalyzed by the membrane-bound, proton-translocating PntAB (EC 1.6.1.2) or the soluble, energy-independent UdhA (EC 1.6.1.1) (Sauer et al., 2004; Pedersen et al., 2008). Up to now, only Enterobacteriaceae are known to contain both enzymes; all other microbes contain either one or none. Cyanobacteria harbor the genes for PntAB only, which was found to be particularly important for NADPH production under low-light mixotrophic conditions (Kämäräinen et al., 2017). Using mutant *Escherichia coli* strains and metabolic flux analysis (MFA), Sauer et al. (Sauer et al., 2004) identified PntAB as major source of NADPH and reported that it provides 35–45% of the NADPH required during standard aerobic batch growth on glucose, whereas PPP and isocitrate dehydrogenase contributed 35–45% and 20–25%, respectively. On the other hand, hydride transfer from NADPH to NAD^+ by UdhA was found to be essential for growth under metabolic conditions with excess NADPH formation, such as growth on acetate or with inactivated glucose-6-phosphate isomerase (PGI). Canonaco et al. (2001) demonstrated that, in a Δ*pgi* mutant with the PPP as primary route of glucose catabolism, UdhA activity could efficiently restore the redox balance and improve the growth rate by 25%. They concluded that, in prokaryotes, PntAB catalyzes energy- and NADH-dependent $NADP^+$ reduction at low intracellular NADPH levels, whereas UdhA oxidizes NADPH at high intracellular NADPH levels (Sauer et al., 2004).

The function of the transhydrogenases in phototrophic prokaryotes is thought to be similar, maintaining redox homeostasis under imbalanced conditions. Normally, PntAB activity can be neglected during photoautotrophic growth (Kämäräinen et al., 2017). In *Synechocystis* sp. PCC 6803, however, *pntA* transcription was shown to be high under nitrogen and phosphate limitation (Kopf et al., 2014), conditions known to involve an unbalanced NADH/NADPH ratio, suggesting that PntAB plays an important role for redox homeostasis under such conditions. Similarly, it was found that mixotrophic growth, with an enhanced NADH level, depends on PntAB in cyanobacteria (Kämäräinen et al., 2017). A *pntAB*-deficient mutant exhibited growth defects under low-light conditions and day-night rhythm in the presence of glucose. However, the redox state in terms of the NADPH/NADP ratio also appears to be subject of large diurnal variation and to play an important role in respective global regulation (Saha et al., 2016). Further studies on the function of transhydrogenases in phototrophs are missing.

The transhydrogenase systems constitute promising engineering targets to enhance NAD(P)H-dependent biotransformations both in phototrophs and heterotrophs. Because membrane proteins are usually considered more tedious to be heterologously expressed, soluble UdhA is more commonly used in metabolic engineering. Such engineering was successfully employed for the syntheses of several industrially useful compounds. In the study of Xu et al. (2019), a highly NADPH-demanding squalene synthesis pathway was established in *E. coli* to create a squalene-producing bacterial strain. Thereby, *udhA* was overexpressed and obviously enabled an improved intracellular NADPH/$NADP^+$ ratio, resulting in a 59% increase in squalene titer. For (S)-2-chloropropionate production from 2-chloroacrylate catalyzed by the NADPH-dependent 2-haloacrylate reductase, Jan et al. (2013) found that the presence of UdhA increases product yield and NADPH availability while the presence of PntAB has the opposite effect. UdhA also conveyed an increase in polyhydroxybutyrate (PHB) productivity and yield in engineered *E. coli* (Sanchez et al., 2006). Coexpression of native *udh*A from *E. coli* together with the *phb* operon from *Alcaligenes eutrophus* H16 from high copy plasmids resulted in an increase in PHB yield from 49 to 66% of total cell dry weight and an increase in final concentration from 3.52 to 6.42 g L^{-1} compared to the control strain expressing only the *phb* operon. These results are somewhat in contrast to those reported by Sauer et al. for redox balancing during growth and indicate that UdhA not only oxidizes NADPH at high NADPH levels, but also contributes to NADPH formation at low NADPH levels caused by a strong NADPH sink (Schroer et al., 2009). Using a thymidine-overproducing *E. coli* strain, the NADPH availability increased by disrupting PGI and overexpressing *nadK* (NAD kinase) or *udhA*. In chemostat cultures, the NADPH/$NADP^+$ ratios at steady state correlated positively with thymidine yields (Lee et al., 2010). Fatty acid production also depends on NADPH and has been reported to decrease by 88.8% upon deletion of *pntB* and *udhA* in *E. coli*. Whereas the deactivation of the *zwf* gene decreased production, fatty acid biosynthesis in the *zwf* mutant was recovered upon co-expression of *pntAB* and *nadK* (Li et al., 2018).

In cyanobacteria, the production of lactic acid is the first example of how the heterologous coexpression of *udhA* (e.g., from *E. coli*, *B. subtilis*) together with lactate dehydrogenase (e.g., from *E. coli, P. aeruginosa*) improves the production due to enhanced NADH supply (Angermayr et al., 2012; Varman et al., 2013). Whereas overexpression of *E. coli udhA* in cyanobacteria improved NADH-dependent production of lactate, phototrophic growth was reduced, probably due to NADPH consumption by UdhA (Niederholtmeyer et al., 2010). Conversely, overexpression of endogenous *pntAB* in *Synechocystis* increased the NADPH-dependent production of 3-hydroxypropionic acid without inhibition of phototrophic growth (Wang et al., 2016). Similarly, *pntAB* overexpression was shown to support NADPH-dependent sorbitol production in *Synechocystis* sp. PCC 6803 (Chin et al., 2018). Also here, a rebalancing of NADPH availability obviously was necessary, enabling, together with an increase in the fructose bisphosphatase level, a nearly 27-fold increase in sorbitol titer compared to the initial strain just overexpressing a sorbitol-6-phosphate dehydrogenase gene.

As mentioned above, transhydrogenases are lacking in some biotechnologically interesting microorganisms. Yamauchi et al. (2014) introduced the *E. coli udhA* and *pntAB* genes into glutamic

acid-producing *Corynebacterium glutamicum* and examined the metabolic characteristics of the recombinant strains under aerobic and microaerobic conditions. Introduction of the *udh*A gene did not cause major metabolic changes under both conditions. However, the introduction of *pnt*AB increased the NADH/NAD^+ ratio under microaerobic conditions and thereby lactic, acetic, and succinic acid formation, pointing towards the potential of PntAB to catalyze a rebalancing towards NADH formation depending on growth conditions. In *Rhodospirillum rubrum*, a purple non-sulfur alphaproteobacterium, the overexpression of *E. coli pntAB* together with *Ralstonia eutropha phaB1*, encoding an NADPH-dependent polyhydroxyalkanoate (PHA)-precursor synthesizing reductase, accumulated poly(3-hydroxybutyrate-co-3-hydroxyvalerate) with a 13-fold higher 3-hydroxyvalerate content compared to the wild type strain (Heinrich et al., 2015). The engineered *R. rubrum* strain was also able to synthesize this industrially relevant copolymer from CO_2 and CO in syngas. The increased incorporation of 3-hydroxyvalerate was attributed to an excess of the PHA precursor propionyl-CoA, which was generated from aspartate via threonine, thereby consuming two NADPH and producing one NADH, to compensate for PntAB-catalyzed electron transfer from NADH to $NADP^+$. The increased 3-hydroxyvalerate incorporation possibly also involved a shortage of the otherwise preferred PHA precursor acetyl-CoA consumed by the NADH generating TCA cycle (Heinrich et al., 2015). Obviously, the function of the two types of transhydrogenases (UdhA and PntAB) is not unidirectional and, depending on the conditions and host organism applied, both can support NADPH or NADH supply.

2.2 Overexpression of NAD^+ kinases

NAD^+ kinases (NADKs) catalyze the phosphorylation of NAD^+ to $NADP^+$ using ATP as the phosphoryl donor (Kawai et al., 2001). These enzymes are key to balance the ratio of NAD(H) to NADP(H). In an engineered thymidine producing *E. coli* strain, it was reported that *nadK* overexpression resulted in a shift of the NADPH/$NADP^+$ ratio from 0.184 to 0.267. However, the overall (NADH + $NADP^+$)/(NADPH + NAD^+) ratio remained constant probably by regulating *pntAB* and *udhA* expression levels to compensate for the effects of *nad*K overexpression (Lee et al., 2009). The *nad*K overexpression in a recombinant *E. coli* harboring a polyhydroxybutyrate (PHB) synthesis pathway doubled the overall PHB accumulation in a bioreactor experiment and came along with a 3- to 6-fold increase in $NADP^+$ concentration (Li et al., 2009). The overexpression of the NADK gene *yfjB* together with *pntAB* in *E. coli* was reported to increase NADPH availability and thereby isobutanol production to a larger extent than that of *pntAB* alone, whereas *yfjB* overexpression alone had no effect (Shi et al., 2013). This beneficial synergistic effect was more prominent under anaerobic conditions, when NADH constitutes the main electron carrier, PPP and TCA cycle are usually not functional, and transhydrogenases are the only source for NADPH. In general, NADPH-dependent bioproduction routes of thymidine (Lee et al., 2010), isobutanol (Shi et al., 2013), PHB (Li et al., 2009; Zhang et al., 2015), and shikimic acid (Cui et al., 2014) in *E. coli* and of L-arginine (Rahman et al., 2012) and L-isoleucine (Shi et al., 2012) in *Corynebacterium* species were enhanced via *nadK* overexpression alone or combined with genes encoding other NADPH-related enzymes.

In cyanobacteria, NADKs have several functions. Proteome search for NADK homologs of the 72 species registered in CyanoBase revealed 69 species having two typical NADKs classified as Slr0400 type (group 1) and Sll1415 type (group 2) (Ishikawa and Kawai-Yamada, 2019). It is hypothesized that the two NADK types possess distinct functions in cyanobacteria. Ishikawa et al. (2019) reported that a sll1415-deficient mutant showed a growth-impaired phenotype under conditions that would typically yield photomixotrophy (12-h light/12-h dark cycling), or heterotrophy (light-activated heterotrophic growth, LAHG, with cells in darkness exposed to light for 15 min every 24 h) and that wild type cells exhibited 2.2- and 1.8-fold increased $NADP^+$ and NADPH levels, respectively, 96 h after shifting from autotrophic to photomixotrophic conditions. This suggests a key role of group 2 NADKs in photoheterotrophic growth. On the other hand, it is speculated that group 1 NADKs play a key role in suppressing heterotrophic metabolism in *Synechocystis* sp. PCC 6803 under photoautotrophic conditions (Ishikawa and Kawai-Yamada, 2019). A *slr0400*-deficient mutant accumulated NAD^+, resulting in unsuppressed activity of glycolysis and TCA cycle enzymes (Ishikawa et al., 2021). Further research is necessary to clarify the exact role of the two NADK types in cyanobacteria. Effects of NADK gene overexpression and deletion on target product formation have not been investigated, yet.

2.3 Exploiting Heterologous NAD(P)H Generating Systems

Apart from the metabolic engineering of intrinsic NAD(P)H generating pathways, studies have focused on exploiting heterologous systems to increase intracellular NAD(P)H availability and enhance the efficiency and productivity of NAD(P)H-dependent whole-cell biotransformations (**Figure 2**). Of those, glucose dehydrogenases (GDHs) and formate dehydrogenases (FDHs) are most widely used. The first catalyzes the oxidation of β-D-glucose to β-D-glucono-1,5-lactone with simultaneous reduction of $NAD(P)^+$ to NAD(P)H, the latter the NAD^+-dependent oxidation of formate to CO_2.

Berríos-Rivera et al. (2002) manipulated the NADH availability in *E. coli* by regenerating NADH through the heterologous expression of *Candida boidinii* FDH regenerating one mole of NADH per mole of formate converted to CO_2. Natively, this FDH converts formate to CO_2 and H_2 without cofactor involvement. Under anaerobic conditions, the NADH availability increased from 2 to 4 mol NADH per mol glucose consumed and promoted ethanol formation. Under aerobic conditions, when formate was not

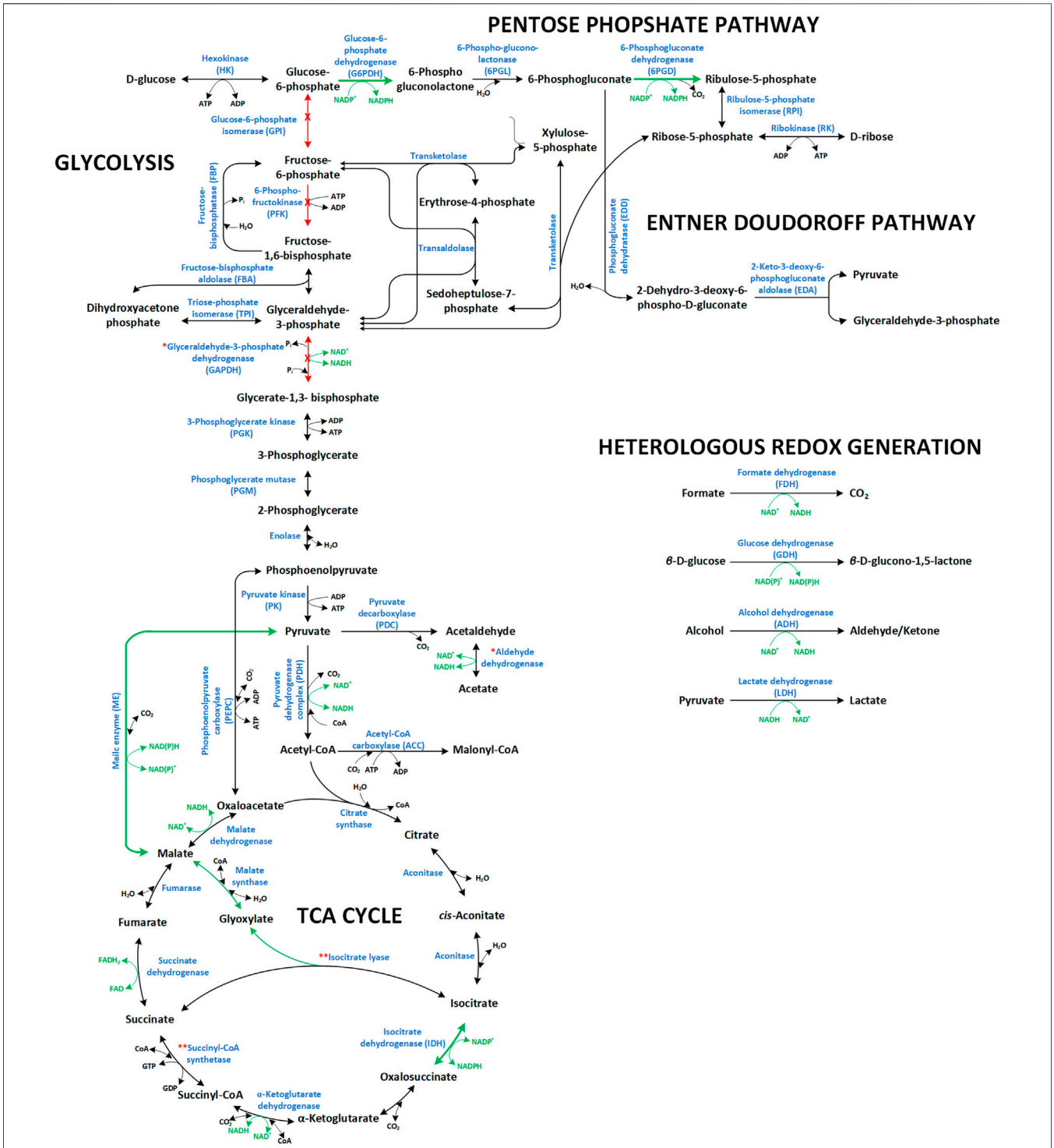

FIGURE 2 | Overview of the NAD(P)$^+$/NAD(P)H dependent reactions in central carbon metabolic modules (glycolysis, pentose phosphate pathway, TCA cycle, and Entner-Doudoroff pathway) and heterologous redox cofactor regeneration systems commonly used to fuel redox-intensive production processes. Green arrows and red arrows indicate reactions, which have been upregulated and downregulated/deleted, respectively, to promote/improve redox intensive production schemes. Enzyme names are accompanied by their abbreviations as cited in the text. Respective genes are: the PPP genes *zwf* (glucose 6-phosphate dehydrogenase, **G6PDH**) and *gnd* (6-phosphogluconate dehydrogenase, **6PGD**) both encoding NADPH forming enzymes (Lim et al., 2002; Poulsen et al., 2005; Zhang et al., 2016a); the glycolytic genes *pgi* (glucose-6-phosphate isomerase, **GPI**), *pfkA*/B (phosphofructokinase I/II, **PFK**), and *gap*A (G3P dehydrogenase, **GAPDH**); the TCA cycle genes *maeA/B* (malic enzyme, **ME**) and *icd* (Isocitrate dehydrogenase, **IDH**). The symbol (*) denotes enzymes that can be exchanged with functionally equivalent isozymes but with different cofactor preference (i.e., NADP$^+$-dependent variants of aldehyde dehydrogenase and GAPDH). The symbol (**) denotes reactions that have been either

(*Continued*)

FIGURE 2 | activated or deactivated depending on the envisaged redox related metabolic engineering target, as in the case of isocitrate lyase and succinyl-coA synthetase. With activated glyoxylate shunt, more malate is formed which in turn can be converted to pyruvate by the ME involving NADPH formation. In order to promote α-KG dependent redox biotransformations, the glyoxylate shunt has been deactivated forcing metabolic flux through the introduced enzyme (e.g., proline or isoleucine dioxygenases). Succinyl-CoA synthetase activity significantly promotes NADPH allocation (*via* IDH) for NADPH-dependent syntheses (e.g., xylitol production). On the other hand, deletion or reduction of this activity promotes α-KG-dependent redox biotransformations.

formed by metabolism but added to the medium, the increased NADH availability stimulated usually inactive fermentation pathways, i.e., ethanol, lactate, and succinate formation (Berríos-Rivera et al., 2002). Wang et al. (2013) introduced either GDH from *B. subtilis* or FDH from *C. boidinii* into a 2,3-butanediol (BD) dehydrogenase bearing *E. coli* for the production of (2S, 3S)-2,3-BD from diacetyl, i.e., a liquid fuel and a building block in asymmetric synthesis. The engineering not only improved the efficiency of (2S, 3S)-2,3-BD production, but also simplified product isolation by driving the reaction to completion and preventing the accumulation of gluconic, acetic, and lactic acid that are by-produced when only glucose is used for internal cofactor regeneration. Introduction of FDH resulted in higher (2S, 3S)-2,3-BD concentration, productivity, and yield, coming along with a large increase in the intracellular NADH concentration. However, GDH introduction poorly improved whole-cell biocatalysis efficiency, probably due to poor glucose permeation over cellular membranes and intracellular gluconic acid accumulation. *E. coli* essentially takes up glucose *via* active transport, i.e., the phosphotransferase system (PTS). Thereby, glucose is directly phosphorylated and does not become available for GDH. In crude extracts, GDH showed high activity, whereas the slow glucose permeation into cells limited GDH-mediated NADH regeneration (Wang et al., 2013). Schewe et al. showed that the introduction of the glucose facilitator from *Zymomonas mobilis*, mediating energy-independent glucose diffusion into cells, can overcome this limitation in CYP450 bearing *E. coli* for the NADPH-dependent oxyfunctionalization of α-pinene to α-pinene oxide, verbenol, and myrtenol (Schewe et al., 2008). FDH from *Mycobacterium vaccae* was applied for efficient NADH supply in *E. coli* for D-fructose reduction of to D-mannitol by coexpressed mannitol dehydrogenase from *Leuconostoc pseudomesenteroides* (Kaup et al., 2004). The additional introduction of the *Z. mobilis* glucose facilitator thereby improved D-fructose uptake, enabling 84% yield. Whereas GDH from *B. subtilis* has been extensively used for *in vivo* NAD(P)H regeneration, mainly because of its dual cofactor specificity and ease of expression in *E. coli*, interesting biochemical properties (e.g., activity and stability) and cofactor preference have been reported for GDHs from different organisms (Pongtharangkul et al., 2015). Pongtharangkul et al. (2015) cloned and expressed in both *E. coli* and *B. subtilis* a GDH gene from *B. amyloliquefaciens* (GDH-BA) and evaluated the kinetics and biochemical properties of the purified enzyme. They suggested that the high specific activity as well as the low K_M-value towards glucose and $NADP^+$ make this GDH a promising candidate for *in vivo* applications. Recombinant *B. subtilis* harboring GDH-BA was successfully used to regenerate NADPH for n-hexane hydroxylation catalyzed by *B. subtilis* containing the CYP450 BM3 variant F87V (Pongtharangkul et al., 2015).

By expressing *adh* from *Lactobacillus brevis* in *E. coli*, Ernst et al. (2005) developed whole-cell biotransformation systems for the reduction of prochiral carbonyl compounds to chiral hydroxy acid derivatives. The *fdh* gene from *M. vaccae* N10 thereby was coexpressed for NADH regeneration and, in the presence of formate, increased the intracellular $NADH/NAD^+$ ratio 7-fold. This enabled the formation of 40 mM methyl (R)-3-hydroxy butanoate from methyl acetoacetate with 100% yield. Also *gdh* coexpression together with genes encoding carbonyl reductases in *E. coli* has been shown to be valuable for the production of chiral alcohols (Kataoka et al., 2003).

For the production of chemicals from CO_2, also the photoautotrophic redox metabolism gains increasing attention. However, the cofactor bias of phototrophs, with NADPH as main source of reduction equivalents, differs from that of heterotrophs. For D-lactate production, Li et al. changed the cofactor preference of the key enzyme D-lactate dehydrogenase (LdhD) from NADH to NADPH. The engineered LdhD in *Synechococcus elongatus* PCC 7942 then enabled efficient light-driven production of optically pure D-lactate from CO_2. Mutation of LdhD increased D-lactate productivity by over 3.6-fold. The additional introduction of a lactic acid transporter and bubbling CO_2-enriched air further enhanced D-lactate concentration and productivity (Li et al., 2015a). For phototrophic D-lactate synthesis from CO_2 by *Synechocystis* sp. PCC 6803, Varman et al. (2013) utilized a mutated GDH. Together with codon optimization and heterologous expression of a soluble transhydrogenase, this approach significantly improved D-lactate synthesis. Whereas *in vivo* NAD(P)H regeneration systems have been widely studied, $NAD(P)^+$ regeneration has been less explored and can be considered less demanding. Using the H_2O producing NADH oxidase from *L. brevis* as heterologous NAD^+ regenerating enzyme together with a NAD^+-dependent (2R, 3R)-2,3-BD dehydrogenase from *B. subtilis*, Xiao et al. (2010) developed an *E. coli* biocatalyst for the production of (3S)-acetoin from meso-2,3-BD, (3R)-acetoin from (2R, 3R)-2,3-BD, and (2S, 3S)-2,3-BD from a substrate mixture. Their work demonstrated that coupling NADH oxidase from *L. brevis* with NAD^+-dependent dehydrogenases provides an efficient platform for NAD^+-dependent whole-cell biotransformations.

TABLE 1 | NAD(P)H generating enzymes in central carbon metabolism.

Enzyme	Reaction	Involved pathway
Glucose-6-phosphate dehydrogenase (G6PDH; EC:1.1.1.49)	D-glucose 6-phosphate + $NADP^+$ → 6-phospho-D-glucono-1,5-lactone + NADPH + H^+	PPP, EDP
$NAD(P)^+$ glucose dehydrogenase (GDHs; EC:1.1.1.47, EC:1.1.1.119)	D-glucose + $NAD(P)^+$ → D-glucono-1,5-lactone + NAD(P)H + H^+	PPP, EDP
6-Phospho-D-gluconate dehydrogenase (6PGDH; EC:1.1.1.44)	6-phospho-D-gluconate + $NADP^+$ → D-ribulose 5-phosphate + CO_2 + NADPH + H^+	PPP
$NADP^+$-dependent non-phosphorylating glyceraldehyde 3-phosphate dehydrogenase (GAPN; EC:1.2.1.9)	D-glyceraldehyde 3-phosphate + $NADP^+$ + H_2O → 3-phospho-D-glycerate + NADPH + 2 H^+	EMPP, PPP
$NAD(P)^+$-dependent phosphorylating glyceraldehyde 3-phosphate dehydrogenase ($NAD(P)^+$-GAPDH; EC:1.2.1.12, 1.2.1.13)	D-glyceraldehyde 3-phosphate + phosphate + $NAD(P)^+$ → 3-phospho-D-glyceroyl phosphate + NAD(P)H + H^+	EMPP
NAD^+-dependent glycerol-3-phosphate dehydrogenase (GPDH; EC: 1.1.1.8)	Glycerate 3-phosphate + NAD^+ → Phosphoenolpyruvate + NADH	EMPP
$NAD(P)^+$-dependent isocitrate dehydrogenase (IDH; EC:1.1.1.41, 1.1.1.42)	Isocitrate + $NAD(P)^+$ → α-ketoglutarate + CO_2 + NAD(P)H + H^+	TCA cycle
$NAD(P)^+$-specific malate dehydrogenase (ME; EC:1.1.1.37, 1.1.1.40)	Malate + $NADP^+$ → pyruvate + CO_2 + NADPH; malate + NAD^+ → oxaloacetate + NADH + H^+	TCA cycle, Anaplerotic node
α-Ketoglutarate dehydrogenase complex (αKGDH; EC: 1.2.4.2, 2.3.1.6, 1.8.1.4)	α-ketoglutarate + NAD^+ + CoA → Succinyl CoA + CO_2 + NADH	TCA cycle
Pyruvate dehydrogenase complex (PDC; EC: 1.2.4.1)	Pyruvate + NAD^+ + CoA → Acetyl-CoA + NADH + CO_2	EMPP, TCA cycle
NAD^+-D-xylose dehydrogenase (XDH; EC: 1.1.1.175)	D-xylose + NAD^+ → D-xylonolactone + NADH + H^+	Dahms pathway

3 PATHWAY ENGINEERING

Central carbon metabolism generally refers to the main NAD(P)H-generating catabolic pathways. Whereas NADH especially fuels aerobic energy metabolism, NADPH is consumed especially in anabolic pathways. In photoautotrophs, NADPH additionally functions as provider of reduction equivalents for CO_2 fixation and thus constitutes the main carrier of reduction equivalents under light conditions. Heterotrophs rely on catabolism for NAD(P)H regeneration with a bias towards NADH. Catabolic modules have been widely exploited to fuel redox-intensive production processes. Key enzymes involved in catabolic NAD(P)H regeneration are summarized in **Table 1**, which gives respective reactions, cofactor specificities, and pathway affiliations. In the following **Sections 3.1** and **3.2**, approaches followed for the engineering of these pathways for NADPH and NADH regeneration are summarized and discussed. Further, the main approaches for heterotrophic metabolism are visualized in **Figure 2**. **Section 3.3** then focusses on the engineering of phototrophic metabolic modules for whole-cell redox biocatalysis. At this point, the value of NAD(P)H biosensors as useful tools to identify genetic manipulations leading to improved NADPH availability is highlighted (Zhang et al., 2016a).

3.1 Engineering the Glycolytic and the Pentose Phosphate Pathways

3.1.1 Overexpression of PPP Genes

Metabolic engineering to increase the NADPH yield per glucose consumed focused on the overexpression of the PPP genes *zwf* (glucose 6-phosphate dehydrogenase, G6PDH, EC 1.1.1.49) and *gnd* (6-phosphogluconate dehydrogenase, 6PGD, EC 1.1.1.44) both encoding NADPH forming enzymes (Lim et al., 2002; Poulsen et al., 2005) and/or the deletion of the glycolytic genes *pgi* (glucose-6-phosphate isomerase, GPI, EC 5.3.1.9) and *pfkA/B* (phosphofructokinase I/II, PFK, EC 2.7.1.11) (Canonaco et al., 2001; Lee et al., 2010) (**Figure 2**). Fuhrer et al. (2005) estimated that in growing *E. coli* cells, 12% of the glucose is catabolized *via* the PPP. The deletion of *pgi* prohibits glucose catabolism *via* glycolysis and enforces catabolism via the PPP, with 2 mol NADPH mol^{-1} glucose in a linear, non-cyclic fashion, plus the NADPH regenerated in the TCA cycle. Complete oxidation of glucose *via* a cyclic PPP requires complete cycling of both fructose 6-phosphate and triose phosphate and theoretically yields 12 mol NADPH per mole glucose (Kruger and von Schaewen, 2003). The Δ*pgi* mutant shows slower glucose uptake and a growth defect probably due to limited PPP flux capacity or regulatory effects on enzymes involved in glucose uptake or the PPP (Fuhrer et al., 2005). While deletion of *pgi* renders cyclization impossible, deletions in *pfkAB* redirect fructose 6-phosphate into the PPP further promoting catabolism *via* the PPP (Siedler et al., 2011).

Overexpression of *zwf* and *gnd* also was found to enhance NADPH-dependent PHB synthesis by recombinant *E. coli*, with *zwf* overexpression being three times more effective than *gnd* overexpression for increasing the NADPH (Lim et al., 2002). Lee et al. (2007) produced ε-caprolactone from cyclohexanone using whole cells of recombinant *E. coli* expressing cyclohexanone monooxygenase of *Acinetobacter calcoaceticus*. The maximum ε-caprolactone concentration was achieved by coexpression of the *zwf* gene enabling a 39% enhancement compared with the control. For (R)-3-hydroxybutyrate (3HB) production, Perez-Zabaleta et al. (2016) introduced the 3HB pathway of *Halomonas boliviensis* into *E. coli*, involving acetoacetyl-CoA reductase, which accepts both NADH and NADPH. The V_{max} for the latter is however eight times higher so that the less abundant NADPH limits production. Overexpression of *zwf* together with nitrogen depletion gave the highest yield and a 50% increase in 3HB concentration. Overexpression of PPP genes also has successfully been applied in organisms other than *E. coli*. For instance, the production of the poly-γ-glutamic acid

(γ-PGA), a multifunctional non-toxic, biodegradable biopolymer, in *Bacillus licheniformis* was improved by 35% when *zwf* was overexpressed (Cai et al., 2017). In *Aspergillus niger*, 13-fold 6PGD overproduction increased the intracellular NADPH concentration 2- to 9-fold (Poulsen et al., 2005). It should however be noted that the overexpression of PPP genes may compromise target product formation if the substrate is used for growth, cofactor regeneration, as well as product formation as one carbon atom is lost *via* decarboxylation (6PGD-catalyzed reaction). In the case of NADPH-dependent GDP-L-fucose biosynthesis from glucose, for instance, *zwf* overexpression decreased the production under glucose-limiting condition even though the intracellular NADPH level was increased compared to the control strain. Fine-tuning of the glucose feeding strategy improved the GDP-L-fucose production by 21% with *zwf* overexpression, highlighting that sufficient supplementation of the carbon and energy source is critical when the PPP is engineered for NADPH-dependent biotransformations (Lee et al., 2011; Lee et al., 2013).

3.1.2 Redirection of Glycolytic Fluxes to the PPP

Apart from overexpressing *zwf* and *gnd*, deletion of *pgi*, *pfkA*, and/or *pfkB* can also redirect the metabolic flux from glycolysis into the PPP (**Figure 2**) and has been employed in the NADPH-dependent production of various chemicals (e.g., hydrogen, amino acids, lycopene, 2-chloropropionic acid, terpenoids) (Aslan et al., 2017). Canonaco et al. (2001) showed via ^{13}C-MFA that glucose catabolism in *E. coli* Δ*pgi* proceeds predominantly (almost 100%) *via* the PPP. Using a theoretical approach, the NADPH production rate was proposed to increase by 300% upon *pgi* deletion (Chemler et al., 2010). The complete flux through the PPP in the Δ*pgi* mutant was also independent of the growth phase in batch cultivation (Toya et al., 2010). In thymidine production, an important precursor of various antiviral drugs, NADPH is used not only for the conversion of uridine diphosphate to deoxyuridine monophosphate, but also for the recycling of tetrahydrofolate to dihydrofolate, a co-substrate for thymidine biosynthesis. Similarly, to *zwf* overexpression, Lee et al. (2010) reported that *pgi* deletion resulted in a 39% higher NADPH/NADP$^+$ ratio which led to a 5-fold enhancement in thymidine yield on glucose. In the same manner, the NADPH-dependent production of leucocyanidin and catechin from dihydroquercetin increased upon *pgi* deletion in *E. coli* (Chemler et al., 2010).

Deletions in *pfkAB* theoretically can afford even higher NADPH yields on glucose by recycling fructose 6-phosphate to glucose 6-phosphate (Kruger and von Schaewen, 2003). This partial cycling involves catabolism of PPP-derived glyceraldehyde 3-phosphate (G3P) *via* the lower part of glycolysis (EMPP) and the TCA cycle. Under resting cell conditions, this flux through EMPP and TCA cycle is necessary and beneficial for energy generation and PTS-driven glucose uptake (Siedler et al., 2011). For the production of methyl 3-hydroxybutyrate (MHB), a building block for widely used cholesterol-lowering statins (Poulsen et al., 2005), the prochiral β-ketoester methyl acetoacetate was reduced in recombinant *E. coli* by the NADPH-dependent R-specific alcohol dehydrogenase (ADH) from *L. brevis*. The MHB yield on glucose was almost doubled *via pfk*A deletion, which was attributed to partial PPP cyclization, which was confirmed by ^{13}C-MFA revealing a negative net flux *via* PGI (Siedler et al., 2012). For further process optimization, Siedler et al. (2012) overexpressed the glucose facilitator and glucokinase genes of *Z. mobilis* and deleted either *pgi*, *pfk*A, or *pfk*A plus *pfk*B. In all cases, the glucose uptake rate increased (30–47%), and, for the Δ*pgi* and Δ*pfk*A strains, the specific MHB production rate increased by 15 and 20%, respectively. Siedler et al. (2013) also investigated *pfk*A or *gap*A (encoding G3P dehydrogenase) deletion in ADH carrying *C. glutamicum*. The WT showed a specific MHB production rate of 3.1 mmol g_{CDW}^{-1} h^{-1} and a MHB yield of 2.7 mol per mol glucose, whereas the Δ*pfkA* mutant showed a similar rate, but a yield of 4.8 mol mol^{-1}. The specific activity of the Δ*gapA* mutant decreased by 62% compared to the other strains, but the MHB yield increased to 7.9 mol per mol glucose.

Likewise, the PPP of *Streptomyces*, a genus widely used for the synthesis of various antibiotics, was successfully modulated. Borodina et al. (2008) deleted the *pfkA2* gene, one of the three annotated *pfkA* homologues in *S. coelicolor* A3, for the overproduction of the pigmented antibiotics actinorhodin and undecylprodigiosin. The *pfkA2* deletion increased the carbon flux through the PPP, as measured by ^{13}C-MFA, involving increased intracellular glucose 6-phosphate and fructose 6-phosphate levels. Similarly, PPP flux was enhanced by deleting *gap*1 and *gap*2 *in S. clavuligerus*, thereby increasing the supply of the precursor G3P for the production of clavulanic acid, a β-lactamase inhibitor (Li and Townsend, 2006).

It is well reported that the NADPH supply, e.g., *via* the PPP, also is crucial for lipid and isoprenoid production by yeast (Zu et al., 2020; Lazar et al., 2018; Qiao et al., 2017; Wasylenko et al., 2015; Runguphan and Keasling, 2014). Apart from diverting carbon flux from glycolysis to the PPP through genetic manipulations (**Figure 2**), medium engineering (i.e., synergistic cofeeding) is also reported to be effective. Park et al. (2019) report that the coordination of carbons, ATP, and reduction equivalents required for lipid synthesis can be optimized by feeding substrate mixtures fueling diverse pathways. Controlled cofeeding of superior ATP and NADPH generating substrates, i.e., glucose to support H_2-driven CO_2 reduction and gluconate to drive acetate reduction, enabled not only circumvention of catabolite repression, but also synergistic co-metabolism in two divergent organisms, i.e., *Moorella thermoacetica* and *Yarrowia lipolytica*. Glucose doping of *M. thermoacetica* stimulated CO_2 reduction into acetate by augmenting ATP synthesis *via* pyruvate kinase (PEP + ADP → pyruvate + ATP), and gluconate doping of *Y. lipolytica* accelerated acetate-driven lipogenesis by NADPH synthesis through cyclic PPP. Together, synergistic cofeeding was calculated to produce CO_2-derived lipids with up to 38% energy yield (referred to H_2 energy). Their stoichiometric analysis suggested that glucose and gluconate complemented ATP and NADPH generation, alleviating limitations seen in acetogenesis and lipogenesis, respectively. Tracing ^{13}C-labelled glucose and gluconate revealed that cells used these substrates almost exclusively for ATP and NADPH production locally within

glycolysis and the PPP, respectively. In particular, PPP activation by gluconate cofeeding solved the challenge of NADPH limitation in acetate-fed cells.

It should be noted that strategies involving a PPP knockout in combination with attenuated glycolysis can also be beneficial for biosynthetic processes, e.g., hyaluronic acid production. Based on a genome-scale metabolic model and respective simulation, Cheng et al., constructed a superior *C. glutamicum* strain for high-titer hyaluronic acid biosynthesis (Cheng et al., 2019). Genetic modulations included enhancement of the hyaluronic acid biosynthesis pathway, *zwf* deletion, fructose bisphosphate aldolase (FBA) attenuation, lactate/acetate pathway knockout, and pyruvate dehydrogenase complex (PDH) attenuation to drive carbon flux from the precursor metabolites glucose-6-phosphate (G6P), fructose-6-phosphate (F6P), and byproducts (lactate, acetate, succinate) to hyaluronic acid biosynthesis. The engineered *C. glutamicum* strain produced 28.7 g L^{-1} HA in a fed-batch culture, while the byproduct concentration was reduced by half.

3.1.3 Switching the Cofactor Preference of Glycolytic Enzymes

Since the first report on redesigning the coenzyme specificity of a dehydrogenase by directed mutagenesis and molecular modelling (Scrutton et al., 1990), switching cofactor preference has been a target not only for enzymatic biocatalysis but also for engineering cellular metabolism towards increased product yields. The case of ethanol production from pentoses by *Saccharomyces cerevisiae* is one of the most studied examples of how switching the cofactor dependency of the involved metabolic pathways can enhance product yield and decrease unwanted side products such as xylitol and CO_2 (Jeppsson et al., 2002; Verho et al., 2003; Petschacher and Nidetzky, 2008; Bengtsson et al., 2009). Apart from microbial platforms for ethanol or other fermentation product formation, switching cofactor preference of glycolytic enzymes also was applied for the bioproduction of industrially relevant terpenoids. These secondary metabolites are synthesized in dedicated biosynthetic pathways linked to the primary metabolism by specific precursors and various cofactors. Kim et al. (2018) engineered *S. cerevisiae* for the production of protopanaxadiol, a type of aglycone ginsenoside, by introducing the respective biosynthetic pathway and rerouting the redox metabolism to improve NADPH availability. By replacing the cytoplasmic NAD^+-utilizing aldehyde dehydrogenase converting acetaldehyde to acetate with a functionally equivalent $NADP^+$-dependent isozyme (**Figure 2**), the final protopanaxadiol titer could be increased more than 11-fold (Kim et al., 2018). Kildegaard et al. (2016) engineered *S. cerevisiae* for high-level 3-hydroxypropionic acid (3HP) production by increasing biosynthetic gene copy numbers and improving flux towards precursors and redox cofactors. 3HP was produced *via* a malonyl-CoA reductase (MCR) that reduces malonyl-CoA to 3HP at the expense of two NADPH. Genomic integration of multiple copies of *Chloroflexus aurantiacus* MCR and phosphorylation-deficient acetyl-CoA carboxylase genes increased the 3HP titer 5-fold in comparison with single integration. Furthermore, the native NAD^+-dependent glyceraldehyde-3-phosphate dehydrogenase (GAPDH) was exchanged with a heterologous $NADP^+$-dependent version from *Chlostridium acetobutylicum* to increase NADPH formation (**Figure 2**) and thus improve 3HP production. However, even though the two major pathways for NADPH regeneration (i.e., PPP and TCA cycle) were upregulated and carried higher flux in the engineered strain, both NADPH/$NADP^+$ as well as NADH/NAD^+ ratios increased, underlining the complexity of redox metabolism (Kildegaard et al., 2016). The same GAPDH exchange was reported to enhance lycopene and ε-caprolactone production in *E. coli* (Martínez et al., 2008).

3.1.4 Engineering the Entner–Doudoroff Pathway

Microorganisms utilize three major pathways to break down glucose into pyruvate, i.e., EMPP, EDP, and oxidative PPP (OPPP) (**Figure 2**). *E. coli* mainly relies on the EMPP and the OPPP, while the EDP is mainly inactive except during growth on gluconate. Interestingly, the EDP was found to be active in the cyanobacterium *Synechocystis* sp. PCC 6803, whose nutrient- rather than ATP-limited lifestyle profits from the lower costs for enzyme synthesis (Chen et al., 2016). In these phototrophs, the EDP seems to be important for the internal glycogen breakdown under fluctuating carbon availability (Lucius et al., 2021). Physiological analyses of different glycolytic strategies revealed that the EDP could be a preferred pathway based on both thermodynamics and the considerably lower enzyme costs. The EMPP operates 10 enzymatic reactions to yield two pyruvates, two ATP, and two NADH per glucose molecule, the OPPP provides two NADPH at the expense of one carbon atom lost as CO_2, and the EDP operates five enzymes to produce one pyruvate, one glyceraldehyde-3-phosphate, one ATP, one NADH and one NADPH per glucose molecule often constituting a well-balanced product mix. Further, the EDP bypasses the two thermodynamic bottlenecks of the EMPP, i.e., fructose 1,6-bisphosphate aldolase and triose-phosphate isomerase but at the expense of ATP yield. This characterizes EMPP and EDP as routes with high protein synthesis costs and poor ATP yield, respectively (Hollinshead et al., 2016). With an active EMPP, GAPDH is the enzyme showing the highest NADH formation rate during aerobic as well as anaerobic growth of *E. coli*. Many organisms lack this route and use the EDP instead with both GAPDH and glucose-6-phosphate dehydrogenase showing high rates (Schrewe et al., 2013). EDP-derived NADPH supports oxidative stress responses and, in contrast to PPP-derived NADPH, is formed without carbon loss (i.e., CO_2 formation) (Hollinshead et al., 2016; Jojima et al., 2021). Recently, EDP upregulation in *E. coli* was shown to enhance glucose consumption as well as G3P and pyruvate formation serving as precursors of isoprenoid synthesis *via* the methylerythritol 4-phosphate (MEP) pathway (Jojima et al., 2021). The latter depends on high and balanced flux among precursors, cofactors, and cellular energy and is limited by the imbalanced supply of G3P and pyruvate in *E. coli*. To address this problem, Li et al. (2015b) either knocked out or overexpressed multiple gene targets to redistribute fluxes among EMPP, EDP, and PPP and thus improve carotenoid production. Directing metabolic flux from EMPP towards EDP together with an enhanced MEP

pathway improved carotenoid synthesis, which was further improved by *pgi* deletion. On the contrary, *pfkAB* deletion had a negative effect. Whereas *pgi* deletion blocks the recycling of F6P and G3P into the OPPP and supports flux towards the MEP substrates pyruvate and G3P, *pfkAB* deletion enables F6P cyclization into the PPP. Importantly, improved carotenoid yields were accompanied by increased biomass growth and decreased acetate overflow, indicating a good balance between carotenoid biosynthesis and cell metabolism (Li et al., 2015b).

In a similar attempt to improve isoprenoid biosynthesis from glucose and xylose in *E. coli*, Liu et al. (2013) evaluated EMPP, EDP, PPP, as well as the Dahms pathway as MEP feeding modules differing in their modes of G3P, pyruvate, and reducing equivalent generation. In EMPP and PPP, G3P generation precedes pyruvate formation, whereas the Dahms pathway generates pyruvate from G3P. Only the EDP simultaneously produces the two MEP precursors in one reaction. Although lower amounts of precursors are produced when glucose is metabolized via the PPP, more reducing equivalents can be generated compared to EMPP and EDP. From glucose, feeding modules containing the EDP enabled three and six times higher isoprene titers and yields, respectively, compared to the EMPP. From xylose, the PPP module was significantly more effective than the Dahms pathway. In terms of precursor generation and energy/reducing-equivalent supply from glucose, the EDP together with the PPP was found to be the optimal module combination (Liu et al., 2013).

Furthermore, OPPP and EDP were investigated as engineering targets for mevalonate production. In an *E. coli* strain expressing the *Enterococcus faecalis* genes *mvaE* and *mvaS*, one mevalonate molecule is synthesized from three acetyl-CoA molecules using two molecules of NADPH in a 3-step reaction. Nagai et al. studied thermodynamic states of the central metabolism to identify metabolic reactions with regulatory function. Based on metabolite concentration data, they calculated ΔG and substrate saturation for each metabolic reaction, comparing control and mevalonate producing strains. Their analyses showed that further activation of thermodynamically feasible reactions in the upper part of glycolysis and the PPP appeared difficult and that metabolic bypassing *via* the EDP was a promising strategy to increase acetyl-CoA and NADPH supply. Deletion of *gnd* and *gntR* (encoding a negative regulator of the expression of two EDP genes) increased mevalonate yield and specific production rate by 113 and 158%, respectively (Nagai et al., 2018). Redirection to the EDP has also been employed for the production of isopropyl alcohol (Okahashi et al., 2017), poly(3-hydroxybutyrate) (Zhang et al., 2014), and isobutanol (Noda et al., 2019) with *E. coli*. Instead of using existing operons, Ng et al. (2015), rationally engineered synthetic operons for the 5-enzyme pathway of *Z. mobilis* and increased the NADPH regeneration rate 25-fold. By combining the synthetic EDP with an optimized terpenoid pathway, the terpenoid titer was increased by 97% (Ng et al., 2015). These successful attempts clearly show that even though microbial cells prefer EMPP for optimal growth, metabolic engineering strategies involving the EDP appear very promising to improve product formation rates and yields.

3.2 Increasing the Availability of Redox Cofactors and Cosubstrates Derived From the TCA Cycle

The TCA cycle is the primary metabolic pathway enabling aerobic organisms to oxidize diverse organic compounds, such as carbohydrates, lipids, or amino acids, to provide redox equivalents, energy, and precursors for biomass formation to the cell. Biotransformations can profit from the TCA cycle for the provision not only of redox cofactors but also of TCA intermediates as cosubstrates, as in the case of α-ketoglutarate (α-KG) dependent dioxygenases (**Figure 2**). Here, it has to be considered that the TCA cycle of cyanobacteria is different from that of heterotrophic bacteria (Knoop et al., 2013; Xiong et al., 2014; Zhang et al., 2016b), as it lacks α-KG dehydrogenase and thus cannot convert α-KG to succinyl–CoA. The cycle was however shown to be completed by two alternative enzymes, a novel α-KG decarboxylase and a succinic semialdehyde dehydrogenase. This corrected the misconception that these organisms have an incomplete TCA cycle and shed light on new metabolic potentials for biotechnological exploitation (Zhang et al., 2016b). The synthesis of *trans*-4-hydroxy-L-proline by both heterotrophic and photosynthetic cells using an α-KG dependent L-proline-4-hydroxylase is such a successful example (Falcioni et al., 2015; Theodosiou et al., 2017; Zhang et al., 2021a; Brandenburg et al., 2021). This and other examples for TCA dependent biocatalytic reactions are discussed in the following.

3.2.1 Engineering Redox Cofactor Supply *via* TCA Cycle and Anaplerotic Pathways

Apart from the PPP and the proton-translocating transhydrogenase PntAB, the malic enzyme (ME) is also considered a major source of NAD(P)H and a promising target for redox metabolism engineering (**Figure 2**). ME catalyzes the reversible oxidative decarboxylation of malate to pyruvate. MEs can reduce NAD^+, $NADP^+$, or both cofactors. In *E. coli*, there are 2 genes, i.e., *maeA* (encoding a NAD^+-ME) and *maeB* (encoding a $NADP^+$-ME), which are part of the anaplerotic node that links glycolysis and gluconeogenesis to the TCA cycle (Sauer and Eikmanns, 2005). Isocitrate dehydrogenase (*icd*) can also be an important NAD(P)H supplier (Sauer et al., 2004). Whereas *E. coli* IDH depends on $NADP^+$, eukaryotes also contain a NAD^+-dependent IDH playing an important role in the TCA cycle (Cupp and McAlister-Henn, 1991). Finally, the glyoxylate shunt can have an effect on the NADPH generation and is often manipulated to redirect fluxes. It bypasses the conversion of isocitrate to succinate and respective NAD(P)H generation in the TCA cycle. When the glyoxylate shunt is activated (e.g., by deletion of the respective repressor gene *iclR*), more malate is formed, which in turn can be converted to pyruvate by the ME involving NADPH formation (Lin et al., 2013).

Lee et al. (2011) overexpressed *zwf*, *icd*, and *maeB* genes in order to improve NADPH-dependent GDP-l-fucose productivity in recombinant *E. coli* bearing GDP-l-fucose biosynthetic enzymes. Overexpression of *icd* resulted in 30% higher GDP-L-fucose production compared with the control, similarly as *zwf*

overexpression. Overexpression of *maeB* however resulted in a 24% reduction of GDP-L-fucose production. Liu et al. (2018) overexpressed isocitrate dehydrogenase and citrate synthase genes in *B. licheniformis* DW2 to allow a high TCA cycle flux and study whether the improved ATP and NADPH levels could concomitantly enhance bacitracin biosynthesis. What they found was that the increased TCA cycle flux resulted in more energy generation and improved amino acid uptake and intracellular biosynthesis leading to larger pools of precursor amino acids for bacitracin biosynthesis. The contribution of the TCA cycle in NADPH regeneration was also confirmed by Chin et al. (2009) who worked with *E. coli* bearing NADPH-dependent xylose reductase from *C. boidinii*. They reported that succinyl-CoA synthetase (*sucC*) deletion significantly reduced the xylitol yield on glucose provided as cosubstrate, indicating that a functional TCA cycle contributes to NADPH allocation for xylitol production.

ME has a decisive role as major NADPH provider for fatty acid biosynthesis in oleaginous microorganisms and is often considered rate-limiting (Liang and Jiang, 2013; Ratledge, 2014). It was shown that *maeB* overexpression in *Mucor cicinelloides*, a commercial oil-producing fungus, resulted in a 2.5-fold increase in lipid accumulation (Zhang et al., 2007). This *mae*B gene also was overexpressed in the oleaginous yeast *Rhodotorula glutinis* and improved its lipid content by more than 2-fold (from 18.74 to 39.35% w/w) without affecting fatty acid profiles (Li et al., 2013). *E. coli* could be an alternative fatty acid producer even though it provides only a small amount of the precursor malonyl-CoA. Meng et al. (2011) simulated the lipogenesis of oleaginous microorganisms in *E. coli* by coexpressing the acetyl-CoA carboxylase genes (*accABCD*) from *A. calcoaceticus* to improve malonyl-CoA formation and the *maeB* gene from *E. coli* to improve NADPH availability. The overexpression of the *acc* genes alone improved malonyl-CoA formation resulting in a 3-fold increase in intracellular lipids, whereas *maeB* overexpression together with the addition of malate resulted in a 4-fold increase in intracellular lipids (197.74 mg g^{-1}). Combining the approaches, a 5.6-fold increase of intracellular lipids was achieved (284.56 mg g^{-1}). Similarly, the overexpression of ME from the oleaginous fungus *Mortierell alpine* in fatty alcohol producing *S. cerevisiae* strains lead to increased final fatty alcohol titers, with the reduction of fatty acyl-CoA to fatty alcohol requiring stoichiometric amounts of NADPH (Runguphan and Keasling, 2014).

These studies implicate ME to be a key supplier of lipogenic NADPH. However, ^{13}C-MFA by Wasylenko et al. revealed that, in engineered *Y. lipolytica* showing a two-fold increased fatty acid yield compared to the control strain, NADPH formation via the oxidative PPP was approximately doubled while the ME flux did not differ significantly between the two strains (Wasylenko et al., 2015). Moreover, they found that the PPP-related NADPH formation rate was in good agreement with the estimated NADPH demand for fatty acid biosynthesis in both strains, identifying the oxidative PPP as the primary source of lipogenic NADPH in *Y. lipolytica*. Based on this finding, Qiao et al. increased lipid synthesis by engineering pathways in *Y. lipolytica* that utilize glycolytic NADH to promote the synthesis of the lipid precursors NADPH or acetyl-CoA (Qiao et al., 2017). For this purpose, they constructed 13 novel strains based on a *Y. lipolytica* variant with overexpressed acetyl-CoA carboxylase and diacylglyceride acyltransferase. They concluded that at least three strategies can be applied to convert most of the cytosolic NADH to NADPH leading to overall process yield improvement: 1) high-level expression of the $NADP^+$-dependent glyceraldhyde-3-phosphate dehydrogenase (GAPDH) from *C. acetobutylicum*, 2) overexpression of NAD^+ kinase, and 3) introduction of cytosolic $NADP^+$-dependent malic enzyme. Interestingly, the conversion of NADH to NADPH reduced the O_2 demand of the culture enabling higher cell densities with the same aeration capacity.

MFA has shown that the competition for NAD(P)H between redox biocatalysis and the energy metabolism becomes critical during asymmetric styrene epoxidation catalyzed by growing *E. coli* containing recombinant NADH-dependent styrene monooxygenase (Bühler et al., 2008). Engineering TCA-cycle regulation allowed increased TCA-cycle activities, a delay of acetate formation, and enhanced NAD(P)H yields during batch cultivation (Kuhn et al., 2013). This, however, could not improve whole-cell styrene epoxidation activities, whereas elevated product concentrations were found to cause a significantly increased NAD(P)H demand and a compromised efficiency of metabolic operation. Higher styrene epoxidation activities however were obtained with constitutively solvent-tolerant *Pseudomonas taiwanensis* VLB120ΔCΔ*ttgV* (Volmer et al., 2014) as host strain with an inherently higher glucose uptake rate and TCA cycle activity (Volmer et al., 2019).

3.2.2 Engineering Cosubstrate Supply *via* the TCA Cycle

As mentioned above, synthetically interesting biocatalytic reactions can directly depend on central carbon metabolites that serve as cosubstrates. The hydroxylation of L-proline to trans-4-hydroxy-L-proline (hyp) using an α-KG dependent L-proline-4-hydroxylase (P4H) is such an example (Shibasaki et al., 2000). The reaction catalyzed by recombinant *E. coli* cells bearing P4H from *Dactylosporangium* sp. strain RH1 requires stoichiometric amounts of the TCA cycle intermediate α-KG. In this hydroxylation reaction, one atom of molecular oxygen is introduced into L-proline to yield hyp, while the other oxygen atom is used for oxidative decarboxylation of α-KG giving rise to succinate and CO_2. This decarboxylation added a shortcut of the TCA. For the synthesis of hyp from proline, a commercially used whole-cell process has been reported (Shibasaki et al., 2000) and the interdependency of process conditions, host metabolism, and catalyst performance was resolved (Theodosiou et al., 2015). In an attempt to evaluate TCA cycle engineering strategies to enforce and increase α-KG flux through P4H, Theodosiou et al. (2017) deleted the TCA-cycle genes *sucA* (α-KG dehydrogenase E1 subunit) or *sucC* (succinyl-CoA synthetase β subunit) together with *aceA* (isocitrate lyase), disrupting both glyoxylate shunt and TCA cycle (**Figure 2**), in a proline degradation-deficient *E. coli* strain (Δ*putA*) expressing the *p4h* gene. Whereas the Δ*sucC*Δ*aceA*Δ*putA* strain grew in minimal medium in the absence of P4H, relying on the

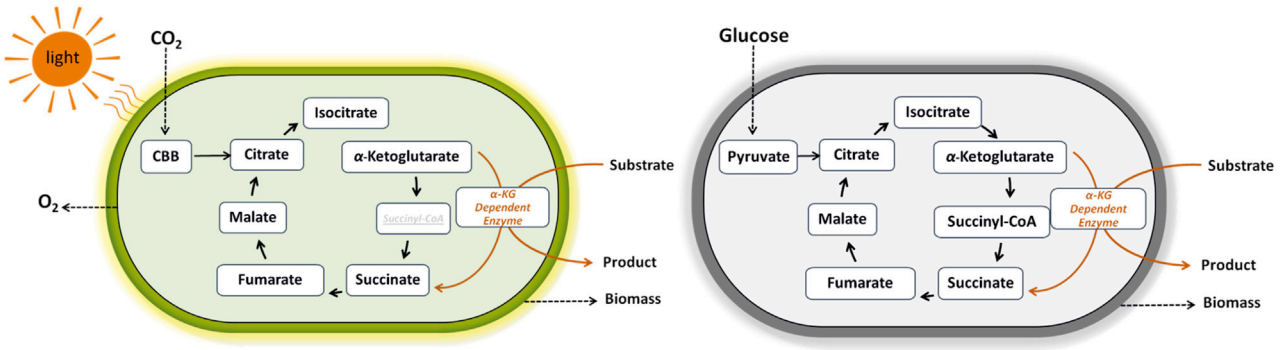

FIGURE 3 | Coupling of α-ketoglutarate dependent oxygenases to phototrophic and heterotrophic metabolism. These enzymes catalyze a remarkable range of reactions, such as hydroxylation, desaturation, and epoxidation. They utilize iron (II) as the metallo-cofactor and α-ketoglutarate as the co-substrate that is oxidatively decarboxylated to succinate and CO_2.

activity of fumarate reductase, growth of the Δ*sucA*Δ*aceA*Δ*putA* strictly depended on P4H activity, thus coupling growth to proline hydroxylation. Employing a Na^+/L-proline transporter (*putP* gene) in the Δ*sucA*Δ*aceA*Δ*putA* strain, the specific proline hydroxylation rate doubled (Theodosiou et al., 2017). In a similar approach, Smirnov et al. (2010) produced (2S,3R, 4S)-4-hydroxyisoleucine from L-isoleucine by means of recombinant *E. coli* carrying an α-ketoglutarate-dependent L-isoleucine dioxygenase (IDO) (Kodera et al., 2009). Also here, IDO introduction was able to shunt the TCA cycle in an *E. coli* mutant with both glyoxylate shunt and TCA-cycle disrupted, forcing metabolic flux through the hydroxylation reaction. The same engineering was successfully applied for the synthesis of G-7-aminodeacetoxycephalosporanic acid (G-7-ADCA) from penicillin G (Lin et al., 2015). In that case, an *E. coli* strain expressing α-KG-dependent deacetoxycephalosporin C synthase (DAOCS) was used to reconstitute the TCA cycle. Additional engineering (*poxB* deletion and *acs* overexpression) reduced acetate accumulation in order to prevent medium acidification and carbon loss. Together with the deletion of the host *β*-lactamase involved in penicillin G and G-7-ADCA degradation, the G-7-ADCA titer could be increased 11-fold to 29.01 mM. Interestingly, the constructed vector systems did not require antibiotic selection, as survival depended on the expression of the dioxygenase encoded on the vector.

Whilethe exploitation of α-KG dependent dioxygenases in heterotrophic bacteria requires organic carbon to fuel the TCA cycle, cyanobacterial reliance on CO_2 offers a promising sustainable alternative (**Figure 3**). The first exploitation of the cyanobacterial TCA cycle was reported in 1994 for the production of ethylene, a widely used feedstock in plastic industry, by introducing the *efe* gene from *Pseudomonas syringae pv. phaseolicola* PK2 into *S. elongatus* PCC 7942 (Fukuda et al., 1994). Since then, metabolic engineering and synthetic biology of cyanobacteria greatly advanced photoautotrophic ethylene production as recently reviewed by Kallio et al. (2021). Regarding amino acid hydroxylation with high potential in food and pharmaceutical industries, the work of Brandenburg et al. (2021) describes the first successful example of photosynthetic hyp production directly from CO_2, by genetic engineering of the cyanobacterium *Synechocystis* sp. PCC 6803 bearing the *p4h* gene from *Dactylosporangium*.

3.3 Engineering Phototrophic Metabolic Modules for Whole-Cell Biocatalysis

3.3.1 Direct Utilization of Light

Biocatalytic redox reactions depend not only on suitable enzymes, but also on efficient and sustainable redox cofactor supply. To find the optimal electron transfer partner, both the redox potential and the supply rate of this carrier have to be considered. Most commonly, NADH- or NADPH-dependent enzymes are used. However, photosynthetic cells offer various other electron carriers, such as ferredoxin (Fd), the primary electron acceptor of photosystem I. **Figure 4** displays the photosynthetic electron transport chain (PETC) and the variety of electron carriers involved as well as possible homo-/heterologous electron sinks.

Due to the relatively low redox potential of Fd (Wlodarczyk et al., 2015; Berepiki et al., 2016; Hoschek et al., 2019a), application of Fd-dependent enzymes seems to be highly promising. Several Fd-dependent oxygenases have been applied and specific activities up to 40 U g_{CDW}^{-1} were achieved. Both enzyme specific and host intrinsic Fds have been found to shuttle electrons, with differing efficiency. Phototrophs contain multiple Fds with, e.g., at least nine Fd in the model cyanobacterium *Synechocystis* sp. PCC 6803 (Cassier-Chauvat and Chauvat, 2014). This complicates the prediction of electron transfer efficiencies towards Fd-dependent enzymes. NADPH (Böhmer et al., 2017; Tüllinghoff et al., 2022), NADH, flavodoxins or plastochinones also have the potential to be used as electron donors. Enzymes depending on NADPH as a main product of the light reaction may benefit from the relatively large NADPH pool, but may suffer from competition with electron consuming metabolic routes, especially CO_2 fixation and nitrate assimilation (Mellor et al., 2017). A study investigating the most suitable carrier for a CYP450 showed that 1) the type of available electron carrier determines the biocatalytic reaction rate and 2) this rate profits from electron carrier-CYP450

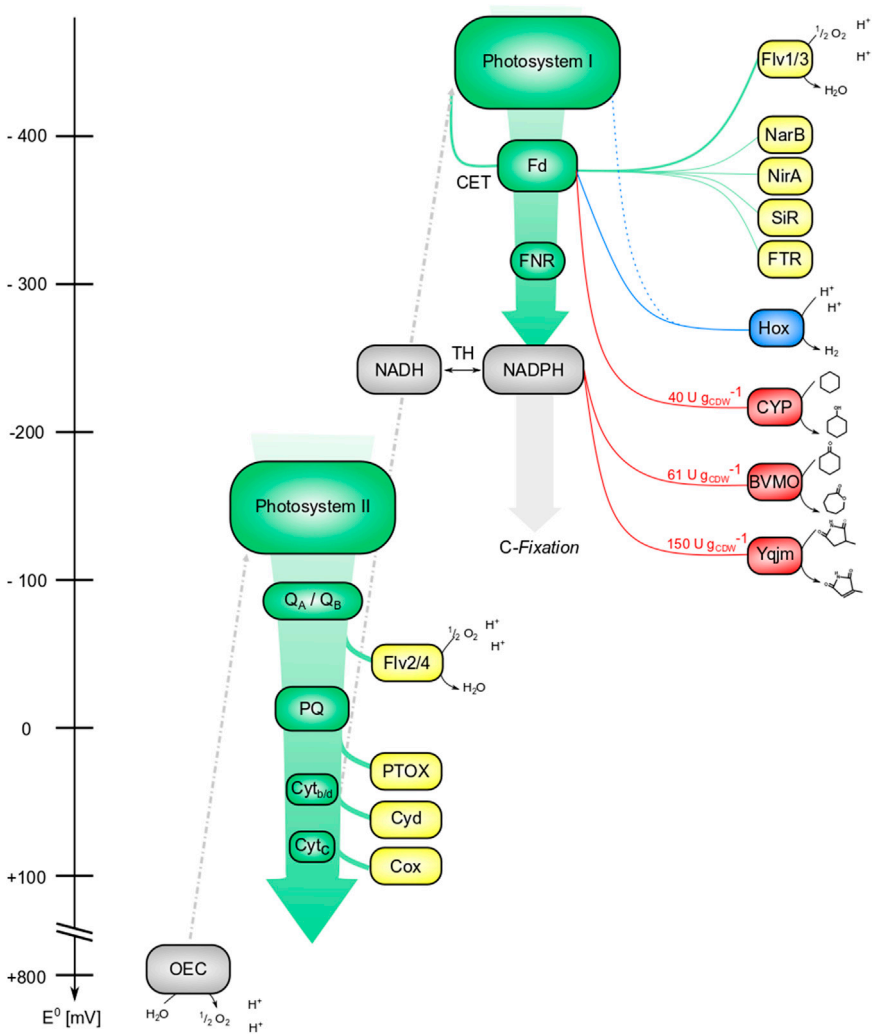

FIGURE 4 | Tapping the reductive potential of photosynthesis. Green: components of the photosynthetic electron transfer chain (PETC); yellow: internal electron sinks; blue: (native) hydrogenase (Hox); red: (recombinant) redox enzymes. Electrons derived from water splitting enter the photosynthetic electron transport chain at photosystem II, where energy from light quanta promotes them to a higher excitation state (a more negative potential). This excited state can be used for photochemistry, i.e., the reduction of the primary acceptor Q_A/Q_B, followed by electron transport over plastoquinone (PQ) and cytochromes ($Cyt_{b/d}$ and Cyt_c) along a gradient of redox potentials. Photosystem I again absorbs light energy and constitutes a reducing agent strong enough to transfer electrons to Ferredoxin (Fd). The minimal redox potentials in photosystems are not drawn to scale. Ferredoxin-NADPH-reductase (FNR) allocates a big share of these electrons to NADPH, which either can be used for C-fixation or can be converted to NADH by transhydrogenases (TH). Alternatively, electrons can be distributed to N- and S-assimilation (Fd-nitrate-reductase NarB, Fd-nitrite-reductase NirA, and Fd-sulfite-reductase SiR), regulatory elements (e.g., Fd-thioredoxin-reductase FTR), or back to photosystem I, referred to as cyclic electron transfer (CET). At different points of the PETC, reductive stress can be released by transferring electrons to acceptors like the flavodiiron proteins Flv2/4 and Flv1/3 and respiratory oxidases like the PQ-terminal oxidase PTOX, $Cyt_{b/d}$- oxidase Cyd, and Cyt_c-oxidase Cox. Redox potentials of electron sinks are not drawn to scale. So far, the reductive potential of photosynthesis was tapped at or downstream of PS I, by fusion constructs (dotted line), at the level of Fd (Hox and CYP450), and at the level of NADPH (Baeyer-Villiger monooxygenase BVMO and ene-reductase Yqjm).

fusion (Mellor et al., 2019). Methods to improve intracellular CYP450 catalysis, including enzyme-, redox-partner-, and substrate engineering recently were nicely reviewed by Li et al. (2020). An improved connection to the PETC has the potential to significantly increase production rates, as shown for the linkage of a CYP450 to the thylakoid membrane (Lassen et al., 2014a). A direct connection to the photosynthetic apparatus, as demonstrated for hydrogenases (Appel et al., 2020; Kanygin et al., 2020), allowed a direct electron transfer, mitigating unwanted electron leakage. As a strategy to avoid intracellular competition for redox equivalents, FNR affinity for ferredoxin can be attenuated, thereby making more ferredoxin available for target reactions, e.g., hydrogen formation catalyzed by Fd-accepting hydrogenases (Kannchen et al., 2020). The plastochinone pool in principle constitutes another attractive point to tap reducing power from photosynthesis, with native transfer to the terminal oxidase as an example (Feilke et al., 2017). Its relatively positive redox potential however limits the amount of reactions to be potentially fueled by plastochinone.

The implementation of biocatalytic reactions in phototrophs mostly constituted an iterative process. Several CYP450, BVMOs,

TABLE 2 | Recombinant redox biotransformations in cyanobacteria and microalgae. Adapted from Jodlbauer et al. (2021) und updated.

Host	Enzyme	Tapping Point	Product	Max. Activity/*Scale*	References
Synechocystis sp. PCC 6803	Yqjm ene reductase (*Bacillus subtilis*)	NADPH	2-methyl-succinimide	150 U g_{CDW}^{-1}, *1 ml, 5–30 min*, 25.7 U g_{CDW}^{-1a}, *200 ml, 22 h*	Assil-Companioni et al. (2020), (Hobisch et al., 2021)
	Cytochrome P450 monoxygenase (*Acidovorax* sp. CHX100)	Fd	Cyclohexanol	39.2 U g_{CDW}^{-1}, *2 L, 52 h*	Hoschek et al. (2019a)
	Alkane monooxygenase (*Pseudomonas putida*)	NADH	H-NAME	1.5 U g_{CDW}^{-1}, *1 ml, 30 min*	Hoschek et al. (2017)
	Baeyer-Villiger-Monoxygenase (*Acidovorax* sp. CHX100)	NADPH	ε—Caprolactone	60.9 U g_{CDW}^{-1}, *2 L, 24 h*	Tüllinghoff et al. (2022)
	Imine reductase (*Streptomyces* sp. GF3587)	NADPH	Cyclic amines	21.8 U g_{CDW}^{-1a}	Büchsenschütz et al. (2020)
	Cytochrome P450 monoxygenase CYP79A1 and CYP71E1 and glycosyltransferase (*Sorghum bicolor*)	Fd	*p*-Hydroxyphenylacetaloxim	1.0 U g_{CDW}^{-1}	Wlodarczyk et al. (2015)
Synechococcus elongatus PCC 7942	Alcohol dehydrogenase (*Lactobacillus kefir*)	NADPH	Dhurrin 1-phenylethanol	0.03 U g_{CDW}^{-1}, 84 U g_{CDW}^{-1a}	Sengupta et al. (2019)
Synechococcus sp. PCC 7002	Cytochrome P450 monoxygenase CYP79A1 (*Sorghum bicolor*)	Fd	*p*-Hydroxyphenylacetaloxim	(26 μM titer with OD_{730} = 2.5)[d]	Lassen et al. (2014a)
Chlamydomonas reinhardtii	Amine dehydrogenase (*Exiguobacterium sibiricum*)	NADH[b]	Linear and cylcic amines	<0.5 U 10_{cells}^{-8} ≈ 0.5 U g_{CDW}^{-1c}, *2 ml, 40 h*	Löwe et al. (2018)

[a]—*Calculated from substrate consumption.*
[b]—*Regenerated by formate reduction by* C. reinhardtii.
[c]—*Estimation based on (Fan et al., 2017).*
[d]—*Time of biotransformation not available.*
H-NAME—ω-hydroxynanoic acid methyl ester, Fd—Ferredoxin.

reductases, hydrogenases, etc., have been applied with specific activities up to 150 U g_{CDW}^{-1} as summarized in **Table 2**. Interestingly, electron drainage *via* biotransformation reactions appeared to cause an ATP/NADPH imbalance, (possibly) affecting both the biocatalytic reaction and the host metabolism. The introduction of heterologous pathways relying on C-fixation and reducing power showed a way to avoid such imbalance (Berepiki et al., 2018; Santos-Merino et al., 2021). Thus, the balance of sources and sinks should be considered. As with heterotrophic microbes, substrate and product inhibition, toxicity, and volatility also have to be considered with substrate supply as a biochemical engineering target (Lin and Tao, 2017). For BVMO catalysis in *Synechocystis* sp. PCC 6803 for instance, kinetic constraints have been found to be more relevant and thus overlay photosynthesis-related effects such as light limitation (Tüllinghoff et al., 2022).

In contrast to cyanobacteria, which have been used in various studies for biocatalysis, examples employing green algae are scarce (Zheng et al., 2018), which is mostly due to the limited molecular biology toolbox for such strains. *Chlorella vulgaris* or *Chlamydomonas reinhardtii* were recently applied as whole-cell biocatalysts, using the photosynthetic reduction power for either dehalogenations (Khan et al., 2021) or aliphatic amine formation via an amine dehydrogenase (Löwe et al., 2018; Gröger, 2019). The presented examples indicate a limited applicability of phototrophs for NADH-dependent reactions, which only indirectly couple to the photosynthetic light reaction. Application of such enzymes in cyanobacteria/green algae requires either a change in enzymatic cofactor preference (Park and Choi, 2017; Wang et al., 2017) or redirection of electrons towards NADH. Implementation of NADH-dependent nitrate assimilation led to enhanced NADH production, supporting the target pathways and finally the NADPH-dependent butanol formation (Purdy et al., 2022).

Besides providing reduction power, the photosynthetic light reaction can supply O_2 and thus overcome one major limitation in the application of oxygenases in heterotrophs. Theoretical calculations indicate that optimally aerated growing heterotrophic cells can reach productivities up to 3.5 g L^{-1} h^{-1} without oxygen limitation (Pedersen et al., 2015). For CYP catalysis in cyanobacteria (Hoschek et al., 2018), external O_2 supply could even be completely omitted and the reaction be fueled by photosynthesis-derived O_2. Additionally, an indirect O_2 supply was demonstrated in a mixed species approach, in which phototrophs provided heterotrophic whole-cell biocatalysts with O_2 (Hoschek et al., 2019b; Heuschkel et al., 2019). Furthermore, photosynthetic *in situ* O_2 supply makes application of other O_2-dependent enzymes not relying on reduction power conceivable, e.g., alcohol oxidases, amine oxidases, laccases, and dioxygenases. The oxidation of alcohols to aldehydes or ketones by alcohol oxidases is of particular interest for the production of flavors and fragrances. Examples include benzaldehyde (bitter almond), cinnamaldehyde (cinnamon), octanal (citrus), 2-heptanone (banana), ionones (rose), and vanillin (vanilla) (Berger, 2009; Berger, 2015). Laccases, which gained interest in recent years (Bassanini et al., 2021), are present in phototrophic species and have the potential to be used for degradation processes (Afreen et al., 2017; Liang et al., 2018).

TABLE 3 | Photosynthetic rates of phototrophic host organisms applied for redox biocatalysis.

Host	O_2-evolution rate (mol O_2 $g_{Chl\ a}^{-1}$ h^{-1})	e^- supply rate (mol e^- $g_{Chl\ a}^{-1}$ h^{-1})	μ_{max} (h^{-1})
Synechocystis sp. PCC 6803	0.34–1.01[a] (Zavřel et al., 2019)	1.08–2.16[b] (Kauny and Sétif, 2014)	0.135 (Zavrel et al., 2015)
Synechococcus elongatus UTEX 2973	0.82 (Ungerer et al., 2018)	—	0.365 (Yu et al., 2015)
Chlamydomonas reinhardtii	0.15 ± 0.01 (Langner et al., 2009)	1.08 ± 0.06[c] (Langner et al., 2009)	0.059 (Boyle and Morgan, 2009)
Chlorella vulgaris	0.11 ± 0.01 (Wagner et al., 2006)	0.94 ± 0.02[c] (Wagner et al., 2006)	0.07 (Schuurmans et al., 2015)

[a]*Depending on light conditions.*
[b]*Assessed via NADPH-fluorescence measurements.*
[c]*Assessed via Chl_a measurements at PS II.*

3.3.2 Calculations Regarding Light-to-Product Efficiency

For the envisioned photosynthesis-driven redox biocatalysis, the light-to-product efficiency is of special interest. Major questions to be answered, are:

1) How efficiently does the biocatalyst use the incident light? What are the resulting electron transfer rates (ETRs)?
2) At which point can photosynthesis be tapped with what efficiency?
3) Which strains or strain character traits are desirable to improve photosynthesis-driven biotechnology?

The light-to-biomass efficiency is maximal at the light saturation point E_k, where the incident light is just sufficient to supply the metabolism with the reductive power needed, e.g., for biomass production. In natural environments, phototrophic organisms face a "light usage dilemma" (Wilhelm et al., 2021), consisting of the incident light being either below or above E_k, impairing overall photosynthetic efficiency. In fact, 82% of the incident photosynthetically active radiation (PAR) reach the surface with light intensities above E_k (Wilhelm et al., 2021). Consequently, the photosynthetic apparatus is evolutionarily optimized to handle over-excitation rather than to maximize light usage efficiency.

Within the photosynthetic apparatus, (excess) energy is lost at different levels, often by mechanisms important to protect the apparatus from over-excitation: 1) Depending on their pigmentation, photosynthetic organisms absorb only a share of PAR, expressed as the share of photosynthetically absorbed quanta Q_{phar}. 2) At photosystem II (PSII), a part of the energy is dissipated via heat or fluorescence emission and non-photochemical quenching (NPQ), which decreases the operative quantum yield at PSII (Φ_{PSII}). Φ_{PSII} can be assessed *via* pulse-amplitude-modulation (PAM) fluorometry to calculate the ETR in PSII. 3) Alternative electron flux (AEF) via terminal oxidases and Mehler- or Mehler-type reactions further compromises the light-to-biomass efficiency. As a result, only a fraction of the incident light energy can be used for biomass formation or productive (biocatalytic) reactions. To illustrate these theoretical considerations, **Table 3** summarizes relevant rates of O_2 evolution, electron supply, and growth for typical phototrophic microorganisms.

Due to the energy losses along the photosynthetic electron transfer chain, it is obvious that the closer a reaction is situated to the water splitting, the higher are electron supply rate and light use efficiencies. About 50–60% (Wilhelm et al., 2021) of the light energy can in principle be tapped at PSII or directly downstream to it, at the plastoquinone pool, where losses only result from heat and fluorescence dissipation and non-photochemical quenching. Tapping reductive power at PS I or at its acceptor side (*via* Fd or NADPH as described above) involves electron losses to respiratory elements, like oxidases, or Mehler- and Mehler-type reactions. Taken together, these losses account for 20–30%, reducing the light use efficiency to 15–20%. Beside these theoretical efficiencies, the redox potentials of tapped PETC cofactors or electron carriers are of practical importance as reviewed by Mellor et al. (2017): PSII [~−110 mV in *Synechocystis* sp. PCC 6803 (Allakhverdiev et al., 2011)] and plastoquinone [+80 to +110 mV (Antal et al., 2013)] have a by far lower reductive power than already used electron carriers like Fd [−430 mV to −300 mV (Cammack et al., 1977)] and NADPH (−320 mV), which makes the latter ones highly suitable electron donors for redox biocatalysis.

In agreement with these theoretical considerations regarding light-to-product efficiencies, potential hosts for light-driven biotechnology require special character traits to ensure powerful and robust processes. High-light- and high-temperature-tolerances are especially important for outdoor applications. Adaptive laboratory evolution (ALE) in combination with systems biology approaches, were successfully applied for *Chlamydomonas, Synechocystis*, and *Synechococcus* (Zhang et al., 2021b; Srivastava et al., 2021; LaPanse et al., 2021; Dann et al., 2021; Mukherjee et al., 2020). *Synechocystis* sp. PCC 6803, for instance, was adapted to cope with additional (light) energy on account of a higher light harvesting capacity (Dann et al., 2021), auguring well for an effective use of high light intensities. Relatively low growth rates constitute another obstacle for photo-biotechnology (**Table 3**). Here, the fast growing *Synechococcus elongatus* UTEX 2973 (Ungerer et al., 2018) and the recently described *Synechococcus* sp. PCC 11901 represent a significant progress (Włodarczyk et al., 2020). For the production of fuels or chemicals with (phototrophic) whole-cell factories, solvent tolerance is another desirable trait, for which considerable ALE-based progress recently has been reported for *Synechococcus* (Srivastava et al., 2021).

As mentioned above, phototrophs experience light excess under normal/natural conditions and have evolved multiple mechanisms for excessive energy dissipation (Muramatsu and Hihara, 2012; Canonico et al., 2021). Approaches are needed to avoid such energy loss by overflow valves and to control electron flow. Several studies tackled this aspect in cyanobacteria and green algae. The major protection mechanisms in cyanobacteria are cyclic electron flow around PSI consuming up to 35% of the photosynthetically captured electrons (Theune et al., 2020), flavodiiron proteins, the orange carotenoid protein as main energy dissipater in cyanobacterial antenna systems, and adaptations of the photosynthetic apparatus, e.g., state transitions, antenna sizes, etc. Flavodiiron proteins (Bao et al., 2017) were targeted in several studies (Allahverdiyeva et al., 2015). Knock out strategies increased electron flow and desired product formation (Thiel et al., 2019; Assil-Companioni et al., 2020). As recently reviewed (Bassi and Dall'Osto, 2021; Magdaong and Blankenship, 2018), numerous mechanisms protect green algae from photoinhibition, which should be tackled in a holistic approach.

3.3.3 Biotechnological Application/Engineering of Phototrophs

Several challenges have to be addressed to apply phototrophic organisms for production purposes. Respective processes are often hindered by light limitation, inefficient light utilization, low biomass concentrations, and low production rates. As light supply is a key aspect and a major limiting factor for high-density cultivation of phototrophs, measures are needed to improve light supply and utilization (Stephens et al., 2021). Major factors are the limited absorption capacities and self-shading effects in outdoor applications (Socher et al., 2016). Systems and synthetic biology approaches aim at the engineering of strains with improved photosynthetic performance based on, e.g., improved photosystems, optimal protein allocation, and/or efficient carbon concentration and fixation (Burnap, 2015; Ort et al., 2015; Jahn et al., 2018; Luan et al., 2020; Miao et al., 2020; Roussou et al., 2021). Strategies include the reduction of antenna systems for more efficient light absorption in high-density cultures (Kirst et al., 2014), attenuation of protection mechanisms (Allahverdiyeva et al., 2015; Bassi and Dall'Osto, 2021; Kirilovsky et al., 2014), and streamlining of carbon, energy, and redox metabolism (Veaudor et al., 2020; Roussou et al., 2021; Santos-Merino et al., 2021; Zhou et al., 2021; Jaiswal et al., 2022). Furthermore, operating costs and costs for product removal have to be considered. Substrate and product toxicity constitute a general critical factor for industrial application, which can be mitigated by *in situ* product removal (ISPR) concepts. As an example, a two-liquid-phase system has been demonstrated to stabilize a cyanobacterial CYP450-based process by reducing substrate toxicity and volatility (Hoschek et al., 2019a).

Conventional photobioreactor systems are often limited by low cell densities (Chanquia et al., 2021). Therefore, innovative approaches to overcome light limitation have been developed recently (Johnson et al., 2018; Kirnev et al., 2020; Chanquia et al., 2021), including bioreactors with internal illumination (Heining et al., 2015; Hobisch et al., 2021), biofilm-based concepts (Li et al., 2017), and cell immobilization approaches (Léonard et al., 2010; Polakovič et al., 2017). Biofilm bioreactors enable high surface to volume ratios and thus high biomass concentrations and high light utilization efficiency. Bioreactors with internal light supply enabled a reduced light limitation of suspended cells and a more than two-fold increase in volumetric productivity for photosynthesis-driven 2-methylmaleimide reduction (Hobisch et al., 2021). Further, natural or synthetic consortia recently attracted attention (Hays et al., 2017; Weiss et al., 2017), offering benefits regarding process stability, multistep enzyme cascades, cofactor supply, and light utilization (Fedeson et al., 2021). Hoschek et al. (2019b) demonstrated that a two species biofilm approach enables a process duration of several weeks for cyclohexane hydroxylation at a rate of up to 3.76 $g_{cyclohexanol}$ m^{-2} day^{-1} with reduction equivalents and O_2 provided by the photosynthetic light reaction in cyanobacteria.

Other critical factors in photobiotechnology, not further addressed here, include temperature and pH control, gas (CO_2, O_2) mass transfer, strain-specific nutrient supply, water evaporation, harvesting costs, and sterility. Interested readers are referred to relevant reviews (Fabris et al., 2020; Ullmann and Grimm, 2021; van den Berg et al., 2019; Fernandes et al., 2015).

4 CONCLUSIONS AND PERSPECTIVES

Transhydrogenases and NAD^+ kinases have been shown to be promising targets to tune redox metabolism towards an efficient support of NAD(P)H-dependent productive reactions. The introduction of heterologous NAD(P)H generating enzyme systems into whole-cell biocatalysts on the other hand relieves the dependency of target reactions on the cellular redox metabolism and can be suitable for specific biotransformations. Targeted modifications in central carbon metabolism, such as overexpression and deletion of genes encoding critical enzymes or regulators, can effectively enhance redox-dependent production processes. Respective investigations also provide insight into the intricate regulatory network guiding future pathway and genome-scale engineering efforts to further boost productivities. Whereas the PPP has high potential for the optimization of NADPH availability, EDP, TCA cycle, and respective engineering have been shown to be valuable targets to achieve high NAD(P)H regeneration rates. The TCA-cycle also has high value to drive redox reactions depending on metabolites other than NAD(P)H, e.g., α-KG for oxyfunctionalizations catalyzed by α-KG-dependent dioxygenases.

Cyanobacteria and green algae have great potential as whole-cell redox biocatalysts, making use of water and sunlight to provide reduction equivalents. Recent studies showed that introduction of an artificial electron sink could not only benefit from, but also enhance photosynthetic performance. For high light-to-product efficiencies, efficient electron transport in the photosynthetic apparatus is required. Promising strategies include overexpression of limiting

elements, e.g., cytochrome b_6f, attachment to PSI, and targeted manipulation of protection mechanisms. Further, strategies to avoid intracellular competition are needed, such as attenuating FNR affinity for ferredoxin and thereby making more ferredoxin available for target reactions. Finally, future approaches have to tackle imbalances among redox and energy status of the cells.

AUTHOR CONTRIBUTIONS

ET and BB developed conception and design of the review. ET, AT, and JT wrote the original draft of the manuscript. BB contributed in terms of article structuring and editing. All authors approved the submitted version.

ACKNOWLEDGMENTS

We acknowledge the use of the facilities of the Centre for Biocatalysis (MiKat) at the Helmholtz Centre for Environmental Research, which is supported by European Regional Development Funds (EFRE, Europe funds Saxony) and the Helmholtz Association.

REFERENCES

Afreen, S., Shamsi, T. N., Baig, M. A., Ahmad, N., Fatima, S., Qureshi, M. I., et al. (2017). A Novel Multicopper Oxidase (Laccase) from Cyanobacteria: Purification, Characterization with Potential in the Decolorization of Anthraquinonic Dye. *PLOS ONE* 12, e0175144. doi:10.1371/journal.pone.0175144

Allahverdiyeva, Y., Isojärvi, J., Zhang, P., and Aro, E.-M. (2015). Cyanobacterial Oxygenic Photosynthesis Is Protected by Flavodiiron Proteins. *Life* 5, 716–743. doi:10.3390/life5010716

Allakhverdiev, S. I., Tsuchiya, T., Watabe, K., Kojima, A., Los, D. A., Tomo, T., et al. (2011). Redox Potentials of Primary Electron Acceptor Quinone Molecule $(Q_A)^-$ and Conserved Energetics of Photosystem II in Cyanobacteria with Chlorophyll a and Chlorophyll D. *Proc. Natl. Acad. Sci. U.S.A.* 108, 8054–8058. doi:10.1073/pnas.1100173108d

Angermayr, S. A., Gorchs Rovira, A., and Hellingwerf, K. J. (2015). Metabolic Engineering of Cyanobacteria for the Synthesis of Commodity Products. *Trends Biotechnol.* 33, 352–361. doi:10.1016/j.tibtech.2015.03.009

Angermayr, S. A., Paszota, M., and Hellingwerf, K. J. (2012). Engineering a Cyanobacterial Cell Factory for Production of Lactic Acid. *Appl. Environ. Microbiol.* 78, 7098–7106. doi:10.1128/aem.01587-12

Antal, T. K., Kovalenko, I. B., Rubin, A. B., and Tyystjärvi, E. (2013). Photosynthesis-Related Quantities for Education and Modeling. *Photosynth Res.* 117, 1–30. doi:10.1007/s11120-013-9945-8

Appel, J., Hueren, V., Boehm, M., and Gutekunst, K. (2020). Cyanobacterial *In Vivo* Solar Hydrogen Production Using a Photosystem I-Hydrogenase (PsaD-HoxYH) Fusion Complex. *Nat. Energ.* 5, 458–467. doi:10.1038/s41560-020-0609-6

Arias, D. M., Ortíz-Sánchez, E., Okoye, P. U., Rodríguez-Rangel, H., Balbuena Ortega, A., Longoria, A., et al. (2021). A Review on Cyanobacteria Cultivation for Carbohydrate-Based Biofuels: Cultivation Aspects, Polysaccharides Accumulation Strategies, and Biofuels Production Scenarios. *Sci. Total Environ.* 794, 148636. doi:10.1016/j.scitotenv.2021.148636

Aslan, S., Noor, E., and Bar-Even, A. (2017). Holistic Bioengineering: Rewiring Central Metabolism for Enhanced Bioproduction. *Biochem. J.* 474, 3935–3950. doi:10.1042/bcj20170377

Assil-Companioni, L., Büchsenschütz, H. C., Solymosi, D., Dyczmons-Nowaczyk, N. G., Bauer, K. K. F., Wallner, S., et al. (2020). Engineering of NADPH Supply Boosts Photosynthesis-Driven Biotransformations. *ACS Catal.* 10, 11864–11877. doi:10.1021/acscatal.0c02601

Baldwin, C. V. F., and Woodley, J. M. (2006). On Oxygen Limitation in a Whole Cell Biocatalytic Baeyer-Villiger Oxidation Process. *Biotechnol. Bioeng.* 95, 362–369. doi:10.1002/bit.20869

Bao, H., Melnicki, M. R., and Kerfeld, C. A. (2017). Structure and Functions of Orange Carotenoid Protein Homologs in Cyanobacteria. *Curr. Opin. Plant Biol.* 37, 1–9. doi:10.1016/j.pbi.2017.03.010

Bassanini, I., Ferrandi, E. E., Riva, S., and Monti, D. (2021). Biocatalysis with Laccases: An Updated Overview. *Catalysts* 11, 26. doi:10.3390/catal11010026

Bassi, R., and Dall'Osto, L. (2021). Dissipation of Light Energy Absorbed in Excess: The Molecular Mechanisms. *Annu. Rev. Plant Biol.* 72, 47–76. doi:10.1146/annurev-arplant-071720-015522

Batista-Silva, W., da Fonseca-Pereira, P., Martins, A. O., Zsögön, A., Nunes-Nesi, A., and Araújo, W. L. (2020). Engineering Improved Photosynthesis in the Era of Synthetic Biology. *Plant Commun.* 1, 100032. doi:10.1016/j.xplc.2020.100032

Bengtsson, O., Hahn-Hägerdal, B., and Gorwa-Grauslund, M. F. (2009). Xylose Reductase from *Pichia stipitis* with Altered Coenzyme Preference Improves Ethanolic Xylose Fermentation by Recombinant *Saccharomyces cerevisiae*. *Biotechnol. Biofuels* 2, 9. doi:10.1186/1754-6834-2-9

Berepiki, A., Gittins, J. R., Moore, C. M., and Bibby, T. S. (2018). Rational Engineering of Photosynthetic Electron Flux Enhances Light-Powered Cytochrome P450 Activity. *Synth. Biol. (Oxf)* 3, ysy009. doi:10.1093/synbio/ysy009

Berepiki, A., Hitchcock, A., Moore, C. M., and Bibby, T. S. (2016). Tapping the Unused Potential of Photosynthesis with a Heterologous Electron Sink. *ACS Synth. Biol.* 5, 1369–1375. doi:10.1021/acssynbio.6b00100

Berger, R. G. (2015). Biotechnology as a Source of Natural Volatile Flavours. *Curr. Opin. Food Sci.* 1, 38–43. doi:10.1016/j.cofs.2014.09.003

Berger, R. G. (2009). Biotechnology of Flavours-The Next Generation. *Biotechnol. Lett.* 31, 1651–1659. doi:10.1007/s10529-009-0083-5

Berríos-Rivera, S., Bennett, G. N., and San, K. Y. (2002). Metabolic Engineering of *Escherichia coli*: Increase of NADH Availability by Overexpressing an NAD+-Dependent Formate Dehydrogenase. *Metab. Eng.* 4, 217–229. doi:10.1006/mben.2002.0227

Blank, L. M., Ebert, B. E., Bühler, K., and Bühler, B. (2010). Redox Biocatalysis and Metabolism: Molecular Mechanisms and Metabolic Network Analysis. *Antioxid. Redox Signaling* 13, 349–394. doi:10.1089/ars.2009.2931

Blank, L. M., Ebert, B. E., Bühler, B., and Schmid, A. (2008). Metabolic Capacity Estimation of *E. coli* as a Platform for Redox Biocatalysis: Constraint-Based Modeling and Experimental Verification. *Biotechnol. Bioeng.* 100, 1050–1065. doi:10.1002/bit.21837

Böhmer, S., Köninger, K., Bojarra, S., Mügge, C., Schmidt, S., Nowaczyk, M. M., et al. (2017). Enzymatic Oxyfunctionalization Driven by Photosynthetic Water-Splitting in the Cyanobacterium *Synechocystis* sp. PCC 6803. *Catalysts* 7, 240. doi:10.3390/catal7080240

Borodina, I., Siebring, J., Zhang, J., Smith, C. P., van Keulen, G., Dijkhuizen, L., et al. (2008). Antibiotic Overproduction in *Streptomyces coelicolor* A3(2) Mediated by Phosphofructokinase Deletion. *J. Biol. Chem.* 283, 25186–25199. doi:10.1074/jbc.m803105200

Boyle, N. R., and Morgan, J. A. (2009). Flux Balance Analysis of Primary Metabolism in *Chlamydomonas reinhardtii*. *BMC Syst. Biol.* 3, 4. doi:10.1186/1752-0509-3-4

Brandenburg, F., Theodosiou, E., Bertelmann, C., Grund, M., Klähn, S., Schmid, A., et al. (2021). *Trans*-4-Hydroxy-L-Proline Production by the Cyanobacterium *Synechocystis* sp. PCC 6803. *Metab. Eng. Commun.* 12, e00155. doi:10.1016/j.mec.2020.e00155

Büchsenschütz, H. C., Vidimce-Risteski, V., Eggbauer, B., Schmidt, S., Winkler, C. K., Schrittwieser, J. H., et al. (2020). Stereoselective Biotransformations of Cyclic Imines in Recombinant Cells of *Synechocystis* sp. PCC 6803. *Chem. Cat Chem.* 12, 726–730. doi:10.1002/cctc.201901592

Bühler, B., Park, J. B., Blank, L. M., and Schmid, A. (2008). NADH Availability Limits Asymmetric Biocatalytic Epoxidation in a Growing Recombinant *Escherichia coli* Strain. *Appl. Environ. Microbiol.* 74, 1436–1446. doi:10.1128/AEM.02234-07

Burnap, R. L. (2015). Systems and Photosystems: Cellular Limits of Autotrophic Productivity in Cyanobacteria. *Front. Bioeng. Biotechnol.* 3, 1. doi:10.3389/fbioe.2015.00001

Cai, D., He, P., Lu, X., Zhu, C., Zhu, J., Zhan, Y., et al. (2017). A Novel Approach to Improve Poly-γ-Glutamic Acid Production by NADPH Regeneration in *Bacillus licheniformis* WX-02. *Sci. Rep.* 7, 43404. doi:10.1038/srep43404

Cammack, R., Rao, K. K., Bargeron, C. P., Hutson, K. G., Andrew, P. W., and Rogers, L. J. (1977). Midpoint Redox Potentials of Plant and Algal Ferredoxins. *Biochem. J.* 168, 205–209. doi:10.1042/bj1680205

Canonaco, F., Hess, T. A., Heri, S., Wang, T., Szyperski, T., and Sauer, U. (2001). Metabolic Flux Response to Phosphoglucose Isomerase Knock-Out in *Escherichia coli* and Impact of Overexpression of the Soluble Transhydrogenase UdhA. *FEMS Microbiol. Lett.* 204, 247–252. doi:10.1111/j.1574-6968.2001.tb10892.x

Canonico, M., Konert, G., Crepin, A., Šedivá, B., and Kaňa, R. (2021). Gradual Response of Cyanobacterial Thylakoids to Acute High-Light Stress-Importance of Carotenoid Accumulation. *Cells* 10 (8), 1916. doi:10.3390/cells10081916

Cassier-Chauvat, C., and Chauvat, F. (2014). Function and Regulation of Ferredoxins in the Cyanobacterium, *Synechocystis* sp. PCC 6803: Recent Advances. *Life* 4, 666–680. doi:10.3390/life4040666

Chae, T. U., Choi, S. Y., Kim, J. W., Ko, Y.-S., and Lee, S. Y. (2017). Recent Advances in Systems Metabolic Engineering Tools and Strategies. *Curr. Opin. Biotechnol.* 47, 67–82. doi:10.1016/j.copbio.2017.06.007

Chanquia, S. N., Vernet, G., and Kara, S. (2021). Photobioreactors for Cultivation and Synthesis: Specifications, Challenges, and Perspectives. *Eng. Life Sci.* 1–11. doi:10.1002/elsc.202100070

Chemler, J. A., Fowler, Z. L., McHugh, K. P., and Koffas, M. A. G. (2010). Improving NADPH Availability for Natural Product Biosynthesis in *Escherichia coli* by Metabolic Engineering. *Metab. Eng.* 12, 96–104. doi:10.1016/j.ymben.2009.07.003

Chen, X., Schreiber, K., Appel, J., Makowka, A., Fähnrich, B., Roettger, M., et al. (2016). The Entner-Doudoroff Pathway Is an Overlooked Glycolytic Route in Cyanobacteria and Plants. *Proc. Natl. Acad. Sci. U.S.A.* 113, 5441–5446. doi:10.1073/pnas.1521916113

Cheng, F., Yu, H., and Stephanopoulos, G. (2019). Engineering *Corynebacterium glutamicum* for High-Titer Biosynthesis of Hyaluronic Acid. *Metab. Eng.* 55, 276–289. doi:10.1016/j.ymben.2019.07.003

Chin, J. W., Khankal, R., Monroe, C. A., Maranas, C. D., and Cirino, P. C. (2009). Analysis of NADPH Supply During Xylitol Production by Engineered *Escherichia coli*. *Biotechnol. Bioeng.* 102, 209–220. doi:10.1002/bit.22060

Chin, T., Okuda, Y., and Ikeuchi, M. (2018). Sorbitol Production and Optimization of Photosynthetic Supply in the Cyanobacterium *Synechocystis* sp. PCC 6803. *J. Biotechnol.* 276-277, 25–33. doi:10.1016/j.jbiotec.2018.04.004

Cui, Y.-Y., Ling, C., Zhang, Y.-Y., Huang, J., and Liu, J.-Z. (2014). Production of Shikimic Acid from *Escherichia coli* Through Chemically Inducible Chromosomal Evolution and Cofactor Metabolic Engineering. *Microb. Cel. Fact.* 13, 21. doi:10.1186/1475-2859-13-21

Cupp, J. R., and McAlister-Henn, L. (1991). NAD(+)-Dependent Isocitrate Dehydrogenase. Cloning, Nucleotide Sequence, and Disruption of the IDH2 Gene from *Saccharomyces cerevisiae*. *J. Biol. Chem.* 266, 22199–22205. doi:10.1016/s0021-9258(18)54554-3

Dann, M., Ortiz, E. M., Thomas, M., Guljamow, A., Lehmann, M., Schaefer, H., et al. (2021). Enhancing Photosynthesis at High Light Levels by Adaptive Laboratory Evolution. *Nat. Plants* 7, 681–695. doi:10.1038/s41477-021-00904-2

Duetz, W. A., van Beilen, J. B., and Witholt, B. (2001). Using Proteins in Their Natural Environment: Potential and Limitations of Microbial Whole-Cell Hydroxylations in Applied Biocatalysis. *Curr. Opin. Biotechnol.* 12, 419–425. doi:10.1016/s0958-1669(00)00237-8

Ernst, M., Kaup, B. r., Moller, M., Bringer-Meyer, S., and Sahm, H. (2005). Enantioselective Reduction of Carbonyl Compounds by Whole-Cell Biotransformation, Combining a Formate Dehydrogenase and a (R)-Specific Alcohol Dehydrogenase. *Appl. Microbiol. Biotechnol.* 66, 629–634. doi:10.1007/s00253-004-1765-5

Fabris, M., Abbriano, R. M., Pernice, M., Sutherland, D. L., Commault, A. S., Hall, C. C., et al. (2020). Emerging Technologies in Algal Biotechnology: Toward the Establishment of a Sustainable, Algae-Based Bioeconomy. *Front. Plant Sci.* 11, 279. doi:10.3389/fpls.2020.00279

Falcioni, F., Bühler, B., and Schmid, A. (2015). Efficient Hydroxyproline Production from Glucose in Minimal Media by *Corynebacterium glutamicum*. *Biotechnol. Bioeng.* 112, 322–330. doi:10.1002/bit.25442

Fan, J., Zheng, L., Bai, Y., Saroussi, S., and Grossman, A. R. (2017). Flocculation of *Chlamydomonas reinhardtii* with Different Phenotypic Traits by Metal Cations and High pH. *Front. Plant Sci.* 8, 1997. doi:10.3389/fpls.2017.01997

Fedeson, D. T., and Ducat, D. C. (2021). "Symbiotic Interactions of Phototrophic Microbes: Engineering Synthetic Consortia for Biotechnology, P 37-62," in *Role of Microbial Communities for Sustainability*. Editors G. Seneviratne and J. S. Zavahir (Singapore: Springer Singapore).

Feilke, K., Ajlani, G., and Krieger-Liszkay, A. (2017). Overexpression of Plastid Terminal Oxidase in *Synechocystis* sp. PCC 6803 Alters Cellular Redox State. *Philos. Trans. R. Soc. Lond. B Biol. Sci.* 372. doi:10.1098/rstb.2016.0379

Fernandes, B. D., Mota, A., Teixeira, J. A., and Vicente, A. A. (2015). Continuous Cultivation of Photosynthetic Microorganisms: Approaches, Applications and Future Trends. *Biotechnol. Adv.* 33, 1228–1245. doi:10.1016/j.biotechadv.2015.03.004

Fernández, F. G. A., Reis, A., Wijffels, R. H., Barbosa, M., Verdelho, V., and Llamas, B. (2021). The Role of Microalgae in the Bioeconomy. *New Biotechnol.* 61, 99–107. doi:10.1016/j.nbt.2020.11.011

Fuhrer, T., Fischer, E., and Sauer, U. (2005). Experimental Identification and Quantification of Glucose Metabolism in Seven Bacterial Species. *J. Bacteriol.* 187, 1581–1590. doi:10.1128/jb.187.5.1581-1590.2005

Fukuda, H., Sakai, M., Nagahama, K., Fujii, T., Matsuoka, M., Inoue, Y., et al. (1994). Heterologous Expression of the Gene for the Ethylene-Forming Enzyme from *Pseudomonas syringae* in the Cyanobacterium *Synechococcus*. *Biotechnol. Lett.* 16, 1–6. doi:10.1007/bf01022614

Gröger, H. (2019). Biocatalytic Concepts for Synthesizing Amine Bulk Chemicals: Recent Approaches towards Linear and Cyclic Aliphatic Primary Amines and ω-Substituted Derivatives Thereof. *Appl. Microbiol. Biotechnol.* 103, 83–95. doi:10.1007/s00253-018-9452-0

Grund, M., Jakob, T., Wilhelm, C., Bühler, B., and Schmid, A. (2019). Electron Balancing Under Different Sink Conditions Reveals Positive Effects on Photon Efficiency and Metabolic Activity of *Synechocystis* sp. PCC 6803. *Biotechnol. Biofuels* 12, 43. doi:10.1186/s13068-019-1378-y

Hays, S. G., Yan, L. L. W., Silver, P. A., and Ducat, D. C. (2017). Synthetic Photosynthetic Consortia Define Interactions Leading to Robustness and Photoproduction. *J. Biol. Eng.* 11, 4. doi:10.1186/s13036-017-0048-5

Heining, M., Sutor, A., Stute, S. C., Lindenberger, C. P., and Buchholz, R. (2015). Internal Illumination of Photobioreactors via Wireless Light Emitters: A Proof of Concept. *J. Appl. Phycol* 27, 59–66. doi:10.1007/s10811-014-0290-x

Heinrich, D., Raberg, M., and Steinbüchel, A. (2015). Synthesis of Poly(3-Hydroxybutyrate-Co-3-Hydroxyvalerate) from Unrelated Carbon Sources in Engineered *Rhodospirillum rubrum*. *FEMS Microbiol. Lett.* 362, fnv038. doi:10.1093/femsle/fnv038

Heuschkel, I., Hoschek, A., Schmid, A., Bühler, B., Karande, R., and Bühler, K. (2019). Mixed-Trophies Biofilm Cultivation in Capillary Reactors. *MethodsX* 6, 1822–1831. doi:10.1016/j.mex.2019.07.021

Hobisch, M., Spasic, J., Malihan-Yap, L., Barone, G. D., Castiglione, K., Tamagnini, P., et al. (2021). Internal Illumination to Overcome the Cell Density Limitation in the Scale-up of Whole-Cell Photobiocatalysis. *ChemSusChem* 14, 3219–3225. doi:10.1002/cssc.202100832

Hollinshead, W. D., Rodriguez, S., Martin, H. G., Wang, G., Baidoo, E. E. K., Sale, K. L., et al. (2016). Examining *Escherichia coli* Glycolytic Pathways, Catabolite Repression, and Metabolite Channeling Using Δpfk Mutants. *Biotechnol. Biofuels* 9, 212. doi:10.1186/s13068-016-0630-y

Holm, A. K., Blank, L. M., Oldiges, M., Schmid, A., Solem, C., Jensen, P. R., et al. (2010). Metabolic and Transcriptional Response to Cofactor Perturbations in *Escherichia coli*. *J. Biol. Chem.* 285, 17498–17506. doi:10.1074/jbc.m109.095570

Hoschek, A., Toepel, J., Hochkeppel, A., Karande, R., Bühler, B., and Schmid, A. (2019a). Light-Dependent and Aeration-Independent Gram-Scale Hydroxylation of Cyclohexane to Cyclohexanol by CYP450 Harboring *Synechocystis* sp. PCC 6803. *Biotechnol. J.* 14, e1800724. doi:10.1002/biot.201800724

Hoschek, A., Bühler, B., and Schmid, A. (2017). Overcoming the Gas-Liquid Mass Transfer of Oxygen by Coupling Photosynthetic Water Oxidation with Biocatalytic Oxyfunctionalization. *Angew. Chem. Int. Ed.* 56, 15146–15149. doi:10.1002/anie.201706886

Hoschek, A., Heuschkel, I., Schmid, A., Bühler, B., Karande, R., and Bühler, K. (2019b). Mixed-Species Biofilms for High-Cell-Density Application of *Synechocystis* sp. PCC 6803 in Capillary Reactors for Continuous Cyclohexane Oxidation to Cyclohexanol. *Bioresour. Technology* 282, 171–178. doi:10.1016/j.biortech.2019.02.093

Hoschek, A., Schmid, A., and Bühler, B. (2018). *In Situ* O_2 Generation for Biocatalytic Oxyfunctionalization Reactions. *ChemCatChem* 10, 5366–5371. doi:10.1002/cctc.201801262

Ishikawa, Y., Cassan, C., Kadeer, A., Yuasa, K., Sato, N., Sonoike, K., et al. (2021). The NAD Kinase *Slr0400* Functions as a Growth Repressor in *Synechocystis* sp. PCC 6803. *Plant Cel. Physiol.* 62, 668–677. doi:10.1093/pcp/pcab023

Ishikawa, Y., and Kawai-Yamada, M. (2019). Physiological Significance of NAD Kinases in Cyanobacteria. *Front. Plant Sci.* 10, 847. doi:10.3389/fpls.2019.00847

Ishikawa, Y., Miyagi, A., Ishikawa, T., Nagano, M., Yamaguchi, M., Hihara, Y., et al. (2019). One of the NAD Kinases, Sll1415, is Required for the Glucose Metabolism of *Synechocystis* sp. PCC 6803. *Plant J.* 98, 654–666. doi:10.1111/tpj.14262

Jahan, N., Maeda, K., Matsuoka, Y., Sugimoto, Y., and Kurata, H. (2016). Development of an Accurate Kinetic Model for the Central Carbon Metabolism of *Escherichia coli*. *Microb. Cel. Fact.* 15, 112. doi:10.1186/s12934-016-0511-x

Jahn, M., Vialas, V., Karlsen, J., Maddalo, G., Edfors, F., Forsström, B., et al. (2018). Growth of Cyanobacteria Is Constrained by the Abundance of Light and Carbon Assimilation Proteins. *Cel. Rep.* 25, 478–486. doi:10.1016/j.celrep.2018.09.040

Jaiswal, D., Sahasrabuddhe, D., and Wangikar, P. P. (2022). Cyanobacteria as Cell Factories: The Roles of Host and Pathway Engineering and Translational Research. *Curr. Opin. Biotechnol.* 73, 314–322. doi:10.1016/j.copbio.2021.09.010

Jan, J., Martinez, I., Wang, Y., Bennett, G. N., and San, K.-Y. (2013). Metabolic Engineering and Transhydrogenase Effects on NADPH Availability in *E. coli*. *Biotechnol. Prog.* 29, 1124–1130. doi:10.1002/btpr.1765

Jeppsson, M., Johansson, B., Hahn-Hägerdal, B., and Gorwa-Grauslund, M. F. (2002). Reduced Oxidative Pentose Phosphate Pathway Flux in Recombinant Xylose-Utilizing *Saccharomyces cerevisiae* Strains Improves the Ethanol Yield from Xylose. *Appl. Environ. Microbiol.* 68, 1604–1609. doi:10.1128/aem.68.4.1604-1609.2002

Jodlbauer, J., Rohr, T., Spadiut, O., Mihovilovic, M. D., and Rudroff, F. (2021). Biocatalysis in Green and Blue: Cyanobacteria. *Trends Biotechnol.* 39, 875–889. doi:10.1016/j.tibtech.2020.12.009

Johnson, T. J., Katuwal, S., Anderson, G. A., Gu, L., Zhou, R., and Gibbons, W. R. (2018). Photobioreactor Cultivation Strategies for Microalgae and Cyanobacteria. *Biotechnol. Prog.* 34, 811–827. doi:10.1002/btpr.2628

Jojima, T., Igari, T., Noburyu, R., Watanabe, A., Suda, M., and Inui, M. (2021). Coexistence of the Entner-Doudoroff and Embden-Meyerhof-Parnas Pathways Enhances Glucose Consumption of Ethanol-Producing *Corynebacterium glutamicum*. *Biotechnol. Biofuels* 14, 45. doi:10.1186/s13068-021-01876-3

Kadisch, M., Willrodt, C., Hillen, M., Bühler, B., and Schmid, A. (2017). Maximizing the Stability of Metabolic Engineering-Derived Whole-Cell Biocatalysts. *Biotechnol. J.* 12, 8. doi:10.1002/biot.201600170

Kallio, P., Kugler, A., Pyytövaara, S., Stensjö, K., Allahverdiyeva, Y., Gao, X., et al. (2021). Photoautotrophic Production of Renewable Ethylene by Engineered Cyanobacteria: Steering the Cell Metabolism towards Biotechnological Use. *Physiologia Plantarum* 173, 579–590. doi:10.1111/ppl.13430

Kämäräinen, J., Huokko, T., Kreula, S., Jones, P. R., Aro, E. M., and Kallio, P. (2017). Pyridine Nucleotide Transhydrogenase PntAB Is Essential for Optimal Growth and Photosynthetic Integrity Under Low-light Mixotrophic Conditions in *Synechocystis* sp. PCC 6803. *New Phytol.* 214, 194–204. doi:10.1111/nph.14353

Kannchen, D., Zabret, J., Oworah-Nkruma, R., Dyczmons-Nowaczyk, N. G., Wiegand, K., Löbbert, P., et al. (2020). Remodeling of Photosynthetic Electron Transport in *Synechocystis* sp. PCC 6803 for Future Hydrogen Production from Water. *BBA Bioenerg.* 1861, 148208. doi:10.1016/j.bbabio.2020.148208

Kanygin, A., Milrad, Y., Thummala, C., Reifschneider, K., Baker, P., Marco, P., et al. (2020). Rewiring Photosynthesis: A Photosystem I-Hydrogenase Chimera that Makes H_2 *in vivo*. *Energy Environ. Sci.* 13, 2903–2914. doi:10.1039/c9ee03859k

Kataoka, M., Kita, K., Wada, M., Yasohara, Y., Hasegawa, J., and Shimizu, S. (2003). Novel Bioreduction System for the Production of Chiral Alcohols. *Appl. Microbiol. Biotechnol.* 62, 437–445. doi:10.1007/s00253-003-1347-y

Kato, Y., Inabe, K., Hidese, R., Kondo, A., and Hasunuma, T. (2022). Metabolomics-Based Engineering for Biofuel and Bio-Based Chemical Production in Microalgae and Cyanobacteria: A Review. *Bioresour. Technol.* 344, 126196. doi:10.1016/j.biortech.2021.126196

Kauny, J., and Sétif, P. (2014). NADPH Fluorescence in the Cyanobacterium *Synechocystis* sp. PCC 6803: A Versatile Probe for *In Vivo* Measurements of Rates, Yields and Pools. *Biochim. Biophys. Acta (Bba) - Bioenerg.* 1837, 792–801. doi:10.1016/j.bbabio.2014.01.009

Kaup, B., Bringer-Meyer, S., and Sahm, H. (2004). Metabolic Engineering of *Escherichia coli*: Construction of an Efficient Biocatalyst for D-Mannitol Formation in a Whole-Cell Biotransformation. *Appl. Microbiol. Biotechnol.* 64, 333–339. doi:10.1007/s00253-003-1470-9

Kawai, S., Mori, S., Mukai, T., Matsukawa, H., Matuo, Y., and Murata, K. (2001). Establishment of a Mass-Production System for NADP Using Bacterial Inorganic Polyphosphate/ATP-NAD Kinase. *J. Biosci. Bioeng.* 92, 447–452. doi:10.1016/s1389-1723(01)80294-2

Khan, S., Fu, P., Di Fonzo, A., Marasca, I., and Secundo, F. (2021). Enhanced Whole-Cell Biotransformation of 3-Chloropropiophenone into 1-Phenyl-1-Propanone by Hydrogel Entrapped *Chlorella emersonii* (211.8b). *Biotechnol. Lett.* 43, 2259–2272. doi:10.1007/s10529-021-03194-y

Kildegaard, K. R., Jensen, N. B., Schneider, K., Czarnotta, E., Özdemir, E., Klein, T., et al. (2016). Engineering and Systems-Level Analysis of *Saccharomyces cerevisiae* for Production of 3-hydroxypropionic Acid via Malonyl-CoA Reductase-Dependent Pathway. *Microb. Cel. Fact.* 15, 53. doi:10.1186/s12934-016-0451-5

Kim, J.-E., Jang, I.-S., Sung, B. H., Kim, S. C., and Lee, J. Y. (2018). Rerouting of NADPH Synthetic Pathways for Increased Protopanaxadiol Production in *Saccharomyces cerevisiae*. *Sci. Rep.* 8, 15820. doi:10.1038/s41598-018-34210-3

Kirilovsky, D., Kaňa, R., and Prášil, O. (2014). "Mechanisms Modulating Energy Arriving at Reaction Centers in Cyanobacteria, P 471-501," in *Non-Photochemical Quenching and Energy Dissipation in Plants, Algae and Cyanobacteria*. Editors B. Demmig-Adams, G. Garab, W. Adams III, and Govindjee (Dordrecht Netherlands: Springer Netherlands).

Kirnev, P. C. S., Carvalho, J. C., Vandenberghe, L. P. S., Karp, S. G., and Soccol, C. R. (2020). Technological Mapping and Trends in Photobioreactors for the Production of Microalgae. *World J. Microbiol. Biotechnol.* 36, 42. doi:10.1007/s11274-020-02819-0

Kirst, H., Formighieri, C., and Melis, A. (2014). Maximizing Photosynthetic Efficiency and Culture Productivity in Cyanobacteria upon Minimizing the Phycobilisome Light-Harvesting Antenna Size. *Biochim. Biophys. Acta (Bba) - Bioenerg.* 1837, 1653–1664. doi:10.1016/j.bbabio.2014.07.009

Knoop, H., Gründel, M., Zilliges, Y., Lehmann, R., Hoffmann, S., Lockau, W., et al. (2013). Flux Balance Analysis of Cyanobacterial Metabolism: The Metabolic Network of *Synechocystis* sp. PCC 6803. *Plos Comput. Biol.* 9, e1003081. doi:10.1371/journal.pcbi.1003081

Kodera, T., Smirnov, S. V., Samsonova, N. N., Kozlov, Y. I., Koyama, R., Hibi, M., et al. (2009). A Novel L-Isoleucine Hydroxylating Enzyme, L-Isoleucine Dioxygenase from *Bacillus thuringiensis*, Produces (2S,3R,4S)-4-Hydroxyisoleucine. *Biochem. Biophysical Res. Commun.* 390, 506–510. doi:10.1016/j.bbrc.2009.09.126

Kopf, M., Klähn, S., Scholz, I., Matthiessen, J. K. F., Hess, W. R., and Voss, B. (2014). Comparative Analysis of the Primary Transcriptome of *Synechocystis* sp. PCC 6803. *DNA Res.* 21, 527–539. doi:10.1093/dnares/dsu018

Kruger, N. J., and von Schaewen, A. (2003). The Oxidative Pentose Phosphate Pathway: Structure and Organisation. *Curr. Opin. Plant Biol.* 6, 236–246. doi:10.1016/s1369-5266(03)00039-6

Kuhn, D., Fritzsch, F. S. O., Zhang, X., Wendisch, V. F., Blank, L. M., Bühler, B., et al. (2013). Subtoxic Product Levels Limit the Epoxidation Capacity of Recombinant *E. coli* by Increasing Microbial Energy Demands. *J. Biotechnol.* 163, 194–203. doi:10.1016/j.jbiotec.2012.07.194

Ladkau, N., Assmann, M., Schrewe, M., Julsing, M. K., Schmid, A., and Bühler, B. (2016). Efficient Production of the Nylon 12 Monomer ω-Aminododecanoic Acid Methyl Ester from Renewable Dodecanoic Acid Methyl Ester with Engineered *Escherichia coli*. *Metab. Eng.* 36, 1–9. doi:10.1016/j.ymben.2016.02.011

Ladkau, N., Schmid, A., and Bühler, B. (2014). The Microbial Cell - Functional Unit for Energy Dependent Multistep Biocatalysis. *Curr. Opin. Biotechnol.* 30, 178–189. doi:10.1016/j.copbio.2014.06.003

Langner, U., Jakob, T., Stehfest, K., and Wilhelm, C. (2009). An Energy Balance from Absorbed Photons to New Biomass for *Chlamydomonas reinhardtii* and *Chlamydomonas acidophila* under Neutral and Extremely Acidic Growth Conditions. *Plant Cel. Environ.* 32, 250–258. doi:10.1111/j.1365-3040.2008.01917.x

LaPanse, A. J., Krishnan, A., and Posewitz, M. C. (2021). Adaptive Laboratory Evolution for Algal Strain Improvement: Methodologies and Applications. *Algal Res.* 53, 102122. doi:10.1016/j.algal.2020.102122

Lassen, L. M., Nielsen, A. Z., Olsen, C. E., Bialek, W., Jensen, K., Møller, B. L., et al. (2014b). Anchoring a Plant Cytochrome P450 via PsaM to the Thylakoids in *Synechococcus* sp. PCC 7002: Evidence for Light-Driven Biosynthesis. *PLoS One* 9, e102184. doi:10.1371/journal.pone.0102184

Lassen, L. M., Nielsen, A. Z., Ziersen, B., Gnanasekaran, T., Møller, B. L., and Jensen, P. E. (2014a). Redirecting Photosynthetic Electron Flow into Light-Driven Synthesis of Alternative Products Including High-Value Bioactive Natural Compounds. *ACS Synth. Biol.* 3, 1–12. doi:10.1021/sb400136f

Lazar, Z., Liu, N., and Stephanopoulos, G. (2018). Holistic Approaches in Lipid Production by *Yarrowia lipolytica*. *Trends Biotechnol.* 36, 1157–1170. doi:10.1016/j.tibtech.2018.06.007

Lee, H. C., Kim, J. S., Jang, W., and Kim, S. Y. (2010). High NADPH/$NADP^+$ Ratio Improves Thymidine Production by a Metabolically Engineered *Escherichia coli* Strain. *J. Biotechnol.* 149, 24–32. doi:10.1016/j.jbiotec.2010.06.011

Lee, H. C., Kim, J. S., Jang, W., and Kim, S. Y. (2009). Thymidine Production by Overexpressing NAD^+ Kinase in an *Escherichia coli* Recombinant Strain. *Biotechnol. Lett.* 31, 1929–1936. doi:10.1007/s10529-009-0097-z

Lee, W.-H., Chin, Y.-W., Han, N. S., Kim, M.-D., and Seo, J.-H. (2011). Enhanced Production of GDP-L-Fucose by Overexpression of NADPH Regenerator in Recombinant *Escherichia coli*. *Appl. Microbiol. Biotechnol.* 91, 967–976. doi:10.1007/s00253-011-3271-x

Lee, W.-H., Kim, M.-D., Jin, Y.-S., and Seo, J.-H. (2013). Engineering of NADPH Regenerators in *Escherichia coli* for Enhanced Biotransformation. *Appl. Microbiol. Biotechnol.* 97, 2761–2772. doi:10.1007/s00253-013-4750-z

Lee, W.-H., Park, J.-B., Park, K., Kim, M.-D., and Seo, J.-H. (2007). Enhanced Production of ε-Caprolactone by Overexpression of NADPH-Regenerating Glucose 6-Phosphate Dehydrogenase in Recombinant *Escherichia coli* Harboring Cyclohexanone Monooxygenase Gene. *Appl. Microbiol. Biotechnol.* 76, 329–338. doi:10.1007/s00253-007-1016-7

Léonard, A., Rooke, J. C., Meunier, C. F., Sarmento, H., Descy, J.-P., and Su, B.-L. (2010). Cyanobacteria Immobilised in Porous Silica Gels: Exploring Biocompatible Synthesis Routes for the Development of Photobioreactors. *Energ. Environ. Sci.* 3, 370–377. doi:10.1039/b923859j

Li, C., Tao, F., Ni, J., Wang, Y., Yao, F., and Xu, P. (2015a). Enhancing the Light-Driven Production of D-Lactate by Engineering Cyanobacterium Using a Combinational Strategy. *Sci. Rep.* 5, 9777. doi:10.1038/srep09777

Li, C., Ying, L.-Q., Zhang, S.-S., Chen, N., Liu, W.-F., and Tao, Y. (2015b). Modification of Targets Related to the Entner-Doudoroff/pentose Phosphate Pathway Route for Methyl-D-Erythritol 4-Phosphate-Dependent Carotenoid Biosynthesis in *Escherichia coli*. *Microb. Cel. Fact.* 14, 117. doi:10.1186/s12934-015-0301-x

Li, R., and Townsend, C. A. (2006). Rational Strain Improvement for Enhanced Clavulanic Acid Production by Genetic Engineering of the Glycolytic Pathway in *Streptomyces clavuligerus*. *Metab. Eng.* 8, 240–252. doi:10.1016/j.ymben.2006.01.003

Li, T., Strous, M., and Melkonian, M. (2017). Biofilm-Based Photobioreactors: Their Design and Improving Productivity through Efficient Supply of Dissolved Inorganic Carbon. *FEMS Microbiol. Lett.* 364. doi:10.1093/femsle/fnx218

Li, W., Wu, H., Li, M., and San, K.-Y. (2018). Effect of NADPH Availability on Free Fatty Acid Production in *E. coli*. *Biotechnol. Bioeng.* 115, 444–452. doi:10.1002/bit.26464

Li, Z.-J., Cai, L., Wu, Q., and Chen, G.-Q. (2009). Overexpression of NAD Kinase in Recombinant *Escherichia coli* Harboring the phbCAB Operon Improves Poly(3-Hydroxybutyrate) Production. *Appl. Microbiol. Biotechnol.* 83, 939–947. doi:10.1007/s00253-009-1943-6

Li, Z., Jiang, Y., Guengerich, F. P., Ma, L., Li, S., and Zhang, W. (2020). Engineering Cytochrome P450 Enzyme Systems for Biomedical and Biotechnological Applications. *J. Biol. Chem.* 295, 833–849. doi:10.1074/jbc.rev119.008758

Li, Z., Sun, H., Mo, X., Li, X., Xu, B., and Tian, P. (2013). Overexpression of Malic Enzyme (ME) of *Mucor circinelloides* Improved Lipid Accumulation in Engineered *Rhodotorula glutinis*. *Appl. Microbiol. Biotechnol.* 97, 4927–4936. doi:10.1007/s00253-012-4571-5

Liang, M.-H., and Jiang, J.-G. (2013). Advancing Oleaginous Microorganisms to Produce Lipid via Metabolic Engineering Technology. *Prog. Lipid Res.* 52, 395–408. doi:10.1016/j.plipres.2013.05.002

Liang, Y., Hou, J., Liu, Y., Luo, Y., Tang, J., Cheng, J. J., et al. (2018). Textile Dye Decolorizing *Synechococcus* PCC 7942 Engineered with CotA Laccase. *Front. Bioeng. Biotechnol.* 6, 95. doi:10.3389/fbioe.2018.00095

Liao, J. C., Mi, L., Pontrelli, S., and Luo, S. (2016). Fuelling the Future: Microbial Engineering for the Production of Sustainable Biofuels. *Nat. Rev. Microbiol.* 14, 288–304. doi:10.1038/nrmicro.2016.32

Lim, S.-J., Jung, Y.-M., Shin, H.-D., and Lee, Y.-H. (2002). Amplification of the NADPH-Related Genes *Zwf* and *Gnd* for the Oddball Biosynthesis of PHB in an *E. coli* Transformant Harboring a Cloned phbCAB Operon. *J. Biosci. Bioeng.* 93, 543–549. doi:10.1016/s1389-1723(02)80235-3

Lin, B., Fan, K., Zhao, J., Ji, J., Wu, L., Yang, K., et al. (2015). Reconstitution of TCA Cycle with DAOCS to Engineer *Escherichia coli* into an Efficient Whole Cell Catalyst of Penicillin G. *Proc. Natl. Acad. Sci. U.S.A.* 112, 9855–9859. doi:10.1073/pnas.1502866112

Lin, B., and Tao, Y. (2017). Whole-Cell Biocatalysts by Design. *Microb. Cel. Fact* 16, 106. doi:10.1186/s12934-017-0724-7

Lin, F., Chen, Y., Levine, R., Lee, K., Yuan, Y., and Lin, X. N. (2013). Improving Fatty Acid Availability for Bio-Hydrocarbon Production in *Escherichia coli* by Metabolic Engineering. *PLoS One* 8, e78595. doi:10.1371/journal.pone.0078595

Liu, H., Sun, Y., Ramos, K. R. M., Nisola, G. M., Valdehuesa, K. N. G., Lee, W. K., et al. (2013). Combination of Entner-Doudoroff Pathway with MEP Increases Isoprene Production in Engineered *Escherichia coli*. *PLoS One* 8, e83290. doi:10.1371/journal.pone.0083290

Liu, Z., Yu, W., Nomura, C. T., Li, J., Chen, S., Yang, Y., et al. (2018). Increased Flux through the TCA Cycle Enhances Bacitracin Production by *Bacillus licheniformis* DW2. *Appl. Microbiol. Biotechnol.* 102, 6935–6946. doi:10.1007/s00253-018-9133-z

Löwe, J., Siewert, A., Scholpp, A. C., Wobbe, L., and Gröger, H. (2018). Providing Reducing Power by Microalgal Photosynthesis: A Novel Perspective Towards Sustainable Biocatalytic Production of Bulk Chemicals Exemplified for Aliphatic Amines. *Sci. Rep.* 8, 10436. doi:10.1038/s41598-018-28755-6

Luan, G., Zhang, S., and Lu, X. (2020). Engineering Cyanobacteria Chassis Cells Toward More Efficient Photosynthesis. *Curr. Opin. Biotechnol.* 62, 1–6. doi:10.1016/j.copbio.2019.07.004

Lucius, S., Makowka, A., Michl, K., Gutekunst, K., and Hagemann, M. (2021). The Entner-Doudoroff Pathway Contributes to Glycogen Breakdown during High to Low CO_2 Shifts in the Cyanobacterium *Synechocystis* sp. PCC 6803. *Front. Plant Sci.* 12, 787943. doi:10.3389/fpls.2021.787943

Lupacchini, S., Appel, J., Stauder, R., Bolay, P., Klähn, S., Lettau, E., et al. (2021). Rewiring Cyanobacterial Photosynthesis by the Implementation of an Oxygen-Tolerant Hydrogenase. *Metab. Eng.* 68, 199–209. doi:10.1016/j.ymben.2021.10.006

Macnab, R. M. (1990). Cultural Exchange. *Nature* 348, 401. doi:10.1038/348401a0

Magdaong, N. C. M., and Blankenship, R. E. (2018). Photoprotective, Excited-State Quenching Mechanisms in Diverse Photosynthetic Organisms. *J. Biol. Chem.* 293, 5018–5025. doi:10.1074/jbc.tm117.000233

Martínez, I., Zhu, J., Lin, H., Bennett, G. N., and San, K.-Y. (2008). Replacing *Escherichia coli* NAD-Dependent Glyceraldehyde 3-Phosphate Dehydrogenase (GAPDH) with a NADP-Dependent Enzyme from *Clostridium acetobutylicum* Facilitates NADPH Dependent Pathways. *Metab. Eng.* 10, 352–359. doi:10.1016/j.ymben.2008.09.001

Mellor, S. B., Vavitsas, K., Nielsen, A. Z., and Jensen, P. E. (2017). Photosynthetic Fuel for Heterologous Enzymes: The Role of Electron Carrier Proteins. *Photosynth Res.* 134, 329–342. doi:10.1007/s11120-017-0364-0

Mellor, S. B., Vinde, M. H., Nielsen, A. Z., Hanke, G. T., Abdiaziz, K., Roessler, M. M., et al. (2019). Defining Optimal Electron Transfer Partners for Light-Driven Cytochrome P450 Reactions. *Metab. Eng.* 55, 33–43. doi:10.1016/j.ymben.2019.05.003

Meng, X., Yang, J., Cao, Y., Li, L., Jiang, X., Xu, X., et al. (2011). Increasing Fatty Acid Production in *E. coli* by Simulating the Lipid Accumulation of Oleaginous Microorganisms. *J. Ind. Microbiol. Biotechnol.* 38, 919–925. doi:10.1007/s10295-010-0861-z

Miao, R., Xie, H., Liu, X., Lindberg, P., and Lindblad, P. (2020). Current Processes and Future Challenges of Photoautotrophic Production of Acetyl-CoA-Derived Solar Fuels and Chemicals in Cyanobacteria. *Curr. Opin. Chem. Biol.* 59, 69–76. doi:10.1016/j.cbpa.2020.04.013

Mukherjee, B., Madhu, S., and Wangikar, P. P. (2020). The Role of Systems Biology in Developing Non-Model Cyanobacteria as Hosts for Chemical Production. *Curr. Opin. Biotechnol.* 64, 62–69. doi:10.1016/j.copbio.2019.10.003

Muramatsu, M., and Hihara, Y. (2012). Acclimation to High-Light Conditions in Cyanobacteria: From Gene Expression to Physiological Responses. *J. Plant Res.* 125, 11–39. doi:10.1007/s10265-011-0454-6

Nagai, H., Masuda, A., Toya, Y., Matsuda, F., and Shimizu, H. (2018). Metabolic Engineering of Mevalonate-Producing *Escherichia coli* Strains Based on Thermodynamic Analysis. *Metab. Eng.* 47, 1–9. doi:10.1016/j.ymben.2018.02.012

Ng, C. Y., Farasat, I., Maranas, C. D., and Salis, H. M. (2015). Rational Design of a Synthetic Entner-Doudoroff Pathway for Improved and Controllable NADPH Regeneration. *Metab. Eng.* 29, 86–96. doi:10.1016/j.ymben.2015.03.001

Niederholtmeyer, H., Wolfstädter, B. T., Savage, D. F., Silver, P. A., and Way, J. C. (2010). Engineering Cyanobacteria to Synthesize and Export Hydrophilic Products. *Appl. Environ. Microbiol.* 76, 3462–3466. doi:10.1128/aem.00202-10

Noda, S., Mori, Y., Oyama, S., Kondo, A., Araki, M., and Shirai, T. (2019). Reconstruction of Metabolic Pathway for Isobutanol Production in *Escherichia coli*. *Microb. Cel. Fact* 18, 124. doi:10.1186/s12934-019-1171-4

Okahashi, N., Matsuda, F., Yoshikawa, K., Shirai, T., Matsumoto, Y., Wada, M., et al. (2017). Metabolic Engineering of Isopropyl Alcohol Producing *E. coli* strains with ^{13}C-Metabolic Flux Analysis. *Biotechnol. Bioeng.* 114, 2782–2793. doi:10.1002/bit.26390

Ort, D. R., Merchant, S. S., Alric, J., Barkan, A., Blankenship, R. E., Bock, R., et al. (2015). Redesigning Photosynthesis to Sustainably Meet Global Food and Bioenergy Demand. *Proc. Natl. Acad. Sci. U.S.A.* 112, 8529–8536. doi:10.1073/pnas.1424031112

Ouyang, P., Wang, H., Hajnal, I., Wu, Q., Guo, Y., and Chen, G.-Q. (2018). Increasing Oxygen Availability for Improving Poly(3-Hydroxybutyrate) Production by *Halomonas*. *Metab. Eng.* 45, 20–31. doi:10.1016/j.ymben.2017.11.006

Panke, S., and Wubbolts, M. (2005). Advances in Biocatalytic Synthesis of Pharmaceutical Intermediates. *Curr. Opin. Chem. Biol.* 9, 188–194. doi:10.1016/j.cbpa.2005.02.007

Park, J. B. (2007). Oxygenase-Based Whole-Cell Biocatalysis in Organic Synthesis. *J. Microbiol. Biotechnol.* 17, 379–392.

Park, J., and Choi, Y. (2017). Cofactor Engineering in Cyanobacteria to Overcome Imbalance between NADPH and NADH: A Mini Review. *Front. Chem. Sci. Eng.* 11, 66–71. doi:10.1007/s11705-016-1591-1

Park, J. O., Liu, N., Holinski, K. M., Emerson, D. F., Qiao, K., Woolston, B. M., et al. (2019). Synergistic Substrate Cofeeding Stimulates Reductive Metabolism. *Nat. Metab.* 1, 643–651. doi:10.1038/s42255-019-0077-0

Pedersen, A., Karlsson, G. B., and Rydström, J. (2008). Proton-Translocating Transhydrogenase: An Update of Unsolved and Controversial Issues. *J. Bioenerg. Biomembr.* 40, 463–473. doi:10.1007/s10863-008-9170-x

Pedersen, A. T., Rehn, G., and Woodley, J. M. (2015). "Oxygen Transfer Rates and Requirements in Oxidative Biocatalysis," in *Comput Aided Chem Eng*. Editors K. V. Gernaey, J. K. Huusom, and R. Gani (Elsevier), 37, 2111–2116. doi:10.1016/b978-0-444-63576-1.50046-7

Perez-Zabaleta, M., Sjöberg, G., Guevara-Martínez, M., Jarmander, J., Gustavsson, M., Quillaguamán, J., et al. (2016). Increasing the Production of (R)-3-Hydroxybutyrate in Recombinant *Escherichia coli* by Improved Cofactor Supply. *Microb. Cel. Fact.* 15, 91. doi:10.1186/s12934-016-0490-y

Petschacher, B., and Nidetzky, B. (2008). Altering the Coenzyme Preference of Xylose Reductase to Favor Utilization of NADH Enhances Ethanol Yield from Xylose in a Metabolically Engineered Strain of *Saccharomyces cerevisiae*. *Microb. Cel. Factories* 7, 9. doi:10.1186/1475-2859-7-9

Polakovič, M., Švitel, J., Bučko, M., Filip, J., Neděla, V., Ansorge-Schumacher, M. B., et al. (2017). Progress in Biocatalysis with Immobilized Viable Whole Cells: Systems Development, Reaction Engineering and Applications. *Biotechnol. Lett.* 39, 667–683. doi:10.1007/s10529-017-2300-y

Pongtharangkul, T., Chuekitkumchorn, P., Suwanampa, N., Payongsri, P., Honda, K., and Panbangred, W. (2015). Kinetic Properties and Stability of Glucose Dehydrogenase from *Bacillus amyloliquefaciens* SB5 and its Potential for Cofactor Regeneration. *AMB Expr.* 5 (1), 68. doi:10.1186/s13568-015-0157-9

Poulsen, B. R., Nohr, J., Douthwaite, S., Hansen, L. V., Iversen, J. J. L., Visser, J., et al. (2005). Increased NADPH Concentration Obtained by Metabolic Engineering of the Pentose Phosphate Pathway in *Aspergillus niger*. *FEBS J.* 272, 1313–1325. doi:10.1111/j.1742-4658.2005.04554.x

Purdy, H. M., Pfleger, B. F., and Reed, J. L. (2022). Introduction of NADH-Dependent Nitrate Assimilation in *Synechococcus* sp. PCC 7002 Improves Photosynthetic Production of 2-Methyl-1-Butanol and Isobutanol. *Metab. Eng.* 69, 87–97. doi:10.1016/j.ymben.2021.11.003

Qiao, K., Wasylenko, T. M., Zhou, K., Xu, P., and Stephanopoulos, G. (2017). Lipid Production in *Yarrowia lipolytica* Is Maximized by Engineering Cytosolic Redox Metabolism. *Nat. Biotechnol.* 35, 173–177. doi:10.1038/nbt.3763

Rahman, M. M., Qin, Z. Q., Dou, W. F., Rao, Z. M., and Xu, Z. H. (2012). Over-Expression of NAD Kinase in *Corynebacterium crenatum* and its Impact on L-Arginine Biosynthesis. *Trop. J. Pharm. Res.* 11, 909–916. doi:10.4314/tjpr.v11i6.6

Ratledge, C. (2014). The Role of Malic Enzyme as the Provider of NADPH in Oleaginous Microorganisms: A Reappraisal and Unsolved Problems. *Biotechnol. Lett.* 36, 1557–1568. doi:10.1007/s10529-014-1532-3

Roussou, S., Albergati, A., Liang, F., and Lindblad, P. (2021). Engineered Cyanobacteria with Additional Overexpression of Selected Calvin-Benson-Bassham Enzymes Show Further Increased Ethanol Production. *Metab. Eng. Commun.* 12, e00161. doi:10.1016/j.mec.2021.e00161

Runguphan, W., and Keasling, J. D. (2014). Metabolic Engineering of *Saccharomyces cerevisiae* for Production of Fatty Acid-Derived Biofuels and Chemicals. *Metab. Eng.* 21, 103–113. doi:10.1016/j.ymben.2013.07.003

Saha, R., Liu, D., Hoynes-O'Connor, A., Liberton, M., Yu, J., Bhattacharyya-Pakrasi, M., et al. (2016). Diurnal Regulation of Cellular Processes in the Cyanobacterium *Synechocystis* sp. Strain PCC 6803: Insights from Transcriptomic, Fluxomic, and Physiological Analyses. *mBio* 7, e00464–16. doi:10.1128/mBio.00464-16

Sanchez, A. M., Andrews, J., Hussein, I., Bennett, G. N., and San, K.-Y. (2006). Effect of Overexpression of a Soluble Pyridine Nucleotide Transhydrogenase (UdhA) on the Production of Poly(3-Hydroxybutyrate) in *Escherichia coli*. *Biotechnol. Prog.* 22, 420–425. doi:10.1021/bp050375u

Santos-Merino, M., Torrado, A., Davis, G. A., Rottig, A., Bibby, T. S., Kramer, D. M., et al. (2021). Improved Photosynthetic Capacity and Photosystem I Oxidation via Heterologous Metabolism Engineering in Cyanobacteria. *Proc. Natl. Acad. Sci. U S A.* 118, 171–209. doi:10.1073/pnas.2021523118

Sauer, U., Canonaco, F., Heri, S., Perrenoud, A., and Fischer, E. (2004). The Soluble and Membrane-Bound Transhydrogenases UdhA and PntAB Have Divergent Functions in NADPH Metabolism of *Escherichia coli*. *J. Biol. Chem.* 279, 6613–6619. doi:10.1074/jbc.m311657200

Sauer, U., and Eikmanns, B. J. (2005). The PEP-Pyruvate-Oxaloacetate Node as the Switch point for Carbon Flux Distribution in Bacteria. *FEMS Microbiol. Rev.* 29, 765–794. doi:10.1016/j.femsre.2004.11.002

Schewe, H., Kaup, B.-A., and Schrader, J. (2008). Improvement of P450BM-3 Whole-Cell Biocatalysis by Integrating Heterologous Cofactor Regeneration Combining Glucose Facilitator and Dehydrogenase in *E. coli*. *Appl. Microbiol. Biotechnol.* 78, 55–65. doi:10.1007/s00253-007-1277-1

Schipper, K., Al-Jabri, H. M. S. J., Wijffels, R. H., and Barbosa, M. J. (2021). Techno-Economics of Algae Production in the Arabian Peninsula. *Bioresour. Technology* 331, 125043. doi:10.1016/j.biortech.2021.125043

Schrewe, M., Julsing, M. K., Bühler, B., and Schmid, A. (2013). Whole-Cell Biocatalysis for Selective and Productive C-O Functional Group Introduction and Modification. *Chem. Soc. Rev.* 42, 6346–6377. doi:10.1039/c3cs60011d

Schroer, K., Zelic, B., Oldiges, M., and Lütz, S. (2009). Metabolomics for Biotransformations: Intracellular Redox Cofactor Analysis and Enzyme Kinetics Offer Insight into Whole Cell Processes. *Biotechnol. Bioeng.* 104, 251–260. doi:10.1002/bit.22390

Schuurmans, R. M., van Alphen, P., Schuurmans, J. M., Matthijs, H. C. P., and Hellingwerf, K. J. (2015). Comparison of the Photosynthetic Yield of Cyanobacteria and Green Algae: Different Methods Give Different Answers. *PLoS One* 10, e0139061. doi:10.1371/journal.pone.0139061

Scrutton, N. S., Berry, A., and Perham, R. N. (1990). Redesign of the Coenzyme Specificity of a Dehydrogenase by Protein Engineering. *Nature* 343, 38–43. doi:10.1038/343038a0

Sengupta, A., Sunder, A. V., Sohoni, S. V., and Wangikar, P. P. (2019). The Effect of CO_2 in Enhancing Photosynthetic Cofactor Recycling for Alcohol Dehydrogenase Mediated Chiral Synthesis in Cyanobacteria. *J. Biotechnol.* 289, 1–6. doi:10.1016/j.jbiotec.2018.11.002

Shi, A., Zhu, X., Lu, J., Zhang, X., and Ma, Y. (2013). Activating Transhydrogenase and NAD Kinase in Combination for Improving Isobutanol Production. *Metab. Eng.* 16, 1–10. doi:10.1016/j.ymben.2012.11.008

Shi, F., Huan, X., Wang, X., and Ning, J. (2012). Overexpression of NAD Kinases Improves the L-Isoleucine Biosynthesis in *Corynebacterium glutamicum* sp. *lactofermentum*. *Enzyme Microb. Technol.* 51, 73–80. doi:10.1016/j.enzmictec.2012.04.003

Shibasaki, T., Mori, H., and Ozaki, A. (2000). Enzymatic Production of Trans-4-Hydroxy-L-Proline by Regio- and Stereospecific Hydroxylation of L-Proline. *Biosci. Biotechnol. Biochem.* 64, 746–750. doi:10.1271/bbb.64.746

Siedler, S., Bringer, S., Blank, L. M., and Bott, M. (2012). Engineering Yield and Rate of Reductive Biotransformation in *Escherichia coli* by Partial Cyclization of the Pentose Phosphate Pathway and PTS-Independent Glucose Transport. *Appl. Microbiol. Biotechnol.* 93, 1459–1467. doi:10.1007/s00253-011-3626-3

Siedler, S., Bringer, S., and Bott, M. (2011). Increased NADPH Availability in *Escherichia coli:* Improvement of the Product Per Glucose Ratio in Reductive Whole-Cell Biotransformation. *Appl. Microbiol. Biotechnol.* 92, 929–937. doi:10.1007/s00253-011-3374-4

Siedler, S., Lindner, S. N., Bringer, S., Wendisch, V. F., and Bott, M. (2013). Reductive Whole-Cell Biotransformation with *Corynebacterium glutamicum*: Improvement of NADPH Generation from Glucose by a Cyclized Pentose Phosphate Pathway Using *pfkA* and *gapA* Deletion Mutants. *Appl. Microbiol. Biotechnol.* 97, 143–152. doi:10.1007/s00253-012-4314-7

Smirnov, S. V., Kodera, T., Samsonova, N. N., Kotlyarova, V. A., Rushkevich, N. Y., Kivero, A. D., et al. (2010). Metabolic Engineering of *Escherichia coli* to Produce (2S, 3R, 4S)-4-Hydroxyisoleucine. *Appl. Microbiol. Biotechnol.* 88, 719–726. doi:10.1007/s00253-010-2772-3

Socher, M. L., Löser, C., Schott, C., Bley, T., and Steingroewer, J. (2016). The Challenge of Scaling up Photobioreactors: Modeling and Approaches in Small Scale. *Eng. Life Sci.* 16, 598–609. doi:10.1002/elsc.201500134

Srivastava, V., Amanna, R., Rowden, S. J. L., Sengupta, S., Madhu, S., Howe, C. J., et al. (2021). Adaptive Laboratory Evolution of the Fast-Growing Cyanobacterium *Synechococcus elongatus* PCC 11801 for Improved Solvent Tolerance. *J. Biosci. Bioeng.* 131, 491–500. doi:10.1016/j.jbiosc.2020.11.012

Stephens, S., Mahadevan, R., and Allen, D. G. (2021). Engineering Photosynthetic Bioprocesses for Sustainable Chemical Production: A Review. *Front. Bioeng. Biotechnol.* 8, 610723. doi:10.3389/fbioe.2020.610723

Sudarsan, S., Dethlefsen, S., Blank, L. M., Siemann-Herzberg, M., and Schmid, A. (2014). The Functional Structure of Central Carbon Metabolism in *Pseudomonas putida* KT2440. *Appl. Environ. Microbiol.* 80, 5292–5303. doi:10.1128/aem.01643-14

Tanvir, R. U., Zhang, J., Canter, T., Chen, D., Lu, J., and Hu, Z. (2021). Harnessing Solar Energy Using Phototrophic Microorganisms: A Sustainable Pathway to Bioenergy, Biomaterials, and Environmental Solutions. *Renew. Sustainable Energ. Rev.* 146, 111181. doi:10.1016/j.rser.2021.111181

Theodosiou, E., Breisch, M., Julsing, M. K., Falcioni, F., Bühler, B., and Schmid, A. (2017). An Artificial TCA Cycle Selects for Efficient α-Ketoglutarate Dependent Hydroxylase Catalysis in Engineered *Escherichia coli*. *Biotechnol. Bioeng.* 114, 1511–1520. doi:10.1002/bit.26281

Theodosiou, E., Frick, O., Bühler, B., and Schmid, A. (2015). Metabolic Network Capacity of *Escherichia coli* for Krebs Cycle-Dependent Proline Hydroxylation. *Microb. Cel. Fact.* 14, 108. doi:10.1186/s12934-015-0298-1

Theune, M. L., Hildebrandt, S., Steffen-Heins, A., Bilger, W., Gutekunst, K., and Appel, J. (2020). *In-vivo* Quantification of Electron Flow through Photosystem I - Cyclic Electron Transport Makes up about 35% in a Cyanobacterium. *BBA Bioenerg.* 1862, 148353. doi:10.1016/j.bbabio.2020.148353

Thiel, K., Patrikainen, P., Nagy, C., Fitzpatrick, D., Pope, N., Aro, E.-M., et al. (2019). Redirecting Photosynthetic Electron Flux in the Cyanobacterium *Synechocystis* sp. PCC 6803 by the Deletion of Flavodiiron Protein Flv3. *Microb. Cel. Fact.* 18, 189. doi:10.1186/s12934-019-1238-2

Till, P., Toepel, J., Bühler, B., Mach, R. L., and Mach-Aigner, A. R. (2020). Regulatory Systems for Gene Expression Control in Cyanobacteria. *Appl. Microbiol. Biotechnol.* 104, 1977–1991. doi:10.1007/s00253-019-10344-w

Toya, Y., Ishii, N., Nakahigashi, K., Hirasawa, T., Soga, T., Tomita, M., et al. (2010). 13C-Metabolic Flux Analysis for Batch Culture of *Escherichia coli* and its Pyk and Pgi Gene Knockout Mutants Based on Mass Isotopomer Distribution of Intracellular Metabolites. *Biotechnol. Prog.* 26, 975–992. doi:10.1002/btpr.420

Tsuzuki, M., Okada, K., Isoda, H., Hirano, M., Odaka, T., Saijo, H., et al. (2019). Physiological Properties of Photoautotrophic Microalgae and Cyanobacteria Relevant to Industrial Biomass Production. *Mar. Biotechnol.* 21, 406–415. doi:10.1007/s10126-019-09890-1

Tüllinghoff, A., Uhl, M. B., Nintzel, F. E., Schmid, A., Bühler, B., and Toepel, J. (2022). Maximizing Photosynthesis-Driven Baeyer-Villiger Oxidation Efficiency in Recombinant *Synechocystis* sp. PCC 6803. *Front. Catal.* 1. doi:10.3389/fctls.2021.780474

Ullmann, J., and Grimm, D. (2021). Algae and Their Potential for a Future Bioeconomy, Landless Food Production, and the Socio-Economic Impact of an Algae Industry. *Org. Agr.* 11, 261–267. doi:10.1007/s13165-020-00337-9

Ungerer, J., Lin, P. C., Chen, H. Y., and Pakrasi, H. B. (2018). Adjustments to Photosystem Stoichiometry and Electron Transfer Proteins Are Key to the Remarkably Fast Growth of the Cyanobacterium *Synechococcus elongatus* UTEX 2973. *mBio* 9 (1), e02327. doi:10.1128/mBio.02327-17

van den Berg, C., Eppink, M. H. M., and Wijffels, R. H. (2019). Integrated Product Recovery Will Boost Industrial Cyanobacterial Processes. *Trends Biotechnol.* 37, 454–463. doi:10.1016/j.tibtech.2018.11.006

Varman, A. M., Yu, Y., You, L., and Tang, Y. J. (2013). Photoautotrophic Production of D-Lactic Acid in an Engineered Cyanobacterium. *Microb. Cel. Fact.* 12, 117. doi:10.1186/1475-2859-12-117

Vavitsas, K., Kugler, A., Satta, A., Hatzinikolaou, D. G., Lindblad, P., Fewer, D. P., et al. (2021). Doing Synthetic Biology with Photosynthetic Microorganisms. *Physiologia Plantarum* 173, 624–638. doi:10.1111/ppl.13455

Veaudor, T., Blanc-Garin, V., Chenebault, C., Diaz-Santos, E., Sassi, J.-F., Cassier-Chauvat, C., et al. (2020). Recent Advances in the Photoautotrophic Metabolism of Cyanobacteria: Biotechnological Implications. *Life* 10, 71. doi:10.3390/life10050071

Verho, R., Londesborough, J., Penttilä, M., and Richard, P. (2003). Engineering Redox Cofactor Regeneration for Improved Pentose Fermentation in *Saccharomyces cerevisiae*. *Appl. Environ. Microbiol.* 69, 5892–5897. doi:10.1128/aem.69.10.5892-5897.2003

Volmer, J., Lindmeyer, M., Seipp, J., Schmid, A., and Bühler, B. (2019). Constitutively Solvent-Tolerant *Pseudomonas taiwanensis* VLB Supports Particularly High-Styrene Epoxidation Activities when Grown Under Glucose Excess Conditions. *Biotechnol. Bioeng.* 116, 1089–1101. doi:10.1002/bit.26924

Volmer, J., Neumann, C., Bühler, B., and Schmid, A. (2014). Engineering of *Pseudomonas taiwanensis* VLB120 for Constitutive Solvent Tolerance and Increased Specific Styrene Epoxidation Activity. *Appl. Environ. Microbiol.* 80, 6539–6548. doi:10.1128/aem.01940-14

Volmer, J., Schmid, A., and Bühler, B. (2015). Guiding Bioprocess Design by Microbial Ecology. *Curr. Opin. Microbiol.* 25, 25–32. doi:10.1016/j.mib.2015.02.002

Wagner, H., Jakob, T., and Wilhelm, C. (2006). Balancing the Energy Flow from Captured Light to Biomass under Fluctuating Light Conditions. *New Phytol.* 169, 95–108. doi:10.1111/j.1469-8137.2005.01550.x

Wang, M., Chen, B., Fang, Y., and Tan, T. (2017). Cofactor Engineering for More Efficient Production of Chemicals and Biofuels. *Biotechnol. Adv.* 35, 1032–1039. doi:10.1016/j.biotechadv.2017.09.008

Wang, Y., Li, L., Ma, C., Gao, C., Tao, F., and Xu, P. (2013). Engineering of Cofactor Regeneration Enhances (2S,3S)-2,3-Butanediol Production from Diacetyl. *Sci. Rep.* 3, 2643. doi:10.1038/srep02643

Wang, Y., Sun, T., Gao, X., Shi, M., Wu, L., Chen, L., et al. (2016). Biosynthesis of Platform Chemical 3-Hydroxypropionic Acid (3-HP) Directly from CO_2 in Cyanobacterium *Synechocystis* sp. PCC 6803. *Metab. Eng.* 34, 60–70. doi:10.1016/j.ymben.2015.10.008

Wasylenko, T. M., Ahn, W. S., and Stephanopoulos, G. (2015). The Oxidative Pentose Phosphate Pathway Is the Primary Source of NADPH for Lipid Overproduction from Glucose in *Yarrowia lipolytica*. *Metab. Eng.* 30, 27–39. doi:10.1016/j.ymben.2015.02.007

Weiss, T. L., Young, E. J., and Ducat, D. C. (2017). A Synthetic, Light-Driven Consortium of Cyanobacteria and Heterotrophic Bacteria Enables Stable

Polyhydroxybutyrate Production. *Metab. Eng.* 44, 236–245. doi:10.1016/j.ymben.2017.10.009

Wilhelm, C., and Wagner, H. (2021). "6 Rate-Limiting Steps in Algal Energy Conversion from Sunlight to Products – the Role of Photosynthesis, P 149-174," in *Photosynthesis: Biotechnological Applications with Microalgae*. Editor R. Matthias (Berlin: De Gruyter).

Wlodarczyk, A., Gnanasekaran, T., Nielsen, A. Z., Zulu, N. N., Mellor, S. B., Luckner, M., et al. (2015). Metabolic Engineering of Light-Driven Cytochrome P450 Dependent Pathways into *Synechocystis* sp. PCC 6803. *Metab. Eng.* 33, 1–11. doi:10.1016/j.ymben.2015.10.009

Włodarczyk, A., Selão, T. T., Norling, B., and Nixon, P. J. (2020). Newly Discovered *Synechococcus* sp. PCC 11901 Is a Robust Cyanobacterial Strain for High Biomass Production. *Commun. Biol.* 3, 215. doi:10.1038/s42003-020-0910-8

Woo, J.-M., Jeon, E.-Y., Seo, E.-J., Seo, J.-H., Lee, D.-Y., Yeon, Y. J., et al. (2018). Improving Catalytic Activity of the Baeyer-Villiger Monooxygenase-Based *Escherichia coli* Biocatalysts for the Overproduction of (Z)-11-(heptanoyloxy)undec-9-Enoic Acid from Ricinoleic Acid. *Sci. Rep.* 8, 10280. doi:10.1038/s41598-018-28575-8

Xiao, Z., Lv, C., Gao, C., Qin, J., Ma, C., Liu, Z., et al. (2010). A Novel Whole-Cell Biocatalyst with NAD^+ Regeneration for Production of Chiral Chemicals. *Plos One* 5 (1), e8860. doi:10.1371/journal.pone.0008860

Xiong, W., Brune, D., and Vermaas, W. F. J. (2014). The γ-Aminobutyric Acid Shunt Contributes to Closing the Tricarboxylic Acid Cycle in *Synechocystis* sp. PCC 6803. *Mol. Microbiol.* 93, 786–796. doi:10.1111/mmi.12699

Xu, W., Yao, J., Liu, L., Ma, X., Li, W., Sun, X., et al. (2019). Improving Squalene Production by Enhancing the NADPH/NADP+ Ratio, Modifying the Isoprenoid-Feeding Module and Blocking the Menaquinone Pathway in *Escherichia coli*. *Biotechnol. Biofuels* 12, 68. doi:10.1186/s13068-019-1415-x

Yamauchi, Y., Hirasawa, T., Nishii, M., Furusawa, C., and Shimizu, H. (2014). Enhanced Acetic Acid and Succinic Acid Production Under Microaerobic Conditions by *Corynebacterium glutamicum* Harboring *Escherichia coli* Transhydrogenase Gene pntAB. *J. Gen. Appl. Microbiol.* 60, 112–118. doi:10.2323/jgam.60.112

Yu, J., Liberton, M., Cliften, P. F., Head, R. D., Jacobs, J. M., Smith, R. D., et al. (2015). *Synechococcus elongatus* UTEX 2973, A Fast Growing Cyanobacterial Chassis for Biosynthesis Using Light and CO_2. *Sci. Rep.* 5, 8132. doi:10.1038/srep08132

Yu, Y., You, L., Liu, D., Hollinshead, W., Tang, Y., and Zhang, F. (2013). Development of *Synechocystis* sp. PCC 6803 as a Phototrophic Cell Factory. *Mar. Drugs* 11, 2894–2916. doi:10.3390/md11082894

Zavřel, T., Faizi, M., Loureiro, C., Poschmann, G., Stühler, K., Sinetova, M., et al. (2019). Quantitative Insights into the Cyanobacterial Cell Economy. *Elife* 8, e42508. doi:10.7554/eLife.42508

Zavrel, T., Sinetova, M. A., Buzova, D., Literakova, P., and Cerveny, J. (2015). Characterization of a Model Cyanobacterium *Synechocystis* sp. PCC 6803 Autotrophic Growth in a Flat-Panel Photobioreactor. *Eng. Life Sci.* 15, 122–132. doi:10.1002/elsc.201300165

Zhang, B., Wu, J., and Meng, F. (2021a). Adaptive Laboratory Evolution of Microalgae: A Review of the Regulation of Growth, Stress Resistance, Metabolic Processes, and Biodegradation of Pollutants. *Front. Microbiol.* 12, 737248. doi:10.3389/fmicb.2021.737248

Zhang, J., Gao, X., Hong, P.-H., Li, Z.-J., and Tan, T.-W. (2015). Enhanced Production of Poly-3-Hydroxybutyrate by *Escherichia coli* Over-Expressing Multiple Copies of NAD Kinase Integrated in the Host Genome. *Biotechnol. Lett.* 37, 1273–1278. doi:10.1007/s10529-015-1797-1

Zhang, J., Sonnenschein, N., Pihl, T. P. B., Pedersen, K. R., Jensen, M. K., and Keasling, J. D. (2016a). Engineering an NADPH/$NADP^+$ Redox Biosensor in Yeast. *ACS Synth. Biol.* 5, 1546–1556. doi:10.1021/acssynbio.6b00135

Zhang, S., Qian, X., Chang, S., Dismukes, G. C., and Bryant, D. A. (2016b). Natural and Synthetic Variants of the Tricarboxylic Acid Cycle in Cyanobacteria: Introduction of the GABA Shunt into *Synechococcus* sp. PCC 7002. *Front. Microbiol.* 7, 1972. doi:10.3389/fmicb.2016.01972

Zhang, Y., Adams, I. P., and Ratledge, C. (2007). Malic Enzyme: The Controlling Activity for Lipid Production? Overexpression of Malic Enzyme in *Mucor circinelloides* Leads to a 2.5-Fold Increase in Lipid Accumulation. *Microbiology* 153, 2013–2025. doi:10.1099/mic.0.2006/002683-0

Zhang, Y., Lin, Z., Liu, Q., Li, Y., Wang, Z., Ma, H., et al. (2014). Engineering of Serine-Deamination Pathway, Entner-Doudoroff Pathway and Pyruvate Dehydrogenase Complex to Improve Poly(3-Hydroxybutyrate) Production in *Escherichia coli*. *Microb. Cel. Fact.* 13, 172. doi:10.1186/s12934-014-0172-6

Zhang, Z., Liu, P., Su, W., Zhang, H., Xu, W., and Chu, X. (2021b). Metabolic Engineering Strategy for Synthetizing *Trans*-4-Hydroxy-L-Proline in Microorganisms. *Microb. Cel. Fact.* 20, 87. doi:10.1186/s12934-021-01579-2

Zhao, H., and van der Donk, W. A. (2003). Regeneration of Cofactors for Use in Biocatalysis. *Curr. Opin. Biotechnol.* 14, 583–589. doi:10.1016/j.copbio.2003.09.007

Zheng, L., Zhang, X., Bai, Y., and Fan, J. (2018). Using Algae Cells to Drive Cofactor Regeneration and Asymmetric Reduction for the Synthesis of Chiral Chemicals. *Algal Res.* 35, 432–438. doi:10.1016/j.algal.2018.09.019

Zhou, J., Yang, F., Zhang, F., Meng, H., Zhang, Y., and Li, Y. (2021). Impairing Photorespiration Increases Photosynthetic Conversion of CO_2 to Isoprene in Engineered Cyanobacteria. *Bioresour. Bioproc.* 8, 42. doi:10.1186/s40643-021-00398-y

Zu, Y., Prather, K. L., and Stephanopoulos, G. (2020). Metabolic Engineering Strategies to Overcome Precursor Limitations in Isoprenoid Biosynthesis. *Curr. Opin. Biotechnol.* 66, 171–178. doi:10.1016/j.copbio.2020.07.005

Conflict of Interest: The authors declare that the research was conducted in the absence of any commercial or financial relationships that could be construed as a potential conflict of interest.

Publisher's Note: All claims expressed in this article are solely those of the authors and do not necessarily represent those of their affiliated organizations, or those of the publisher, the editors and the reviewers. Any product that may be evaluated in this article, or claim that may be made by its manufacturer, is not guaranteed or endorsed by the publisher.

frontiers | Frontiers in Bioengineering and Biotechnology

TYPE Mini Review
PUBLISHED 22 July 2022
DOI 10.3389/fbioe.2022.944226

OPEN ACCESS

EDITED BY
Jennifer Ann Littlechild,
University of Exeter, United Kingdom

REVIEWED BY
Robson Carlos Alnoch,
University of São Paulo, Brazil

*CORRESPONDENCE
Selin Kara,
selin.kara@bce.au.dk

SPECIALTY SECTION
This article was submitted to Bioprocess Engineering,
a section of the journal
Frontiers in Bioengineering and Biotechnology

RECEIVED 14 May 2022
ACCEPTED 30 June 2022
PUBLISHED 22 July 2022

CITATION
Ma Y, Zhang N, Vernet G and Kara S (2022), Design of fusion enzymes for biocatalytic applications in aqueous and non-aqueous media.
Front. Bioeng. Biotechnol. 10:944226.
doi: 10.3389/fbioe.2022.944226

Design of fusion enzymes for biocatalytic applications in aqueous and non-aqueous media

Yu Ma[1], Ningning Zhang[2], Guillem Vernet[2] and Selin Kara[1,2]*

[1]Biocatalysis and Bioprocessing Group, Department of Biological and Chemical Engineering, Aarhus University, Aarhus, Denmark, [2]Institute of Technical Chemistry, Leibniz University Hannover, Hannover, Germany

Biocatalytic cascades play a fundamental role in sustainable chemical synthesis. Fusion enzymes are one of the powerful toolboxes to enable the tailored combination of multiple enzymes for efficient cooperative cascades. Especially, this approach offers a substantial potential for the practical application of cofactor-dependent oxidoreductases by forming cofactor self-sufficient cascades. Adequate cofactor recycling while keeping the oxidized/reduced cofactor in a confined microenvironment benefits from the fusion fashion and makes the use of oxidoreductases in harsh non-aqueous media practical. In this mini-review, we have summarized the application of various fusion enzymes in aqueous and non-aqueous media with a focus on the discussion of linker design within oxidoreductases. The design and properties of the reported linkers have been reviewed in detail. Besides, the substrate loadings in these studies have been listed to showcase one of the key limitations (low solubility of hydrophobic substrates) of aqueous biocatalysis when it comes to efficiency and economic feasibility. Therefore, a straightforward strategy of applying non-aqueous media has been briefly discussed while the potential of using the fusion oxidoreductase of interest in organic media was highlighted.

KEYWORDS

fusion enzymes, biocatalytic cascades, oxidoreductases, fusion linkers, aqueous and non-aqueous media

1 Introduction

Biocatalytic cascades have been widely explored to mimic natural biosynthetic routes to produce high value-added chemicals (Muschiol et al., 2015; France et al., 2017; Huffman et al., 2019; Walsh and Moore, 2019; Zhou et al., 2021; Benítez-Mateos et al., 2022). In this context, the spatial organization of multi-enzymes plays a pivotal role in surmounting barriers between different enzyme classes, averting the mutual inhibition, limiting the long-range diffusion of intermediates, and enhancing the reaction efficiency (Quin et al., 2017). Up to now, a variety of enzyme co-localization strategies have been developed including 1) enzyme fusion (Elleuche, 2015; Aalbers and Fraaije,

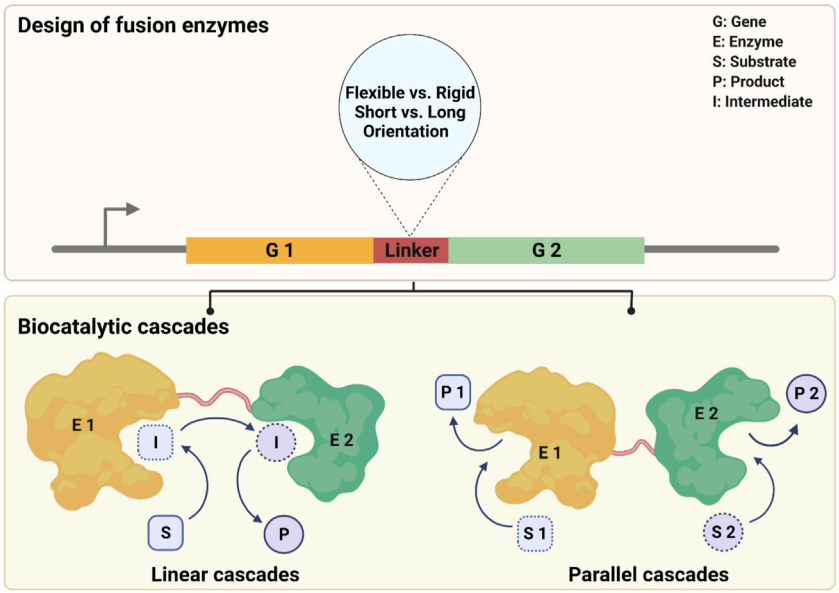

SCHEME 1
Design of fusion enzymes for two biocatalytic cascade processes.

2019), 2) co-immobilization (attachment on a carrier or encapsulation in a matrix) (Ren et al., 2019; Xu et al., 2020), and 3) scaffolding (Kuchler et al., 2016; Ellis et al., 2019). In particular, the direct fusion of enzymes has emerged as a fascinating toolbox in its own right (Quin et al., 2017; Rabe et al., 2017; Aalbers and Fraaije, 2019). It brings multiple enzymes in close proximity to form a single multifunctional catalyst through genetic fusion (Aalbers and Fraaije, 2017) or covalent bonds between proteins formed post-transcriptionally (Keeble and Howarth, 2020). By enzyme fusion, the sequential channeling of substrates between enzyme active sites can be easily achieved with a high degree of controllability (Huang et al., 2001; Wilding et al., 2018). Consequently, the delicately tethered enzymes gain many benefits, such as improved stability and catalytic efficiency, as well as enhanced expression and ease of production as a single construct.

Fusion approaches have been well-illustrated with many types of cofactor-dependent enzymes including the combination of cytochrome P450 with their redox partners (Munro et al., 2007; Bakkes et al., 2017; Kokkonen et al., 2019; Belsare et al., 2020; Kokorin et al., 2021; Kokorin and Urlacher, 2022), and Baeyer-Villiger monooxygenases (BVMOs) with alcohol dehydrogenases and transaminases (Torres Pazmiño et al., 2008; Peters et al., 2017; Aalbers and Fraaije, 2019) (Scheme 1). These studies have largely demonstrated the practicability and effectiveness of the fusion approach. However, there are still some limitations to overcome in order to make it practicable. The trial-and-error in the design of linkers and time-consuming molecular experiments can lead to a huge workload. Furthermore, most of these proofs of concept were explored at low substrate loadings usually in μM ranges, which lags far behind practical applications at a technical scale.

Some enzymes are of high interest for their use in cascades for the biocatalytic production of valuable chemicals. In particular, cyclohexanone monooxygenase (CHMO) has been extensively investigated for the synthesis of ε-caprolactone, an important precursor for polymer synthesis (Schmidt et al., 2015; Scherkus et al., 2016; Engel et al., 2019a). Generally, most cascades have been developed by coupling various alcohol dehydrogenases (ADHs) (Bornadel et al., 2015; Schmidt et al., 2015; Scherkus et al., 2016; Scherkus et al., 2017; Engel et al., 2019b; de Gonzalo and Alcántara, 2021) as well as newly reported thioredoxin/thioredoxin reductases pairs (Zhang et al., 2022) with CHMO to form redox-neutral self-sufficient systems. Despite these advances, in most one-pot systems, substrate concentrations have been used up to 100 mM given the strong substrate and product inhibition. By harnessing the fusion approach not only the inhibition caused by substrates and intermediates could be relieved but also the transport distance of cofactors between active sites can be shortened to avoid the degradation of nicotinamide cofactors in non-aqueous media (Huang et al., 2019). This has inspired the design and generation of various fusions of CHMO with its cofactor regenerating enzymes as effective catalysts for cascades, demonstrating the practicality of fusions for this type of enzyme (Aalbers and Fraaije, 2017).

TABLE 1 List of fused and non-fused oxidoreductases, and their biocatalytic applications with varying substrate concentrations in various aqueous and non-aqueous media.

Entry	Enzyme pairs	Fusion name	Linker	Application of enzyme pairs	Substrate concentration (mM)	Reaction media	Organic solvent (vol%)	References
1	ADH, BVMO	CHMO-ADHA	L1: (13) SSGGSGGSGGSAG	cascade reaction, cyclic alcohol to lactone	0.25, 10	water	0	Aalbers and Fraaije, (2017)
		CHMO-ADHM						
		ADH-CHMO						
2	ADH, BVMO	FDH-CHMO	L1: (6) SGSAAG L2: (6) SRSAAG	NADPH-recycling system	5	water, MTBE, DES (choline chloride and glycerol)	0, 10, 40, 20	Mourelle-Insua et al. (2019)
		GDH-CHMO						
		PTDH-CHMO						
		FDH-ADH						
		GDH-ADH						
		PTDH-ADH						
3	ADH, BVMO	ADH-Gly-BVMO	L1: (12) SGGSGGSGGSAG L2: (30) SASNCLIGLFLNDQELKKKAKVYDKIAKDV L3: none	cascade reaction, alcohol to ester	0.2	water	0	Jeon et al. (2015)
		ADH-FOM-BVMO						
		ADH-BVMO						
4	Ene reductase, BVMO	XenB-CHMO	L1: (13) SSGGSGGSGGSAG L2: (12) SSATGSATGSAG L3: (1) W	cascade reaction, unsaturated cyclic alcohols to chiral lactones	3	water	0	Peters et al. (2017)
5	PTDH, P450	BF2	L1: (6) SGGGGS L2: (6) EPPPPK L3: (24) (SGGGGS) × 4	NADPH-recycling system	0.2	water	0	Kokorin et al. (2021)
		F2B						
		F2B-P1						
		F2B-G1						
		F2B-G4						
6	PTDH, P450	pCRE2-P450-BM3	L1: (6) SRSAAG	NADPH-recycling system	0.1	water	0	Beyer et al. (2018)
7	Styrene monooxygenase (StyA), Flavin reductase (StyB)	Fus-SMO	L1: (30) ASGGGGSGGGGSGGGGSGGGGSGGGGSGAS L2: (20) (GGGGS) × 4	electron transfer for epoxidation of styrene	0.5	water	0	Corrado et al. (2018)
8	P450, Alcohol oxidase	OleTJE-AldO	L1: (18) GSGLEVLFQGPGSGGGGS L2: (45) A (EAAAK) × 4-LEA-(EAAAK) × 4A	hydrogen peroxide supply for decarboxylation reaction	0.5–10	water	0	Matthews et al. (2017)

(Continued on following page)

10.3389/fbioe.2022.944226

TABLE 1 (*Continued*) List of fused and non-fused oxidoreductases, and their biocatalytic applications with varying substrate concentrations in various aqueous and non-aqueous media.

Entry	Enzyme pairs	Fusion name	Linker	Application of enzyme pairs	Substrate concentration (mM)	Reaction media	Organic solvent (vol%)	References
9	Formate dehydrogenase	FDH-AzoRo	L1: (30) His Tag × 10	NAD^+ regeneration	0.025	water	0	Ngo et al. (2022)
10	ADH, aminotransferase	ADH-AT	L1: PAS linker: (20) ASPAAPAPASPAAPAPSAPA L2: (40) PAS × 2 L3: (60) PAS × 3	cascade reaction, alcohol to amine, stabilization through linker	300	water	0	Lerchner et al. (2016)
11	Formate dehydrogenase, Leucine dehydrogenase	FDH-LeuDH	L1: none L2: (5) EAAAK L3: (10) (EAAAK) × 2 L4: (15) (EAAAK) × 3 L5: (5) GGGGS L6: (10) (GGGGS) × 2 L7: (15) (GGGGS) × 3	L-tert leucine biotransformation	4.5	water	0	Zhang et al. (2017)
12	P450 BM3	BM3-ADH ADH-BM3	L1: none L2: (10) (GGGGS) × 2 L3: (9) A × 9 L4: (10) (EAAAK) × 2	NADPH-recycling system	0.2, 0.5, 10	water	0	Kokorin and Urlacher, (2022)
13	Flavin-dependent halogenase, flavin reductase	FH-FR	L1: (10) PSPSTDQSPS L2: (16) VLHRHQPVTIGEPAAR L3: (22) VLHRHQPVSPIHSRTIGEPAAR	electron transfer for halogenation	0.5	water	0	Andorfer et al. (2017)
14	CHMO, ADH, CAL-A	No fused	—	—	20, 100	water	0	Schmidt et al. (2015)
15	CHMO	No fused	—	—	3.4–11	water	0	Romero et al. (2016)
16	CHMO, ADH, CAL-B	No fused	—	—	1–25	water	0	Scherkus et al. (2016)
17	P450, ADH	No fused	—	—	2, 20	water	0	Tavanti et al. (2017)
18	PTDH, BVMO	PockeMO-PTDH CPDMO-PTDH CHMO-PTDH	L1: (6) SRSAAG	NADPH-recycling system	0.2–0.8	water, dioxane	10	Furst et al. (2017)
19	CHMO, ADH, CAL-B	No fused	—	—	20	water	0	Scherkus et al. (2017)
20	CHMO, ADH, CAL-B	No fused	—	—	40–100	water	0	Wedde et al. (2017)
21	CHMO, ADH	No fused	—	—	0, 100	water	0	Engel et al. (2019b)
22	CHMO, GDH	No fused	—	—	10, 140	water, methanol	10	Delgove et al. (2019)
23	CHMO, GDH	No fused	—	—	30, 240	water, methanol	1.25, 10	Solé et al. (2019)
24	FMO, ADH	FMO-ADH	L1: (6) SGSAAG	NADPH-recycling system	10–20	microaqueous	95	Huang et al. (2019)
25	PSMO, FDH	No fused	—	—	10	water, methanol	10	Zhu et al. (2022)
26	CHMO, FDH	No fused	—	—	5	water, methanol	10	Zhu et al. (2022)

CHMO, Cyclohexanone monooxygenase; ADH, Alcohol dehydrogenase; PTDH, Phosphite dehydrogenase; FDH, Formate dehydrogenase; GDH, Glucose dehydrogenase; PockeMO, Polycyclic ketone monooxygenase; CPDMO, Pseudomonad cyclopentadecanone monooxygenase; MTBE, Methyl tert-butyl ether; DES, Deep eutectic solvent.

10.3389/fbioe.2022.944226

Enzymes have naturally evolved to function optimally in aqueous media. Accordingly, most enzyme-catalyzed transformations take place in buffer systems to maintain enzymatic stability and activity. However, for industrial applications that mostly use hydrophobic non-natural substrates, this can be a key obstacle (Holtmann and Hollmann, 2022). In most studies, the concentrations of poorly water-soluble reagents are often adjusted to the millimolar range. The 'diluted' biocatalysis with low substrate loadings is both poorly economical and unsustainable (Hollmann et al., 2021). Using non-aqueous media with the presence of co-solvents can effectively enable high substrate loadings required by the industrial scale-up and commercialization (Dominguez de Maria and Hollmann, 2015; Illanes, 2016). Biocatalysis in non-aqueous media has seen a big rise since the pioneering work of Klibanov (1989) on enzyme catalysis in organic solvents (Zaks and Klibanov, 1988), which mainly focused on lipases with distinctive stability (Kumar et al., 2016). However, applying redox biocatalysis in non-aqueous media confronts several major concerns, e.g., enzyme stability and cofactor recycling (Kara et al., 2013; Huang et al., 2018; Vidal et al., 2018). A recent study proved the feasibility of using a fused type II flavin-containing monooxygenase (FMO-E) and horse liver alcohol dehydrogenase (HLADH) in organic media (Huang et al., 2019). Benefits can be promisingly envisioned by applying these fusions for cascades with high substrate loadings in non-aqueous media (Holtmann and Hollmann, 2022). Inspiringly, many enzymes of interest especially the above-mentioned CHMO can be optimized by a similar way for the cascades toward an industrial application.

Here we present recent advances in the design and application of fusion enzymes, which cover not only the traditional aqueous systems but also non-aqueous media (e.g., organic solvents, and deep eutectic solvents). In detail, the development and application of various fusion enzymes in an aqueous environment (Section 1) and some recent examples especially about oxidoreductases in non-aqueous media (Section 2) have been outlined. Meanwhile, the linker design regarding classification, flexibility and rigidity, length, and orientation is discussed in both sections. In particular, the potential of using fusion enzymes for redox cascades with high substrate loadings in pursuit of satisfactory space-time-yields is highlighted.

2 Fusion enzymes in aqueous media

Most fused enzymes are constructed by genetic fusion, which requires a linker peptide to connect target proteins. A linker peptide is a segment of the polypeptide, consisting of several or hundreds of amino acids in length (Arai, 2021). The presence of linkers allows for the separation of two enzymes and thus avoids mutual interference during the folding and catalytic processes. There are at least two factors to consider when designing an enzyme fusion: 1) which type of linker to use and 2) in which order proteins should be placed. In the first aspect, the composition and length of a linker are two determining factors of its physicochemical properties regarding flexibility vs. rigidity and hydrophilicity vs. hydrophobicity. This can highly affect the spatial distribution of fused subunits. According to the characteristics of linkers, they are generally classified into two types: 1) flexible linker peptides and 2) linker peptides that can form α-helices (Chen et al., 2013). As a simple summary, Table 1 lists the enzyme pairs in fused or non-fused forms and the used linkers of mainly oxidoreductases described in this mini-review. All examples are explained in more detail in the entries.

The composition is a determinant factor for the flexibility or rigidity of linkers. Flexible linkers are glycine-rich and can produce a disordered loop, which usually could improve protein solubility and provide flexibility for catalysis domain separation (Arai et al., 2001). The flexible linker peptide does not interfere with the folding domain of the protein, thus theoretically allowing for natural folding and other conformational movements (Reddy Chichili et al., 2013). This type of linker has been widely used in biocatalysis with relative success, such as cytochrome P450 fusions (Matthews et al., 2017; Beyer et al., 2018; Kokorin et al., 2021; Kokorin and Urlacher, 2022), flavin reductase (FR) fusions (Andorfer et al., 2017; Corrado et al., 2018), formate dehydrogenase (FDH) fusions (Zhang et al., 2017), and Baeyer-Villiger Monooxygenases (BVMOs) fusions (entries 1–13, Table 1). In detail, Fraaije and coworkers reported a fusion of an ADH from *Thermoanaerobacter brockii* (*Tb*ADH) and a CHMO from *Thermocrispum municipal* (*Tm*CHMO) with a glycine-rich linker, which was used in a linear cascade fashion to synthesize ε-caprolactone (entry 1, Table 1) (Aalbers and Fraaije, 2017). They found the fused *Tm*CHMO exhibited around two-fold higher oxygenation activity compared to the individual protein. The obtained fusion achieved 99% conversion using 200 mM substrate (substrate-feeding applied) and gave a turnover number (TON) of >13,000 (Aalbers and Fraaije, 2017). Glycine-rich peptide linkers are structurally flexible and thus hardly restrict the natural movement of enzymes, which to a high extent leads to a more favourable performance of fusion enzymes compared to that with rigid linkers. There is another example of such enzyme that *Tm*CHMO was fused with three different cofactor regeneration enzymes using short flexible linkers. Therein all fusion enzymes resulted in good soluble expression and excellent conversions (entry 2, Table 1) (Mourelle-Insua et al., 2019). Not only for isolated enzyme fusions, but also the biotransformation activity of recombinant cells containing overexpressed fusion enzymes was markedly influenced by the type of fusion linkers. Therein, it turned out that flexible linkers allowed for higher conversions than rigid α-helix linkers (entry 3, Table 1) (Jeon et al., 2015). In general, other studies have shown some similar effects by using flexible linkers, reaching higher

conversions (Peters et al., 2017; Kokorin et al., 2021), improving catalytic activities (Beyer et al., 2017; Beyer et al., 2018; Corrado et al., 2018), and yielding higher productions (Peters et al., 2017) (entries 4–7, Table 1). Therefore, flexible glycine-rich linkers are safe options to try when it comes to the preliminary linker design.

The inclusion of helix-associated amino acids such as alanine and lysine enables the introduction of stiff tethers in glycine-rich linkers, providing the advantage of being resistant to proteolysis and the well-controlled domain separation (Chen et al., 2013). In some research, it has been studied that fusions with rigid peptide linkers exhibited better activities than that with flexible linkers due to the effective separation of protein moieties (Zhang et al., 2017; Huang et al., 2021). For example, the α-helix-based rigid linker between alditol oxidase (AldO) and cytochrome P450 OleTJE (CYP152L1) highly contributed to the improved decarboxylation of myristic acid in the presence of peroxide (H_2O_2) when compared to equal amounts of isolated OleTJE and AldO (entry 8, Table 1). The authors also mentioned the enhanced activity may be attributed to the more efficient channeling of H_2O_2 between enzyme active sites within the proximity of these domains (Matthews et al., 2017).

Despite the potential of rigid linkers, flexible linkers have received more attention than the research done so far on rigid linkers. Overall, various studies have described glycine-rich linkers are beneficial by enhancing flexibility between the two partners, which could provide degrees of freedom for proper folding and conformational changes (Chen et al., 2013). When most studies have focused on the use of flexible or rigid linkers, there is an interesting study that reported a fusion of FDH from *Candida boidinii* and azoreductase from *Rhodococcus opacus 1CP* (AzoRo) with His 10-tag as the linker (Ngo et al., 2022). Due to its high affinity for nickel-containing resins, histidine (His) is often designed as a tag for affinity purification of recombinant proteins. Since most recombinant proteins usually have His-tags at the N or C-terminal, His-tags are used to combine the two proteins with the expectation that it can have multiple biological functions of proteins purification and fusion linkers at the same time. The result showed using His-tag as a linker is achievable, but it might affect the solubility of the fusion protein (entry 9, Table 1). Evidently, each of these linkers has its own pros and cons, and the application will depend on the specific reaction to be achieved.

Besides the composition of linkers, the length of linkers has recently been found to have a pronounced effect on the properties of fusion enzymes. In one case, the effect of the length of a glycine-rich linker with 15 amino acids as the basic linker on the biocatalytic properties of *Tb*ADH-*Tm*CHMO fusion was investigated by evaluating 14 lengths (Gran-Scheuch et al., 2021). All variants exhibited a high expression level but varying activities. The fusions with linker lengths of 10, 12, and 15 amino acids, showed a slight increase in k_{obs} for both activities while the fusions with 2, 3, 6, 7, 13, and 14 amino acid linkers resulted in the highest TONs (Gran-Scheuch et al., 2021). Despite that, no clear correlation between linker length and the catalytic performance of fusions was established within limited studies. Nevertheless, the length of linkers can be adjusted to make space for proper folding of both enzymes, which consequently affects the expression and activity of fusions. For example, three linkers consisting of repeated PAS sequences (20, 40, and 60 amino acids) (entry 10, Table 1) were used in the fusion of an ADH with an aminotransferase (AT) to synthesize amines from alcohols. Therein, they found specific effects for each linker, from short to long: PAS20 achieved two-fold higher conversion compared to the individual enzymes; PAS40 showed the highest activity while PAS60 resulted in the highest soluble expression (Lerchner et al., 2016). Likewise, in another study using NHase as a subunit, proper longer linkers resulted in higher stability while overlong linkers had a negative effect on the activity and expression of NHase. (Guo et al., 2021). Based on current studies, there is still no clear consensus on whether longer or shorter linkers are better. Therefore, it is necessary to design and evaluate different lengths of linkers in a certain case, which, obviously, can be time-consuming. For this reason, a recent study reported a three-step process in straightforward PCR that utilized reiterative primer design, PCR-mediated linker library generation, and restriction enzyme-free cloning methods to generate linker libraries. The authors stated it to be applicable for most fusion constructs (Norris and Hughes, 2018).

In addition to the composition and length of linkers, the order of fused moieties is also critical for the catalytic performance of fusions. An in-depth study of loops and linkers illustrated that linkers are not just 'connectors' but have a significant impact on the microenvironment and orientation of fusions (Huang et al., 2021). The order of protein sequences (N and C-terminal orientation) can influence the correct folding, oligomerization state, stability, and activity of the fusion constructs (Lai et al., 2015). Given that, the gene order for a fusion enzyme was exemplarily optimized by using simulations (Lai et al., 2015; Papaleo et al., 2016). Zhang et al. (2017) predicted the orientation of the cofactor binding domain of leucine dehydrogenase (LeuDH) and formate dehydrogenase (FDH) by structural modelling approach with an online server to ensure the favorable orientation of active sites in the fusion enzyme complex (entry 11, Table 1). This simulation revealed that fusing the C-terminus of FDH with the N-terminus of LeuDH formed a favorable face-to-face active cleft orientation. This would promote the formation of intramolecular tunnelling and accelerate the cofactor channel between FDH and LeuDH. However, such a result could not be obtained in the other direction (Zhang et al., 2017). In the case of BVMOs, changing the order of the same linker led to a significant increase in ADH activity: *Tb*ADH-*Tm*CHMO showed higher k_{cat} than *Tm*CHMO-*Tb*ADH (Aalbers and Fraaije, 2017). While in another study of P450, there is no difference (entry 12, Table 1)

(Kokorin and Urlacher, 2022). In general, the orientation between the two enzymes can have a significant impact on the efficiency of the reaction. Although, with the assistance of computational simulations or using linker databases, the orientation between enzymes can be designed in a more rational way. However, in practice, this is still difficult to control (Lai et al., 2015).

In addition to genetic fusion, post-transcriptional interactions between tags have become popular to bring multiple enzymes in close proximity to form a single multifunctional catalyst (Keeble and Howarth, 2020). SpyTag/SpyCatcher is one such protein coupling approach and it is by far the most used tag. Schoene et al. (2014) reported that locking the termini (often the most flexible part of a protein) together through SpyTag/SpyCatcher altered the enzyme robustness. The thermal and proteolytic stability of β-lactamase has been improved significantly. Another proven way to enhance stability and performance was to encapsulate enzymes with SpyTag/SpyCatcher in protein cages (Mittmann et al., 2022). For example, Pamela and coworkers encapsulated two enzymes via SpyTag/SpyCatcher for the biosynthesis of indigo, enhancing intracellular indigo production and increasing the stability by 90% (Giessen and Silver, 2016). SpyTag/SpyCatcher was shown to facilitate substrate recruitment, thus improving enzyme performance (Wang et al., 2017). Moreover, Spy technology has increased resilience, promoted substrate channeling, and assembled hydrogels for continuous flow biocatalysis (Keeble and Howarth, 2020). Based on these studies, we can see that using a combination of these tags could contribute to a better enzymic performance, especially improving the stability of enzymes. It will be exciting to see how the Spy toolbox develops in the field of biocatalysis in the future.

3 Oxidoreductases in organic media and perspectives

As aforementioned, the use of fusion proteins is mostly documented for aqueous media. However, the use of water as a "green" solvent has been intensely debated within the biocatalysis field, which made it clear that the impact of contaminated water surely needs to be quantified when assessing the greenness of an enzymatic process (Ni et al., 2014). For this reason, water has been included in the recently modified E-factor to emphasize a fair comparison between the use of water and other solvents (Tieves et al., 2019). When using water as reaction media for chemical synthesis, not only wastewater but also several other limitations should be considered, such as 1) lower substrate solubility, 2) laborious downstream processing, 3) unwanted water-related side reactions, 4) enzyme inhibition, and 5) microbial contamination. Given these problems especially the limited substrate loadings, there is a high interest in the use of non-aqueous media for enzymatic catalysis (Osterberg et al., 2015; Rosinha Grundtvig et al., 2018; Bollinger et al., 2020). In this context, organic solvents are often widely used in most synthetic processes, especially in the pharmaceutical industry (Caron et al., 2006; van Schie et al., 2021) and can be seen as a possible improvement for different biocatalytic systems.

Research on biocatalysis in organic media has focused on hydrolases (EC 3) mainly lipases some of which have been applied at technical scales. Although oxidoreductases-mediated selective oxidation is considered one of the most important transformations in organic chemistry, studies on oxidoreductases (EC 1) are still limited (Hollmann et al., 2011; Ringborg et al., 2017; Dong et al., 2018). Between 2000 and 2015, 68% of the patents covering biocatalytic applications were based on oxidoreductases, despite the fact that they account for "only" one-third approximately of all the known enzymes (Drenth et al., 2021). The limited use of oxidoreductase at technical scales in organic media is not only due to the instability of redox enzymes *per se* but also the fact that up to 50% approximately of known oxidoreductases are cofactor-dependent [NAD(P)H]. Given the expensive and unstable nature of NAD(P)H, their regeneration and re-utilization are often necessary for the economic feasibility on an industrial scale (Velasco-Lozano et al., 2017; Selles Vidal et al., 2018). In this case, enzyme-coupled cofactor regeneration approaches have emerged as powerful tools to meet this demand. In particular, dehydrogenase-promoted *in situ* cofactor regeneration in whole cells (so-called "designer cells") (Groger et al., 2006) and *in vitro* multi-enzymatic cascades have been widely reported in aqueous media. In the case of cascade reactions, the distance between enzymes' active sites has a significant effect. Fusing enzymes or co-immobilizing enzymes are some of the different approaches that can be used to shorten the transport distance of reaction intermediates between active sites while increasing the enzyme stability, jointly contributing to the improved efficiency of cofactor regeneration (Hollmann et al., 2018; Zhu et al., 2022).

Baeyer-Villiger monooxygenases (BVMOs) can oxidize ketones to furnish value-added esters and lactones, which rely on both NADPH and molecular oxygen (Schmidt et al., 2015; Scherkus et al., 2016). One preparative application of BVMO overexpressed in whole cells has been demonstrated in an *in situ* substrate feeding and product removal process by using adsorbent resin within a bubble column reactor (Hilker et al., 2004a; Hilker et al., 2004b; Hilker et al., 2005). This set-up has been scaled up to the kilogram level in a 50 L reactor. Therein, it is concluded that overcoming the oxygen limitation could afford higher productivity. Given the use of organic solvents offers magnitudes higher oxygen solubility than water (Ramesh et al., 2016), applying BVMOs in organic media to achieve oxygen limitation removal is appealing. Furthermore, Sato et al. (2014)

reported that the oxygen solubility increases with larger alkyl chains of alcohol solvents while with decreased alkyl chains of alkane solvents, which provided a basic guideline for solvent selection.

Various multi-enzymatic cascades have been designed and established involving oxidoreductases mostly in water and water-organic mixtures to produce bulk and fine chemicals especially active pharmaceutical ingredients (APIs). Some of representative studies have been summarized in Table 1 which has a focus on cyclohexanone monooxygenases and widely used cofactor regeneration enzymes ADHs. These studies demonstrated the screening, the characterization including mutation and fusion (entries 1, 18, 2, and 24, Table 1) for more stable enzymes, and the application of these enzymes in different reaction conditions and set-ups. In addition, the optimization of an oxidative process by using air or pure oxygen was illustrated. All these studies were performed with a broad range of substrate concentrations and various enzymes for the cofactor regeneration (14–17, 19–22, 25, and 26, Table 1). A successful scale-up of a sequential cascade reaction has been reported by adding the two enzymes separately, optimizing the dosing factor, and increasing the reaction volume up to 100 L in a 200 L-reactor (entry 23, Table 1) (Solé et al., 2019). Despite these advances, there is still room for further improvement especially concerning the cofactor recycling, substrate loadings, oxygen supply, and enzyme stability. This is where enzyme fusions in organic media can fit in and provide counterpart solutions.

To the best of our knowledge, there has been only one study on the use of fused oxygenating enzymes in low-water media (micro-aqueous media) so far. Huang et al. (2019) reported the use of fused type II flavin-containing monooxygenase (FMO-E) and horse liver alcohol dehydrogenase (HLADH) by using a flexible linker in micro-aqueous media (5 vol% aqueous buffer in organic solvent) for the synthesis of γ-butyrolactone. It was reported that the enzymes' tolerance toward organic solvents could be transmitted when enzymes are fused. Depending on the art of combination, different stabilities can be obtained. For instance, Mourelle-Insua et al. (2019) reported that *Bs*FDH-*Tm*CHMO fusion achieved around 10% conversion in 1 vol% 1,4-dioxane, while fusing *Ps*PTDH with *Tm*CHMO by using two different short-flexible linkers led to full conversion. These examples demonstrate the great potential of applying fusion enzymes in organic media. However, it is undoubtable that the rational design of fusion enzymes with suitable linkers and the application of fused enzymes for biocatalytic cascades in non-aqueous media still remains complex and challenging. Moreover, further research is urgently needed to bridge the gap between laboratory-level study and the application under industrially relevant conditions.

4 Conclusion and outlook

Overall, the development of fusion enzymes has highly facilitated the design and application of enzymatic cascades to produce valuable compounds in a more efficient manner. Many gains have been firmly demonstrated. The fusion approach enables the combination of target functional domains to easily modularize these multifunctional catalysts for custom applications. For cofactor-dependent enzymes, especially oxidoreductases, fusions have been used to provide efficient cofactor regeneration by shortening diffusion pathways and stabilizing unstable cofactors both in whole cells and *in vitro* using enzyme systems. Not only the improved catalytic performance but also the enhanced co-expression is achievable by optimizing fusion linkers. Given complicated structure-function correlations, rational and efficient design of linkers has so far remained a challenge. However, it is becoming easier with the help of *in-silico* modeling and the establishment of linker database libraries. Along this path, more and more studies have emerged, some of which have been outlined here to provide a general overview. In particular, fusions of oxidoreductase have been highlighted due to high interest in them as well as their infinite potential for chemical synthesis. Benefiting from the fusion mode, the applications of cofactor-dependent oxidoreductases not only in aqueous media but also in non-aqueous media can be realized, expanding the biocatalytic toolbox for sustainable industrial chemistry.

Author contributions

Conception of the work: SK, NZ, YM, and GV; Drafting the article: YM, NZ, and GV. Critical revision of the article: all authors.

Funding

SK thanks to Aarhus University Research Foundation (AUFF). YM thanks the China Scholarship Council (CSC) for the financial support (No. 202108610066).

Conflict of interest

The authors declare that the research was conducted in the absence of any commercial or financial relationships that could be construed as a potential conflict of interest.

Publisher's note

References

Aalbers, F. S., and Fraaije, M. W. (2017). Coupled reactions by coupled enzymes: Alcohol to lactone cascade with alcohol dehydrogenase-cyclohexanone monooxygenase fusions. *Appl. Microbiol. Biotechnol.* 101 (20), 7557–7565. doi:10.1007/s00253-017-8501-4

Aalbers, F. S., and Fraaije, M. W. (2019). Enzyme fusions in biocatalysis: Coupling reactions by pairing enzymes. *ChemBioChem* 20 (1), 20–28. doi:10.1002/cbic.201800394

Andorfer, M. C., Belsare, K. D., Girlich, A. M., and Lewis, J. C. (2017). Aromatic halogenation by using bifunctional flavin reductase-halogenase fusion enzymes. *ChemBioChem* 18 (21), 2099–2103. doi:10.1002/cbic.201700391

Arai, R. (2021). Design of helical linkers for fusion proteins and protein-based nanostructures. *Methods Enzymol.* 647, 209–230. doi:10.1016/bs.mie.2020.10.003

Arai, R., Ueda, H., Kitayama, A., Kamiya, N., and Nagamune, T. (2001). Design of the linkers which effectively separate domains of a bifunctional fusion protein. *Protein Eng. Des. Sel.* 14 (8), 529–532. doi:10.1093/protein/14.8.529

Bakkes, P. J., Riehm, J. L., Sagadin, T., Rühlmann, A., Schubert, P., Biemann, S., et al. (2017). Engineering of versatile redox partner fusions that support monooxygenase activity of functionally diverse cytochrome P450s. *Sci. Rep.* 7 (1), 9570. doi:10.1038/s41598-017-10075-w

Belsare, K. D., Ruff, A. J., Martinez, R., and Schwaneberg, U. (2020). Insights on intermolecular fmn-heme domain interaction and the role of linker length in cytochrome P450cin fusion proteins. *Biol. Chem.* 401 (11), 1249–1255. doi:10.1515/hsz-2020-0134

Benítez-Mateos, A. I., Roura Padrosa, D., and Paradisi, F. (2022). Multistep enzyme cascades as a route towards green and sustainable pharmaceutical syntheses. *Nat. Chem.* 14 (5), 489–499. doi:10.1038/s41557-022-00931-2

Beyer, N., Kulig, J. K., Bartsch, A., Hayes, M. A., Janssen, D. B., Fraaije, M. W., et al. (2017). P450bm3 fused to phosphite dehydrogenase allows phosphite-driven selective oxidations. *Appl. Microbiol. Biotechnol.* 101 (6), 2319–2331. doi:10.1007/s00253-016-7993-7

Beyer, N., Kulig, J. K., Fraaije, M. W., Hayes, M. A., and Janssen, D. B. (2018). Exploring PTDH-P450BM3 variants for the synthesis of drug metabolites. *ChemBioChem* 19 (4), 326–337. doi:10.1002/cbic.201700470

Bollinger, A., Molitor, R., Thies, S., Koch, R., Coscolín, C., Ferrer, M., et al. (2020). Organic-solvent-tolerant carboxylic ester hydrolases for organic synthesis. *Appl. Environ. Microbiol.* 86 (9), e00106–20. doi:10.1128/AEM.00106-20

Bornadel, A., Hatti-Kaul, R., Hollmann, F., and Kara, S. (2015). A Bi-enzymatic convergent cascade for ε-caprolactone synthesis employing 1,6-hexanediol as a 'double-smart cosubstrate'. *ChemCatChem* 7 (16), 2442–2445. doi:10.1002/cctc.201500511

Caron, S., Dugger, R. W., Ruggeri, S. G., Ragan, J. A., and Ripin, D. H. (2006). Large-scale oxidations in the pharmaceutical industry. *Chem. Rev.* 106 (7), 2943–2989. doi:10.1021/cr040679f

Chen, X., Zaro, J., and Shen, W.-C. (2013). Fusion protein linkers: Property, design and functionality. *Adv. Drug Deliv. Rev.* 65 (10), 1357–1369. doi:10.1016/j.addr.2012.09.039

Corrado, M. L., Knaus, T., and Mutti, F. G. (2018). A chimeric styrene monooxygenase with increased efficiency in asymmetric biocatalytic epoxidation. *ChemBioChem* 19 (7), 679–686. doi:10.1002/cbic.201700653

de Gonzalo, G., and Alcántara, A. R. (2021). Multienzymatic processes involving baeyer-villiger monooxygenases. *Catalysts* 11 (5), 605. doi:10.3390/catal11050605

Delgove, M. A. F., Valencia, D., Solé, J., Bernaerts, K. V., De Wildeman, S. M. A., Guillén, M., et al. (2019). High performing immobilized Baeyer-Villiger monooxygenase and glucose dehydrogenase for the synthesis of ε-caprolactone derivative. *Appl. Catal. A General* 572, 134–141. doi:10.1016/j.apcata.2018.12.036

Domínguez de María, P., and Hollmann, F. (2015). On the (Un)Greenness of biocatalysis: Some challenging figures and some promising options. *Front. Microbiol.* 6, 1257. doi:10.3389/fmicb.2015.01257

Dong, J., Fernández-Fueyo, E., Hollmann, F., Paul, C. E., Pesic, M., Schmidt, S., et al. (2018). Biokatalytische oxidationsreaktionen - aus der sicht eines chemikers. *Angew. Chem.* 130 (30), 9380–9404. doi:10.1002/ange.201800343

Drenth, J., Yang, G., Paul, C. E., and Fraaije, M. W. (2021). A tailor-made deazaflavin-mediated recycling system for artificial nicotinamide cofactor biomimetics. *ACS Catal.* 11 (18), 11561–11569. doi:10.1021/acscatal.1c03033

Elleuche, S. (2015). Bringing functions together with fusion enzymes-from nature's inventions to biotechnological applications. *Appl. Microbiol. Biotechnol.* 99 (4), 1545–1556. doi:10.1007/s00253-014-6315-1

Ellis, G. A., Klein, W. P., Lasarte-Aragonés, G., Thakur, M., Walper, S. A., Medintz, I. L., et al. (2019). Artificial multienzyme scaffolds: Pursuing *in vitro* substrate channeling with an overview of current progress. *ACS Catal.* 9 (12), 10812–10869. doi:10.1021/acscatal.9b02413

Engel, J., Cordellier, A., Huang, L., and Kara, S. (2019a). Enzymatic ring-opening polymerization of lactones: Traditional approaches and alternative strategies. *ChemCatChem* 11 (20), 4983–4997. doi:10.1002/cctc.201900976

Engel, J., Mthethwa, K. S., Opperman, D. J., and Kara, S. (2019b). Characterization of new baeyer-villiger monooxygenases for lactonizations in redox-neutral cascades. *Mol. Catal.* 468, 44–51. doi:10.1016/j.mcat.2019.02.006

France, S. P., Hepworth, L. J., Turner, N. J., and Flitsch, S. L. (2017). Constructing biocatalytic cascades: *in vitro* and *in vivo* approaches to de novo multi-enzyme pathways. *ACS Catal.* 7 (1), 710–724. doi:10.1021/acscatal.6b02979

Fürst, M. J., Savino, S., Dudek, H. M., Gómez Castellanos, J. R., Gutiérrez de Souza, C., Rovida, S., et al. (2017). Polycyclic ketone monooxygenase from the thermophilic fungus thermothelomyces thermophila: A structurally distinct biocatalyst for bulky substrates. *J. Am. Chem. Soc.* 139 (2), 627–630. doi:10.1021/jacs.6b12246

Giessen, T. W., and Silver, P. A. (2016). A catalytic nanoreactor based on *in vivo* encapsulation of multiple enzymes in an engineered protein nanocompartment. *ChemBioChem* 17 (20), 1931–1935. doi:10.1002/cbic.201600431

Gran-Scheuch, A., Aalbers, F., Woudstra, Y., Parra, L., and Fraaije, M. W. (2021). Optimizing the linker length for fusing an alcohol dehydrogenase with a cyclohexanone monooxygenase. *Methods Enzymol.* 647, 107–143. doi:10.1016/bs.mie.2020.09.008

Gröger, H., Chamouleau, F., Orologas, N., Rollmann, C., Drauz, K., Hummel, W., et al. (2006). Enantioselective reduction of ketones with "designer cells" at high substrate concentrations: Highly efficient access to functionalized optically active alcohols. *Angew. Chem. Int. Ed.* 45 (34), 5677–5681. doi:10.1002/anie.200503394

Guo, J., Cheng, Z., Berdychowska, J., Zhu, X., Wang, L., Peplowski, L., et al. (2021). Effect and mechanism analysis of different linkers on efficient catalysis of subunit-fused nitrile hydratase. *Int. J. Biol. Macromol.* 181, 444–451. doi:10.1016/j.ijbiomac.2021.03.103

Hilker, I., Alphand, V., Wohlgemuth, R., and Furstoss, R. (2004a). Microbial transformations, 56. Preparative scale Asymmetric baeyer-villiger oxidation using a highly Productive"Two-in-one" resin-based*in situ* SFPR concept. *Adv. Synthesis Catal.* 346 (23), 203–214. doi:10.1002/adsc.200303183

Hilker, I., Gutiérrez, M. C., Alphand, V., Wohlgemuth, R., and Furstoss, R. (2004b). Microbiological transformations 57. Facile and efficient resin-based *in situ* SFPR preparative-scale synthesis of an enantiopure "unexpected" lactone regioisomer via a Baeyer–Villiger oxidation process. *Org. Lett.* 6 (12), 1955–1958. doi:10.1021/ol049508n

Hilker, I., Wohlgemuth, R., Alphand, V., and Furstoss, R. (2005). Microbial transformations 59: First kilogram scale Asymmetric microbial baeyer-villiger oxidation with optimized productivity using a resin-based *in situ* sfpr strategy. *Biotechnol. Bioeng.* 92 (6), 702–710. doi:10.1002/bit.20636

Hollmann, F., Arends, I. W. C. E., Buehler, K., Schallmey, A., and Bühler, B. (2011). Enzyme-mediated oxidations for the chemist. *Green Chem.* 13 (2), 226–265. doi:10.1039/c0gc00595a

Hollmann, F., Kara, S., Opperman, D. J., and Wang, Y. (2018). Biocatalytic synthesis of lactones and lactams. *Chem. Asian J.* 13 (23), 3601–3610. doi:10.1002/asia.201801180

Hollmann, F., Opperman, D. J., and Paul, C. E. (2021). Biocatalytic reduction reactions from a chemist's perspective. *Angew. Chem. Int. Ed.* 60 (11), 5644–5665. doi:10.1002/anie.202001876

Holtmann, D., and Hollmann, F. (2022). Is water the best solvent for biocatalysis? *Mol. Catal.* 517, 112035. doi:10.1016/j.mcat.2021.112035

Huang, L., Aalbers, F. S., Tang, W., Röllig, R., Fraaije, M. W., Kara, S., et al. (2019). Convergent cascade catalyzed by monooxygenase-alcohol dehydrogenase fusion applied in organic media. *ChemBioChem* 20 (13), 1653–1658. doi:10.1002/cbic.201800814

Huang, L., Domínguez de María, P., and Kara, S. (2018). The 'water challenge': Opportunities and challenges of using oxidoreductases in non-conventional media. *Chim. Oggi* 36, 48–56.

Huang, X., Holden, H. M., and Raushel, F. M. (2001). Channeling of substrates and intermediates in enzyme-catalyzed reactions. *Annu. Rev. Biochem.* 70 (1), 149–180. doi:10.1146/annurev.biochem.70.1.149

Huang, Z., Zhang, C., and Xing, X.-H. (2021). Design and construction of chimeric linker library with controllable flexibilities for precision protein engineering. *Methods Enzymol.* 647, 23–49. doi:10.1016/bs.mie.2020.12.004

Huffman, M. A., Fryszkowska, A., Alvizo, O., Borra-Garske, M., Campos, K. R., Canada, K. A., et al. (2019). Design of an *in vitro* biocatalytic cascade for the manufacture of islatravir. *Science* 366 (6470), 1255–1259. doi:10.1126/science.aay8484

Illanes, A. (2015). CHAPTER 3. Biocatalysis in organic media. *White Biotechnol. Sustain. Chem.*, 36–51. doi:10.1039/9781782624080-00036

Jeon, E.-Y., Baek, A. H., Bornscheuer, U. T., and Park, J.-B. (2015). Enzyme fusion for whole-cell biotransformation of long-chain sec-alcohols into esters. *Appl. Microbiol. Biotechnol.* 99 (15), 6267–6275. doi:10.1007/s00253-015-6392-9

Kara, S., Schrittwieser, J. H., and Hollmann, F. (2013). Strategies for cofactor regeneration in biocatalyzed reductions. *Synthetic Methods Biol. Act. Mol.*, 209–238. doi:10.1002/9783527665785.ch08

Keeble, A. H., and Howarth, M. (2020). Power to the protein: Enhancing and combining activities using the Spy toolbox. *Chem. Sci.* 11 (28), 7281–7291. doi:10.1039/d0sc01878c

Klibanov, A. M. (1989). Enzymatic catalysis in anhydrous organic solvents. *Trends Biochem. Sci.* 14 (4), 141–144. doi:10.1016/0968-0004(89)90146-1

Kokkonen, P., Bednar, D., Pinto, G., Prokop, Z., and Damborsky, J. (2019). Engineering enzyme access tunnels. *Biotechnol. Adv.* 37 (6), 107386. doi:10.1016/j.biotechadv.2019.04.008

Kokorin, A., Parshin, P. D., Bakkes, P. J., Pometun, A. A., Tishkov, V. I., Urlacher, V. B., et al. (2021). Genetic fusion of P450 Bm3 and formate dehydrogenase towards self-sufficient biocatalysts with enhanced activity. *Sci. Rep.* 11 (1), 21706. doi:10.1038/s41598-021-00957-5

Kokorin, A., and Urlacher, V. B. (2022). Artificial fusions between P450 BM3 and an alcohol dehydrogenase for efficient (+)-Nootkatone production. *ChemBioChem* 23 (12), e202200065. doi:10.1002/cbic.202200065

Küchler, A., Yoshimoto, M., Luginbühl, S., Mavelli, F., and Walde, P. (2016). Enzymatic reactions in confined environments. *Nat. Nanotech* 11 (5), 409–420. doi:10.1038/nnano.2016.54

Kumar, A., Dhar, K., Kanwar, S. S., and Arora, P. K. (2016). Lipase catalysis in organic solvents: Advantages and applications. *Biol. Proced. Online* 18 (1), 2. doi:10.1186/s12575-016-0033-2

Lai, Y.-T., Jiang, L., Chen, W., and Yeates, T. O. (2015). On the predictability of the orientation of protein domains joined by a spanning alpha-helical linker. *Protein Eng. Des. Sel.* 28 (11), 491–500. doi:10.1093/protein/gzv035

Lerchner, A., Daake, M., Jarasch, A., and Skerra, A. (2016). Fusion of an alcohol dehydrogenase with an aminotransferase using a pas linker to improve coupled enzymatic alcohol-to-amine conversion. *Protein Eng. Des. Sel.* 29 (12), 557–562. doi:10.1093/protein/gzw039

Matthews, S., Tee, K. L., Rattray, N. J., McLean, K. J., Leys, D., Parker, D. A., et al. (2017). Production of alkenes and novel secondary products by P450 Oletje using novel H2O2-generating fusion protein systems. *FEBS Lett.* 591 (5), 737–750. doi:10.1002/1873-3468.12581

Mittmann, E., Mickoleit, F., Maier, D. S., Stäbler, S. Y., Klein, M. A., Niemeyer, C. M., et al. (2022). A magnetosome-based platform for flow biocatalysis. *ACS Appl. Mat. Interfaces* 14, 22138–22150. doi:10.1021/acsami.2c03337

Mourelle-Insua, Á., Aalbers, F. S., Lavandera, I., Gotor-Fernández, V., and Fraaije, M. W. (2019). What to sacrifice? Fusions of cofactor regenerating enzymes with baeyer-villiger monooxygenases and alcohol dehydrogenases for self-sufficient redox biocatalysis. *Tetrahedron* 75 (13), 1832–1839. doi:10.1016/j.tet.2019.02.015

Munro, A. W., Girvan, H. M., and McLean, K. J. (2007). Cytochrome P450-redox partner fusion enzymes. *Biochimica Biophysica Acta (BBA) - General Subj.* 1770 (3), 345–359. doi:10.1016/j.bbagen.2006.08.018

Muschiol, J., Peters, C., Oberleitner, N., Mihovilovic, M. D., Bornscheuer, U. T., Rudroff, F., et al. (2015). Cascade catalysis - strategies and challenges en route to preparative synthetic biology. *Chem. Commun.* 51 (27), 5798–5811. doi:10.1039/C4CC08752F

Ngo, A. C. R., Schultes, F. P. J., Maier, A., Hadewig, S. N. H., and Tischler, D. (2022). Improving biocatalytic properties of an azoreductase via the N- terminal fusion of formate dehydrogenase. *Chembiochem.* 23 (6), e202100643. doi:10.1002/cbic.202100643

Ni, Y., Holtmann, D., and Hollmann, F. (2014). How green is biocatalysis? To calculate is to know. *ChemCatChem* 6 (4), 930–943. doi:10.1002/cctc.201300976

Norris, J. L., and Hughes, R. M. (2018). protaTETHER - a method for the incorporation of variable linkers in protein fusions reveals impacts of linker flexibility in a PKAc-GFP fusion protein. *FEBS Open Bio* 8 (6), 1029–1042. doi:10.1002/2211-5463.12414

Osterberg, P. M., Niemeier, J. K., Welch, C. J., Hawkins, J. M., Martinelli, J. R., Johnson, T. E., et al. (2015). Experimental limiting oxygen concentrations for nine organic solvents at temperatures and pressures relevant to aerobic oxidations in the pharmaceutical industry. *Org. Process Res. Dev.* 19 (11), 1537–1543. doi:10.1021/op500328f

Papaleo, E., Saladino, G., Lambrughi, M., Lindorff-Larsen, K., Gervasio, F. L., Nussinov, R., et al. (2016). The role of protein loops and linkers in conformational dynamics and allostery. *Chem. Rev.* 116 (11), 6391–6423. doi:10.1021/acs.chemrev.5b00623

Peters, C., Rudroff, F., Mihovilovic, M. D., and T. Bornscheuer, U. T. (2017). Fusion proteins of an enoate reductase and a baeyer-villiger monooxygenase facilitate the synthesis of chiral lactones. *Biol. Chem.* 398 (1), 31–37. doi:10.1515/hsz-2016-0150

Quin, M. B., Wallin, K. K., Zhang, G., and Schmidt-Dannert, C. (2017). Spatial organization of multi-enzyme biocatalytic cascades. *Org. Biomol. Chem.* 15 (20), 4260–4271. doi:10.1039/c7ob00391a

Rabe, K. S., Müller, J., Skoupi, M., and Niemeyer, C. M. (2017). Cascades in compartments: En route to machine-assisted Biotechnology. *Angew. Chem. Int. Ed.* 56 (44), 13574–13589. doi:10.1002/anie.201703806

Ramesh, H., Mayr, T., Hobisch, M., Borisov, S., Klimant, I., Krühne, U., et al. (2016). Measurement of oxygen transfer from air into organic solvents. *J. Chem. Technol. Biotechnol.* 91 (3), 832–836. doi:10.1002/jctb.4862

Reddy Chichili, V. P., Kumar, V., and Sivaraman, J. (2013). Linkers in the structural biology of protein-protein interactions. *Protein Sci.* 22 (2), 153–167. doi:10.1002/pro.2206

Ren, S., Li, C., Jiao, X., Jia, S., Jiang, Y., Bilal, M., et al. (2019). Recent progress in multienzymes Co-immobilization and multienzyme system Applications. *Chem. Eng. J.* 373, 1254–1278. doi:10.1016/j.cej.2019.05.141

Ringborg, R. H., Toftgaard Pedersen, A., and Woodley, J. M. (2017). Automated determination of oxygen-dependent enzyme kinetics in a tube-in-tube flow reactor. *ChemCatChem* 9 (17), 3285–3288. doi:10.1002/cctc.201700811

Romero, E., Castellanos, J. R. G., Mattevi, A., and Fraaije, M. W. (2016). Characterization and crystal structure of a robust cyclohexanone monooxygenase. *Angew. Chem.* 128 (51), 16084–16087. doi:10.1002/ange.201608951

Rosinha Grundtvig, I. P., Heintz, S., Krühne, U., Gernaey, K. V., Adlercreutz, P., Hayler, J. D., et al. (2018). Screening of organic solvents for bioprocesses using aqueous-organic two-phase systems. *Biotechnol. Adv.* 36 (7), 1801–1814. doi:10.1016/j.biotechadv.2018.05.007

Sato, T., Hamada, Y., Sumikawa, M., Araki, S., and Yamamoto, H. (2014). Solubility of oxygen in organic solvents and calculation of the hansen solubility parameters of oxygen. *Ind. Eng. Chem. Res.* 53 (49), 19331–19337. doi:10.1021/ie502386t

Scherkus, C., Schmidt, S., Bornscheuer, U. T., Gröger, H., Kara, S., Liese, A., et al. (2016). A fed-batch synthetic strategy for a three-step enzymatic synthesis of poly-ϵ-caprolactone. *ChemCatChem* 8 (22), 3446–3452. doi:10.1002/cctc.201600806

Scherkus, C., Schmidt, S., Bornscheuer, U. T., Gröger, H., Kara, S., Liese, A., et al. (2017). Kinetic insights into ϵ-caprolactone synthesis: Improvement of an enzymatic cascade reaction. *Biotechnol. Bioeng.* 114 (6), 1215–1221. doi:10.1002/bit.26258

Schmidt, S., Scherkus, C., Muschiol, J., Menyes, U., Winkler, T., Hummel, W., et al. (2015). An enzyme cascade synthesis of ε-caprolactone and its oligomers. *Angew. Chem. Int. Ed.* 54 (9), 2784–2787. doi:10.1002/anie.201410633

Schoene, C., Fierer, J. O., Bennett, S. P., and Howarth, M. (2014). Spytag/spycatcher cyclization confers resilience to boiling on a mesophilic enzyme. *Angew. Chem. Int. Ed.* 53 (24), 6101–6104. doi:10.1002/anie.201402519

Sellés Vidal, L., Kelly, C. L., Mordaka, P. M., and Heap, J. T. (2018). Review of nad(P)H-dependent oxidoreductases: Properties, engineering and application. *Biochimica Biophysica Acta (BBA)—Proteins Proteomics* 1866 (2), 327–347. doi:10.1016/j.bbapap.2017.11.005

Solé, J., Brummund, J., Caminal, G., Álvaro, G., Schürmann, M., Guillén, M., et al. (2019). Enzymatic synthesis of trimethyl-ε-caprolactone: Process intensification and demonstration on a 100 L scale. *Org. Process Res. Dev.* 23 (11), 2336–2344. doi:10.1021/acs.oprd.9b00185

Tavanti, M., Parmeggiani, F., Castellanos, J. R. G., Mattevi, A., and Turner, N. J. (2017). One-pot biocatalytic double oxidation of α-isophorone for the synthesis of ketoisophorone. *ChemCatChem* 9 (17), 3338–3348. doi:10.1002/cctc.201700620

Tieves, F., Tonin, F., Fernández-Fueyo, E., Robbins, J., Bommarius, B., Bommarius, A., et al. (2019). Energising the e-factor: The E&-Factor. *Tetrahedron* 75, 1311–1314. doi:10.1016/j.tet.2019.01.065

Torres-Pazmiño, D. E., Snajdrova, R., Baas, B.-J., Ghobrial, M., Mihovilovic, M. D., Fraaije, M. W., et al. (2008). Self-sufficient baeyer-villiger monooxygenases: Effective coenzyme regeneration for biooxygenation by fusion engineering. *Angew. Chem.* 120 (12), 2307–2310. doi:10.1002/ange.200704630

van Schie, M., Spöring, J. D., Bocola, M., Domínguez de María, P., and Rother, D. (2021). Applied biocatalysis beyond just buffers - from aqueous to unconventional media. Options and guidelines. *Green Chem.* 23 (9), 3191–3206. doi:10.1039/d1gc00561h

Velasco-Lozano, S., Benítez-Mateos, A. I., and López-Gallego, F. (2017). Co-immobilized phosphorylated cofactors and enzymes as self-sufficient heterogeneous biocatalysts for chemical processes. *Angew. Chem. Int. Ed.* 56 (3), 771–775. doi:10.1002/anie.201609758

Vidal, L. S., Kelly, C. L., Mordaka, P. M., and Heap, J. T. (2018). Review of NAD(P)H-Dependent oxidoreductases: Properties, engineering and application. *Bba-Proteins Proteom.* 1866 (2), 327–347. doi:10.1016/j.bbapap.2017.11.005

Walsh, C. T., and Moore, B. S. (2019). Enzymatic cascade reactions in biosynthesis. *Angew. Chem. Int. Ed.* 58 (21), 6846–6879. doi:10.1002/anie.201807844

Wang, H. H., Altun, B., Nwe, K., and Tsourkas, A. (2017). Proximity-based sortase-mediated ligation. *Angew. Chem. Int. Ed.* 56 (19), 5349–5352. doi:10.1002/anie.201701419

Wedde, S., Rommelmann, P., Scherkus, C., Schmidt, S., Bornscheuer, U. T., Liese, A., et al. (2017). An alternative approach towards poly-ε-caprolactone through a chemoenzymatic synthesis: Combined hydrogenation, bio-oxidations and polymerization without the isolation of intermediates. *Green Chem.* 19 (5), 1286–1290. doi:10.1039/c6gc02529c

Wilding, M., Scott, C., and Warden, A. C. (2018). Computer-guided surface engineering for enzyme improvement. *Sci. Rep.* 8 (1), 11998. doi:10.1038/s41598-018-30434-5

Xu, K., Chen, X., Zheng, R., and Zheng, Y. (2020). Immobilization of multi-enzymes on support materials for efficient biocatalysis. *Front. Bioeng. Biotechnol.* 8, 660. doi:10.3389/fbioe.2020.00660

Zaks, A., and Klibanov, A. M. (1988). Enzymatic catalysis in nonaqueous solvents. *J. Biol. Chem.* 263 (7), 3194–3201. doi:10.1016/s0021-9258(18)69054-4

Zhang, N., Müller, B., Kirkeby, T. Ø., Kara, S., and Loderer, C. (2022). Development of a thioredoxin-based cofactor regeneration system for NADPH-dependent oxidoreductases. *ChemCatChem* 14 (7), e202101625. doi:10.1002/cctc.202101625

Zhang, Y., Wang, Y., Wang, S., and Fang, B. (2017). Engineering Bi-functional enzyme complex of formate dehydrogenase and leucine dehydrogenase by peptide linker mediated fusion for accelerating cofactor regeneration. *Eng. Life Sci.* 17 (9), 989–996. doi:10.1002/elsc.201600232

Zhou, Y., Wu, S., and Bornscheuer, U. T. (2021). Recent advances in (Chemo)Enzymatic cascades for upgrading bio-based resources. *Chem. Commun.* 57 (82), 10661–10674. doi:10.1039/D1CC04243B

Zhu, J., Geng, Q., Liu, Y.-Y., Pan, J., Yu, H. L., Xu, J.-H., et al. (2022). Co-Cross-Linked aggregates of baeyer-villiger monooxygenases and formate dehydrogenase for repeated use in asymmetric biooxidation. *Org. Process Res. Dev.* doi:10.1021/acs.oprd.1c00382

frontiers | Frontiers in Bioengineering and Biotechnology

TYPE Review
PUBLISHED 22 July 2022
DOI 10.3389/fbioe.2022.958606

OPEN ACCESS

EDITED BY
Helen Treichel,
Universidade Federal da Fronteira Sul, Brazil

REVIEWED BY
Suzana Fátima Bazoti,
Universidade Federal da Fronteira Sul, Brazil
Nadia Guajardo,
Metropolitan University of Technology, Chile

*CORRESPONDENCE
Roland Wohlgemuth,
roland.wohlgemuth.1@p.lodz.pl
Jennifer Littlechild,
J.A.Littlechild@exeter.ac.uk

SPECIALTY SECTION
This article was submitted to Bioprocess Engineering, a section of the journal Frontiers in Bioengineering and Biotechnology

RECEIVED 31 May 2022
ACCEPTED 28 June 2022
PUBLISHED 22 July 2022

CITATION
Wohlgemuth R and Littlechild J (2022), Complexity reduction and opportunities in the design, integration and intensification of biocatalytic processes for metabolite synthesis. *Front. Bioeng. Biotechnol.* 10:958606. doi: 10.3389/fbioe.2022.958606

Complexity reduction and opportunities in the design, integration and intensification of biocatalytic processes for metabolite synthesis

Roland Wohlgemuth[1,2]* and Jennifer Littlechild[3]*

[1]Institute of Molecular and Industrial Biotechnology, Lodz University of Technology, Lodz, Poland, [2]Swiss Coordination Committee for Biotechnology, Zurich, Switzerland, [3]Henry Wellcome Building for Biocatalysis, Biosciences, University of Exeter, Exeter, United Kingdom

The biosynthesis of metabolites from available starting materials is becoming an ever important area due to the increasing demands within the life science research area. Access to metabolites is making essential contributions to analytical, diagnostic, therapeutic and different industrial applications. These molecules can be synthesized by the enzymes of biological systems under sustainable process conditions. The facile synthetic access to the metabolite and metabolite-like molecular space is of fundamental importance. The increasing knowledge within molecular biology, enzyme discovery and production together with their biochemical and structural properties offers excellent opportunities for using modular cell-free biocatalytic systems. This reduces the complexity of synthesizing metabolites using biological whole-cell approaches or by classical chemical synthesis. A systems biocatalysis approach can provide a wealth of optimized enzymes for the biosynthesis of already identified and new metabolite molecules.

KEYWORDS

cell-free biocatalysis, enzyme development, enzyme function, reaction engineering, biocatalytic process design, metabolite synthesis, bioprocess navigation

Introduction

The quality of human life has continued to benefit from the rapid development of new medicines for the treatment of many diseases. The tremendous growth of knowledge in the discovery, isolation, structural characterization and man-made synthetic replication of small molecules formed naturally in living organisms represents a new domain of synthetic biology. The man-made synthesis of the metabolites has been of fundamental importance in this area. The first demonstration of this approach was using urea or acetic acid characterised as organic molecules from living organisms that could be synthesized from inorganic starting materials. Today this has developed into the total synthesis of metabolites having the most complex molecular structures (Nicolaou et al., 2000; Nicolaou and

Rigol, 2020). The development of broadly applicable synthetic methodologies for the construction of the carbon backbone and for the selective introduction of a large diversity of functional groups, has created the necessary knowledge base for human creativity to find sequences of reactions for targeting products that can be prepared from available starting materials (Woodward, 1966; Eschenmoser and Wintner, 1977; Corey, 1991; Eschenmoser, 2015; Nicolaou and Rigol, 2020). As chirality is a key feature of the small molecules of living organisms, the analysis and synthesis of the absolute configuration of the metabolites involved in the metabolic pathways of interest are of central importance. The synthetic methodologies rely either on the introduction of new chiral centers into the starting materials by asymmetric synthesis or by the utilization of bio-based starting materials with the naturally occurring stereochemical configuration such as the chiral pool of compounds, including amino acids, carbohydrates, or terpenes. Apart from the selection of the most suitable and easily available starting materials and a classical primary criteria for evaluating a synthetic route, such as yield, number of reaction steps, safety, health, environment or cost aspects, there are additional factors that have an influence on what is considered as the ideal synthesis of a given target compound (Gaich and Baran, 2010; Wender 2014; Peters et al., 2021). Highly chemoselective reactions which do not require the initial introduction of protecting groups and their later removal, not only reduce complexity and the waste generated, but are also a clear goal to provide support towards the ideal synthetic process (Young and Baran, 2009). The total time needed to prepare a metabolite from the starting materials available can be the predominant determining criterion for determining the ideal synthetic route (Hayashi, 2021). This can either be man-made in the laboratory or using the metabolic pathway adopted by biological organisms or a combination of both.

The goals of synthetic chemistry towards the ideal synthesis in the laboratory can be greatly facilitated by the metabolomic information available from the highly evolved thousands of biocatalytic reactions that occur naturally in biological cells. This provides a complimentary and fruitful interface for making use of "natures enzymes" to catalyze protecting-group free reactions with reduced complexity and minimal waste. The development and application of biocatalysis is therefore key to the science of small molecule synthesis and is enabling the move towards sustainable synthetic routes that contribute to the UN Sustainable Development Goals and the European Green Deal.

The first man-made synthesis of a metabolite occurring in living organisms from inorganic starting material (Wöhler, 1828), namely the synthesis of urea outside the kidney from ammonium cyanate, represented a milestone achievement and is

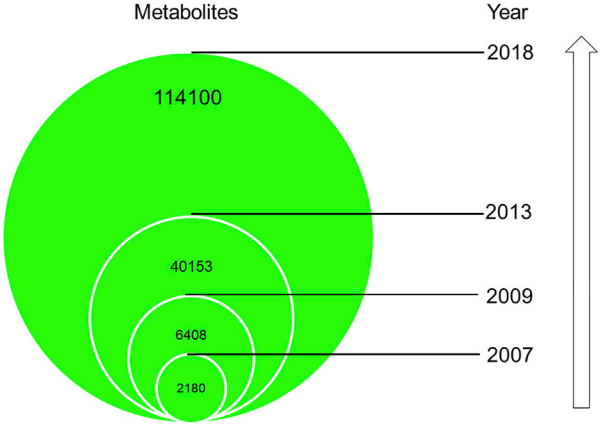

FIGURE 1
A diagrammatic representation of the growth of described metabolites from 2007 in the Human Metabolome Database (HMDB) as reported by Wishart et al. (2018).

of fundamental interest. From that time until today great advances have enabled the development of a large variety of synthetic processes for valuable metabolites. From the beginning, the question of fossil or bio-based starting materials can be illustrated by the initial development of the coal tar based chemical synthesis of indigo (Baeyer, 1900), which took over industrial manufacturing leading to a large increase in synthetic indigo production from petrochemicals, whereas the natural plant-based indigo production decreased. While economic determinants such as overall production costs are still prevailing, the increasing importance of health and environmental aspects are changing the boundary conditions and have revitalized the interest in bioprocesses towards one of the oldest and most often used indigo dyes (Mendoza-Avila et al., 2020). In addition, the industrial large-scale manufacturing of metabolites today needs to deal with new boundary conditions and increased attention to the safety, sustainability of the involved reactions and chemicals, industry sector-specific strategies and customer preferences for biobased starting materials. These conditions as well as numerous other factors, solubilities, thermodynamics, kinetics, downstream processing, product recovery and purification, have an influence on the final process design.

Biocatalysis and the exploration of its frontiers have inspired numerous biocatalytic process designs with high molecular economy (Wohlgemuth 2021; Alcántara et al., 2022). These have been realized in various ways, ranging from single step reactions to their combination with other biocatalytic or chemocatalytic reactions. This can be achieved by a variety of methods ranging from the use of purified enzymes or cell-free extracts, to the organization of the required enzymes in multi-enzyme assemblies both *in vitro* or *in vivo* using engineered whole-cells.

Synthetic access to the metabolite and metabolite-like molecular space

The interest and knowledge in the total metabolite molecular space of a biological organism, the metabolome, and the related metabolite-like small molecules interacting with enzymes has increased tremendously over the past 15 years. The metabolomes of biological organisms are of key importance together with its genomes, transcriptomes and proteomes. This is very clearly illustrated by the growth of the world's largest organism-specific metabolome database, the human metabolome database HMDB (Figure 1). The first release, HMDB 1.0 described 2,180 metabolites and its fourth release increased to 114,100 metabolites (Wishart et al., 2018).

Although the synthesis of metabolites goes back to the origins of organic chemistry and to the historic milestones in biochemistry, the actual gap between the number of known metabolites and the ones for which the synthesis has been reported is widening (Wohlgemuth, 2018). The question of why there is this widening gap and why the synthetic access to natural metabolites and metabolite-like molecules is important and relevant beyond the fundamental aspects of the science of synthesis, is connected with different areas of the life sciences, including biomedicine and industry. Having sufficient amounts of pure metabolites or metabolite-like compounds is essential in the analysis and identification of metabolites for the areas of metabolomics, enzyme assays, and discovery of novel biological functions. Enantiomerically pure metabolites are key to the precise kinetic characterization of enzymes and understanding their substrate enantioselectivity.

Chiral metabolites are more challenging to synthesize by traditional synthetic chemical methods, which often involve many steps including protection and deprotection of functional groups due to non-selective synthetic methods. Nature synthesizes chiral metabolites naturally in specific stereochemical configurations since enzymes themselves are chiral and are made up of L-aminoacids. This property means that enzymes will usually only use one enantiomer of a specific substrate. However some enzymes do show promiscuity especially when non-natural substrates are used in biocatalytic synthetic reactions. It has been shown that a change in L to D configuration in specific amino acids within a protein can result in its misfolding. When the protein structure cannot fold correctly this can lead to the production of amyloid deposits that cannot be degraded by natural proteases, so they accumulate in specific tissues such as the eyes and the brain. Specific racemase enzymes have been found in human tissue which can be responsible for this change (Ohide et al., 2011). The analysis of the chiral identity of metabolites is a powerful biomarker for monitoring of human disease and is an area for development within clinical medicine. The importance of being able to have standard metabolite molecules to identify these changes is of increasing importance. D-amino acids are naturally found in bacterial cell walls and are therefore associated with our microbiome (Bastings et al., 2019). The importance of understanding of an individual's microbiome and its symbiotic importance to human health is a topical research area. It is known that our microbiome is involved in immunity and the function of the gut barrier (Ruth and Field, 2013).

The synthesis of metabolites is essential in the development of new chemical entities intended for interacting with biological organisms, such as drugs for human and veterinary use or agrochemicals for plant protection. As the multitude of metabolites in a biological cell is achieved through a variety of natural biocatalytic reactions, the reduction of the complexity in the synthesis of a desired single metabolite can be carried out using a systems biocatalysis approach. This can use only the required biocatalytic reactions in cell free biocatalysis (Schmid-Dannert and López-Gallego, 2019; Bergquist et al., 2020; Sutiono et al., 2021), use cell-free biosynthesis (Morgado et al., 2016), use artificial metabolism (Fessner, 2015) or synthetic metabolism (Erb, 2019), all providing attractive strategies for the design of new biocatalytic processes for metabolite synthesis. The substrate scope of metabolic enzymes provides also an opportunity for the synthesis of metabolite-like molecules, which are of interest for potential new pharmaceuticals, since a major fraction of approved drugs have been shown to have a similarity to metabolites (Swainston et al., 2015). Although the importance of metabolites and metabolic pathways in connection with disease has long been known, it is only through recent scientific advances and discoveries that metabolites have attracted much attention, for example in metabolites as signatures of altered cancer cell metabolism associated with specific types of cancer (Ward and Thompson, 2012). Certain cancer-specific metabolites which are no longer seen as an indirect response to cancer cell proliferation but have themselves been shown to be oncogenic, have been designated as onco-metabolites (Leca et al., 2021).

Search and selection of optimal route, starting materials and biocatalysts

A key success factor for facile synthetic access to metabolites is the identification of the optimal route to the target molecules (Figure 2), whereby database, experience and retrosynthetic analysis tools in both the biochemical and chemical domains can provide valuable guidance. Suitable starting materials resulting from the disconnection of bonds of the target molecules in the retrosynthetic analysis can be evaluated according to criteria such as commercial availability, cost, fossil or biobased origin.

The starting materials for metabolite synthesis are an important consideration, also with respect to the reduction of

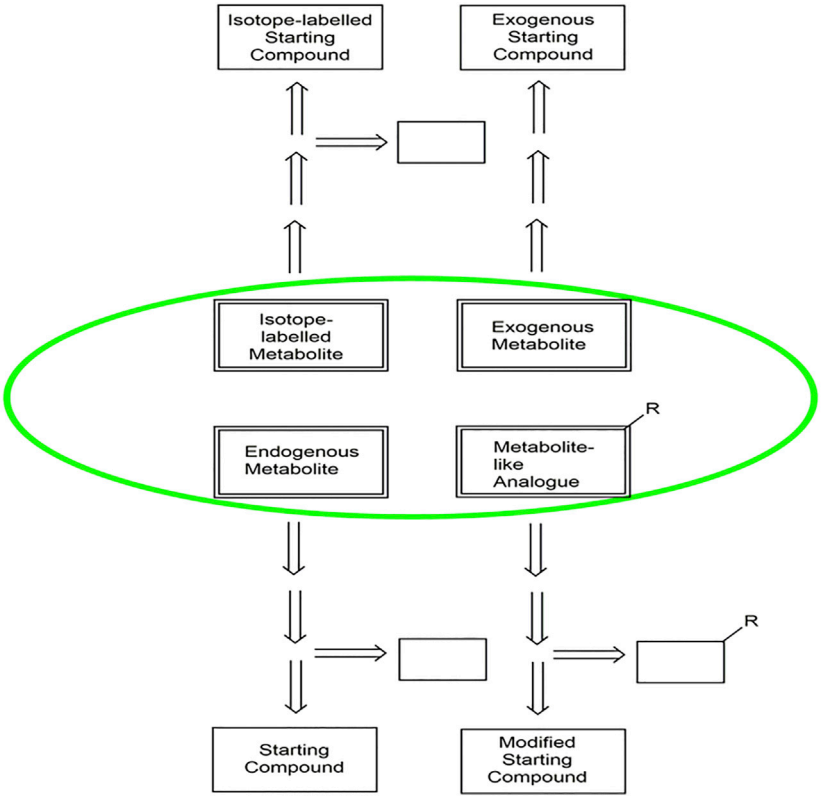

FIGURE 2
An overview of the selection of synthetic routes for endogenous metabolites, exogenous. metabolites, isotope-labelled metabolites and metabolite-like analogues, highlighted in. green. The arrows indicate the retrosynthetic pathways from the different classes of. metabolites to the starting compounds. The open boxes represent additional auxiliary. molecules in the different pathways.

complexity, because starting from highly reduced fossil-based starting materials the synthetic route to the metabolite can involve many more reaction steps and be more challenging than a straightforward defunctionalization reaction from a biobased starting material containing already many oxygen- and nitrogen-containing functional groups (Wohlgemuth, 2022).

The selection of suitable starting materials depends on various factors, such as availability, quality, stability, customer requirements, safety, health and environment aspects, economic conditions, or the supply chain. The stability of the supply chain in the long term, amid needs and sustainability considerations may also affect the choice of fossil-based versus biobased starting materials. A number of parallel developments are supporting research and development on the transition from fossil-based to biobased starting materials. The number and molecular diversity of biobased starting materials is continuously increasing, with many classical compounds already been traditionally manufactured from bioresources. Top platform chemicals have been identified, starting in 2004 by the United States Department of Energy (Werpy and Petersen, 2004) and updated in 2010 (Bozell and Petersen, 2010). Many more platform chemicals derived from bioresources are becoming available as biobased starting materials and new compounds derived by novel routes from bioresources are being developed (Jang et al., 2012; Choi et al., 2015). In order to develop syntheses using biobased resources which can replace petrochemicals, knowledge of the production of the starting material needs to be considered. A globally standardized and simple descriptor for the source of each compound is not only facilitating the clear choice between fossil-based and biobased starting materials, but is also beneficial for quality purposes.

Examples of biobased starting materials which are available at industrial large scale and can be considered as a substitute for the corresponding fossil-based starting materials can include a mix of older and newer compounds. These could be ethanol and related alcohols, 1,3-propanediol, glycerol, sugar alcohols like sorbitol and xylitol, organic acids like acetic acid, 3-hydroxypropanoic acid, lactic acid enantiomers, levulinic acid and succinic acid, furans like furfural, 5-hydroxymethylfurfural, and furan-2,5-dicarboxylic acid, or hydrocarbons like farnesene, isoprene and limonene. Matrices and biological materials which can be used as biobased starting materials are mainly derived

from natural photosynthesis, which provides inexpensive and renewable polysaccharides and biomass.

The move away from fossil based starting materials is being driven by the push towards a sustainable circular bioeconomy. With this in mind the optimal route and starting materials should be determined by the search and availability of the optimal biocatalysts. Enzymes have traditionally been classified into six main classes which is based on the type of reaction that they catalyze. This first classification was introduction by Dixon and Webb and was establishment as a fundamental enzyme classification scheme by the enzyme commission more than 60 years ago (McDonald and Tipton, 2022). However a major change of the system was introduced by the enzyme commission in 2018 with the establishment of a new seventh class named as translocases describing enzymes catalyzing transport across cell membranes (McDonald and Tipton, 2022). The concept of enzyme engineering for optimization of a particular process is now generally accepted. Hence a key factor is the initial selection of the most suitable biocatalysts, that can carry out the desired reactions in a highly selective, sustainable and energy efficient manner.

Gene sequencing techniques have rapidly developed in the last few years allowing the genomes of many animal, plant and microbial species to be available for identification of a host of new enzymes which can be characterised and produced for different metabolite synthesis. In addition the concept of metagenomics has allowed DNA to be isolated and sequenced from different unique environments. It is estimated that we can only cultivate 5% of the existing microorganisms found in nature so metagenomics allows identification of a wealth of new enzymes which would have escaped our current knowledge. New genes can be identified using a bioinformatic approach to search for a known class of enzyme using the amino acid sequence and known protein structural motifs. These motifs identified in known proteins are often specific for the binding of ATP and cofactors necessary for enzyme activity which can help with annotation. Protein structural space is restricted to a limited number of overall folds (arrangement of α-helices and β-sheets) that can be used in different proteins with a variety of different catalytic activities which can make the specific identification of many proteins difficult. However the increasing number of protein structures deposited in the Protein Data Bank, which currently exceeds 180,000, together with new improved modelling techniques based on artificial intelligence such as Alphafold2 (Jumper et al., 2021), have increased the amount of protein structural information available.

The use of expression libraries generated from available DNA sequences is another approach to identify new enzymes, which relies directly on enzyme activity. The DNA is cleaved into "gene size" fragments and inserted into expression plasmids which can be induced to over-express a library of many different gene products in a suitable host such as *Escherichia coli*. This library can be screened to identify single bacterial colonies that are able to grow on the selected substrate of interest by either direct visualisation of clearing zones on agar plates containing the substrate of interest or by colorimetric identification specific for a particular product. This technique allows the identification of enzyme activities against non-natural substrates and can identify different enzyme classes that are active against a particular substrate for example racemic γ-lactam (Taylor et al., 1993).

The metabolic pathways and genes are easier to identify from bacterial species since they are often encoded in tandem within the genome allowing one messenger RNA (polycistronic mRNA) to be expressed when the whole enzyme synthetic pathway is required by the microorganism. Also many bacteria have a secondary metabolism that it only turned on in response to different growth conditions hence it is important to consider genomics and proteomics. In addition to genomic DNA many bacteria carry genes on large plasmids which enable them to grow under specific conditions such as in the presence of camphor (McGhie and Littlechild, 2017).

In eukaryotes the genes within in a metabolic pathway are often more difficult to identify since they can be distributed over the genome and each gene contains several introns (uncoded regions) that have to be removed from the mature mRNA before it leaves the cell nucleus. Molecular biology techniques are used to copy the mature messenger mRNA to DNA using a viral reverse transcriptase enzyme to produce cDNA that can be cloned directly using suitable host systems such as *E. coli*. The cost and availability of synthetic gene synthesis now allows the rapid cloning of codon optimised DNA sequences which can be tailored to a chosen expression host. Advances in genome annotation and improved bioinformatic techniques will continue to allow the identification of new novel biocatalysts for metabolite synthesis.

As there can be a mismatch between the reaction requirements and the enzyme properties and performance, regarding activity, stability or enzyme inhibition, this can cause a problem. However enzyme engineering approaches provide a powerful tool for the optimization of enzyme performance. The enzymes can be evolved and optimised for the reaction conditions by directed evolution (Reetz, 2016; Arnold, 2018; Chen and Arnold, 2020) or rational protein engineering methods that are directed by the structural knowledge of the enzyme of interest and an understanding of its mechanism. Enzymes can also be identified from organisms that grow naturally at high temperatures which have evolved to be more robust and stable to extreme conditions and as such are better for industrial processes (Littlechild, 2015a,b; Littlechild, 2017).

While this enzyme optimization applies to both whole-cell and cell-free approaches, the effective contribution of metabolic engineering differs in whole-cell systems, cell-free lysates and cell-free systems using purified enzymes. While the blocking or repression of an enzyme which catalyzes the further conversion

of the metabolite in whole-cell systems is a well-established methodology, the large diversity of other enzymes in whole cells increase the likelihood of diverting the desired metabolite to by-products, which may be difficult to separate due to similar properties as the desired metabolite. Therefore, the contribution of metabolic engineering for optimizing the flux to the desired metabolite and reducing unwanted by-product formation is very important.

Enzyme optimisation for *in vitro* synthesis can be directly carried out with each enzyme optimised for stability and/or substrate specificity based on its structure and mechanistic properties. Other desired properties can be introduced using directed evolution as mentioned above. If whole cells are used for an *in vivo* synthesis using a synthetic cascade of enzymes this can be more challenging, however the designed cascade can be introduced into the host cells using a suitable plasmid and promotors for each individual enzyme. This can be approached using BioBricks cloning methodology (http://hdl.handle.net/10871/27323) where different genes are assembled with their own promotors within an expression vector. This is easier to carry out if a natural pathway is to be used, for example the synthesis of the natural extremolyte molecule 2,3-diphospho-D-glycerate that can protect cellular components to high temperatures (De Rose et al., 2021). However if a new synthetic pathway is designed problems of flux need to be addressed. Genetic manipulation of the host organism is often required to overcome these problems. It has been possible to alter the steady state flux in a cell by knockout of specific genes, replacing promotors and introduction of heterologous genes in a systems metabolic engineering approach (Brockman and Prather, 2015; Ko et al., 2020). Other approaches involve so called "precision engineering" where the design and engineering of systems use a cellular response to specific signals to optimise production strategies (McNerney et al., 2015). Computational modelling can address different problems in optimising metabolite production, for example control of enzyme expression, toxic pathway intermediates, and product inhibition of upstream enzymes.

Fast and meaningful experimental analytical assays are a key success factor for all types of enzyme optimizations. Analytical advances in droplet-based microfluidics and ultrahigh-throughput screening methods have led to practical benefits for rapid enzyme improvements (Colin et al., 2015; Bunzel et al., 2018; Gielen et al., 2018). Tremendous methodological advances in MS and NMR have enabled the combining of high information content with simplified, fast and sensitive analysis. The development of desorption electrospray ionization (DESI) mass spectrometry (Takáts et al., 2004) has provided a powerful analytical technology for rapid and direct analysis of enzymatic reactions without having to use labels (Morato et al., 2020; Morato et al., 2020; Kulathunga et al., 2022). Another powerful label-free analytical technology has been demonstrated by using micro-fluidics to sort nanoliter droplets whereby the droplets are split with direct detection by ESI-MS on one side, and on the second side with sorting according to the result of the ESI-MS analysis (Holland-Moritz et al., 2020).

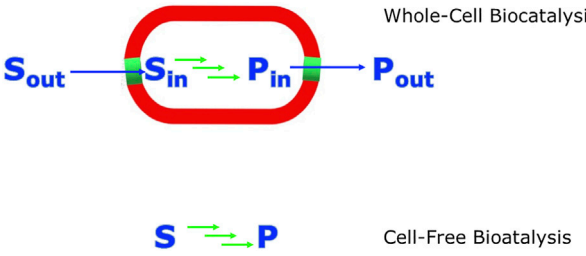

FIGURE 3
A schematic comparison of biocatalytic synthesis in whole-cell versus cell-free systems. The green arrows indicate the biocatalytic reaction steps involved. The blue arrows. indicate the transport of substrates and products across the cell membrane.

Advances in enzyme immobilisation techniques (Sheldon et al., 2021) have provided a cost-effective and sustainable way of using enzymes as recyclable heterogeneous catalysts, which are easier to be removed from the bioreactor vessels by either centrifugation or filtration.

Cell-free versus whole-cell biocatalytic systems

While the use of whole cells for producing metabolites has a long history, the use of cell free biocatalytic systems has attracted increasing interest over the last 20 years (Hodgman and Jewett, 2012; Swartz, 2018). To carry out biocatalytic reactions outside a living cell (cell-free, *in vitro*) the respective enzymes need to satisfy certain requirements, such as stability for the synthetic process. The thermodynamics and kinetics of natural pathways can facilitate the design of similar new bioprocess learning from naturally evolved flux of the enzymes which allow the pathway to flow in the desired direction. For newly designed synthetic and non-natural pathways where the energetics and flux is not favourable suitable adaptations need to be designed considering both thermodynamic and kinetic aspects. Metabolic engineering of whole-cells as well as cell-free systems can allow the choice of enzyme activities and their sequential arrangement to allow a favourable flux to drive the system to completion. Some interventions are much simpler for cell-free systems, for example precise coordination and temporal control of the reactions in a sequence by modifying the quantities of the enzyme catalysts used in relation to their different turnover rates. However this is more challenging in whole cell systems since the enzymes converting precursors into the desired

metabolite need to be optimized for their increased and coordinated expression. At the same time enzymes diverting precursors towards side products need to be repressed (Zalatan et al., 2015). A variety of molecular and engineering tools can be utilized for both whole-cell and cell-free systems to provide more favourable energetics. As whole-cell and cell-free systems (Figure 3) have their advantages and disadvantages the design of a hybrid bioprocess could divide the parts of a bioprocess which are best supported by a whole-cell and those by a cell-free system. The choice of the system depends on various boundary conditions which may also change over time such as economic aspects (Claassens et al., 2019).

If the process of biosynthesis is carried out *in vivo* by a natural pathway or the construction of synthetic enzyme cascades/pathways in whole cells, the cellular environment provides some protein stability and also the vital co-factors that are required for the activity of many of the natural enzymes. On the other hand this *in vivo* approach also requires that there is effective transport of the required substrates into the whole cells. In addition the transport of the synthesized metabolite products out of the whole cells needs to be optimized to avoid mass transport limitations, or the whole cells need to be disintegrated before the metabolites can be isolated and purified. The efficient and selective transport of products through the cell membranes out of the cells can be an advantage for the use of whole-cell systems. However the energetics of having in addition to the desired bioprocess, the need to sustain various other processes in whole-cells and the kinetics of the reactions and transport issues may limit the efficiency of the whole-cell bioprocesses. Another challenge for the use of whole cells in metabolite synthesis is the need to genetically delete enzymes which catalyze undesired side reactions of substrates, intermediates and products, thereby decreasing the efficiency of the bioprocess.

From the perspective of complexity reduction, carrying out a biosynthetic process *in vitro*, or *ex vivo*, as described over 25 years ago (Roessner and Scott, 1996), can overcome limitations of whole-cell approaches by the opportunity to focus only on the required reactions for optimizing productivity, diversity or new-to-nature metabolites. The use of cell-free systems, whether in the form of a crude cell lysate or composed of a number of isolated and purified enzymes, has some fundamental advantages compared to whole cell systems. This approach gives the opportunity to focus only on the required reactions and their optimization towards high productivity by avoiding product losses by unwanted side reactions, bypassing complex interactions of substrates, intermediates or products resulting in toxicity to whole cells, and simplifying product recovery and purification as the cell membrane/cell wall and complex cellular components are removed. The first demonstration of cell free biocatalytic processes was carried out in the 19th century by Eduard Buchner, who received the 1907 Nobel Prize in Chemistry "for his biochemical researches and his discovery of cell-free fermentation" (Buchner, 1897; Buchner 1907). Great advances have enabled the assembly of recombinant enzymes in a modular fashion, such as in the biocatalytic synthesis of metabolites of the natural aerobic and anaerobic vitamin B_{12} pathways using cell-free systems (Scott, 2003). Reproducible and stable biosynthesis of metabolic intermediates at submicromolar scale was the reason for moving from whole cell preparations of *Propionibacterium shermanii* to the cell-free synthesis of corrin metabolites such as cobyrinic acid from uroporphyrinogen III and aminolevulinic acid (Scott et al., 1973). The cell-free biocatalytic synthesis of the corrin metabolite hydrogenobyrinic acid from aminolevulinic acid, which uses 12 overexpressed enzymes for catalyzing 17 reaction steps in one pot, has been achieved with an overall yield of 20% (Roessner et al., 1994; 1995). A cell-free system containing nine enzymes, including auxiliary enzymes and cofactor regenerating enzymes, enabled the one-pot synthesis of nepetalactol or nepetalactone starting from geraniol at a much higher product concentration of about 1 g L^{-1} than the highest titer described for microbial systems (Bat-Erdene et al., 2021). The use of cell-free systems is highly attractive due to its modularity and continues to attract much interest in cell-free metabolic engineering (Dudley et al., 2015; Swartz, 2018) and synthetic biochemistry (Bowie et al., 2020).

Design of biocatalytic processes

Before starting the design of a biocatalytic process in the context of metabolite synthesis it is important to define the design goals. The most common design goal is to find the optimal synthetic route towards a desired metabolite in a target-oriented synthesis. There may however be other situations where the design goal is to find suitable targets which can be synthesized from a common starting material in a diversity-oriented synthesis, or to reduce complexity towards obtaining a compound most suited for a particular application in a function-oriented synthesis. While in target-oriented synthesis a major reason for synthesizing natural products has been to provide simplified access to the desired target product in a defined quality for its function, whereas the strategy of function-oriented synthesis is to achieve a desired function of the target product by design and with synthetic economy (Wender et al., 2008; Wender et al., 2015). Bioactive small molecules from natural resources are of great value for drug development and medicine, but simplification of their structural complexity by removing unnecessary or even disturbing substructures can overcome bottlenecks and limitations of their drug properties, pharmacokinetics, and synthesis (Wang et al., 2019).

This paper will concentrate on target-oriented synthesis for which Figure 4 highlights a number of key design tools. In this synthetic approach, retrosynthetic analysis in the chemical and

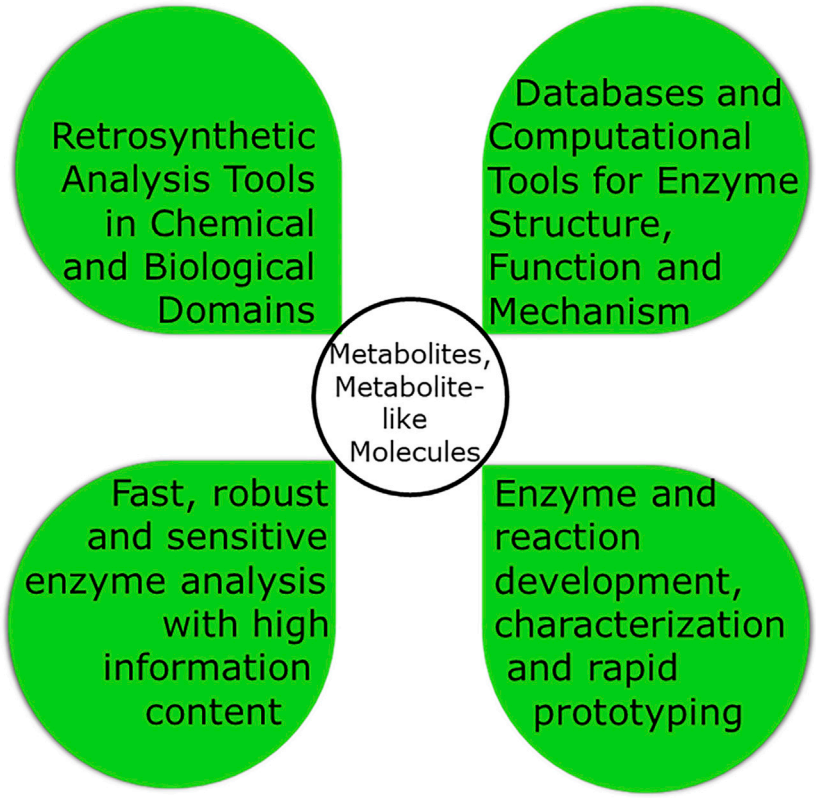

FIGURE 4
The four key aspects for the design of a biocatalytic process in target-oriented. synthesis of metabolites and metabolite-like molecules.

biological reaction space provides the background for navigating through the various routes which can be thought of from starting material to the product. Considering molecular economy aspects together with the lowest number of reaction steps is important for integrating multiple steps. Finally process intensification not only for the reaction but also for the product recovery and purification is essential for practical implementation. While biocatalytic process design is a complex task the increased experience with the innovation steps for successfully implemented bioprocesses provides an excellent practical knowledge base for innovation in systematic process design methods and for integrating various methodologies, such as protein and process engineering (Woodley, 2017).

Retrosynthetic analysis from both the biological as well a chemical perspective provides a design framework with which the most promising solutions can be used for rapid prototyping and obtaining a proof of principle (Wohlgemuth, 2017). The analysis of chemical and biological routes for the synthesis of metabolites often shows large differences in the number of reaction steps required to construct highly and differentially functionalized small molecules. Designing highly selective and straightforward biocatalytic one-step synthesis methods instead of lengthy and challenging chemical routes has been established as the preferred method for preparative access to a large number of valuable metabolites (Richter et al., 2009; Schell et al., 2009; Matsumi et al., 2014; Schoenenberger et al., 2017a; Hardt et al., 2017; Schoenenberger et al., 2018; Krevet et al., 2020; Schoenenberger et al., 2020; Sun et al., 2021). As the finding and selection of routes is a key task in target-oriented synthesis the development of appropriate methodologies has attracted much interest in both chemistry and biology. New tools for retrosynthetic analysis have been developed both in the domain of biochemical (Delépine et al., 2018; Lin et al., 2019; Hafner et al., 2021; MohammadiPeyhani et al., 2022) as well as chemical reactions (Mikulak-Klucznik et al., 2020).

Suitable methods with the necessary high information content, such as MS and NMR, for the analysis of the biocatalytic transformations and products are therefore a key success factor, both for the development and in-process control in the production phase (Jani et al., 2008; Gauss et al., 2014; Matsubara et al., 2014; Schoenenberger et al., 2017b).

The complexity of the downstream processing, product recovery and purification steps can be greatly reduced if simple purification methods such as crystallization,

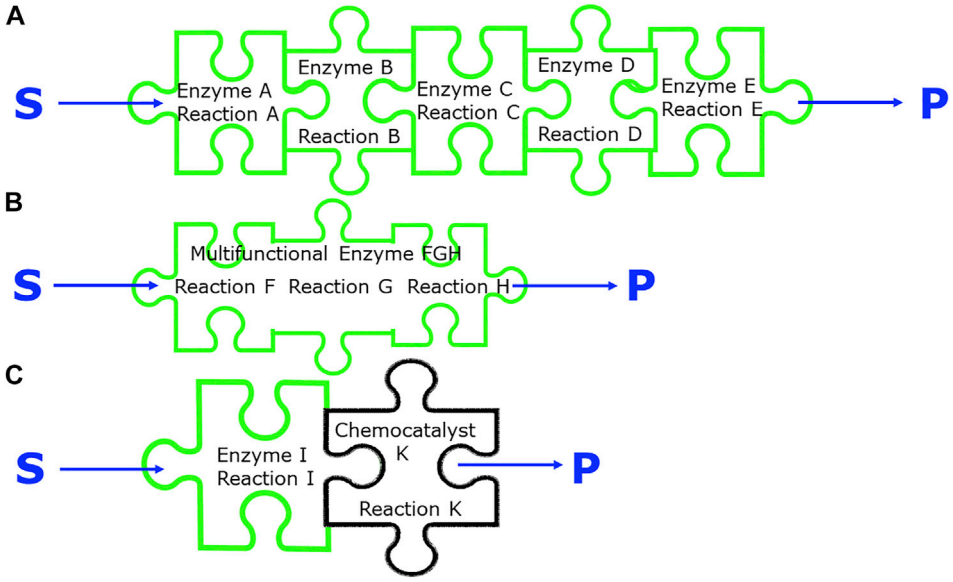

FIGURE 5
Different integration strategies of biocatalytic processes, **(A)** use of five different enzymes. in a sequential reaction cascade or simultaneously in a one-pot reaction, **(B)** use of one multifunctional enzyme catalyzing three related reactions, **(C)** use of a biocatalytic and a chemocatalytic reaction in a sequential reaction or in a one-pot reaction.

precipitation, extraction, phase separation, or distillation, which have been successfully designed for one metabolite, can be transferred to other metabolites of the same class (Wohlgemuth, 2011).

Integration of biocatalytic reactions

Biocatalytic reactions can be integrated along the paths of multiple biocatalytic reactions steps (Figure 5), or along biocatalytic and classical chemical reaction steps, or along the reaction, downstream processing and product recovery steps. Considering molecular economy aspects together with the lowest number of reaction steps is important for integrating multiple steps. The relevant aspects of molecular economy for step integration include the optimization of the step economy by reducing the number of reaction steps, by more direct transformations or by eliminating protection-deprotection schemes, by avoiding intermediate isolation and downstream processing steps through coupling several reaction steps in one pot. The examples of the manufacturing processes for mevalonate 5-phosphate (Matsumi et al., 2014), shikimate-3-phosphate (Schoenenberger et al., 2018), tagatose-1,6-diphosphate (Schoenenberger et al., 2020), 2-keto-3-deoxy-D-gluconate (Matsubara et al., 2014) and L-argininosuccinate (Schoenenberger et al., 2017a) demonstrate the importance of complexity reduction. This can be achieved by reducing the number of steps, avoiding protecting groups, selective biocatalytic phosphorylation reactions, selective defunctionalization and simple addition reactions reducing complex chemical multi-step routes.

Multiple biocatalytic reaction steps can be achieved by having a multifunctional biocatalyst catalyzing more than one reaction step, a principle used by nature, for example in case of the polyketide synthases and the non-ribosomal peptide synthetases (Adrover-Castellano et al., 2021). This is also of much interest for biocatalytic synthesis as demonstrated by the recent discovery of a multifunctional biocatalyst EneIRED, which can catalyse conjugate reduction, as well as imine reduction and reductive amination of a broad range of simple prochiral substrates to diastereomeric amines in one-pot (Thorpe et al., 2022). An already classical way of integration is the assembly of multiple biocatalysts acting in a reaction sequence, with each biocatalyst catalyzing one specific reaction step (Roessner and Scott, 1996; Cutlan et al., 2020).

There are many examples of enzyme cascades being effectively used in "one pot" reactions such as the production of plant benzylisoquinoline alkaloids using purified enzymes (Lichman et al., 2015; Zhao et al., 2018). The construction of process models is commonly carried out to help understand the enzyme reactions and their optimisation for scale-up (Finnigan et al., 2019). The biocatalytic conversion of 4-methyl toluate to 4-tolyl alcohol, which involved at least seven enzymes in three reaction steps and included cofactor recycling, has been optimized by the use and validation of process models based on characterized enzyme parts (Finnigan et al., 2019). An

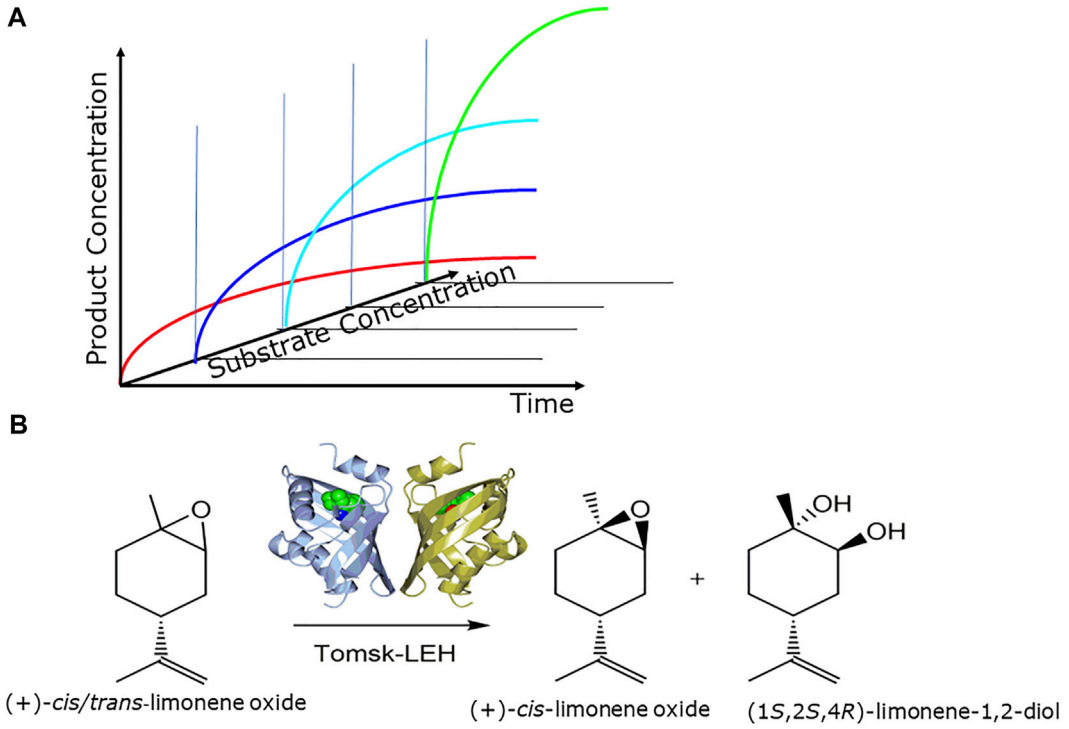

FIGURE 6
(A) Optimizing process metrics by increasing substrate concentration while maintaining complete conversion, **(B)** intensification of epoxide-hydrolase catalyzed resolutions of (+)-and (−)-cis/trans-limonene oxides, as illustrated for the Tomsk limonene epoxide hydrolase (LEH) for the production of (+)-cis-limonene oxide and the (1S,2S,4R)- limonene-1,2-diol (Ferrandi et al., 2015b).

approach combining experimental enzyme kinetics with pathway modelling has been successfully applied to a reaction sequence for the preparation of 2-ketoglutarate from D-xylose, using five enzymes of the Weimberg pathway in a cell-free system (Shen et al., 2020). Linear biocatalytic reaction cascades have attracted increasing interest over the last years and offer excellent synthetic opportunities with the reduced complexity of designing biocatalytic reaction sequences from well-characterized single biocatalytic reactions operating in a simultaneous or sequential mode (Schrittwieser et al., 2018). In cases where some biocatalysts of a reaction sequence show only sufficient activities in whole cells, for example membrane-bound enzymes for which no active variant is available in soluble form, the combination of biocatalysts in purified form as well as in whole cells represents another integration opportunity. The plant metabolite *cis*-(+)-12-oxophytodienoic acid has been synthesized in good yield, high diastereoselectivity and low side product formation from linolenic acid by a cascade of three biocatalytic reactions involving lipoxygenase 13-LOX as an isolated enzyme and recombinant *E. coli* whole cells expressing the *Arabidopsis thaliana* genes encoding allene oxide synthase AOS and allene oxide cyclase AOC2 (Löwe et al., 2020). Integration of several biocatalytic reaction steps can be achieved by searching for a novel biocatalyst which is able to catalyze a more direct reaction route to the target product. It is important to know all of the enzymes in the natural biosynthetic route to a metabolite and any missing enzymes need to be identified (Caputi et al., 2018).

While natural pathway enzymes provide within their substrate scope facile synthetic access to metabolites or metabolite-like molecules, more diversified and non-natural metabolite-like compounds can become accessible by broadening of the substrate by enzyme engineering, by introducing new catalytic activities with non-natural substrates and by developing new chemical transformations by combining chemistry and protein engineering (Miller et al., 2022). The transformations which can effectively be performed by either a classical chemical reaction, a chemocatalytic or a biocatalytic reaction can enable the combination of the two worlds of classical organic synthesis and biocatalysis (Wohlgemuth, 2007; Roberts et al., 2010; Rudroff et al., 2018; Bering et al., 2022).

In cases where no enzymes are known to catalyze a particular reaction, the integration of chemocatalytic and enzymatic transformations in a one-pot process offers a synthetic opportunity, if mutually compatible reaction conditions can be found and any interfering cross-reactions and

incompatibilities can be overcome. Regioselective C–H bond functionalization methods have been developed with halogenase enzymes and palladium-catalysed cyanation together with the incorporation of nitrile hydratase or nitrilase enzymes. This type of two- or three-component chemobiocatalytic system can be carried out in "one pot" at gram scale (Craven et al., 2021).

Intensification of biocatalytic processes

The increase of the overall productivity of the prototype of the integrated biocatalytic procedure is essential for reaching a viable manufacturing process. The intensification of biocatalytic processes needs to take into account upstream, biocatalytic reaction and downstream phases (Boodhoo et al., 2022). The use of simple process metrics such as reaction yield, space-time yield, product concentration (Figure 6A) is thereby not only valuable for characterizing and comparing process performance in the course of intensifying, scaling and implementing biocatalytic processes, but also for setting targets for protein engineering and process engineering (Woodley 2017).

An important starting point for process development are the available process windows for favorable thermodynamics and stabilities of the components of the biocatalytic reactions, such as enzymes, substrates, intermediates and products, under the reaction conditions. While a variety of powerful methodologies are available for engineering the properties and stabilities of enzymes to match the optimum reaction conditions, the properties and stabilities of products can determine the reaction conditions, or otherwise product modifications need to be considered. In a next intensification phase biocatalytic reaction engineering aiming at complete substrate to product conversion and minimizing the formation of side products is an essential intermediate phase. In the final intensification phase the increase of the substrate concentration and the decrease of the enzyme usage is optimized for achieving the highest space-time yield, while maintaining the complete conversion and highest product purity from the previous intensification phase.

Overall biocatalytic process intensification builds on optimizing each biocatalytic reaction involved, since one single bottleneck in a biocatalytic reaction affects the entire process. This is illustrated with the biocatalytic process intensification for the synthesis of important chiral lactaldehyde and limonene oxide metabolites. The application of novel thermostable epoxide hydrolases (Ferrandi et al., 2015a). which are also stable in organic solvents, facilitates the use of poorly water-soluble substrates at high substrate concentrations. Complementary limonene-1,2-epoxide hydrolases have been applied in the process intensification up to 2 M substrate concentrations for the synthesis of all limonene oxide enantiomers as well as (1*S*,2*S*,4*R*)-limonene-1,2-diol and (1*R*,2*R*,4*S*)-limonene-1,2-diol (Ferrandi et al., 2015b) as illustrated in Figure 6B. The key ketoreductase-catalyzed asymmetric reduction steps in the synthesis of enantiomerically pure (*R*)- and (*S*)-lactaldehydes have been intensified in two development phases, whereby the substrate concentration could be increased from 6 to 250 g L^{-1}, the cofactor concentration could be decreased from 0.8 to 0.05 g L^{-1}, while maintaining complete conversion and excellent chemical and enantiomeric purity (Vogel et al., 2016).

Downstream processing methods with full product recovery in high quality are as important as the intensification of the reaction with complete conversion and are a key success factor for achieving viable processes with high overall resource efficiency. A variety of methodologies and tools are available for the intensification of metabolite downstream processing, recovery and purification (Wohlgemuth, 2009). Simple extraction optimization is illustrated by the examples of the complete extraction of enantiomerically pure 1,1-dimethoxy-2-propanols, which has been achieved by saturating the aqueous reaction solution with sodium chloride (Vogel et al., 2016). Working within process windows for product stability is essential in case of labile products for maintaining the product quality during downstream operations (Gauss et al., 2016). Simple product recovery and purification methodologies, such as phase separation, crystallization, or extraction, are attractive for intensification. However chromatographic separation may be needed, where simulated moving bed chromatography can be successfully used in the intensification of efficient separations of equimolar mixtures, such as enantiomerically pure regioisomeric lactones (Kaiser et al., 2009).

Process intensification over a convergent multistep reaction cascade in one pot has been demonstrated by the biocatalytic synthesis of MK-1454 (McIntosh et al., 2022). Process intensification phases involved classical optimization of reaction conditions, directed evolution of cyclic guanosine-adenosine synthase, optimizing cofactors and cosolvents, increasing substrate concentration, enzyme engineering of cyclic guanosine-adenosine synthase under optimized reaction conditions (Benkovics et al., 2022), which has intensified this biocatalytic process and improved the initial yield of less than 1%–91% (Benkovics et al., 2022).

Discussion

The large "natural" reserve of known biocatalysts and the tremendous advances in tools and methodologies for designing, integrating and intensifying biocatalytic reactions are providing benefits and opportunities for future biocatalytic processes for the synthesis of metabolites and metabolite-like molecules. The

high selectivity of natural biocatalysts removes the need for protection and deprotection reactions and reduces the complexity of functional group transformations thereby significantly simplifying the synthesis of more complex products. The metabolic pathways in biological cells and new synthetic pathways for metabolites and metabolite-like molecules, can provide blueprints and starting points for biocatalytic platform technologies. The interaction of scientific disciplines of classical organic chemistry and biocatalysis in total synthesis, microbial whole-cell and cell-free approaches in design and integration, or reaction/process engineering with protein engineering has allowed a multidisciplinary research community to be established to drive forward the synthesis of metabolite and metabolite-like molecules for their many potential future applications.

Author contributions

JL and RW have contributed equally to the writing and preparation of this manuscript.

Acknowledgments

The COST organization is gratefully acknowledged for supporting the SysBiocat COST Action CM1303.

Conflict of interest

The authors declare that the research was conducted in the absence of any commercial or financial relationships that could be construed as a potential conflict of interest.

Publisher's note

All claims expressed in this article are solely those of the authors and do not necessarily represent those of their affiliated organizations, or those of the publisher, the editors and the reviewers. Any product that may be evaluated in this article, or claim that may be made by its manufacturer, is not guaranteed or endorsed by the publisher.

References

Adrover-Castellano, M. L., Schmidt, J. J., and Sherman, D. H. (2021). Biosynthetic cyclization catalysts for the assembly of peptide and polyketide natural products. *ChemCatChem* 13 (9), 2095–2116. doi:10.1002/cctc.202001886

Alcántara, A. R., Domínguez de María, P., Littlechild, J. A., Schürmann, M., Sheldon, R. A., and Wohlgemuth, R. (2022). Biocatalysis as key to sustainable industrial chemistry. *ChemSusChem* 15 (9), e202102709. doi:10.1002/cssc.202102709

Arnold, F. H. (2018). Directed evolution: Bringing new chemistry to life. *Angew. Chem. Int. Ed.* 57 (16), 4143–4148. doi:10.1002/anie.201708408

Baeyer, A. V. (1900). Zur geschichte der indigo-synthese. *Ber. Dt. Ges. Chem.* 33, LI–LXX. doi:10.1002/cber.190003303211

Bastings, J. J. A. J., Eijk, H. M., Olde Damink, S. W., and Rensen, S. S. (2019). D-Amino acids in health and disease: A focus on cancer. *Nutrients* 11, 2205. doi:10.3390/nu11092205

Bat-Erdene, U., Billingsley, J. M., Turner, W. C., Lichman, B. R., Ippoliti, F. M., Garg, N. K., et al. (2021). Cell-free total biosynthesis of plant terpene natural products using an orthogonal cofactor regeneration system. *ACS Catal.* 11 (15), 9898–9903. doi:10.1021/acscatal.1c02267

Benkovics, T., Peng, F., Phillips, E. M., An, C., Bade, R. S., Chung, C. K., et al. (2022). Diverse catalytic reactions for the stereoselective synthesis of cyclic dinucleotide MK-1454. *J. Am. Chem. Soc.* 144, 5855–5863. doi:10.1021/jacs.1c12106

Bergquist, P. L., Siddiqui, S., and Sunna, A. (2020). Cell-free biocatalysis for the production of platform chemicals. *Front. Energy Res.* 8, 193. doi:10.3389/fenrg.2020.00193

Bering, L., Thompson, J., and Micklefield, J. (2022). New reaction pathways by integrating chemo- and biocatalysis. *Trends Chem.* 4, 392–408. doi:10.1016/j.trechm.2022.02.008

Boodhoo, K. V. K., Flickinger, M. C., Woodley, J. M., and Emanuelsson, E. A. C. (2022). Bioprocess intensification: A route to efficient and sustainable biocatalytic transformations for the future. *Chem. Eng. Process. - Process Intensif.* 172, 108793. doi:10.1016/j.cep.2022.108793

Bowie, J. U., Sherkhanov, S., Korman, T. P., Valliere, M. A., Opgenorth, P. H., Liu, H., et al. (2020). Synthetic biochemistry: The bio-inspired cell-free approach to commodity chemical production. *Trends Biotechnol.* 38 (7), 766–778. doi:10.1016/j.tibtech.2019.12.024

Bozell, J. J., and Petersen, G. R. (2010). Technology development for the production of biobased products from biorefinery carbohydrates - The US Department of Energy's "Top 10" revisited. *Green Chem.* 12 (4), 539. doi:10.1039/B922014C

Brockman, I, M., and Prather, K. L. J. (2015). Dynamic metabolic engineering: New strategies for developing responsive cell factories. *Biotechnol. J.* 10 (9), 1360–1369. doi:10.1002/biot.201400422

Buchner, E. (1897). Alkoholische Gährung ohne Hefezellen. *Ber. Dtsch. Chem. Ges.* 30 (1), 117–124. doi:10.1002/cber.18970300121

Buchner, E. (1907). *Cell-free fermentation*. Nobel Lecture. Available at: https://www.nobelprize.org/uploads/2018/06/buchner-lecture.pdf.

Bunzel, H. A., Garrabou, X., Pott, M., and Hilvert, D. (2018). Speeding up enzyme discovery and engineering with ultrahigh-throughput methods. *Curr. Opin. Struct. Biol.* 48, 149–156. doi:10.1016/j.sbi.2017.12.010

Caputi, L., Franke, J., Farrow, S. C., Chung, K., Payne, R. M., Nguyen, T. D., et al. (2018). Missing enzymes in the biosynthesis of the anticancer drug vinblastine in Madagascar periwinkle. *Science* 360 (6394), 1235–1239. doi:10.1126/science.aat4100

Chen, K., and Arnold, F. H. (2020). Engineering new catalytic activities in enzymes. *Nat. Catal.* 3 (3), 203–213. doi:10.1038/s41929-019-0385-5

Choi, S., Song, C. W., Shin, J. H., and Lee, S. Y. (2015). Biorefineries for the production of top building block chemicals and their derivatives. *Metab. Eng.* 28, 223–239. doi:10.1016/j.ymben.2014.12.007

Claassens, N. J., Burgener, S., Vögeli, B., Erb, T. J., and Bar-Even, A. (2019). A critical comparison of cellular and cell-free bioproduction systems. *Curr. Opin. Biotechnol.* 60, 221–229. doi:10.1016/j.copbio.2019.05.003

Colin, P. Y., Kintses, B., Gielen, F., Miton, C. M., Fischer, G., Mohamed, M. F., et al. (2015). Ultrahigh-throughput discovery of promiscuous enzymes by picodroplet functional metagenomics. *Nat. Commun.* 6, 10008. doi:10.1038/ncomms10008

Corey, E. J. (1991). The logic of chemical synthesis: Multistep synthesis of complex carbogenic molecules (Nobel lecture). *Angew. Chem. Int. Ed. Engl.* 30 (5), 455–465. doi:10.1002/anie.199104553

Craven, E. J., Latham, J., Shepherd, S. A., Khan, I., Diaz-Rodriguez, A., Greaney, M. F., et al. (2021). Programmable late-stage C–H bond functionalization enabled by integration of enzymes with chemocatalysis. *Nat. Catal.* 4, 385–394. doi:10.1038/s41929-021-00603-3

Cutlan, R., De Rose, S., Isupov, M. N., Littlechild, J. A., and Harmer, N. J. (2020). Using enzyme cascades in biocatalysis: Highlight on transaminases and carboxylic

acid reductases. *Biochimica Biophysica Acta - Proteins Proteomics* 1868, 140322. doi:10.1016/j.bbapap.2019.140322

De Rose, S, A., Finnigan, W., Harmer, N. J., and Littlechild, J. A. (2021). Production of the extremolyte cyclic 2, 3-diphosphoglycerate using *Thermus thermophilus* as a whole-cell factory. *Front. Catal.* 1, 803416. doi:10.3389/2fctls.2021.803416

Delépine, B., Duigouc, T., Carbonell, P., and Faulon, J. L. (2018). RetroPath2.0: A retrosynthesis workflow for metabolic engineers. *Metab. Eng.* 45, 158–170. doi:10.1016/j.ymben.2017.12.002

Dudley, Q. M., Karim, A. S., and Jewett, M. C. (2015). Cell-free metabolic engineering: Biomanufacturing beyond the cell. *Biotechnol. J.* 10 (1), 69–82. doi:10.1002/biot.201400330

Erb, T. J. (2019). Structural organization of biocatalytic systems: The next dimension of synthetic metabolism. *Emerg. Top. Life Sci.* 3, 579–586. doi:10.1042/ETLS20190015

Eschenmoser, A. (2015). Introductory remarks on the publication series 'corrin syntheses-parts I-vi'. *Helv. Chim. Acta* 98, 1475–1482. doi:10.1002/hlca.201400399

Eschenmoser, A., and Wintner, C. E. (1977). Natural Product Synthesis and Vitamin B12: Total synthesis of vitamin B12 provided a framework for exploration in several areas of organic chemistry. *Science* 196 (4297), 1410–1420. doi:10.1126/science.867037

Ferrandi, E. E., Marchesi, C., Annovazzi, C., Riva, S., Monti, D., Wohlgemuth, R., et al. (2015b). Efficient epoxide hydrolase catalyzed resolutions of (+)-and (−)-cis/trans-Limonene oxides. *ChemCatChem* 7 (19), 3171–3178. doi:10.1002/cctc.201500608

Ferrandi, E. E., Sayer, C., Isupov, M. N., Annovazzi, C., Marchesi, C., Iacobone, G., et al. (2015a). Discovery and characterization of thermophilic limonene-1, 2-epoxide hydrolases from hot spring metagenomic libraries. *FEBS J.* 282 (15), 2879–2894. doi:10.1111/febs.13328

Fessner, W. D. (2015). Systems Biocatalysis: Development and engineering of cell-free "artificial metabolisms" for preparative multi-enzymatic synthesis. *N. Biotechnol.* 32, 658–664. doi:10.1016/j.nbt.2014.11.007

Finnigan, W., Cutlan, R., Snajdrova, R., Adams, J. P., Littlechild, J. A., Harmer, N. J., et al. (2019). Engineering a seven enzyme biotransformation using mathematical modelling and characterized enzyme parts. *ChemCatChem* 11, 3474–3489. doi:10.1002/cctc.201900646

Gaich, T., and Baran, P. S. (2010). Aiming for the ideal synthesis. *J. Org. Chem.* 75, 4657–4673. doi:10.1021/jo1006812

Gauss, D., Schoenenberger, B., Molla, G. S., Kinfu, B. M., Chow, J., Liese, A., et al. (2016). "Biocatalytic phosphorylation of metabolites," in *Applied biocatalysis – from fundamental science to industrial applications*. Editors A. Liese, L. Hilterhaus, U. Kettling, and G. Antranikian (Weinheim, Germany: Wiley VCH).

Gauss, D., Schoenenberger, B., and Wohlgemuth, R. (2014). Chemical and enzymatic methodologies for the synthesis of enantiomerically pure glyceraldehyde 3-phosphates. *Carbohydr. Res.* 389, 18–24. doi:10.1016/j.carres.2013.12.023

Gielen, F., Colin, P-Y., Mair, P., and Hollfelder, F. (2018). Ultrahigh-throughput screening of single-cell lysates for directed evolution and functional metagenomics. *Methods Mol. Biol.* 1685, 297–309. doi:10.1007/978-1-4939-7366-8_18

Hafner, J., Payne, J., MohammadiPeyhani, H., Hatzimanikatis, V., and Smolke, C. A. (2021). A computational workflow for the expansion of heterologous biosynthetic pathways to natural product derivatives. *Nat. Commun.* 12, 1760. doi:10.1038/s41467-021-22022-5

Hardt, N., Kinfu, B. M., Chow, J., Schoenenberger, B., Streit, W. R., Obkircher, M., et al. (2017). Biocatalytic asymmetric phosphorylation catalyzed by recombinant glycerate-2-kinase. *ChemBioChem* 18 (15), 1518–1522. doi:10.1002/cbic.201700201

Hayashi, Y. (2021). Time economy in total synthesis. *J. Org. Chem.* 86, 1–23. doi:10.1021/acs.joc.0c01581

Hodgman, C. E., and Jewett, M. C. (2012). Cell-free synthetic biology: Thinking outside the cell. *Metab. Eng.* 14, 261–269. doi:10.1016/j.ymben.2011.09.002

Holland-Moritz, D. A., Wismer, M. K., Mann, B. F., Farasat, I., Devine, P., Guetschow, E. D., et al. (2020). Mass activated droplet sorting (mads) enables high-throughput screening of enzymatic reactions at nanoliter scale. *Angew. Chem. Int. Ed.* 59 (11), 4470–4477. doi:10.1002/anie.201913203

Jang, Y.-S., Kim, B., Shin, J. H., Choi, Y. J., Choi, S., Song, C. W., et al. (2012). Bio-based production of C2–C6 platform chemicals. *Biotechnol. Bioeng.* 109 (10), 2437–2459. doi:10.1002/bit.24599

Jani, P., Emmert, J., and Wohlgemuth, R. (2008). Process analysis of macrotetrolide biosynthesis during fermentation by means of direct infusion LC-MS. *Biotechnol. J.* 3 (2), 202–208. doi:10.1002/biot.200700174

Jumper, J., Evans, R., Pritzel, A., Green, T., Figurnov, M., Ronneberger, O., et al. (2021). Highly accurate protein structure prediction with alphafold. *Nature* 596 (7873), 583–589. doi:10.1038/s41586-021-03819-2

Kaiser, P., Ottolina, G., Carrea, G., and Wohlgemuth, R. (2009). Preparative-scale separation by simulated moving bed chromatography of biocatalytically produced regioisomeric lactones. *New Biotechnol.* 25 (4), 220–225. doi:10.1016/j.nbt.2009.01.005

Ko, Y. S., Kim, J. W., Lee, J. A., Han, T., Kim, G. B., Park, J. E., et al. (2020). Tools and strategies of systems metabolic engineering for the development of microbial cell factories for chemical production. *Chem. Soc. Rev.* 49 (14), 4615–4636. doi:10.1039/D0CS00155D

Krevet, S., Shen, L., Bohnen, T., Schoenenberger, B., Meier, R., Obkircher, M., et al. (2020). Enzymatic synthesis of 2-keto-3-deoxy-6-phosphogluconate by the 6-phosphogluconate-dehydratase from *Caulobacter crescentus*. *Front. Bioeng. Biotechnol.* 8, 185. doi:10.3389/fbioe.2020.00185

Kulathunga, S. C., Morato, N. M., Zhou, Q., Cooks, R. G., and Mesecar, A. D. (2022). Desorption electrospray ionization mass spectrometry assay for label-free characterization of SULT2B1b enzyme kinetics. *ChemMedChem* 17 (9), e202200043. doi:10.1002/cmdc.202200043

Leca, J., Fortin, J., and Mak, T. W. (2021). Illuminating the cross-talk between tumor metabolism and immunity in IDH-mutated cancers. *Curr. Opin. Biotechnol.* 68, 181–185. doi:10.1016/j.copbio.2020.11.013

Lichman, B. R., Lamming, E. D., Pesnot, T., Smith, J. M., Hailes, H. C., and Ward, J. M. (2015). One-pot triangular chemoenzymatic cascades for the syntheses of chiral alkaloids from dopamine. *Green Chem.* 17 (2), 852–855. doi:10.1039/C4GC02325K

Lin, G. M., Warden-Rothman, R., and Voigt, C. A. (2019). Retrosynthetic design of metabolic pathways to chemicals not found in nature. *Curr. Opin. Syst. Biol.* 14, 82–107. doi:10.1016/j.coisb.2019.04.004

Littlechild, J. A. (2015a). Archaeal enzymes and applications in industrial biocatalysts. *Archaea* 2015, 147671. doi:10.1155/2015/147671

Littlechild, J. A. (2015b). Enzymes from extreme environments and their industrial applications. *Front. Bioeng. Biotechnol.* 3, 161. doi:10.3389/fbioe.2015.00161

Littlechild, J. A. (2017). Improving the 'tool box' for robust industrial enzymes. *J. Ind. Microbiol. Biotechnol.* 44, 711–720. doi:10.1007/s10295-017-1920-5

Löwe, J., Dietz, K. J., and Gröger, H. (2020). From a biosynthetic pathway toward a biocatalytic process and chemocatalytic modifications: Three-step enzymatic cascade to the plant metabolite cis-(+)-12-OPDA and metathesis-derived products. *Adv. Sci.* 7 (13), 1902973. doi:10.1002/advs.201902973

Matsubara, K., Köhling, R., Schönenberger, B., Kouril, T., Esser, D., Bräsen, C., et al. (2014). One-step synthesis of 2-keto-3-deoxy-D-gluconate by biocatalytic dehydration of D-gluconate. *J. Biotechnol.* 191, 69–77. doi:10.1016/j.jbiotec.2014.06.005

Matsumi, R., Hellriegel, C., Schoenenberger, B., Milesi, T., Van Der Oost, J., Wohlgemuth, R., et al. (2014). Biocatalytic asymmetric phosphorylation of mevalonate. *RSC Adv.* 4, 12989. doi:10.1039/C4RA01299B

McDonald, A., and Tipton, K. F. (2022). Enzyme nomenclature and classification: The state of the art. *FEBS J.* doi:10.1111/febs.16274

McGhie, E. J., and Littlechild, J. A. (2017). The purification and crystallisation of 2, 5-diketocamphane 1, 2-monooxygenase and 3, 6-diketocamphane 1, 6-monooxygenase from *Pseudomonas putida* NCIMB 10007. *Biochem. Soc. Trans.* 24 (1), 29S. doi:10.1042/bst024029s

McIntosh, J. A., Liu, Z., Andresen, B. M., Marzijarani, N. S., Moore, J. C., Marshall, N. M., et al. (2022). A kinase-cGAS cascade to synthesize a therapeutic STING activator. *Nature* 603 (7901), 439–444. doi:10.1038/s41586-022-04422-9

McNerney, M. P., Watstein, D. N., and Styczynski, M. P. (2015). Precision metabolic engineering: The design of responsive, selective, and controllable metabolic systems. *Metab. Eng.* 31, 123–131. doi:10.1016/j.ymben.2015.06.011

Mendoza-Avila, J., Chauhan, K., and Vazquez-Duhalt, R. (2020). Enzymatic synthesis of indigo-derivative industrial dyes. *Dyes Pigments* 178, 108384. doi:10.1016/j.dyepig.2020.108384

Mikulak-Klucznik, B., Gołębiowska, P., Bayly, A. A., Popik, O., Klucznik, T., Szymkuć, S., et al. (2020). Computational planning of the synthesis of complex natural products. *Nature* 588, 83–88. doi:10.1038/s41586-020-2855-y

Miller, D. C., Athavale, S. V., and Arnold, F. H. (2022). Combining chemistry and protein engineering for new-to-nature biocatalysis. *Nat. Synth.* 1, 18–23. doi:10.1038/s44160-021-00008-x

MohammadiPeyhani, H., Hafner, J., Sveshnikova, A., Viterbo, V., and Hatzimanikatis, H. (2022). Expanding biochemical knowledge and illuminating metabolic dark matter with ATLASx. *Nat. Commun.* 13, 1560. doi:10.1038/s41467-022-29238-z

Morato, N. M., Holden, D. T., and Cooks, R. G. (2020). High-throughput label-free enzymatic assays using desorption electrospray-ionization mass spectrometry. *Angew. Chem. Int. Ed.* 59, 20459–20464. doi:10.1002/anie.202009598

Morgado, G., Gerngross, D., Roberts, T. M., and Panke, S. (2016). "Synthetic biology for cell-free biosynthesis: Fundamentals of designing novel *in vitro* multi-enzyme reaction networks," in *Synthetic biology-metabolic engineering. Adv. Biochem. Eng./Biotechnol.* Editors H. Zhao and A. P. Zeng (Cham: Springer), 162, 117–146. doi:10.1007/10_2016_13

Nicolaou, K. C., and Rigol, S. (2020). Perspectives from nearly five decades of total synthesis of natural products and their analogues for biology and medicine. *Nat. Prod. Rep.* 37, 1404–1435. doi:10.1039/D0NP00003E

Nicolaou, K. C., Vourloumis, D., Winssinger, N., and Baran, P. S. (2000). The art and science of total synthesis at the dawn of the twenty-first century. *Angew. Chem. Int. Ed.* 39 (1), 44–122. doi:10.1002/(sici)1521-3773(20000103)39:1<44::aid-anie44>3.0.co;2-l

Ohide, H., Miyoshi, Y., Maruyama, R., Hamase, K., and Konno, R. (2011). D-Amino acid metabolism in mammals: Biosynthesis, degradation and analytical aspects of the metabolic study. *J. Chromatogr. B* 879, 3162–3168. doi:10.1016/j.jchromb.2011.06.028

Peters, D. S., Pitts, C. R., McClymont, K. S., Stratton, T. P., Bi, C., Baran, P. S., et al. (2021). Ideality in context: Motivations for total synthesis. *Acc. Chem. Res.* 54, 605–617. doi:10.1021/acs.accounts.0c00821

Reetz, M. T. (2016). *Directed evolution of selective enzymes: Catalysts for organic chemistry and Biotechnology*. Weinheim: Wiley VCH. ISBN 978-3-527-31660-1.

Richter, N., Neumann, M., Liese, A., Wohlgemuth, R., Eggert, T., Hummel, W., et al. (2009). Characterisation of a recombinant NADP-dependent glycerol dehydrogenase from *Gluconobacter oxydans* and its application in the production of L-glyceraldehyde. *ChemBioChem* 10 (11), 1888–1896. doi:10.1002/cbic.200900193

Roberts, A. R., Ryan, K. S., Moore, B. S., and Gulder, T. A. M. (2010). Total (Bio) Synthesis: Strategies of nature and of chemists. *Top. Curr. Chem.* 297, 149–203. doi:10.1007/128_2010_79

Roessner, C. A., and Scott, A. I. (1996). Achieving natural product synthesis and diversity via catalytic networking *ex vivo*. *Chem. Biol.* 3 (5), 325–330. doi:10.1016/S1074-5521(96)90114-3

Roessner, C. A., Spencer, J. B., Ozaki, S., Min, C. H., Atshaves, B. P., Nayar, P., et al. (1995). Overexpression in *Escherichia coli* of 12 vitamin B12 biosynthetic enzymes. *Protein Expr. Purif.* 6, 155–163. doi:10.1006/prep.1995.1019

Roessner, C. A., Spencer, J. B., Stolowich, N. J., Wang, J., Nayar, G. P., Santander, P. J., et al. (1994). Genetically engineered synthesis of precorrin-6x and the complete corrinoid, hydrogenobyrinic acid, an advanced precursor of vitamin B12. *Chem. Biol.* 1 (2), 119–124. doi:10.1016/1074-5521(94)90050-7

Rudroff, F., Mihovilovic, M. D., Gröger, H., Snajdrova, R., Iding, H., Bornscheuer, U. T., et al. (2018). Opportunities and challenges for combining chemo- and biocatalysis. *Nat. Catal.* 1 (1), 12–22. doi:10.1038/s41929-017-0010-4

Ruth, M. R., and Field, C. J. (2013). The immune modifying effects of amino acids on gut-associated lymphoid tissue. *J. Anim. Sci. Biotechnol.* 4 (27), 27. doi:10.1186/2049-1891-4-27

Schell, U., Wohlgemuth, R., and Ward, J. M. (2009). Synthesis of pyridoxamine 5′-phosphate using an MBA:pyruvate transaminase as biocatalyst. *J. Mol. Catal. B Enzym.* 59 (4), 279–285. doi:10.1016/j.molcatb.2008.10.005

Schmid-Dannert, C., and López-Gallego, F. (2019). Advances and opportunities for the design of self-sufficient and spatially organized cell-free biocatalytic systems. *Curr. Opin. Chem. Biol.* 49, 97–104. doi:10.1016/j.cbpa.2018.11.021

Schoenenberger, B., Kind, S., Meier, R., Eggert, T., Obkircher, M., Wohlgemuth, R., et al. (2020). Efficient biocatalytic synthesis of D-tagatose 1, 6-diphosphate by LacC-catalysed phosphorylation of D-tagatose 6-phosphate. *Biocatal. Biotransformation* 38 (1), 53–63. doi:10.1080/10242422.2019.1634694

Schoenenberger, B., Wszolek, A., Meier, R., Brundiek, H., Obkircher, M., Wohlgemuth, R., et al. (2017a). Biocatalytic asymmetric Michael addition reaction of L-arginine to fumarate for the green synthesis of N-(([(4S)-4-amino-4-carboxy-butyl]amino)iminomethyl)-L-aspartic acid lithium salt (L-argininosuccinic acid lithium salt). *RSC Adv.* 7, 48952–48957. doi:10.1039/C7RA10236D

Schoenenberger, B., Wszolek, A., Meier, R., Brundiek, H., Obkircher, M., Wohlgemuth, R., et al. (2018). Recombinant AroL-catalyzed phosphorylation for the efficient synthesis of shikimic acid 3-phosphate. *Biotechnol. J.* 13 (8), 1700529. doi:10.1002/biot.201700529

Schoenenberger, B., Wszolek, A., Milesi, T., Brundiek, H., Obkircher, M., Wohlgemuth, R., et al. (2017b). Synthesis of *N*ω-phospho-L-arginine by biocatalytic phosphorylation of L-arginine. *ChemCatChem* 9 (1), 121–126. doi:10.1002/cctc.201601080

Schrittwieser, J. H., Velikogne, S., Hall, M., and Kroutil, W. (2018). Artificial biocatalytic linear cascades for preparation of organic molecules. *Chem. Rev.* 118 (1), 270–348. doi:10.1021/acs.chemrev.7b00033

Scott, A. I. (2003). Discovering nature's diverse pathways to vitamin B12: A 35-year odyssey. *J. Org. Chem.* 68 (7), 2529–2539. doi:10.1021/jo020728t

Scott, A. I., Yagen, B., and Lee, E. (1973). Biosynthesis of corrins. Cell-free system from *Propionibacterium shermanii*. *J. Am. Chem. Soc.* 95, 5761–5762. doi:10.1021/ja00798a054

Sheldon, R. A., Basso, A., and Brady, D. (2021). New frontiers in enzyme immobilisation: robust biocatalysts for a circular bio-based economy. *Chem. Soc. Rev.* 50 (10), 5850–5862. doi:10.1039/D1CS00015B

Shen, L., Kohlhaas, M., Enoki, J., Meier, R., Schönenberger, B., Wohlgemuth, R., et al. (2020). A combined experimental and modelling approach for the Weimberg pathway optimisation. *Nat. Commun.* 11, 1098. doi:10.1038/s41467-020-14830-y

Sun, Q., Lv, Y., Zhang, C., Wu, W., Zhang, R., Zhu, C., et al. (2021). Efficient preparation of c-di-AMP at gram-scale using an immobilized *Vibrio cholerae* dinucleotide cyclase DncV. *Enzyme Microb. Technol.* 143, 109700. doi:10.1016/j.enzmictec.2020.109700

Sutiono, S., Pick, A., and Sieber, V. (2021). Converging conversion–using promiscuous biocatalysts for the cell-free synthesis of chemicals from heterogeneous biomass. *Green Chem.* 23 (10), 3656–3663. doi:10.1039/D0GC04288A

Swainston, N., Handl, J., and Kell, D. B. (2015). A 'rule of 0.5'for the metabolite-likeness of approved pharmaceutical drugs. *Metabolomics* 11 (2), 323–339. doi:10.1007/s11306-014-0733-z

Swartz, J. R. (2018). Expanding biological applications using cell-free metabolic engineering: An overview. *Metab. Eng.* 50, 156–172. doi:10.1016/j.ymben.2018.09.011

Takáts, Z., Wiseman, J. M., Gologan, B., and Cooks, R. G. (2004). Mass spectrometry sampling under ambient conditions with desorption electrospray ionization. *Science* 306, 471–473. doi:10.1126/science.1104404

Taylor, S. J., McCague, R., Wisdom, R., Lee, C., Dickson, K., Ruecroft, G., et al. (1993). Development of the biocatalytic resolution of 2-azabicyclo[2.2.1]hept-5-en-3-one as an entry to single-enantiomer carbocyclic nucleosides. *Tetrahedron Asymmetry* 4 (6), 1117–1128. doi:10.1016/S0957-4166(00)80218-9

Thorpe, T. W., Marshall, J. R., Harawa, V., Ruscoe, R. E., Cuetos, A., Finnigan, J. D., et al. (2022). Multifunctional biocatalyst for conjugate reduction and reductive amination. *Nature* 604 (7904), 86–91. doi:10.1038/s41586-022-04458-x

Vogel, M. A. K., Burger, H., Schläger, N., Meier, R., Schönenberger, B., Bisschops, T., et al. (2016). Highly efficient and scalable chemoenzymatic syntheses of (R)-and (S)-lactaldehydes. *React. Chem. Eng.* 1 (2), 156–160. doi:10.1039/C5RE00009B

Wang, S., Dong, G., and Sheng, C. (2019). Structural simplification of natural products. *Chem. Rev.* 119, 4180–4220. doi:10.1021/acs.chemrev.8b00504

Ward, P. S., and Thompson, C. B. (2012). Metabolic reprogramming: A cancer hallmark even warburg did not anticipate. *Cancer Cell* 21, 297–308. doi:10.1016/j.ccr.2012.02.014

Wender, P. A., Quiroz, R. V., and Stevens, M. C. (2015). Function through synthesis-informed design. *Acc. Chem. Res.* 48, 752–760. doi:10.1021/acs.accounts.5b00004

Wender, P. A. (2014). Toward the ideal synthesis and molecular function through synthesis-informed design. *Nat. Prod. Rep.* 31, 433–440. doi:10.1039/C4NP00013G

Wender, P. A., Verma, V. A., Paxton, T. J., and Pillow, T. H. (2008). Function-oriented synthesis, step economy, and drug design. *Acc. Chem. Res.* 41, 40–49. doi:10.1021/ar700155p

T. Werpy and G. Petersen (Editors) (2004). *Top value added chemicals from biomass, volume I, results of screening for potential candidates from sugars and synthesis gas* (Golden, Colorado, USA: U.S. Department of Energy (DOE), National Renewable Energy Laboratory). No. DOE/GO-102004-1992.

Wishart, D. S., Feunang, Y. D., Marcu, A., Guo, A. C., Liang, K., Vazquez-Fresno, R., et al. (2018). HMDB 4.0: The human metabolome database for 2018. *Nucleic Acids Res.* 46 (D1), D608–D617. doi:10.1093/nar/gkx1089

Wöhler, F. (1828). Ueber künstliche Bildung des Harnstoffs. *Ann. Phys. Chem.* 12, 253–256. doi:10.1002/andp.18280880206

Wohlgemuth, R. (2017). Biocatalytic process design and reaction engineering. *Chem. Biochem. Eng. Q.* 31, 131–138. doi:10.15255/CABEQ.2016.1029

Wohlgemuth, R. (2018). Horizons of systems biocatalysis and renaissance of metabolite synthesis. *Biotechnol. J.* 13 (6), 1700620. doi:10.1002/biot.201700620

Wohlgemuth, R. (2007). Interfacing biocatalysis and organic synthesis. *J. Chem. Technol. Biotechnol.* 82 (12), 1055–1062. doi:10.1002/jctb.1761

Wohlgemuth, R. (2021). Key advances in biocatalytic phosphorylations in the last two decades: Biocatalytic syntheses *in vitro* and biotransformations *in vivo* (in humans). *Biotechnol. J.* 16 (4), 2000090. doi:10.1002/biot.202000090

Wohlgemuth, R. (2011). "Product recovery," in *Comprehensive Biotechnology*. Editors M. Moo-Young, M. Butler, C. Webb, A. Moreira, B. Grodzinski, Z. F. Cui, et al. 2, 591–601. doi:10.1016/B978-0-444-64046-8.00096-3

Wohlgemuth, R. (2022). Selective biocatalytic defunctionalization of raw materials. *ChemSusChem* 15 (9), e202200402. doi:10.1002/cssc.202200402

Wohlgemuth, R. (2009). Tools and ingredients for the biocatalytic synthesis of metabolites. *Biotechnol. J.* 4 (9), 1253–1265. doi:10.1002/biot.200900002

Woodley, J. M. (2017). Integrating protein engineering with process design for biocatalysis. *Phil. Trans. R. Soc. A* 376, 20170062. doi:10.1098/rsta.2017.0062

Woodward, R. B. (1966). Recent advances in the chemistry of natural products. *Science* 153 (3735), 487–493. doi:10.1126/science.153.3735.487

Young, I. S., and Baran, P. S. (2009). Protecting-group-free synthesis as an opportunity for invention. *Nat. Chem.* 1 (3), 193–205. doi:10.1038/nchem.216

Zalatan, J. G., Lee, M. E., Almeida, R., Gilbert, L. A., Whitehead, E. H., La Russa, M., et al. (2015). Engineering complex synthetic transcriptional programs with CRISPR RNA scaffolds. *Cell* 160 (0), 339–350. doi:10.1016/j.cell.2014.11.052

Zhao, M., Qin, Z., Abdullah, A., and Xiao, Y. (2022). Construction of biocatalytic cascades for the synthesis of benzylisoquinoline alkaloids from p-coumaric acid derivatives and dopamine. *Green Chem.* 24 (8), 3225–3234. doi:10.1039/D1GC04759K

Advantages of publishing in Frontiers

OPEN ACCESS
Articles are free to read for greatest visibility and readership

FAST PUBLICATION
Around 90 days from submission to decision

HIGH QUALITY PEER-REVIEW
Rigorous, collaborative, and constructive peer-review

TRANSPARENT PEER-REVIEW
Editors and reviewers acknowledged by name on published articles

Frontiers
Avenue du Tribunal-Fédéral 34
1005 Lausanne | Switzerland

Visit us: www.frontiersin.org
Contact us: frontiersin.org/about/contact

REPRODUCIBILITY OF RESEARCH
Support open data and methods to enhance research reproducibility

DIGITAL PUBLISHING
Articles designed for optimal readership across devices

FOLLOW US
@frontiersin

IMPACT METRICS
Advanced article metrics track visibility across digital media

EXTENSIVE PROMOTION
Marketing and promotion of impactful research

LOOP RESEARCH NETWORK
Our network increases your article's readership